Porphyrins
for
Surface Modification

A Thesis Presented in Partial Fulfilment of the

Requirements for the Degree of

Doctor of Philosophy

in

Chemistry

at Massey University, Palmerston North,

New Zealand.

Wayne Mason Campbell

2001

MASSEY UNIVERSITY
APPLICATION FOR APPROVAL OF REQUEST TO EMBARGO A THESIS
(Pursuant to AC98/168 (Revised 2), Approved by Academic Board 16.02.99)

Name of Candidate: _Warren Mason Campbell_ I.D. Number: _91063166_

Degree: _Doctor of Philosophy_ Dept / Institute / School: _Chemistry, IFS_

Thesis Title: _Porphyrins for Surface Modification_

Name of Chief Supervisor: _David L. Officer_ Telephone Ext: _3565_

As author of the above named thesis, I request that my thesis be embargoed from public

access until (date)_____ 9 / 2003 _____ for the following reasons:

[✓] Thesis contains commercially sensitive information.

[ ] Thesis contains information which is personal or private and / or which was given on the basis that it not be disclosed.

[ ] Immediate disclosure of thesis contents would not allow the author a reasonable opportunity to publish all or part of the thesis.

[ ] Other (specify) : _____

Please explain here why you think this request is justified:

A patent on this work is currently
being prepared.

Signed (Candidate): _W.M.C._ Date: _18/09/01_

Endorsed (Chief Supervisor): _____ Date: _18/09/01_

Approved / ~~Not Approved~~ (Representative of VC): _H.K. Long_ Date: _18/09/01_

Note: Copies of this form, once approved by the representative of the Vice Chancellor, must be bound into <u>every</u> copy of the thesis.

[MURET appl form Disk 15]

Abstract

The controlled synthesis of a variety of benzoic acid porphyrins ranging from monomers to arrays for the modification of TiO_2 and GaAs semiconductors, and sulfur functionalised porphyrin monomers for attachment to GaAs and Au surfaces was achieved. A semi-quantitative study of the photosensitisation of TiO_2 by the porphyrin acids was carried out.

The syntheses of β-styryl linked porphyrin benzoic acids and some *meso*-substituted benzoic acid porphyrins was successfully carried out employing Wittig chemistry and classical porphyrin-forming condensation reactions with appropriate formyl methyl esters. Hydrolysis of the resulting porphyrin esters provided a facile and reliable acid synthesis, particularly where multi-step reactions were necessary. It was also demonstrated that acid functionality on porphyrins could be generated from aldehydes via esters, even though direct oxidation of the aldehydes to acids could not be achieved. The syntheses of "dipole" and "collinear" diporphyrins were achieved, providing two different porphyrin light harvesting arrays for evaluation on semiconductor surfaces. As a result of the synthesis of a new linear diporphyrin Building Block C, an alternative pathway to the controlled syntheses of mixed-metal and mixed-porphyrin arrays was achieved. This provided an alternative strategy for the controlled placement of three different metals into three different porphyrins of a linear triporphyrin, pentaporphyrin and a larger star-shaped nonaporphyrin.

The exploitation of the stepwise controlled synthesis of the triporphyrin systems was expanded to include mixed-porphyrin systems synthesised with a unique tetraester porphyrin phosphonium salt. This phosphonium salt afforded mixed-diporphyrin and mixed-triporphyrin arrays, which were hydrolysed to give "sticky" mixed-diporphyrin and triporphyrin acid arrays.

An alternative milder and higher yielding stepwise Wittig method was developed for the synthesis of a star shaped TXP pentaporphyrin. This new method involving milder base conditions gives advantages over the traditional acid catalysed approach developed in these laboratories. It is now possible to build these arrays in a stepwise manner with

acid labile metals present in the porphyrin moieties. Access to the controlled synthesis of "sticky" mixed-pentaporphyrin arrays was then achieved using this new methodology.

With the synthesis of a variety of unique benzoic acid functionalised porphyrin monomers and multiporphyrin array systems, evaluation of their performance in the dye-sensitised TiO_2 Grätzel cell was carried out. The development of a reliable solar cell testing apparatus and procedures required to assess the solar cell performance of these chromophores is presented. None of the conditions employed have been optimised, but insights into the significance of the porphyrin photoelectrochemical cell variables has been obtained. It was determined that the porphyrin acids are better photosensitisers than their salts, and that $Zn(II)$ metalloporphyrins performed best as dyes. The results also suggest that $Cu(II)$ metalloporphyrins are worth pursuing in future where long term stability of the chromophores is required in solar cells. It was also found that adsorption solvent choice, electrolyte composition and dye concentrations are all critical to cell performance, and should all be optimised in future studies. The tetraaryl β-substituted monoporphyrin acids were found to have a significant advantage over the multiporphyrin arrays and other monoporphyrins synthesised and examined in this work.

A variety of new disulfide porphyrins and some new 2- and 3-thienylporphyrins were successfully synthesised. A new class of terthiophene-appended porphyrins was also synthesised. Using a combination of Wittig chemistry and classical condensation reactions, β-substituted, and bis- and tetra-*meso*-porphyrin variants were synthesised and characterised. Both the bis- and tetraterthienylpoprhyrins were isolated as mixtures of atropisomers.

Acknowledgments

Table of Contents

Appendix C

List of Figures

List of Tables

List of Equations

Abbreviations

AFM	atomic force microscopy
AM1.0	air mass 1.0 (shortest path length for solar radiation through the atmosphere)
AM1.5	air mass 1.5 (1.5 times the shortest path length for solar radiation through the atmosphere)
AR	analytical reagent
app	apparent
aq.	aqueous
Ar	aryl group
avg	average
Au	gold
BAP	5,15-bis-*aryl*-porphyrin
BAcP	bis-*acetal*-porphyrin
BCP	bis-*carboxy*-porphyrin
BEP	bis-*ester*-porphyrin
BDP	bis-*disulfide*-porphyrin
BFP	bis-*formyl*-porphyrin
BP	3,5-di-*tert*-butylphenyl group
B2TP	bis-2-*thienyl*-porphyrin
B3TP	bis-3-*thienyl*-porphyrin
BTTP	bis-*terthienyl*-porphyrin
Calcd	calculated
CHCA	α-cyano-4-hydroxycinnamic acid
conc.	concentrated
COSY	correlated spectroscopy
d	doublet
DBU	1,8-diazabicyclo[5.4.0]undec-7-ene
DCE	1,2-dichloroethane
DCM	dichloromethane or CH_2Cl_2
DMF	*N,N*-dimethylformamide
DMSO	dimethylsulfoxide

dia	circular diameter
DPM	dipyrrylmethane
EI	electron ionisation
eq	equivalent
ES	electrospray
Et	ethyl
Et_2O	diethyl ether
EDW	electron donating group
Et_3N	triethylamine
EWG	electron withdrawing group
FAB	fast atom bombardment
FET	field-effect-transistor
FF	fill factor (ratio of the maximum output of the photovoltaic device, to the product of I_{sc} and V_{oc})
GaAs	gallium arsenide
GP	general-purpose reagent
h	hours
hept	heptet
hex	hextet
HMTA	hexamethylenetetramine
HR	high resolution
HRMS	high resolution mass spectrometry
HOMO	highest occupied molecular orbital
IPCE	incident photon-to-current conversion efficiency
I_{sc}	short circuit current
ITO	indium-tin-oxide (conductive glass coating)
LUMO	lowest unoccupied molecular orbital
LR	low resolution
LRMS	low resolution mass spectrometry
min	minutes
M	$mol\ L^{-1}$
M	a metal ion
m	multiplet, milli
MALDI	matrix assisted laser desorption ionisation spectroscopy

Me	methyl
MeOH	methanol
mp	melting point
MS	mass spectrometry
NMR	nuclear magnetic resonance
[O]	oxidation
oct	octet
P(A-D)	TiO_2 coated ITO glass (batches A-D)
Pc	phthalocyanine
PEC	photoelectrochemical cell
pent	pentet
Ph	phenyl
ppm	parts per million
ps	phosphonium salt
q	quartet
[R]	reduction
R_f	retention factor
RT	room temperature
RO	reverse osmosis
ROSEY	rotating frame overhauser enhancement spectroscopy
sat.	saturated
SC	semiconductor
SEM	scanning electron microscopy
sh	shoulder
SP	"sticky" porphyrin
SS	steady state
STM	scanning tunnelling microscopy
t	triplet
TAcP	tetra-*acetal*-porphyrin
TAP	5,10,15,20-tetra-*aryl*-porphyrin
TBM	tetrabutyltetramethyl
TBMP	2,8,12,18-tetra-*n*-butyl-3,7,13,17-tetramethylporphyrin
TBP	5,10,15,20-tetrakis(3',5'-di-*tert*-butylphenyl)porphyrin
TCA	trichloroacetic acid

TCP	tetra-4'-*carboxy*-porphyrin
T3CP	tetra-3'-*carboxy*-porphyrin
T3,5CP	tetra-3',5'-*dicarboxy*-porphyrin
TEP	tetra-*4'-ester*-porphyrin
T3EP	tetra-*3'- ester*-porphyrin
T3,5EP	tetra-*3',5'-diester*-porphyrin
TFA	trifluoroacetic acid
TFP	tetra-*4'-formyl*-porphyrin
THF	tetrahydrofuran
TiO_2	titanium dioxide
TLC	thin layer chromatography
TMS	tetramethylsilane
TOF	time-of-flight
TOPP	5,10,15,20-tetra(4-octylphenyl)porphyrin
TPP	5,10,15,20-tetraphenylporphyrin
TR	all-*trans*-retinoic acid
TTTP	tetra-*3"-terthienyl*-porphyrin
TXP	tetra-*xylyl*-porphyrin or
	5,10,15,20-tetrakis(3',5'-dimethylphenyl)porphyrin
UV-vis	ultraviolet-visible spectroscopy
Xyl	xylyl (3,5-dimethylphenyl group)
V_{oc}	open circuit voltage

TAP

BAP (TBMP)

TAP	Ar	#
TPP	Ph	1
TXP	Xyl	2
TBP	BP	3
TEP	CO_2Me	85
TCP	CO_2H	8
T3EP	CO_2Me Est	93
T3CP	CO_2H Acid	95
T3,5EP	CO_2Me CO_2Me	74
T3,5CP	CO_2H CO_2H	75
TAcP		114
TFP	CHO	110
TTTP		139

BAP	Ar	#
BAcP		62
BFP	CHO	76
BEP	CO_2Me	60
BCP	CO_2H	73
BDP	Me	150
B2TP		134
B3TP		135
BTTP		138

See Back Page for Foldout Index

Introduction

1.1   Molecules on Surfaces

Molecules have been attached to surfaces for a wide variety of reasons. By binding a molecule to a surface through chemisorption or physisorption, the functionality and properties of individual molecules may be immobilised to a specific location, phase and orientation. Immobilisation can take place with little change in properties of the surface or molecule. However, more frequently binding molecules to surfaces emanates from the desire to enhance the properties of the molecule or surface or even produce completely new properties. In short, the physical and chemical intra/inter-molecular properties of attached molecular systems may be transmitted through to the surface/substrate where they can be measured or transformed into other useful physical and chemical processes.

Table 1-1. Common surfaces modified by molecules.

Insulators	Semiconductors (SCs)	Metals
SiO_2	SnO_2, TiO_2	Au
Al_2O_3	Ge/GeO	Pt
	Si, InP	Ag
	CdSe, CdS	Cu
	GaAs	

Molecular surface modification has been applied extensively to three important classes of materials: insulators, semiconductors (SC) and metals (Table 1-1).[1-4] These surface/substrates could be comprised of metal or inorganic/organic SC compounds. The surface component could differ from that of the substrate component or the bulk may consist of a matrix of these components.

The types of molecules used and their applications vary considerably. However at the forefront of current research is the modification of electronic materials like gold (Au) and SCs like gallium arsenide (GaAs) and titanium dioxide (TiO_2) with photo/redox-active chromophore molecules.[5] The photosensitisation of wide-bandgap (≥ 3.0 eV, corresponding to photons with wavelength ≤ 413 nm) SCs such as ZnO, TiO_2 and SnO_2 (Figure 1-1) over the visible and near-IR parts of the electromagnetic spectrum have already shown application in photonic[2,6,7] and optoelectronic devices.[8] In particular,

photosensitisation of TiO_2 shows promise for the commercialisation of the dye-sensitised photoelectrochemical cells (PECs, Grätzel cell)[9] and solid state n-p junction solar cells[10]. Applications in electro/photo-chromic[11-16] and optoelectronic write-read-erase[17] devices have already been realised. Development of photo/electrocatalysis for the production of H_2 from water and the photo-oxidation/degradation of organic contaminants is progressing.[18-21]
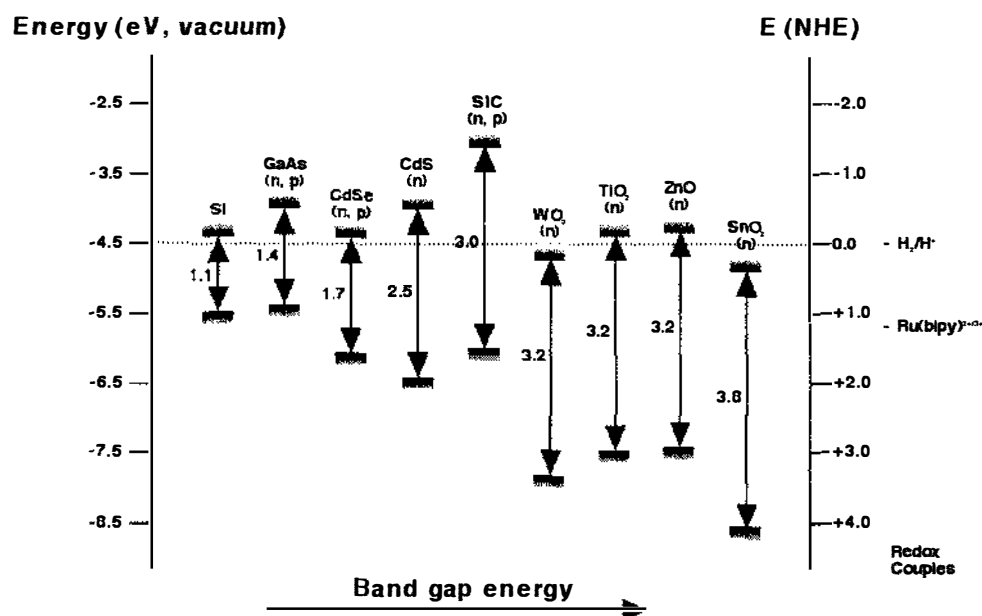
Figure 1-1. Band edge positions of TiO_2 and other SCs at pH 1 (adapted from Grätzel et al.).[22]

Chromophores coupled to GaAs SC surfaces are showing promise for optoelectronic field effect transistor (FET) devices[23] and chemical sensors[24]. The modification of Au surfaces with photo/redox-active chromophore molecules has been of considerable interest for the study of light induced charge transfer processes[25,26] and has also shown potential for use in optoelectronic devices[27].

To date a diverse range of chromophores have been used as photosensitisers. Generally, transition metal complexes derived from polypyridines **A**, porphine **B** or phthalocyanine **C** (Figure 1-2) have been preferred. These ligands are all nitrogen heterocycles with a delocalised π or aromatic ring system and are capable of complexing with a variety of metal ions. The complexes exhibit a number of low-lying electronic excited states. They have long-lived d-d* and d-π* metal-to-ligand charge transfer (MLCT) and ligand-centred π-π* excited states, which can participate in electron transfer processes.

Through molecular engineering, these metal complexes can be readily anchored to SC surfaces.

Ru polypyridine complex   Metalloporphyrin   Metallophthalocyanine

A   B   C
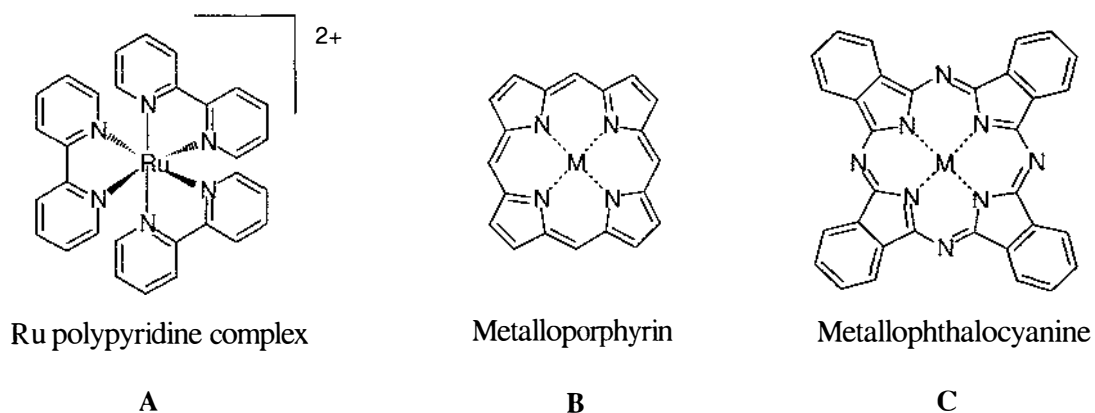
Figure 1-2. Common photosensitisers.

These chromophores have characteristics fundamentally required for light-harvesting dyes, namely:

- The complexes have broad and intense light absorptions in the visible, near-IR and IR regions. For solar energy conversion, a large spectral absorption range is necessary, whereas for wavelength specific photonic devices a narrower spectral range is more suitable.
- Functionalisation of the ligands allows tuning of the absorption bands.
- They have long-lived excited states.
- The dyes have been shown to be stable in the oxidised, reduced and excited states, and resist photochemical and chemical degradation.

The ability to organise molecules on a surface with control over their arrangement, distribution, mobility, photophysical and redox properties is important. In addition, many advances into improving the efficiency of surface photosensitisation have been explored and achieved with high surface area films and the construction of multi-component molecular antennae array systems. The porphyrin-based chromophores are of most interest to us as we have well-established synthetic methodologies allowing the rapid and efficient synthesis of some unique variants.

1.2   Chromophores on Metal and Semiconductor Surfaces

The binding of a chromophore to a metal or SC surface can take place in various ways: The binding can consist of covalent anchoring, electrostatic interactions, hydrogen bonding or physisorption (van der Waals interactions) (Figure 1-3). Chromophores could also be immobilised on a surface by polymerisation or physical entrapment within the substrate bulk.
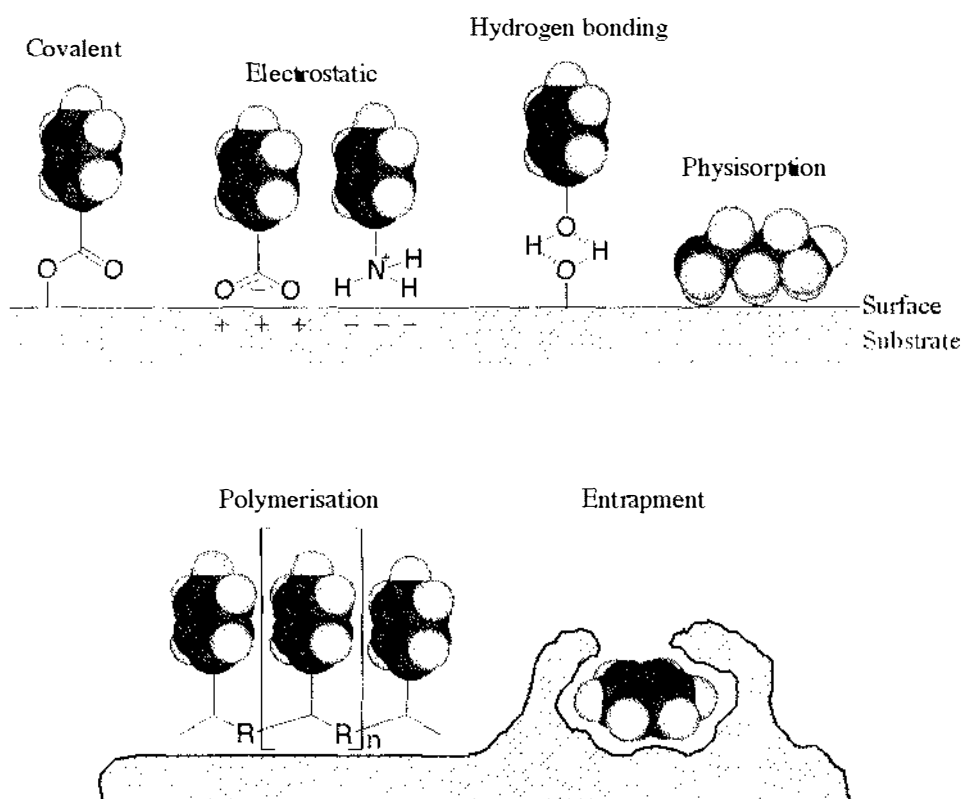
Figure 1-3. Anchoring molecules to surfaces.

The spatial organization of molecules on a surface can be established by a combination of surface structure, binding interactions and weak-to-strong intermolecular interactions between molecules bound to the surface. Intermolecular interactions can consist of hydrophobic, π-π, hydrogen-bonding and electrostatic interactions or a combination of these (Figure 1-4). The molecule-to-molecule and molecule-to-surface interactions can lead to the controlled formation of self-assembled monolayers (SAMs) of discrete and larger multi-component array assemblies on a surface.
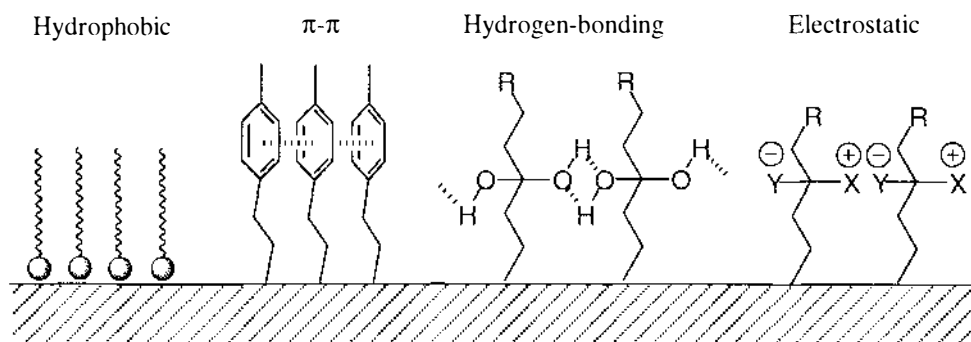
Figure 1-4. Intermolecular interactions on a surface

All of these factors are critical for the effective photosensitisation of SC and metal surfaces. The fundamental processes of photosensitisation are briefly discussed in the following sections. Following this, chromophoric excitation and the subsequent electronic energy-transfer processes in discrete and multi-component array systems are reviewed.

1.2.1 Photosensitisation of TiO$_2$

Titanium dioxide (TiO$_2$) is a chemically inert, non-toxic and biocompatible white pigment that is readily available in high purity. It represents an economical and ecologically safe SC material for photonic and optoelectronic devices, with specific applications in photovoltaics and photocatalysis. Of the oxide SCs, TiO$_2$, is by far the most commonly used.[28] Its extensive usage in industrial applications (paints, paper, coatings, plastics, fibres and cosmetics) comes from its high refractive index and easy preparation into fine particles. Thin films of TiO$_2$ have been prepared by many different physical and chemical techniques such as thermal oxidation, sputtering and chemical vapour deposition. Such films have found application for anti-reflective coatings for glass, dielectric materials, sensors and wave-guides.[11]

Rutile, anatase and brookite are the three common crystalline polymorphs of TiO$_2$, rutile being the thermodynamically most stable form ($\approx$ 5.0-12 kJ mol^{-1} more stable than anatase). The rutile to anatase transformation occurs in the temperature range 700-1000°C depending on the crystalline size and purity. Anatase TiO$_2$ is a wide band gap

n-type SC (Figure 1-1). Because its band gap energy E_{BG} is ≥ 3.2 eV (corresponding to photons with wavelength ≤ 390 nm), it is nearly transparent to the major part of the solar spectrum. The process of photosensitisation can improve the photo-response of wide band gap SC materials, such as TiO_2, towards low energy excitations in the visible and near-IR regions of the solar spectrum. Figure 1-5 compares the optimum excitation wavelengths for TiO_2 and some other common SCs versus the AM1.5 solar irradiation spectrum. AM1 refers to air mass = 1, the shortest path length of solar radiation through the atmosphere, i.e. the sun is directly overhead. Therefore, AM1.5 is 1.5 times the shortest solar path length, where the sun is at an angle of 42°. The global normalised AM1.5g spectrum is scaled to integrate to intensity of 1000 W m^{-2} for solar cell testing (often referred to as 1 sun).
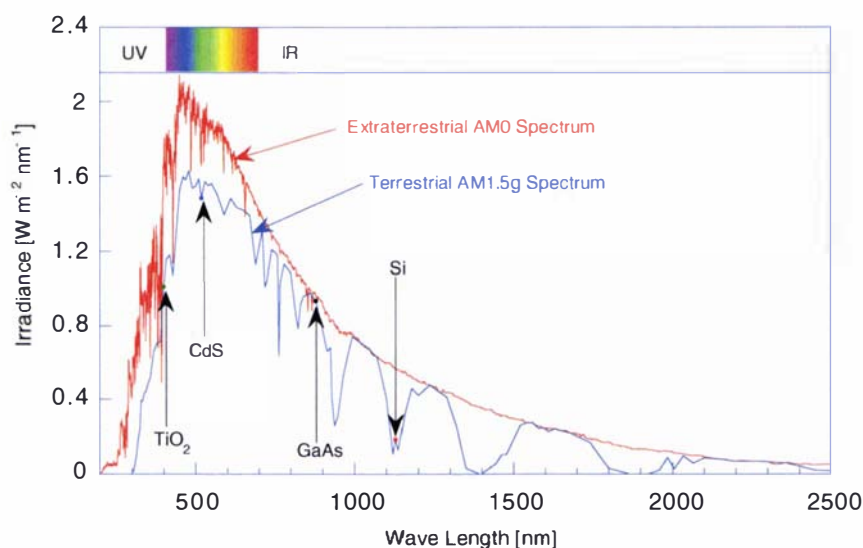
Figure 1-5. Photoresponse of TiO_2 and other SCs vs. AM1.5g and AM0 spectrum.[29]

Efficient capture of solar energy requires good photoresponse. This can be achieved by coating the SC with a thin layer of a sensitising dye (chromophore) that absorbs in the visible and near-IR regions. Photoexcitation of the sensitiser will then be followed by electron transfer (ET) to the SC conduction band, allowing photochemical and photocatalytic processes to occur.

Excitation of an electron in the chromophore occurs in the singlet or triplet excited state of the molecule. If the oxidative energy level of the excited state of the dye molecule is favourable (i.e. more negative) with respect to the conduction band energy level of the

SC, then the dye molecule can transfer an electron to the conduction band of the SC (Figure 1-6).
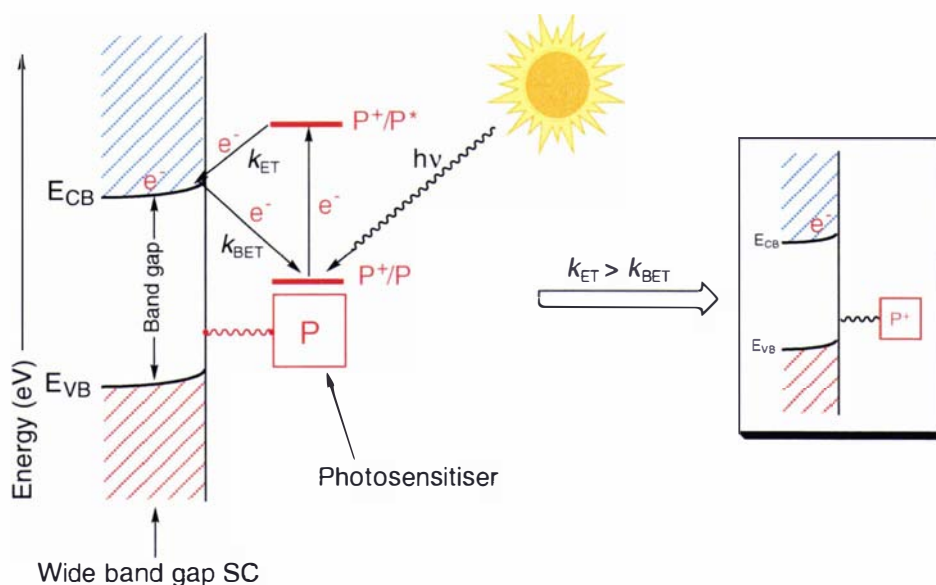
Figure 1-6. Photoinduced charge separation on TiO_2 surface

(k_{ET} and k_{BET} represent rate constants for charge injection and back electron transfer, respectively).

The surface acts as a quencher accepting an electron from the excited chromophore donor. The electron in turn can be transferred to reduce another organic molecule on the surface (i.e. catalysis), or collected for other useful work (i.e. generating electricity). Surprisingly, back electron transfer (BET) or charge recombination from the SC to the dye is slow compared to charge injection, the ratio k_{ET}/k_{BET} is often greater than 10^3. The reasons for this are yet not fully understood.[30] It is proposed that recombination is suppressed by band bending that drives the electron into the bulk of TiO_2 and/or by slow kinetics from back electron transfer. The back electron transfer rates to the electrolyte (dark current) can be reduced even further by blocking the exposed TiO_2 surface with other non-acceptor molecules such as 4-*tert*-butylpyridine ($k_{ET}/k_{BET} > 10^6$), thereby inhibiting back electron transfer of injected electrons.[31] This is especially important in the photoelectrochemical cell where there are other redox acceptor molecules in solution, at the solution-SC interface. Recently Zaban et al. reported the fabrication of a TiO_2 electrode with an inherent energy barrier at its surface.[32] By coating, the TiO_2 surface with a thin layer of Nb_2O_5 the conduction band potential at the surface is raised about 100 mV more negative (Figure 1-7) forming an energy barrier at the electrode-electrolyte interface. Herein lies the usefulness of sensitised TiO_2 for

photoinduced charge transfer applications, where the difference in rates of charge injection and charge recombination can be exploited.
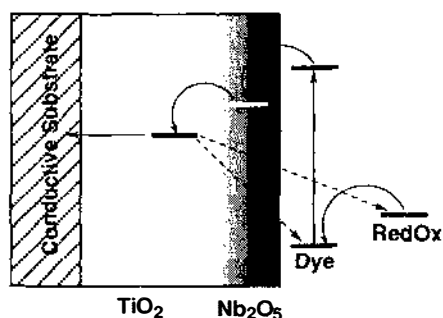
Figure 1-7. Schematic of energy barrier modified electrode.[32]
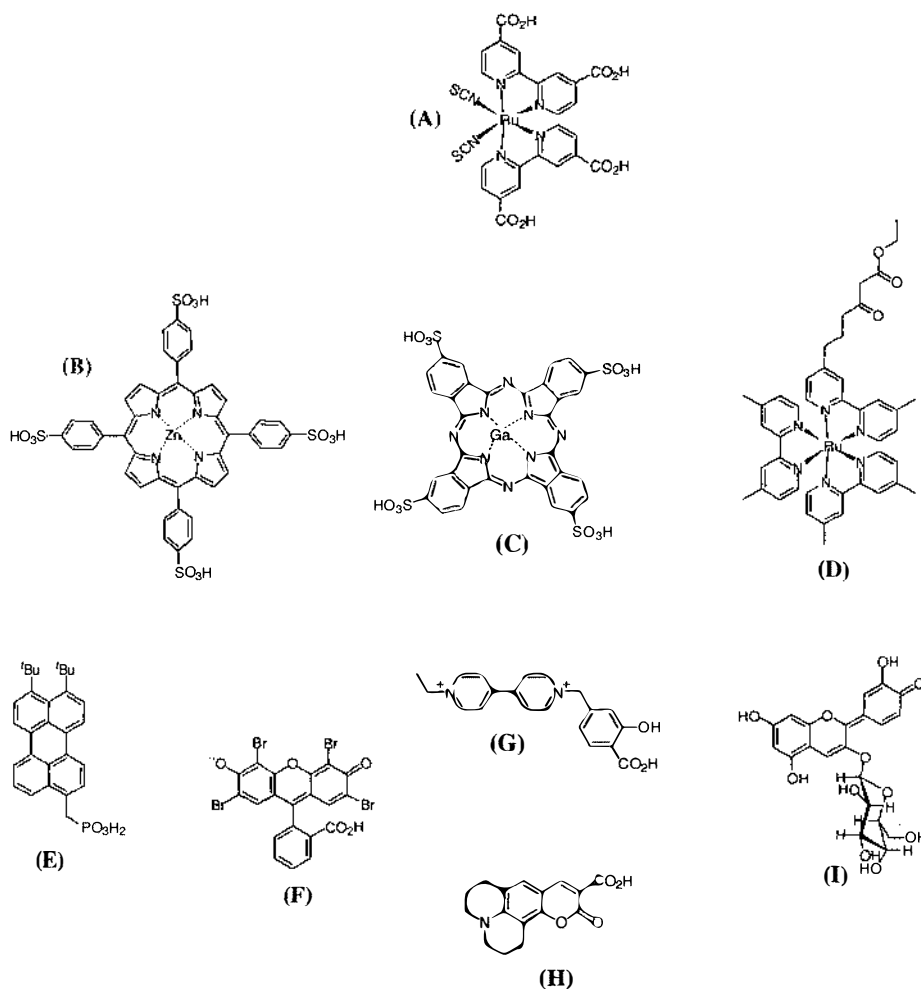
Figure 1-8. Chromophores and anchoring systems used on TiO_2.

(Ruthenium carboxypolypyridine complex (A)[33], zinc tetrasulfonatephenylporphyrin and (B) tetrasulfonatephthalocyanine (C)[34], ruthenium acetylacetonate polypyridine complex (D)[35], perylene dye (E)[36], xanthene dye (Eosin Y) (F)[37-39], viologen dye (G)[40], Coumarin 343 (H)[41], natural flavonoid anthocyanin dye extracted from California blackberries dye (I)[42].)

Anchoring of the chromophores to TiO_2 has been achieved through a number of functional groups. The most common functional groups have been salicylate, carboxylic acid, sulfonic acid, phosphonic acid and acetylacetonate derivatives. Figure 1-8 shows some of the wide range of chromophores and the anchoring groups that have been successfully attached to TiO_2. The most widely used and successful to date have been the carboxylic acid and phosphonic acid functionalities. The carboxylic acid groups, while ensuring efficient adsorption of the dye on the surface, promote electronic coupling through coupling of the donor levels of the excited chromophore and the acceptor levels of the SC. Some of the possible modes of chelation/derivatisation, ranging from chemical bonding (chelating or bridging mode) to H-bonding are shown in Figure 1-9.
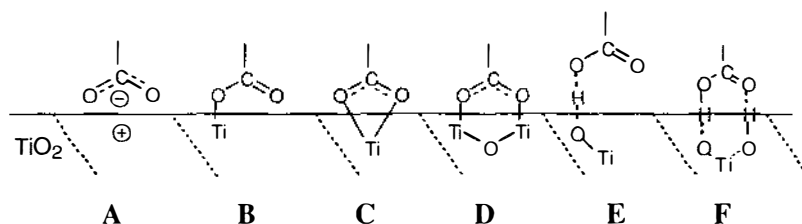
Figure 1-9. Possible binding modes for carboxylic acid groups on TiO_2.

Conflict exists in the literature about the specific binding mode. Falaras suggest their IR and Raman spectra support chemical bonding through ester formation **B** on the surface.[43] However, Duffy et al. strongly suggest surface coordination involves *syn-syn* bridging between two surface titanium atoms (eg. **D**).[44] One drawback of the COOH anchoring group is that the dye desorbs in the presence of water. This has been rectified to some extent by the use of a stronger binding group such as phosphonic acid. However, there is little information about the binding mode of phosphonic acid derivatives in the literature, although an ester type formation can be proposed (Figure 1-10). The photosensitiser $\{Ru(PO_3\text{-terpy})(Me_2bpy)(NCS)\}$ shows monochromatic and overall light-to-electrical conversion efficiency comparable to Ru dicarboxypolypyridine-based complexes (Figure 1-8, (A)). This phosphonic acid derivative has been shown to bind strongly to the TiO_2 surface (about 80 times more strongly than carboxylated analogues), and is not displaced easily by water. The adsorbed state is maintained over a wide pH domain (pH = 0-9) and excellent solar cell performance is obtained.[45,46]
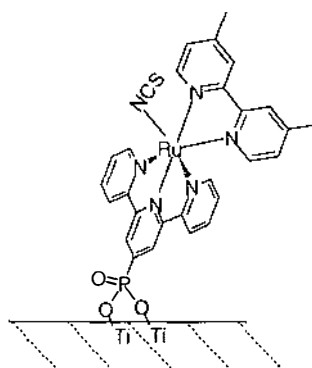
Figure 1-10. Possible mode of phosphonic acid ester surface binding on TiO_2.[45,46]

The type of anchor functionality and linker used between the sensitiser and SC surface can enhance electronic coupling and/or alter the surface state energetics so that electron injection is faster and more efficient. However, experiments suggest that the distance of the chromophoric ligand from the surface is critical to the design of molecular sensitisers, more so than the type of anchor.[35] For example, Ru(II) polypyridyl sensitisers on TiO_2 with an *n*-propyl spacer between a bipyridine ring and an acetylacetonate group (Figure 1-11, **A**), give comparable corrected IPCE (incident monochromatic photon-to-current conversion efficiency) values to a related sensitiser with a carboxylic acid group bound to the *n*-propyl spacer (Figure 1-11, **B**). However, neither of these gives as good a result as the sensitiser with a directly bound carboxylic acid (Figure 1-11, **C**).

IPCE = 0.292 ± 0.148   IPCE = 0.263 ± 0.120   IPCE = 0.495 ± 0.061

A   **B**   **C**
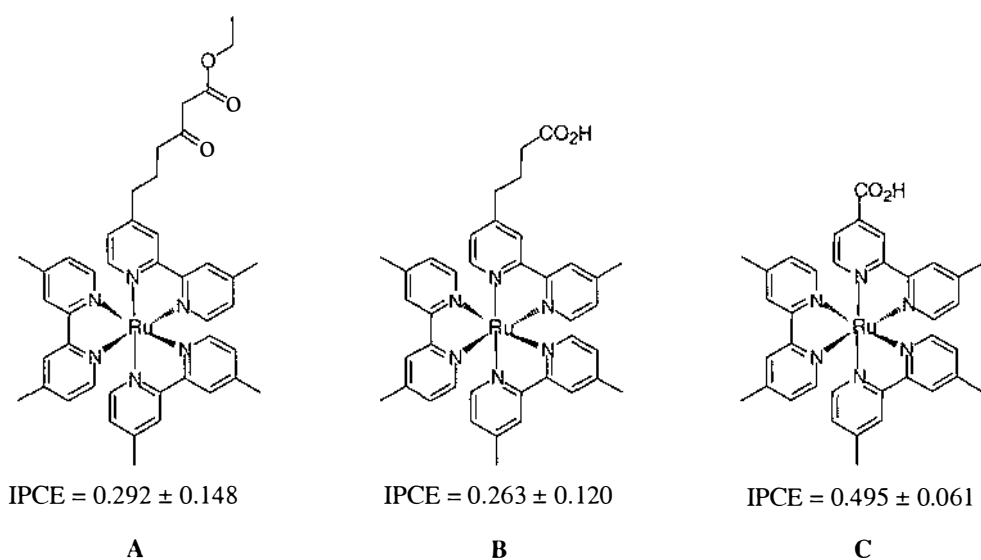
Figure 1-11. $IPCE_{max}$ results for model Ru polypyridyl complexes.[35]

The results suggest that there may be an optimum sensitiser orientation (or distance from surface) and possible linker (i.e. conjugation) dependence, wherein interfacial charge separation is still efficient but the charge recombination is inhibited enough to give high IPCE values.[35]

In order to explore the effect of sensitiser orientation, a bimetallic coordination compound was prepared, which when coordinated to TiO_2, holds a Ru sensitiser close to the surface (Figure 1-12).
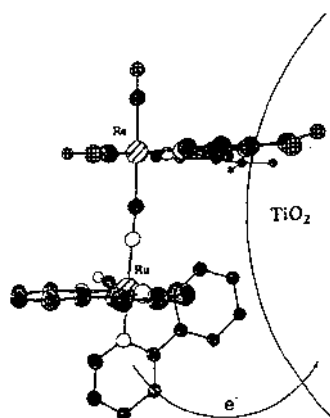
Figure 1-12. Through-space charge transfer (Reproduced from Meyer et al.).[47]

Visible light excitation of this sensitiser bound to TiO_2 leads to efficient photocurrent production. The Ru(bpy)$_2$ group absorbs most of the visible light, and since it is not bound to the SC surface it was concluded that direct attachment[47] or intimate contact[48] is not required for efficient solar conversion. However close proximity of the sensitiser to the surface may be more crucial; this does not diminish the importance of the anchoring group, as it must still hold the chromophore to the surface and/or potentially provide favourable electronic coupling between the donor levels of the sensitiser and the acceptor levels of the SC. Further research on the importance of these points is necessary. These principles as applied to the Grätzel cell will be more fully discussed in Chapter 5.

1.2.2   Photosensitisation of GaAs and Au

The modification of other SCs and metals, such as GaAs and Au is also of interest to us. Naaman et al. found that GaAs field-effect-transistors (FETs) could be modified by the adsorption of carboxylic acids and disulfides on to an exposed gate surface.[49]
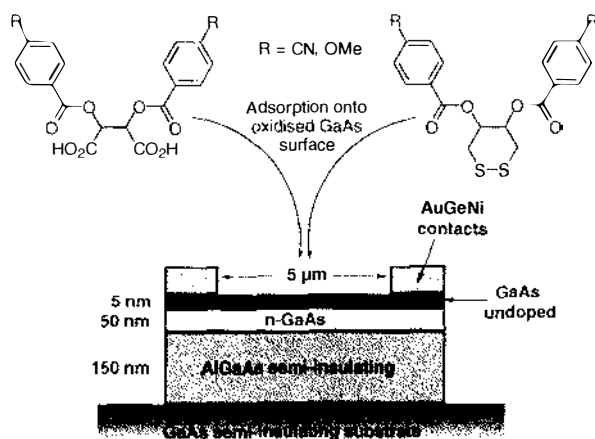
Figure 1-13. Molecularly modified FET device (Adapted from Naaman et al.).[49]

Figure 1-13 is a schematic of a FET device developed to monitor adsorption kinetics in real time. Naaman et al. discovered that by attaching light absorbing groups, the photocurrent decay times of the FET were modified by orders of magnitudes.[23] These effects were molecule specific, as they depend on the electronic properties and on the absorption spectra of the molecules. Naaman's group have also attached iron porphyrins through modified ligands as above to produce a novel NO biosensor (Figure 1-14).[24]
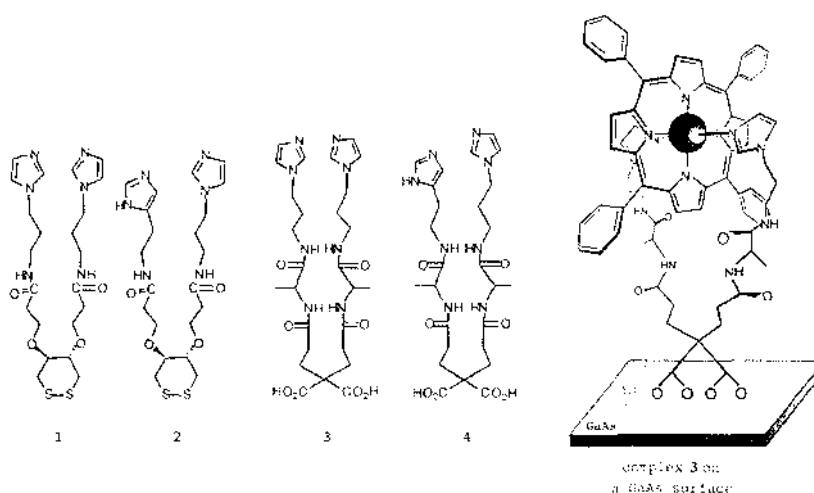
Figure 1-14. Bidentate binding of iron porphyrin to GaAs (Reproduced from Wu et al.).[24]

The photosensitisation of n-Si and n-GaAs with cationic porphyrin chromophores has also been studied by Zhang et al.[50] The functional groups showing most promise on GaAs are carboxylic acid and sulfur bearing chromophores. Sulfur functionalised chromophores are also desirable for the functionalisation of Au surfaces.[51] These could be applied to the pure metal or coatings on other SC surfaces. A variety of sulfur groups are known to bind to Au surfaces, these ranging from thiols, disulfides, sulfides, xanthates, thiocarbamates[3,52] to thiophene[53-55] derivatives (Figure 1-15).

| Thiol | Disulfide | Sulfide | Xanthate | Thiocarbamate | Thiophene |
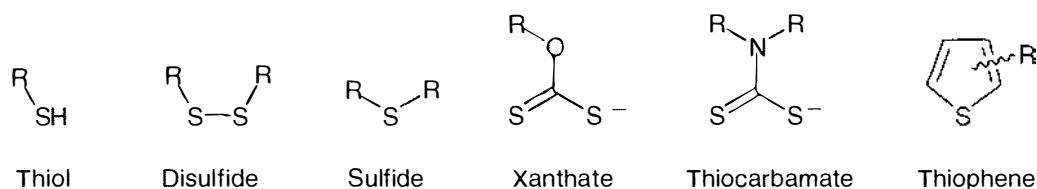
Figure 1-15. Sulfur compounds binding to Au surfaces.

1.3   *Improving Surface Photosensitisation*

Much research into dye sensitised molecular photovoltaic devices (solar cells) has been carried out. Initially, the efficiency of such devices based on dye sensitised wide band gap SCs and metals was low. This was largely due to the limited light absorption by a monolayer of the dye adsorbed onto an essentially smooth surface. Therefore, there was intense effort to improve the efficiency of dye-sensitised systems.

Two approaches have been investigated:

1. Increasing the projected surface area of SC based systems with mesoporous films.
2. Improving the light harvesting efficiency of a single chromophore by constructing multi-component "molecular antennae" where energy transfer processes convey the excitation energy on a number of chromophoric components to a common final acceptor, where the energy can be transferred to the surface.

The majority of the work relating to increased surface area has been carried out on wide band gap SCs like TiO_2 and ZnO. In contrast, the molecular antennae approach is applicable to both smooth or porous SCs, and metals surfaces.

1.3.1   Mesoporous Surfaces

Transparent mesoporous nanocrystalline TiO_2 film electrodes (larger surface area) provide a way to amplify the light absorption of a molecular monolayer, giving highly efficient light induced charge transfer devices based on wide band gap SCs. These surfaces have a roughness factor of over 500 (i.e. projected surface area is 500 times greater than a smooth surface). When light penetrates these films, it crosses the equivalent of several hundreds of adsorbed dye monolayers (Figure 1-16).
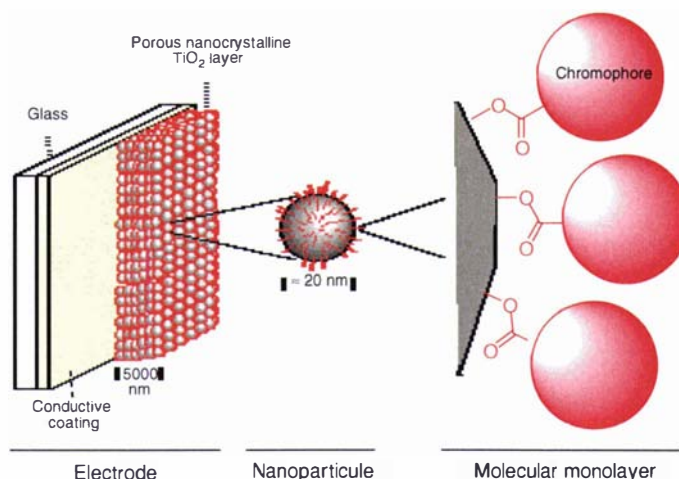
Figure 1-16. Structure of TiO_2 mesoporous nanocrystalline electrode derivatised with chromophores (adapted from Grätzel).[16]

Nanocrystalline TiO_2 SC surfaces are now easily prepared by depositing nanosized colloidal TiO_2 SC particles on a conducting glass support. This film is often then heated to sinter the nanoparticles, forming a porous high surface area, TiO_2 membrane.
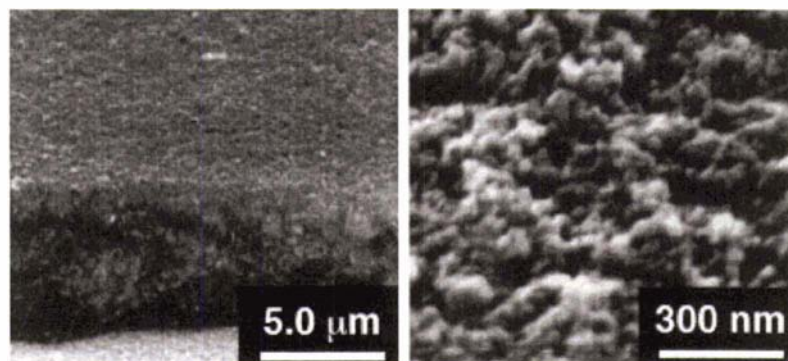
Figure 1-17. High and low-resolution SEM pictures of P-25 TiO_2 (reproduced from Kambe).[56]

Displayed in Figure 1-17 is a representative low and high-resolution SEM image of a mesoporous nanocrystalline TiO_2 electrode surface. Typically, the surface of a 5 μm thick layer is 500 times the projected area. The conductivity of these films under vacuum is very low, $\approx 10^{-9}$ S cm^{-1} at room temperature. Under exposure to UV light, the conductivity increases significantly indicating that the poor conductivity in the dark is due to a small electron concentration in the conduction band rather than low electrical contact between particles.[22] As the TiO_2 SC band-gap energy is ≥ 3.2 eV (≤ 390 nm), it is nearly transparent to the major part of the solar spectrum. This means that absorption

of light by a chromophore is not hindered by the optical properties of the SC itself, when buried deep within the porous nanocrystalline films.

1.3.2   Molecular Antennae Effect

Another approach to harvesting photons more efficiently by chromophores has been to attach arrays of chromophores, "molecular antennae", to SCs and metals. By linking a graded series of chromophores in an array or assembly, using appropriate spacers or bridging units, the higher energy chromophore transfers excitation energy to the lowest energy unit, which injects charge into the acceptor surface. The efficiency of the intramolecular energy and electron transfer processes in antennae assemblies will depend on the extent of electronic coupling between chromophores, modulated both by the bridge and the spatial orientation of individual chromophoric units. While any type of chemical forces in principle could be used to link molecular components, covalent bonding via an appropriate bridging group seems to be the best choice for a stable antennae system. The antennae effect can be conceived to increase efficiency of light harvesting on a SC surface by two models; **A** branched, or **B** linear one-dimensional (Figure 1-18).[6,7] The obvious requirements for an antenna are, 1) an efficient antennae effect channelling the absorbed energy towards the surface component, and 2) the capability of the excited molecular component bound to the SC or metal surface to inject electrons into the conduction band.
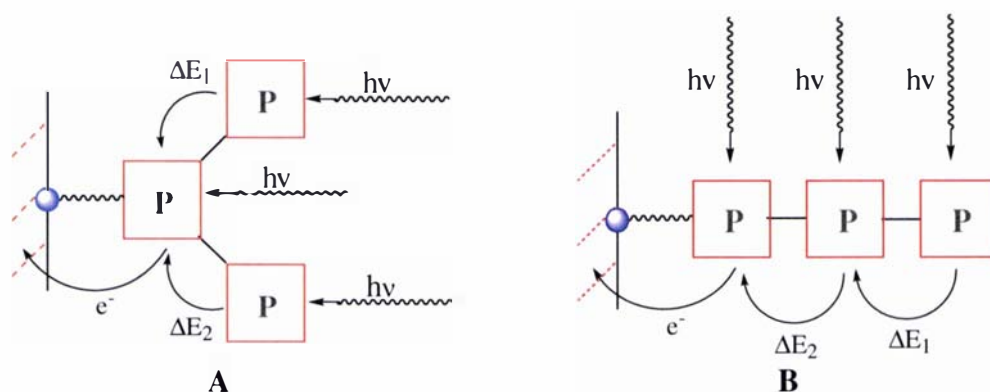
Figure 1-18. Branched **A** and linear **B** approaches to chromophore antenna systems.

There are significant energy-related problems associated with multi-component chromophore systems. If a finite energy demand (ΔE) exists for each parallel transfer step, a branch design, with extensive use of parallel energy processes ($\Delta E_{total} = (1/\Delta E_1 + 1/\Delta E_2)^{-1}$), is clearly energy saving relative to the linear design where all processes are in series and energy demands are additive ($\Delta E_{total} = \Delta E_1 + \Delta E_2$). The dimensions of the antennae system cannot be increased without introducing energy losses. For an array system considered as an independent photochemical molecular device, one expectation is that the larger the antennae system, the larger the light harvesting efficiency. This is not necessarily true for light energy conversion on a SC. A highly branched antenna species occupies a much larger surface area on the SC than a simple molecular sensitiser. At saturation coverage, this would strongly reduce the gain represented by the antennae effect. From this point of view, the one-dimensional design would look superior to the branched one, as one could think of increasing indefinitely the nuclearity of the array without substantially increasing the occupied surface area. These arguments, however, should be treated with caution as the SC surface available for absorption is far from being an idealised flat surface. In nanocrystalline photoanodes, an extremely rough surface is present, mostly made up of pores and cavities with nanometre dimensions. As such dimensions are comparable to those of large molecular systems, the fitting requirements of such arrays in pores may be the ultimate determining condition. One current approach in this area has been to synthesise arrays of ruthenium polypyridyl complexes using dendrimer synthesis.[57,58]

1.4   *Porphyrins as Photosensitisers*

Along with polypyridines, metalloporphyrins have great potential as metal and SC photosensitisers.   The ability to tune the photochemical, redox and molecular recognition properties of synthetic porphyrins offers unprecedented opportunities to develop new and more efficient chromophores for photonic applications.

1.4.1   The Porphyrin Chromophore

A) T●p view   B) Side view

Figure 1-19. Space filling representations of tetraphenylporphyrin (TPP).

Porphyrin-type compounds are found throughout nature, where they are employed in a myriad of biological roles in which photophysical and redox processes are occurring. As a consequence they have attracted the attention of photochemists wanting to exploit their attractive light absorbing and excited state properties. They are essentially flat and exhibit a high degree of aromaticity, resulting in high symmetry (up to D_{4h}) (Figure 1-19). The simplest porphyrin is porphin (Figure 1-20). All other porphyrin analogues have substituents on the *mes●* and/or *β*-pyrrolic carbons around the porphyrin ring.
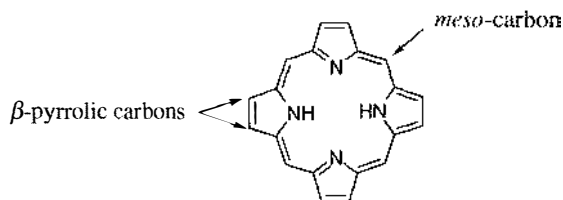
Figure 1-20. Porphin

The tetrapyrrolic porphyrin macrocycle system can be viewed as two planar delocalised 18 π–electron tautomers (Figure 1-21).[59]

A   B
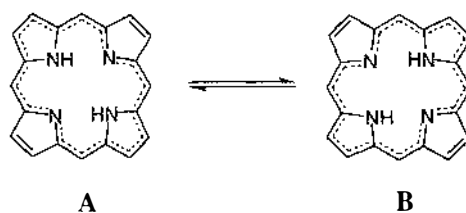
Figure 1-21. Tautomerism in free-base porphyrins.

These are the only two significant tautomers as other forms are too high in energy to be considered. In free-base porphyrins, two protons exist bound to the nitrogens as in tautomers **A** and **B**. The free-base porphyrin can accept two protons to form the 2^+ diacid, or donate two protons to form the dianion (Figure 1-22).
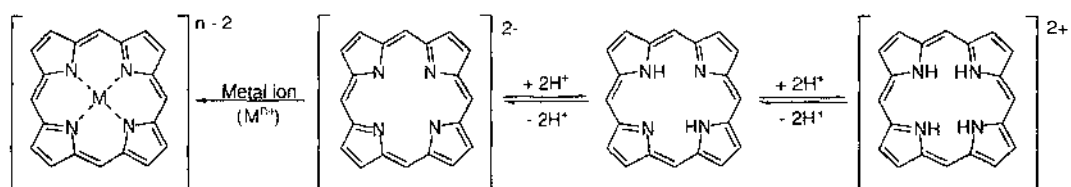
Figure 1-22. Metallation and acid-base chemistry of porphyrins.

The dianion can coordinate almost every metal ion in the Periodic Table, to form metalloporphyrins. The flatness and aromaticity results in a tendency for these macrocycles to aggregate through π–π interactions. The aromaticity also confers considerable chemical and thermal stability.

Porphyrins are highly coloured and have characteristic electronic absorption spectra with π-π^* and n-π^* transitions predominating. The π-π^* transitions dominate the spectra due to their high molar absorptivities. The 'Soret' band (380-420 nm) is the most intense in the porphyrins with molar absorptivities commonly of the order of

several hundred thousand. This band is regarded as a characteristic of the macrocycle conjugation and is absent in non-conjugated rings of unoxidised porphyrinogens. In the visible region, a free–base porphyrin spectrum exhibits a number of smaller satellite bands (typically four), known as 'Q' bands (generally $\varepsilon < 20,000$ L mol^{-1} cm^{-1}) (Figure 1-23). The absorption spectra of metalloporphyrins containing divalent metal ions have a Soret band and two visible α and β bands (Figure 1-23).
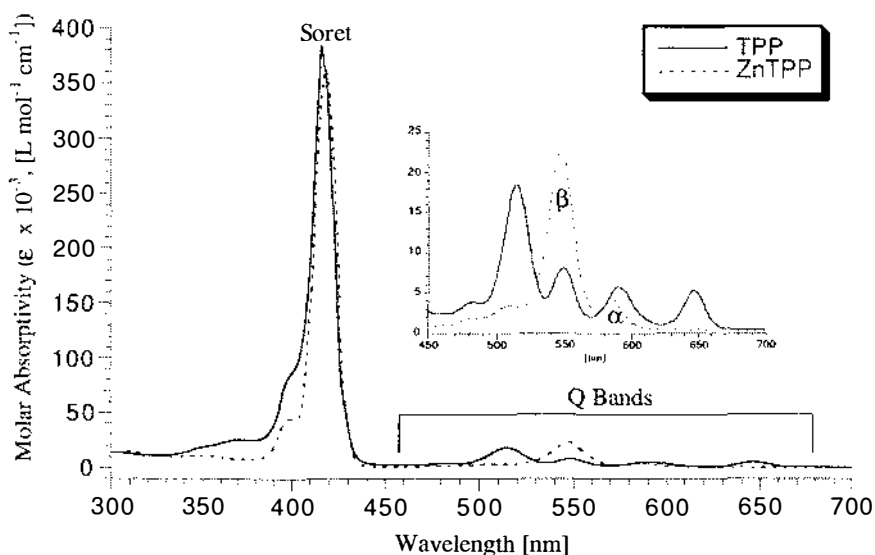
Figure 1-23. Typical UV-vis absorption spectra of a free-base porphyrin (TPP) and Zn(II) metalloporphyrin (ZnTPP) in CH$_2$Cl$_2$. Insert: expanded Q band region.
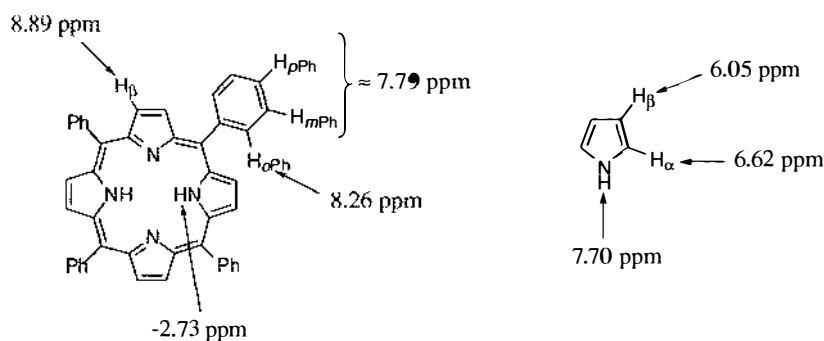
Figure 1-24. ^{1}H NMR chemical shifts of TPP and pyrrole protons in CDCl$_3$.

The ^{1}H NMR spectrum of TPP demonstrates the effect of the large anisotropic ring current that results from the delocalised aromatic ring system (Figure 1-24). This results in the observed downfield shift in the resonances of the β-pyrrolics and *meso*-phenyl protons on the periphery of the ring, relative to those of pyrrole and benzene. The broad inner **NH** proton resonances are shifted upfield by 10.43 ppm relative to

pyrrole.

The unique properties of porphyrins extend to the electrochemistry of the macrocycle where a well-studied four-step single-electron redox process is typically observed.[60]

In both free-base and metallated porphyrins, the photophysical and photochemical properties of the macrocycle are greatly influenced by the various substituents attached to the perimeter (β-pyrrolic and *meso* positions) of the porphyrin ring. These substituents by their electron-donating or electron-withdrawing nature have the ability to "tune" the delocalised molecular orbitals of the compound or complex, and thus vary all its chemical and physical properties.[59] Synthetic porphyrins for this reason have long been used to study charge transfer reactions as models for the photosynthesis process.

1.4.2 Porphyrins on TiO_2, GaAs and Au surfaces

The efficiency of charge injection by the porphyrin chromophore depends on the interaction with the surface and neighbouring chromophores (Figure 1-25). This is influenced by:

- The type, strength and number of anchoring groups,
- The type, length and number of linking groups,
- The spatial relationship of chromophore to the surface,
- Chromophore assembly (discrete molecules or arrays),
- Inter-chromophore spatial requirements.

These five factors are discussed more fully below and specific examples of porphyrins relating to TiO_2, GaAs and Au surfaces are more fully reviewed in Chapters 5 and 6.

Anchoring Groups: The attachment of a porphyrin to a SC or metal surface can range from chemisorption, covalent, non-covalent bonding (such as H-bonding or ionic bonding) or a combination of these. As discussed in Section 1.2, the strength and type of surface binding, as well as the number of binding sites, can have a major effect on photosensitisation. Although numerous studies involving the chemisorption of porphyrins onto surfaces like these have been carried out, the focus of this thesis is on

the stronger covalent type attachment. Porphyrins have in general, been most commonly attached to TiO_2 via carboxylic and sulfonic acid groups; for an in-depth review see Chapter 5. Specific examples of porphyrins attached to Au via a variety of sulfur functional groups are reviewed in Chapter 6. For GaAs, both carboxylic acid and disulfide groups are known to bind (see Section 1.2.2).
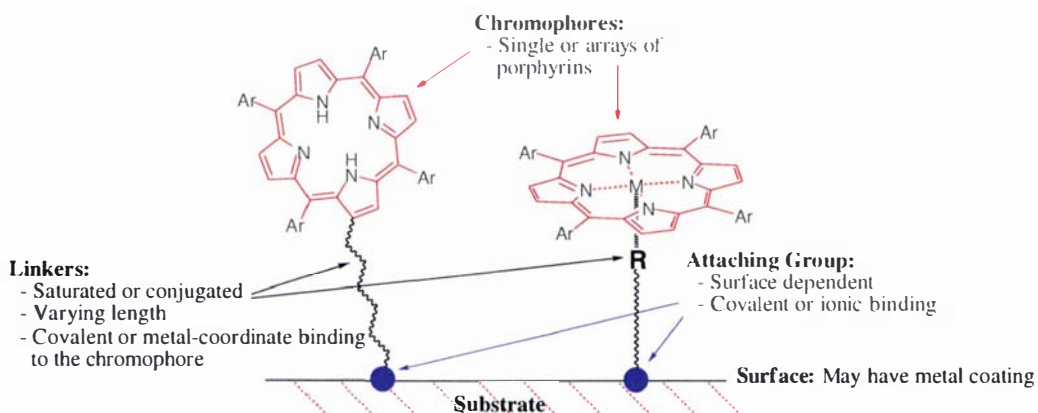
Figure 1-25. Summary of porphyrin attaching modes to surfaces.

Linking Groups and Spatial Relationships: It is still unresolved as to whether the linker type is more important than the proximity and orientation of the chromophore to the surface. Consideration of the type of linker must also include the number of linkers employed and if a delocalised electron-conducting pathway is necessary. The linker can be attached to the porphyrin via covalent bonding through the β-pyrrolic or *meso* positions, or by axial coordinate binding to a metal (Figure 1-25). Various perpendicular or planar porphyrin-to-surface geometries can be envisaged by using the appropriate linker connections. It is also possible to have the porphyrin as a ligand on a metal complex bound to the surface, however this is beyond the scope of this thesis.

Very few examples of porphyrins attached via the β-pyrrolic position to any of the surfaces of interest exist in the literature; most involve a *meso*-type linkage system. There are some literature examples of natural metallo-chlorophyll, natural metallo-mesoporphyrins and natural metallo-uroporphyrins for the photosensitisation of TiO_2 by Kalyanasundaram and Grätzel et al. (see Chapter 5).[61-63] None of these examples have conjugated linker systems between the macrocycle and surface. Sulfur functionalised porphyrins attached through linkers at the β-pyrrolic position are rare; a few modified natural heme derivatives by Willner et al.[64] and Kobayashi et al.[65] are known (see

Chapter 6). A few examples of porphyrins and related phthalocyanines attached by axial metal coordination linkers have been reported (see Figure 1-14 and Figure 1-29 C).[51,66-68]

Chromophore Assembly: Various porphyrin assemblies, from monomers **A** to branched **B** and linear **C** arrays can be envisaged attached to a surface. Alternatively, arrays can be constructed where each chromophore has a number of attaching groups **D** (known as the "sticky" porphyrin approach). Up until recently, only single porphyrins had been attached to TiO_2, GaAs and Au surfaces (see Chapters 5 and 6). There are now however, a small number of examples of dimer type porphyrins on these surfaces.[69-72] Nonetheless, it is still unclear whether discrete porphyrin chromophores or assemblies will give the best photosensitisation efficiencies (Figure 1-26). For multi-component arrays, the type of bonding between pendant chromophores moieties in the structure will affect the energy transfer and will need to be considered in developing antenna arrays.
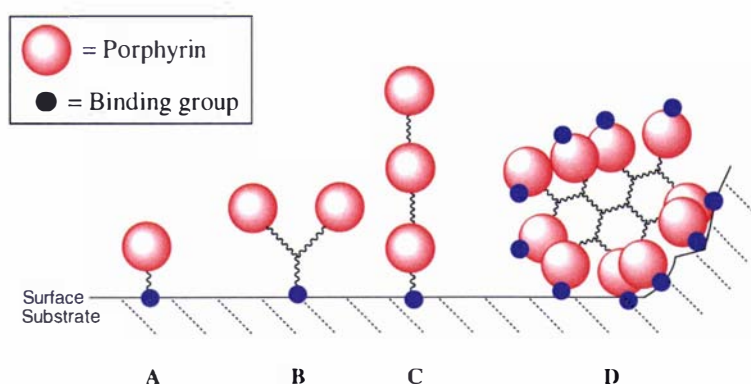
Figure 1-26. Discrete and antennae approaches to chromophore surface assembly.

Inter-chromophore Spatial Requirements: As is well demonstrated by the efficient light harvesting of chlorophyll, inter-chromophore spatial requirements are important (for both discrete and supramolecular assemblies).[73,74] Here strategically placed porphyrin derivatives can result in efficient collection and transfer of solar energy. Excited state quenching occurs in porphyrins that have aggregated due to strong π-π interactions.[75] Organic dyes, and particularly metalloporphyrins and phthalocyanines, are known to aggregate in solution even at low concentrations (10^{-5} M) via π-π interactions. It has been suggested that solar energy conversion efficiencies obtained

with metalloporphyrins are generally low, due to poor absorption in the major part of the visible spectrum. However many porphyrin species have absorptions in this region that are equally as intense as the other common photosensitisers, metal polypyridyl complexes (i.e. $(Ru(bpy)_3)$ $\varepsilon_{480} \approx 14,000$ M^{-1} cm^{-1}).[76] Poor efficiencies are more likely to result from quenching of the excited states because of molecular aggregation (Figure 1-27).
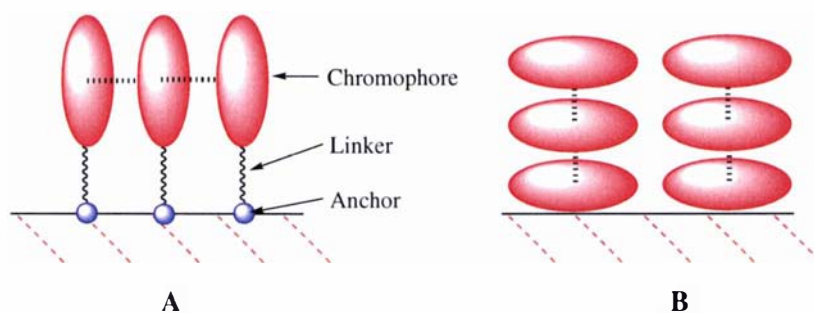
Figure 1-27. Representation of π-π interactions amongst flat aromatic chromophores on surfaces.

There are a number of potential ways to reduce this aggregation. Additives (co-adsorbates) that separate neighbouring chromophores and disrupt π-π interactions have been employed (Figure 1-28, **A**).[27] It has been found that the presence of additives such as bile acid derivatives significantly improve the light conversion efficiency for phthalocyanine sensitised TiO_2 electrodes.[68] The concentrations of sensitiser and additive in the coating solutions have to be optimised to limit aggregation but still achieve a high sensitiser loading. The addition of the sensitiser and additive in this manner may result in groupings of chromophores and additives on the surface, thus not achieving disruption of π-π interactions.
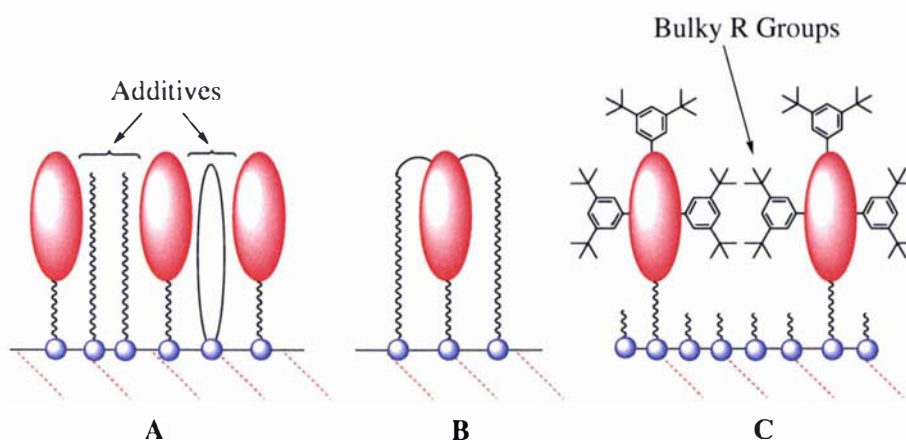
Figure 1-28. Methods for eliminating aggregation.

The drawback of competitive absorption of sensitiser and additive isolator on TiO_2 could be avoided by linking the additive directly to the dye molecule (Figure 1-28, **B**) before adsorption. This will have the advantage of fixing the ratio of dye and additive on the surface. Another method to reduce aggregation would be to use bulky substituents attached to the chromophores (Figure 1-28, **C**). While this may increase the chromophore spacing slightly, it avoids the need to control additive insertion between chromophores. The uncovered surface could then be filled with a smaller surface blocker that does not affect sensitiser loading, but reduces unwanted surface-electrolyte interaction.
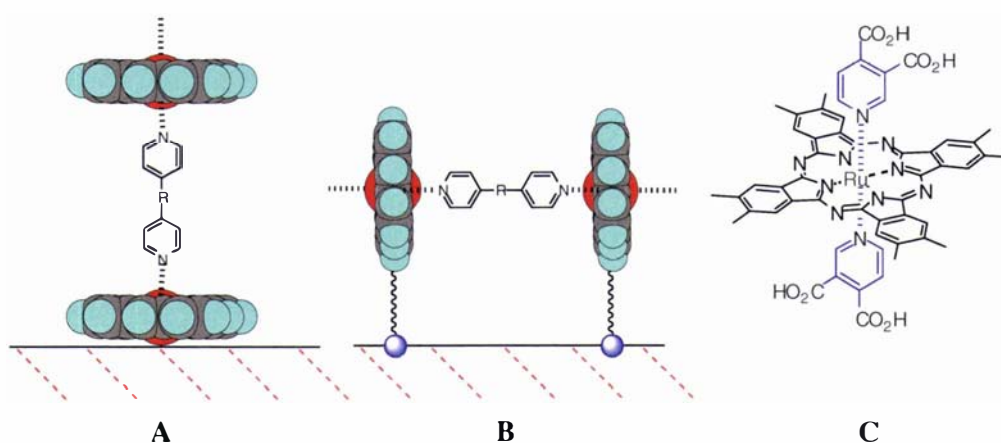
Figure 1-29. Axial coordination of porphyrins and phthalocyanine chromophores.

The presence of axial ligands such as pyridine compounds coordinated to Zn, Mg, and Ru metalloporphyrins and metallophthalocyanines complexes is also expected to inhibit π-π stacking interactions (Figure 1-29 **A** and **B**).[77] Recently excellent IPCE results ($IPCE_{660 nm} \approx 60\%$) were obtained with a ruthenium phthalocyanine complex to support this (Figure 1-29, **C**).[68] Attachment was made to the TiO_2 surface through axially attached pyridine ligands and the co-use of a bile acid additive. π-π stacking was prevented by the second coordinated pyridine group. For multi-chromophore arrays, aggregation may be inhibited by controlling the array geometry via the type of linker between individual chromophores, or again the use of bulky substituents and/or axial ligand coordination.

1.5 Synthesis of Porphyrins and Thesis Structure (Monomers to Arrays)

The aim of this thesis was to set up reliable synthetic procedures to allow the synthesis of a variety of new carboxylic acid functionalised porphyrins from monomers to arrays. These were then to be evaluated as photosensitisers in the TiO_2 Grätzel cell. In addition, the synthesis of some new disulfide and thienyl sulfur-functionalised porphyrins for attaching to Au surfaces was to be investigated.

1.5.1   Porphyrin Synthesis

The following is an overview of the strategy used in this thesis for synthesising aryl carboxylic acids and sulfur functionalised porphyrin chromophores, primarily for the modification of TiO_2, GaAs and Au surfaces. The goals of this research were to develop dependable synthetic routes to monomeric porphyrin systems and then exploit them in larger arrays. Classical porphyrin forming condensation reactions together with the Wittig chemistry of Officer et al. using tetraarylporphyrin phosphonium salts[78,79], lends itself well to the development of flexible synthetic strategies.. The condensation reactions used in this thesis, involve the condensation of pyrrole (Figure 1-30) or a dipyrrylmethane (DPM) (Figure 1-31) with an appropriately functionalised benzaldehyde, to produce tetra-*meso*-aryl (TAP) or bis-*meso*-aryl (BAP) substituted porphyrins.
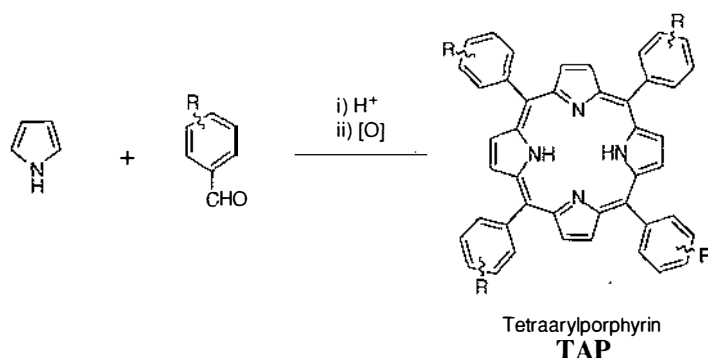
Figure 1-30. Condensation of pyrrole with aldehydes.
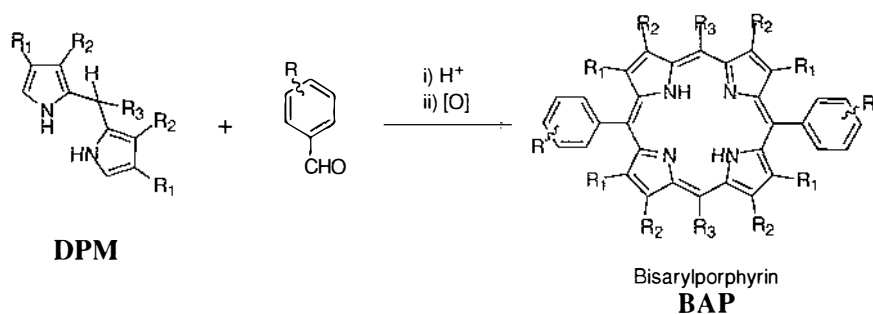
Figure 1-31. 2+2 Condensation of dipyrrylmethanes with aldehydes.

This requires suitable acid catalysts for the condensation, and oxidants for the conversion of the resulting porphyrinogen intermediates to the corresponding porphyrin.
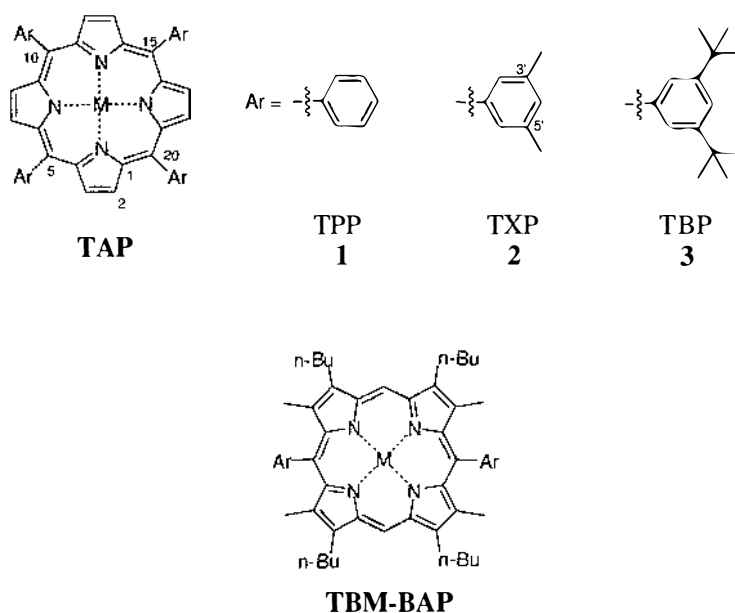
Figure 1-32. TAPs and BAP commonly used in this thesis.

The TAPs commonly generated by pyrrole condensations are the TPP, TXP, and TBP derivatives (Figure 1-32). The most common BAP used is the tetrabutyltetramethyl (TBM-BAP) derivative. A full foldout index of abbreviations and structures for TAPs and the TBM-BAPs synthesised in this thesis is inserted inside the back cover. Porphyrin compounds are numbered in the style of **M-#**. Thus, tetraphenylporphyrin **1** containing zinc(II) is referred to as **Zn-1**.

The reaction of TAP phosphonium salts (TAPps) with appropriately functionalised benzaldehydes under basic conditions, results in β-styrylporphyrins (Figure 1-33). The

all-*trans* product can be obtained by appropriate isomerization techniques. Metallo derivatives are easily obtained by metallation of a free-base porphyrin (M = 2H). This can in practice be carried out at any step along the reaction pathway.
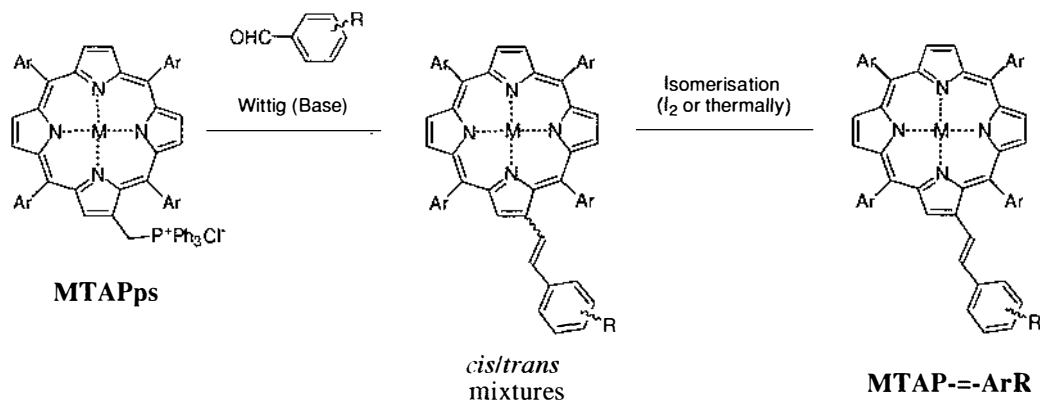
Figure 1-33. TAPps Wittig chemistry.

The synthesis of a number of different TAPps was required. This was based on the methodology developed by Officer et al. as depicted in Figure 1-34.[78,79]
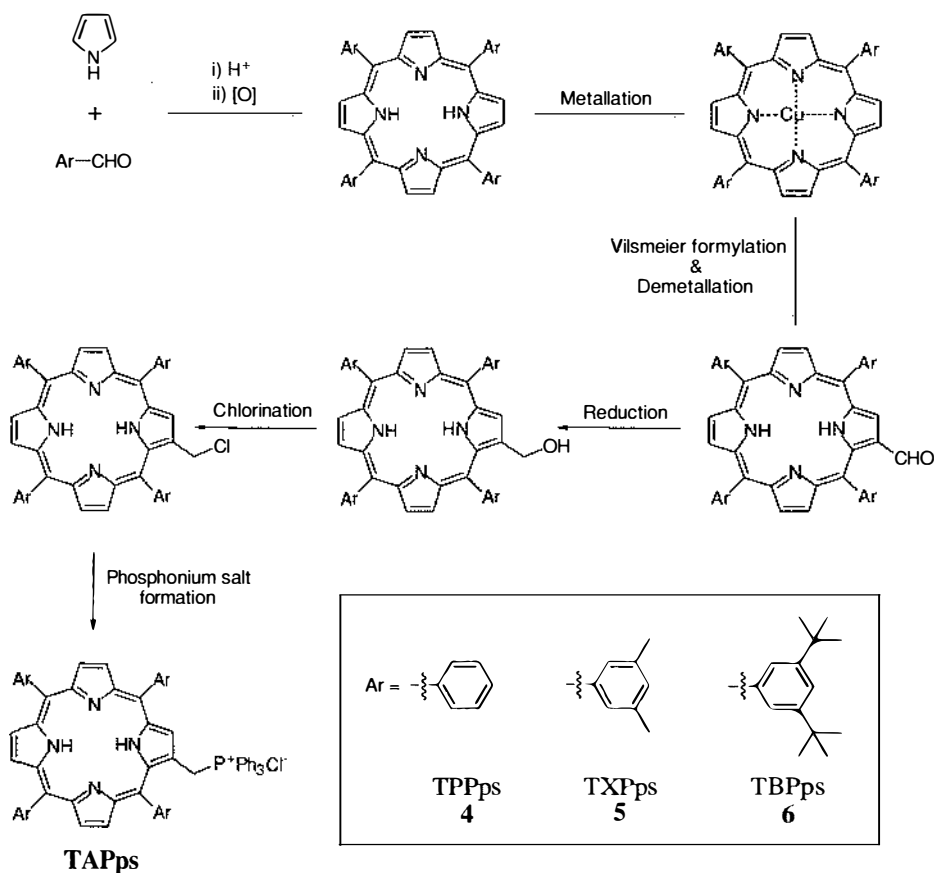
Figure 1-34. TAPps synthesis.

The three commonly used TAPps are the TPP, TXP and TBP derivatives **4**, **5** and **6** respectively. The xylyl derivative, TXPps **2** is generally the most used due to its enhanced solubility in organic solvents.

1.5.2   Thesis Structure

Chapter 2 describes the development of reliable synthetic strategies to porphyrin benzoic acids. The syntheses of a number of monoporphyrin and diporphyrin (branched and linear diporphyrin arrays) benzoic acids are presented. The synthesis of a linear diporphyrin required the use of protected aldehyde chemistry. This opened new synthetic routes to the controlled synthesis of mixed-metal and mixed-porphyrin arrays exploited in Chapter 3.

In Chapter 3, controlled syntheses of mixed-metal and mixed-porphyrin arrays from linear triporphyrins and pentaporphyrins to a large nonaporphyrin are realised. This methodology was developed and later applied to the synthesis of some unique "sticky" mixed-triporphyrins in Chapter 4.

Chapter 4 develops a second methodology for the synthesis of acid porphyrin arrays. In this approach, the acid functionality is built into the porphyrin, which is then used as the building block, to construct arrays using the established Wittig and condensation chemistry. This required the evolution of a "sticky" porphyrin phosphonium salt. A series of diporphyrins, triporphyrins and pentaporphyrins were synthesised based on this methodology.

Chapter 5 evaluates the porphyrinic acids synthesised in the preceding synthetic chapters, in the TiO_2 based photoelectrochemical solar cell (Grätzel cell).

In Chapter 6, the synthesis of sulfur functionalised porphyrins for attachment to Au surfaces is described. A range of porphyrin disulfides and thiophene derivatives were synthesised, the later having potential application in polymerisation studies. A new class of terthiophene-appended porphyrins were synthesised. Using a combination of Wittig chemistry and classical condensation reactions, β-substituted, and bis- and tetra-

meso-porphyrin variants were synthesised and characterised. Both the bis- and tetraterthienylporphyrins were isolated as mixtures of atropisomers.

Synthesis of Benzoic Acid

Porphyrins

2.1   Introduction

This thesis is principally focused on the synthesis of porphyrins containing aryl-carboxylic acid functionality for surface attachment to TiO_2 or GaAs. In the literature, there exists an enormous assortment of porphyrin carboxylic acids or ester derivatives. The most commonly used synthetic porphyrin acid is the tetra-*meso*-benzoic acid 5,10,15,20-tetra(4-carboxyphenyl)porphyrin (TCP) **8**, (Figure 2-1). This is synthesised by the condensation of pyrrole with 4-formylbenzoic acid **7**.[80]
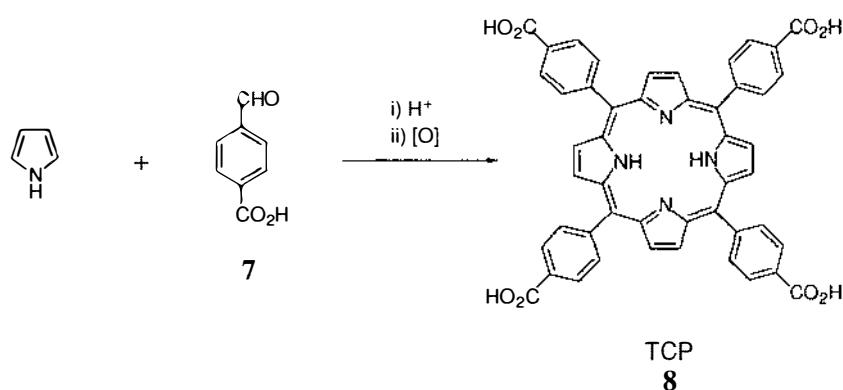
Figure 2-1. The synthesis of 5,10,15,20-tetra(4-carboxyphenyl)porphyrin (TCP) **8**.[80]

While TCP **8** shows some promise as a photosensitiser on SCs, this and many other porphyrin acid derivatives rely on attachment through a *meso*-benzoic acid group (see Chapter 5, Section 5.1.2). The geometry of **8** to the surface cannot be effectively controlled due to the multiple binding points. Although the synthesis of monoacid porphyrins with a single binding group has been achieved and evaluated, most synthetic strategies involve mixed aldehyde condensations with statistical product outcomes. Attachment of a porphyrin to a SC, through a single *β*-pyrrolic position is unknown; a few examples exist with multiple binding groups at the *β*-pyrrolic position from some natural metallo-chlorophyll, natural metallo-mesoporphyrins and natural metallo-uroporphyrins for the photosensitisation of TiO_2 (see Chapter 5).[61-63] None of these examples have conjugated linkers systems between the macrocycle and surface. Using our TAPps Wittig methodology we had the ability not only to synthesis some new *β*-pyrrolic substituted monoacid porphyrins TAP-=-PhCO₂H (Figure 2-2), but also a way

to gain some control over surface orientation of the porphyrin in relation to a surface by using formylbenzoic acids of varying geometry.
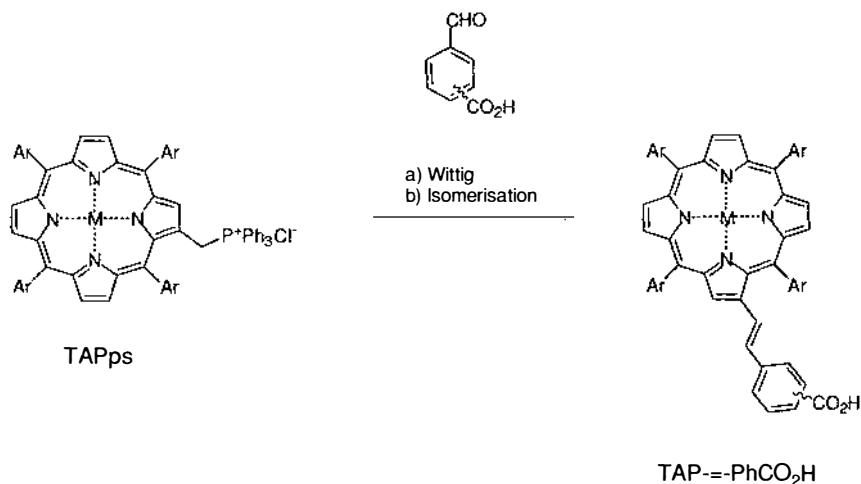
Figure 2-2. Synthesis of TAP-=-PhCO$_2$H.

Initial synthesis of the vinyl-linked benzoic acid TPP-=-PhCO$_2$H **9** by the Wittig reaction of *meso*-tetraphenylporphyrin phosphonium salt (TPPps) **4** and 4-formylbenzoic acid **7** was carried out in these laboratories by Grant (Figure 2-3).[81]
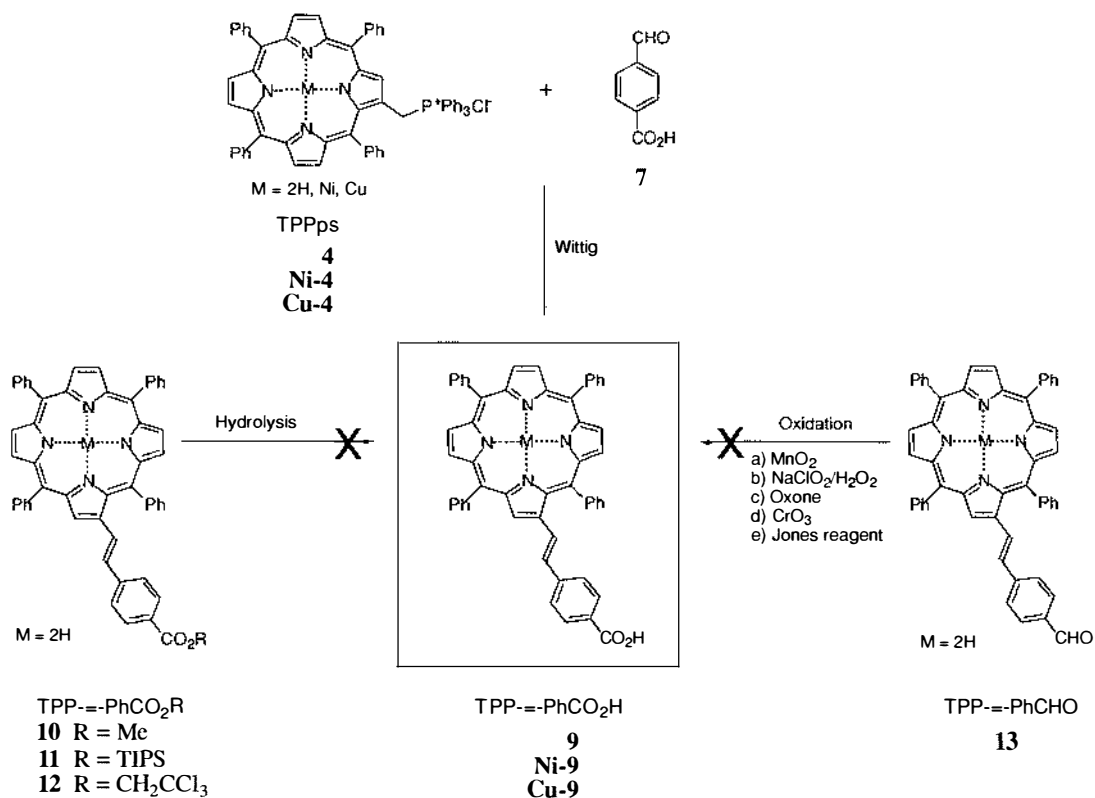
Figure 2-3. Synthesis and attempted syntheses of TPP-=-PhCO$_2$H **9**.

However, there was a notable problem in obtaining pure **9**. The direct synthesis of a β-pyrrolic benzoic acid porphyrin from a formylbenzoic acid initially appears trivial, but there are major solubility and purification problems. This becomes a significant issue in array formation where multi-step reactions are performed in organic solvents. Alternative syntheses of TAP-=-PhCO$_2$H by the hydrolysis of ester derivatives (**10, 11, 12**) or oxidation of aldehyde **13** were not successful.
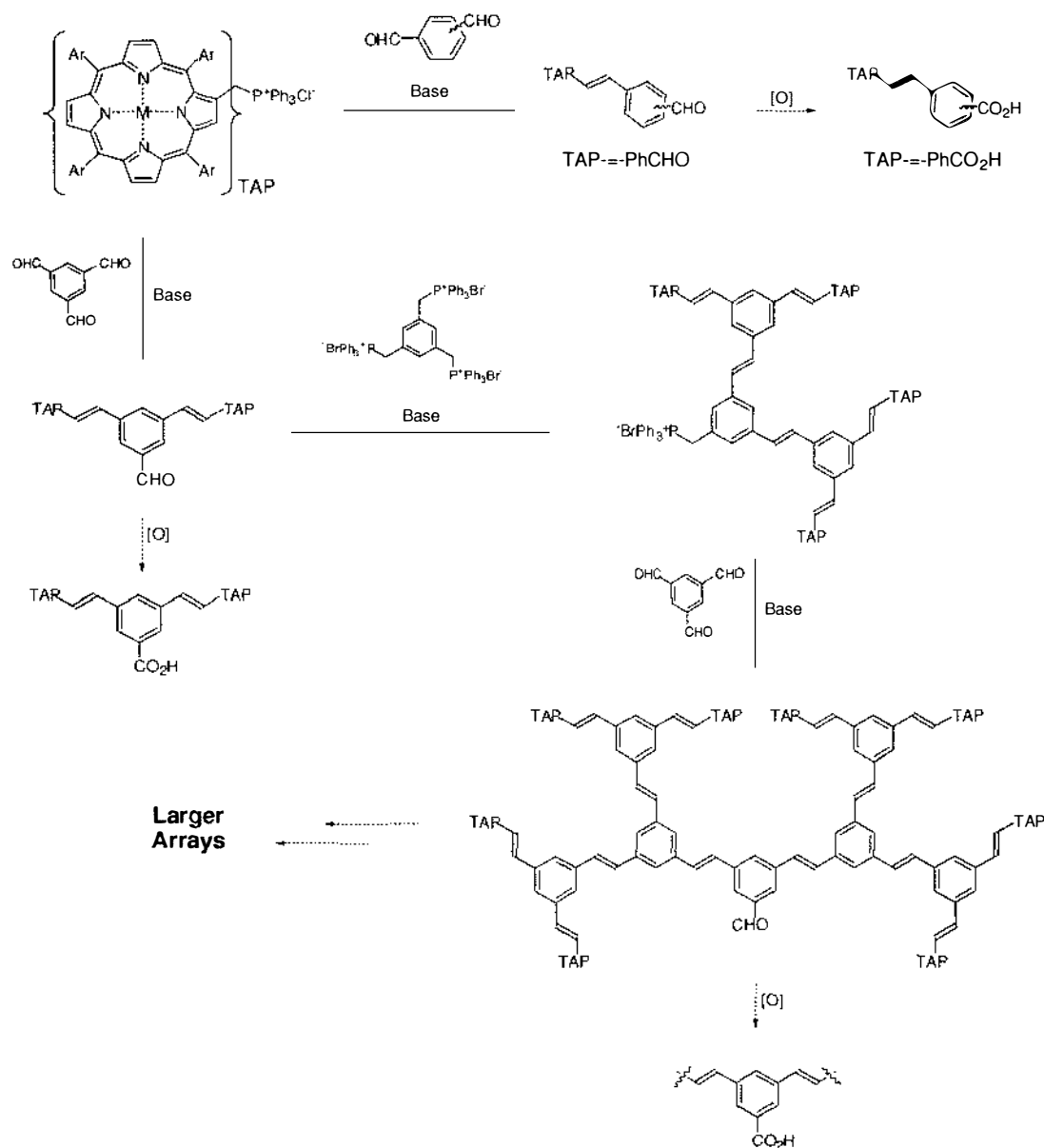
Figure 2-4. Potentially oxidisable aldehyde porphyrins used in 'building block' and dendrimer synthesis.

Certainly, the most efficient way to simplify purification in multi-step reactions is to form the required acid as the last step of a synthetic route using a single final functional

group transformation. As this would provide a general approach to a wide variety of porphyrin acids, it seemed appropriate to reinvestigate alternative ester hydrolysis and/or oxidation procedures. The development of oxidation procedures of porphyrin aldehydes was also of importance due to the ready availability of benzaldehyde functionalised porphyrins from the 'building block' approach and 'dendrimer' synthesis under development in these laboratories (Figure 2-4).[79,82] Porphyrin arrays of varying sizes could already be made with aldehyde functionalities, and an efficient oxidation procedure could provide a variety of arrays suitable for binding to surfaces.

In the following section the oxidations of TXP-=-PhCHO **M-14** porphyrins are initially explored, followed by the reinvestigation of ester formation and hydrolysis.

2.2 *Synthesis*

2.2.1   Oxidations

Figure 2-5 gives an overview of the initial oxidations that were attempted on styryl TXP aldehydes **M-14**. Previously, oxidations using TPP derivatives had been investigated. We were interested in developing synthesis of soluble arrays utilising the *meso*-tetraxylylporphyrin **2** (TXP) derivative. This type of porphyrin has a greater solubility in dichloromethane (DCM), CHCl$_3$, toluene and THF than the TPP derivative. In addition, the TXP derivative has greater solubility in polar organic solvents such as MeOH, acetone and acetonitrile, than the TPP derivative.

a) AgO (> 4 eq), THF:H$_2$O (9:1), RT (21 h). b) NaClO$_2$-DMSO (> 6 eq), NaH$_2$PO$_4$/H$_2$O/toluene, RT (12 h). c) NaBO$_3$ ·4H$_2$O (5 eq), acetic acid, 100°C (3.5 h). d) Peroxyacetic acid (5 eq), acetic acid, 50°C (10 min). e) KMnO$_4$ (4.5 eq), acetone, RT
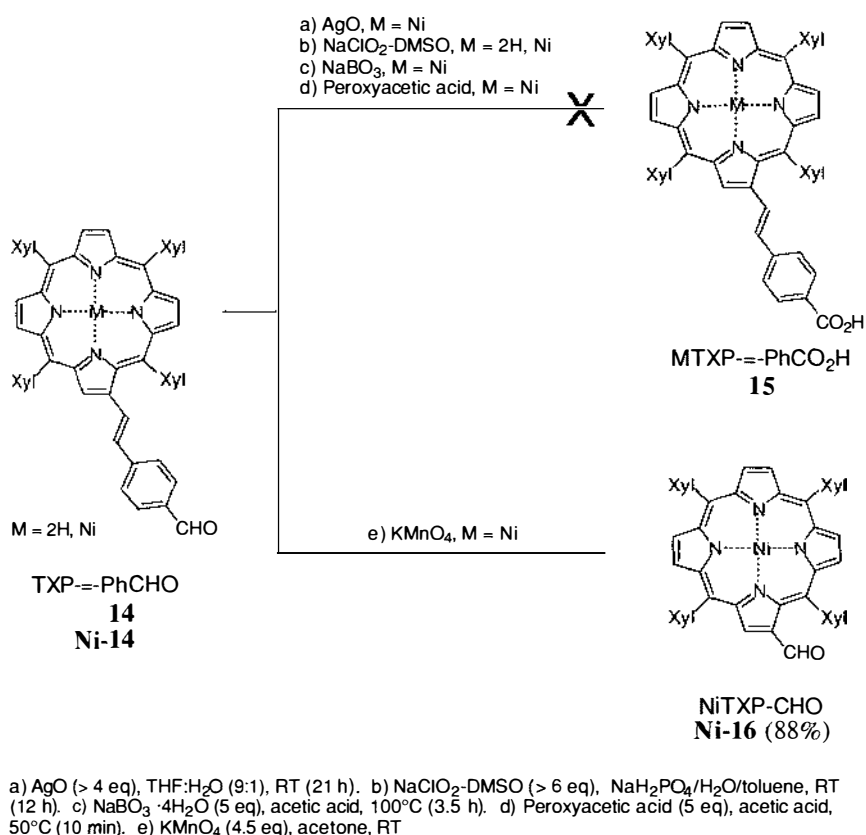
Figure 2-5. Oxidations attempted on TXP-=-PhCHO **14**.

Oxidations that could be performed in these organic solvents were pursued. Aqueous oxidising reagents were considered only if phase transfer catalysis (PTC) conditions

could be employed or where the free-base porphyrin could be solubilised by protonation of the porphyrin core.
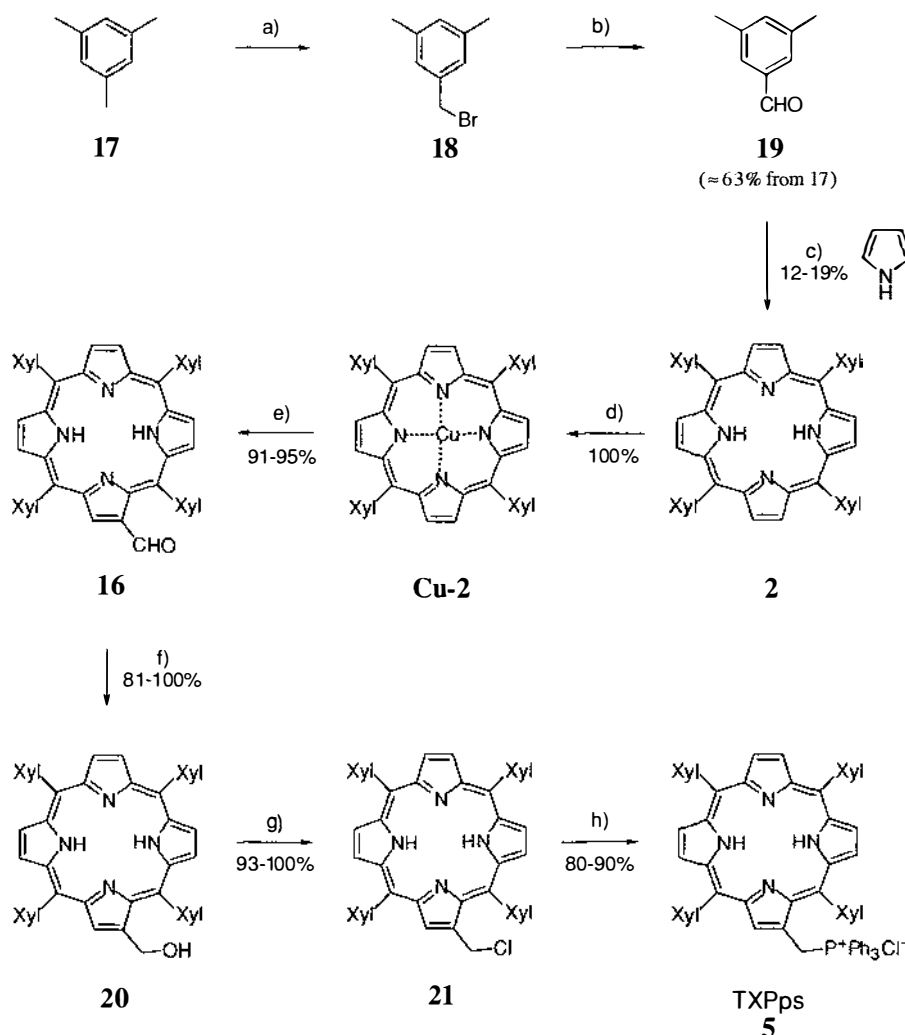
a) NBS, CH$_2$Cl$_2$, hv, reflux (1 h). b) i) HMTA, EtOH/H$_2$O, reflux (4 h). ii) Conc. HCl, reflux (1 h). c) Propanoic acid, reflux (1 h). d) Cu(OAc)$_2$·H$_2$O (1.2 eq), CHCl$_3$/MeOH, reflux (2 h). e) i) POCl$_3$/DMF, 1,2-DCE, reflux (2 h). ii) Conc. H$_2$SO$_4$. f) NaBH$_4$, THF/H$_2$O, RT (15 min). g) SOCl$_2$/pyridine, CH$_2$Cl$_2$, 0°C to RT (1 h). h) PPh$_3$ (20 eq), CHCl$_3$, reflux (19 h).

Figure 2-6. The synthesis of TXPps **5**.

The required free-base **14** and Ni(II) **Ni-14** derivatives were first prepared in good yields (89% and 82% respectively, Figure 2-7) after the synthesis of TXPps **5** according to established procedures of Belcher et al. (Figure 2-6).[83] The lengthy 8-step synthesis of TXPps **5** was required and repeated a number of times during the course of this thesis according to established procedure of Reid.[79] During the course of this thesis the

synthesis of TXPps **5** was successfully scaled up from the usual 2-3 g to 10-11 g batch sizes.
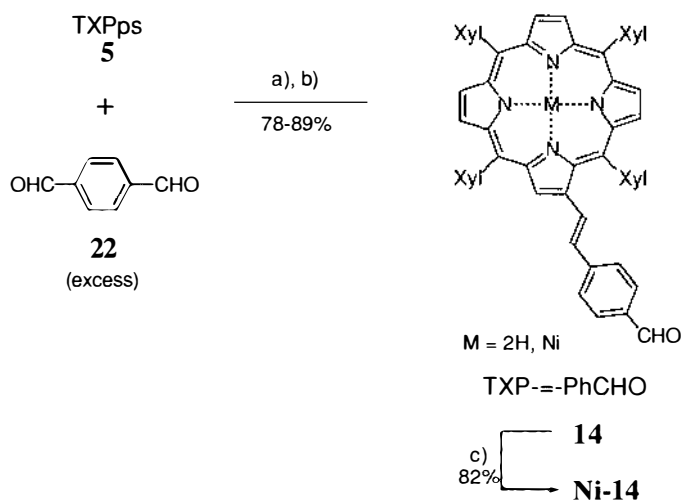
a) DBU (>1.0 eq), CHCl$_3$, reflux (10 min). b) i) I$_2$ (3.0 eq), CH$_2$Cl$_2$, RT (3 h). ii) Sat. aq. Na$_2$S$_2$O$_3$ (excess). c) Ni(OAc)$_2$·4H$_2$O (14 eq), reflux (18 h).

Figure 2-7. The synthesis of TXP-=-PhCHO **M-14**.

The various oxidations a), b), c) and d) that were attempted on TXP-=-PhCHO **M-14** (Figure 2-5), were carried out according to literature procedures. All methods were tested by oxidising *p*-nitrobenzaldehyde to *p*-nitrobenzoic acid, ensuring satisfactory reproducibility of the literature conditions. Monitoring of the reactions was performed by TLC, looking for changes in R_f and/or colour. In reactions a)-c), the starting material persisted with no observed reaction. The use of freshly prepared argentic oxide[84] (AgO) under the conditions in reaction a) gave no reaction.[85] These conditions, although unsuccessful for oxidation of the aldehyde, were later found by accident to be exceptional method for the insertion of Ag(II) into free-base porphyrins (see Chapter 3). In b) the use of sodium chlorite, with DMSO as a HOCl scavenger according to the procedure of Dalcanale et al., also gave no reaction.[86] Procedure c) of Banerjee et al., with sodium perborate showed no reaction.[87] Clezy et al. had used peroxyacetic acid for the oxidation of *β*-formylporphyrins to acids.[88] However, use of peroxyacetic acid[85] d) resulted in the formation of multiple products; none of these proved to be the desired acid. These conditions were assumed to be too harsh, and were not pursued any further.

Potassium permanganate is frequently used to prepare aromatic carboxylic acids from aldehydes. In organic solvents, it has been shown to be advantageous to use the quaternary ammonium salt form, and for biphasic systems, a PTC is necessary. Iihama et al. demonstrated that a good yield of an aromatic carboxylic acid could be obtained by using potassium permanganate in acetone/water solution.[89] With this knowledge a range of organic solvent systems were tested using potassium permanganate (1.5 equivalents) on p-nitrobenzaldehyde (Table 2-1). In all cases, only one new spot of lower R_f corresponding to the acid was observed by TLC, indicating efficient oxidation.

Table 2-1. Solvent systems for oxidations with $KMnO_4$.

Solvent System	Ratio
Acetone	1
Acetone:H_2O	3:4
Acetone:H_2O:THF	2:1:2
Acetone:CH_2Cl_2	2:1
Acetone:THF	2:1

Using potassium permanganate on NiTXP-=-PhCHO **Ni-14** in pure acetone, the appearance of a single new band of *higher* R_f than the starting material was observed. Driving the reaction to completion by adding an excess of potassium permanganate gave NiTXP-CHO **Ni-16** as the product in 88% yield (Figure 2-5). At no time during the reaction was any other porphyrinic product of lower R_f than the starting material observed. Under these conditions, it appears that oxidation at the alkene proceeds instead of aldehyde oxidation. No further oxidation of NiTXP-CHO **Ni-16** was observed, even with a large excess of oxidant present. This is consistent with that observed for other β-pyrrolic substituted TAPs by Crossley.[90]

Oxidations of aldehydes to carboxylic acids with permanganate can be carried out under acidic, neutral or basic conditions. Neutral or acidic permanganate solutions are commonly used for double bond cleavage.[91] The oxidations of benzaldehydes with permanganate in organic solvents has been shown to be very efficient and facile irrespective of *para* electron withdrawing (-NO_2) or electron donating groups (-Cl, -OMe).[92] It is therefore surprising that oxidation of the aldehyde is not observed. Generally, these oxidations require less than stoichiometric ratios of oxidant to aldehyde, however oxidation of stilbenes (alkenes) although efficient, do necessitate

higher stoichiometric ratios. A similar oxidation mechanism to that proposed by Sam et al. can be applied **Ni-14** (Figure 2-8).[93] It is speculated that the appended porphyrin and vinyl linkage must be exhibiting a significant deactivating (electron donating) influence all the way through to the aldehyde of the phenyl ring, making the oxidation of the ethenyl bond more favourable.
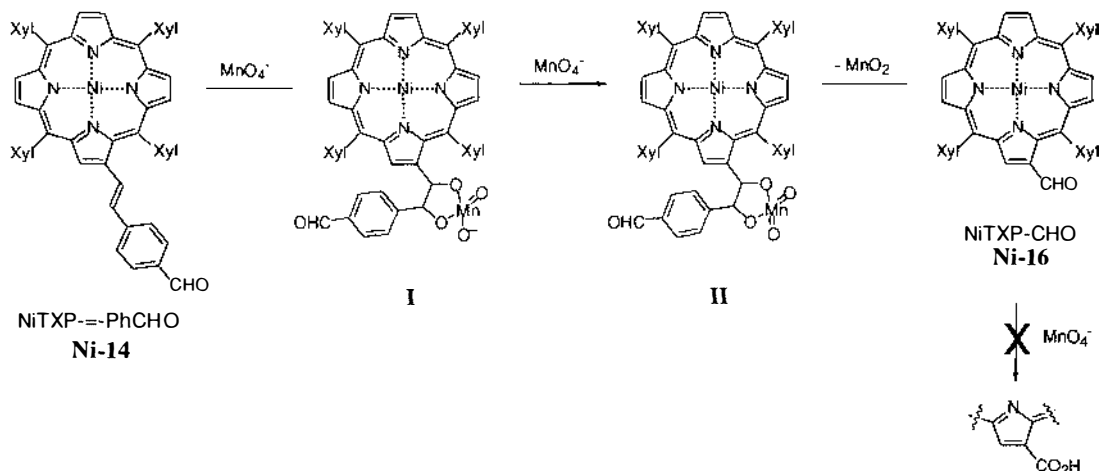
Figure 2-8. Postulated oxidation mechanism of NiTXP-=-PhCHO **Ni-14**.

Given the difficulty of directly oxidising these porphyrin aldehydes to acids, an alternative oxidative method for converting aromatic aldehydes into esters was investigated (Figure 2-9).
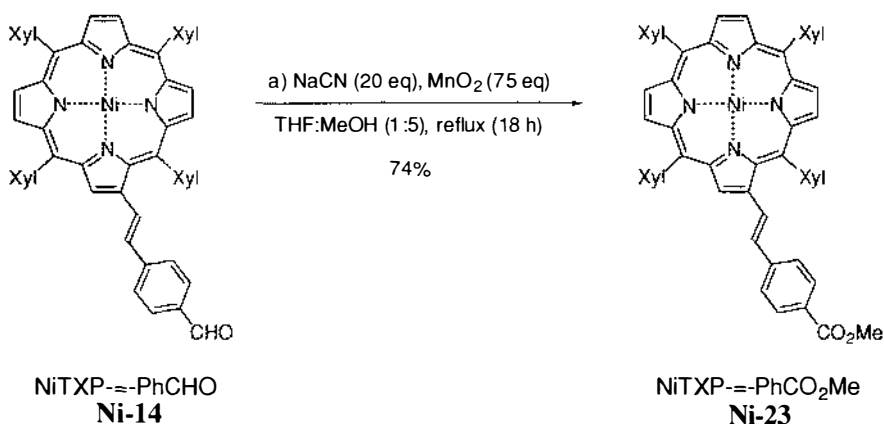
Figure 2-9. Oxidation of NiTXP-=-PhCHO **Ni-14** to methyl ester **Ni-23**.

The procedure of Lai et al.[94] employs mild conditions and is a modification on the original of Corey et al.[84] The Lai procedure was further modified in this thesis by the

use of a THF:MeOH solvent mixture to ensure the solubility of the **Ni-14** porphyrin aldehyde starting material (Figure 2-9). After the addition of NaCN (5 eq) and active MnO$_2$ [95] (15 eq) with stirring at room temperature, a reaction was seen to be proceeding slowly by TLC. By heating the reaction to reflux temperature with more NaCN and MnO$_2$, the reaction proceeded to near completion. The product NiTXP-=-PhCO$_2$Me **Ni-23** was isolated by column chromatography from the remaining starting material in 74% yield. The ester **Ni-23** was characterised by ^{1}H NMR, FAB HRMS and UV-vis. The spectra were similar to that of the analogous free-base TPP derivative **10** synthesised by Grant.[81] This reaction is assumed to proceed through a cyanohydrin, which is oxidised to an α-keto nitrile (Figure 2-10).[85] The α-keto nitrile is in turn converted into an ester by manganese dioxide in MeOH.
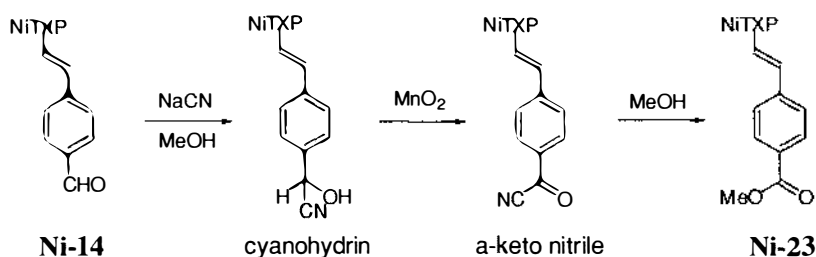
Figure 2-10. Oxidation of cyanohydrin to methyl ester **Ni-23**.

As the synthesis of porphyrin benzoate esters offers a viable synthetic route to porphyrin acids where multi-step reactions are required, the development of reliable hydrolysis procedures as the last step to the acid should allow easy handling of porphyrin benzoate intermediates along the reaction pathway.

2.2.2   Porphyrin Benzoic Acids via Esters

Ester Hydrolysis

With the ability to directly synthesise porphyrin benzoate esters from appropriate methyl formylbenzoates[81] or the conversion of porphyrin-appended benzaldehydes to

methyl esters (Figure 2-11), the development of reliable ester hydrolysis procedures was undertaken.
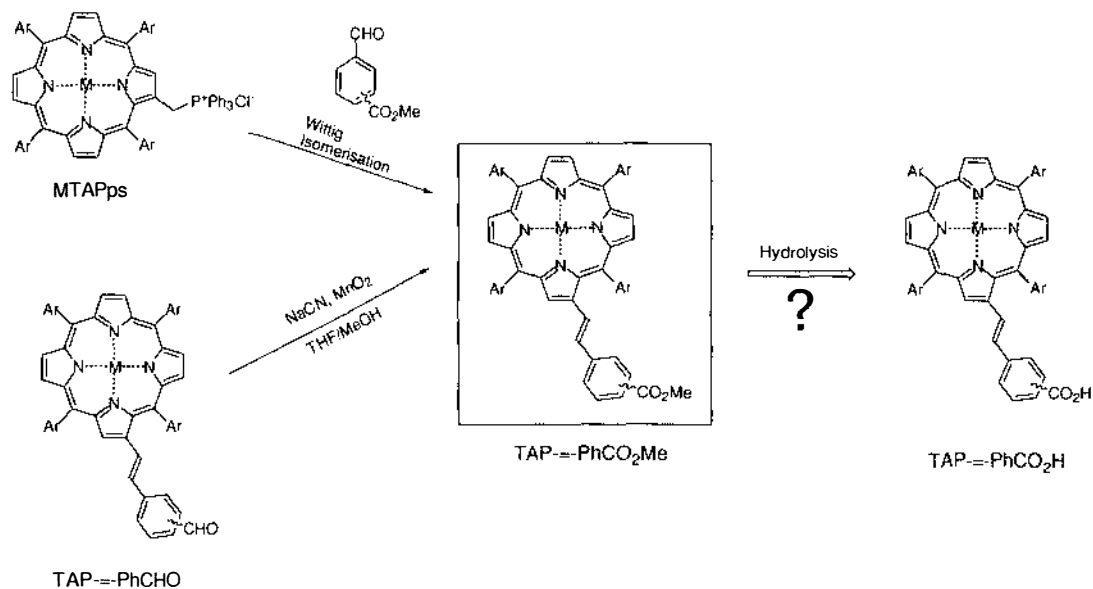
Figure 2-11. Routes to porphyrin-appended methyl benzoates.

Initial hydrolysis attempts by Grant on TPP-=-PhCO$_2$Me **10** using KOH (2 M) were unsuccessful.[81] The conditions used resulted in nucleophilic attack at the ethenyl double bond, giving unwanted TPP-Me **24** and TPP-CHO **25** products (Figure 2-12).
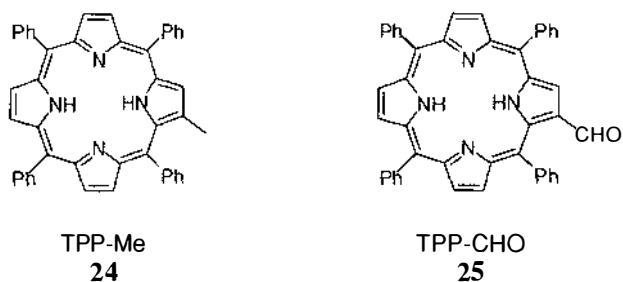
Figure 2-12. Hydrolysis reaction side products of **10** (TPP-Me & TPP-CHO).

A recent hydrolysis of (*m e s o*-tetrakis(3-carboxymethoxyphenyl)porphyrinato)-manganese(III) acetate using KOH (15 eq per CO$_2$Me) in refluxing MeOH:water (10:1), followed by acidification with HCl was attempted on *para*-NiTPP-=-PhCO$_2$Me **Ni-10** (see Figure 2-15).[96] Initially monitoring of the reaction by TLC revealed no reaction; this was undoubtedly due to the insolubility of the porphyrin in the solvent mixture. It was found that with the addition of THF to solubilise the porphyrin, hydrolysis of the

methyl ester was accomplished. After hydrolysis, the reaction was cooled to room temperature and diluted with water. In general, the addition of an organic layer (DCM or $CHCl_3$) followed by acidification resulted in an observed movement of porphyrin colour from the aqueous layer to the organic layer. The reactions were monitored by TLC, and the most identifiable feature of ester hydrolysis is the increased product polarity and the absence of the methyl ester ($PhCO_2CH_3$, ≈ 3.9 ppm) proton resonance in the ^1H NMR spectra. Further modification of this procedure by replacing HCl with H_3PO_4 allowed the hydrolysis and acid workup of metalloporphyrin carboxylic acids containing a labile metal, such as zinc.

Figure 2-13. General hydrolysis conditions for porphyrin methyl esters.

Using this general hydrolysis procedure (Figure 2-13), a diverse range of β-styryl linked porphyrin benzoic acids ($TAP-=-Ph_{o,m,p}CO_2H$) were synthesised from their methyl porphyrin benzoates.

Monoporphyrin Acids

The ability to produce a variety of monoporphyrin benzoic acids provides the opportunity to study the effect on surface modification by systematically varying the nature and geometry of the porphyrin acid. Thus, regio-isomeric acids could be made with different *meso*-aryl substituents and metals. Different surface orientations and steric interactions can be envisaged by changing the nature of the conjugation through the linker (Figure 2-14).

Figure 2-14. Surface orientations with TAP-=-Ph$_{o,m,p}$CO$_2$H derivatives.

The synthesis of TAP-=-Ph$_{o,m,p}$CO$_2$Me derivatives using established Wittig chemistry was achieved using methyl 2-, 3- and 4-formylbenzoates (**26, 27, 28**) and TPP, TXP and TBP phosphonium salts (**4, Ni-4, 5, 6**, Figure 2-15). Hydrolysis of the esters afforded the corresponding TAP-=-Ph$_{o,m,p}$CO$_2$H carboxylic acids displayed in Figure 2-15. In practice, quantitative metallation (step c), Figure 2-15) can be carried out at any step during the synthesis to give the required metalloporphyrin derivative. Generally the metalloporphyrin ester derivatives TAP-=-PhCO$_2$Me were prepared via metallation of their parent free-base ester; CuTXP-=-PhCO$_2$H **Cu-15** being the only exception being synthesised from its free-base acid **15** form. The ester derivatives are reasonably soluble in halogenated solvents, except for the ZnTPP derivative **Zn-10**, which has limited solubility in DCM. Hydrolysis of the *ortho*-ester derivative **Zn-29** required additional KOH and a longer reflux time, as starting material persisted after 19 h by TLC. The *ortho*-ester position may perhaps be slowing hydrolysis due to steric hindrance. Solubility of the acids was limited in most organic solvents. ZnTBP acid **Zn-34** was not appreciably soluble in either DMSO or CHCl$_3$. It was expected it to be more soluble in CHCl$_3$ than the TPP and TXP monoacids, but this proved not to be the case. The characterisation of all products was by ^{1}H NMR, FAB HRMS and UV-vis; this is discussed in Section 2.3.2 (pg 68).

TAPps

4, Ni-4, 5, 6

Ar = TPP

TXP

TBP

OHC

CO$_2$Me

o, m, p
(1.5-3.0 eq)
26, 27, 28

a) Wittig
b) Isomerisation
c) Metallation

CO$_2$Me

TAP-=-Ph$_{o,m,p}$CO$_2$Me

d) Hydrolysis
c) Metallation
→

CO$_2$H

TAP-=-Ph$_{o,m,p}$CO$_2$H

TPP *para*-ester:
10 (64%), **Zn-10** (63%), **Ni-10** (51%)
TXP *ortho*-ester:
29 (80%), **Zn-29** (66%)
TXP *meta*-ester:
30 (74%), **Zn-30** (55%)
TXP *para*-ester:
23 (73%), **Zn-23** (71%)
TBP *para*-ester:
30 (53%), **Zn-31** (52%)

TPP *para*-acid:
Zn-9 (96%), **Ni-9** (92%)
TXP *ortho*-acid:
Zn-32 (95%)
TXP *meta*-acid:
Zn-33 (99%)
TXP *para*-acid:
Zn-15 (96%), **15** (96%), **Cu-15** (9●%)
TBP *para*-acid:
Zn-34 (94%)

a) DBU (> 3.0 eq). b) i) I$_2$ (2.5 eq), RT (3 h). ii) Na$_2$S$_2$O$_3$ (excess). c) M(OAc)$_2$·XH$_2$O (1-14 eq), CHCl$_3$/MeOH, RT/reflux.d) i) KOH (15-30 eq per CO$_2$Me). ii) H$_3$PO$_4$ (≈ 7% excess, 2 mol L^{-1}), MeOH:H$_2$O:THF (10:1:10), reflux (4-23 h).

Figure 2-15. Synthesis of TAP-=-Ph$_{o,m,p}$CO$_2$H derivatives.

ZnTXP-=-PhCO$_2^-$ Salts

As the effect on surface binding to TiO$_2$ with different salts of ZnTXP-=-PhCO$_2$H **Zn-15** was of interest, the sodium and tetra-*n*-butylammonium salts ZnTXP-=-PhCO$_2^-$Na$^+$ **Zn-35** and ZnTXP-=-PhCO$_2^-$(*n*-Bu)$_4$N$^+$ **Zn-36** were prepared using an excess of sodium hydroxide and tetra-*n*-butylammonium hydroxide, respectively (Figure 2-16).

a) NaOH (4 eq), MeOH, RT. b) (*n*-Bu)$_4$N$^+$OH$^-$$_{aq}$ (4 eq), MeOH, RT.
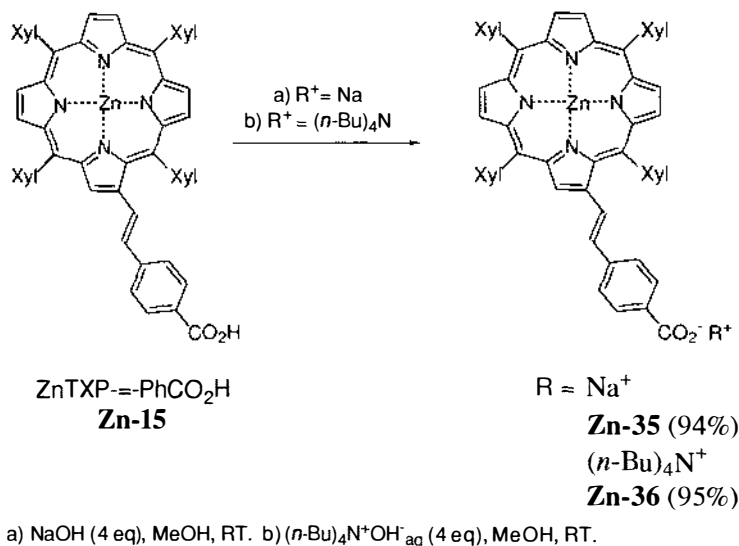
Figure 2-16. Preparation of ZnTXP-=-PhCO$_2^-$R$^+$ salts **Zn-35** and **Zn-36**.

Formation of salts was inferred by the disappearance of the starting material and the appearance of a new more-polar spot by TLC. The resulting salts had higher solubility in a polar solvent such as MeOH. Excess sodium hydroxide was eliminated from **Zn-35** by removing the solvent from the reaction mixture followed by redissolving the resulting solid in benzene and filtering. Excess tetra-*n*-butylammonium hydroxide was washed out with water after the product **Zn-36** was suspended in DCM. The spectral characterisation of these salts was similar to that of their parent acids. The FAB MS of the sodium salt **Zn-35** showed only the parent protonated molecular ion minus the sodium [M − Na + H]$^+$. As for the tetrabutylammonium salt **Zn-36** both anion and cation were observed, [M − (*n*-Bu)$_4$N + H]$^+$ and (*n*-Bu)$_4$N$^+$.

ZnTXP-=-Ph$_m$(CO$_2$H)$_2$

In order to obtain further insight into the binding of porphyrin acids to SC surfaces the 3,5-dicarboxylphenyl ZnTXP-=-Ph$_m$(CO$_2$H)$_2$ **Zn-37** derivative was synthesised. This

isophthalic acid derivative offers the possibility of dual or single binding modes (Figure 2-17).
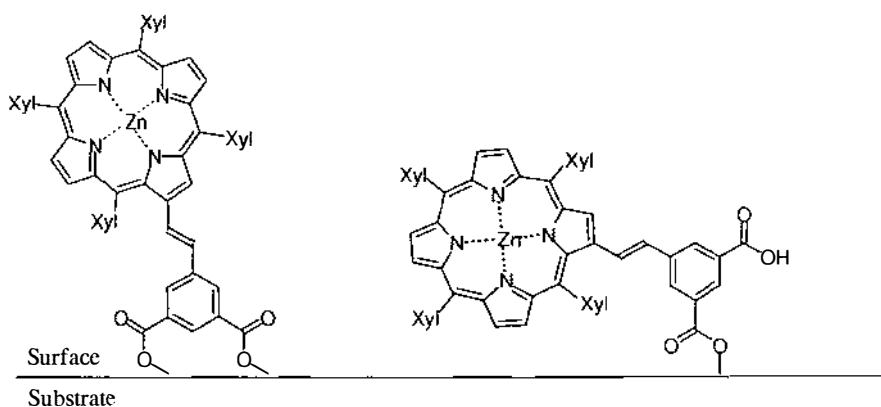
Figure 2-17. Surface orientations of ZnTXP-=-Ph$_m$(CO$_2$H)$_2$ **Zn-37.**

The appropriate aldehyde **40** (Figure 2-18) was first required. Dimethyl 5-formyl-1,3-benzenedicarboxylate **40** has been made before using two different approaches. Both methods utilise dimethyl 5-methylisophthalate **38** as the starting material. This is not commercially available and was made via the oxidation of mesitylene.[97] The first method by Bonar-Law involves the Fieser chromic anhydride oxidation of **38** (no yield was reported).[98] The second method involves Sommelet oxidation of the bromomethyl derivative **39** (no yield is reported for bromination).[99]
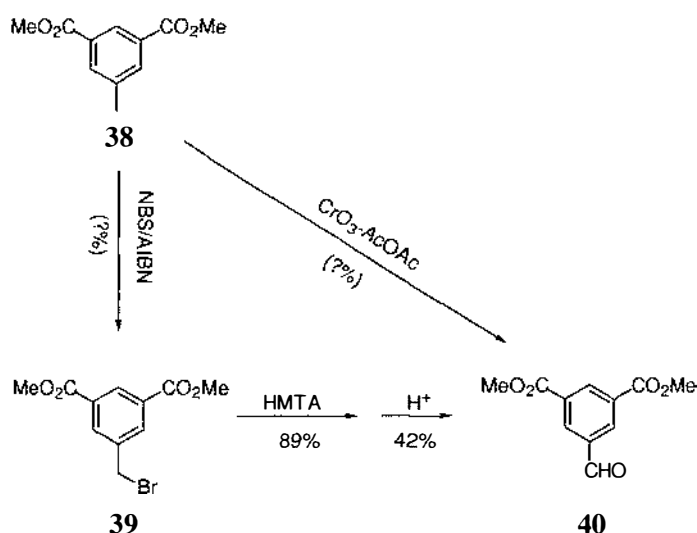
Figure 2-18. Known syntheses of diester **40**.[98,99]

Since completing this work, another plausible method has appeared in the literature by Fudickar et al., synthesising the diethyl diester **43** analogue (Figure 2-19).[100] A 54% overall yield was obtained based on the monoreduction of the triester **41** to alcohol **42**, followed by oxidation to the formyl-diester **43**.

Figure 2-19. Synthesis of diethyl diester **43** by Fudickar et al.[100]

A different synthetic route to aldehyde **40** was proposed and undertaken (Figure 2-20). This proposed synthesis required the monohydrolysis of the trimethyl trimesate **44** to the acid **45**, followed by acylation to give acid chloride **46**, and then reduction to give aldehyde **40**.

Figure 2-20. Proposed alternative synthetic route to the dimethyl formyl-diester **40**.

Firstly, the synthesis of the diester acid **45** was achieved by the hydrolysis of triester **44**. This produced mixtures of starting material **44**, monohydrolysis product **45**, dihydrolysis product **47** and trihydrolysis product **48** (Figure 2-21). The optimisation of the hydrolysis conditions was investigated and pure **45** was eventually obtained in 87% yield after column chromatography of the product mixture (entry 4, Table 2-2).

Figure 2-21. Synthesis of acid esters **45** and **47**.

Table 2-2. Hydrolysis of ester **44** with methanolic KOH.

#	KOH (eq)	Reflux time (h)	44:45:47:48*
1	1.0	16	33:67:0:0
2	1.5	2	29:71:0:0
3	1.5	14	9:91:0:0
4	1.5	16.5	4:94:2:0
5	1.5	23	3:92:4:0
6	2.1	48	0:50:50:0
7	2.5	17	0:91:9:0
8	2.5	48	0:15:78:7
9	2.9	22	0:5:84:10

*Product ratios were determined by ^{1}H NMR Spectroscopy.

An alternative synthesis of **45** is that reported by Kasina et al.[101] They obtained a partially purified yield of 90% by monodemethylation of the trimethyl trimesate **44** using an excess of 1,1-dimethylhydrazine (Figure 2-22).
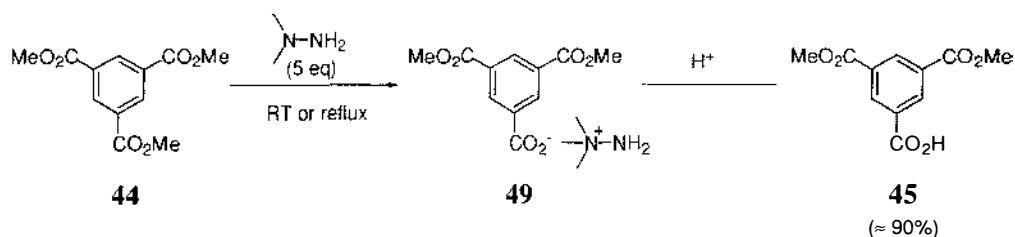
Figure 2-22. Synthesis of **45** by Kasina et al.[101]

Acid **45** was converted in 96% yield to acid chloride **46** using excess oxalyl chloride with catalytic DMF using a similar procedure to that of Melvin et al.[102] The procedure differed slightly from that of Melvin et al. with the use of a larger excess of oxalyl chloride and a higher reaction temperature. These changes resulted in a reduced reaction time and higher yields (Figure 2-23).
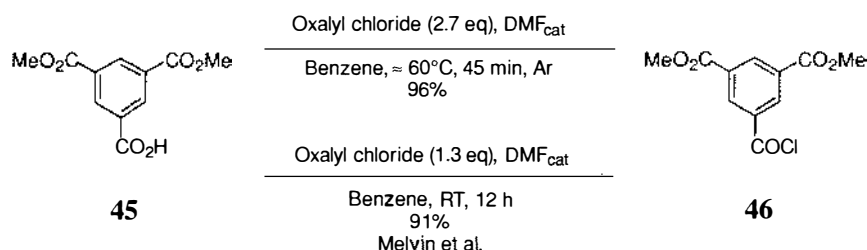
Figure 2-23. Synthesis of acid chloride **46**.[102]

Rosenmund reduction of acid chloride **46** gave the desired aldehyde **40** in a 90% isolated yield (Figure 2-24). The reaction was judged complete by the titration of the liberated HCl.
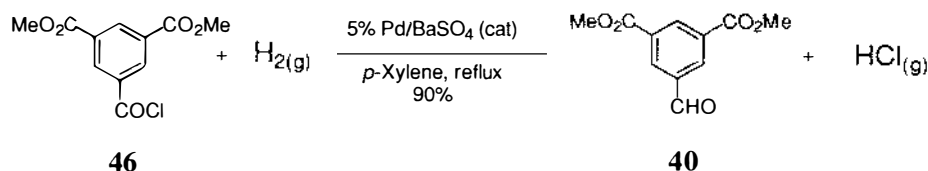
Figure 2-24. Rosenmund reduction of **46** to aldehyde **40**.

This sequence of three reactions leading to the synthesis of **40**, proceeds in an excellent overall yield of 75%. This compares very favourably with the 2-step 54% yielding procedure of Fudickar (Figure 2-19).[100] The synthesis of ZnTXP-=-Ph$_m$(CO$_2$H)$_2$ **Zn-37**

was achieved using the standard Wittig procedure as outlined in (Figure 2-15). The Wittig reaction of TXPps **5** with aldehyde **40** resulted in a *cis/trans* (1:9) mixture of diester **50** (Figure 2-25). Isomerisation with iodine afforded *trans* diester **50** in 82% overall yield. Metallation with zinc acetate gave metalloporphyrin diester **Zn-50** (80%). Hydrolysis of diester **Zn-50** gave the desired diacid **Zn-37**. The characterisation of diester **Zn-50** and diacid **Zn-37** is consistent with the analogous monoester and monoacid compounds, and is briefly commented on in Section 2.3.2.

a) DBU (3.0 eq), CHCl$_3$, reflux (15 min), N$_2$. b) i) I$_2$ (3.0 eq), CH$_2$Cl$_2$, RT (3 h). ii) Na$_2$S$_2$O$_3$ (excess). c) Zn(OAc)$_2$·2H$_2$O (1.2 eq), CHCl$_3$/MeOH, RT (30 min). d) i) KOH (10 eq per CO$_2$Me). ii) H$_3$PO$_4$ (21 eq, 2 M), MeOH:H$_2$O:THF (10:1:10), reflux (17 h), N$_2$.
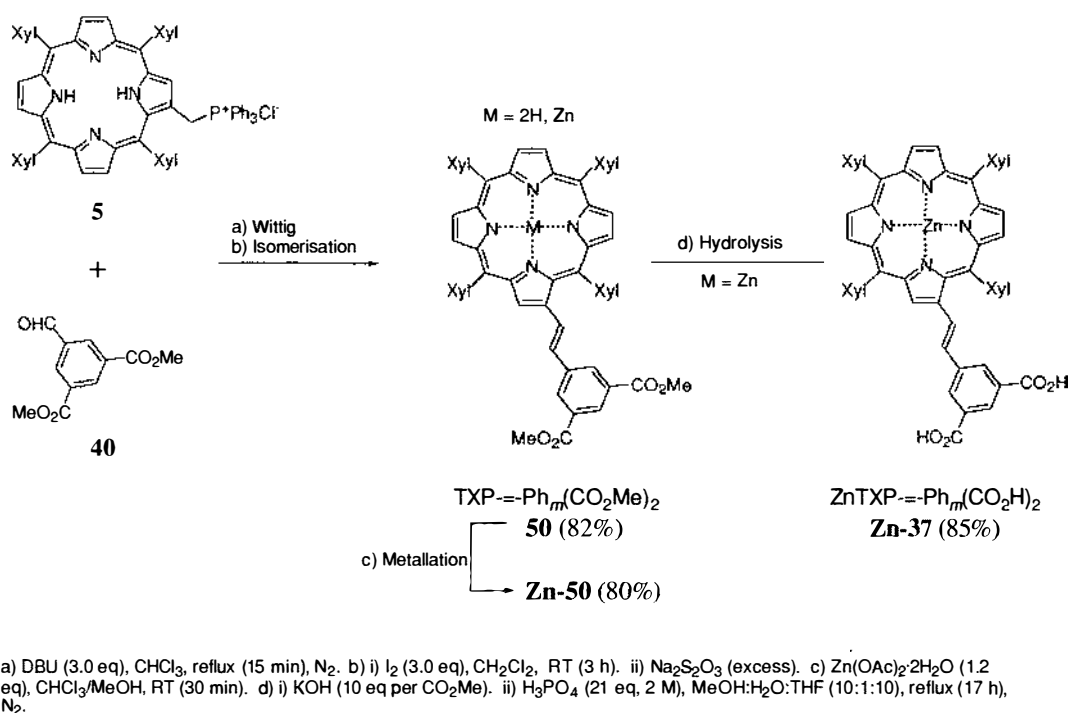
Figure 2-25. Synthesis of ZnTXP-=-Ph$_m$(CO$_2$H)$_2$ **Zn-37**.

Diporphyrin Acids

The synthesis of geometrically diverse porphyrin arrays was one of the objectives of this thesis. Two types of diporphyrin benzoic acid arrays attached through a common single benzoic acid group were targeted (Figure 2-26). The first is a branched "dipole" diporphyrin array, and the second is a linear "collinear" diporphyrin array.
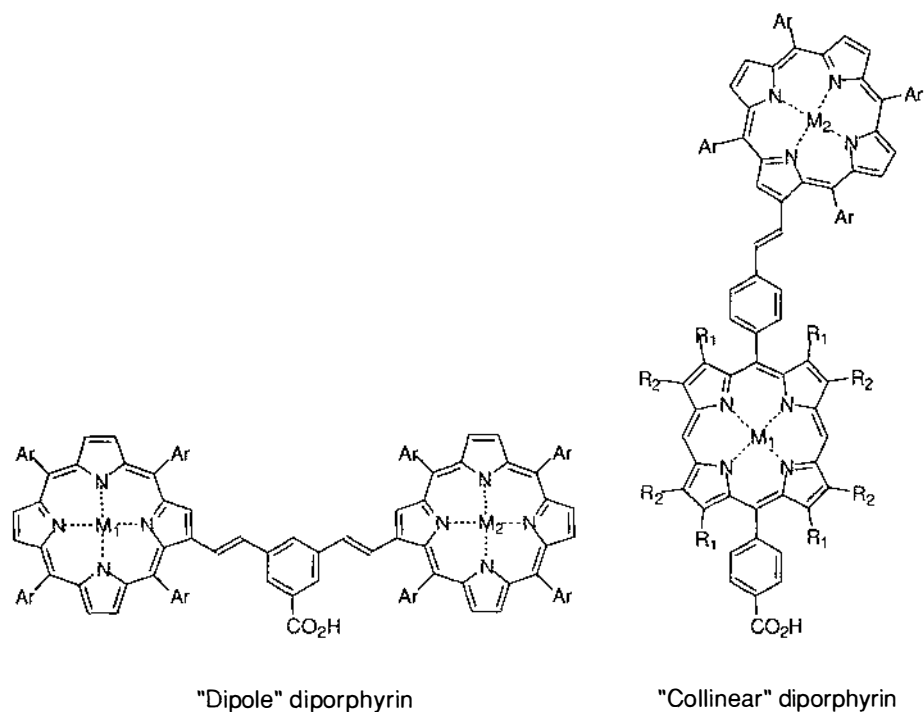
Figure 2-26. Branched and linear diporphyrin arrays.

"Dipole" diporphyrin

The proposed synthesis of the ZnTXP "dipole" diporphyrin acid **Zn$_2$-53** is given in Figure 2-27, based on the Wittig reaction of TXPps **5** with dialdehyde ester **51**.
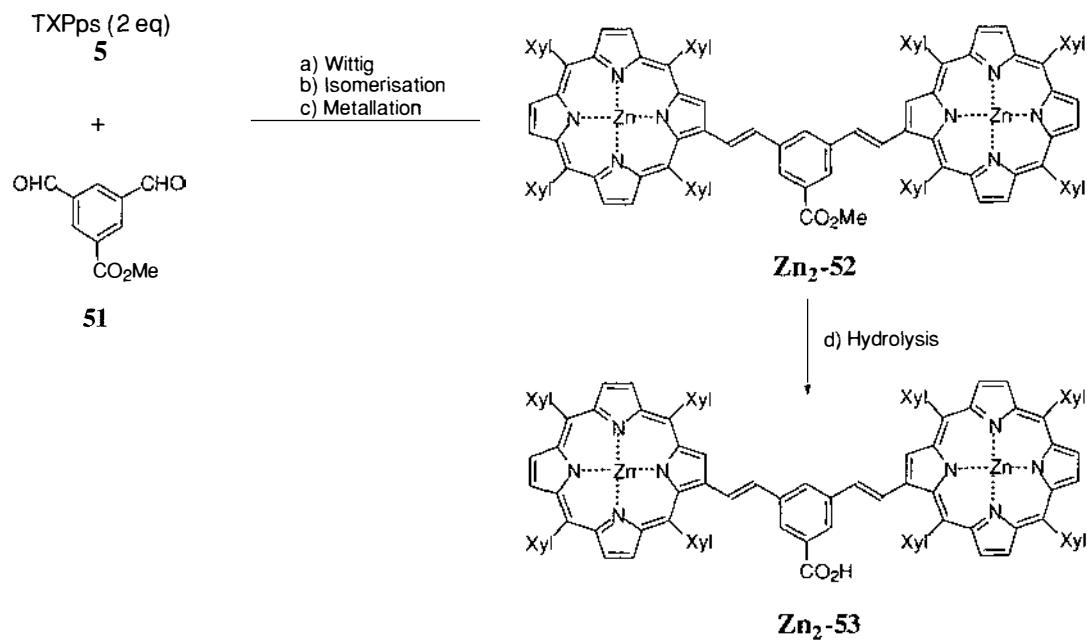
Figure 2-27. Proposed synthesis of "Dipole" diporphyrin **Zn$_2$-53**.

The synthesis of dialdehyde ester **51** has been reported in the literature as a by-product of the oxidation of the bis(bromomethyl) ester **54** using bis(tetrabutylammonium) dichromate by Keana et al. (Figure 2-28).[103]
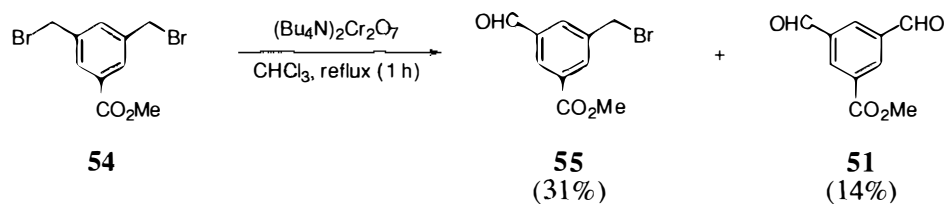
Figure 2-28. Synthesis of dialdehyde **51** by Keana et al.[103]

As this method (Keana) required the synthesis of bis(bromomethyl) ester **54** first, a different approach was taken using the same methodology developed for the synthesis of formyl-diester **40** (Figure 2-29).
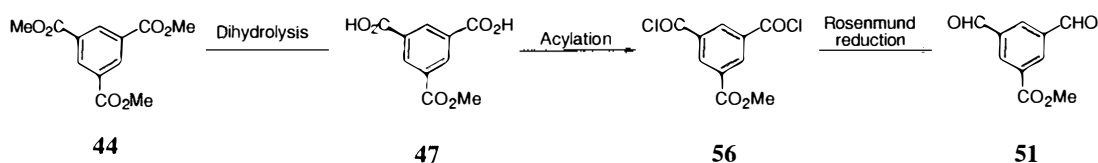
Figure 2-29. Alternative synthetic route to the dialdehyde ester **51**.

Firstly, diacid **47** was obtained as reported previously (entry 9, Table 2-2) from the hydrolysis of triester **44**. A mixture of monoacid **45** and diacid **47** was isolated from the trinary reaction mixture via Soxhlet extraction (Figure 2-30). This two-component mixture proved difficult to separate on large scale, and the binary mixture was carried through subsequent reactions without further purification. The bis(chlorocarbonyl) compound **56** has been synthesised previously by Atwell et al. from **47** with SOCl$_2$/DMF (Figure 2-31).[104] Neither the yield or spectral characterisation of **56** is reported. Nor is the synthesis and spectral characterisation of **47** reported, but it is referenced to a very early (1891) procedure by Von Pechmann.[105]
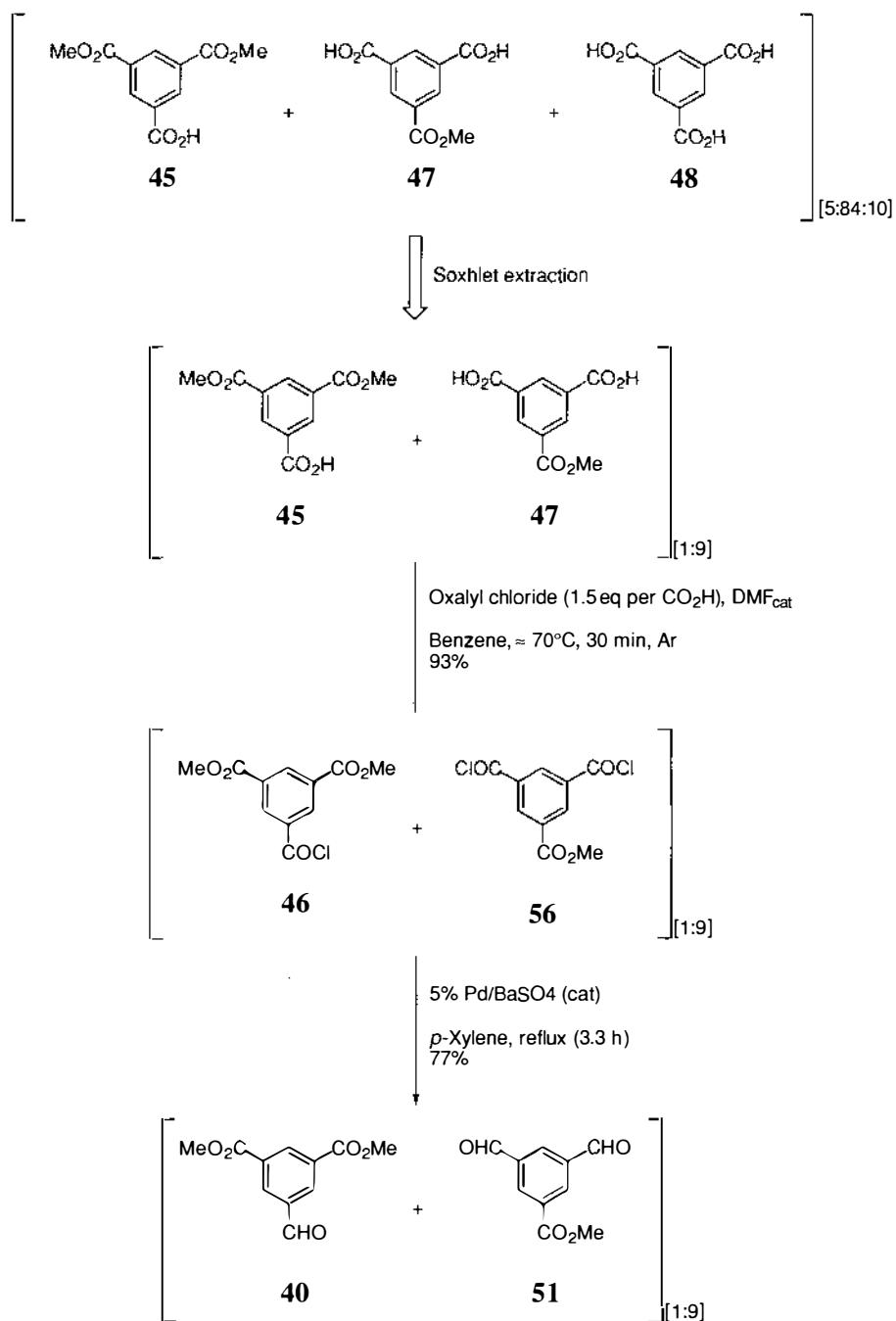
Figure 2-30. Synthesis of dialdehyde **51**.
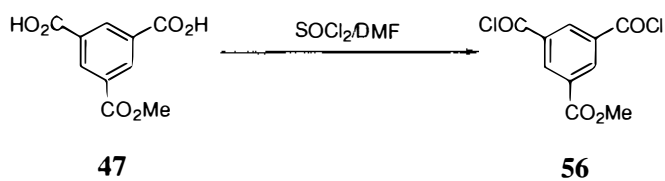
Figure 2-31. Synthesis of **56** by Atwell et al.[104]

Treating the mixture of **45:47** with oxalyl chloride gave the mixture of chlorocarbonyl compounds **46** and **56** in good yield (Figure 2-30). No attempts were made to separate the resulting mixtures. Rosenmund reduction of this mixture yielded a 1:9 mixture of formyl diester **40** and dialdehyde **51** (Figure 2-30). This mixture was used 'as is', in the following porphyrin Wittig chemistry. Pure samples of diacid **47** and dialdehyde **51** were obtained by careful column chromatography for characterisation purposes. Also a pure sample of bis(chlorocarbonyl) **56** was synthesised from pure **47** for characterisation. The methyl ester ^{1}H NMR proton resonances for the dialdehyde **51** were incorrectly reported at 4.62 ppm (instead of 4.03 ppm) by Keana et al.[103] This and additional ^{13}C NMR and HRMS data have been supplied in this thesis. The diacid **47** and bis(chlorocarbonyl) **56** were characterised by ^{1}H, ^{13}C NMR and HRMS.

The Wittig reaction between the aldehyde mixture **40:51** (1:9) and excess TXPps **5** under basic conditions gave, after column chromatography, a mixture of *cis* and *trans* isomers of the free-base diporphyrin ester **52** (Figure 2-32). The presence of *cis* isomers was evident from AB quartet vinylic signals at 6.431 and 6.585 ppm ($^3J = 12$ Hz). The monoporphyrin isophthalate TXP-=-Ph$_m$(CO$_2$Me)$_2$ **50** was also isolated as expected, along with TXP-Me **57**. Treating the isomeric mixture of ester **52** with iodine gave the all *trans* ester in 78% yield (based on dialdehyde **51**). Near quantitative metallation with zinc(II) afforded **Zn$_2$-52**, followed by hydrolysis to give the required acid **Zn$_2$-53**. Hydrolysis was incomplete, as 17% of the starting material **Zn$_2$-52** was recovered during chromatography. The spectral characterisation was similar to the analogous TXP diporphyrin aldehyde prepared by Reid.[79]

Figure 2-32. Synthesis of "dipole" diporphyrin acid **Zn₂-53**.
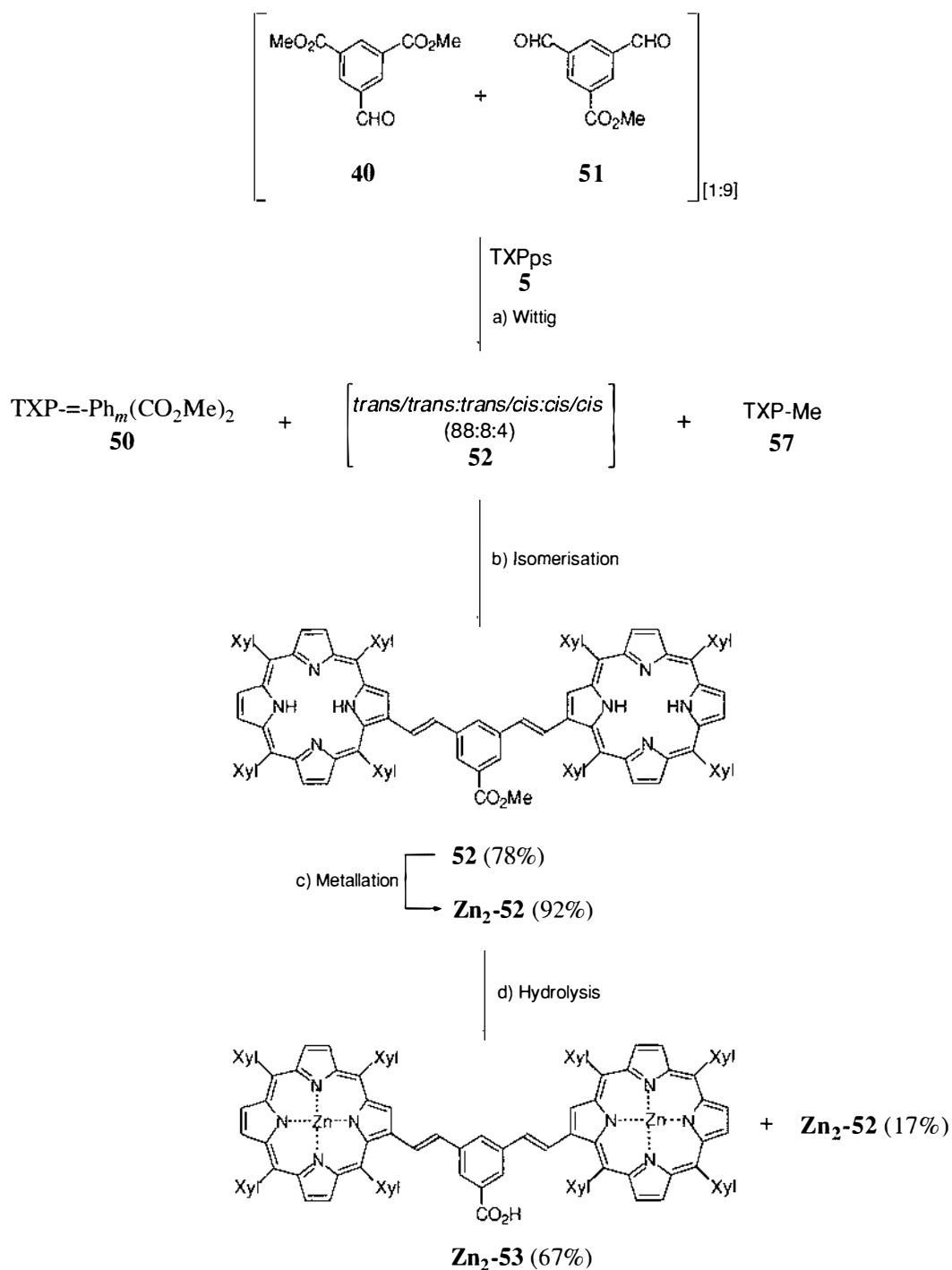
a) **5** (4.5 eq per CHO), DBU (2.0 eq), CH₂Cl₂, RT, 15 min, N₂. b) i) I₂ (≈ 2 eq), CH₂Cl₂, RT, 3 h. ii) Na₂S₂O₃. c) Zn(OAc)₂·2H₂O (2.2 eq), CHCl₃/MeOH, RT (30 min). d) i) KOH (20 eq), THF:H₂O:MeOH (10:1:10), reflux (17 h), N₂.

"Collinear" diporphyrin

Two alternative synthetic pathways to the "collinear" diporphyrin **Zn$_2$-66** were postulated (Figure 2-33). Both approaches involve the 2+2 condensation of dipyrrylmethane (DPM) **58**[106,107] with methyl 4-formylbenzoate **28** and a second functionalised aldehyde. These two methods both employ a binary mixture of aldehydes, which should produce a mixture with the desired unsymmetrical product **61** or **64** statistically favoured (Figure 2-33).

The first approach (Method A) involves the use of protected aldehyde chemistry to form the formylporphyrin ester **63**. The subsequent Wittig chemistry with TXPps **5**, followed by metallation and hydrolysis should afford the desired "collinear" diporphyrin acid **Zn$_2$-66**. The second alternative approach (Method B) to diporphyrin **Zn$_2$-66** is based on the direct synthesis of diporphyrin ester **64** using a binary aldehyde mixture containing methyl 4-formylbenzoate **28** and the porphyrin aldehyde building block **14**. Following metallation and hydrolysis, the desired "collinear" diporphyrin acid **Zn$_2$-66** should be obtained.

While the second approach (Method B) is appealing, the first route would provide both the unsymmetrical formylporphyrin ester **63** and the symmetrical bisacetalporphyrin **62**, useful intermediates for other syntheses. The use of bisacetal **62** is explored and exploited in Chapter 3. The aldehyde ester **63** could also be exploited in other step-wise synthesis to attach other functionality with the porphyrin to a surface. Due to the relative simplicity of this approach, this route was investigated first.
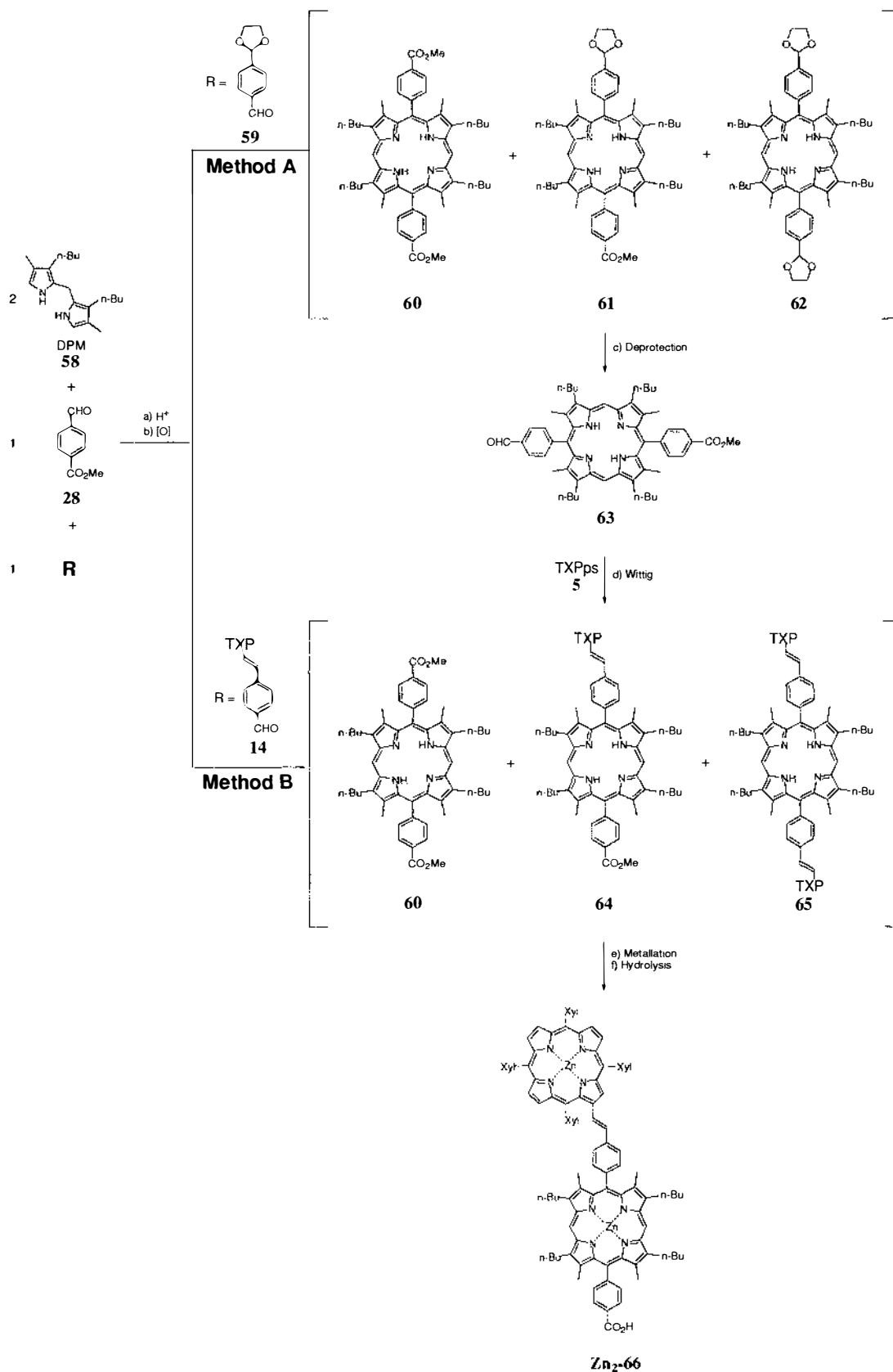
Figure 2-33. Proposed routes to "collinear" diporphyrin **Zn₂-66**.

The unsymmetrical formylporphyrin ester **63** has previously been made and characterised by Kuciauskas et al. via a 5-step synthesis shown in Figure 2-34.[108,109] Method B additionally has the potential advantage of providing a shorter synthesis of the formylporphyrin ester **63** than that of Kuciauskas et al.
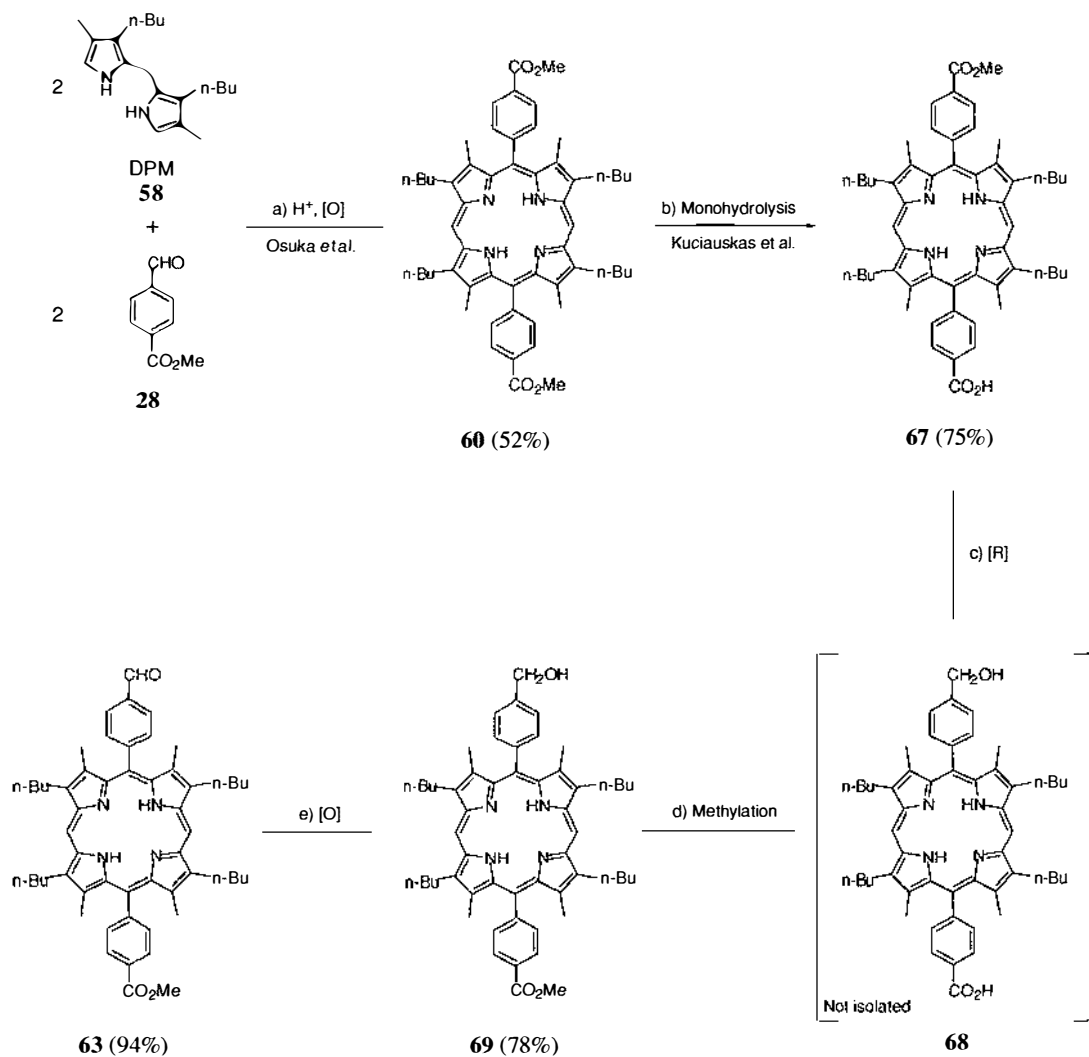
a) i) TCA (0.17 eq), CH₃CN (10⁻¹ M), RT (5 h), N₂. ii) p-chloranil (1.7 eq), THF, RT (3 h). b) TFA/HCl, H₂O, 80°C (2 h). c) LiAlH₄, THF. d) Diazomethane, CH₂Cl₂, RT. e) MnO₂, CH₂Cl₂, RT (1 h).

Figure 2-34. Synthesis of formylporphyrin ester **63** by Kuciauskas et al.[108,109]

The monoacetal 4-(1,3-dioxa-2-cyclopentyl)benzaldehyde acetal **59** was synthesised by modification of a commercial procedure by Ichimura et al.[110] used for the acid catalysed synthesis of terephthalaldehyde mono(diethyl acetal). Optimising 1,2-ethanediol ratios, gave a mixture containing products **22, 59** and **70** in a ratio of 19:69:11 (Figure 2-35).
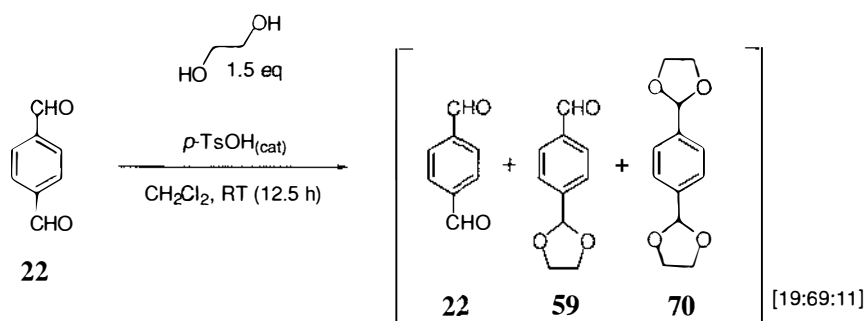
Figure 2-35. Synthesis of monoacetal **59**.

The resulting mixture was separated, first by removing the dialdehyde **22** component with vacuum sublimation, then short path fractional distillation of monoacetal **59**, leaving the diacetal **70** component behind. Fractions containing up to 97% pure monoacetal **59** were isolated. The presence of small amounts of diacetal **70** in the monoacetal **59** was not a concern for the following porphyrin forming reactions, since it would not take part in the condensations under the anhydrous conditions employed. Although alternative syntheses for monoacetal **59** also exist in the literature, but most require the prior preparation of other intermediates first. Castells et al.[111] has synthesised and characterised monoacetal **59** using polymer-supported Wittig reagents, and Blankespooor et al.[112] prepared **59** via photochemical methods from suitably substituted anthraquinones. While this work was being carried out, Ponde and co-workers published an efficient method for the monoprotection of terephthaldicarboxaldehyde **22** using natural kaolinitic clay as a catalyst, claiming a 92% yield of **59**.[113]

The 2+2 condensation of DPM **58** with a mixture methyl 4-formylbenzoate **28** and monoacetal **59** was carried out under Lindsey conditions[114] (Figure 2-36). There appeared to be little acid-catalysed deprotection of either the stating material or products. This is fortunate, as even small amounts for deprotection would have lead to significant amounts of oligomers and polymers and thereby drastically reducing the yields. Isolation of the products by chromatography gave the desired unsymmetrical acetal-porphyrin ester **61** (27%) and the symmetrical bisester **60** (22%) and bisacetal **62** (15%) porphyrins. Deprotection of the acetal-porphyrin ester **61** by transacetalation with *p*-toluenesulfonic acid in acetone, quantitatively gave the formylporphyrin ester **63**.

a) i) TFA (1.0 eq), CH$_2$Cl$_2$ (10^{-2} M), RT (25 min), N$_2$. ii) DBU (1.0 eq), iii) p-Chloranil (2.5 eq), reflux (2.5 h). b) p-TsOH•H$_2$O (6.0 eq), acetone, reflux (1.5 h), N$_2$.
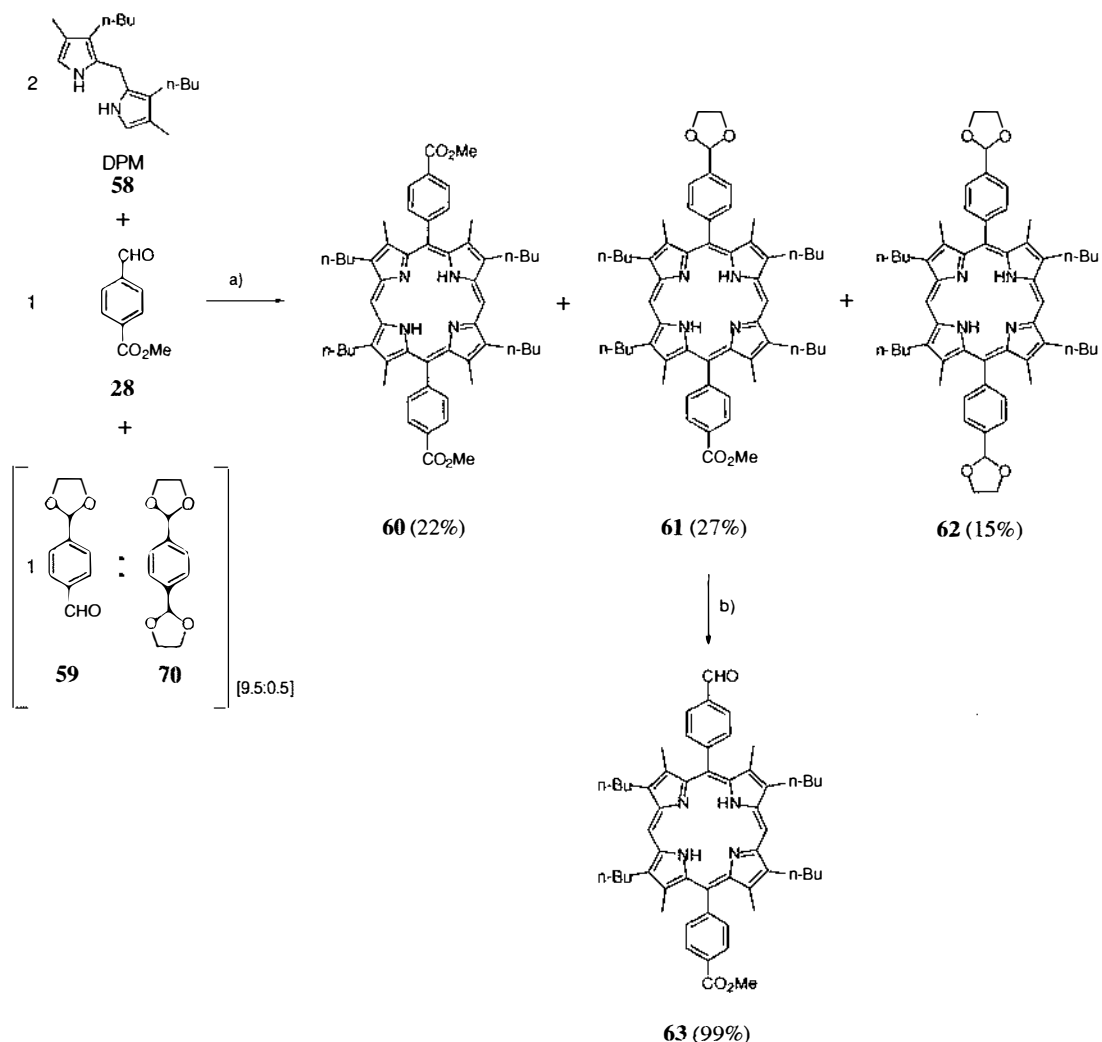
Figure 2-36. Synthesis of unsymmetrical formylporphyrin ester **63**.

The Wittig reaction of **63** with TXPps **5** gave what appeared to be a mixture of compounds (Figure 2-37). ^{1}H NMR spectra showed extra product signals at δ 7.41-7.74, most likely attributed to contamination with triphenylphosphine oxide. In addition, there appeared to be no extra signals in the ^{1}H NMR spectra attributed to the *cis* isomer. This reflects the higher temperatures used in the Wittig reaction and probably unfavourable steric interactions present in the *cis* isomer. Metallation with zinc(II) was carried out after the Wittig reaction on the partially purified mixture to aid in the separation. Chromatographic separation of the metallated derivative gave the *trans* "collinear" diporphyrin ester **Zn$_2$-64** in 82% overall yield, free from contaminants.

Near quantitative hydrolysis of this ester gave the desired *trans* "collinear" diporphyrin acid Zn_2-66.
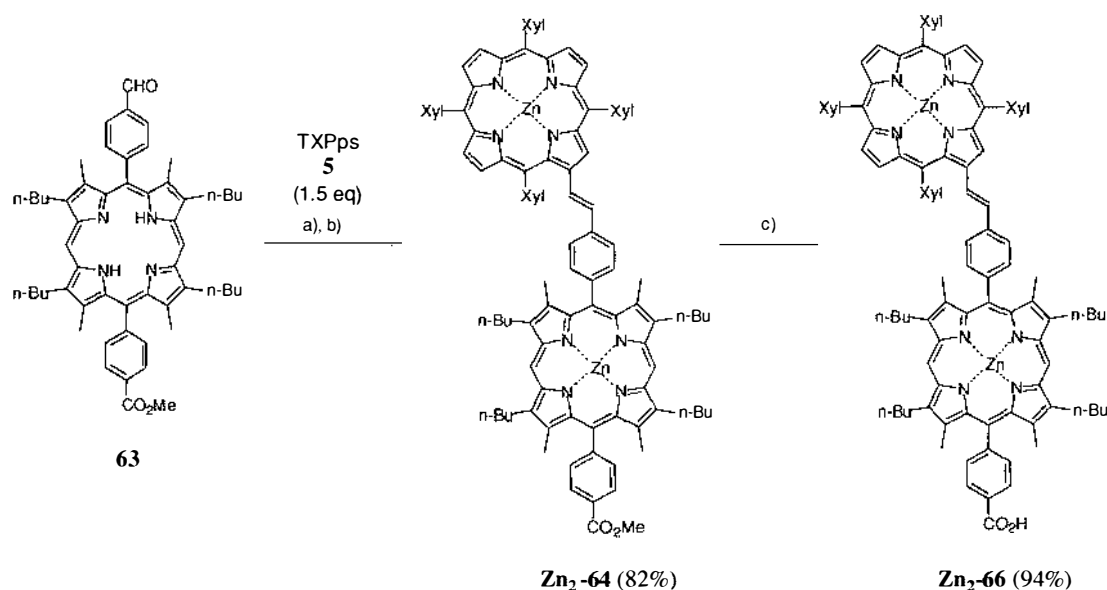
a) DBU (2.0 eq), CHCl$_3$, reflux (20 min), N$_2$. b) Zn(OAc)$_2$·2H$_2$O (1.2 eq), CHCl$_3$, RT (30 min). c) i) KOH (30 eq), THF:MeOH:H$_2$O (10:10:1), reflux (5 h), N$_2$. ii) H$_3$PO$_4$ (32 eq).

Figure 2-37. Synthesis of "collinear" diporphyrin Zn_2-66.

2.2.3   Other Acidic Porphyrins

The methodology developed in the previous section provided the opportunity to explore the synthesis of a variety of other acidic porphyrins for attachment to SC surfaces, allowing alternative surface binding modes to be explored, and being useful as comparison acids systems. Weaker surface binders such as phenols and potentially stronger binders such as diacids and multiacid porphyrins were synthesised from starting materials and by-products previously prepared. The syntheses of these are now discussed.

TXP Phenol derivatives

The β-styryl linked *para*-phenol derivative **Zn-72** was synthesised following the already established Wittig methodology (Figure 2-38). Using an excess of 4-formylphenol **71** with TXPps **5** gave free-base TXP phenol porphyrin **72** in 52% yield.

This slightly below average yield is probably due to losses during separation by column chromatography; significant smearing through the column was noted. The Wittig reaction was performed in refluxing toluene to avoid the requirement for isomerisation with iodine, thus avoiding possible iodination of the phenol moiety. Subsequent metallation with zinc(II) acetate afforded the desired **Zn-72** product in good yield. Spectral characterisation by ^{1}H NMR spectroscopy was typical of the TXP β-styryl substituted porphyrins. The hydroxyl proton resonance for free-base porphyrin **72** was not resolved in the ^{1}H NMR spectrum due to exchange, but for the metallated derivative **Zn-72** it appears as a well-resolved singlet at 4.75 ppm.

a) i) DBU (3.0 eq), toluene, reflux (30 min), N$_2$. ii) H$_3$PO$_4$. b) Zn(OAc)$_2$·2H$_2$O (2.0 eq), CHCl$_3$/MeOH, RT (15 min).
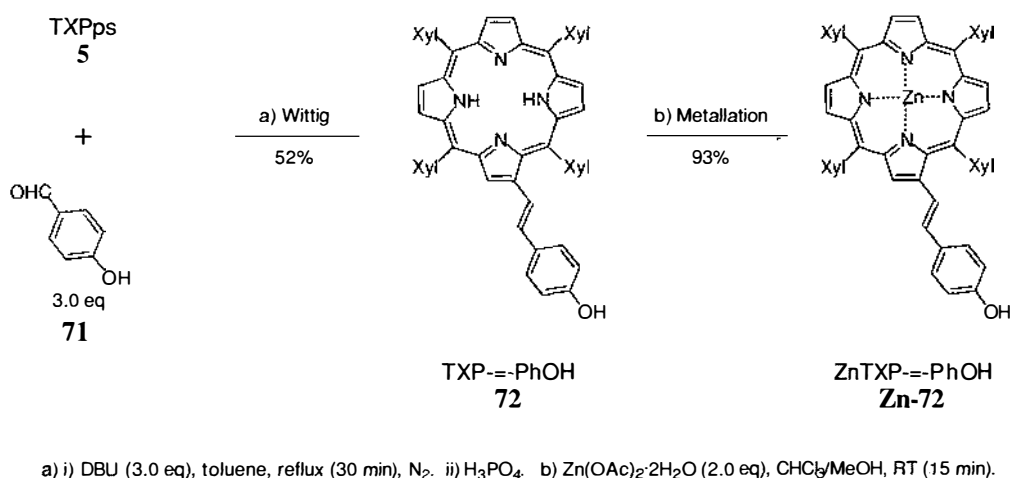
Figure 2-38. Synthesis of phenol porphyrins **72** and **Zn-72**.

5,15-Biscarboxyphenylporphyrin

The synthesis of diacid **Zn-73**, was achieved through the hydrolysis of the diester derivative **Zn-60** (Figure 2-39). Ester **60** has been previously synthesised by Kuciauskas et al. in 52% yield[108] (Figure 2-34) using the method of Osuka and coworkers.[109] It is also a by product of the synthesis of formylporphyrin ester **63** in this thesis (Figure 2-36). Large-scale direct synthesis of **60** was also achieved in this thesis with *p*-toluenesulfonic acid in MeOH, using similar condensation conditions to those of Gunter et al.[115], giving an excellent 64% yield (Figure 2-39). Metallation of with zinc(II) gave **Zn-60** in 80% yield, and subsequent quantitative hydrolysis afforded the desired acid **Zn-73**. Spectral characterisation was typical of the bis-substituted TBMPs. The CO$_2$**H** proton resonances of **Zn-73** were observed at 13.21 ppm as a broad singlet in the ^{1}H NMR (DMSO-d$_6$) spectrum.
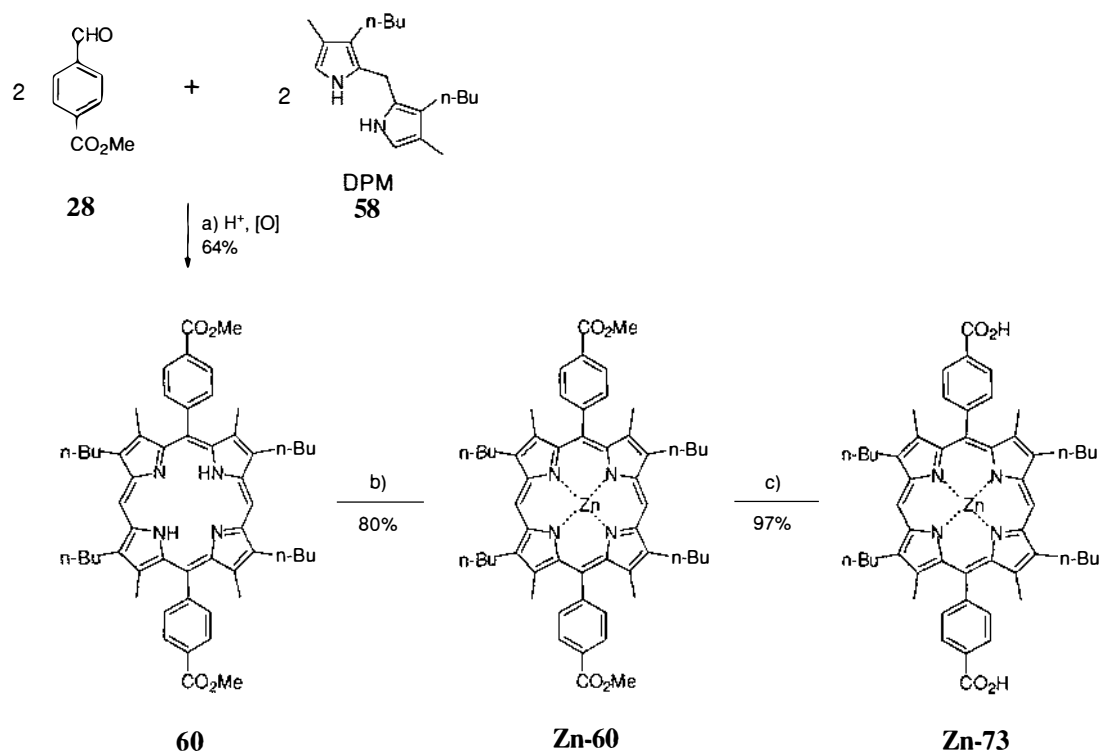
a) i) *p*-TsOH·H$_2$O (0.25 eq), MeOH, RT (20 h), N$_2$. ii) *p*-Chloranil (0.9 eq), CH$_2$Cl$_2$, RT (3.5 h). b) Zn(OAc)$_2$·2H$_2$O (1.2 eq), CHCl$_3$/MeOH, RT (30 min). c) i) KOH (15 eq per CO$_2$Me), THF:MeOH:H$_2$O (10:10:1), reflux (22 h), N$_2$. ii) H$_3$PO$_4$ (excess).

Figure 2-39. Synthesis of Zn(II) 5,15-biscarboxyphenylporphyrinato **Zn-73**.

5,10,15,20-Tetra(3,5-dicarboxyphenyl)porphyrin

The generality of this hydrolysis chemistry is no better exemplified than by its use for the synthesis of the octaacid porphyrin **Zn-75** (Figure 2-40). Although the methyl ester **74** has not been reported previously, other alkyl ester derivatives have.[100,116,117] An ethyl ester derivative was synthesised in a similar way by Fudickar et al. who also carried out hydrolysis producing the free-base acid **75**.[100] A manganese acetate derivative **Mn-75** of the free acid is also known.[118,119] The required octaester **74** was prepared in moderate yield under typical Lindsey pyrrole condensation conditions.[120] Near quantitative metallation of **74** with zinc acetate afforded **Zn-74**. The hydrolysis of the octaester **Zn-74** gave the octaacid **Zn-75** in good yield. Spectral characterisation was straightforward due to the symmetrical nature of the porphyrins. The CO$_2$H proton resonances of octaacid **Zn-75** were observed at 13.5 ppm as a broad singlet of the correct integral in the ^{1}H NMR (DMSO-d$_6$) spectrum. Only a low resolution FAB mass spectrum result

could be obtained for octaacid **Zn-75**. Both +ve and −ve mode FAB MS were attempted with only a weak MH$^+$ being detected.
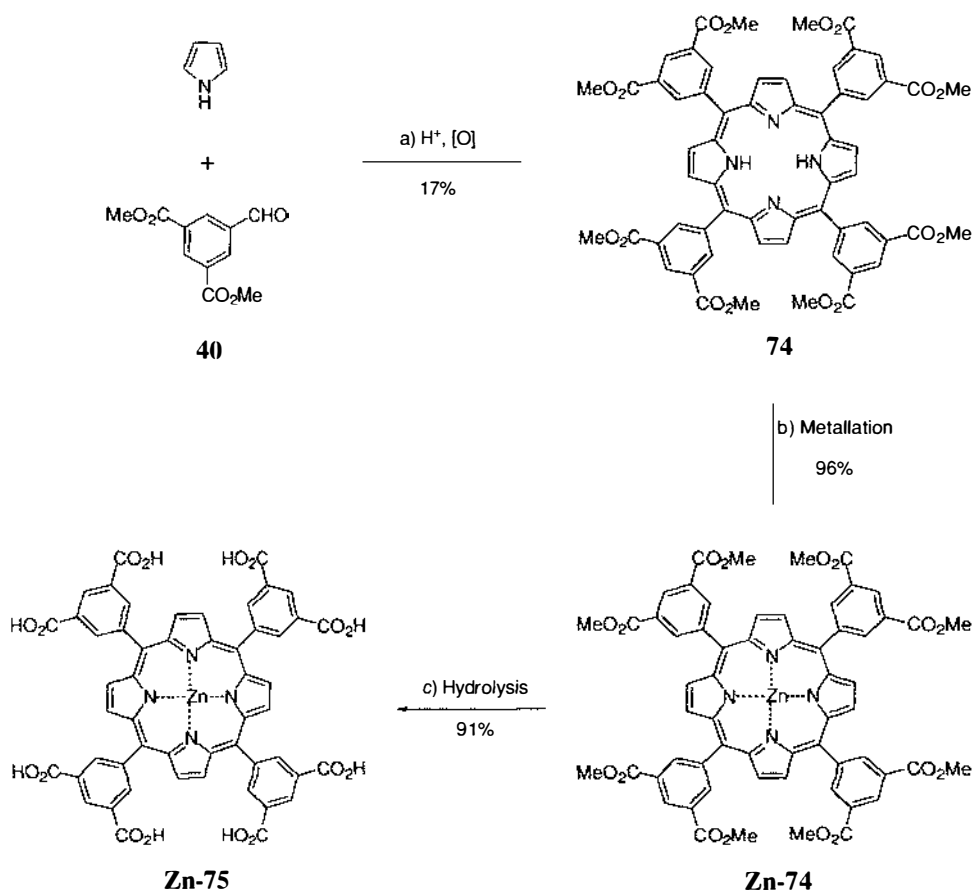
a) i) BF$_3$·OEt$_2$ (0.1 eq), CH$_2$Cl$_2$ (10^{-2}M), RT (3 h). ii) p-Chloranil (0.75 eq), reflux (2 h). iii) Et$_3$N (excess). b) Zn(OAc)$_2$·2H$_2$O (1.2 eq), CHCl$_3$/MeOH, reflux (30 min). c) i) KOH (15 eq per CO$_2$Me), THF:MeOH:H$_2$O (10:10:1), reflux (18 h), N$_2$. ii) H$_3$PO$_4$ (excess).

Figure 2-40. Synthesis of octaacid **Zn-75**.

2.3 *Characterisation*

2.3.1   Reaction Monitoring

Due to the coloured nature of the chromophores, most reactions involving porphyrin compounds were monitored easily by thin layer chromatography (TLC). Metallation of free-base porphyrin moieties with Cu(II) or Ni(II) always gives compounds with higher R_f on silica gel. Metallation of tetraarylporphyrins (TAPs) with Zn(■) generally results in a compound with a slightly lower R_f, however, metallation of the bisaryl TBMP-based porphyrins results in compounds of higher R_f. UV-vis analysis was also routinely used to monitor metallation reactions where TLC observations were not conclusive. Conversion from free-base to metallo species can usually be followed by observing the change in number and position of Q-bands in the absorption spectra.

2.3.2   NMR Spectroscopy

The primary characterisation method for the porphyrin compounds was ^{1}H NMR spectroscopy. Porphyrin solutions of 2 x 10^{-2} M or less were prepared and the 270 and/or 400 MHz spectra obtained. Although these compounds afford what appear to be complex spectra, they are generally first-order in nature and easily assigned. Short and long-range ^{1}H-^{1}H COSY spectra were routinely used to aid assignments. A typical example of a β-styryl linked TAPs is that of the TXP-based, free-base methyl porphyrin ester **23** (Figure 2-41). The same trends and general features are observed for the TPP and TBP derivatives. At high field, this spectrum shows the signal of two highly shielded nitrogen protons at the centre of the aromatic porphyrin ring, as a slightly broadened singlet (-2.63 ppm). This resonance is lost on metallation with diamagnetic metals like Zn(II) and Ni(II). The signals from the methyl groups of the xylene substituents appear around 2.6 ppm, as three signals due to the unsymmetrical nature of the β-substituted porphyrin. The aryl methyl ester resonances always appear at about 4.0 ppm. The most obvious difference between the ester and acid derivatives is the loss

of these methyl ester proton resonances upon hydrolysis. The consequent acid protons are not normally observed, being too broad to identify.
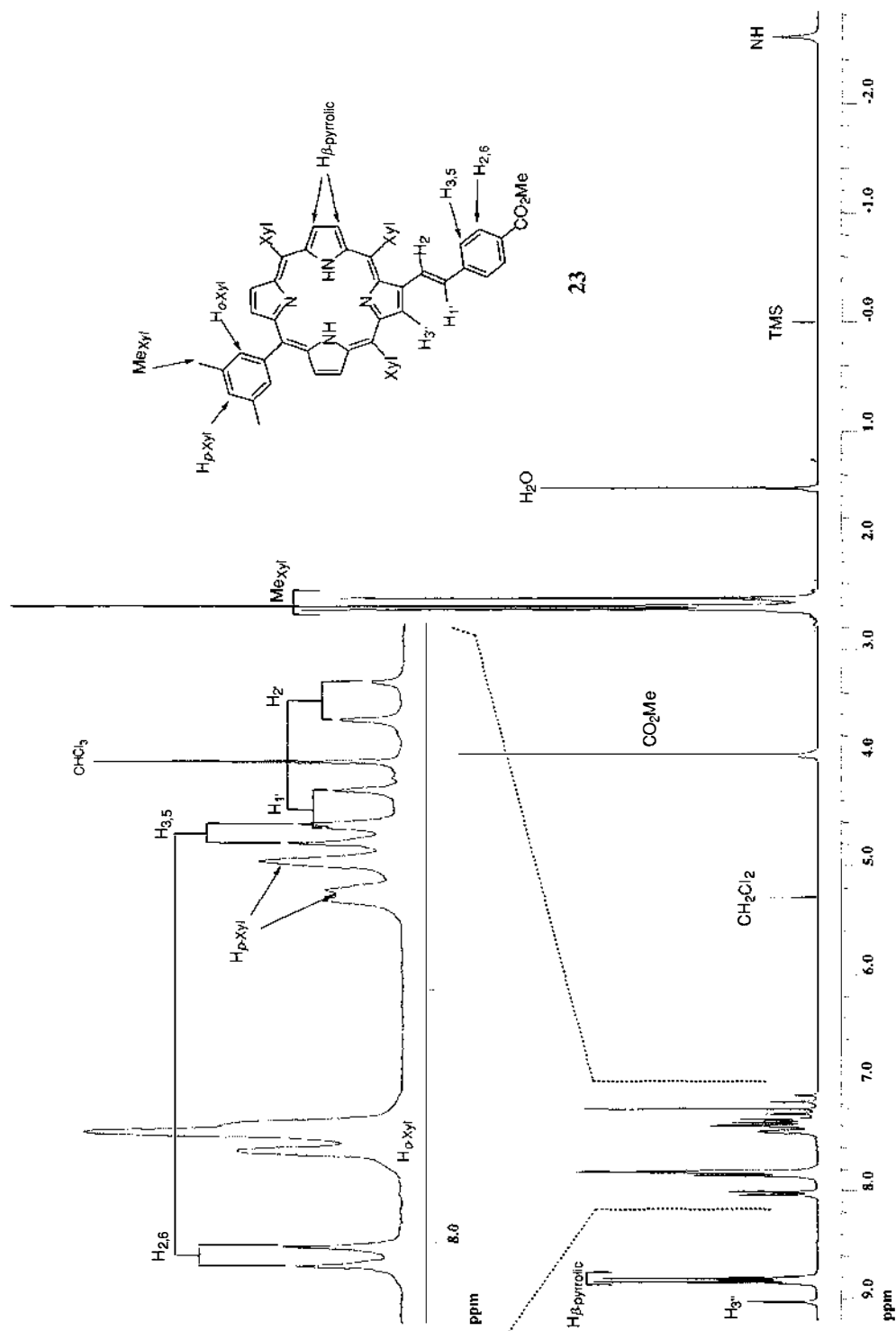
Figure 2-41. ^{1}H NMR spectrum of **23** (CDCl$_3$, 270 MHz).

Moving up-field, the insert shows an expansion of the aromatic region where the signals of the *trans* ethenyl protons of $H_{1'}$ and $H_{2'}$ appear as an AB quartet, having a typical 16 Hz ^3J coupling. A ^4J coupling of about 0.6 Hz can often be seen between ethenyl $H_{2'}$ and β-pyrrolic $H_{3''}$ protons (see **Zn-10** experimental Section 7.2). The *para* xylene proton resonances are split due to lack of symmetry around the porphyrin core and appear up-field from the *ortho* proton signals. The styryl protons $H_{3,5}$ and $H_{2,6}$ generally appear as doublets and are easily assigned from coupling constants or COSY spectra. The β-pyrrolic proton signals are further downfield. The $H_{7',8',12',13',17',18'}$ signals appear as a multiplet, due to the lack of symmetry. For some compounds, a typical spin-spin coupling of $^3J = 4.9$ Hz can be observed for some of these protons, but often they have convergent overlapping chemical shifts. The furthest downfield signal that of the $H_{3''}$ β-pyrrolic proton next to the ethene link. The porphyrin ring current heavily deshields this proton, with an additive contribution from the ethenyl bond. In the TXP *ortho* esters and acid (TXP-=-Ph_oCO_2R, **29**, **Zn-29**, **Zn-32**), there is a downfield shift to from ≈ 7.3 to ≈ 8.0 ppm for the $H_{1'}$ ethenyl proton. This is undoubtedly due to the deshielding influence exhibited by the close proximity of the carbonyl group. Reid also observed this in the spectra of the analogous *ortho* aldehyde compound.[79] Poor solubility of the acid porphyrins was sometimes a problem. In the case of NiTPP-=-$PhCO_2H$ **Ni-9** a suitable solvent was not found, and at best only a broadened ^1H NMR spectra was obtained. However, the absence of the methyl ester (CO_2CH_3) proton resonance was evident. Generally, well-resolved proton spectra were obtained even on precipitated samples by utilising variable temperature NMR with exhaustive shimming. For the zinc isophthalic acid derivative ZnTXP-=-$Ph_m(CO_2H)_2$ **Zn-37**, Et_3N was added to the NMR solvent to improve solubility. Subtraction of the overlapping Et_3N signals integral values, gave the correct integral values expected for the porphyrin moiety.

Another ^1H NMR spectrum of interest is that of the "collinear" diporphyrin **Zn_2-64** (Figure 2-42). This spectrum typifies the first-order nature of some of these more complex molecules. Having an appended-TBMP porphyrin moiety on the styryl TXP does not greatly complicate the spectra.
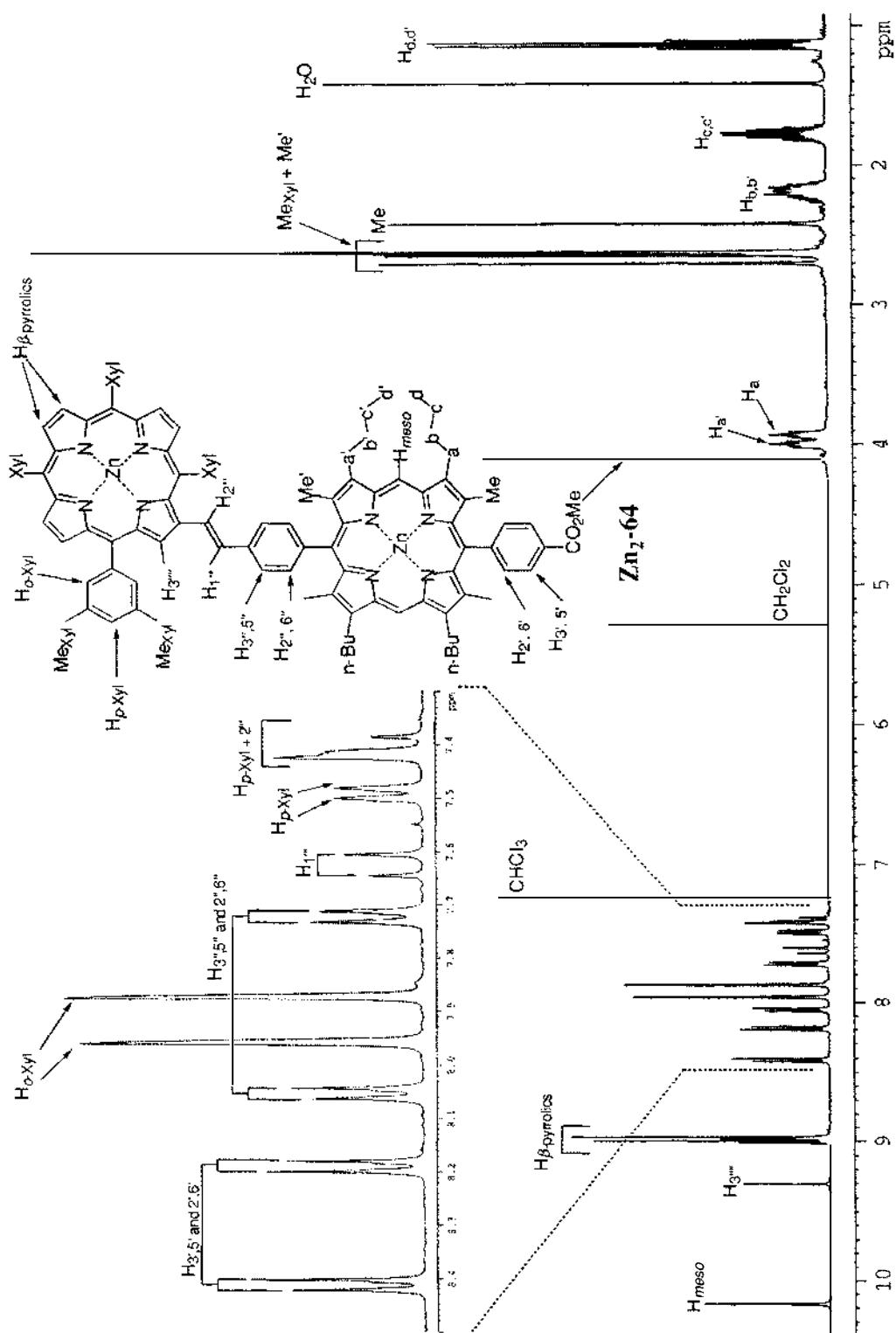
Figure 2-42. ^{1}H NMR spectrum of **Zn$_2$-64** (CDCl$_3$, 400 MHz).

Assignments are easily made from COSY experiments and comparisons to the known symmetrical analogues (bisacetal **Zn-60** and triporphyrin **Zn$_3$-65**) reported elsewhere in this thesis. Notably the aromatic region (Figure 2-42, insert) is simplified due to the

deshielding effect imposed by the TBMP moiety. Due to the unsymmetrical nature of the TBMP group, the $H_{b',b}$ and $H_{c',c}$ alkyl proton resonances appear as complex multiplets, while those of $H_{a',a}$ and $H_{d',d}$ being discernible as separate triplets. The most downfield signal in the spectrum is now that of the highly deshielded *meso* protons.

2.3.3   Mass Spectrometry

Fast-atom-bombardment high-resolution mass-spectrometry (FAB HRMS) techniques were used to identify the parent molecular ions. From FAB HRMS the experimental isotopic patterns of all the molecular ions did mirror the calculated isotopic mass patterns, along with the correct mass, supporting the identification of all the porphyrins. The FAB mass spectra are dominated by the M^+ and MH^+ parent ions although sometimes the isotopic patterns are distorted due to the presence of both species. Weak isotope shadows of ($[M + 16]^+$ and $[M + 32]^+$ are commonly observed in the mass spectra. These result from the addition of molecular oxygen during the ionisation process.[121]

2.3.4   UV-vis Absorption Spectroscopy

Solution UV-vis spectroscopy was carried out on free-base and metalloporphyrin derivatives. DCM solutions were mostly used, however because of poor solubility the acid derivatives were generally run in THF. Typical absorption spectra were observed for all of these species, dominated by the Soret and Q bands as described in Chapter 1 (Section 1.4.1).

Of particular interest are "collinear" diporphyrins **Zn₂-64** and **Zn₂-66**, which have two distinctly separate Soret peaks at 411 and 430 nm (Figure 2-43). The 411 and 430 nm peaks for **Zn₂-64** are indicative of the separate ZnTBMP and ZnTXP moieties respectively. This is clearly demonstrated by comparing it with the overlayed spectra of the monoporphyrin reference compounds **Zn-60** and **Zn-23**. Singular Q-bands are not well resolved, but shoulders can be seen at the appropriate wavelengths in the spectrum of diporphyrin **Zn₂-64**.
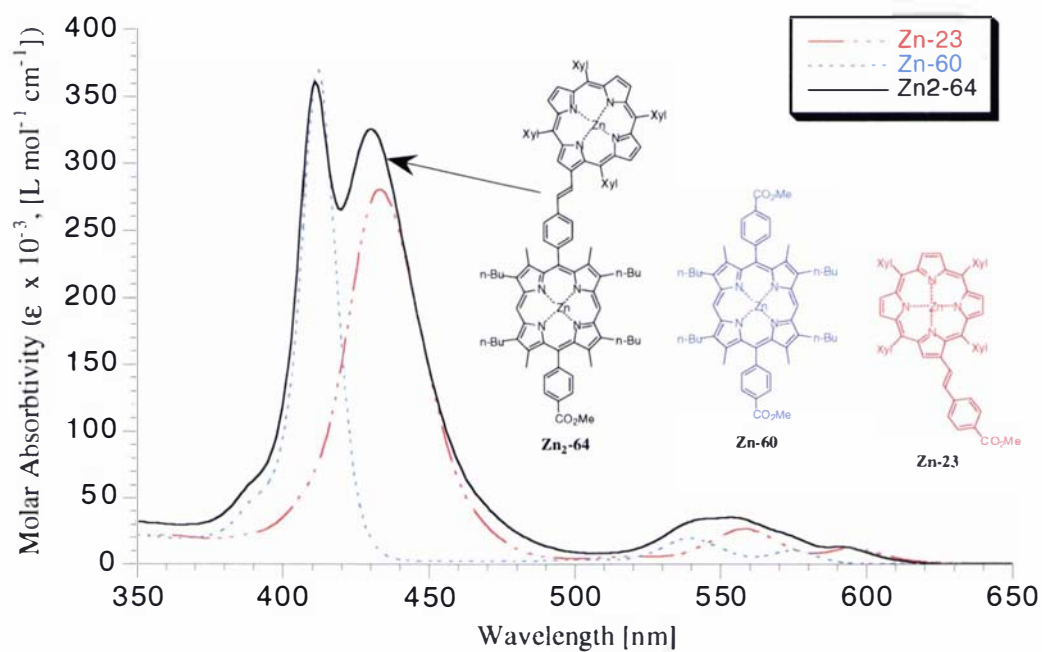
Figure 2-43. UV-vis spectra of "collinear" diporphyrin **Zn₂-64** and monoporphyrins **Zn-60** and **Zn-23** in CH₂Cl₂.

2.4 Conclusion

The syntheses of β-styryl linked porphyrin benzoic acids and some *meso*-substituted benzoic acid porphyrins was achieved by employing Wittig chemistry and classical porphyrin-forming condensation reactions with appropriate formyl methyl esters. Hydrolysis of the resulting porphyrin esters provided a facile and reliable acid synthesis, particularly where multi-step reactions were necessary. It was demonstrated that acid functionality on porphyrins could be generated from aldehydes via esters, even though direct oxidation of the aldehydes to acids could not be achieved.

The synthesis of the "dipole" **Zn$_2$-53** and "collinear" **Zn$_2$-66** diporphyrins were achieved, providing two different porphyrin light harvesting arrays for evaluation on SC surfaces. The methodology for the syntheses of these two arrays could easily be expanded further to unsymmetrical binary chromophore systems as illustrated in Figure 2-44. By the stepwise nature of the synthesis, a second chromophore λ_x (with a different absorption spectrum) or redox system could be attached. In principle, any chromophoric phosphonium salt could be reacted with the primary branched or linear porphyrin aldehydes to give mixed systems.

The synthesis of TBMP bisacetal **Zn-62** by product is exploited further in the following chapter. From the bisaldehyde derivative of this compound, a methodology was developed to allow the controlled synthesis of larger mixed-porphyrin and mixed-metal porphyrin arrays, from linear triporphyrins and pentaporphyrins to a large nonaporphyrin. The methodology developed in Chapter 3 was then applied later to the synthesis of some unique "sticky" mixed-triporphyrins in Chapter 4.
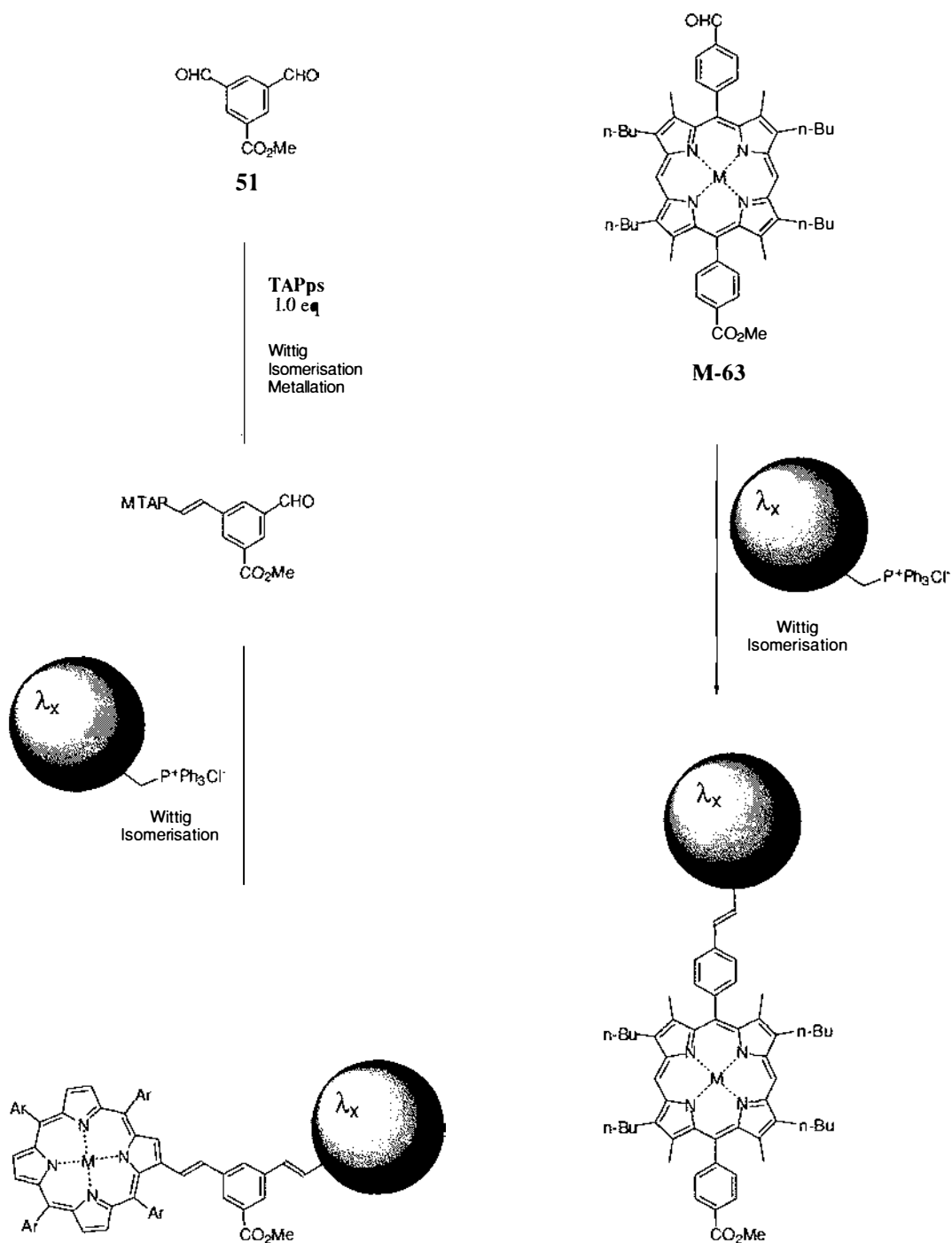
Figure 2-44. Mixed-chromophore "dipole" and "collinear" arrays.

Chapter 3

Synthesis of Mixed-Metal and

Mixed-Porphyrin Arrays

A Building Block Approach to the Controlled Synthesis of Mixed-Metal and Mixed-Porphyrin Arrays

3.1   Introduction

While the synthesis of dimetallo (M_1/M_2 or $M_1/2H$) mixed-porphyrin arrays from diporphyrins and upwards is common[122], the controlled synthesis of trimetallo ($M_1/M_2/M_3$ or $M_1/M_2/2H$) mixed-porphyrin arrays is rare.
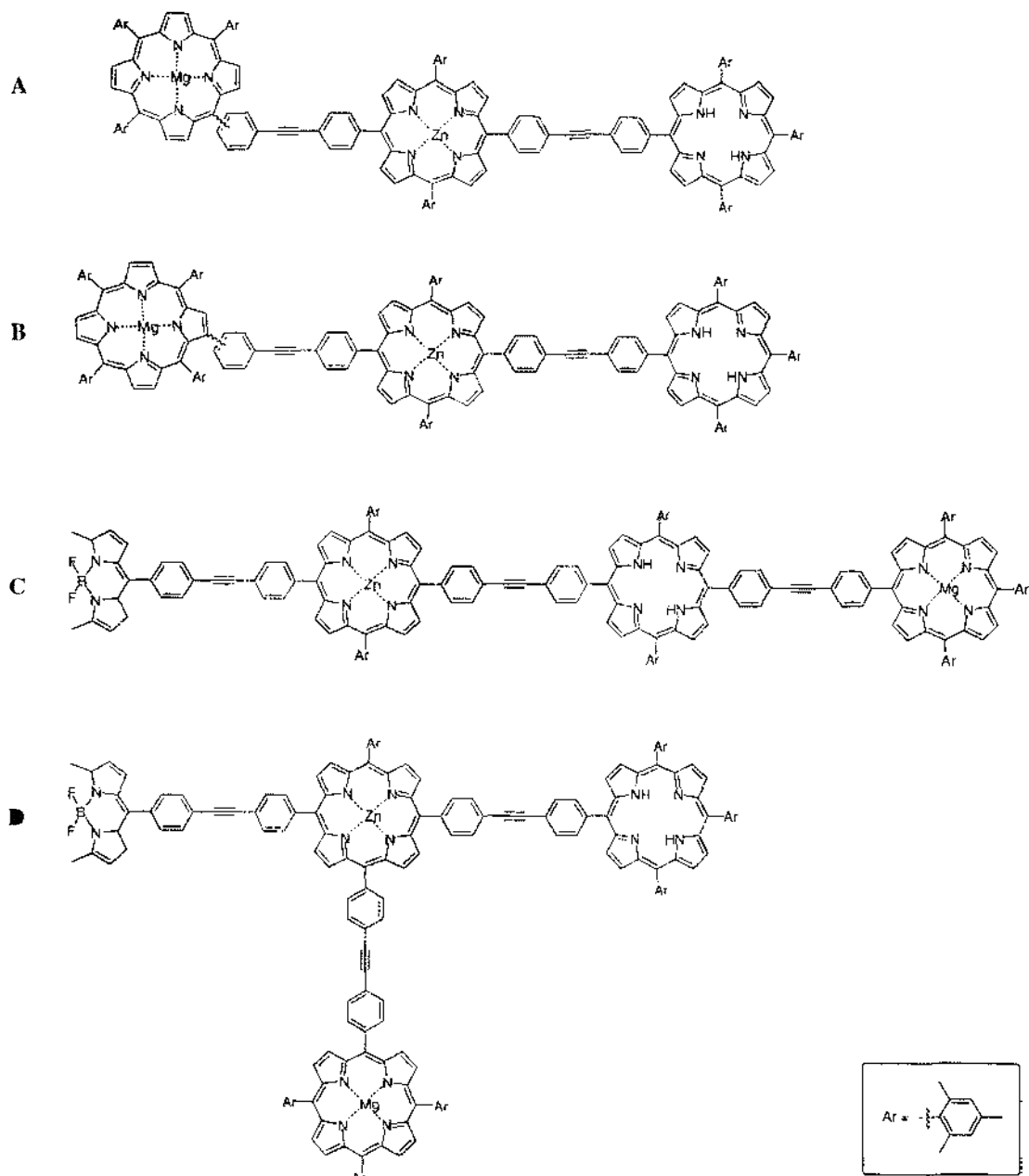
Figure 3-1. Mixed-metal triporphyrins by Lindsey et al.[123,124]

Lindsey et al. has demonstrated the synthesis of a number of Zn/2H/Mg triporphyrins (Figure 3-1) for the development of molecular optoelectronic gates, and the study of energy transfer processes.[123,124] Gossauer et al. have also demonstrated the controlled syntheses of trimetallo planar triporphyrin (Figure 3-2).[125]

	M$_1$	M$_2$	M$_3$
A	Zn	Ni	2H
B	Zn	Ni	Cu
C	2H	Ni	Cu

A, B, C
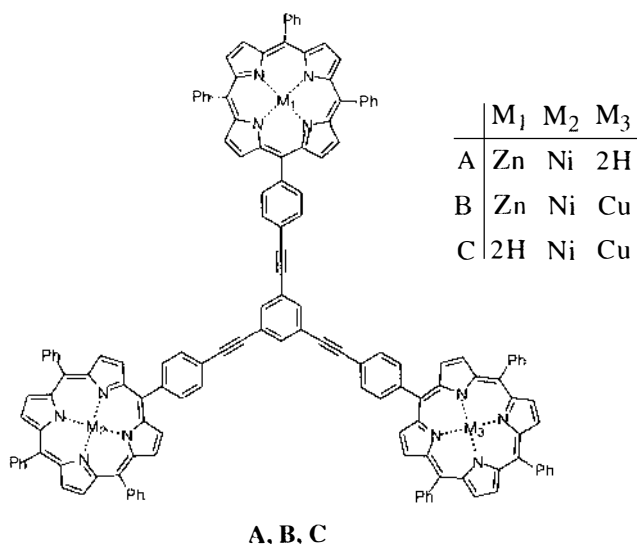
Figure 3-2. Trimetalloporphyrins by Gossauer et al.[125]

Work in our laboratory has previously demonstrated the synthesis of dimetallo mixed-metal triporphyrin systems using Wittig chemistry with a variety of TAPps (Figure 3-3).[83] This Building Block A approach has allowed quick and convenient access to dimetallo, diporphyrins, triporphyrins and a pentaporphyrin.[79,82,126] This methodology was taken a step further with a branched diporphyrin Building Block B that could be exploited for the synthesis of trimetallo mixed-porphyrin systems up to nonaporphyrins (Figure 3-4).[79,82,127]
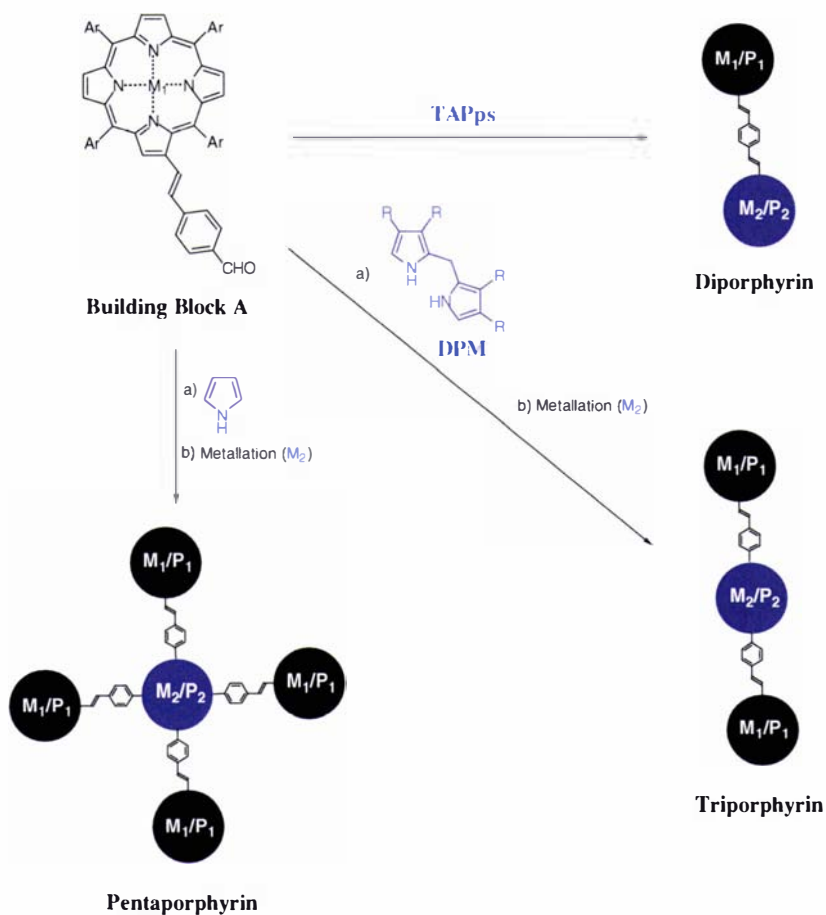
Figure 3-3. Building Block A approach to porphyrin arrays in these laboratories.
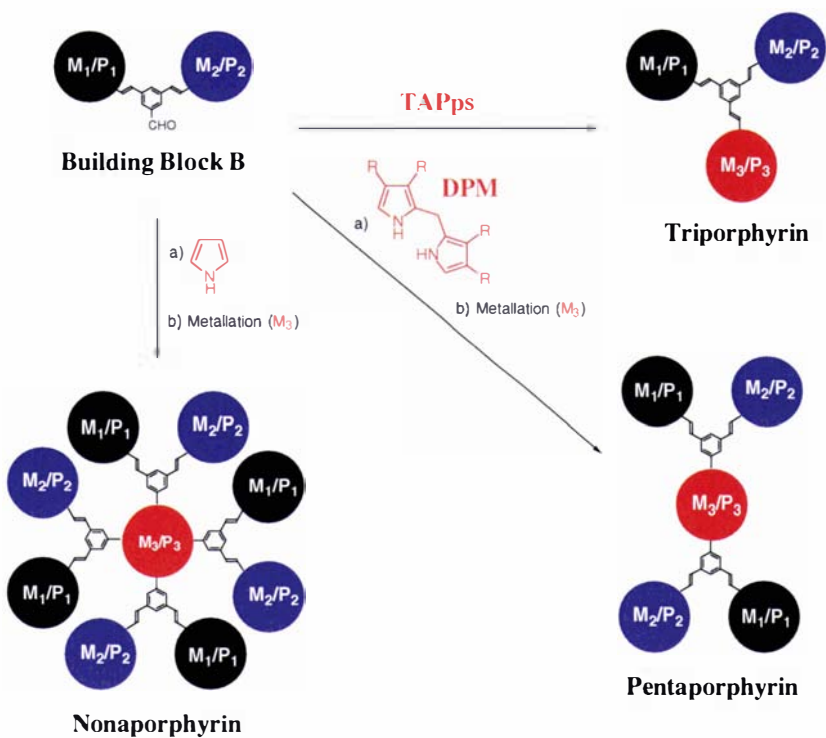
Figure 3-4. Building Block B approach to porphyrin arrays in these laboratories.

Methodologies allowing synthetic control over the placement of three or more different metals or porphyrins from triporphyrins and larger porphyrin systems are of interest for gaining understanding into energy transfer processes for artificial light harvesting and molecular optoelectronic devices.[128] In an extension of this building block approach, it was proposed to exploit the bisacetalporphyrin (BAcP) **62** (Figure 3-5) from Chapter 2. By deprotecting BAcP **62**, the subsequent bisformylporphyrin (BFP) **76** could be reacted with one equivalent of a TAPps (like TXPps **5**) to fabricate a new linear dimetallo diporphyrin Building Block C **M₂/M₁-77**.
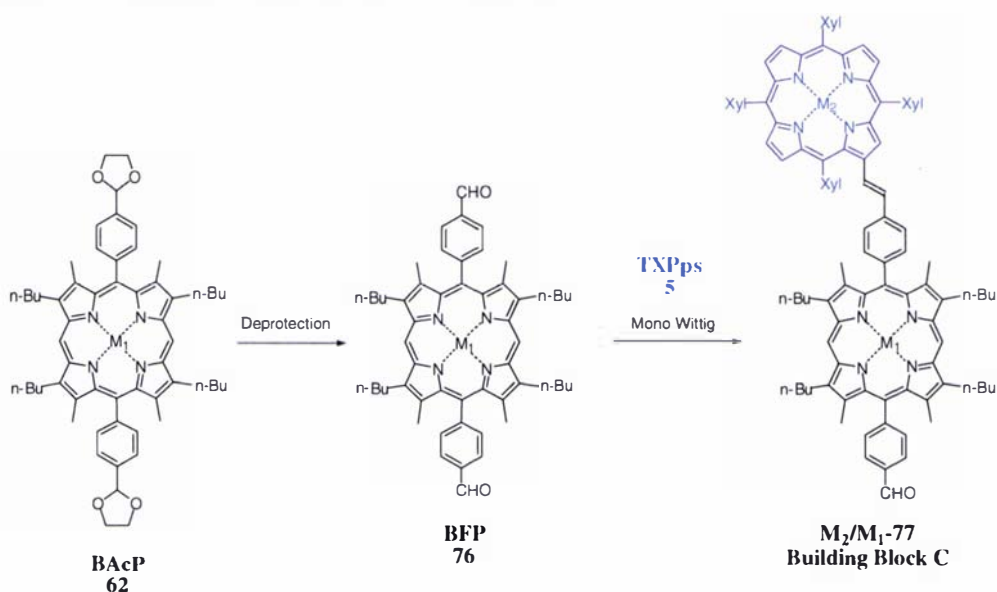
Figure 3-5. Proposed Building Block C synthesis.

The synthesis of Building Block C could allow the stepwise preparation of mixed-metal/mixed-porphyrin diporphyrin, triporphyrin, pentaporphyrin and nonaporphyrin array systems (Figure 3-6). Of importance is that this new approach will allow the placement of at least three different metals as well as three different porphyrin types, to be synthetically controlled using Wittig chemistry and classical porphyrin condensation reactions.
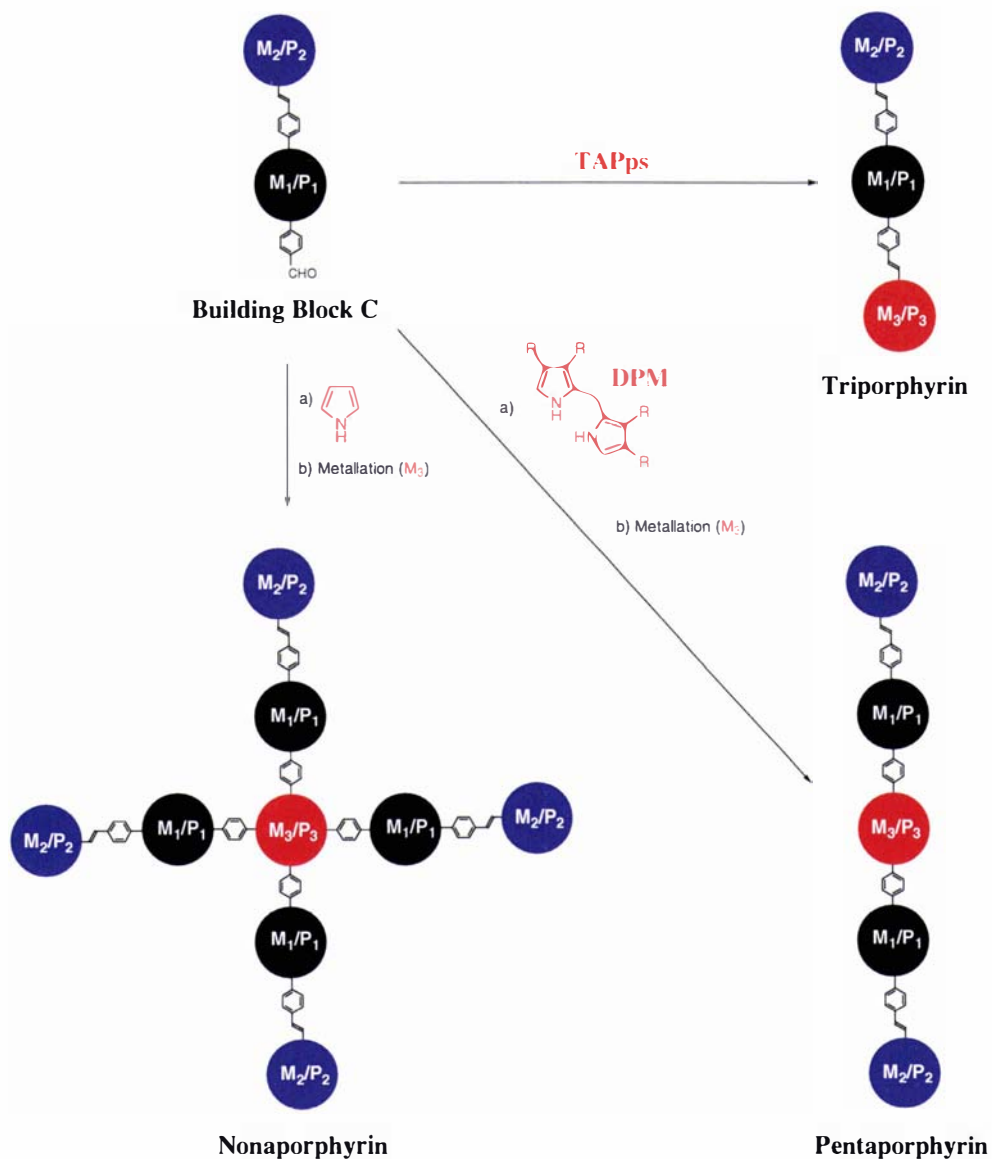
Figure 3-6. New proposed Building Block C approach to porphyrin arrays.

3.2 Synthesis and Characterisation of Mixed-Metal and Mixed-Porphyrin Arrays

3.2.1 Bisformylporphyrin (BFP)

A variety of bisformylporphyrins (BFPs) exist in the literature[129-133], the examples most closely related to **76** are the tetraethyltetramethyl derivatives **81** of Maruyama et al. (Figure 3-7).[109] These were synthesised from the respective acetals.
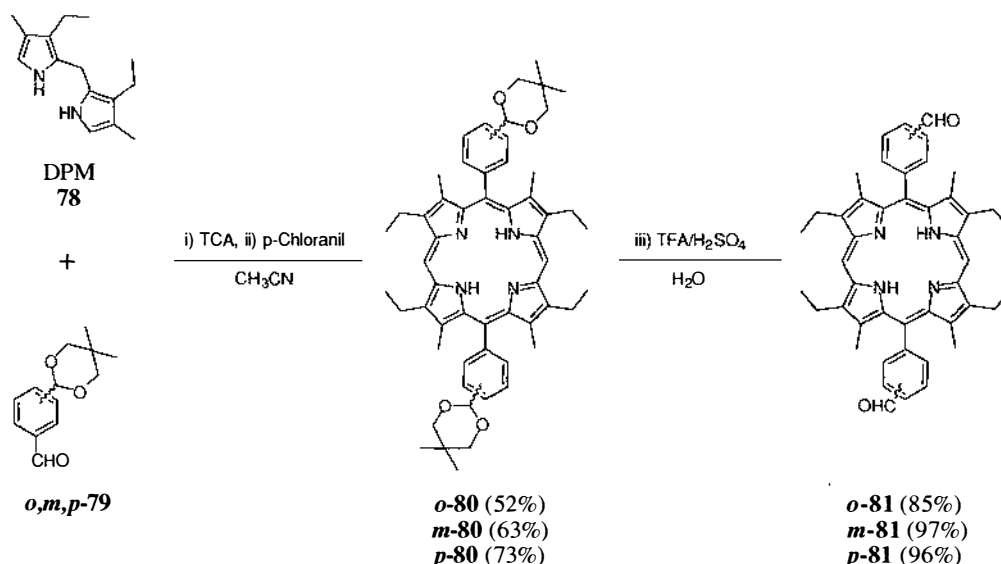
Figure 3-7. Bisformylporphyrins by Maruyama et al.[109]

As DPM **58** and mono-protected dialdehyde **59** were already available in our laboratories, the purposeful synthesis of the bisacetal **62** was undertaken. The condensation between **58** and **59** was carried out using TFA catalyst in DCM under Lindsey conditions[114], affording the desired product **62** in good yield (Figure 3-8). It was found that excess unreacted *p*-chloranil could be conveniently removed by the addition of excess Et₃N. This complexed with *p*-chloranil to form a MeOH soluble product, allowing the bisacetal **62** to be precipitated from DCM with MeOH.
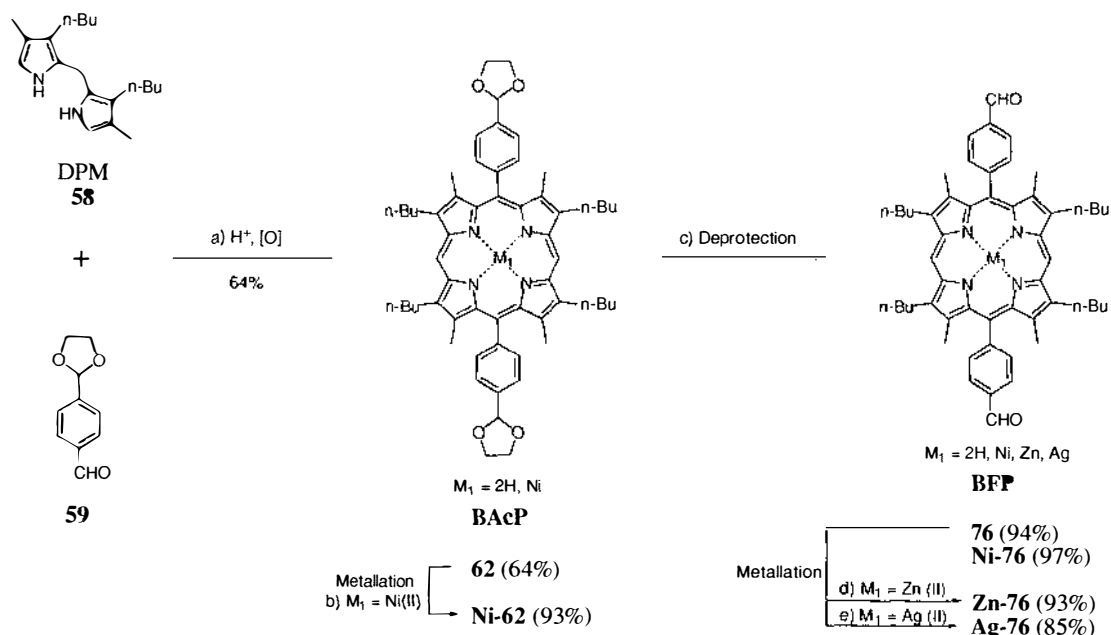
Figure 3-8. Synthesis of bisacetal **M-62** and bisformyl **M-76** porphyrins.

Porphyrin bisacetal **62** can be either deprotected, or metallated prior to deprotection. The metallation of **62** with Ni(II) was near quantitative, using the acetate method.[60] The insertion of Ni(II) into the porphyrin was monitored by TLC, with the disappearance of **62** and subsequent appearance of the new less polar band of **Ni-62**.

The conversion of bisacetals **62** and **Ni-62** to aldehydes was achieved via *trans*-acetalation with *p*-toluenesulfonic acid in refluxing acetone. The deprotection of bisacetal **Ni-62** proceeded more rapidly than that of free-base **62**. The formation of BFPs **76** and **Ni-76** is almost quantitative under these conditions. The zinc derivative **Zn-76** was also easily obtained from the metallation of **76** with Zn(II) using the acetate method.[60] In an attempt to oxidise **76** to its acid analogue **73**, an efficient method was discovered for the insertion of Ag(II) into porphyrins using argentic oxide. The treatment of **76** with argentic oxide gave **Ag-76** in 85% yield.

An x-ray quality crystal of **76** was grown from a diffusion matrix of DCM and MeOH. The structure was solved by Professor A. K. Burrell and refined by B. Therrien and is shown in Figure 3-9. This structure is typical of this type of bisarylporphyrin, with a

planar porphyrin core and near-orthogonal ($\approx 89.23°$) aromatic substituents. The crystal structure refinement data is tabulated in the appendix (Table 7-3, pg 331) and full crystallographic data has been submitted to *Acta Cryst. E.*[134]
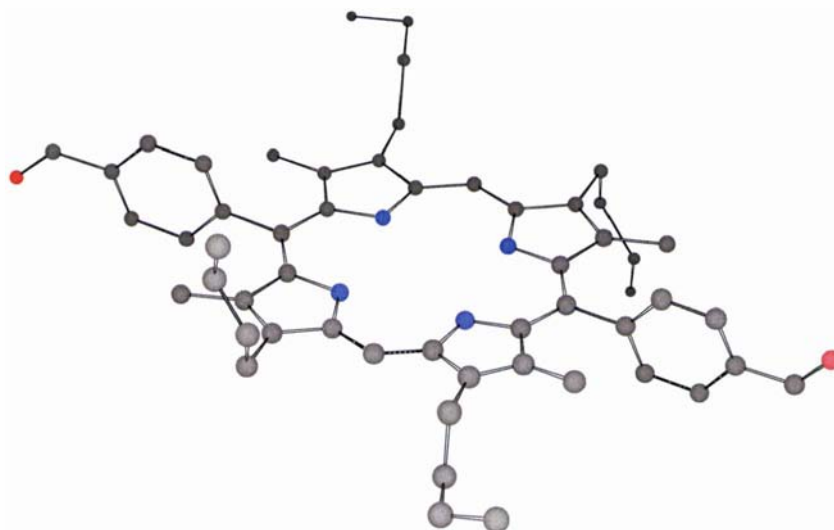
Figure 3-9. Chem3D X-ray structure representation of **76** (hydrogens omitted for clarity).

3.2.2   Diporphyrin Building Block C and Triporphyrins

The Wittig reactions of BFP **76** with TXPps **5** to form Building Block C **M₂/M₁-77** were examined next. Figure 3-10 tabulates the overall results and methods of formation.

In general, the chemistry first involved the synthesis of TXPps **5** (see Figure 2-6, p39). TXPps **5** was then reacted with the BFP **76** under basic conditions using different methods (A, B, C). Generally, two new distinct coloured bands were observed by TLC, these belonging to the mono-Wittig diporphyrin Building Block C and the di-Wittig triporphyrin product. Separation of the products was achieved by column chromatography, the triporphyrin having a lower polarity than the building block. Unreacted BFP **M-76** was also recovered, having a higher polarity than the Building Block C material.
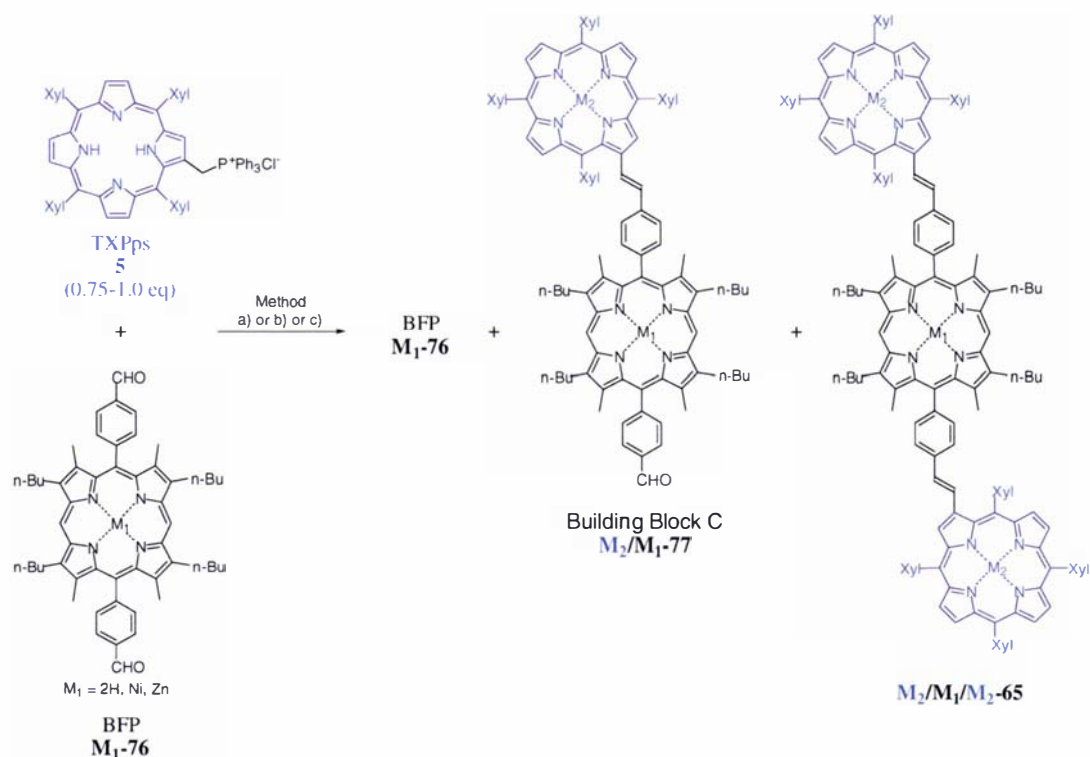
a) i) M_1 = 2H, 5 (1.0 eq), DBU (5.5 eq), CH$_2$Cl$_2$, RT (10 min), N$_2$. ii) Zn(OAc)$_2$·2H$_2$O (> 2.0 eq), CH$_2$Cl$_2$/MeOH, RT (15 min). b) i) M_1 = Ni, 5 (0.76 eq), DBU (5.7 eq), toluene, reflux (50 min), N$_2$. ii) Ni(OAc)$_2$·4H$_2$O (10 eq), CHCl$_3$/MeOH, reflux (13.5 h) iii) I$_2$, CH$_2$Cl$_2$, RT (4.5 h). iv) sat. Na$_2$S$_2$O$_3$ (excess). c) i) M_1 = Zn, 5 (1.0 eq), DBU (6.0 eq), toluene, reflux (1 h), N$_2$.

	Isolated Products (%)		
Method	**BFP**	**Building Block C**	**Triporphyrin**
A	**76** (32)	**Zn/Zn-77** (28)	**Zn/Zn/Zn-65** (7)
B	**Ni-76** (39)	**Ni/Ni-77** (35)	**Ni/Ni/Ni-65** (5)
C	**Zn-76** (40)	**2H/Zn-77** (31)	**2H/Zn/2H-65** (13)

Figure 3-10. Product mixture from synthesis of Building Block C M_2/M_1-77.

Method A

For the Wittig reaction of **76** with TXPps **5** the products proved difficult to separate. Unreacted **76** was isolated through recrystallisation, however metallation of the remaining mixture with Zn(II) was required to aid separation of Building Block C **Zn/Zn-77** and triporphyrin **Zn/Zn/Zn-65** by column chromatography. Both Building Block C and the triporphyrin were found to be pure all *trans* products by ¹H NMR. The absence of the *cis* isomer here presumably reflects some greater steric requirement or electronic effect of the free-base porphyrins during the Wittig reaction. Porphyrin phosphonium salt reactions carried out at room temperature typically give some *cis* product.

Method B

The Wittig reaction of **Ni-76** with TXPps **5** was carried out in refluxing toluene, and the crude porphyrin reaction product was metallated with nickel acetate. The separation of the unreacted BFP **Ni-76**, Building Block C and the triporphyrin was achieved through column chromatography. ^{1}H NMR spectra showed the Building Block C and the triporphyrin products to contain *cis/trans* isomers. Thermal isomerisations in toluene were attempted, but without success. These products were subsequently isomerised using iodine to give pure *trans* Building Block C **Ni/Ni-77** and all *trans* triporphyrin **Ni/Ni/Ni-65** respectively.

Method C

The Wittig reaction of **Zn-76** with TXPps **5** was carried out in refluxing toluene, giving the *trans* Building Block C **2H/Zn-77** and all-*trans* triporphyrin **2H/Zn/2H-65**. These products were easily isolated by column chromatography, allowing access to a mixed metalloporphyrin system.

Characterisation of the diporphyrin Building Block Cs was by ^{1}H NMR and UV-vis spectroscopy, and FAB HRMS. The ^{1}H NMR spectra of the diporphyrin aldehydes were consistent with that of the previously characterised collinear ester **Zn$_2$-64** (see Figure 2-42, pg 71). The ^{1}H NMR spectra of the triporphyrin products were consistent with the analogous compounds made via the Building Block **A** methodology.[83] For **2H/Zn/2H–65** no clean spectrum consistent with only one compound was obtained. The ^{1}H NMR spectrum displayed an additional resonance at 2.85 ppm (**NH**) and extra resonances in the β-pyrrolic region (8.62-8.93 ppm). This is attributed to a small amount of contaminant that is suspected to be the **Zn/2H/2H–65** analogue. This would result from inter- or intra-molecular transmetallation of Zn(II) from the central TBMP moiety to one of the TXP moieties during purification procedures. The FAB MS was consistent with only one triporphyrin parent molecular ion species.

In the UV-vis spectra, most of the diporphyrins and triporphyrins showed well-separated double Soret bands as for the collinear diporphyrin ester **Zn$_2$-64** and acid **Zn$_2$-66** (see Figure 2-43, pg 73). Exceptions to this were the diporphyrin building block

Ni/Ni-77 and the triporphyrin **Ni/Ni/Ni-65**; these had converging adsorptions (see Figure 3-18 for **Ni/Ni-77**).

An x-ray quality crystal of Building Block C **Zn/Zn-77** was grown from a $CHCl_3/n$-butanol diffusion system and the structure determination carried out by Professor A. K. Burrell (Figure 3-11).
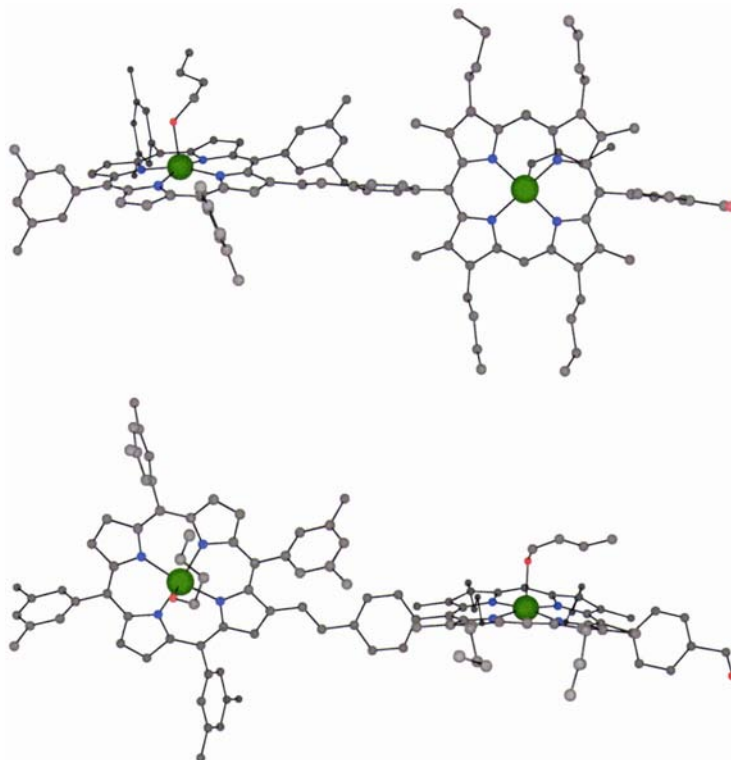
Figure 3-11. Chem3D X-ray structure representation of Building Block C **Zn/Zn-77** (hydrogens omitted for clarity).

The crystal structure refinement data is tabulated in the appendix (Table 7-4, pg 332) and the bond length and angle data will be deposited with the Cambridge Crystallographic Database. n-Butanol is coordinated to the Zn of the porphyrin moieties. The structure shows a degree of planarity (25.8°) through the TXP and styryl linker, but it does not extend through to the TBMP moiety (Figure 3-11). This supports the original finding of Officer et al. of potential conjugation between the β-styryl group and the porphyrin core of **Cu-13** (Figure 3-12).[78,135]
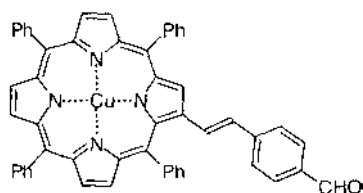
Figure 3-12. CuTPP-=-PhCHO **Cu-13**.

In contrast, a crystal of a **Ni/Zn/Ni-65** triporphyrin grown earlier in these laboratories (synthesised via the Building Block A approach) showed planar porphyrin rings with little evidence of conjugation between the TXP and styryl linker (Figure 3-13).[83] The difference in these two structures can presumably be attributed to different crystal packing forces.
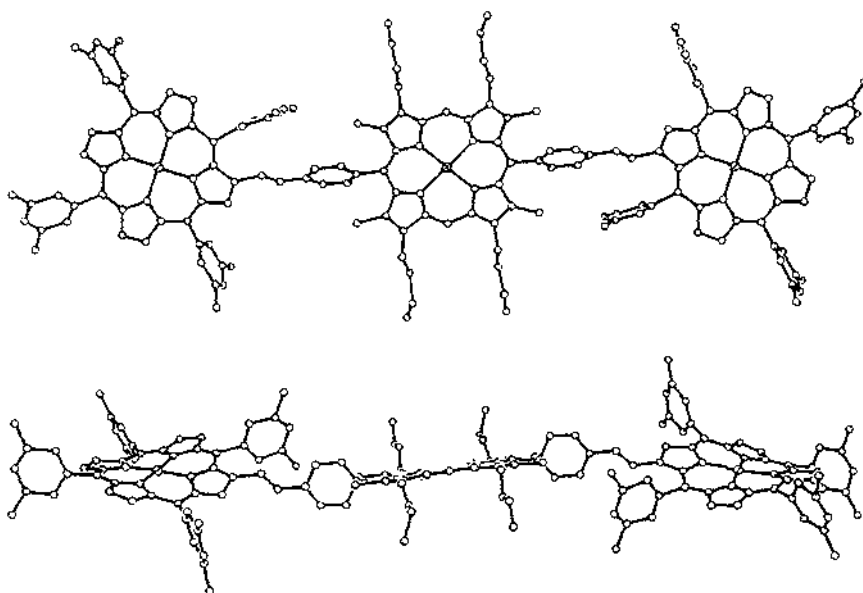
Figure 3-13. X-ray structure of **Ni/Zn/Ni-65** (hydrogens omitted for clarity).[83]

The availability of linear diporphyrin Building Block C **2H/Zn-77** system allowed access to a dimetallo mixed-porphyrin (M_2/M_1-P_2/P_1) building block. This was accomplished through the metallation of **2H/Zn-77** with Ni(II), giving the **Ni/Zn-77** mixed-metal/mixed-porphyrin Building Block C (Figure 3-14). The loss of the **NH** resonances at -2.547 ppm and small shifts in the TXP aromatic proton signals where observed by ^{1}H NMR upon metallation. In addition, the disappearance of some Q-bands in the UV-vis spectrum is seen.
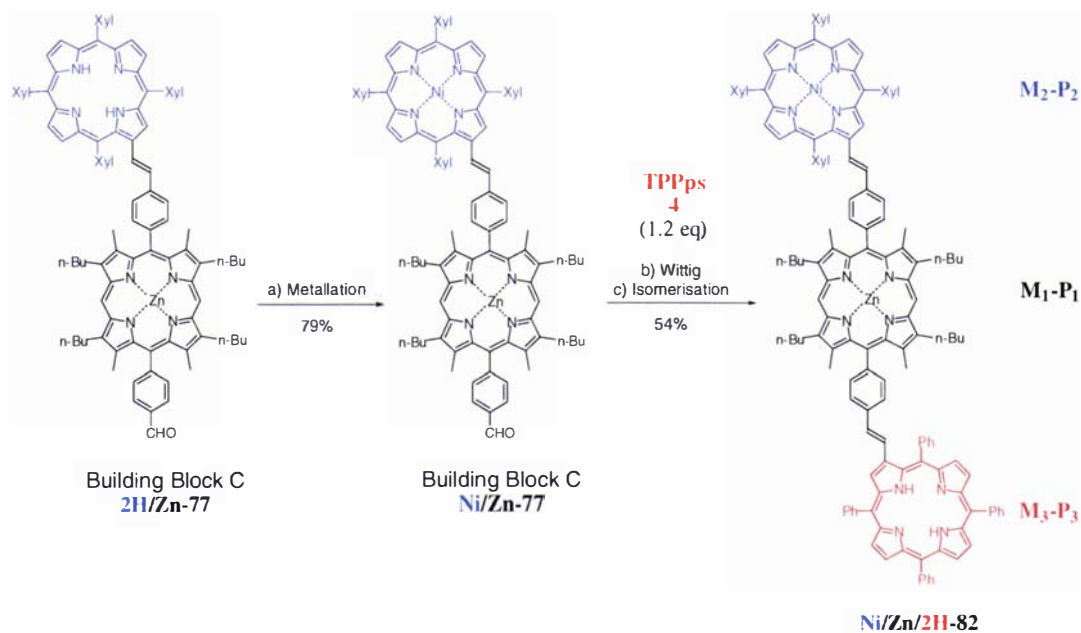
a) Ni(OAc)$_2$·4H$_2$O (10 eq). CHCl$_3$/MeOH. reflux (15 h). b) DBU (37 eq). toluene. reflux (1 h). N$_2$. c) i) Toluene. reflux (28 h). N$_2$.

Figure 3-14. Synthesis of M$_2$/M$_1$/M$_3$-P$_2$/P$_1$/P$_3$ mixed-metal/mixed-triporphyrins.

This dimetallo mixed-porphyrin building block **Ni/Zn-77** provided the opportunity to produce the first fully controlled synthesis of a mixed-metal/mixed-triporphyrin (M$_2$/M$_1$/M$_3$-P$_2$/P$_1$/P$_3$) system. To prove this, the Wittig reaction of **Ni/Zn-77** with TPPps **4** was carried out, yielding the mixed-metal NiTXP-ZnTBMP-TPP triporphyrin **Ni/Zn/2H-82** as a *cis/trans* mixture (54%). Thermal isomerisation of this mixture in refluxing toluene gave all-*trans* **Ni/Zn/2H-82**. Although metallation of the TPP porphyrin moiety (P$_3$) was not carried out, it should be straightforward. This represents unprecedented control in a porphyrin array synthesis. Characterisation was by the usual methods. The ^{1}H NMR spectrum was consistent with two different tetraaryl (NiTXP/TPP) species on the triporphyrin, now showing an **NH** (-2.53 ppm) signal for the introduced TPP moiety, and two separate H$_3$ β-pyrrolic signals (9.080 ppm, TXP), (9.185 ppm, TPP). With the aid of COSY spectra, the required two sets of coupled ethenyl protons were identified, and appropriate couplings were also observed between the phenyl protons on the TPP moiety. Assignments were also aided by comparison to the spectra of building block **Ni/Zn-77** and the known symmetrical triporphyrins **Ni/2H/Ni-65**, **Ni/Zn/Ni-65** and related free-base **TPP-TBMP-TPP**.[83] The FAB HRMS was consistent with the title compound. The UV-vis spectrum showed two Soret peaks (412$_{TBMP}$ and 428$_{TAP}$ nm), however there was a significant increase in intensity of the

428 nm absorption maxima going from building block **Ni/Zn-77** to triporphyrin **Ni/Zn/2H-82**. This suggests that the TPP absorption maxima overlays the TXP absorption maxima at ≈ 430 nm (see Figure 2-43, pg 73).

3.2.3   Pentaporphyrins

The next step in extending the building block approach was to attempt condensations of Building Block C with a dipyrrylmethane and pyrrole for the synthesis of pentaporphyrins and nonaporphyrins respectively. Firstly, the synthesis of a linear pentaporphyrin (Figure 3-15) was carried out using an acid catalysed condensation between Building Block C **Ni/Ni-77** and DPM **58**. After oxidation with p-chloranil, a new coloured band of higher polarity than the starting material was observed by TLC. The product was isolated by column chromatography to yield the pentaporphyrin **Ni/Ni/2H/Ni/Ni-83** in good yield. The centre porphyrin of this pentaporphyrin was metallated with Zn(II) to afford the pentaporphyrin **Ni/Ni/Zn/Ni/Ni-83** in near quantitative yield. The loss of **NH** signals was observed in the ^{1}H NMR. Analysis of the building block **Zn/Zn-77** crystal structure suggests that these pentaporphyrins if planar throughout the central TBMP moieties, will be about 7.3 nm in length (Figure 3-15).

Primary characterisation of the pentaporphyrins **M₅-83** was by ^{1}H NMR spectroscopy. This was supported by UV-vis spectroscopy, ES-MS and MALDI-TOF MS. The ^{1}H NMR spectrum of **Ni/Ni/2H/Ni/Ni-83** is relatively simple given the presence of 50 protons observed in the aromatic region (Figure 3-16), and reflects the high symmetry of this molecule. The spectrum is very similar to that of the diporphyrin ester **Zn₂-64** but shows an additional set of signals for the butyl protons. Larger up-field shifts are experience by those protons closer to the centre porphyrin due to the combined anisotropic ring current effects, these resulting from the close proximity of the centre TBMP cores.
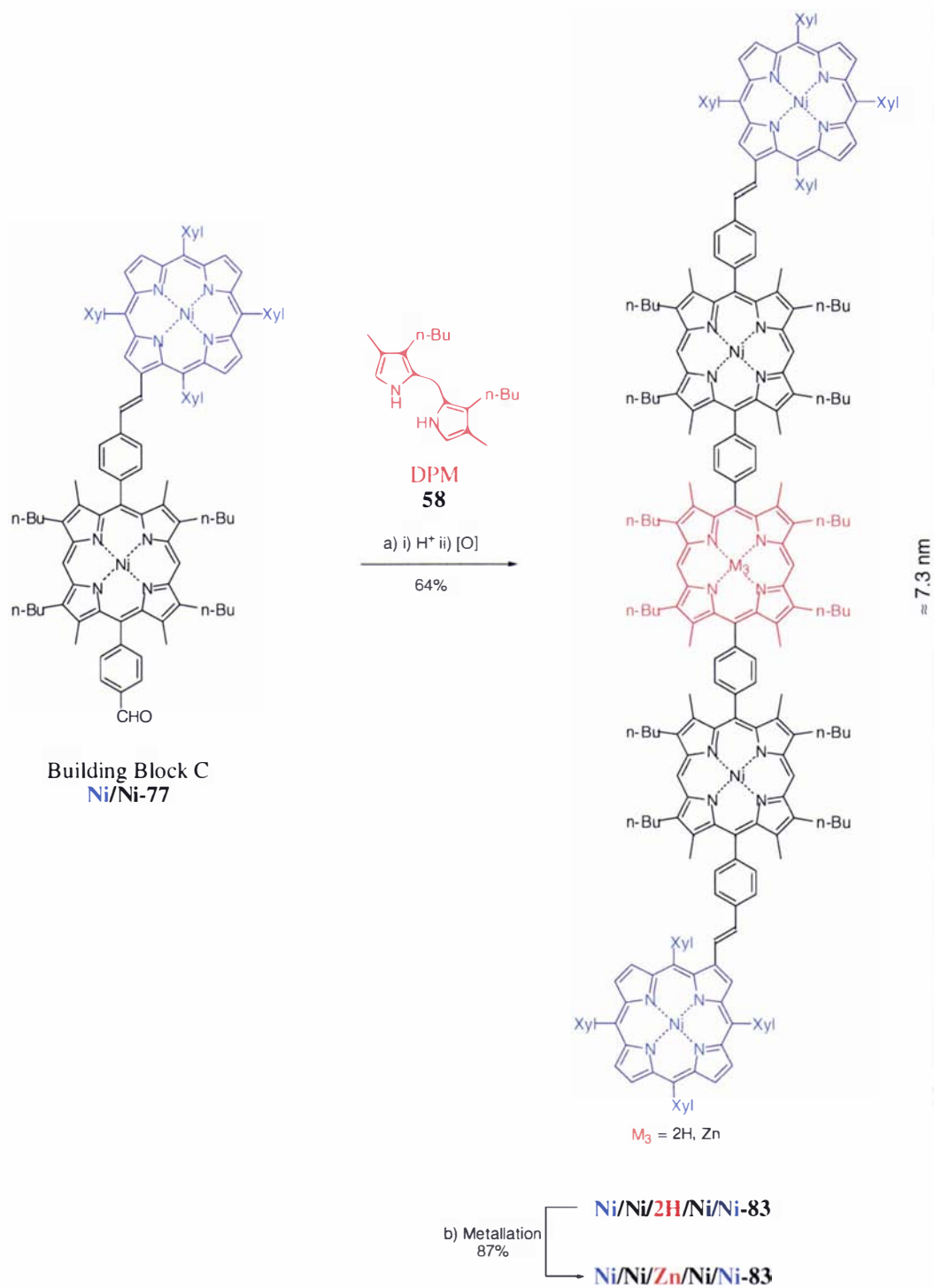
a) i) TFA (1.5 eq), CH$_2$Cl$_2$/MeOH (10^{-2} M), RT (1 h), N$_2$. ii) p-Chloranil (3.5 eq), RT (1.3 h).
b) Zn(OAc)$_2$·2H$_2$O (2.0 eq), CH$_2$Cl$_2$/MeOH, RT (15 min).

Figure 3-15. Synthesis of linear pentaporphyrins.
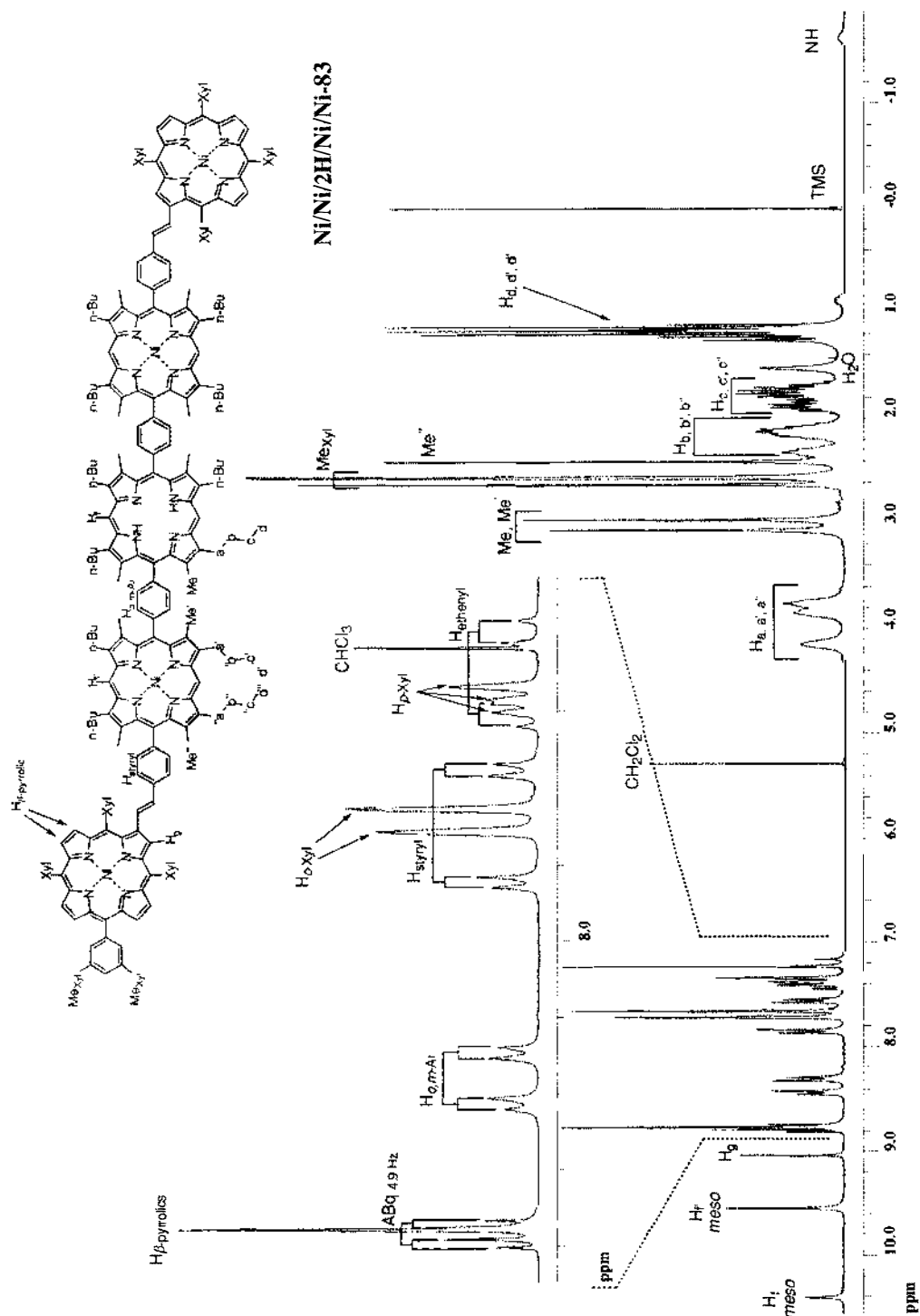
Figure 3-16. ^{1}H NMR of **Ni/Ni/2H/Ni/Ni-83** pentaporphyrin.

As the pentaporphyrins **M$_5$-83** were outside of the range of FAB MS equipment available, ES-MS was initially performed. ES-MS was carried out in CHCl$_3$:MeOH (3:2) on **Ni/Ni/Zn/Ni/Ni-83** allowing the identification of double (1932.7, [M + 2H]$^{2+}$),

triple (288.8, $[M + 3H]^{3+}$) and quadruple (966.9, $[M + 4H]^{4+}$) charged molecular ions in the spectra. With the addition of formic acid to the solvent system, demetallation of the centre ZnTBMP was noted with the appropriate double (1901.7, $[M - Zn + 4H]^{2+}$) and triply (1267.8, $[M - Zn + 5H]^{3+}$) charged molecular ions in the mass spectrum. MALDI-TOF MS results for pentaporphyrins M_5-83 were also obtained from Professor Liang Li at the University of Alberta. The samples were prepared in $CHCl_3$, and all-*trans*-retinoic acid was used as the matrix, giving average mass results close to the calculated values.

3.2.4   Nonaporphyrins

Extending this building block approach, the synthesis of a star shaped nonaporphyrin was carried out (Figure 3-17). The acid catalysed condensation between building block **Ni/Ni-77** and pyrrole was performed using $BF_3 \cdot OEt_2$ as the catalyst, under Lindsey conditions.[136] After oxidation with *p*-chloranil, TLC analysis indicated significant band smearing from what appeared to be multiple products. The crude product was then metallated with zinc acetate to give a major single band when chromatographed, of lower polarity than the starting material **Ni/Ni-77**. Separation was finally gained of nonaporphyrin **(Ni/Ni)₄-Zn-84** in a respectable 22% yield after a combination of flash silica filtrations and two solvent recrystallisations.

Characterisation of nonaporphyrin **(Ni/Ni)₄-Zn-84** was also by ^{1}H NMR and UV-vis spectroscopy, and MALDI-TOF MS. The ^{1}H NMR spectrum was well resolved and uncomplicated due to the high symmetry of the molecule, allowing confident assignment with the aid of COSY spectra. The UV-vis spectra of nonaporphyrin **(Ni/Ni)₄-Zn-84**, pentaporphyrin **Ni/Ni/2H/Ni/Ni-83**, diporphyrin **Ni/Ni-77** and monoporphyrin **Ni-23** (Figure 3-18), show how the combining of porphyrins into covalently linked arrays leads to broadening of the absorption bands, giving high molar absorptivities over a large part of the UV-vis spectrum. The relative areas of the Soret bands displayed on the spectra indicate an additive effect on molar absorptivity as the array size is increased.

Building Block C
Ni/Ni-77

a) i) H⁺ ii) [O]
b) Metallation
22%
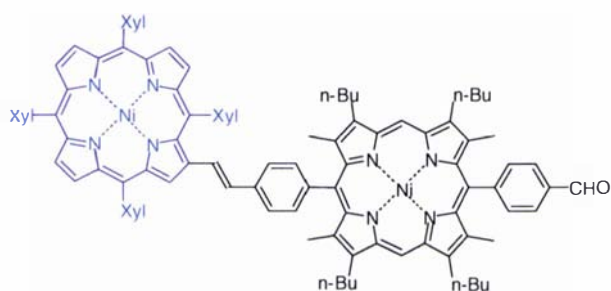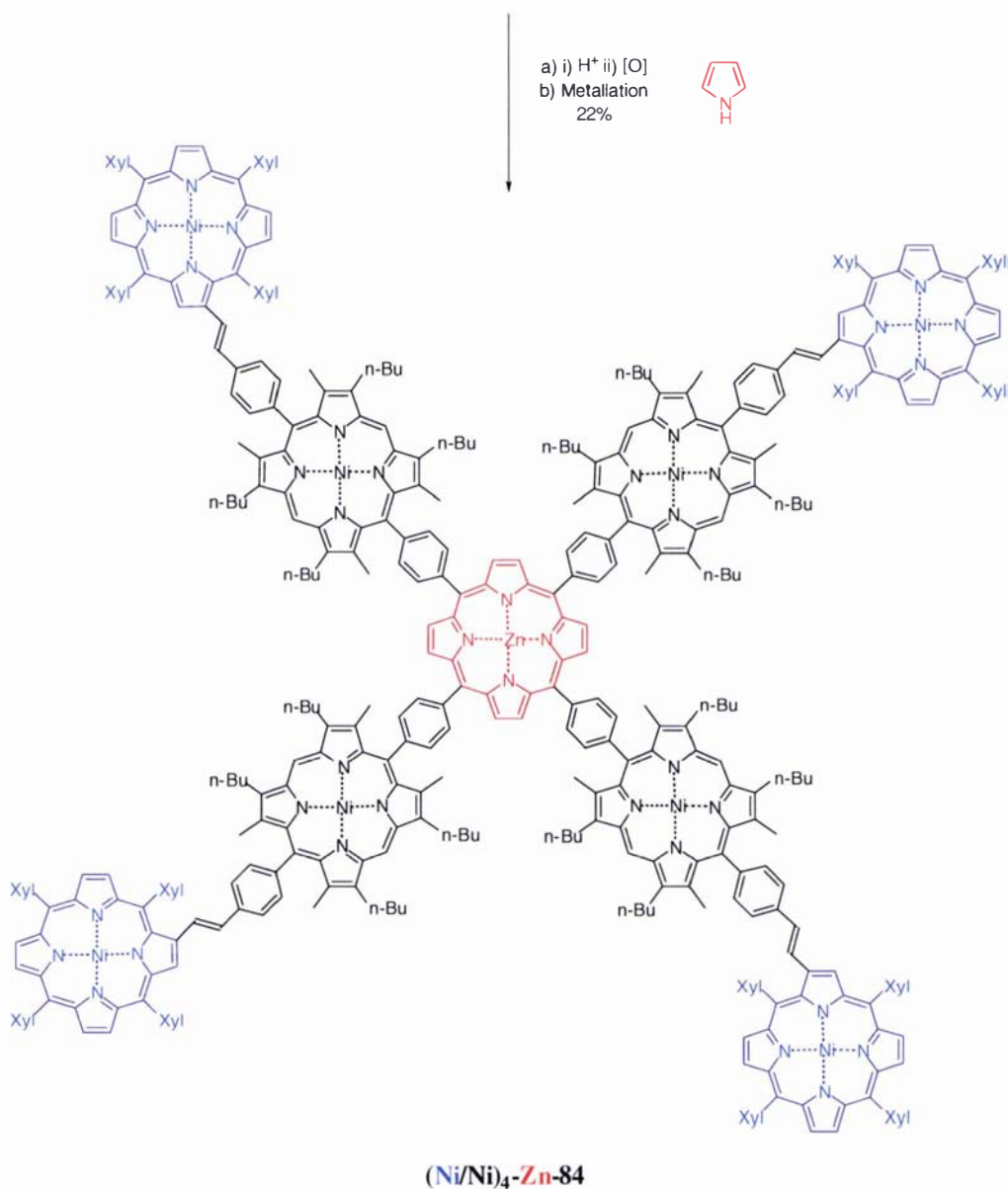
(Ni/Ni)₄-Zn-84

a) i) BF₃·OEt₂ (0.2 eq), CH₂Cl₂/EtOH (10⁻² M), RT (1.5 h), N₂. ii) *p*-Chloranil (1.5 eq), RT (1 h). iii) Et₃N (excess). b) Zn(OAc)₂·2H₂O (> 1 eq), CH₂Cl₂/MeOH, RT (15 min).

Figure 3-17. Synthesis of star nonaporphyrin **(Ni/Ni)₄-Zn-84**.
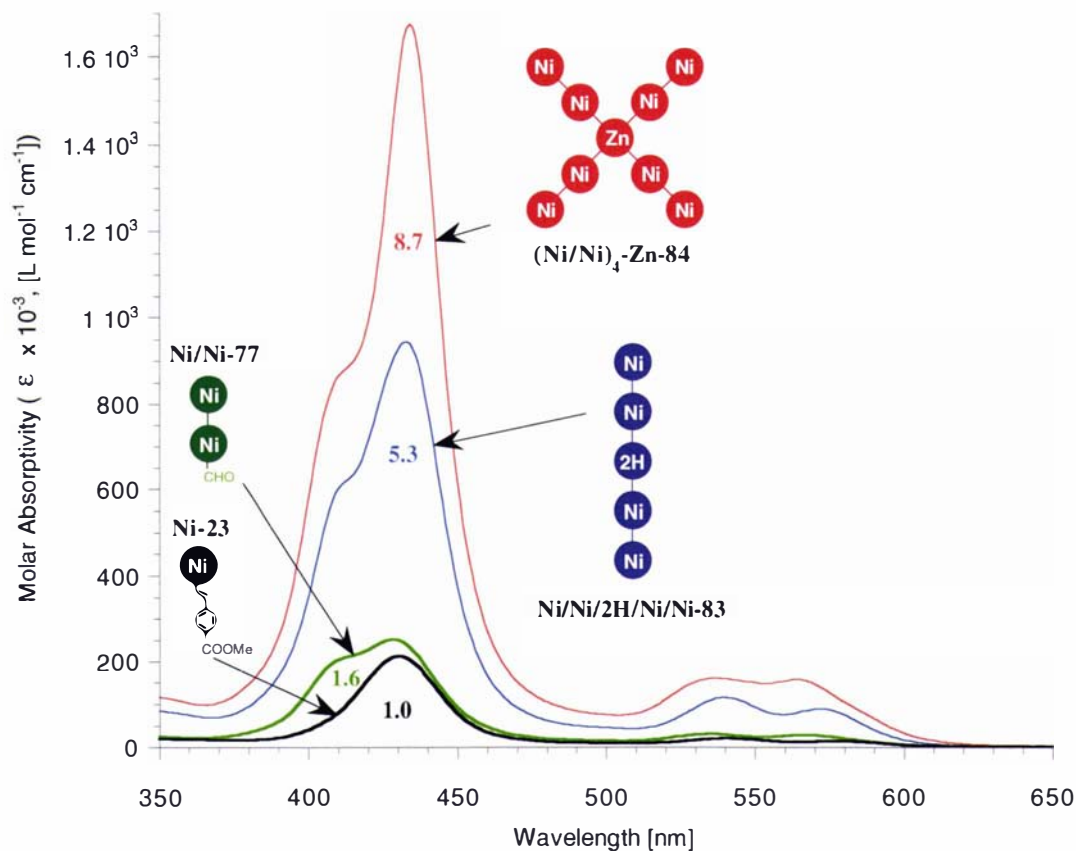
Figure 3-18. UV-vis spectra of **(Ni/Ni)₄-Zn-84**, **Ni/Ni/2H/Ni/Ni-83**, **Ni/Ni-77** and **Ni-23** porphyrins and relative Soret band areas.

3.3   Conclusion

Through the synthesis of a new linear diporphyrin Building Block C **M$_2$/M$_1$-77** from bisformylporphyrin **76**, an alternative pathway allowing the controlled synthesis of mixed-metal and mixed-porphyrin arrays has been achieved.   This provides an alternative strategy for the controlled placement of three different metals into three different porphyrins of a linear triporphyrin and pentaporphyrin and a larger star-shaped planar nonaporphyrin.

Since the development of this methodology, a variety of mixed-metal/mixed-porphyrin linear triporphyrins that were not readily achievable through the pre-existing Building Block A methodology are now been prepared by others in our research group.[137]

The exploitation of the stepwise controlled synthesis of the triporphyrin systems is described in Chapter 4. It is shown that mixed-porphyrin systems are easily synthesised from a unique "sticky" porphyrin phosphonium salt.

Chapter 4

Synthesis of "Sticky" Porphyrin Arrays

4.1   Introduction

The synthesis of "dipole" and "collinear" diporphyrin acids **53** and **66** was one approach to porphyrin array systems for attachment to surfaces, this methodology being based on arrays attached through a single acid linker system (Figure 4-1, **I**). Alternatively, arrays can be constructed where each chromophore has a number of attaching groups, known here as the "sticky" porphyrin (SP) approach (Figure 4-1, **II**). In this alternative approach, the acid functionality is part of the porphyrin itself. Large porphyrin arrays with numerous carboxylic acid groups for binding to surfaces could then be rapidly constructed using the now established building block **A** and **C** approaches discussed and developed in Chapter 3.[79,82,126]
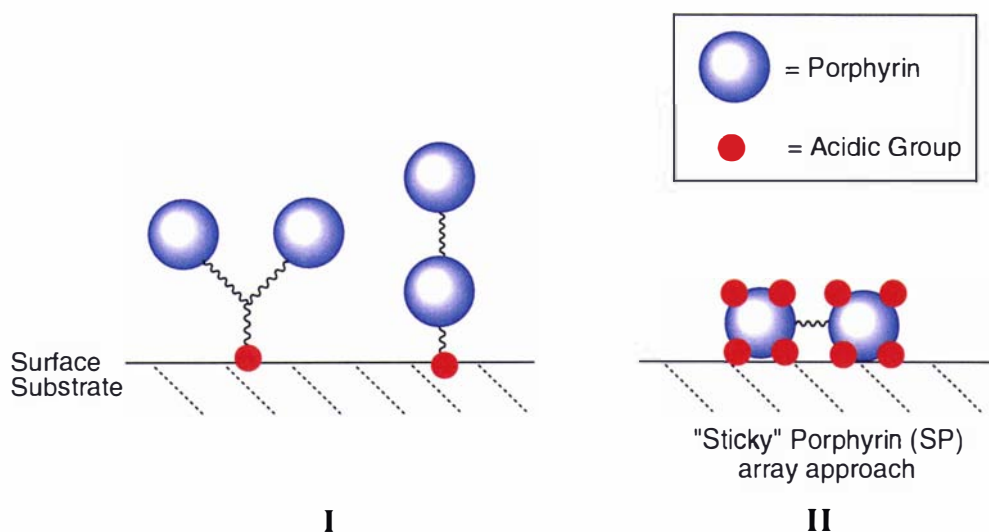
Figure 4-1. Standard **I** and "sticky" porphyrin **II** array approaches.

This SP approach required the development of a SP phosphonium salt, where the porphyrin periphery is functionalised with a number of protected carboxylic acid groups. From this starting material, large SP arrays could then be made via Wittig chemistry with appropriate aldehydes. By having the carboxylic acid groups in the form of esters, the base hydrolysis of the finished arrays would afford the desired acid derivatives. The simplest approach to this was to develop the arrays from a *meso*-tetraarylesterporphyrin and this is described in the next section.

4.2   Synthesis and Characterisation

4.2.1   Attempted Formylation of TEP

The starting point was the development of phosphonium salt **86** using the established TAPps synthesis (Figure 4-2, also see pg 29).[79,138] Due to the number of synthetic steps involved in the synthesis of a TAPps and the difficulty of handling multiacid porphyrins, the methyl tetraester (TEP) porphyrin **85** was the logical starting material. TEP **85** was readily synthesised according to Lindsey et al.[120]
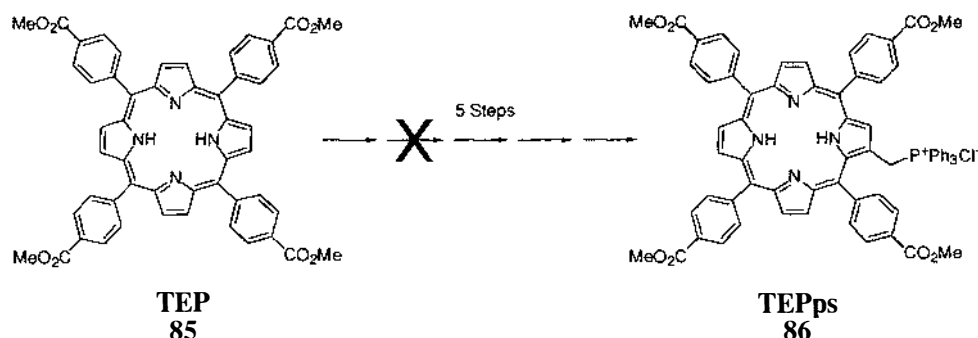
Figure 4-2. Proposed TEPps **86** synthesis.

Quantitative metallation of **85** with Cu(II) by the acetate method[60] afforded **Cu-85**. Unfortunately, attempted formylation of **Cu-85** under standard conditions did not give β-formylporphyrin **87** (Figure 4-3), demetallated starting TEP **85** material being recovered. Employing harsher Vilsmeier conditions (higher temperature) was not successful; no organic soluble porphyrinic compounds were recovered. Deactivation of the β-pyrrolic positions towards electrophilic aromatic substitution was considered likely due to the electron-withdrawing group (EWG) effect associated with the *para*-phenyl methyl ester groups. A simplistic view using electron pushing shows how electron density could be lowered on the porphyrin periphery (Figure 4-3).

CuTEP
Cu-85

Vilsmeier
formylation

X

87
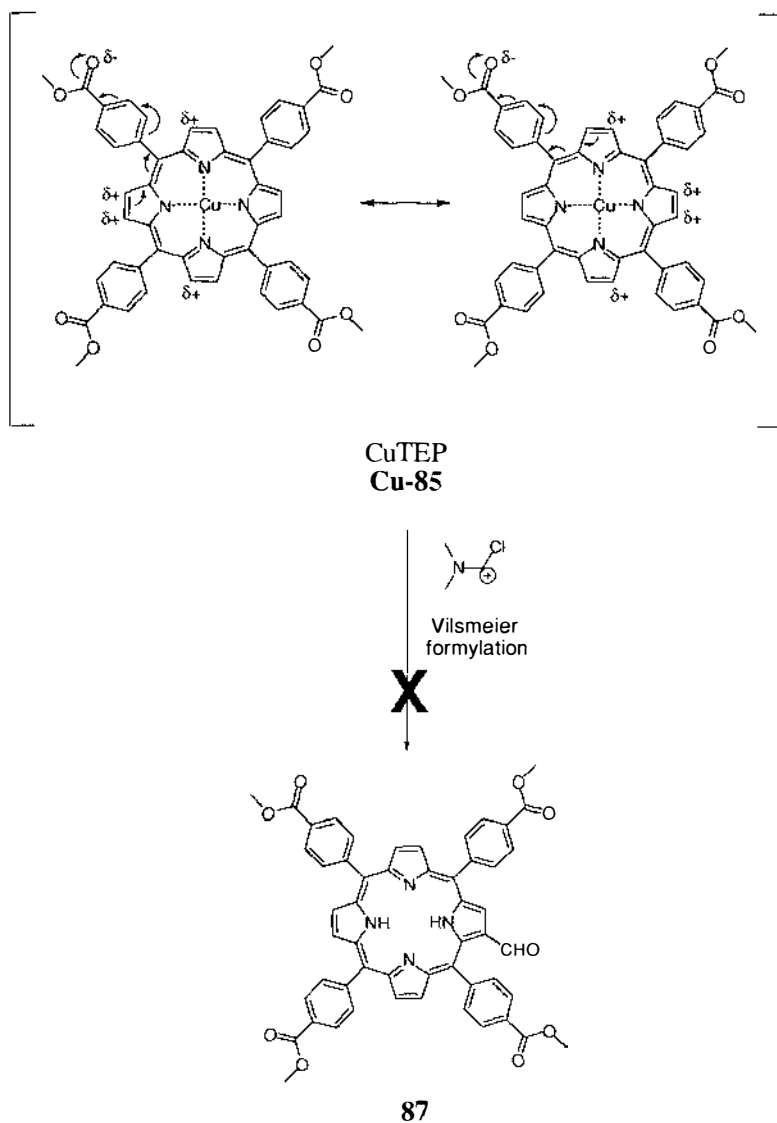
Figure 4-3. Unsuccessful Vilsmeier formylation of Cu-TEP **Cu-85**.

To counteract the deactivation a number of possibilities were considered.

1. Introducing electron-donating groups (EDGs) on the porphyrin periphery to counteract the EWGs.
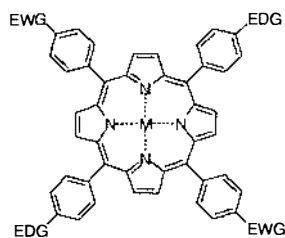
2. Isolating the ester EWG effect by either using the difference in *o,m,p* electronic effects or, spacing the ester group out from the phenyl group with an alkyl spacer.
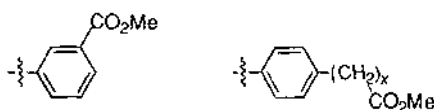
4.2.2 A *Trans*- A₂B₂ Bis(*p*-ester)-Bis(methoxyphenyl) *Meso*- Porphyrin Phosphonium salt!

Counteracting the EWG effect of the carboxyphenyl groups by introducing *p*-methoxyphenyl EDGs onto the *meso*-positions of the porphyrin was attempted (Figure 4-4).

Cu-88

Vilsmeier formylation

89
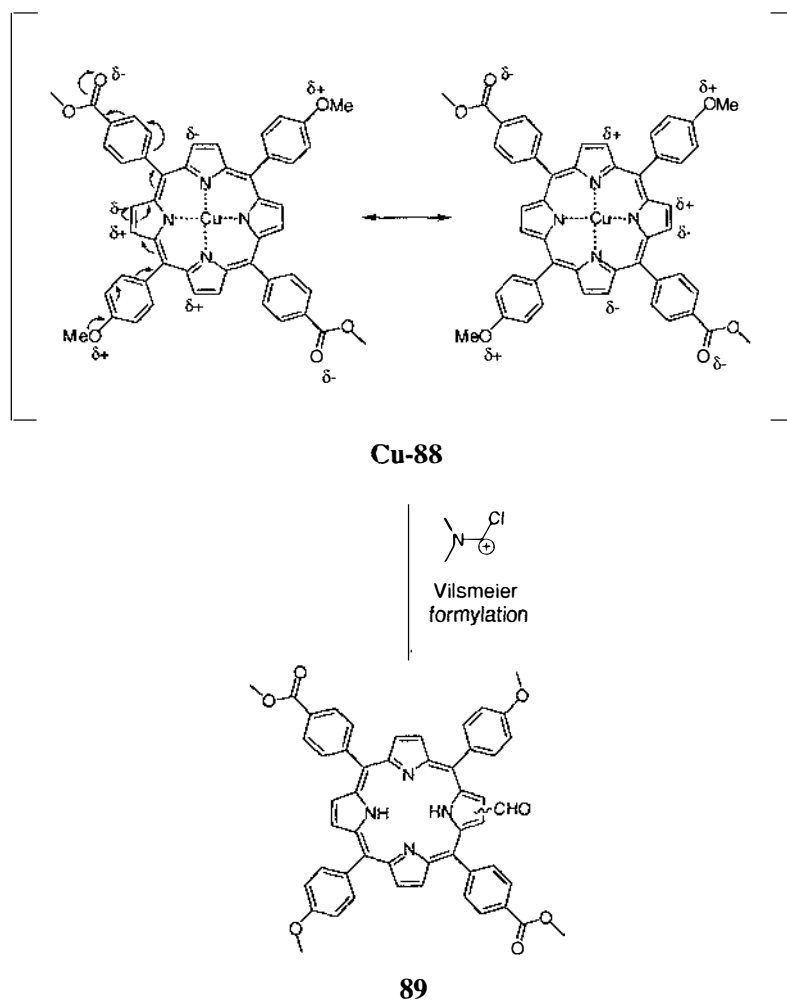
Figure 4-4. EDG reactivation of porphyrin β-pyrrolics positions.

The synthesis of the *trans*-A$_2$B$_2$-porphyrin **88** (Figure 4-5) was required to achieve this. The first step required the preparation of the appropriate 5-(4-methoxyphenyl)dipyrrylmethane **91**.
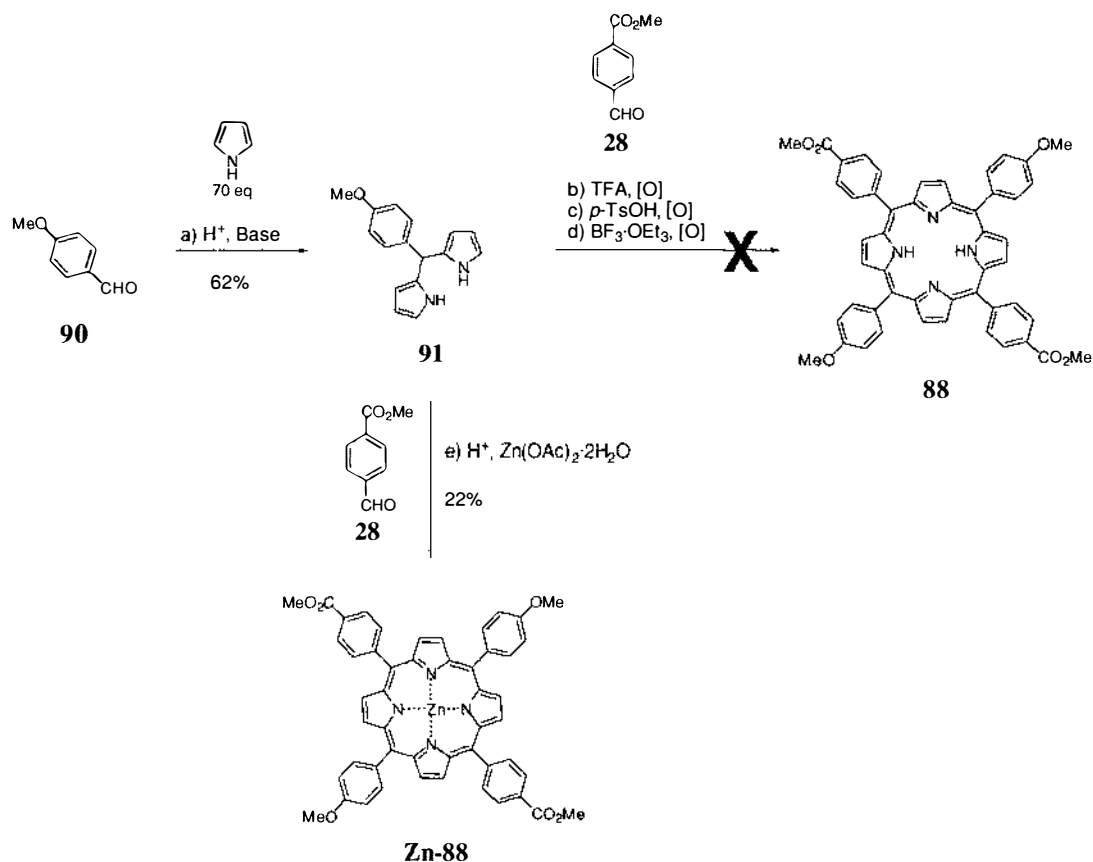
a) i) TFA (0.1 eq), RT (15 min), Ar. ii) Et$_3$N (0.11 eq). b) i) TFA (3 eq), CH$_2$Cl$_2$/MeOH (1:1, 10^{-2} M), RT (30 min), Ar. ii) *p*-Chloranil (0.9 eq), CH$_2$Cl$_2$, RT (3 h). c) i) *p*-TsOH (0.25 eq), MeOH (0.08 M), RT (2.5 d), Ar. ii) *p*-Chloranil (0.9 eq), CH$_2$Cl$_2$, RT (3.5 h). d) i) BF$_3$·OEt$_3$, (0.33 eq), CHCl$_3$ (10^{-2} M), RT (1 h), Ar. ii) *p*-Chloranil (0.8 eq), RT (3 h). e) i) Zn(OAc)$_2$·2H$_2$O (eq), CH$_2$Cl$_2$/propanoic acid (1:2.5), 0°C (2 h), RT (17.5 h), reflux (1 h), air. ii) O$_2$, reflux (1 h).

Figure 4-5. Synthesis of *trans*-A$_2$B$_2$-porphyrin **88**.

This compound was prepared in 62% yield using a procedure based on that of Lindsey et al,[139] This procedure was slightly modified by using Et$_3$N instead of aq. NaOH to neutralise the reaction. *p*-Anisaldehyde **90** was condensed with excess pyrrole in TFA, and subsequently neutralised with Et$_3$N. Removal of excess pyrrole by vacuum distillation and purification via column chromatography on silica gel gave **91** in 62% yield. When this DPM **91** was first synthesised it was fully characterised by ^{1}H and ^{13}C NMR spectroscopy and HRMS spectrometry, giving typical DPM spectra. Subsequently the compound was reported by Lindsey et al. and the data was fully consistent.[140]

The synthesis of *trans*-A$_2$B$_2$-porphyrin **Zn-88** was originally attempted with a variety of acid catalysts under standard porphyrin condensation conditions with little success. TLC analysis of the reaction mixtures after oxidation with *p*-chloranil, showed too many porphyrins formed; these most likely being statistical isomers (A$_4$, B$_4$, A$_3$B, AB$_3$, *cis*-A$_2$B$_2$ and *trans*-A$_2$B$_2$) of the aryl moieties at the meso positions of the porphyrin (Figure 4-6). This undoubtedly arose from acid-catalysed scrambling of the aryl groups at the unoxidised porphyrinogen intermediate stage, as has been observed by Lindsey et al.[120] and Smith et al.[141]
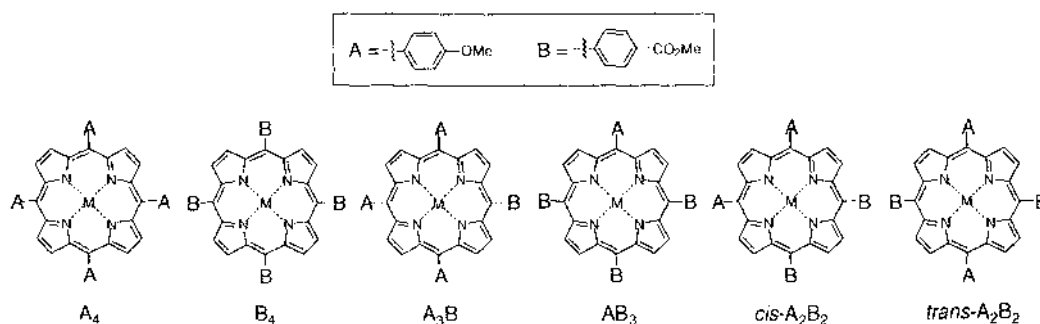
Figure 4-6. Porphyrin isomers from acid scrambling.

To avoid this scrambling, a procedure by Setsune et al.[142] for the synthesis of mixed *meso*-aryl porphyrins using a modified MacDonald [2+2]-type condensation was carried out. The condensation of DPM **91** with methyl 4-formylbenzoate **28** under these conditions gave the *trans*-A$_2$B$_2$-porphyrin **Zn-88** in a respectable 22% yield. This procedure was developed by Setsune et al. to limit the effect of aryl scrambling that occurs during the acid catalysed condensation of aryl-dipyrrylmethanes with an aldehyde. The effectiveness of this approach is probably due to a metal templating effect by the zinc acetate present during the condensation reaction. Characterisation of **Zn-88** was by ^{1}H NMR, UV-vis spectroscopy and FAB HRMS spectrometry. The 400 MHz ^{1}H NMR spectrum displayed signals typical of a symmetrical TAP porphyrin but only one singlet for both the methyl ester and methoxy protons (4.080 ppm) was observed. This is presumably due to the strong anisotropic effect of the porphyrin core.

Transmetallation[60,143] of the Zn(II) porphyrin **Zn-88** in acidified acetone/MeOH with Cu(OAc)$_2$·H$_2$O afforded the **Cu-88** in 90% yield (Figure 4-8). An x-ray quality crystal of **Cu-88** was grown by CHCl$_3$/MeOH diffusion for characterisation (Figure 4-7) and

the structure determined by A. K. Burrell and B. Therrien. The structure is typical of TAPs with near-orthogonal (87° PhCHO and 83° PhCO$_2$Me) aryl substituents to the planar porphyrin core. The crystal structure refinement data is tabulated in the appendix (Table 7-5, pg 332) and full crystallographic data has been submitted to *Acta Cryst. E.*[134]
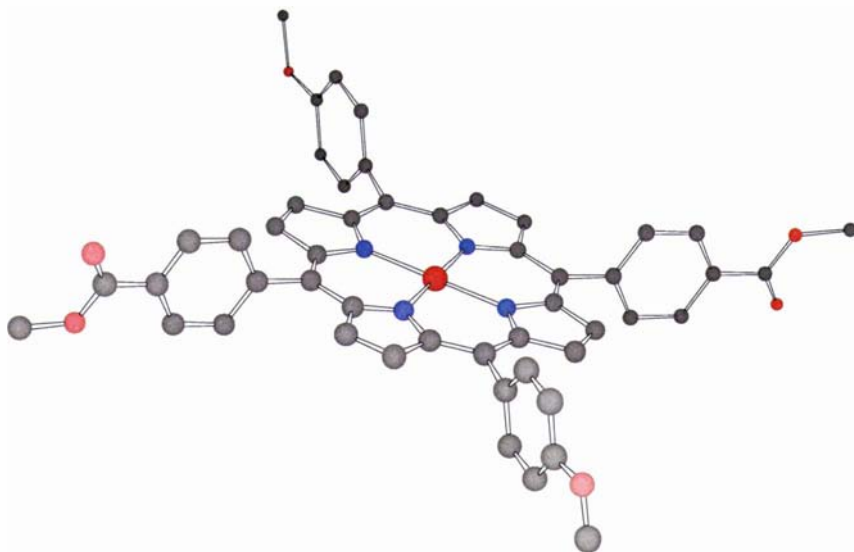
Figure 4-7. Chem3D X-ray structure representation of **Cu-88** (hydrogens omitted for clarity).

Activation of the porphyrin β-pyrrolic positions of **Cu-88** by the introduction of the *meso*-methoxyphenyl groups appeared to be effective with only one major product (by TLC) produced in the subsequent Vilsmeier formylation reaction (Figure 4-8). The ^{1}H NMR spectrum in CDCl$_3$ showed one major aldehyde resonance (9.314 ppm), although in C$_6$D$_6$ two major aldehyde resonances (9.623 and 9.537 ppm) were observed, consistent with the two possible β-formyl isomers of **89a** and **89b**. While two aldehyde resonances could also be due to diformylation the FAB LRMS results gave only one major parent ion consistent with monoformylation. Absence of separate **NH** resonances in the C$_6$D$_6$ ^{1}H NMR spectrum indicated that tautomerism is not the cause of the multiple aldehyde resonances.
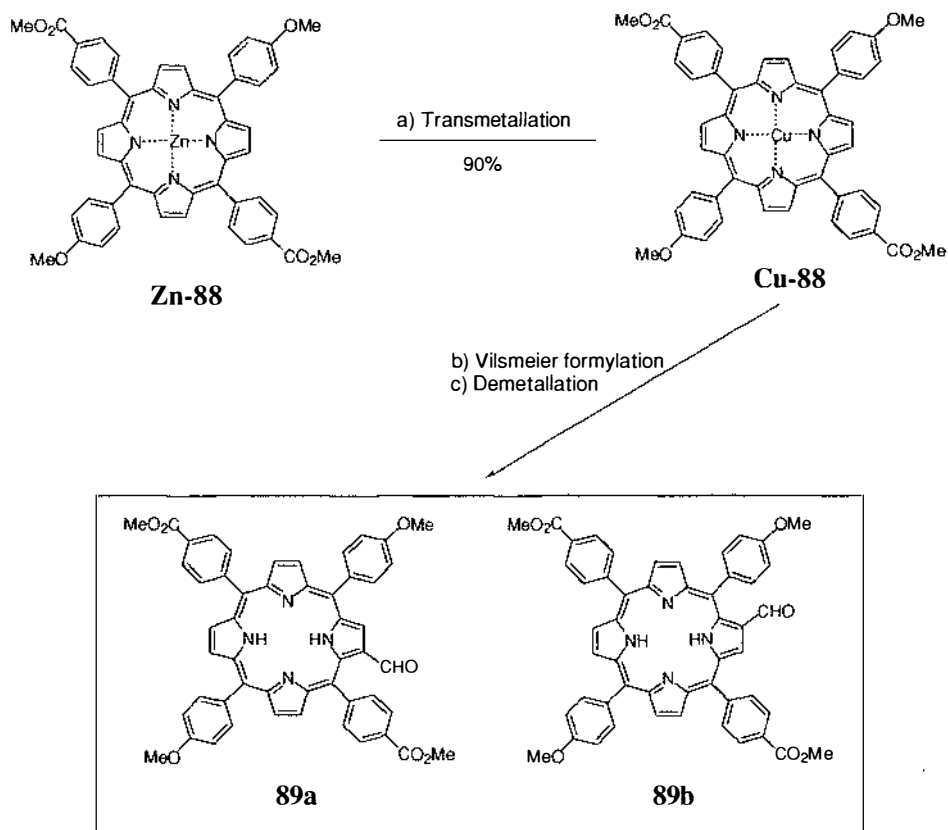
Figure 4-8. Transmetallation and formylation of **M-88**.

Although synthesis of a phosphonium salt could be achieved from this mixture of aldehydes, there would always exist the problem of characterising subsequent arrays by ^{1}H NMR spectroscopy due to the isomeric variations introduced from such a phosphonium salt. Therefore, since it was not possible to separate the aldehyde isomers **89a** and **89b**, the synthesis of the phosphonium salt was not pursued any further.

With the *trans*-bisester **Zn-88** in hand, it was of interest to see what effect the *trans*-EDG would have in the photosensitisation of a surface, therefore liberation of the acid functionalities of the porphyrin was carried out. Base hydrolysis of **Zn-88** was carried out quantitatively affording the *trans*-bisacid **Zn-92** (Figure 4-9). The 400 MHz ^{1}H NMR spectrum in DMSO of **Zn-92** was as expected with a broad singlet (13.3 ppm) observed for the CO$_2$**H** protons.

a) KOH (30 eq), MeOH:H2O:THF (10:1:10), reflux (5 h). ii) H3PO4 (31 eq).
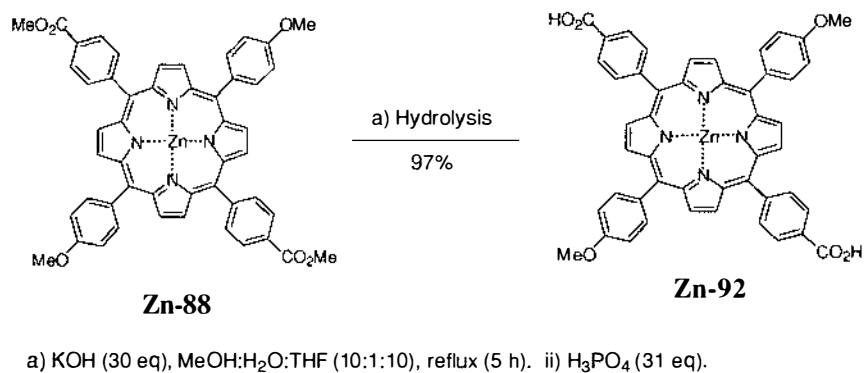
Figure 4-9. Synthesis of *trans*-bisacid **Zn-92**.

4.2.3 Synthesis of a T3EP "Sticky" Porphyrin Phosphonium Salt (T3EPps)

The second approach to SP phosphonium salt synthesis proposed was to diminish the electronic EWG effect by using a *meta*-carboxyphenyl ester derivative T3EP **93** then subsequently transform this into the desired phosphonium salt T3EPps **94** (Figure 4-10) using the established procedures (see Figure 1-34, pg 29).
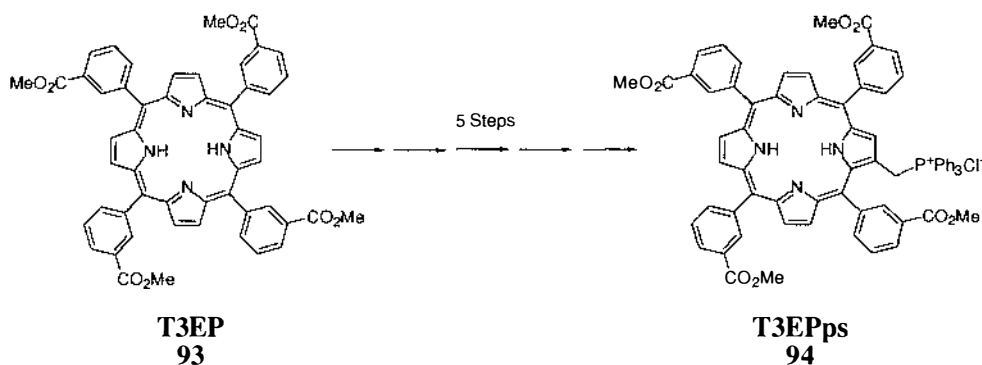
Figure 4-10. Proposed synthesis of T3EPps **94**.

The first step in the synthesis of the SP phosphonium salt (T3EPps) **94** was the synthesis of the precursor porphyrin T3EP **93**. The synthesis of this compound has been reported using two methods by Datta-Gupta et al. (Figure 4-11, Method A and B).[144]

A. The condensation of pyrrole with 3-formylbenzoic acid in refluxing propanoic acid followed by esterification of the porphyrin T3CP **95** with refluxing MeOH and catalytic conc. H_2SO_4.

B. The condensation of pyrrole with methyl 3-formylbenzoate in refluxing propanoic acid.

No yields are reported by Datta-Gupta et al., however yields for this type of reaction conditions rarely exceed 15-20%.
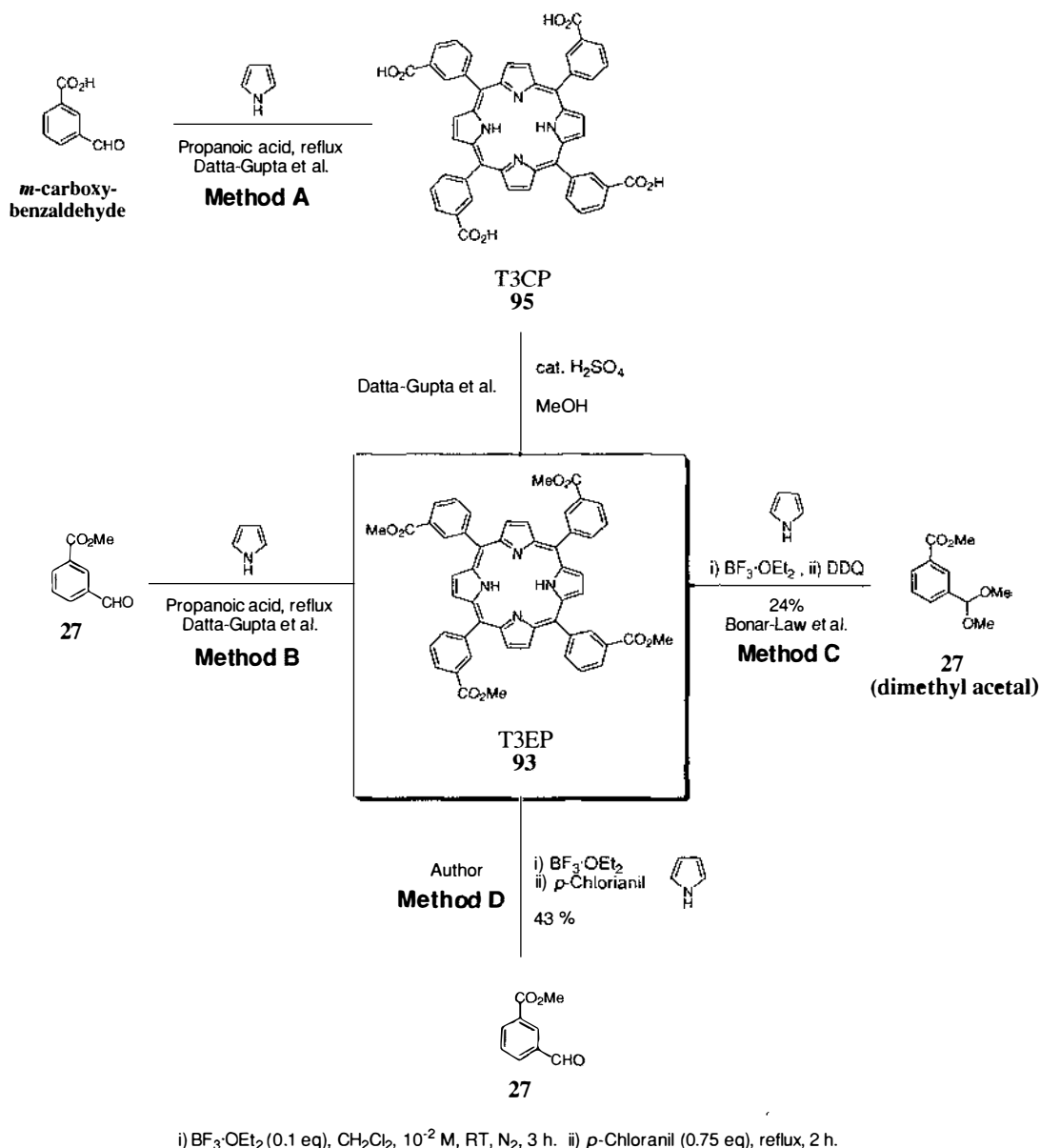
Figure 4-11. Synthesis of T3EP **93** by Datta-Gupta et al.[144], Bonar-Law et al.[145] and the author.

More recently Bonar-Law et al. have prepared this compound in 24% yield via the condensation of the dimethyl acetal of methyl 3-formylbenzoate with pyrrole under Lindsey conditions employing $BF_3 \cdot OEt_2$ as the acid catalyst (Figure 4-11, Method C).[145]

In this thesis, the synthesis of T3EP **93** was achieved using Lindsey conditions[120] but employing pure methyl 3-formylbenzoate in dry degassed DCM to give T3EP **93** in an excellent 43% yield (Method D, Figure 4-11).

The synthesis of T3EPps **94** from T3EP **93** turned out to be relatively straightforward using established TAPps procedures (Figure 4-12).[79,138] Metallation of **93** with copper(II) acetate afforded **Cu-93** quantitatively.

Standard Vilsmeier formylation of **Cu-93** gave the aldehyde **96** in 70% yield. The placement of the ester EWGs in the *meta* positions clearly reduces β-pyrrolic carbon electronic deactivation so as to allow Vilsmeier formylation to proceed. The reaction appeared to be slow, as an extended reaction time (24 h, ca. 7-12 h) was required to give significant conversion, suggesting that there was still a little deactivation by the EWGs. A significant amount of demetallated starting material **93** (17%) was recovered during column chromatography of the product **96**. Optimisation of the Vilsmeier conditions may resolve the problem of incomplete reaction.

Reduction of aldehyde **96** to alcohol **97** using $NaBH_4$ proceeded in near quantitative yield. Subsequent chlorination of **97** with thionyl chloride gave the chloromethyl product **98** in 70% yield. The chloromethyl product **98** was stable enough to be purified by chromatography on silica gel, this not being possible with other TAPs previously synthesised in our laboratories due to decomposition. Treatment of **98** with excess triphenylphosphine gave quantitative conversion to phosphonium salt T3EPps **94**. No other reactions appeared to be significantly influenced by the ester EWGs.
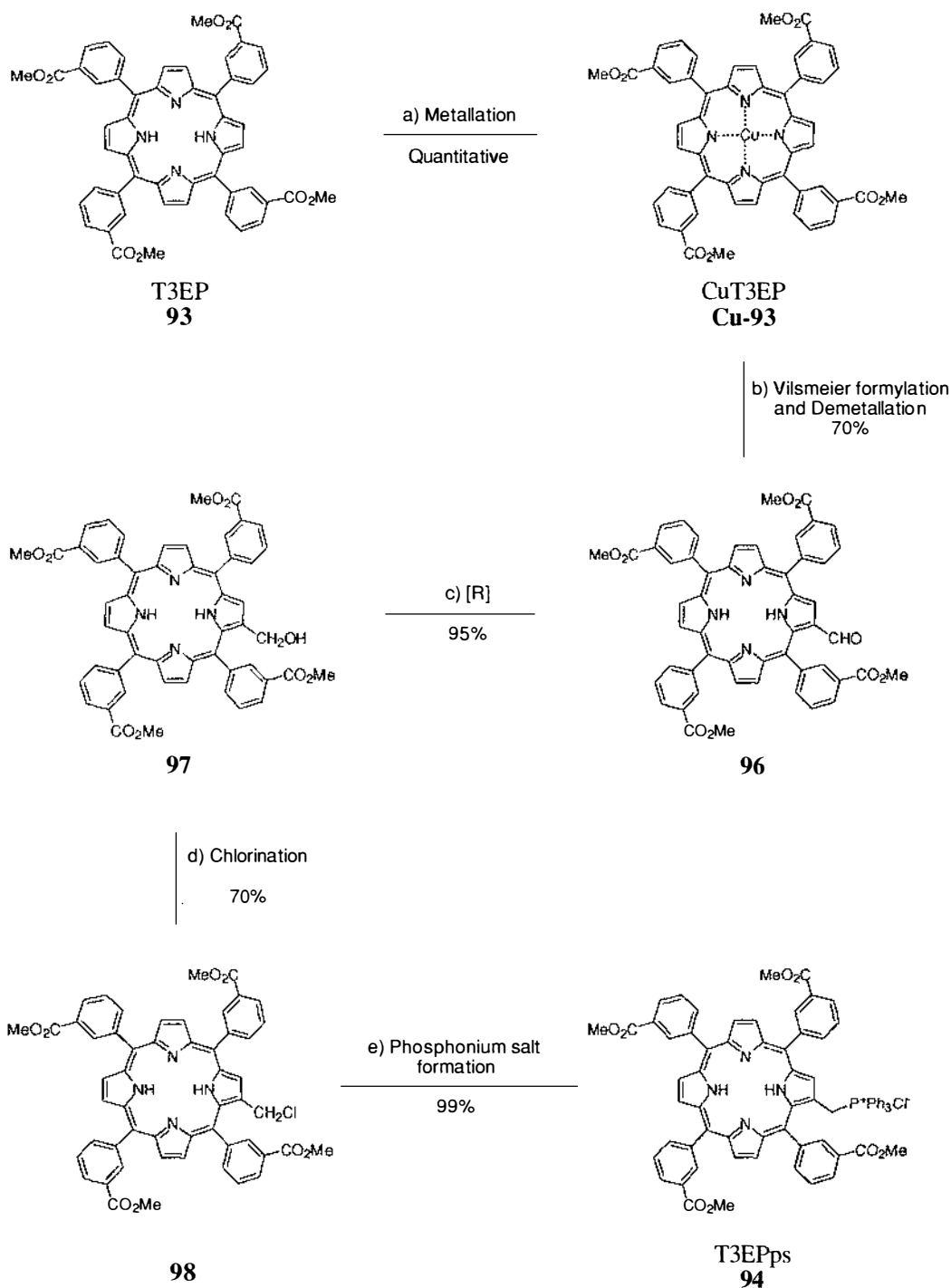
a) Cu(OAc)$_2$·H$_2$O/ MeOH, CHCl$_3$, reflux, 1 h. b) i) POCl$_3$/DMF, DCE, argon, reflux, 24 h. ii) Conc. H$_2$SO$_4$, RT, 15 min. c) NaBH$_4$, THF, H$_2$O, RT, 45 min. d) SOCl$_2$, pyridine, CH$_2$Cl$_2$, 15 min at 0°C and 1.75 h at RT. e) PPh$_3$ (20 eq), reflux, 5 h.

Figure 4-12. Synthesis of "Sticky" porphyrin phosphonium salt (T3EPps) **94.**

Characterisation by ^{1}H NMR of the derivatised T3EPs generally required a mixture of room temperature and variable temperature NMR experiments in a range of different solvents. Generally, the room temperature ^{1}H NMR spectra of the substituted T3EP

compounds gave complex (broadened and multiple signals) for some protons. This was attributed to slowly interconverting atropisomers, and by using elevated temperatures, some of the signals were better resolved. As an example, characterisation of the T3EPps **94** by ^{1}H NMR was difficult due a very broad spectrum at room temperature, but better resolved at 85°C. At ~20°C in C_6D_6 a very broad singlet was just visible at 4.53 ppm and shifts to 4.8 ppm at 85°C. This has been tentatively assigned to the T3EP-CH$_2$P$^+$Ph$_3$Cl$^-$ **94** resonance. The aromatic region of the spectra is too complex to assign. ^{31}P NMR analysis of T3EPps **94** indicates a very similar resonance to that of the characterised TXPps **5** (Table 4-1). At room temperature, there are two separate signals in the ^{31}P NMR spectrum, however these coalesce to one resonance at 85°C.

Table 4-1. Comparison of ^{31}P NMR chemical shifts.

Compound	δ at ≈ 22 °C	δ at 85 °C
Ph$_3$P	-4.03	-
Ph$_3$P=O	26.52	-
TXPps **5**	23.91	-
T3EPps **94**	24.29, 23.95	24.34

Initially a satisfactory FAB HRMS (32 ppm variation) could not be obtained for the phosphonium salt **94** using NBA as the FAB matrix, however in the FAB LRMS the parent ion [M − Cl]$^+$ and the fragment [M − (P$^+$Ph$_3$Cl$^-$)]$^+$) could be assigned. On changing the FAB matrix to 2-nitrophenyl octyl ether, a good HRMS was obtained. Elemental analysis was unsatisfactory for this compound [Elemental: Calcd (found) for (C$_{71}$H$_{54}$Cl$_1$N$_4$O$_8$P$_1$): C, 73.66 (68.79, 68.71); H, 4.70 (4.69, 4.75); Cl, 3.06 (3.56); N, 4.84 (4.28, 4.24); P, 2.68 (2.52)]. Added proof of the structure of T3EPps **94** results from the characterisation of the products obtained from its Wittig reactions.

For the purposes of TiO$_2$ solar cells testing and as a reference compound, the ZnT3CP **Zn-95** was also synthesised (Figure 4-13). The zinc(■) ester **Zn-93** has been reported by Bonar-Law et al., but no experimental data has been published.[145] The metallation of T3EP **93** was achieved quantitatively using the acetate method.[60] The ^{1}H NMR and UV-vis spectra of **Zn-93** were consistent with that previously reported, and extra FAB HRMS data was obtained. The zinc(II) acid analogue **Zn-95** has not been reported in the literature. Base hydrolysis of **Zn-93** gave ZnT3CP **Zn-95** in 97% yield. The 400

MHz ^{1}H NMR spectrum in DMSO of **Zn-95** was as expected with a broad singlet (13.3 ppm) observed for the CO_2H protons.

a) $Zn(OAc)_2 \cdot 2H_2O$ (1.2 eq), $CHCl_3$/MeOH, reflux (1 h). b) i) KOH (15 eq per CO_2Me), MeOH:H_2O (10:1), reflux (2.5 h), N_2
. ii) H_3PO_4 (excess).

Figure 4-13. Synthesis of ZnT3CP **Zn-95**.

4.2.4   "Sticky" Porphyrin Arrays (Wittig Reactions of T3EPps)

"Sticky" Diporphyrins
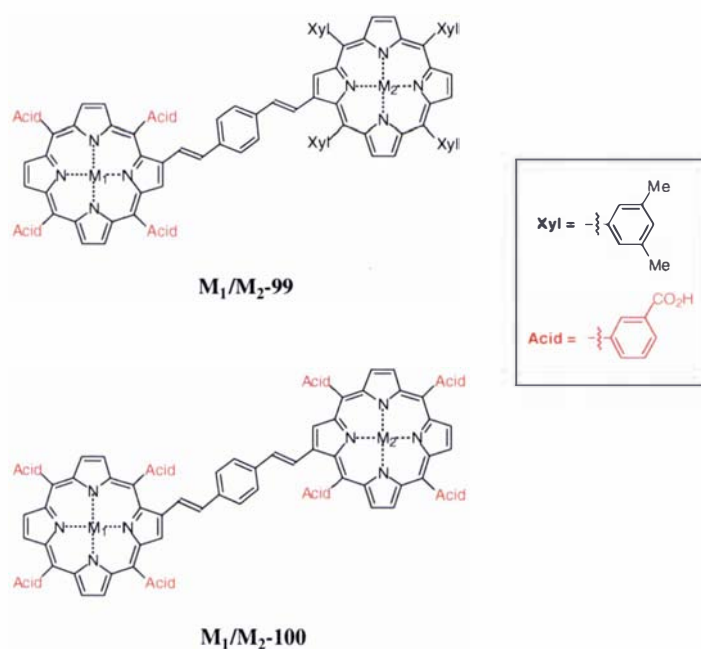
Figure 4-14. Proposed "sticky" diporphyrins.

With the successful synthesis of T3EPps **94**, a series of SP mixed-TXP/T3EP diporphyrin arrays **M₁/M₂-99** and **M₁/M₂-100** were proposed and investigated using the established 'Building Block A' (see Figure 3-3, pg 80) approach of Burrell, Officer and Reid.[79,82,127,135]

The Building Block A starting aldehyde T3EP–PhCHO **101** was first made through the Wittig reaction of T3EPps **94** and terephthaldicarboxaldehyde **22** (Figure 4-15). Under the higher temperature of refluxing CHCl₃, the product **101** was obtained in good yield (90%, based on **94**) as the all *trans* isomer, indicated by the 16 Hz AB quartet in the ¹H NMR spectra. Other spectral data was similar to that reported for the analogous Building Block A TAPs.[78,79,135]
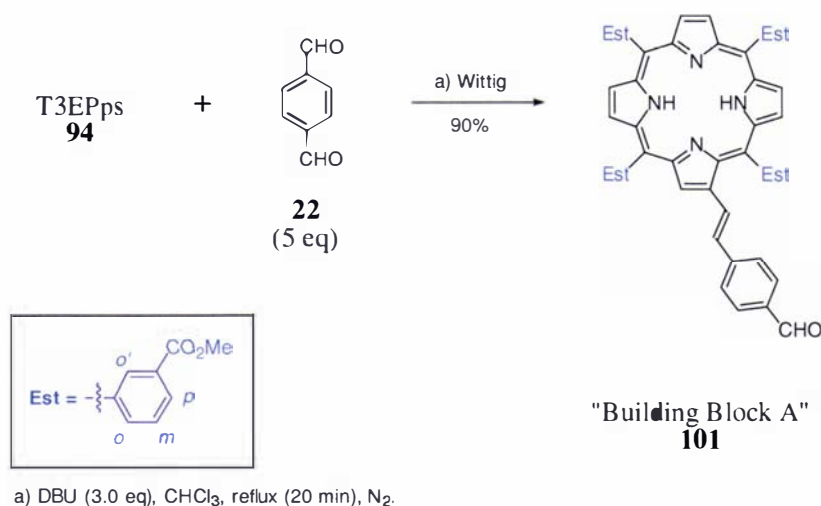
Figure 4-15. Synthesis of T3EP Building Block A **101**.

The Wittig reactions of **101** with either TXPps **5** or T3EPps **94** afforded excellent yields of the mixed-diporphyrin esters T3EP–TXP **102** (91%) and the symmetrical diporphyrin T3EP–T3EP **103** (70%) respectively (Figure 4-16). The ¹H NMR spectrum of the mixed-diporphyrin T3EP–TXP **102** in CDCl₃ gave a singlet for the **NH** protons whereas in C₆D₆ two well-resolved singlets for the different pairs of **NH** protons were observed. The rest of the spectrum contained signals assignable to the two different porphyrins (i.e. separate AB quartets for the two different ethenyl groups). In contrast, the UV-vis spectrum looked essentially like that of a single free-base tetraaryl porphyrin. The

spectral data of the symmetrical free-base dimer **103** was typical of analogous symmetrical dimers.[79,135]
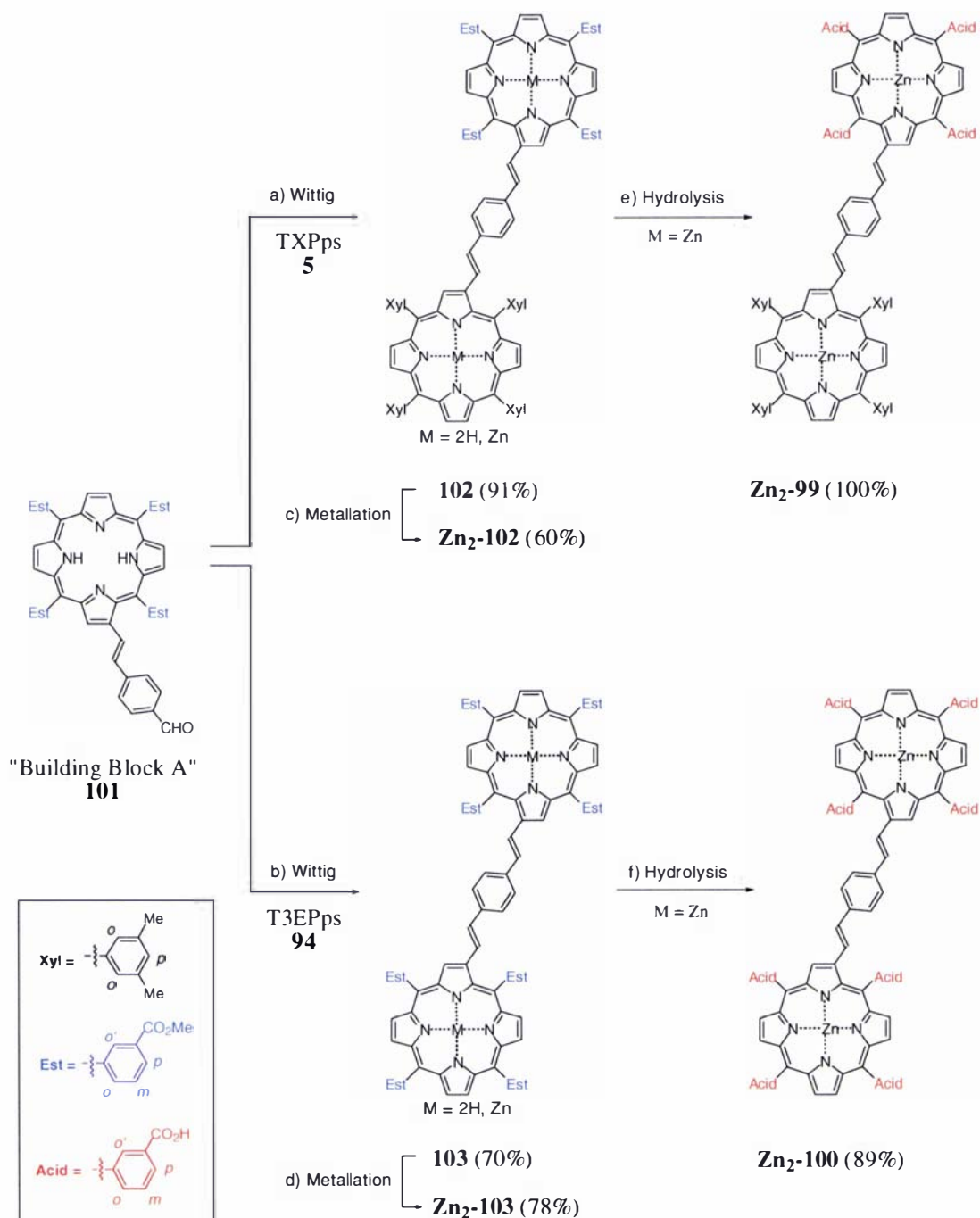
a) **5** (1.5 eq), DBU (1.0 eq h⁻¹), CHCl₃, reflux (3 h), N₂. b) **94** (1.2 eq), DBU (3.0 eq), CHCl₃, reflux (1 h), N₂. c) Zn(OAc)₂·2H₂O (2.4 eq), CHCl₃/MeOH, RT (1 h). d) Zn(OAc)₂·2H₂O (1.3 eq), CHCl₃/MeOH, RT (50 min). e) i) KOH (15 eq per CO₂Me), MeOH:THF:H₂O (10:2:1), reflux (6.5 h), N₂. ii) H₃PO₄ (excess). f) i) KOH (19 eq per CO₂Me), MeOH:THF:H₂O (10:4:1), reflux (4.5 h), N₂. ii) H₃PO₄ (excess).

Figure 4-16. Synthesis of "sticky" diporphyrin acids.

Metallation with zinc(II) was then carried out using the acetate method[60] giving the **Zn$_2$-102** and **Zn$_2$-103** derivatives (Figure 4-16). Similar ^{1}H NMR spectral properties were observed as in the parent free-base compounds, with the obvious absence of the **NH** resonances. The UV-vis spectra were typical of metallo TAPs.

Base hydrolysis of the zinc(II) esters gave the corresponding acids ZnT3CP–ZnTXP **Zn$_2$-99** and ZnT3CP–ZnT3CP **Zn$_2$-100** in good yield (Figure 4-16). Both ZnT3CP–ZnTXP **Zn$_2$-99** and ZnT3CP–ZnT3CP **Zn$_2$-100** were insoluble in CHCl$_3$, semi-soluble in MeOH and soluble in acetone. These compounds stain glass on contact. In the ^{1}H NMR spectrum of the mixed porphyrin ZnT3CP–ZnTXP **Zn$_2$-99**, the absence of methyl ester resonances was observed. With the aid of COSY spectra, a multiplet at 7.09-7.54 ppm could be identified as containing two separate AB quartets for the ethenyl groups along with the aromatic styryl and *para*-xylyl protons. Although soluble in acetone-d$_6$, a well-resolved ^{1}H NMR spectrum could not be obtained for the symmetrical diporphyrin ZnT3CP–ZnT3CP **Zn$_2$-100**. Strong intermolecular hydrogen-bonding between the carboxylic acid groups may be responsible for this. It is however clear from the ^{1}H NMR spectra that the absence of methyl ester resonances indicates successful hydrolysis. The COSY spectrum showed coupling between a broad multiplet at 7.90-8.20 ppm and 8.43-8.54 ppm as expected for coupling of the aromatic H$_{m\text{-Acid}}$ to H$_{o,p\text{-Acid}}$ protons. No AB quartet was visible for the *trans* ethenyl protons, and only one doublet of 16 Hz could be seen. A very weak (~ 10%) M$^+$ molecular ion peak was found in the FAB MS, although high resolution FAB MS gave accurate masses for the parent ion. Due to exchange, no acid resonances were observed in acetone-d$_6$ by ^{1}H NMR for either acid dimer. Typical metallo porphyrin UV-vis spectra were obtained for both acid dimers in THF.

"Sticky" Triporphyrins

Using the new "Building Block C" approach established in Chapter 3, attention turned to mixed-TXP/T3EP triporphyrin acids arrays. A series of SP mixed-TXP/T3EP triporphyrin arrays $M_2/M_1/M_3$-**104** and $M_2/M_1/M_3$-**105** were envisaged based on this approach (Figure 4-17).
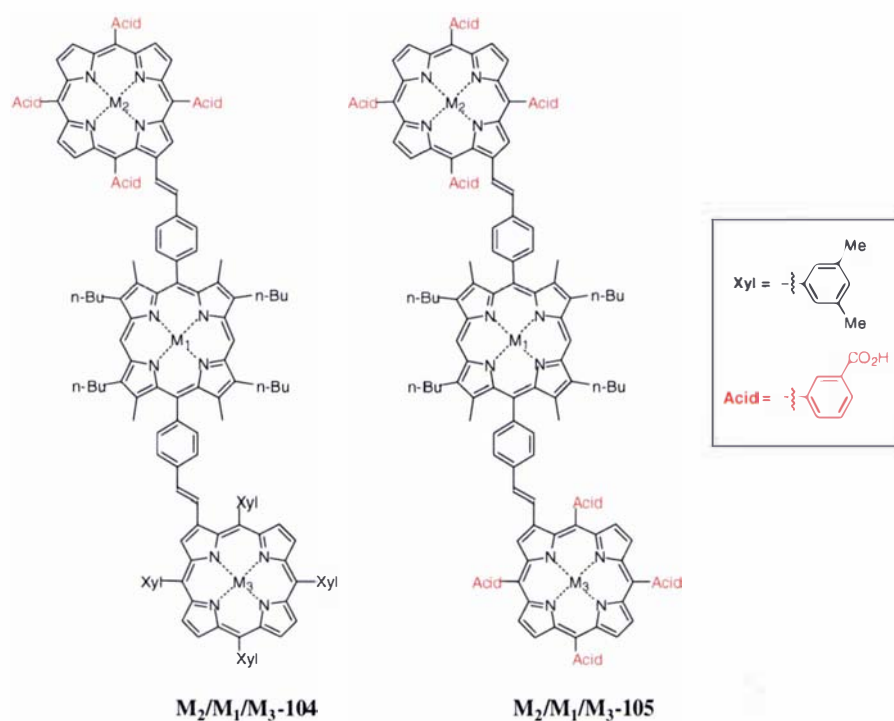
Figure 4-17. Proposed "sticky" linear triporphyrins.

The synthesis of the required mixed-diporphyrin 'Building Block C' aldehyde T3EP–TBMP–CHO **106** was achieved through the Wittig reaction of T3EPps **94** with excess BFP **76** (Figure 4-18). Most of the unreacted BFP **76** was recovered by column chromatography for recycling during isolation of the product. The product T3EP–TBMP–CHO **106** was obtained as a *cis/trans* (<5% *cis*) mixture. The standard I_2 isomerisation conditions (3.0 eq of I_2 per ethenyl) were unsuccessful (no change in *cis/trans* ratio was observed by ^1H NMR). Carrying this Wittig reaction out at higher temperature (i.e. refluxing DCE) may reduce the *cis* isomer content. However, the small amount of *cis* isomer present was deemed insignificant and the product **106** was used in the next synthetic step 'as is'. Building Block **106** was characterised fully by ^1H

NMR, UV-vis spectroscopy and FAB HRMS spectrometry. The ^{1}H NMR spectrum was consistent with that of the previously characterised collinear diporphyrin ester $\mathbf{Zn_2}$-$\mathbf{64}$ of Chapter 2 and the diporphyrin Building Blocks $\mathbf{M_2/M_1}$-$\mathbf{77}$ of Chapter 3.
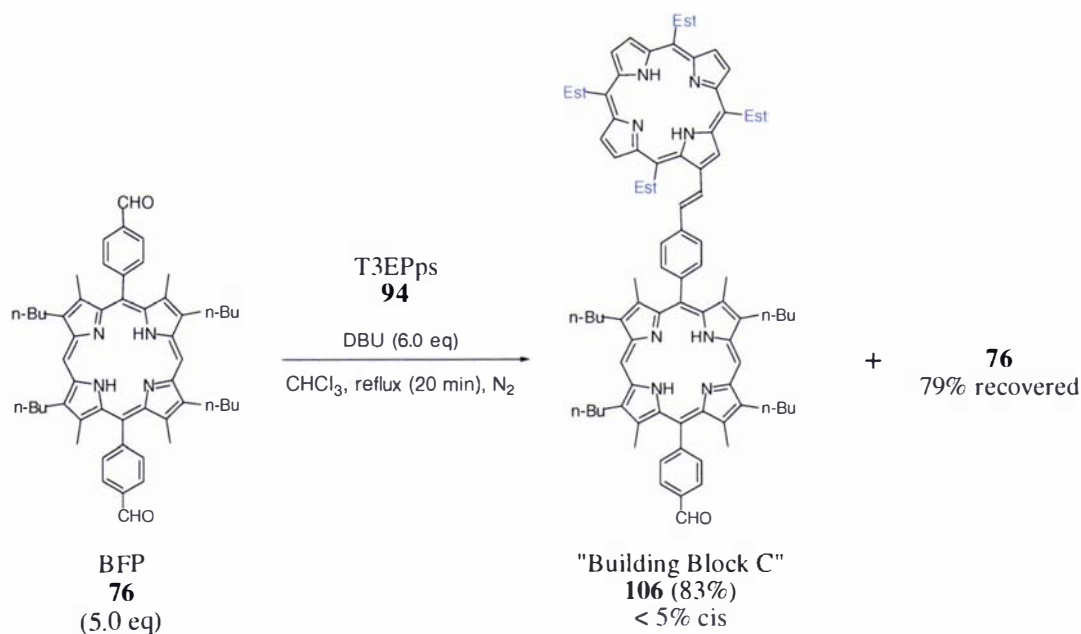
Figure 4-18. Synthesis of the "sticky" porphyrin "Building Block C" T3EP–TBMP–CHO, **106**.

The Wittig reactions of **106** with either TXPps **5** or T3EPps **94** afforded the mixed-triporphyrin T3EP–TBMP–TXP **107** (82%) and the symmetrical triporphyrin T3EP–TBMP–T3EP **108** (66%) respectively (Figure 4-20). The triporphyrins were metallated with zinc(II), using the acetate method[60] giving $\mathbf{Zn_3}$-**107** (75%) and $\mathbf{Zn_3}$-**108** (72%).

In both the mixed T3EP–TBMP–TXP **107** and symmetrical T3EP–TBMP–T3EP **108** triporphyrins the ^{1}H NMR spectra showed the absence of **NH** signals and some small shifts upon metallation with zinc(II). More significantly, there are separate Soret bands for each porphyrin type (TAP and TBMP) evident in the UV-vis spectra, the TAP moiety being slightly red shifted by 6 nm and the TBMP moiety more dramatically blue shifted by 15 nm. The symmetrical T3EP–TBMP–T3EP **108** and $\mathbf{Zn_3}$-**108** triporphyrins gave ^{1}H NMR spectra easily assignable due to their high symmetry, this being consistent with that of previously characterised triporphyrins discussed in Chapter 3 and of those published.[79,83,135]

The mixed T3EP–TBMP–TXP triporphyrins, free-base **107** and metallo **Zn₃-107** afforded a ¹H NMR spectra with most of the signals of the different porphyrins evident and identifiable by COSY spectra. In the ethenyl linked TAP-TBMP-R di- and symmetrical triporphyrins the TAP β-pyrrolic protons H_3 are generally easily recognised as a low field singlet, having long-range coupling (COSY) to their neighbouring ethenyl proton (Figure 4-19).
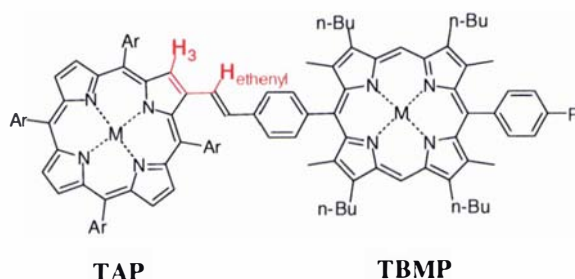
Figure 4-19. H_3 and $H_{ethenyl}$ coupling in TAP-TBMP-R porphyrins.

Comparison of previously assigned H_3 signals in diporphyrin and symmetrical triporphyrin variants allowed us to assign the two different H_3 β-pyrrolic of **107** and **Zn₃-107** to TXP or T3EP (Entries 6 and 12 respectively, Table 4-2).

Table 4-2. Correlation of H_3 β-pyrrolic ¹H NMR resonances at 400 MHz for TXP and T3EP connected to a TBMP.

	Compound*	$H_{3\text{-TXP}}$	$H_{3\text{-ZnTXP}}$	$H_{3\text{-T3EP}}$	$H_{3\text{-ZnT3EP}}$
1	TXP-ZnTBMP-CHO **2H/Zn-77**	9.210 ppm			
2	TXP-ZnTBMP-TXP **2H/Zn/2H-65**	9.206 ppm			
3	TXP-TBMP-CO₂Me **64**	9.187 ppm†			
4	T3EP-TBMP-CHO **106**			9.032 ppm	
5	T3EP-TBMP-T3EP **108**			9.047 ppm	
6	T3EP-TBMP-TXP **107**	9.172 ppm		9.049 ppm	
7	ZnTXP-ZnTBMP-CO₂Me **Zn₂-64**		9.303 ppm		
8	ZnTXP-ZnTBMP-CO₂H **Zn₂-66**		9.303 ppm		
9	ZnTXP-ZnTBMP-CHO **Zn₂-77**		9.306 ppm		
10	ZnTXP-ZnTBMP-ZnTXP **Zn₃-65**		9.306 ppm		
11	ZnT3EP-ZnTBMP-ZnT3EP **Zn₃-108**				9.156 ppm
12	ZnT3EP-ZnTBMP-ZnTXP **Zn₃-107**		9.295 ppm		9.162 ppm

* Spectra of porphyrins containing T3EP moieties were carried out at 55°C in CDCl₃, all other spectra in CDCl₃ at RT. † 270 MHz.
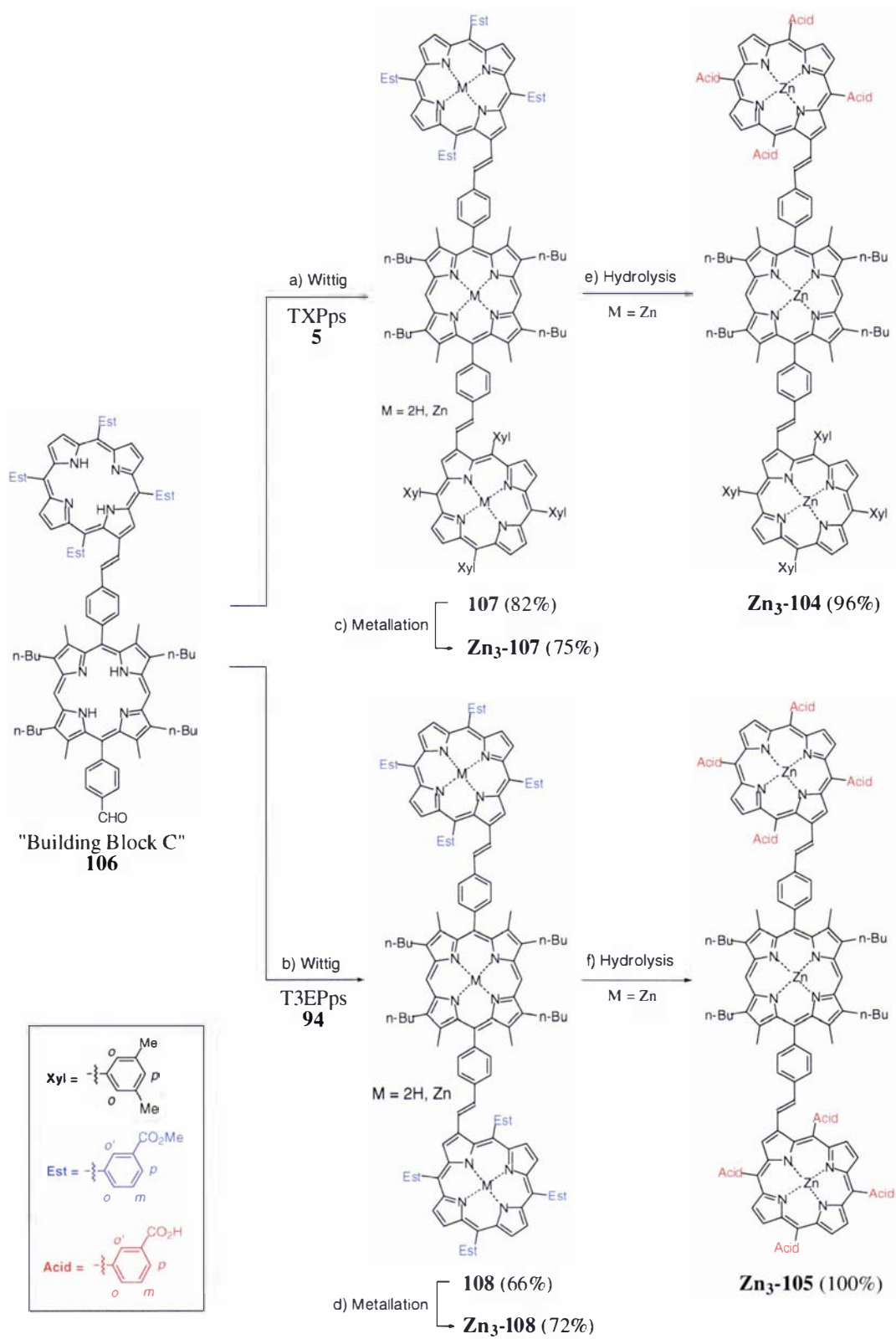
a) 5 (1.5 eq), DBU (1.0 eq h^{-1}), CHCl$_3$, reflux (4 h), N$_2$. b) 94 (1.2 eq), DBU (1.0 eq h^{-1}), CHCl$_3$, reflux (4 h), N$_2$.
c) Zn(OAc)$_2$·2H$_2$O (4 eq), CHCl$_3$/MeOH, RT (3 h). d) Zn(OAc)$_2$·2H$_2$O (4 eq), CHCl$_3$/MeOH, RT (3 h).
e) i) KOH (15 eq per CO$_2$Me), MeOH:THF:H$_2$O (10:10:1), reflux (6.5 h), N$_2$. ii) H$_3$PO$_4$ (excess).
f) i) KOH (15 eq per CO$_2$Me), MeOH:THF:H$_2$O (10:10:1), reflux (4 h), N$_2$. ii) H$_3$PO$_4$ (excess).

Figure 4-20. Synthesis of "sticky" triporphyrins.

Base hydrolysis of the zinc(II) esters gave the corresponding acids ZnT3CP–ZnTBMP–ZnTXP **Zn$_3$-104** and ZnT3CP–ZnTBMP–ZnT3CP **Zn$_3$-105** in high yield. The ^{1}H NMR spectrum of the mixed ZnT3CP–ZnTBMP–ZnTXP **Zn$_3$-104** triporphyrin in CDCl$_3$ was broadened, and no other suitable solvent could be found. Despite the lack of resolution, it was clear that no methyl ester proton resonances were evident. Upfield the appropriate broad resonances are observed for the alkyl groups of the TBMP moiety and the methylaryl groups of the TXP moiety. Downfield the signals are broadened, although a signal for the *meso* protons of TBMP moiety was clearly visible at 10.258 ppm. The ^{1}H NMR in DMSO-d$_6$ at room temperature of the symmetrical ZnT3CP–ZnTBMP–ZnT3CP **Zn$_3$-105** triporphyrin was also broadened, and largely unassignable. Acetone-d$_6$, CD$_3$OD and CDCl$_3$ were also tried as solvents with out success. However, the CO$_2$**H** proton resonances at 13.23 ppm are observed in DMSO. As before, the downfield signals are very broadened, and again the signal for the *meso* protons of TBMP moiety are evident (10.130 ppm). When heated to 100°C in DMSO a single AB quartet representing the *trans* ethenyl protons was identifiable.

The UV-vis spectra of the triporphyrin acids **Zn$_3$-104** and **Zn$_3$-105** was essentially the same as their ester derivatives, giving typical metalloporphyrin spectra with two Soret bands evident. Accurate masses for the parent ions of all the triporphyrins were obtained by high resolution FAB MS.

"Sticky" Pentaporphyrins

The synthesis of a star shaped pentaporphyrin analogous to that of Reid et al. was investigated (Figure 4-21).[127] The pentaporphyrin synthesised by Reid et al. utilised the 'Building Block A' approach. However, an alternative approach was proposed here using the Wittig chemistry of TAP phosphonium salts with tetraformylporphyrin (TFP) **110** (Figure 4-22, Method B). The synthesis via Method B would not only give an alternative route to $(M_1)_4/M_2$-**109**, but also give access to mixed-TXP/T3EP pentaporphyrin variations **111** and **113** (Figure 4-22).
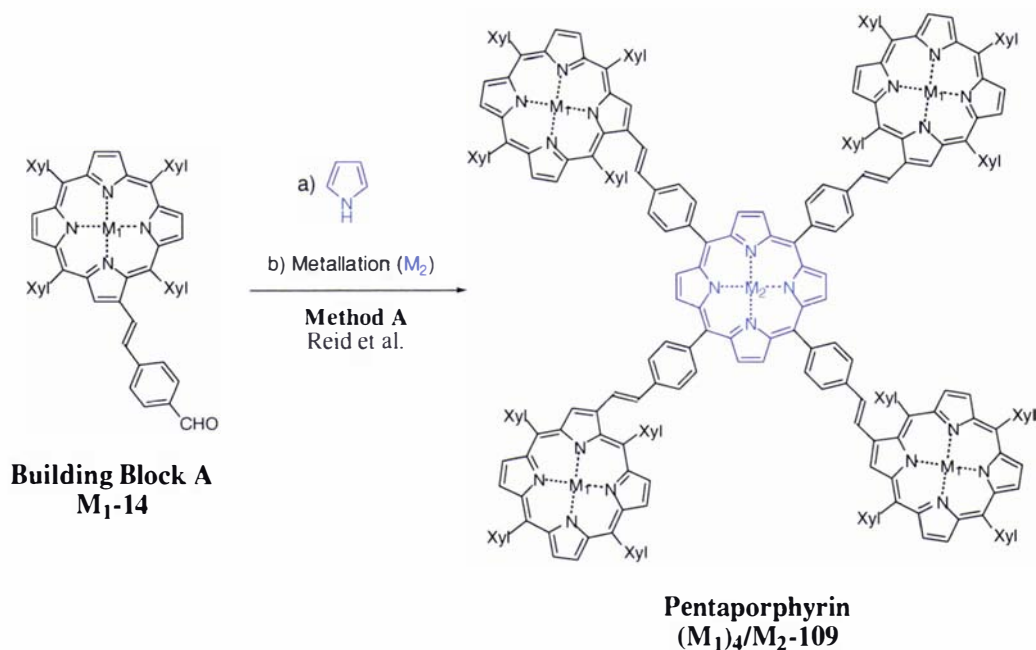
Figure 4-21. Method A, synthesis of pentaporphyrin $(M_1)_4/M_2$-**109** by Reid et al. via 'Building Block A' approach.[127]
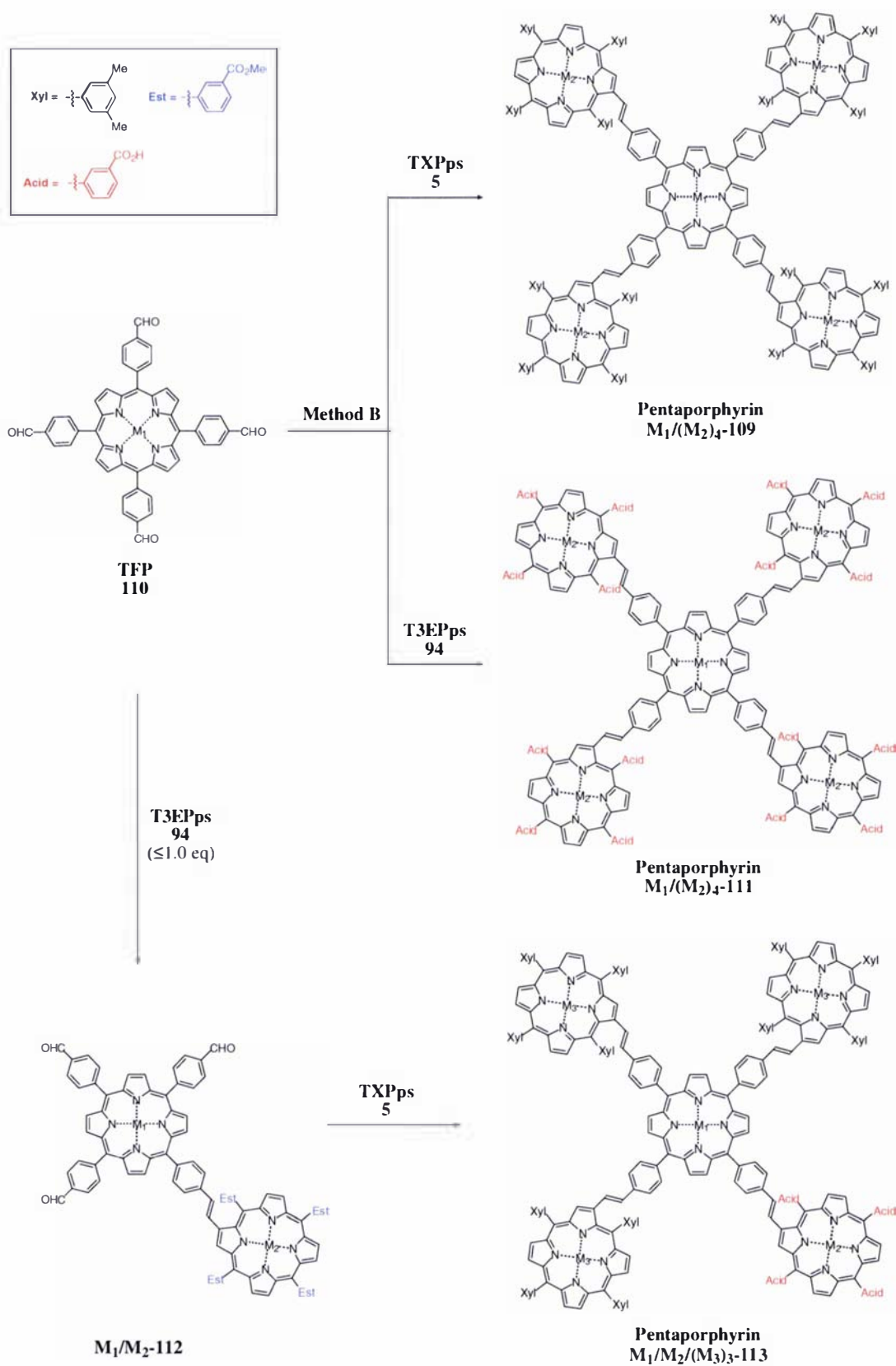
Figure 4-22. Proposed alternative Method B synthesis to pentaporphyrins.

The synthesis of tetra(4-formylphenyl)porphyrin (TFP) **110** was initially required for this Method B approach. TFP **110** is reported by Osuka et al. in multiporphyrin-cyclisation reactions[146] and its preparation is referenced back to an earlier paper by Lindsey et al.[120] However, this paper only gives the synthesis and characterisation of the acetal protected TFP derivative **114** and not TFP **110** itself (Figure 4-23). Deprotection of **114** was expected to be trivial.
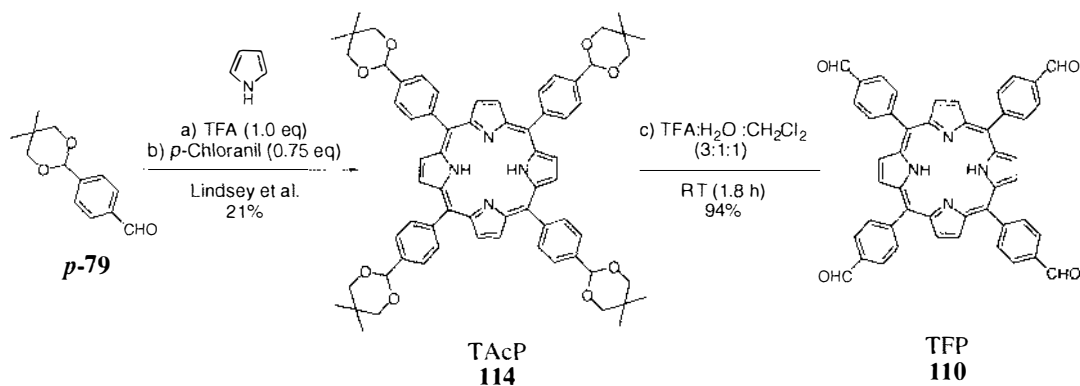
Figure 4-23. Synthesis of tetra-acetal **114**[120] and TFP **110**.

In this work, tetraacetal **114** was synthesised according to Lindsey et al.[120] via the condensation of mono-protected dialdehyde **p-79** with pyrrole (Figure 4-23). The mono-protected dialdehyde was first prepared according to a new procedure by Nierengarten et al. from 4-bromobenzaldehyde.[147] Additional UV-vis spectral data for **114** is presented in the experimental section, this being typical for a free-base TAP. Subsequent deprotection of tetraacetal **114** was carried out using similar conditions to those used by Nierengarten et al for removing this protecting group.[148] The tetra-acetal **114** was hydrolysed using a mixture of TFA/H$_2$O/DCM, to give TFP **110** in 94% yield. TFP **110** was fully characterised by ^{1}H, ^{13}C NMR and UV-vis spectroscopy and FAB HRMS, giving spectra typical of a symmetrical TAP.

TXP Star Pentaporphyrin

As a proof of concept the free-base TXP star pentaporphyrin **109** was first synthesised by this new alternative approach (Figure 4-24).
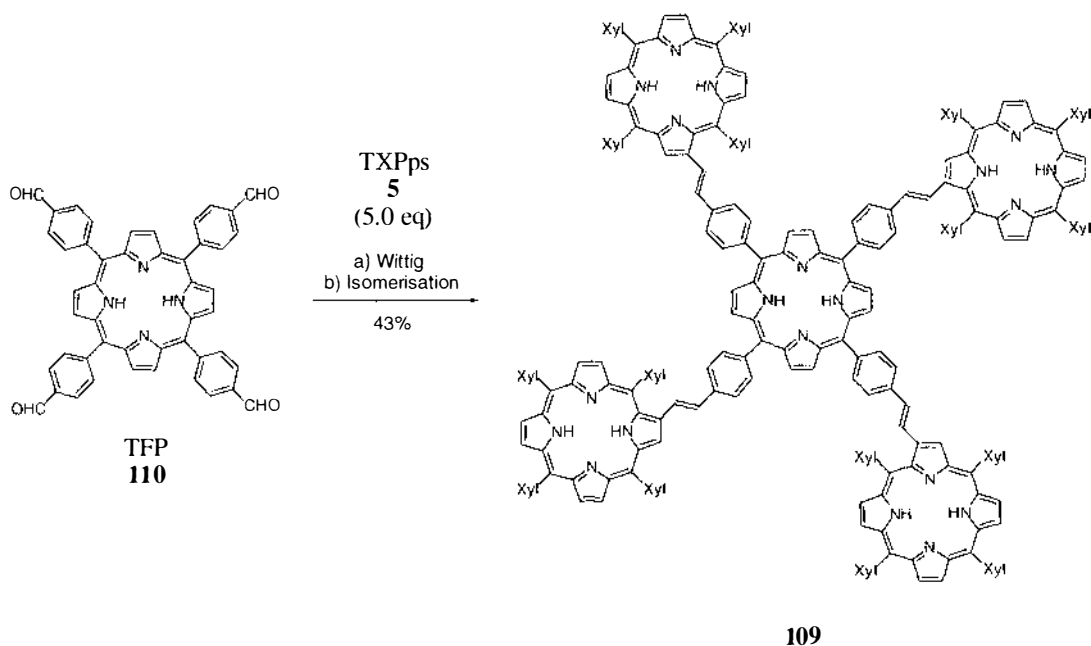
a) DBU (1.0 eq per h^{-1}), CHCl$_3$, reflux (4.5 h), N$_2$. b) i) I$_2$ (3.0 eq per ethenyl), CH$_2$Cl$_2$, RT (3 h), ii) Na$_2$S$_2$O$_3$ (aq), RT (30 min).

Figure 4-24. Synthesis of TXP star pentaporphyrin **109** by Wittig chemistry.

This free-base pentaporphyrin **109** was not accessible by Reid et al.[127] with the previous acid catalysed "Building Block A" method (Figure 4-21, Method A). Reid was only successful in synthesising these arrays using metallo "building block A" derivatives. However, employing the milder Wittig and isomerisation conditions of this new procedure gave the free-base TXP pentaporphyrin **109** in 43% yield (Figure 4-24). This new approach now offers an alternative high yielding stepwise synthesis to **109**-type pentaporphyrins, where labile metals are required in the porphyrin moieties. In particular, this methodology should allow the preparation of the previously unattainable pentaporphyrins with a single central labile metal.

Pentaporphyrin **109** was characterised by ^{1}H NMR and UV-vis spectroscopy and MALDI-TOF MS. Initially, the ^{1}H NMR spectrum of the crude product **109** after the Wittig reaction gave incorrect integral ratios with slight broadening of the resonances. This was attributed to possible *cis/trans* mixtures of the product. Isomerisation with I$_2$ resulted in an all *trans* spectrum having the correct integral ratios. The ^{1}H NMR spectrum was as expected, showing a high degree of symmetry in the signals, allowing full assignment with the aid of long-range and short-range COSY spectra. The β-pyrrolics of the central porphyrins were evident as a singlet at 9.112 ppm and well

separated downfield from the β-pyrrolic multiplet of the TXP moiety. The UV-vis spectrum was typical of a free-base TAP.

T3CP Star Pentaporphyrin

This new approach to the star pentaporphyrin was then extended to the synthesis of SP star pentaporphyrin arrays using T3EPps **94**. The star pentaporphyrin acid **Zn$_5$-111** was made first. The Wittig reaction with excess T3EPps **94** and TFP **110** was carried directly through to the acid **Zn$_5$-111** derivative in 84% yield based on TFP.
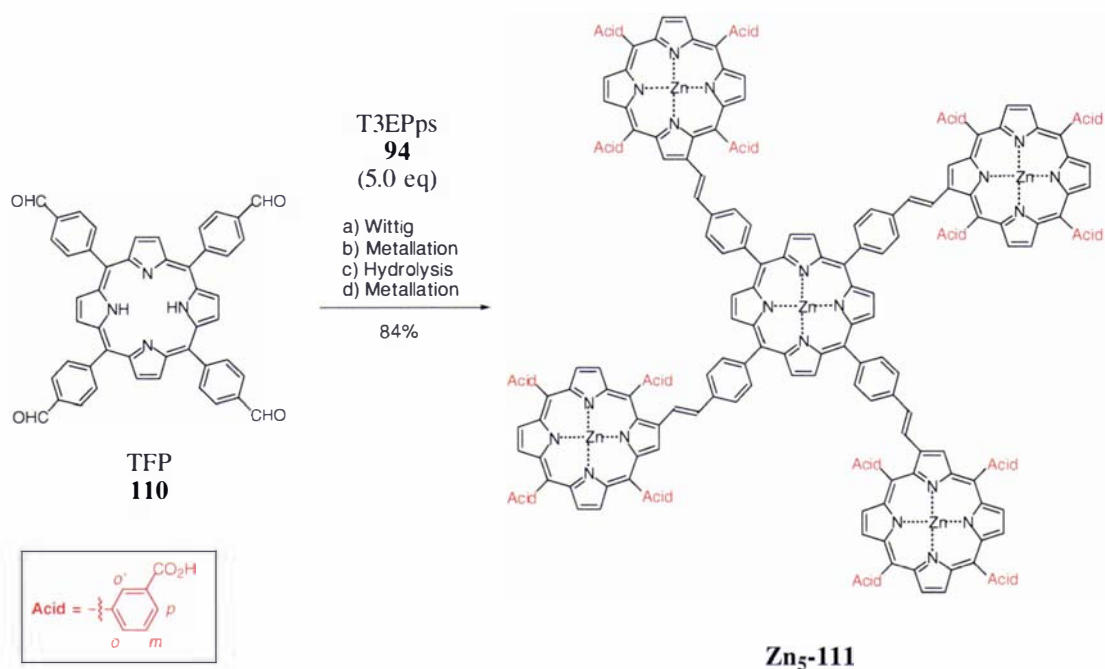
a) DBU (1.0 eq h^{-1}), CHCl$_3$, reflux (4.5 h), N$_2$. b) Zn(OAc)$_2$·2H$_2$O ($\approx$ 7.0 eq), MeOH/CHCl$_3$, reflux (1 h), N$_2$. c) i) KOH (20 eq per CO$_2$Me), H$_2$O:MeOH:THF (1:10:15), reflux (8.5 h), N$_2$. ii) H$_3$PO$_{4(aq)}$. d) Zn(OAc)$_2$·2H$_2$O ($\approx$ 2.0 eq), THF/H$_2$O, reflux (30 min), N$_2$.

Figure 4-25. Synthesis of "sticky" pentaporphyrin **Zn$_5$-111**.

The initial Wittig reaction gave multiple products by ^{1}H NMR, and separation by column chromatography was impractical. The mixture was metallated with zinc(II) acetate to facilitate separation. However, after metallation only a broadened ^{1}H NMR spectrum in CDCl$_3$ could be obtained (a broad resonance for the ester protons was evident at 3.8 ppm). The metallated ester was identified by MALDI-TOF MS analysis. The ester was then subjected to hydrolysis followed by the usual acid work up. The ^{1}H NMR spectrum of the resulting acid in DMSO-d$_6$ showed no ester resonances. A small

NH signal at 2.51 ppm was visible. As this may have resulted from demetallation in the previous acid work up of the product, the solid was treated with more zinc(II) acetate to ensure complete metallation. Upon treatment with base followed by reacidification the resulting acid **Zn$_5$-111** gave a ^{1}H NMR spectrum free of **NH** signals. The ^{1}H NMR spectrum of the acid **Zn$_5$-111** in DMSO-d$_6$ at RT is poorly resolved, however a strong CO$_2$H signal is seen at 13.27 ppm. The integral ratio of 16:124 for the acid signal to the aromatic region (7.2-9.2 ppm) was as expected. On heating the ^{1}H NMR sample to 80°C the acid and residual H$_2$O signals broaden significantly into the base line, however resolution of the aromatic region improves significantly allowing assignment of the AB quartets belong to the ethenyl and styryl protons to be made, aided via COSY spectra.

Pentaporphyrin **Zn$_5$-111** was further characterised by negative mode ESMS. The singly charged parent ion was outside the mass range of the spectrometer used, however the doubly and triply charged species were observed as clusters centred at 2094.42 and 1395.86 (calculated average masses [M – 2H]$^{2-}$ = 2094.39, [M – 3H]$^{3-}$ = 1395.93). ESMS results were later validated by MALDI-TOF MS data.

Quantitative UV-vis analysis of **Zn$_5$-111** proved difficult, due to significant adsorption of the porphyrin onto the glassware used to make up the required dilute solutions. A significant drop in the UV-vis absorption was observed when solutions of porphyrin were left standing in glassware (visible discolouration of the glassware was observed). These effects were overcome by equilibrating all glassware with a primary solution before measurement.

Mixed TXP$_3$/T3CP Star Pentaporphyrin

A mixed-TXP$_3$/T3CP star pentaporphyrin acid array **Zn$_5$-113** was synthesised using stepwise Wittig reactions (Figure 4-26). The idea was to synthesise an antennae array that would be attached through only one porphyrin group allowing the other chromophores to act as photoactive feeders to the attached acid T3CP porphyrin. Using an excess of TFP **110** with T3EPps **94**, the Wittig reaction gave the mono substituted trialdehyde product **112**. A large quantity of the excess TFP **110** was recovered for recycling, during the column chromatography of the product. Trialdehyde **112** was characterised by ^{1}H NMR and UV-vis spectroscopy and FAB HRMS. Separate **NH**

resonances were evident in the ^{1}H NMR spectrum for the two different TAP moieties and assignments to the protons in the aromatic region were made with COSY spectra. Due to the lack of symmetry in the molecule, the aldehyde resonances appear as a two unresolved signals at 10.378 and 10.389 ppm; the higher intensity of the 10.389 ppm signal suggesting it probably belongs to the two equivalent aldehydes. The UV-vis spectrum was essentially the same as a single free-base TAP showing one Soret band and four Q-bands.

The subsequent Wittig reaction of this mono substituted product **112** with excess TXPps **5** gave the all *trans* mixed-pentaporphyrin ester **115** in 54% yield. Near quantitative metallation of **115** with zinc(II) acetate gave metallated pentaporphyrin **Zn₅-115**. The characterisation of **115** and **Zn₅-115** was by ^{1}H NMR and UV-vis spectroscopy and MALDI-TOF MS. The ^{1}H NMR spectra of the mixed free-base pentaporphyrin **115** only displayed two separate signals (-2.463 ppm (8H), -2.413 ppm (2H)) for the three sets of non-equivalent N**H** protons. The TXP and T3EP N**H** signals are expected to be the overlapping in the higher field signal, as is observed for the mixed di- and triporphyrins. Upon metallation, the spectrum of **Zn₅-115** was analogous to that of the free-base compound, with the loss of the N**H** signals. With the aid of the COSY spectra, the ^{1}H NMR assignment of the expected AB quartets belonging to the two different sets of *trans*-ethenyl proton resonances of the TXP and T3EP moieties in **115** and **Zn₅-115** was straightforward. The same applied to the doublets of the aromatic proton resonances for the styryl linkers. The UV-vis spectra of **115** and **Zn₅-115** were essentially typical of free-base and metallo TAPs respectively.

Base hydrolysis of **Zn₅-115** gave the acid derivative **Zn₅-113** in good yield. Again significant binding to glassware was observed. The ^{1}H NMR spectrum of **Zn₅-113** was broadened regardless of the choice of solvent used, however no ester resonances were evident suggesting complete hydrolysis. The only other information that can be obtained from the spectrum was the expected integral ratio of about 1.6:1 for the aromatic region versus the H_{Me-Xyl} region. The UV-vis spectrum of **Zn₅-113** in THF was identical to that of the parent ester **Zn₅-115**.

Figure 4-26. Synthesis of mixed-pentaporphyrin **Zn₅-113** SP array.
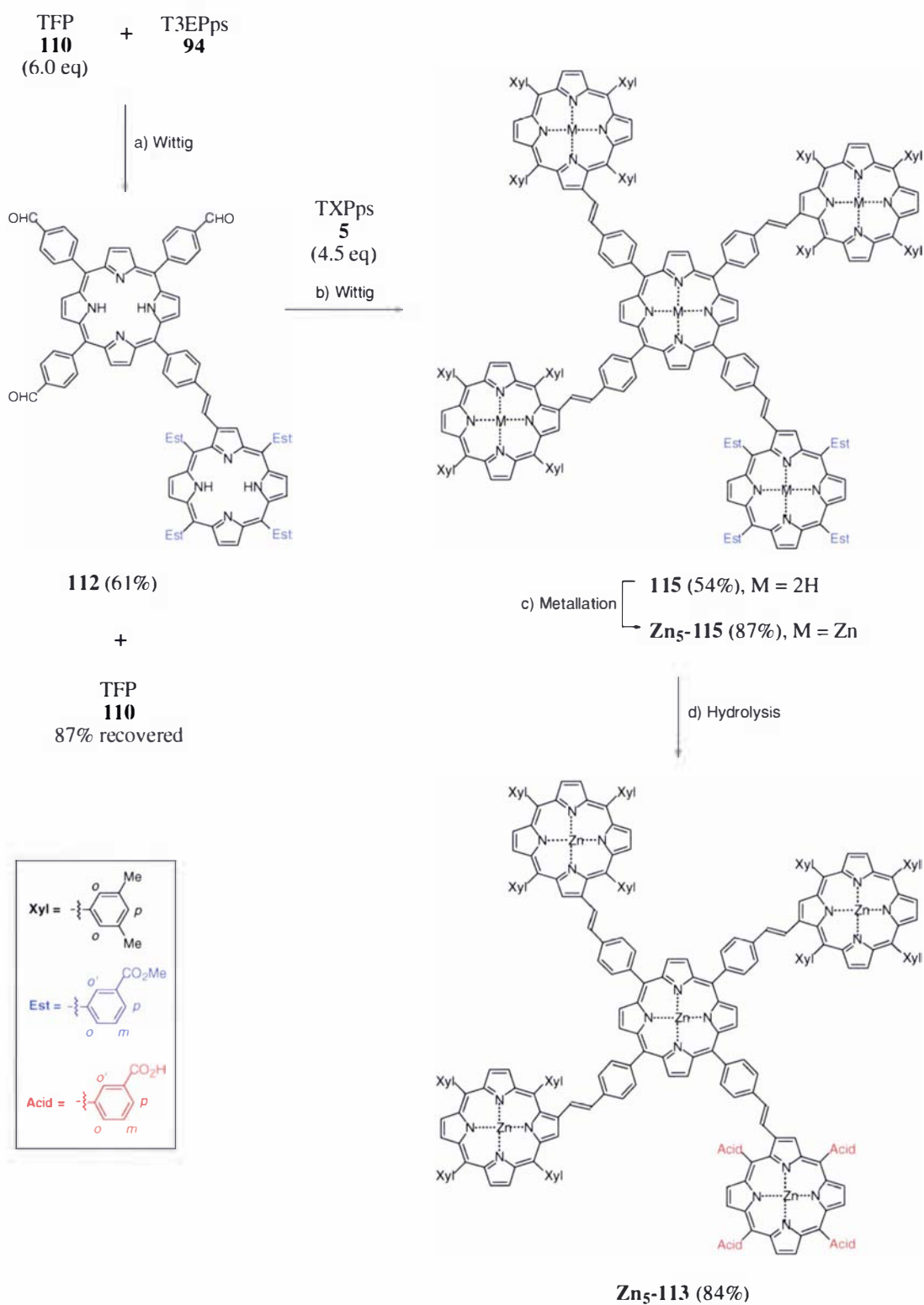
a) DBU (1.0 eq h⁻¹), DCE, reflux (3 h), N₂. b) DBU (1.0 eq h⁻¹), CHCl₃, reflux (4.5 h), N₂. c) Zn(OAc)₂·2H₂O (12 eq), MeOH/CHCl₃, RT (3 h), N₂. d) i) KOH (≈ 30 eq per CO₂Me), H₂O/MeOH/THF (1:10:15), reflux (4 h), N₂. ii) H₃PO₄(aq).

MALDI-TOF MS Characterisation of Pentaporphyrins

MALDI-TOF MS characterisation of the pentaporphyrins was performed by the author. The best matrices found to date were α-cyano-4-hydroxycinnamic acid (CHCA) and all-*trans*-retinoic acid (TR). TR appeared to give good results more consistently. By varying the laser power and detector gain, good quality spectra were obtained where the maximum spectrum intensity was dominated by the analyte (Figure 4-27). The TXP triporphyrin **Ni$_3$-65** ($C_{160}H_{148}N_{12}Ni_3$ = 2411.0010) was used as a calibration standard, giving the predicted isotope pattern in a CHCA matrix. A higher molecular weight calibrant would be more valuable here, to give accurate results in this range (The synthesis of the Ni$_5$-pentaporphyrin of **109** is suggested here).

For those spectra having well resolved isotopic patterns such as **109**, **Zn$_5$-111** and **Zn$_5$-113**, the exact mass peak was not always identifiable due to intrinsically low intensities. For those compounds where isotopic resolution was not obtained (e.g. **Zn$_5$-115**), the acquired mass cluster position and shape at all times matched the simulated spectra pattern (allowing ± 1 amu resolution) (Figure 4-28). For these high molecular weight isotope abundant arrays, the isotopic distributions give clusters that are centred on the average masses, and are reported as so. The mass spectra of the easily protonated free-base compounds **109** and **115** were dominated by MH$^+$ parent ions, whereas the zinc(II) metallo species were typically dominated by M$^+$ ions.
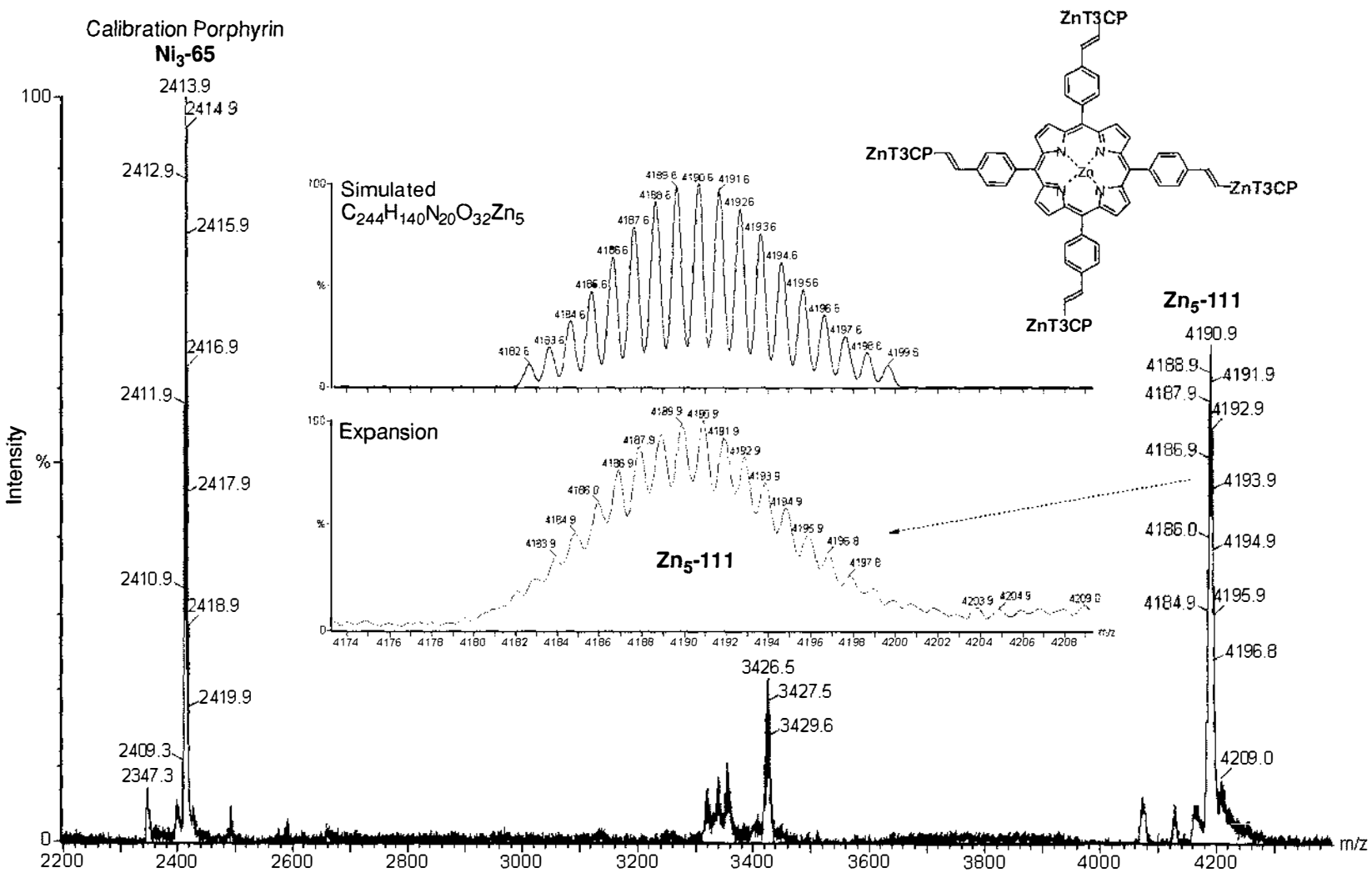
Figure 4-27. MALDI-TOF mass spectrum of **Zn$_5$-111** in a matrix of all-*trans*-retinoic acid.
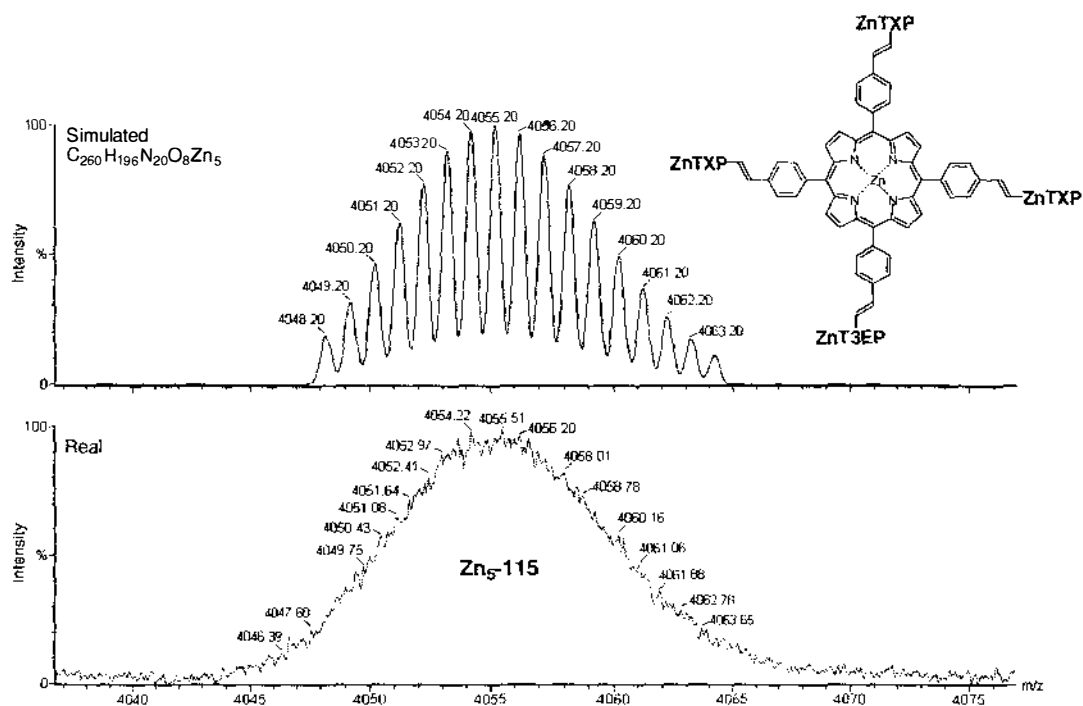
Figure 4-28. MALDI-TOF mass spectrum of **Zn$_5$-115** in a matrix of all-*trans*-retinoic acid.

4.3   Conclusion

The synthesis of a new ester-functionalised porphyrin phosphonium salt (T3EPps, **94**) was developed to allow "sticky" porphyrin array syntheses. By using the "Building Block A" approach of Reid et al.[127] with T3EPps **94**, the synthesis of TXP/T3EP mixed-diporphyrin arrays was achieved. The exploitation of the new "Building Block C" approach developed in Chapter 3 of this thesis, gave access to TXP/T3EP mixed-triporphyrin arrays.

An alternative milder and higher yielding stepwise Wittig method was developed for the synthesis the star TXP pentaporphyrin **109**. This new method under milder base conditions has advantages compared to the initial acid catalysed "Building Block A" approach used. It is now possible to build these arrays in a stepwise manner with acid labile metals present in the porphyrin moieties. Access to the controlled synthesis of the TXP/T3EP mixed-pentaporphyrin arrays **111** and **113** was achieved via this new methodology.

The handling of acid products and obtaining ^{1}H NMR spectra of the acids was often difficult due to solubility and possibly aggregation problems. This was not entirely unexpected with the number of acid groups present in some of these arrays. It does however emphasise the requirement proposed in Chapter 2 that hydrolysis needs to be the final synthetic step.

116
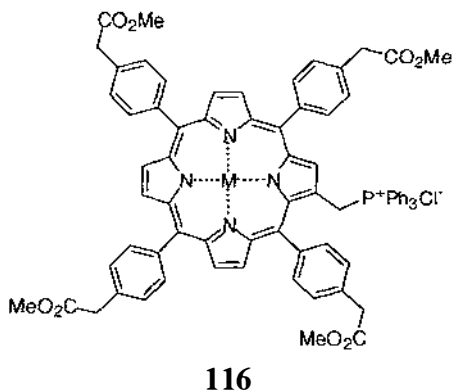
Figure 4-29. Alternative ester porphyrin phosphonium salt.

Although the characterisation of products from this T3EP phosphonium salt were relatively straightforward, a future improvement might be to create a TAP phosphonium salt with alkyl spaces separating the ester group (Figure 4-29). Using a *para*-substituted alkyl spacer group would simplify the characterisation by ^{1}H NMR due to the higher symmetry gained from a *para*-phenyl geometry.

With the synthesis of a variety of unique benzoic acid functionalised porphyrin monomers and array systems outlined here and in Chapter 2, evaluation of their performance in the TiO$_2$ Grätzel cell was carried out. In Chapter 5, the development of testing equipment, and procedures required to assess the performance of these chromophores and their light harvesting ability is presented.

Porphyrins as Sensitisers in a

Grätzel Cell

5.1 Introduction

5.1.1 The Dye-sensitised TiO_2 Photoelectrochemical Solar Cell

At the time of writing high purity inorganic semiconductor (SC) photovoltaic cells typically produce electricity with field efficiencies in excess of 20%. As of 1999, viable efficiencies of 32% have been achieved with a triple junction (GaInP2/GaAs/Ge) concentrator cell.[149] However, to achieve such high efficiencies, expensive materials, processing and packaging costs must be incurred. Numerous research groups are trying to develop alternative systems with better cost/efficiency ratios using inorganic and organic-based photoelectrochemical cells (PECs).

SC-based PECs combine the essential functions of plant energy conversion systems with those of the more technologically advanced current SC-based photovoltaic cells. PEC energy conversion systems, although a relatively new technology, have demonstrated laboratory conversion efficiencies of 10.4%[*] and represent a promising method for obtaining renewable energy from the sun. Their potential cost/efficiency ratios provide a viable option for the widespread implementation of renewable energy. In addition, PECs retain their efficiencies when cheaper polycrystalline SCs are used, in contrast to crystalline p-n junction photovoltaic devices; whose efficiencies decline severely when such materials are employed. The most promising example of PEC is based on dye-sensitised nanocrystalline films of TiO_2 (commonly known as the Grätzel cell). This TiO_2-based PEC has undergone significant development by Grätzel et al. at the Swiss Federal Institute of Technology.[150]

The Grätzel cell consists of two conducting glass electrodes in a sandwich configuration, with a redox electrolyte separating the two (Figure 5-1). One of these electrodes has a nanoporous nanocrystalline TiO_2 layer, a few microns thick, coated with the dye. Absorbances of three and above are readily obtained within the micron-thick layer with a number of Ru-polypyridyl complex dyes. The counter electrode faces the photoanode and is separated by a thin spacer. The gap between the electrodes is filled with a low-volatility electrolyte (such as a molten salt) containing a redox

mediator (generally I^-/I_3^-). Efforts to produce solid non-volatile organic electrolytes are also under investigation.[151-154]
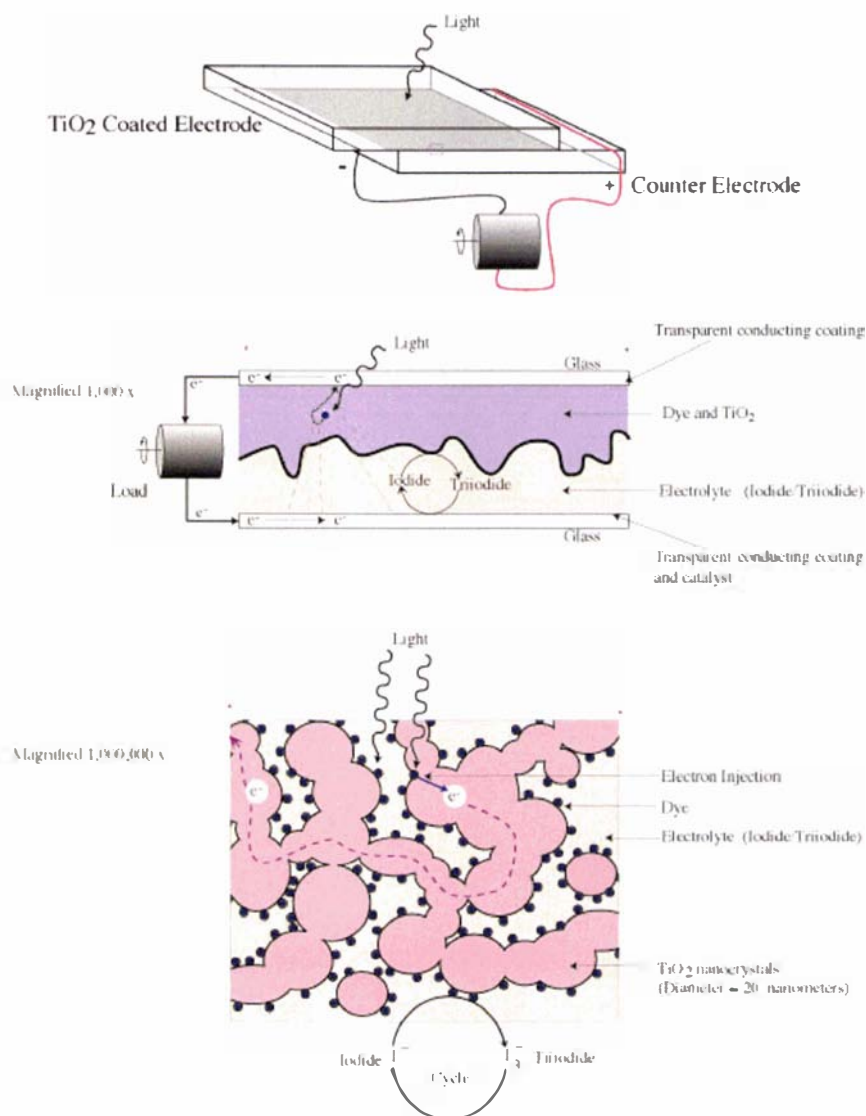
Figure 5-1. Schematic of the Grätzel cell (Reproduced from Grätzel et al.).[42]

The counter-electrode is composed of glass covered with a conducting oxide layer. A trace of platinum (5-10 μg cm²) is deposited on the conducting oxide layer in order to catalyse the cathodic reduction of the triiodide to iodide (I_3^- + 2e- → 3I^-). The whole assembly is hermetically sealed and no other complicated procedures are necessary, thus minimising production costs. Due to their simple construction, the cells offer hope of a significant reduction in the cost of solar electricity.

Theory of Operation

There are a number of key publications, which cover the mechanistic aspects and various components of the cell, and elaborate more on the dye-sensitised solar cell and other optoelectronic applications based on nanocrystalline films.[8,9,11,22,155]
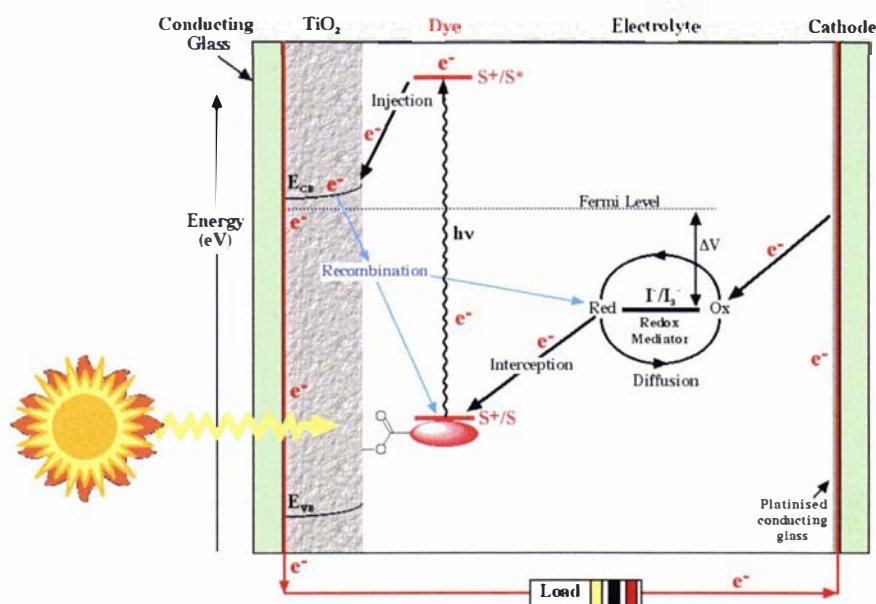
Figure 5-2. Grätzel cell theory.

The Grätzel cell works on the principle in which the process of light absorption by the chromophore is followed by charge separation as outlined in Chapter One (Figure 5-2). Light absorption is performed by a monolayer of dye (S), which is chemically adsorbed at the TiO_2 surface. After excitation by a photon of light, the excited dye (S*) is able to transfer an electron to the TiO_2 ("injection"). The electric field in the bulk material allows extraction of the electron. Positive charge is transferred from the dye (S^+) to a redox mediator (I_3^-) ("interception") in the electrolyte, and thence to the counter electrode. The circuit is closed via this last electron transfer, in which the mediator is returned to its reduced state ($3I^-$). The theoretical maximum voltage (ΔV) that such a device could deliver corresponds to the difference between the redox potential of the mediator and the Fermi level of the SC (for n-type SCs like TiO_2 the Fermi level is close to the conduction band).

Typical Examples of Photosensitisers

The structures of three very efficient photosensitisers from the Ru-polypyridine family used in the above dye-sensitised PEC are shown below (Figure 5-3).
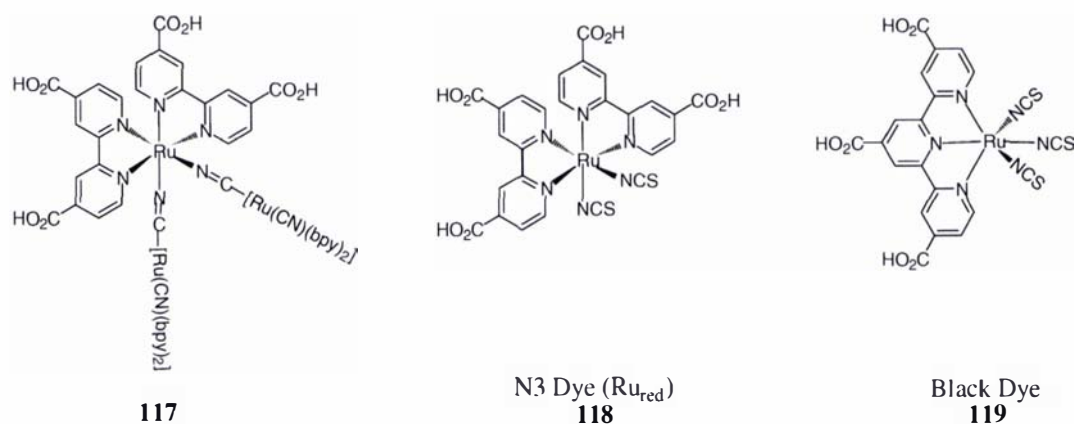
Figure 5-3. Ru-polypyridine based photosensitisers used by Grätzel.

Their photocurrent action spectra, obtained using simulated sunlight (AM 1.5) in the dye-sensitised PEC, are shown in Figure 5-4. Plotted on the left is incident photon-to-current conversion efficiency (IPCE) as a function of the excitation wavelength (monochromatic excitation).
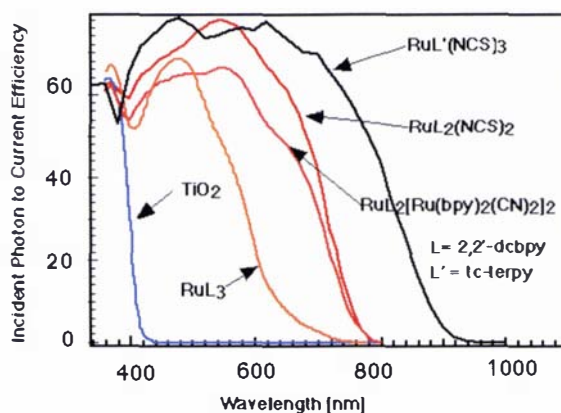
Figure 5-4. Photocurrent action spectra of Ru dyes (AM1.5) (Reproduced from Grätzel et al.).[156]

The IPCE value is the ratio of the observed photocurrent divided by the incident photon flux, uncorrected for transmittance, reflective and other losses from optical excitation

through the conducting glass electrode. Hence, IPCE values of around 80% represent near-quantitative conversion of sunlight energy into electrical energy. The curves represent the increased performance of the cells with an evolving series of photosensitisers. The bis(carboxy)bipyridine (dcbpy) complex, a red dye often known as N3 (Ru$_{red}$ **118**) is used as a standard in many laboratories. Currently the best spectral response is obtained with the triscarboxyterpyridine Ru-complex, [Ru(tcterpy)(NCS)$_3$] (often referred to as the "black" dye **119**).[150] As its absorption covers the entire visible range, the dye appears nearly black.
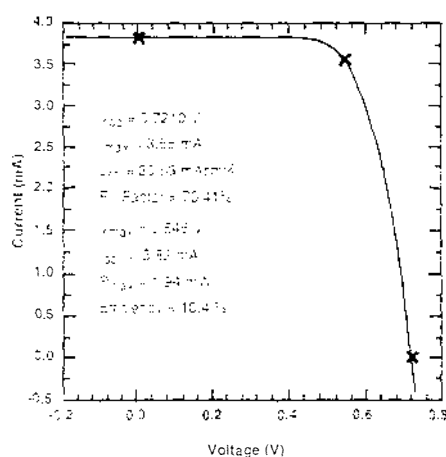
Figure 5-5. Photocurrent-voltage plot for "black" dye from NREL calibration laboratory (AM1.5) (Reproduced from Grätzel et al.)[9].

The photocurrent-voltage plot for the "black" dye under AM1.5 illumination is shown in Figure 5-5. The 10.4% efficiency quoted is termed the normalised AM1.5 efficiency "η", not to be confused with the IPCE monochromatic efficiency values. Caution must be taken in comparing literature IPCE values as monochromatic versus normalised AM1.5 values must be considered. The fill factor (FF) is the ratio of maximum output of the photovoltaic device, under reference conditions, to the product of V_{oc} and I_{sc} under the same conditions. The IPCE value can be considered as the effective quantum yield of the device and it is the product of three important factors:

- Light harvesting efficiency LHE (depends on the spectral and photophysical properties of the dye).

- The charge injection yield (depends on the excited state redox potential and the lifetime).

- The charge collection efficiency (depends on the structure and morphology of the TiO$_2$ layer).

It should be noted that the IPCE values in excess of 85% obtained in the 400-550 nm region correspond to the absorption maximum of the Ru-complexes. Near unity values of IPCE suggest that, in the present case, the charge injection and charge collection steps operate at optimal efficiencies.

5.1.2 Tetrapyrrolic Macrocycles in the PEC Cell

Porphyrin Complexes on TiO$_2$, ZnO, SnO$_2$ and NiO

Various synthetic TAP derivatives have been applied to TiO$_2$ surfaces for photosensitisation studies using physisorption processes. Khairutdinov et al. carried out laser-induced light attenuation studies on aggregates of the free-base and zinc porphyrin derivatives **M-1** (Figure 5-6, M = 2H, Zn) in solution and on TiO$_2$. Their studies show that laser excitation of the aggregates leads to electron transfer from an excited porphyrin to the TiO$_2$.[157] An earlier study by Tsubomura et. al. covered a wide range of MTPP **1** derivatives (Figure 5-6, M = 2H, Zn, Mg, Cd, Pb, Cu, Ni) on ZnO. Quantum efficiency measurements of the photocurrents gave the following decreasing order, Mg>Cd≈Zn>Pb>Cu≈2H>Ni.[158]

M-1
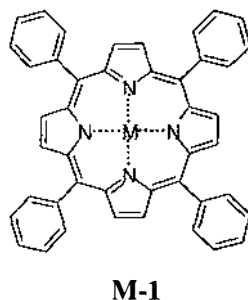
Figure 5-6. Tetraphenylporphyrins **M-1** (MTPP).

The most common porphyrins used for the photosensitization of wide-band-gap SCs like NiO, ZnO and TiO$_2$, have been free-base and zinc derivatives of TCP **8** (Figure 5-7). These porphyrins exhibit long-lived (>1 ns) π* singlet excited states and only

weak singlet/triplet mixing. In 1987, Grätzel et al. reported efficient charge injection from the excited state of ZnTCP **Zn-8** into the conduction band of TiO$_2$ (IPCE$_{Soret}$ = 42%, IPCE$_{Q\,band}$ = 8 - 10%) however no AM1.5 normalised cell efficiency was given.[159] Fox et al. also photosensitised TiO$_2$ with ZnTCP **Zn-8** (IPCE$_{Soret}$ = 9.5%, I$_{sc}$ ≈ 2.5 µA cm^{-2}) again no AM1.5 normalised cell efficiency was given.[160]

M = 2H, Zn

8
Zn-8
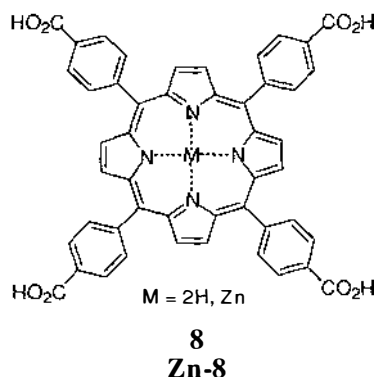
Figure 5-7. Tetrakis(4-carboxyphenyl)porphyrins **M-8** (MTCP)

In 1996, Goossens and Boschloo photosensitised TiO$_2$ with ZnTCP **Zn-8**, giving a low overall solar light energy conversion efficiency (η) of 1.1% (IPCE$_{Soret}$ ≈ 40%, IPCE$_{Q\text{-band}}$ ≈ 10-16%, V$_{oc}$ = 0.36 V, I$_{sc}$ = 0.85 mA cm^{-2}).[161] A more recent and promising result is that from Wamser and Cherian whose TCP **8** based TiO$_2$ photovoltaic cells gave good solar-energy conversion efficiencies under AM1.5 conditions (η of 3.5% and fill factor of 62%, IPCE$_{Soret}$ = 55%, IPCE$_{Q\text{-band}}$ = 25-45%, V$_{oc}$ = 485 mV, I$_{sc}$ = 6 mA cm^{-2}).[162] To date this is the best-reported value for a porphyrin PEC, and was achieved using deoxycholic acid (DCA) as a co-adsorbate. The use of TCP **8** on p-type NiO electrodes was investigated by Lindquist et al. yielding disappointing results (η of 0.0033% and fill factor of 28.5%, IPCE$_{Soret}$ = 0.24%, V$_{oc}$ = 98.5 mV, I$_{sc}$ = 79 µA cm^{-2}).[163] Recently Durrant et al. published a paper comparing the electron injection and charge recombination of Ru$_{red}$ **118**, free-base TCP **8** and Zn(II) TCP **Zn-8**, all on TiO$_2$.[164] Their studies show that these three dyes have almost indistinguishable electron injection and recombination kinetics. They state that the high efficiency reported for Ru$_{red}$ **118** dye probably originates from differences in the rate of electron transfer to the dye cation from the iodide redox-couple used in these devices. It is also possible that the lower efficiency of porphyrin sensitisers results from the increased probability of exciton annihilation from close porphyrin proximity. At high dye coverage, dipole/dipole

interactions are expected to allow rapid migration of the excited state between neighbouring dyes, increasing the probability of exciton annihilation.

The utility of natural porphyrins, zinc and antimony metallo-uroporphyrins were investigated as photosensitisers by Kalyanasundaram et al. (Figure 5-8).[63] They obtained monochromatic IPCE values of 4.5% at 540 nm for the zinc-uroporphyrin **Zn-120** (Q(1,0) band of **Zn-120**).

M = Zn^{II}, Sb^{V} (O, Cl)
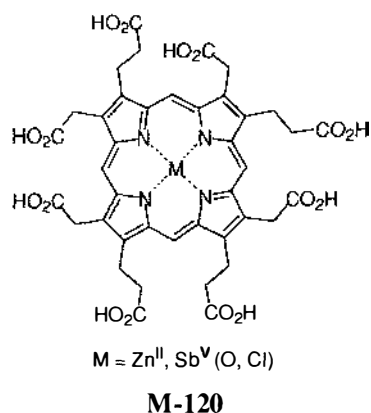
M-120

Figure 5-8. Uroporphyrin **M-120**.[63]

Grätzel et al. have also studied a number of natural metallo chlorophyll derivatives and related natural metallo mesoporphyrins for the photosensitisation of TiO$_2$ solar cells.[61,62] These cells showed efficient sensitisation of TiO$_2$, with near unity quantum efficiency of charge injection for Soret peak illumination of Cu-mesoporphyrin **IX** (Figure 5-9). The overall AM1.5 solar light to energy efficiency of the cell was 2.6%. They concluded that free carboxyl groups are important for adsorption, however conjugation of the carboxyl groups to the π electron system of the chromophore is not necessary for efficient electron transfer with a linker of this length. The study also revealed a strong dependence on the type of solvent and type of co-adsorbates.
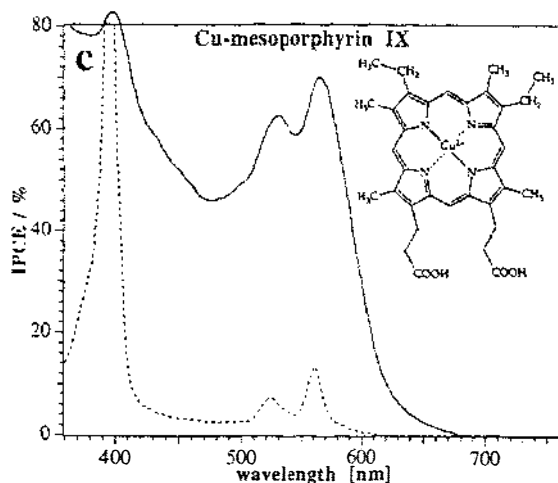
Figure 5-9. Photocurrent action spectrum of TiO_2 electrode sensitised with Cu mesoporphyrin **IX** (solid line) and absorption spectrum in solution (THF + 20 mM deoxycholic acid, dashed line), (Reproduced from Grätzel et al.).[61,62]

Malinka et al. were successful in the production of hydrogen from water by visible light using porphyrin sensitised platinized TiO_2 electrode (Figure 5-10).[165] They used a variety of methylpyridinium- and benzo crown ether-functionalised zinc porphyrins as the sensitisers. Their results showed that hydrogen production was dependent on the concentrations of porphyrins, platinum and the electron donor. They also determined that the photo-stability of zinc porphyrins is increased by attachment to the SC surface.
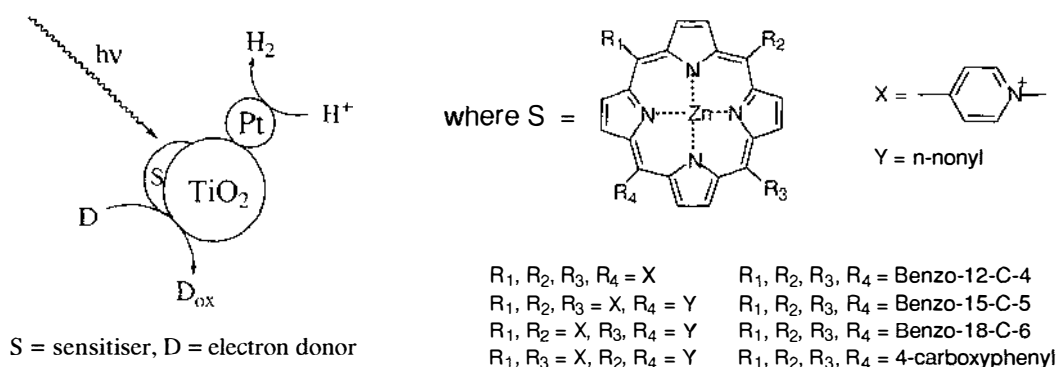
Figure 5-10. The catalytic H_2 production system of Malinka et al.[165]

Schaafsma constructed an organic solar cell made up of an ultrathin layer of a single type of porphyrin or a double layer of an electron donating and accepting (D/A) porphyrin on TiO_2 (Figure 5-11).[166] These porphyrin layers were deposited by a variety of techniques, i.e. modified electro-polymerisation, Langmuir-Blodgett techniques and adsorption from solution. No quantifiable results were presented.
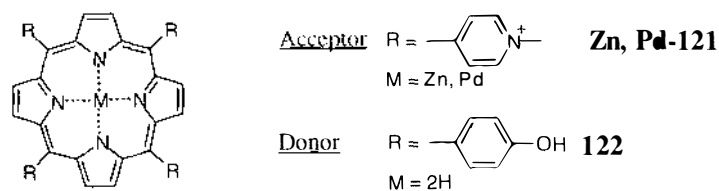
Figure 5-11. Donor and acceptor porphyrins **M-121/122**.[166]

Solid state p-n type organic solar cells have also been constructed on TiO_2 by first depositing a spin coated layer of free-base TOPP **123** acting as an intrinsic SC followed by a second layer of ZnTCP **Zn-8** acting as a p-type SC.[10] The circuit is completed by a Hg counter electrode. TOPP and ZnTCP have HOMO-LUMO gaps of 2.0 and 1.9 eV, respectively (Figure 5-12). The LUMO position of ZnTCP is located about 0.4 eV above that of TOPP making an organic based heterostructure p-i-n solar cell possible. The LUMO positions of these porphyrins are such that unidirectional energy transfer from ZnTCP to TOPP occurs (fill factor of 51%, $IPCE_{440\ nm}$ = 3%, V_{oc} = 650 V, I_{sc} = 85 $\mu A\ cm^{-2}$).
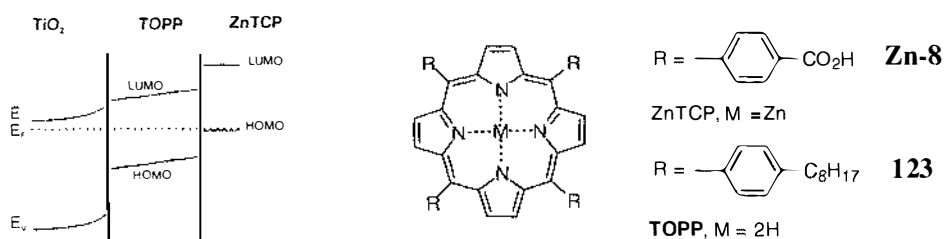
Figure 5-12. HOMO and LUMO bandgaps of TOPP and ZnTCP relative to TiO_2.[10]

Recently, the sensitisation of TiO_2 and SnO_2 by porphyrin dyad systems has appeared in the literature. The first by Koehorst et al. consists of a cell constructed from Zn/free-base diporphyrin heterodimers on TiO_2 (Figure 5-13).[69]
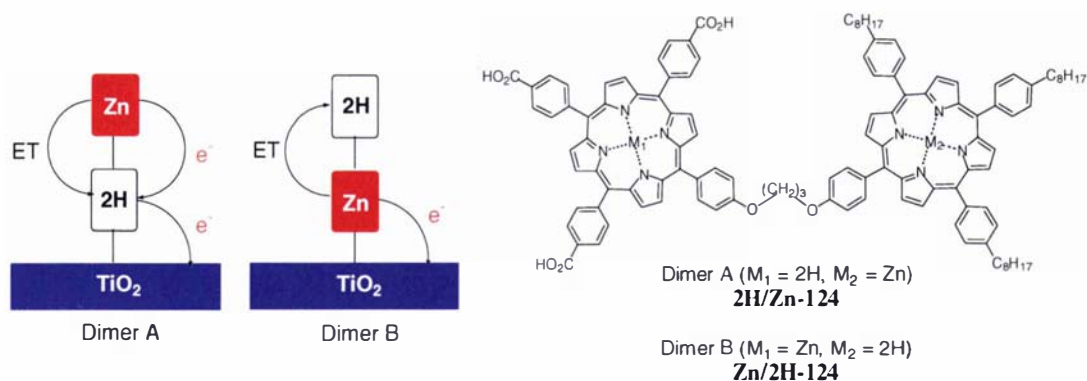
Figure 5-13. Heterodimers **A** and **B** on TiO_2.[69]

Surprisingly both diporphyrins give similar monochromatic IPCE results ($IPCE_{430\,nm}$ = 3%, I_{sc} = 10 mA cm^{-2}). The energy transfer and electron transfer in monolayers of diporphyrin **A** on TiO_2 are shown to be *consecutive* whereas in monolayers of diporphyrin **B** both processes are *competitive* (Figure 5-14).
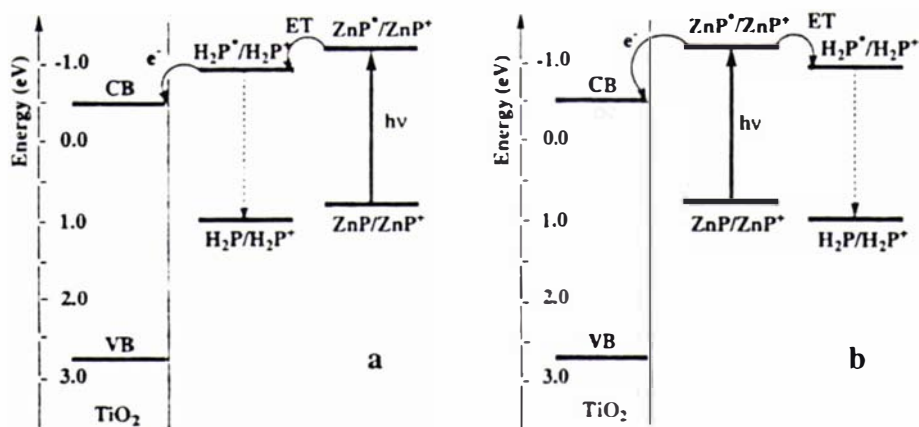
Figure 5-14. Energy transfer in diporphyrin **A** (a) and **B** (b), (Reproduced from Koehorst et al.).[69].

It is suggested that similar IPCE values are the result of a favourable light collecting antennae effect by such diporphyrins.

The photosensitization of SnO_2 with a Zn/free-base diporphyrin dyad P_{Zn}-**P** and monomers **P** and P_{Zn} has been investigated by Sereno et al. (Figure 5-15).[70,71]

P$_{Zn}$-P

125

P, P$_{Zn}$

M-126
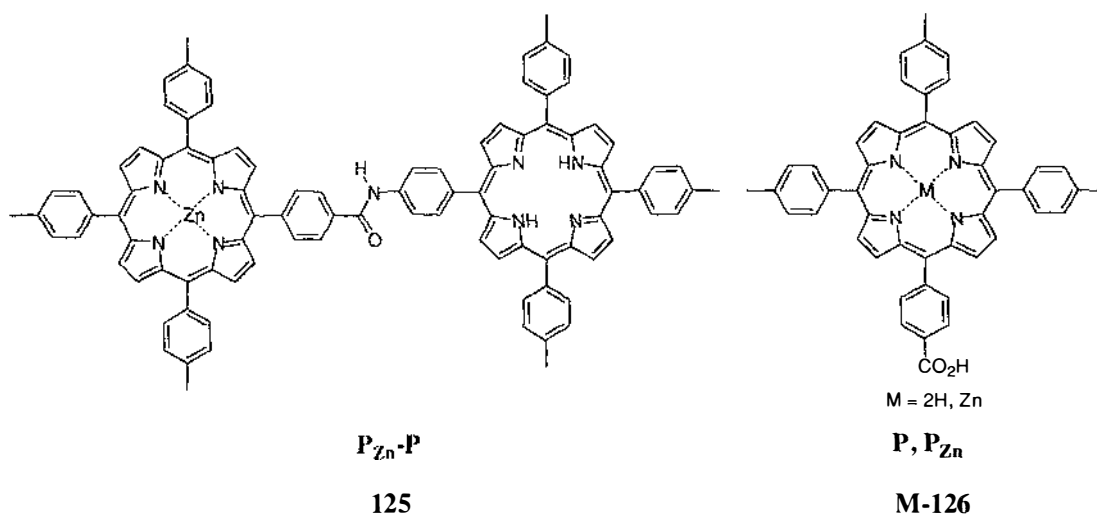
Figure 5-15. Zn/free-base diporphyrin dyad **P$_{Zn}$-P** and monomers **P** and **P$_{Zn}$**.[70,71]

Maximum IPCE values of ≈ 6%, 32% and 11% were obtained at the Soret band of ITO/SnO$_2$/**P$_{Zn}$**, ITO/SnO$_2$/**P** and ITO/SnO$_2$/**P$_{Zn}$-P** respectively. The photocurrent efficiency of the dyad **P$_{Zn}$-P** is low compared to **P**. This was to be expected as there is no control over which porphyrin of the dyad is bound to the surface.

Phthalocyanine Complexes on TiO$_2$

Phthalocyanines (Pc) **M-127** are related to porphyrins, having similar physical and chemical properties (Figure 5-16). Their electronic properties differ in having intense adsorptions that extend into the near-IR region (see Figure 5-21 for an example).

Pc
M-127
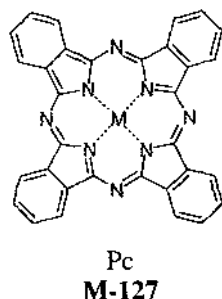
Figure 5-16. Metallophthalocyanine.

In 1980, Bard et al. reported spectral sensitisation of TiO$_2$ and other wide-band gap SC surfaces with a range of metallophthalocyanines (M = Al, 2H, Cu, Co, Zn, Mg, Fe).[167]

Single crystal photosensitization studies have also been carried out on TiO_2 using a vacuum-deposited titanylphthalocyanine (TiOPc) layer.[168] More recently Gregg has developed a solid state TiO_2 organic solar cell using ZnPc and perylene bis(phenethylimide) (PPEI), (I_{sc} = 1.5 mA cm^{-2}, V_{oc} = 447 mV, FF = 33% under simulated AM2 conditions) (Figure 5-17).[169] An average quantum yield of 18% is claimed under 1 sun.
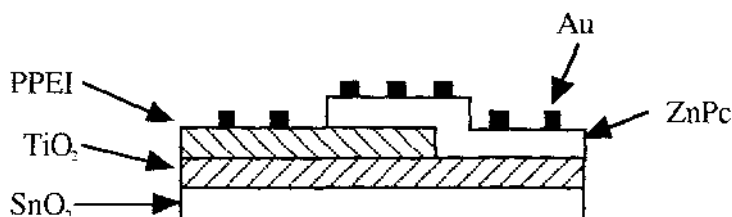
Figure 5-17. Solid state Pc based TiO_2 solar cell of Gregg.[169]

In this cell, the phthalocyanine acts as a p-type SC, forming a p-n junction with the TiO_2. Another variation on this is an $ITO/TiO_2/ZnPc/Au$ structured cell developed by Kajihara et al. running at a low AM1.5 solar light to energy efficiency 0.014% (50 µW cm^{-2}, I_{sc} = 148 µA cm^{-2}, V_{oc} = 338 mV, FF = 29%, Figure 5-18).[170]
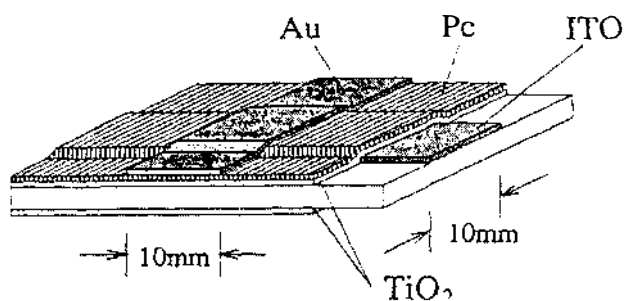
Figure 5-18. Solid state $ITO/TiO_2/ZnPc/Au$ cell (Reproduced from Kajihara et al).[170]

The use of copper phthalocyanine as an efficient dopant in organic solar cells is also currently being explored.[171]

To date, the most efficient phthalocyanine-based nanocrystalline PEC is that of Grätzel et al.[65] Efficient photosensitization in the near-IR region (IPCE$_{660\,nm}$ > 60%, I_{sc} ≈ 10 mA cm^{-2} under AM1.5 illumination) was achieved by grafting the ruthenium phthalocyanine **128** to the TiO_2 surface through axially coordinated 3,5-dicarboxypyridine ligands and

the co-use of a bile acid additive (Figure 5-19).
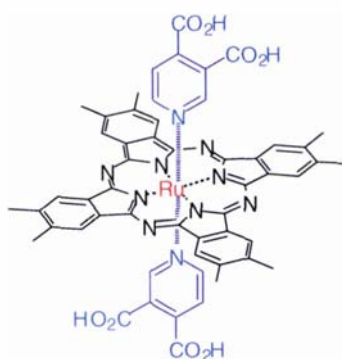
128

Figure 5-19. Bis(3,5-dicarboxypyridine)(1,4,8,11,15,18,22,25-octamethylphthalocyaninato)ruthenium(II) **128**.[68]

This high efficiency may be a direct result of both hindered aggregation of the macrocycle (resulting in less quenching of the excited state of the Pc) and the mode of attachment through axial ligands.

Mixed Porphyrin and Phthalocyanine Complexes on TiO$_2$

The combination of both porphyrins and Pcs together on a TiO$_2$ surface permits the combining their complementary spectral properties, offering the possibility of increased spectral response. Recently Lu et al. cosensitised TiO$_2$ with zinc tetrasulfonylphenyl-porphyrin (ZnTsPP) **Zn-129** and gallium tetrasulfonylphthalocyanine (GaTsPc) **Ga-130** (Figure 5-20).[34,172,173]

ZnTsPP
Zn-129
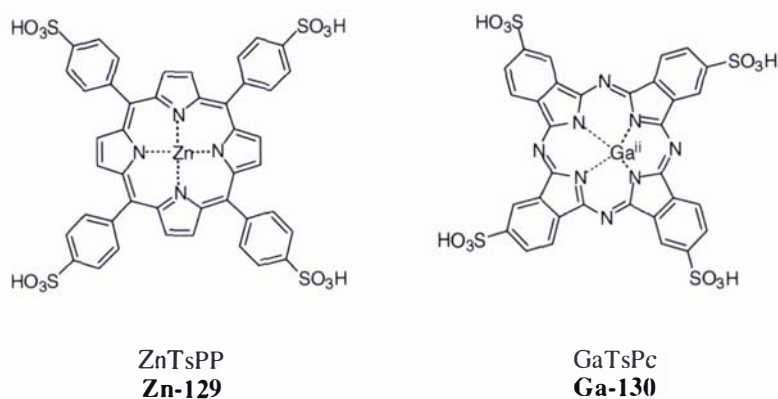
GaTsPc
Ga-130

Figure 5-20. ZnTsPP **Zn-129** and GaTsPc **Ga-130** cosensitizers.[34,172,173]

The cosensitization resulted in a dramatic enhancement in the photoresponse in the long-wavelength region (640-760 nm), with an $IPCE_{700\ nm}$ value of 32% at about 0.14 sun illumination (ca. with about 20 % and 15% for GaTsPc and ZnTsPP respectively). At about 1/3 sun the cell produced an I_{sc} of 771 μA cm^{-2}. However overall cell efficiency under standard AM1.5 illumination has yet to be quantified. Figure 5-21 displays the absorption spectrum resulting from cosensitising TiO$_2$ with GaTsPc and ZnTsPP, relative to the individual chromophores and a bare TiO$_2$ electrode.
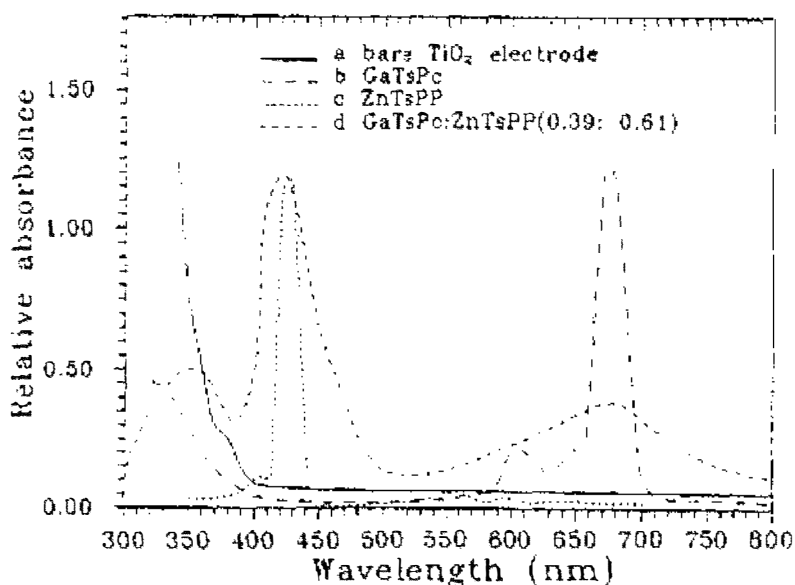
Figure 5-21. Absorption spectra of, a) bare TiO$_2$ electrode, b) GaTsPc in DMSO, c) ZnTsPP in DMSO, d) co-sensitised TiO$_2$ electrode, (Reproduced from Lu et al.).[34,172,173]

5.2 Development and Fabrication of Equipment and Testing Protocols for Reliable Dye Screening

5.2.1 Introduction

The construction of Grätzel cells containing dye-doped TiO_2 is by no means straightforward. The primary problem is the sealing of the liquid electrolyte between the two glass electrodes. In addition, there are many variables difficult to control in the construction of the cells such as:

- ▼ Thickness and quality of TiO_2
- ▼ Control of gap and electrolyte volume between electrodes
- ▼ Cell operating temperature
- ▼ Electrolyte compositions etc.

The effects of some of these variables can be controlled or limited by appropriate design of equipment, cell construction and testing procedures, although the control of some variables like TiO_2 quality was sometimes out of our control. To give reproducible results, significant attention needs to be applied to cell design, construction and materials, as well as testing protocols.

Since quantitative cell measurements could be made in other laboratories equipped to do so, we set out to establish equipment and procedures to develop a semi-quantitative dye screening protocol, that would provide enough information to allow us to identify promising dyes. The whole testing regime needed to be simple and allow many dye samples to be quickly tested.

5.2.2 Design and Fabrication of Test Equipment

The main design requirements of the test equipment were:

▼ A light source whose output resembled the solar spectrum.

▼ A sensor to calibrate the light source between cell tests.

▼ Reliable cell construction and cell holder to hold the cell while testing.

Given that the development of equipment, construction, and dye screening procedures was an evolving process that is described in detail in the following sections, the experimental section in Chapter 7 (section 7.5) contains a summary of the refined final testing protocol.

Light Source

The light source was fabricated[174] to my own design based on an old microscope base with an adjustable X-Y-Z stage (Figure 5-22). The optics were replaced with an adjustable brass tube containing a 12V/50W halogen bulb.[175]
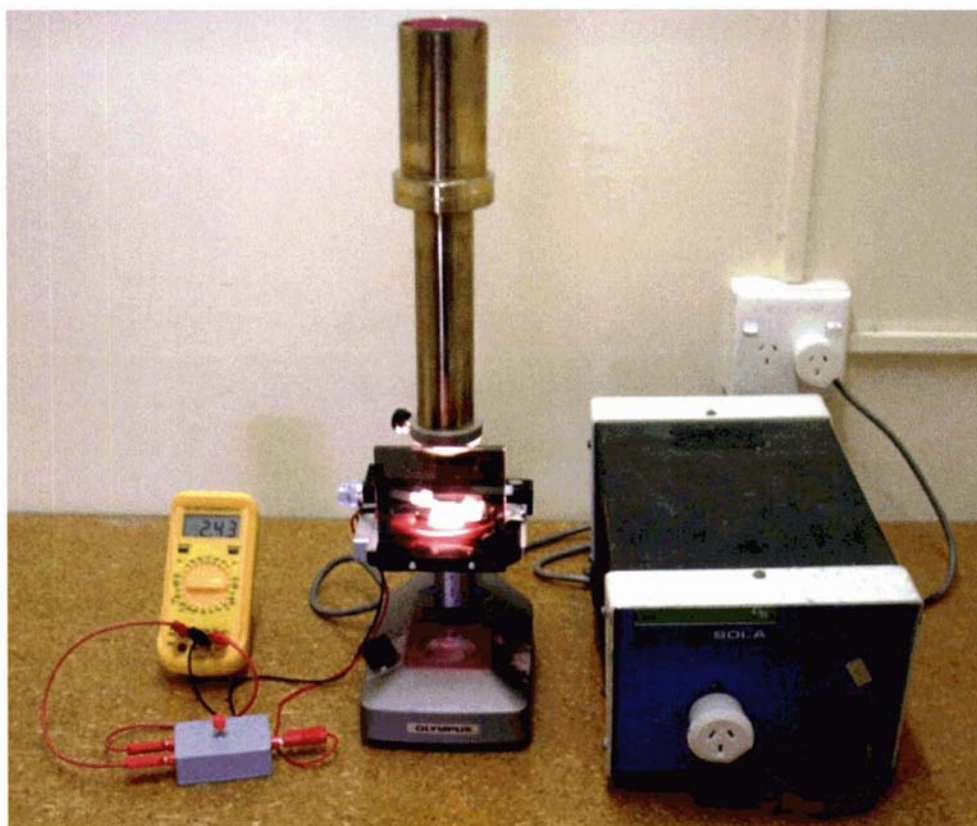
Figure 5-22. Light source set-up for solar cell testing.

Ventilation holes were placed around the lamp to minimise overheating of the bulb. A darkened Perspex glare shield was also fitted on the X-Y-Z stage. After adjusting the tube length to give the desired light intensity, fine adjustments were carried out using the X-Y-Z stage.
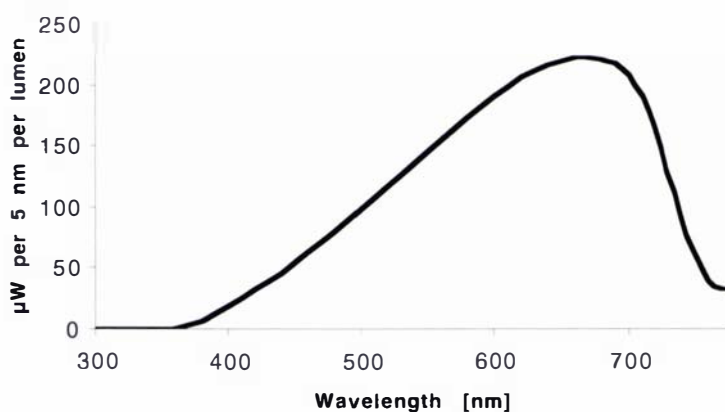
Figure 5-23. Typical irradiance of Philips MASTERline Plus 12V/50W halogen bulb at 1 m.[176]

The typical emission spectrum for this halogen bulb is shown in Figure 5-23.[176] This lamp efficiently covers the visible electromagnetic spectrum without generating too much IR, as is common for normal incandescent sources. In order to give a stable light source a 230V mains power conditioner was essential.

Standardisation Sensors
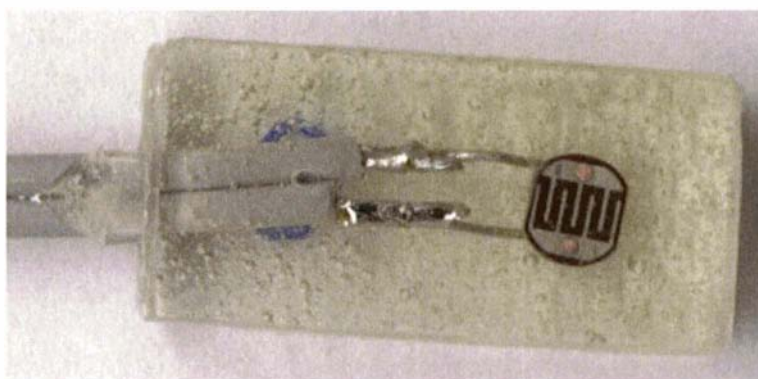
Figure 5-24. LDR1.

In order to standardise the intensity of the light source, two types of light sensors were fabricated. The first, LDR1 (Figure 5-24) was based on a light dependent resistor (LDR) having a peak spectral response of 560-620 nm. This sensor required a long thermal stabilisation period under illumination, so a second type was investigated. The second sensor DPT1 (Figure 5-25) was fabricated from a silicon Darlington phototransistor (DPT). Leads were attached to the 'collector' and 'base' terminals only and voltage readings taken across a 10 kΩ resistor.

Figure 5-25. DPT1.

These sensors were fixed to a small glass window and encased in epoxy resin. Fitted inside a dummy cell holder, they were used to standardise the light source before each cell was tested. DPT1 was the primary sensor used through out this testing. Initially the light source was adjusted to give a sensor output of 124 mV. However, in order to obtain higher solar cell currents (I_{sc}) the light intensity was later increased such that the output of DPT1 was adjusted to 130 mV. A second set of sensors (LDR2 and DPT2) were fabricated and calibrated for use as backups to LDR1 and DPT1.

Cell Construction and Holders

The initial attempts at dye evaluation were carried out in this laboratory by Scott and Evans[177], and involved a cell set-up based on the original Grätzel cell introduced in Section 5.1.1. This consisted of a dye-doped TiO_2-coated glass electrode, backed with a platinised glass counter electrode. The two glass electrodes were held together in a holder by applying pressure from a single screw and the electrolyte was then fed

between the two glass plates by capillary action. However, this design gave no control over the pressure between the two electrodes, and therefore offered little control over the cell width and electrolyte volume. In addition, only poor quality platinised electrodes could be fabricated. As a result, this cell design provided variable results, and so a new cell and cell holder was developed for this work.
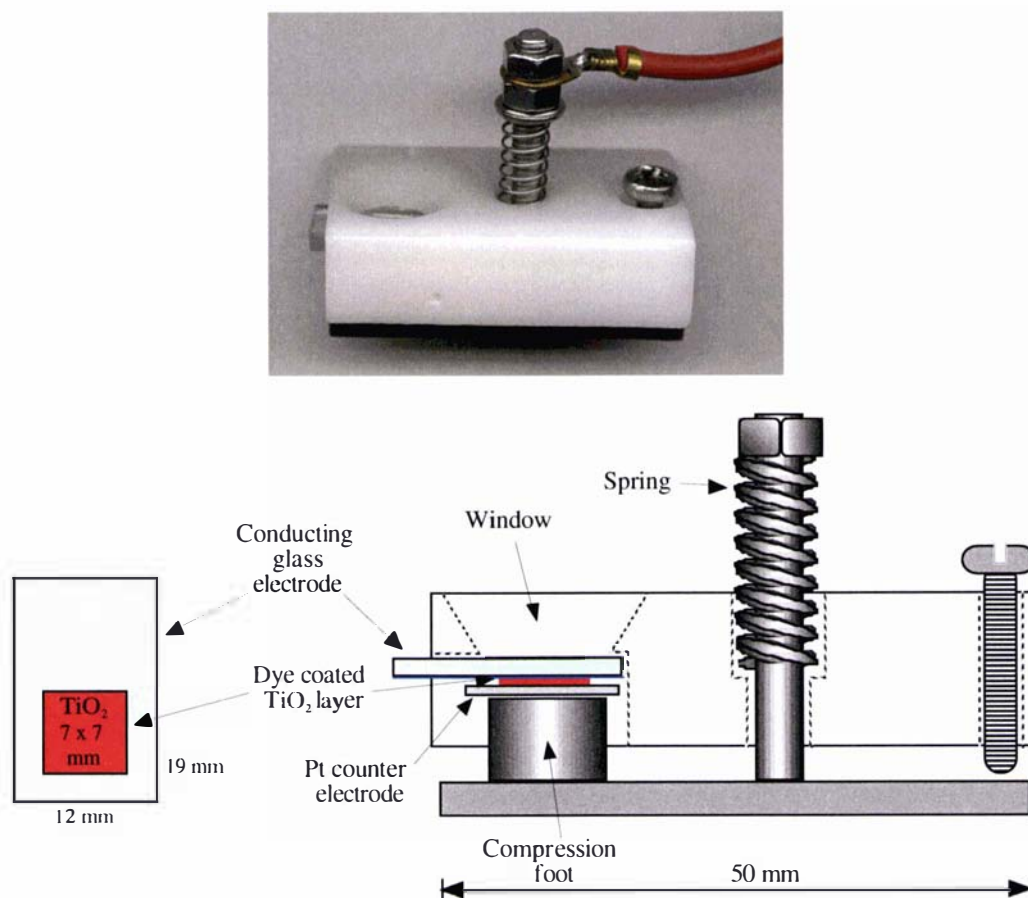
Figure 5-26. Cell holder **CH1**.

The initial cell holder **CH1** was fabricated from plastic and stainless steel (Figure 5-26).[174] This cell holder was designed to hold the TiO_2 plate against a solid platinum counter electrode using a spring-loaded base. The use of a solid Pt plate eliminated surface variations associated with non-homogeneous coated platinised glass counter electrodes. The use of **CH1** with earlier electrode materials proved to be only partially reliable, although consistent results were often obtained. It was noted that when the calibration sensors were inserted in place of the glass cell, that the positioning of the cell holder squarely under the light source was critical in obtaining reproducible light

intensities. This was attributed to shadowing and reflection interference associated with the depth and shape of the window slit cut through the cell holder (Figure 5-26).

So, in order to reduce light obstruction through the window slit, a second variation "**CH2**", was fabricated using some of the existing **CH1** parts (Figure 5-27). This second set-up used a thinner top made of stainless steel, and also accommodated a new glass electrode size to allow insertion of the TiO_2 plates into a standard UV-vis cuvette for monitoring of dye adsorption. Initially, silicon O-rings and teflon washers were used to define the area of TiO_2 in the PEC, and contain the electrolyte between the TiO_2 and counter electrode. This was not satisfactory due to leakage and difficulties in eliminating trapped air bubbles.
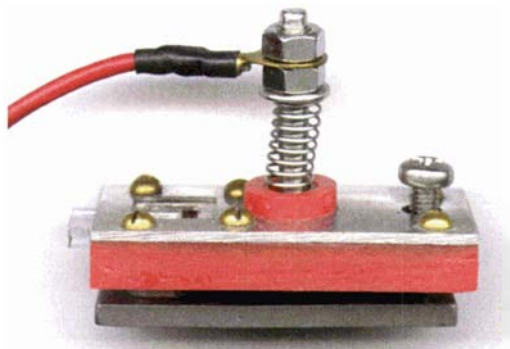
Figure 5-27. Cell holder **CH2**.

The most satisfactory way of controlling the TiO_2 electrode area was by scraping the TiO_2 layer to a specific size. After clamping the Pt counter electrode, the electrolyte was allowed to enter between the two surfaces by capillary action. **CH2** gave good results with the initial samples of TiO_2 coated glass supplied. However, with new supplies of TiO_2-coated glass plates, a large reproducibility problem was again encountered. Apart from a large drop in performance of the cells being tested (TiO_2 quality varied and is discussed fully in Section 5.2.4), there was evidence of short-circuiting between the counter electrode and exposed ITO surface of the conducting glass (where the TiO_2 had been removed). This was attributed to a combination of a thinner TiO_2 layer, and the pressure and position that the Pt counter electrode was held up against the glass TiO_2 electrode by the compression foot. To eliminate the "edge" effects a further improved cell design was needed.
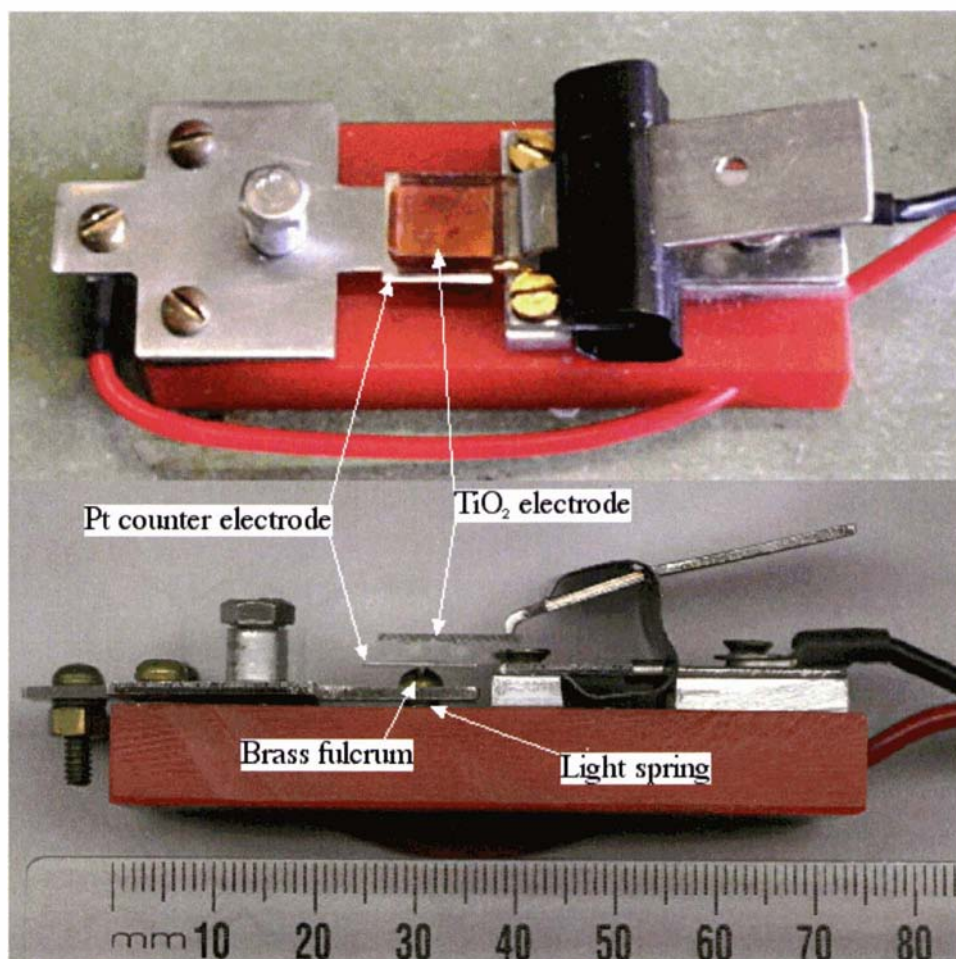
Figure 5-28. Cell holder **CH3**.

A completely new cell holder, **CH3** was designed and fabricated (Figure 5-28). By redesigning the cell holder, the two basic problems with the previous cell holder were overcome; the pressure and means of holding the counter electrode, and the "edge" effects. Removing "edge" effects was achieved by cutting the TiO_2-coated glass plates (10 x 15 mm), then scraping back one edge for an electrode contact point (ca. 10 x 10 mm TiO_2 square), leaving the TiO_2 layer extending fully to 3 edges. An example of this can be seen in Figure 5-29 as a porphyrin dye-coated electrode.

xposed ITO surface   ye coated TiO$_2$
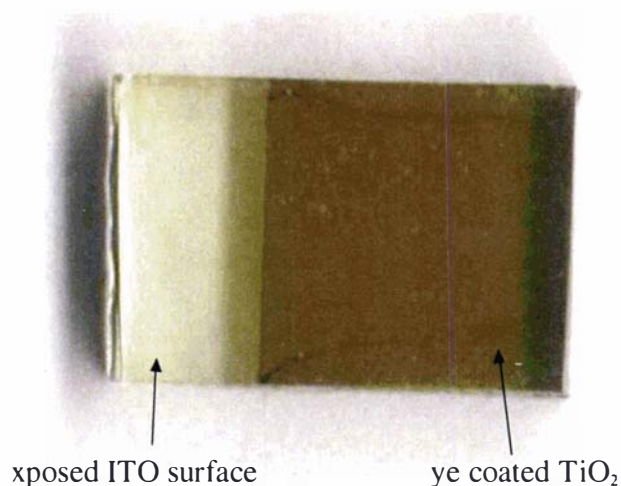
Figure 5-29. Porphyrin dye coated TiO$_2$ electrode.

After testing of the cell, the area of the TiO$_2$ was accurately measured with vernier calipers allowing conversion of I_{sc} values to mA cm^{-2}. The second major improvement came from using a very light spring-loaded platinum counter electrode fulcrum support.[178] The fulcrum point was made via a small brass screw and ensured that the pressure of the Pt counter electrode was spread equally over the entire TiO$_2$ surface, while also acting as an electrical contact for the Pt counter electrode. The glass TiO$_2$ electrode was held in place with a modified bulldog clip (using stainless steel clamps) to hold the glass plate and make electrical contact with the conducting ITO layer. With this mounted on a plastic base, the new cell holder **CH3** gave excellent reproducibility.

5.2.3   Solar Cell Testing Procedure

This section describes the basic testing procedure required to produce reliable and reproducible qualitative results. A more detailed account of the final testing procedure and protocol is given in the experimental section 7.5 of Chapter 7.

The basic procedure involved:

1. TiO$_2$ electrode preparation (cutting of TiO$_2$-coated glass electrodes to appropriate size and pre-treatment).

2. Dye adsorption (firing of TiO_2-coated plates followed by soaking in dye solution). The TiO_2-coated glass as received first required firing prior to dye adsorption.

3. Assembly of dyed TiO_2 electrode and Pt counter electrode in cell holder.

4. Electrolyte addition between electrodes by capillary action.

5. Calibration check of light source.

6. Data Acquisition.

Figure 5-30 shows the final illuminated cell holder **CH3** set-up in the testing apparatus.
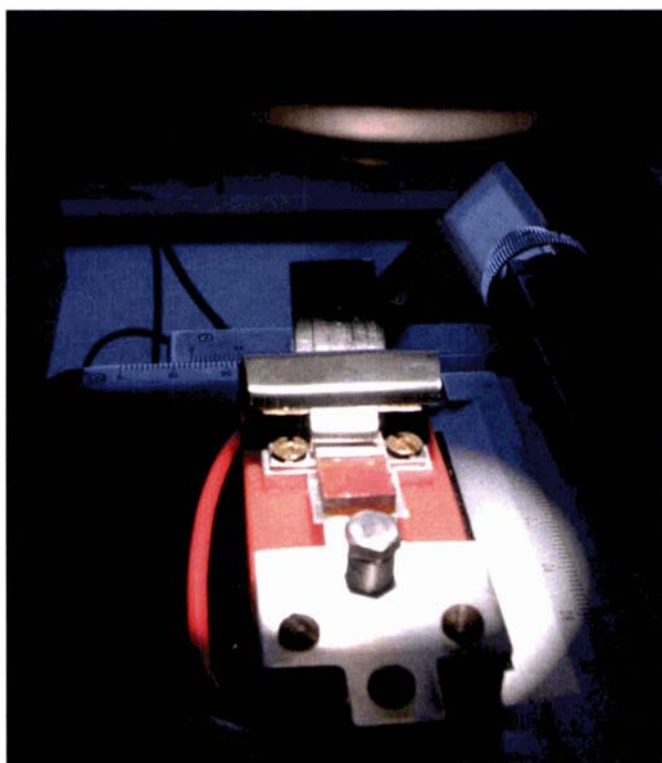
Figure 5-30. Illuminated cell holder **CH3**.

Attempts to follow dye adsorption by UV-vis in a sealed UV-vis cuvette were not very successful. Most significant adsorption appeared to occur in the first 5 to 10 minutes. This did not allow time to set up the instrument to collect absorption readings. Deep colouration of the TiO_2 surface could be seen almost immediately. All adsorptions were carried out overnight (12-20 hours) prior to testing.

5.2.4 TiO$_2$ Electrode Inconsistencies

During the course of testing cells, different batches of TiO$_2$ (PA-PD) were used as supplied by Sustainable Technologies Australia Ltd (STA), NSW, Australia. STA is licensed to produce the Grätzel cells. Variations in the quality and thickness of TiO$_2$ layers from various batches soon became evident, and were evaluated.

Variations in TiO$_2$ Quality

During the initial evaluation of the variables affecting binding of porphyrins to TiO$_2$ cells, only a limited number of cells could be constructed from any one batch of supplied TiO$_2$-coated glass. It was found that every batch of new glass had to be calibrated with a standard dye, as there was no consistency in quality. The differences in TiO$_2$ layers between batches was evident visually (ranging from almost clear to opaque in colour). The first and second batches (PA & PB) supplied gave consistent Isc results and showed good binding of the Ru$_{red}$ and ZnTXP-=-PhCO$_2$H **Zn-15** dye, however the third and fourth batches (PC & PD) initially showed only weak binding of **Zn-15**.

The amount of **Zn-15** dye binding to the electrodes of the same area, was quantified using UV-vis analysis. This was carried out on a series of PC TiO$_2$ electrodes treated under different conditions, comparing to a standard older PB TiO$_2$ electrode. . The dye was absorbed onto the fired TiO$_2$ and the excess dye rinsed off the electrode. The bound dye was then removed from the electrode using Et$_3$N, and the resulting solutions made up to a standard volume, and the UV-vis absorption spectra measured.

Table 5-1. TiO$_2$ Pre-treatment versus dye **Zn-15** adsorption.

#	TiO$_2$ Plate	Treatment	UV-vis Absorbance (λ_{max})
1	PB	None	0.246
2	PC	None	0.111
3	PC	H$_2$O, 2 hr	0.192
4	PC	Et$_3$N (0.029 M), 2 hr	0.192
5	PC	HCl (0.10 M), 2 hr	0.173

As can be seen in Table 5-1, there was a significant difference in the amounts of **Zn-15** adsorbed between the two different batches of TiO_2-coated glass, PB and PC (Entries 1 and 2). In an attempt to correct this, various plate pre-treatments were tried prior to firing and dye adsorption. The result given in Table 5-1 (Entries 3-5) clearly show that either water washing or treatment with Et_3N of the PC plates gave a significant increase in dye binding to that of the untreated PC plate. The treatment of batch PC with HCl also showed significant increase in dye adsorbed. Nonetheless, the PB plate bound significantly more dye than the best PC plates; this may have been due to what appeared visually to be a thinner TiO_2 layer on the PC plates. This is discussed in the following section.

In conclusion, the nature of the PC electrode surface was different from that of the PB surface. The reason for this difference was not investigated. It appears that washing the TiO_2 surface with Mill-Q water is sufficient to restore significant dye binding suggesting surface contamination by a water-soluble species, possibly a salt. All cells made from the PC and PD batches of TiO_2 plates were subsequently treated in this manner.

Non-Uniformity of TiO_2 Thickness

Typically PA and PB TiO_2 electrodes gave consistent I_{sc} cell results for identical dyed cells, when made from the same batch of TiO_2-coated glass. However, the PC and PD electrodes did not. Variations in the I_{sc} values of identical PC and PD dye-coated cells cut from the same batch of TiO_2 were evident, and could not be associated with the physical set-up of the cell. Therefore, it was assumed that varying TiO_2 thickness was a factor. Several methods were considered to quantify the variability in TiO_2 thickness:

- Directly by STM or AFM
- Indirectly:
    - Removal of TiO_2 from a series of known areas and comparison of the weights.
    - Assuming binding sites per volume of TiO_2 are the same then the amount of dye adsorbed is proportional to the volume of TiO_2 on the electrode.

Therefore, by desorbing the dye from known areas the amount can be quantified and compared by spectroscopic methods.

Since neither STM or AFM equipment was readily accessible, the indirect approaches were explored. Removal and weighing of the TiO_2 layer was attempted, but due to the small quantity of TiO_2 present on the electrode surface (0.49 cm^2) the error introduced from the best available balances was too large (> 10%).

The second indirect method was investigated after testing a series of cells containing Grätzel's strongly binding Ru_{red} **118** dye, to see if the differences in I_{sc} readings was reflected in the amount of dye adsorbed onto the electrodes. UV-vis analysis was carried out on two TiO_2 Ru_{red} PD electrodes that showed a large difference in I_{sc} values. The strongest absorption band (308 nm) was measured following desorption of the Ru_{red} dye with methanolic NaOH (0.1 M). The following results were obtained (Table 5-2).

Table 5-2. TiO_2 Thickness variations.

Cell # (Plate)	I_{sc} (mA cm^{-2})	V_{oc} (mV)	Absorbance (A cm^{-2} TiO_2)
203 (PD1)	4.54	580	0.475
207 (PD1)	5.21	590	0.551

The increase in I_{sc} between cell 203 and 207 is 13%, which correlates favourably to an increase of 14% in the absorption value for the desorbed dye between the respective cells. Both TiO_2 plates were cut from the same larger plate and treated in the same manner throughout. It can therefore be assumed that the differences in I_{sc} and absorption values result from a difference in quantity of TiO_2 on those plates in a given area (i.e. thickness). The TiO_2-coated glass is prepared by STA using a screen-printing process. This could provide a variation in TiO_2 thickness, particularly near the glass edges. In addition, variations in float glass thickness will affect TiO_2 thickness. This therefore highlights a large error that is introduced by using plates prepared on normal float glass utilising screen-printing processes. Therefore, an error of this type is expected in any results obtained from this type of TiO_2 glass. The only way to eliminate/reduce this error would be to obtain glass with a guaranteed TiO_2 thickness (not obtainable from the present supplier).

All cells constructed using TiO_2-coated plates PA and PB were tested in the original cell holders **CH1** and **CH2**, and required no pre-treatment of the TiO_2 surface prior to dye adsorption. As discussed later supplies, PC and PD did require pre-treatment to give adequate dye binding and were tested in cell holder **CH3**.

5.2.5   Data Acquisition and Errors

During initial cell testing, data collection was carried out by manually recording the I_{sc} and V_{oc} values from a digital multimeter against time. An improved data collection system was later adopted, collecting the data directly on a computer. The displaying of the data graphically on screen, in real time, allowed better interpretation of cell behaviour. Steady state (SS) I_{sc} and the effects of V_{oc} could be easily observed. All I_{sc} values recorded in the final set-up using cell holder **CH3** were corrected to mA cm^{-2} by accurately measuring the TiO_2 area with vernier calipers after testing.

In order to ascertain the reproducibility of the cell set-up, five Ru_{red} cells (using PD TiO_2 plates) were fabricated and tested. These gave consistent results. Movement of the Pt electrode or contact point rarely affected the cell output. The averages were I_{sc} = 4.45 mA cm^{-2} ± 11% and V_{oc} = 592 mV ± 1%. The results suggest that I_{sc} data from these PD plates could have I_{sc} errors of up to 22% because of the non-uniformity of the TiO_2 layer thickness. In order to account for the variable results, and limit errors arising from the TiO_2 inconsistencies during porphyrin dye evaluation, three identical separate cells were fabricated and tested for each compound. If two consistent results (<10% deviation in I_{sc}) were not obtained, extra cells were constructed and tested. The average I_{sc} and V_{oc} results of these runs are given. Any cell results that appeared as outliers were discarded; if this was a result of poor cell engineering (i.e. short circuiting between electrodes or damaged TiO_2 layer) generally a low V_{oc} resulted allowing a confident exclusion of this result. For cells that never reached a steady state (SS) I_{sc} value, their maximum I_{sc} values are given.

All cells constructed using TiO_2 plates PA and PB were tested in the original cell holders **CH1** and **CH2**, and required no pre-treatment of the TiO_2 surface prior to dye adsorption. As discussed, TiO_2 plates PC and PD did require pre-treatment to give

adequate dye binding and were tested in cell holder **CH3**. Data from cells fabricated from PA and PB plates using the older cell holders **CH1** and **CH2**, generally showed consistently less than 10% variation in the average I_{sc} results of identical cells. Therefore, the errors in I_{sc} measurements for these earlier cells, was believed to be less than 10%.

5.3 Testing of Porphyrin Acids (Monomers to Arrays) in the Grätzel Cell

5.3.1 Introduction

To date, mostly *meso*-substituted TAPs with *para*-benzoic acid groups have been used in the Grätzel cell. The work in this thesis has provided access to a number of new families of porphyrins to allow sequential study. However, initially we needed to optimise and standardise the Grätzel cell conditions. Porphyrin derivative TXP acid **15** was the most appropriate porphyrin to use for this given its ease of synthesis and the availability of metal and structural variants. Since Zn(II) porphyrins have been typically used in other studies (see Section 5.1.2), **Zn-15** was used for these initial studies.
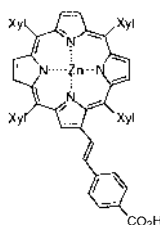
Zn-15

Following this initial determination of the most favourable Grätzel cell conditions for **Zn-15**, the effects of the metal, aryl substituent and acid position could be explored using the regioisomeric porphyrin benzoic acids synthesised in Chapter 2. This data should provide a sound basis for screening the other monoporphyrins and the other multiporphyrin arrays synthesised in Chapters 2 and 4.

The measurement of I_{sc}/V_{oc} data in this chapter required the construction of individual dye-sensitised Grätzel cells as detailed in the previous section. Given the number of variables in such measurements alluded to earlier, a comprehensive study could not be undertaken at this time. Therefore, it was the intention of this work to gain some insight

into the factors influencing the use of porphyrins as dyes, to provide a foundation for a future quantitative study.

5.3.2   Identifying Variables in Porphyrin TiO$_2$ Cell Performance

A number of experiments were carried out using ZnTXP-=-PhCO$_2$H **Zn-15** to investigate some variables in cell preparation guided by previous work.[177]   No optimisation was carried out, but the work highlighted cell variables requiring future optimisation. These investigations were an attempt to lay the basis for a reliable and valuable semi-quantitative screening process. All the following data was obtained from Grätzel cells constructed according to the testing protocols introduced in Section 5.2 (also see experimental Section 7.5.4 for details). In general, the data presented in the following figures are averaged values from two or more cells. The raw data is presented in Appendix B.

Effect of Dye Adsorption Time and Temperature
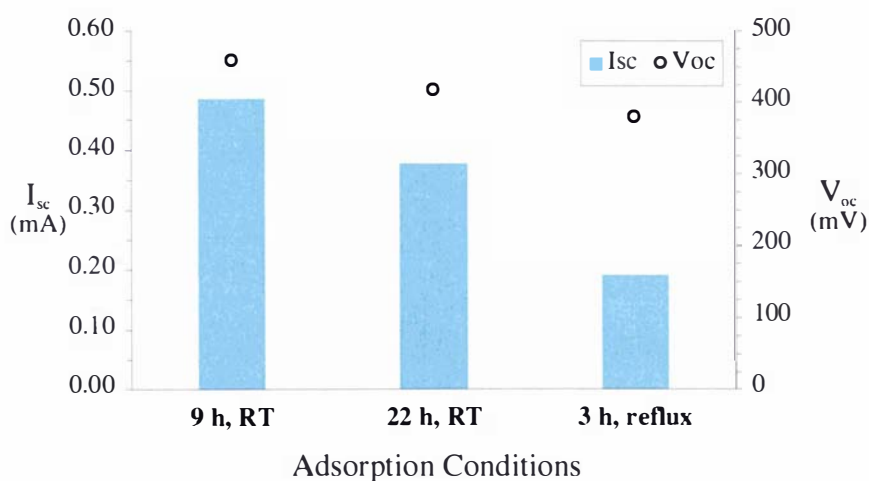
Figure 5-31. Effect of adsorption time.

(**Zn-15**, CH$_2$Cl$_2$ (10^{-5} mol L^{-1}), PA, Electrolyte E)

Figure 5-31 demonstrates the effect different adsorption time and method has on the **Zn-15** cell performance. The drop in I$_{sc}$ and V$_{oc}$ values after a longer period of adsorption suggests that too much porphyrin on the surface is detrimental to cell

efficiency. This could be because of porphyrin aggregation and consequent excited state quenching. The data from a TiO_2 plate dyed under reflux further supports this. Typically, the TiO_2 electrode surface is dyed a light green by this porphyrin. However, the plate dyed under reflux was quite red, similar to solid **Zn-15**, supporting the notion of an increased concentration of porphyrin on the surface. However, much more work needs to be done to ascertain whether aggregation is indeed a problem.

Effect of Adsorption Solvent Type
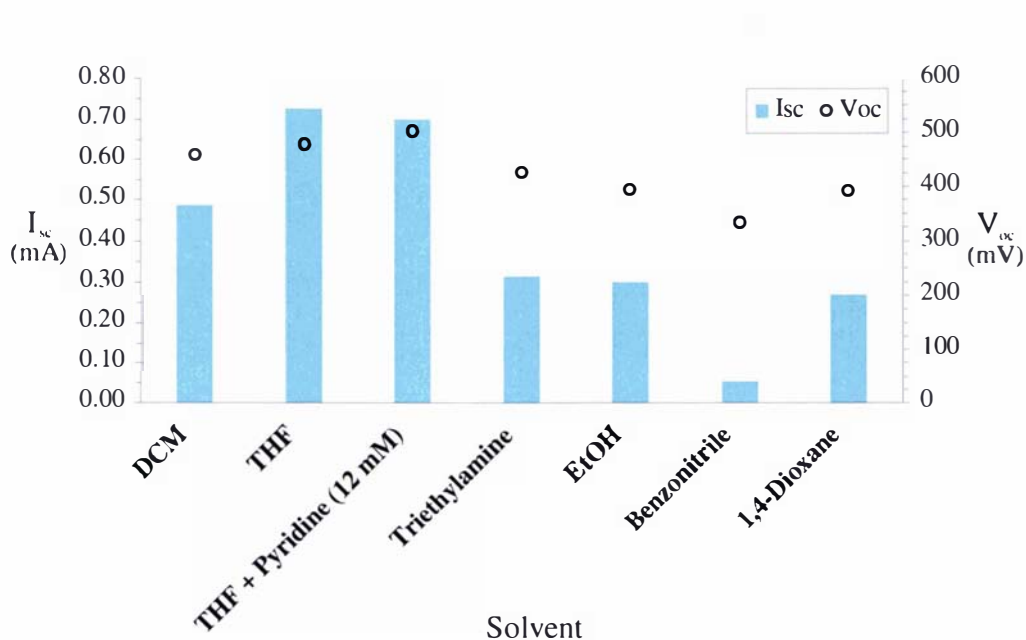
Figure 5-32. Effect of adsorption solvent type.
(**Zn-15**, [solvent] (10^{-5} mol L^{-1}), PA1, Electrolyte E)

Varying the solvent used to adsorb the dye onto the surface was also found to have a significant influence on cell performance. Figure 5-32 displays the dramatic effect that different adsorption solvents can have. THF showed the most significant increase in cell performance. **Zn-15** was soluble in all of the solvents except DCM. Given the effect the solvent could have on dye binding and the nature of the surface, it is difficult to draw any conclusions as to the general characteristics of an effective solvent. However, the results clearly indicate that THF was superior for dye binding and so was chosen as the standard adsorption solvent for further porphyrin solar cell testing.

Effect of Dye Concentration and Rinsing
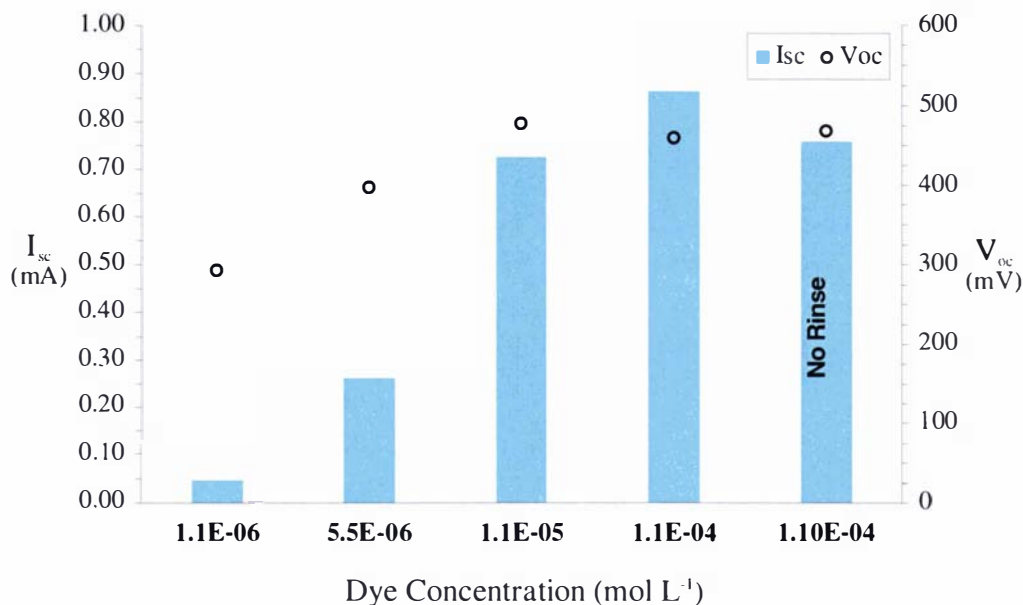
Figure 5-33. Effect of dye concentration.
(**Zn-15**, THF, 9 h, PA1, Electrolyte E)

Dye concentration during adsorption is critical to cell performance (Figure 5-33). As the dye solutions get more dilute, the dyed TiO_2 layer gets visually less intense. For this dye, the optimum concentration appears to be somewhere between 10^{-4} and 10^{-5} M. It should be noted that the porphyrin solutions were still significantly coloured after removal of the dye TiO_2 plates, even at concentrations of 10^{-6} M. Rinsing the dyed plates has a small effect on the cell performance although this is within experimental error. It is apparent however, that if rinsing is carried out for longer than the 5 minutes used in these experiments that discolouration of the solvent continues. Typically, removal of the dyed plates from solutions resulted in coloured patterning known as "shadowing", as the solvent front dried and carried dye across the TiO_2 surface. This all suggests that the porphyrin **Zn-15** is not strongly bound to the TiO_2. In addition, the increase in cell performance as dye concentration is increased, is not inconsistent with a weakly bound dye in equilibrium with the surface. Further work could show a Langmuir type isotherm behaviour as recently proposed by Grätzel et al.[150] We believe the TAPs to be an EDG, therefore expect $pK_a > 4.2$ for **Zn-15** (ca. Benzoic acid, $pK_a =$ 4.2). In contrast the Ru dyes like Ru_{red} **118** and the Black Dye **119** ($pK_a < 3.3$) are known to bind strongly to TiO_2 and are not removed by rinsing.[150,179]

Nonetheless, based on these results, concentrations between of 10^{-4}-10^{-5} M were chosen for the following solar cell testing. In addition, during screening, rinsing was avoided by removal of the plate from the dye solution and quickly mopping up any excess solution with lint-free tissue paper.

Acid Salt Effect on Dye Efficiency
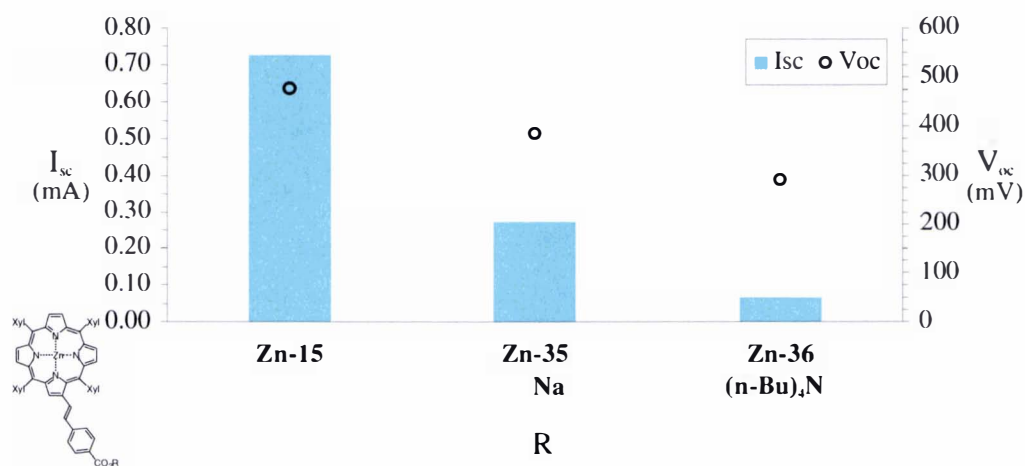
Figure 5-34. Effect of acid salt on cell performance.

(**Zn-15**, **Zn-35**, **Zn-36**, THF (10^{-5} mol L^{-1}), PA1, Electrolyte E)

In order to ascertain whether the free acid or a salt is best for cell efficiency, the Na^+ and $(n\text{-Bu})_4N^+$ derivatives (**Zn-35** and **Zn-36** respectively) of **Zn-15** were synthesised and tested. The free acid form gives significantly superior cell performance (Figure 5-34). Subsequent acids were tested in their free acid form only. This is in agreement with Nazeeruddin et al. who have demonstrated that the fully protonated Ru_{red} dye **118** is more efficient than the deprotonated forms.[179] The drop in performance of the Na^+ salt **Zn-35** suggests that the acid form **Zn-15** is probably not being deprotonated by the electrolyte E containing NaI.

Effect of Electrolyte Composition on Cell Performance

Several electrolyte systems (A-D) as used in previous work[177] were evaluated:

- ▼ Electrolyte A (0.6 M LiI, 0.1 M I_2 in glutaronitrile).
- ▼ Electrolyte B (0.6 M LiI, 0.01 M I_2 in glutaronitrile).
- ▼ Electrolyte C (0.6 M LiI, 0.1 M I_2 in 3-methoxypropionitrile).
- ▼ Electrolyte D (0.6 M LiI, 0.1 M I_2, 4-*t*-butylpyridine (1.0 mM) in glutaronitrile).

Cells using these electrolytes took a long time to stabilise. It was found that the LiI used in these electrolytes was not anhydrous as assumed. NaI was consequently substituted, as it was easier to obtain and prepare in its anhydrous form.

- ▼ Electrolyte E (0.5 M NaI, 0.05 M I_2, in glutaronitrile).

A new electrolyte E, made from iodine, anhydrous NaI in dried glutaronitrile was evaluated. A small amount of fine white precipitate formed on storage, so electrolyte was always shaken prior to use. In contrast to the LiI-based electrolytes, the NaI-based electrolyte E gave cells that rapidly stabilised to steady state (SS) I_{sc} conditions. It appears therefore that water of solvation may affect cell performance.

In order to examine just how critical electrolyte compositions were on cell performance, another electrolyte F was made and tested with the Ru_{red} dye **118**. Electrolyte F contained ethylene glycol instead of glutaronitrile.

- ▼ Electrolyte F (0.5 M NaI, 0.05 M I_2 in ethylene glycol).

Table 5-3. Electrolyte vs. Ru_{Red} **118** cell performance (PD1)

Electrolyte	I_{sc} (mA cm^{-2})	V_{oc} (mV)
E	4.45	592
F	1.31	545

The performance of Ru_{red} dye **118** PECs using electrolyte E and F is summarised in Table 5-3. Electrolyte F performed poorly compared to electrolyte E. Clearly, choice of electrolyte is an important variable and will probably need to be optimised, most probably for each individual porphyrin chromophore system.

As part of this series of optimisation experiments the effect of adding 4-t-butylpyridine on **Zn-15** cell performance was investigated. It was of particular interest to know if the addition of 4-t-butylpyridine in the electrolyte would have any effect on cell performance. Grätzel et al. and other research groups have reported that treating ruthenium dye-coated TiO_2 electrodes with 4-t-butylpyridine results in an increased V_{oc}.[30,180-185] This is presumed to be due to the limiting of back electron transfer from the TiO_2 surface. The Grätzel method of immersing the dye-coated plates in neat 4-t-butylpyridine is however impractical for the **Zn-15** dye, as this dye is easily removed under these conditions. Therefore, a new electrolyte G based on electrolyte E, but containing 0.01 mol L^{-1} 4-t-butylpyridine was evaluated.

▼ Electrolyte G (0.5 M NaI, 0.05 M I_2, 4-t-butylpyridine (0.01 mol L^{-1}) in glutaronitrile).

The results are summarised in Table 5-4. The SS I_{sc} is marginally lower, but the cell appears more stable and recovers well after V_{oc} conditions (This indicated *Type I* cell behaviour in Table 5-4, and is explained in the following section). No increase in V_{oc} was observed. Future experimentation with 4-t-butylpyridine concentrations should be carried out to find optimum concentrations, as stabilisation of V_{oc} conditions is important for long-term PEC applications.

Table 5-4. Effect of 4-t-butylpyridine on ZnTXP-=-PhCO$_2$H **Zn-15** cell performance. (THF (10^{-4} mol L^{-1}), PD2)

Electrolyte (Additive)	I_{sc} (mA cm^{-2})	V_{oc} (mV)	Cell Behaviour
E	0.880	449	*Type II*
G (4-t-butylpyridine)	0.767	429	*Type I*

Typical Cell Behaviours

As discussed in Section 5.2.5 (pg 163) the recording of data with a digital multimeter interfaced to a computer allowed real time displaying of the cell I_{sc}. This provided information about cell behaviour as detailed below.

From the multimeter output, four main types of cell current and voltage behaviours were observed (Figure 5-35). A good cell should ideally show little change in I_{sc} and demonstrate a positive recovery from a lower I_{sc} after V_{oc} conditions.
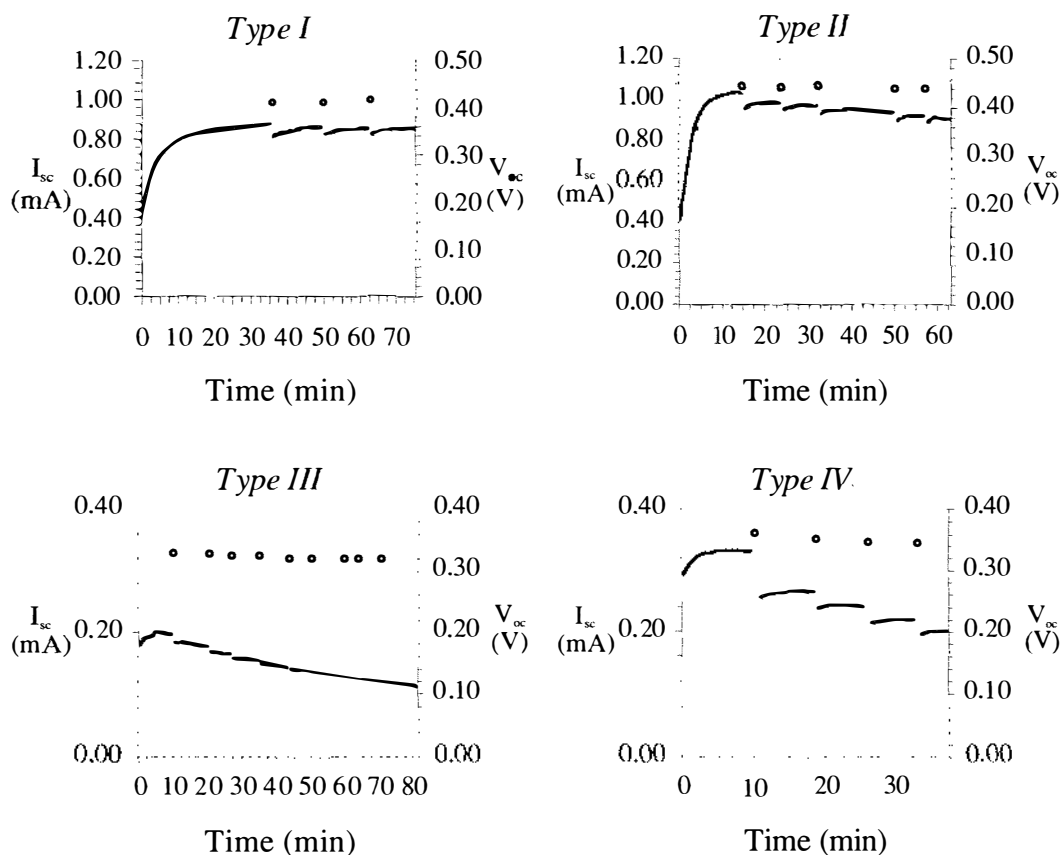
Figure 5-35. Examples of four main cell behaviours

$(- I_{sc} \text{ (mA)}, \text{o } V_{oc} \text{ (V)})$

The four basic cell behaviours can be described as below:

Type I Cell Behaviour

Cells of this type typically reach a SS I_{sc} quickly (< 25 min) and show little drift and good recovery in I_{sc} after V_{oc} conditions. ZnTXP-=-PhCO$_2$H **Zn-15** with electrolyte G is a good example of this.

Type II Cell Behaviour

This behaviour is typified by a drop in I_{sc} during initial V_{oc} conditions, but eventually tend towards a SS I_{sc} with recovery after V_{oc}. ZnTXP-=-PhCO$_2$H **Zn-15** with electrolyte E is and example of this.

Type III Cell Behaviour

These cells never achieve a SS I_{sc} reading. The maximum I_{sc} value is reported for this cell behaviour.

Type IV Cell Behaviour

These cells might achieve a satisfactory SS I_{sc} reading but suffer from significant non-recoverable drop in I_{sc} after each V_{oc} reading. The maximum I_{sc} value is reported here again.

These classifications have been applied to the results of the screening of monomer and array porphyrins where the computer-interfaced digital multimeter was used for data acquisition.

5.3.3 Structural Variants of TXP-=-PhCO$_2$H (15) and Cell Performance

The information and experience obtained in the previous section of this Grätzel cell setup, provided a sound basis from which to assess the effect of the variables in the structure of the porphyrin based on the TXP acid **15**. Changing core metals was initially explored and this was followed by investigating the effect of the regioisomers and the *meso*-aryl substituents around the porphyrin core.

Metalloporphyrins (2H, Zn & Cu)

Given that varieties of free-base and metalloporphyrins are used as photosensitisers by other research groups (see section 5.1.2), it was important to determine what type of porphyrins should be used in this study. Different metalloporphyrins have different excited state lifetimes that can participate in energy transfer processes. They also possess distinct abilities to stabilise the porphyrin core chemically and physically. The cell performance of Zn(II), Cu(II) and the free-base derivatives of **15** are summarised in Figure 5-36.
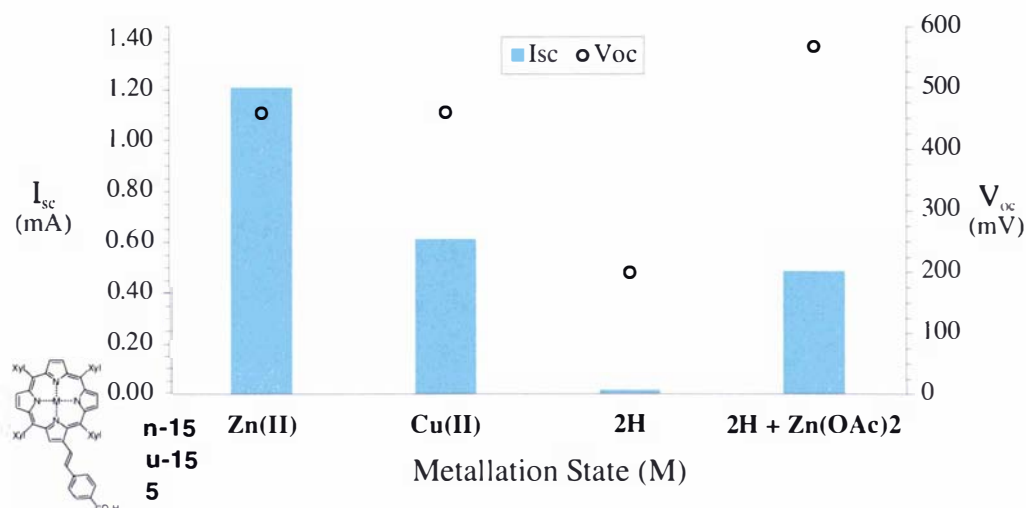
Figure 5-36. Effect of MTXP-=-PhCO$_2$H on cell performance.
(THF (10^{-5} mol L^{-1}), PA2, Electrolyte E)

As previously observed by Tsubomura et al. for metallo TPP **1** derivatives,[158] the Zn(II) derivative **Zn-15** performs better than the other metallo or free-base species. Treatment of the dismantled free-base **18** cell with zinc acetate resulted in a significant increase in cell performance when reconstructed (Figure 5-36). Reconstruction of the cell was achieved by dismantling the electrode and rinsing in acetonitrile, followed by drying under high vacuum. The brown coloured electrode was then immersed in a solution of Zn(OAc)$_2$·2H$_2$O in dry MeOH for 1.5 hours resulting in the typical green coloured electrode associated with ZnTXP-=-Ar-COOH **Zn-15**. It should be noted that reconstructed cells of the same electrode never perform as well as the original cells.

Cu(II) porphyrins are known to have shorter lived excited states compared to the zinc porphyrins, but they are inherently more stable. Although, the **Cu-15** cell performance was half of the **Zn-15** I$_{sc}$ value, these results suggest that Cu(II) porphyrins are worth pursuing in future where long term stability of the chromophores is required in solar cells. The Cu(II) cells also quickly achieved a SS I$_{sc}$ condition (< 10 min) and demonstrated a positive recovery after V$_{oc}$ conditions. The colouring of the TiO$_2$ electrode was a red/brown as compared to the green **Zn-15** electrodes. Shadowing of the TiO$_2$ was evident on removal from the dye solution indicating that poor binding of **Cu-15** may however be a problem.

o,m,p-Carboxylic Acids of ZnTXP-=-Ph(CO₂H)ₓ

The effect on cell performance by the acid regioisomers of **Zn-15** was also investigated (Figure 5-37). The varying steric and electronic effects of these isomers should affect the binding ability of the dye and the relationship of the porphyrin core, to the TiO_2 surface. This study also provided the opportunity to compare the efficiency of a dicarboxylic acid analogue **Zn-37** of the *meta*-regioisomer.
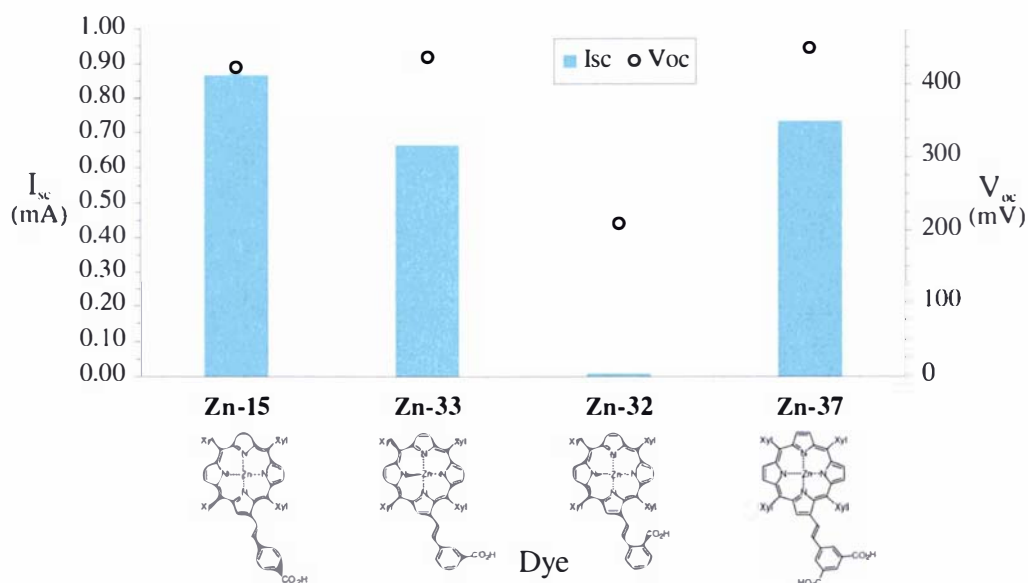
Figure 5-37. *o,m,p*-Acids of ZnTXP-=-Ph(CO₂H)ₓ.
(THF (10^{-5} mol L⁻¹), PB, Electrolyte E, rinsed)

The *para* Zn(II) metalloporphyrin acid **Zn-15** performed the best, with cell performance dropping off from *para, meta* to *ortho*. If the TAP group is electron donating (reducing the acidity) the *meta*-acid derivative might be expected to bind stronger due to greater electronic isolation. This is however not the case, and possibly suggests surface geometry of the porphyrin is more critical. The low I_{sc} value for the *ortho* species **Zn-32** was not unexpected, as a very light colour of porphyrin was observed on the TiO_2 surface after 10 hours of adsorption, suggesting poor binding. Significant steric constraints on binding imposed by the *ortho* acid group would be expected to hinder binding of this dye. The *meta*-diacid ZnTXP-=-Ph$_m$(CO₂H)₂ **Zn-37** gave similar I_{sc} results to the mono *meta* derivative. Strong shadowing was seen on the TiO_2 layer on removal from the dye solution implying weak binding.

Benzoic Acid versus Phenol Binding Group
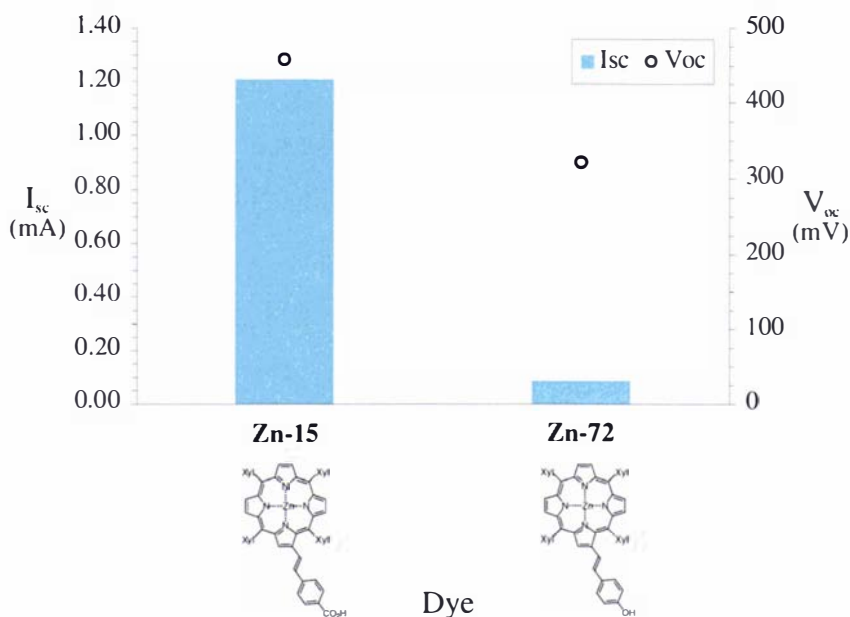
Figure 5-38. PhCO$_2$H vs. PhOH.

(THF (10^{-5} mol L^{-1}), PA2, Electrolyte E)

Phenols are somewhat less acidic in character than benzoic acids (phenol pK_a = 9.9, benzoic acid pK_a = 4.2). The binding of the **Zn-15** phenol analogue **Zn-72**, to the TiO$_2$ electrodes was as expected found to be poor, with a very pale green TiO$_2$ electrode colouration observed. A low I$_{sc}$ value was subsequently recorded for the phenol **Zn-72** (Figure 5-38), supporting the concept that strong surface binding is necessary for cell efficiency.

ZnTXP-=-PhCO$_2$H versus Grätzel's Ru$_{red}$ Dye

The efficiency of ZnTXP-=-PhCO$_2$H **Zn-15** as a light harvester was compared to the Ru$_{red}$ **118** dye, and the results are summarised in Table 5-5. The I$_{sc}$ value of the porphyrin is 20% of that of the ruthenium **118** dye. It could be anticipated that the gap in the performance of these two dyes would be narrowed with further optimisation.

<p align="center">**Table 5-5.** Ru$_{Red}$ vs. ZnTXP-=-PhCO$_2$H (PD1, Electrolyte E)</p>

Dye	I$_{sc}$ (mA cm^{-2})	V$_{oc}$ (mV)
Ru$_{red}$ **118**	4.45	592
Zn-15	0.842	453

One of the **Zn-15** cells was irradiated with natural summer afternoon sunlight, producing about 2 mA cm^{-2} (compared with 0.71 mA cm^{-2} in the testing set-up). This demonstrates that a high current output from porphyrin cells should be possible.

Arylporphyrin Substituents (TPP vs. TXP vs. TBP)
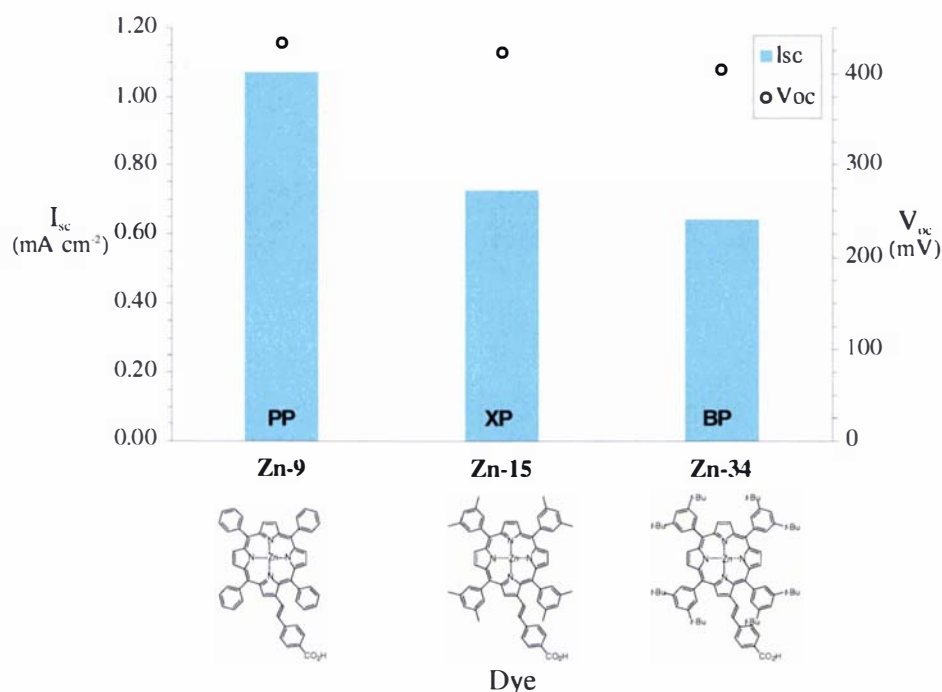
Figure 5-39. TPP vs. TXP vs. TBP derivatives of ZnTAP-=-PhCO$_2$H.
(THF (10^{-4} mol L^{-1}), PD2, Electrolyte G)

The effect of varying the *meso*-aryl groups, modifying the steric bulk and electron donating ability of the ZnTAP-=-PhCO$_2$H acid was investigated. The TPP and TBP analogues of ZnTXP-=-PhCO$_2$H **Zn-15** were absorbed onto TiO$_2$ and their cell characteristics evaluated (Figure 5-39).

Each cell tested exhibited *Type I* cell behaviour (see *Typical Cell Behaviours*, pg 171) and reached a SS I$_{sc}$ showing good stability towards V$_{oc}$ conditions. The TXP and TBP

derivatives (**Zn-15** and **Zn34**) are comparable but the TPP **Zn-9** derivative gave a 47% higher I_{sc} value. Two trends can be postulated from these results. Either cell performance decreases with increasing steric bulk and/or with increasing electron-donating effect of the aryl substituents. Based on electronic effects, the trend suggests that perhaps the acidity of the acid group increases (increased binding) as the electron donating ability of the TAP is reduced. This electronic effect could be further investigated with the synthesis of other EWG and EDG tetra-*meso*-arylporphyrin acid derivatives of **15** (i.e. 4-chlorophenyl or 4-methoxyphenyl variations) for comparison. A steric effect is somewhat more difficult to survey, given the porous nature of the TiO_2 surface and the current lack of data on the way these materials bind.

Quantitative results to verify the performance of the TXP **Zn-15** and TPP **Zn-9** derivatives are presently being sought from the laboratories of Grätzel et al.

5.3.4 Screening of Monoporphyrins and Multiporphyrin Acid Arrays

The types of porphyrin carboxylic acids tested in this section can be arranged into two main groups: monoporphyrin and multiporphyrin acid arrays containing two or more porphyrin units. The screening of a variety of monoporphyrin acids synthesised in Chapters 2 and 4 is presented first.

Screening of Monoporphyrin Acids

A range of *meso*-benzoic acid monoporphyrins was tested in the Grätzel cell and the results compared to those of **Zn-15** (Figure 5-40). Two *trans*-bis(*meso*-benzoic acid)porphyrins were synthesised, one of which has the remaining *meso* positions substituted with *trans*-aryl electron donating groups. The octaacid tetra-*meso*-(isophthalic acid)porphyrin **Zn-75** was also tested. The most commonly used porphyrin photosensitiser, *para* ZnTCP **Zn-8**, was included for comparison. In addition, the *meta* analogue ZnT3CP **Zn-95** was evaluated.
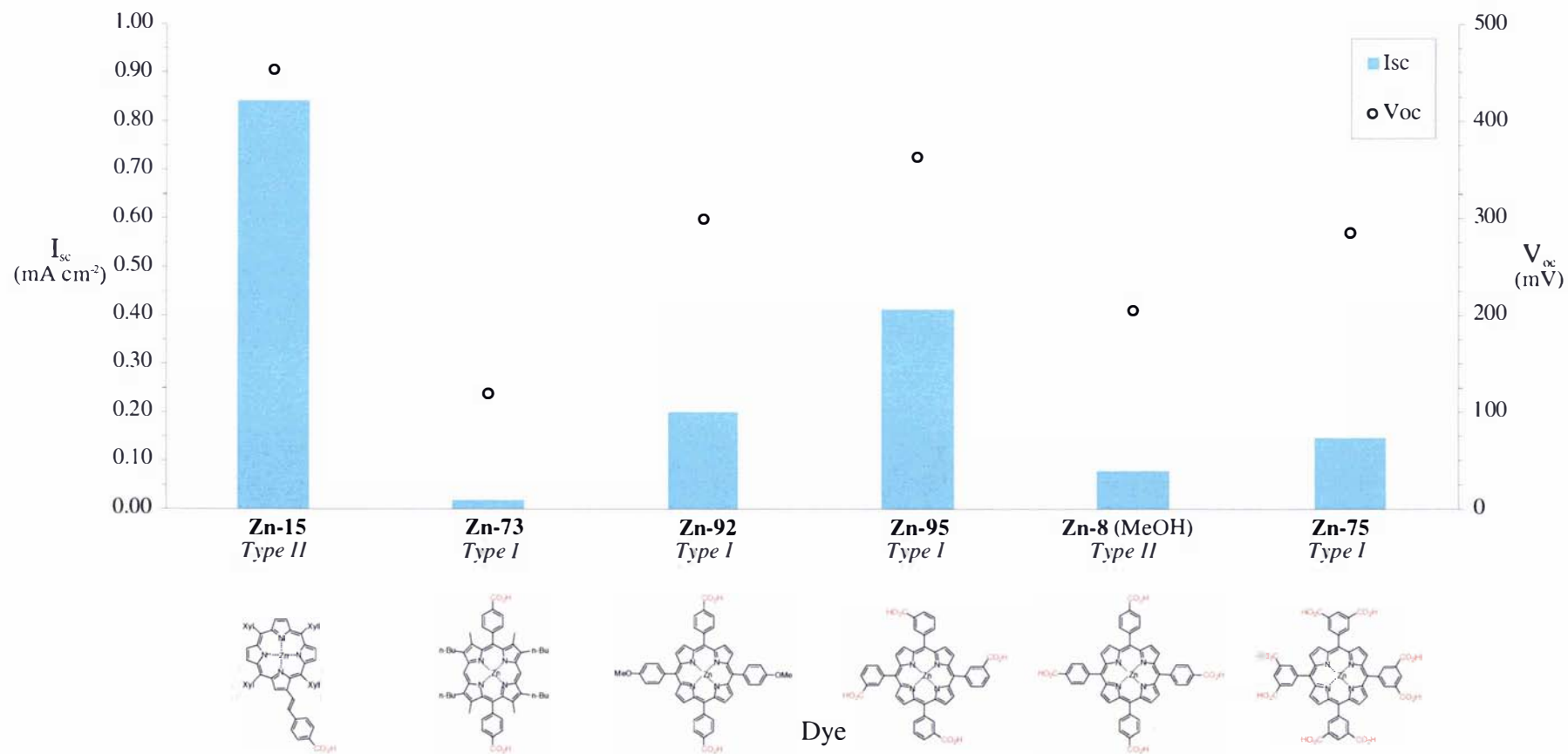
Figure 5-40. Comparison of monoporphyrin acids in the TiO₂ solar cell.

(THF (10^{-4} mol L^{-1}), PD1, Electrolyte E)

Interestingly, the monoacid **Zn-15** performed considerably better than all the *meso*-substituted porphyrin dyes.

The two *meso*-bisbenzoic acids **Zn-73** and **Zn-92** both gave low I_{sc} values compared to **Zn-15**. Of interest is that the current from the **Zn-92** is an order of magnitude larger than that from **Zn-73**, and 24% of the **Zn-15** I_{sc} value. The higher I_{sc} value for **Zn-92** may possibly result from the introduction of electron-donating methoxyphenyl groups to the porphyrin periphery.

Zn-95, **Zn-8** and **Zn-75** are tetra-*meso* acid porphyrins. Of these, the *meta*-substituted monoporphyrin ZnT3CP **Zn-95** gave significantly higher I_{sc} and V_{oc} results. This *meta* acid derivative **Zn-95** gave an I_{sc} value fourfold higher than the *para* acid derivative **Zn-8**, and 50% of ZnTXP-=-PhCO$_2$H **Zn-15**. It should be noted that pure **Zn-8** was found to be insoluble in EtOH and could only be applied in MeOH, contrary to some previous reports.[161,162,164] The octaacid ZnT3,5CP **Zn-75** also gave a poor result.

Generally, low I_{sc} values were accompanied by the observation of faint dye colourations and shadowing on the TiO$_2$ surface after removal from the dye solution, indicating poor binding or low surface coverage. The weak binding of these acids is surprising considering the number carboxylic acid groups (4-8) present on these molecules. Perhaps poor binding of some of these multi-acid porphyrins is a result of the geometry of the porphyrin in relation to the surface (i.e. perpendicular vs. planar) or the pK_a of the carboxylic acid groups. Figure 5-41 demonstrates how the *meta* T3CP porphyrin **95** could adopt a planar geometry with potentially all four acid groups available for surface binding.
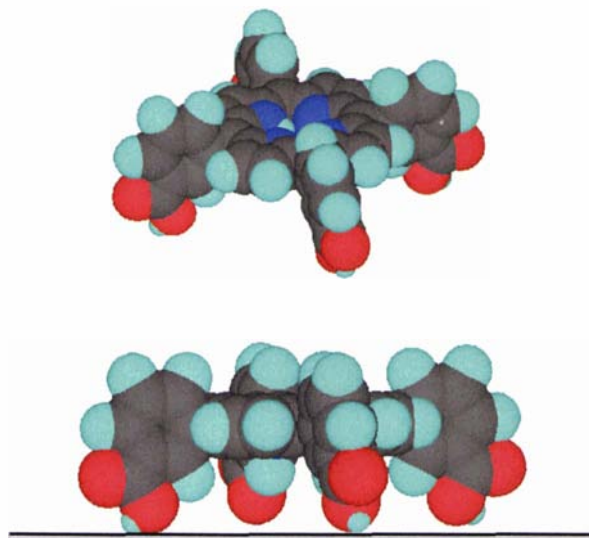
Figure 5-41. T3CP **95** surface orientation.

The *para* derivative TCP **8** does not exhibit this ideal geometry for four site surface binding in the planar geometry, and work by Wamser et al. has suggested it to prefer a more perpendicular stacked type surface binding mode (Figure 5-42).[162] On the other hand, intermolecular aggregation between molecules could be a stronger determining factor in binding efficiency.
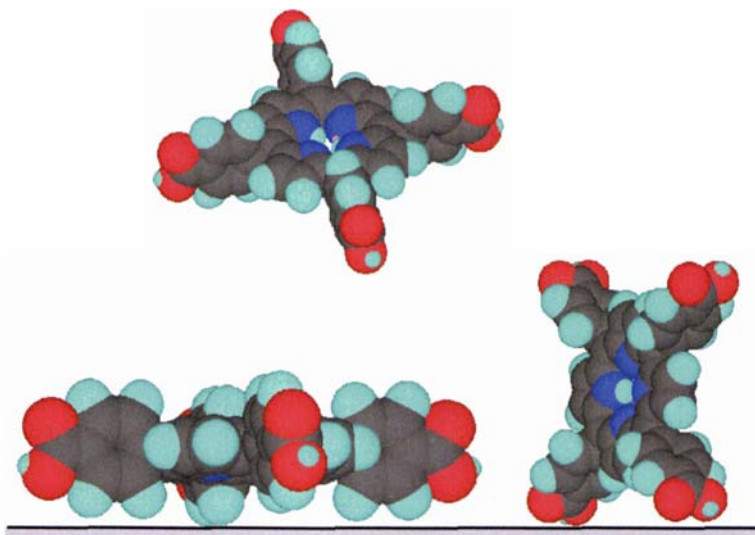
Figure 5-42. TCP **8** surface orientations.

The superior nature of **Zn-15** tempts us to postulate that orthogonal binding through a single acid group is important. This may be due to improved charge transfer through the fully conjugated system rather than the orthogonal *meso*-benzoic acids. Whatever the case, considerable work needs to be done to probe the reasons for the differences.

Screening of Array Porphyrin Acids

Two types of multiporphyrin acid arrays were tested in the Grätzel cell. Firstly, the dipole **Zn$_2$-53** and collinear **Zn$_2$-66** diporphyrin antennae molecules were assessed. A second group, based on the "sticky" porphyrin approach and constructed from T3CP **95** acid porphyrin sub-units, was compared. The PEC results of the multiporphyrin array acids are summarised in Figure 5-43.

"Dipole" and "Collinear" Arrays

Zn$_2$-53   **Zn$_2$-66**
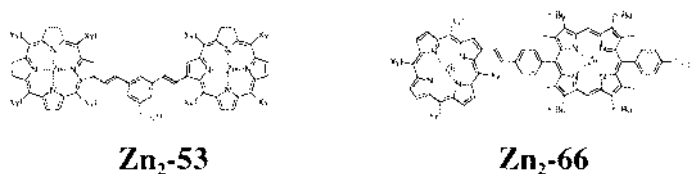
Both the branched "dipole" diporphyrin **Zn$_2$-53** and the "collinear" diporphyrin **Zn$_2$-66**, gave similar, low SS I_{sc} values (11% of ZnTXP-=-PhCO$_2$H **Zn-15**). Adsorption of these dyes resulted in a pale TiO$_2$ colouring, accompanied by significant shadowing of the TiO$_2$ layer after removal from the dye solutions. Rinsing of a used TiO$_2$ plate with THF resulted in removal of most of the dye. This is consistent with weak surface adhesion. These systems were slow to reach a SS I_{sc} (> 100 min). This may result from slow redistribution of the porphyrin molecules within the TiO$_2$ layer or equilibrium with the electrolyte. Clearly, these results do not allow the identification of a significant antennae effect for either of these array systems in this type of PEC, since their overall poor performance may be the result of poor binding.
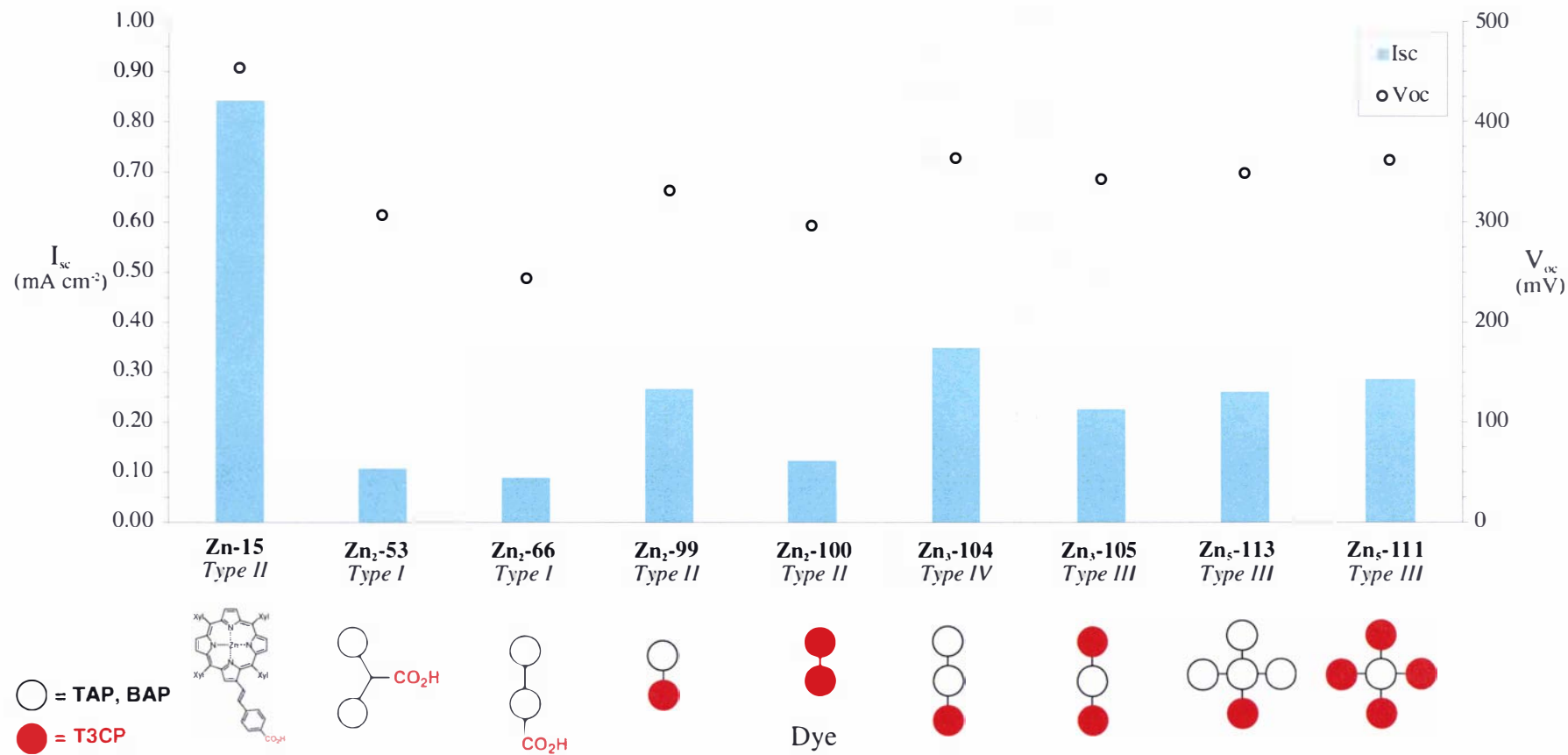
Figure 5-43. Comparison of porphyrin arrays in the TiO₂ solar cell.

(THF (10⁻⁴ mol L⁻¹), PD1, Electrolyte E)

"Sticky" Porphyrin Arrays

There appears to be no difficulty with the binding ability of the "sticky" porphyrin arrays. In contrast to the dipole and collinear arrays, these arrays appeared to bind strongly to the TiO$_2$. A dark green/brown TiO$_2$ surface was evident in all cases after removal from the dye solution.

Zn$_2$-99   **Zn$_2$-100**   **Zn$_3$-104**   **Zn$_3$-105**
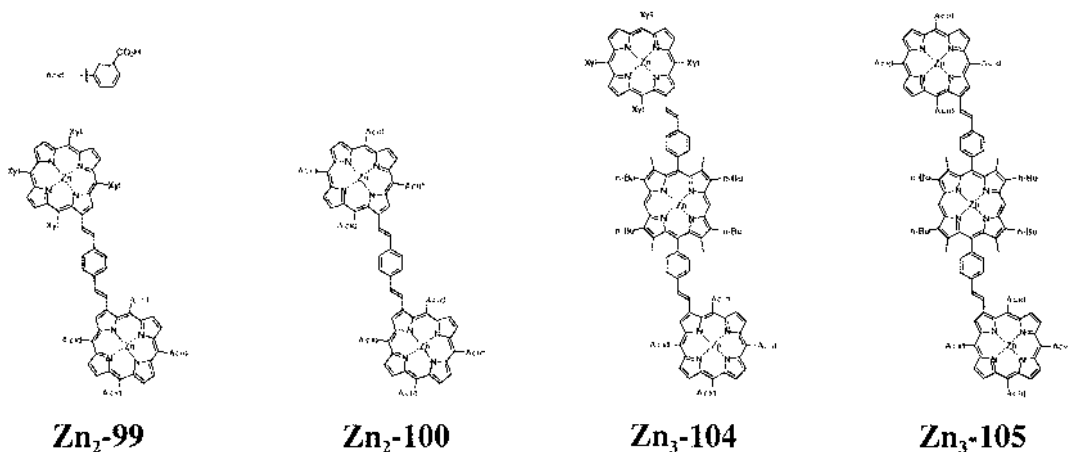
The T3CP based "sticky" array diporphyrins **Zn$_2$-99**, **Zn$_2$-100** and triporphyrins **Zn$_3$-104**, **Zn$_3$-105** revealed a similar trend in their I$_{sc}$ values (Figure 5-43). For each pair, the arrays with more acid groups gave the lower value. Since the arrays with the free TXP moieties (**Zn$_2$-99** and **Zn$_3$-104**) gave the highest outputs, this perhaps suggests that the porphyrin array is a better photosensitiser when it is not held too close to the surface, but tethered in close proximity. The triporphyrins cells did not reach SS, exhibiting *Type III* and *IV* behaviour, indicating poor current stability.
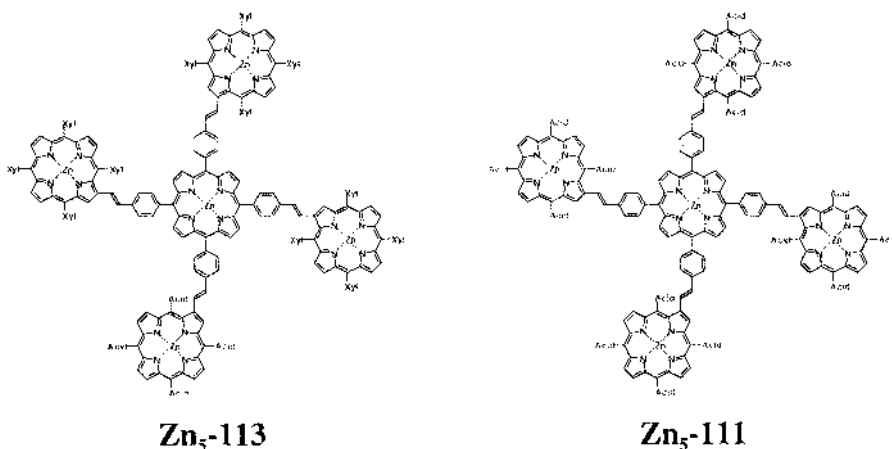
Zn$_5$-113   **Zn$_5$-111**

The star shaped pentaporphyrins **Zn$_5$-113** and **Zn$_5$-111**, gave similar I$_{sc}$ results to those of the triporphyrins (Figure 5-43). Since the triporphyrins and pentaporphyrins cells did

not reach SS, only the maximum I_{sc} values are given, and direct comparisons to those from SS cells cannot be made.

Electrolyte G, containing 4-*t*-butylpyridine, was also tested with the pentaporphyrin **Zn₅-111** cell. There was no significant difference in the maximum I_{sc} value compared to that obtained in electrolyte E (Figure 5-43), and again a SS condition was not obtained (Table 5-6).

Table 5-6. Effect of 4-*t*-butylpyridine on **Zn₅-111** cell performance
(THF (10^{-4} mol L^{-1}), PD2)

Electrolyte	Treatment	I_{sc} (mA cm^{-2})	V_{oc} (mV)	Cell Behaviour
E	-	0.286	362	*Type III*
G	-	0.269	381	*Type III*
G	4-*t*-butylpyridine (soaked)	0.177	395	*Type I*

Following this, a **Zn₅-111** pentaporphyrin cell was soaked in neat 4-*t*-butylpyridine for 15 minutes after removal from the dye solution, prior to cell testing. The immersion of the dyed TiO$_2$ in neat 4-*t*-butylpyridine is only practical with these more strongly binding dyes, where desorption was not an issue. This resulted in the attainment of a *Type I* SS I_{sc} condition quickly (10 min), although an overall decrease in I_{sc} was observed with no significant increase in V_{oc} (Table 5-6). This treatment is worth investigating further on the stronger binding dyes.

All these I_{sc} values are still considerably lower than that of **Zn-15**. Again this supports the notion that it is advantageous for the binding group to be somewhat separated from the chromophore. In addition, low cell performance could result from inter-molecular aggregation, which may be more significant for these larger arrays. There is also the possibility that the small porosity of TiO$_2$ nanocrystalline layer may be preventing adsorption of the dye into its bulk.

5.3.5   Independent Testing by Grätzel
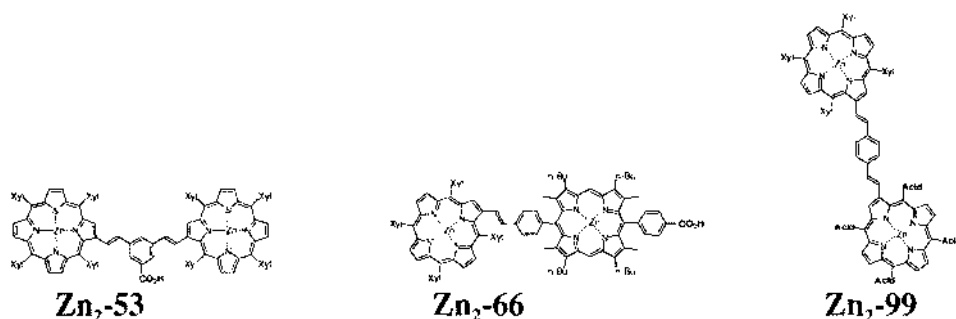
Zn$_2$-53   Zn$_2$-66   Zn$_2$-99

Zn$_2$-53, Zn$_2$-66 and Zn$_2$-99 were tested by the Grätzel group in Switzerland. Their laboratories and testing procedures are well equipped to provide quantitative results on such dyes. The detailed results are given in Appendix B and summarised in Table 5-7. The data was obtained under standard AM1.5 light conditions using a different electrolyte composition from this work. Therefore, while direct comparisons cannot be made with our result, the relative values can be analysed.

Table 5-7. Solar cell performance results from Grätzel's laboratory (AM1.5).

Dye (Cells Tested)	I_{sc} (mA cm^{-2})	V_{oc} (mV)	Efficiency η
Zn$_2$-53 (1)	1.08	470	0.36%
Zn$_2$-66 (1)	0.399	477	0.13%
Zn$_2$-99 (2)	4.40	496	1.50%

The "sticky" diporphyrin Zn$_2$-99 gave a higher I_{sc} output than the dipole Zn$_2$-53 and collinear Zn$_2$-66 diporphyrins. This is in keeping with the trend observed previously in this work. However, the results of the dipole and collinear diporphyrins show a different trend from this work, with little difference between the I_{sc} values. Grätzel's results indicate that the dipole diporphyrin Zn$_2$-53 is more efficient than the collinear Zn$_2$-66 type antenna system.

The cell efficiencies reported here are low compared to those obtained for Ru dyes (up to 10.4%).[150] However, these results were obtained without any attempt to optimise the cell conditions. In particular, solvents such as CHCl$_3$ were used for dye adsorption, whereas this work has shown the optimal solvent for some of these porphyrins is THF.

Currently the best literature results are that of Wamser and Cherian with a η of 3.5% for a ZnTCP **Zn-8** TiO$_2$-dyed PEC.[162]   Therefore an efficiency of 1.5% from an un-optimised cell is excellent.

5.4 Conclusion

With the development of a reliable solar cell testing apparatus and methodology, a number of conclusions can be made giving insight into the future direction this research could take.

The cell conditions employed have not been optimised, but an insight into the significances of some of the variables has been obtained. It is now known that the porphyrin free-acids are superior to their salts, and Zn(II) metalloporphyrins are the most efficient photosensitisers. The results also suggest that Cu(II) porphyrins are worth pursuing in future where long term stability of the chromophores is required in solar cells. Other metals (i.e. Mg, Ru etc.) have yet to be screened. It has been found that the adsorption solvent choice, electrolyte composition, and dye concentrations are all critical to cell performance, and should all be optimised for each dye in future studies. 4-t-Butylpyridine appears to offer stabilisation during V_{oc} conditions and is important for long-term PEC applications (optimal concentrations will need to be found).

The TPP, TXP and TBP monoporphyrin acids (ZnTAP-=-PhCO$_2$H) have a significant advantage over the arrays and other monoporphyrins. It needs to be determined whether cell performance using these dyes increases with decreasing steric bulk and/or with decreasing electron-donating effect of the aryl substituents. The effect of aggregation as controlled by the steric nature of the porphyrin, needs to be determined. Electronic effects may be primarily determining the pK_a of the binding moiety and therefore dramatically affecting binding. This could be further investigated with both EDG and EWG tetra-$meso$-arylporphyrin derivatives (i.e. 4-methoxyphenyl or 4-chlorophenyl), determining pK_as and using stronger binders such as sulfonic acids.

For dipole **Zn$_2$-53** and collinear **Zn$_2$-66** diporphyrins, the overall low performance may be the result of poor binding. Low cell performance of the "sticky" porphyrin arrays could result from inter-molecular aggregation; this would be more significant for the larger arrays. There is also the likelihood that the small porosity of TiO$_2$ nanocrystalline layer may be preventing adsorption of the dye into its bulk.

The excellent Grätzel results for the "sticky" diporphyrin $\mathbf{Zn_2}$-$\mathbf{99}$ ($\eta = 1.5\%$) is up to half that of the best reported by Wamser and Cherian.[162] This shows good promise for the ZnTAP-=-PhCO$_2$H dyes.

An important next step in the design of these porphyrin dyes would be to find a stronger/better-binding group. The synthesis of sulfonates, phosphonates and multi-carboxylic acid functionalities should be further investigated in this regard. The role that the styryl linker plays in cell performance also needs to be evaluated. Long-term stability of these porphyrin PECs towards V_{oc} conditions is unknown and needs be investigated. Techniques for determining the pK_a of these acids were not developed in this thesis but are of interest and warrant future investigation.

Synthesis of Sulfur Functionalised Porphyrins

6.1   Introduction

This chapter describes the synthesis of a number of new derivatised disulfide and thiol porphyrin moieties, along with the development of some novel thiophene-appended porphyrins.   The thiophene derivatives have dual application potential for both photo/redox active Au surface chemistry and polymer applications.

6.1.1   Disulfide and Thiol Porphyrins

The synthesis of disulfide and thiol porphyrin derivatives for functionalisation of Au surfaces has been an active field of research for light harvesting and optoelectronic applications. As discussed in Chapter 1 (section 1.2.2, pg 13) a number of examples of porphyrins coordinated through axial metals[51,66,67] or hydrogen bonding[186] via a thiol or disulfide ligand systems have been reported in the literature. A large number of covalently linked sulfur-functionalised porphyrins have been synthesised for depositing monolayers onto Au surfaces (Figure 6-1). The vast majority of these are linked through a single *meso*-aryl group by various linkers systems (Figure 6-1, **I**). The sulfur-attaching groups range from thiols and their symmetrical disulfide analogues to sulfides and acetylthio derivatives.[26,72,187,188] The linker systems are commonly short to long alkyl chains, with some containing other redox centres like ferrocene.[25,189] There are examples in which there is functionality on the opposing side of the porphyrin (position X, **I**), having photo/redox active centres such as ferrocene[190], porphyrin[72] and C_{60}[25]. Other *meso*-aryl examples that appear in the literature are the bis- and tetra-substituted sulfides of Lindsey et al.[191] **II**, and the bis-substituted thiol, disulfides, sulfides and acetylthiols of Sanders et al.[192] **III**.
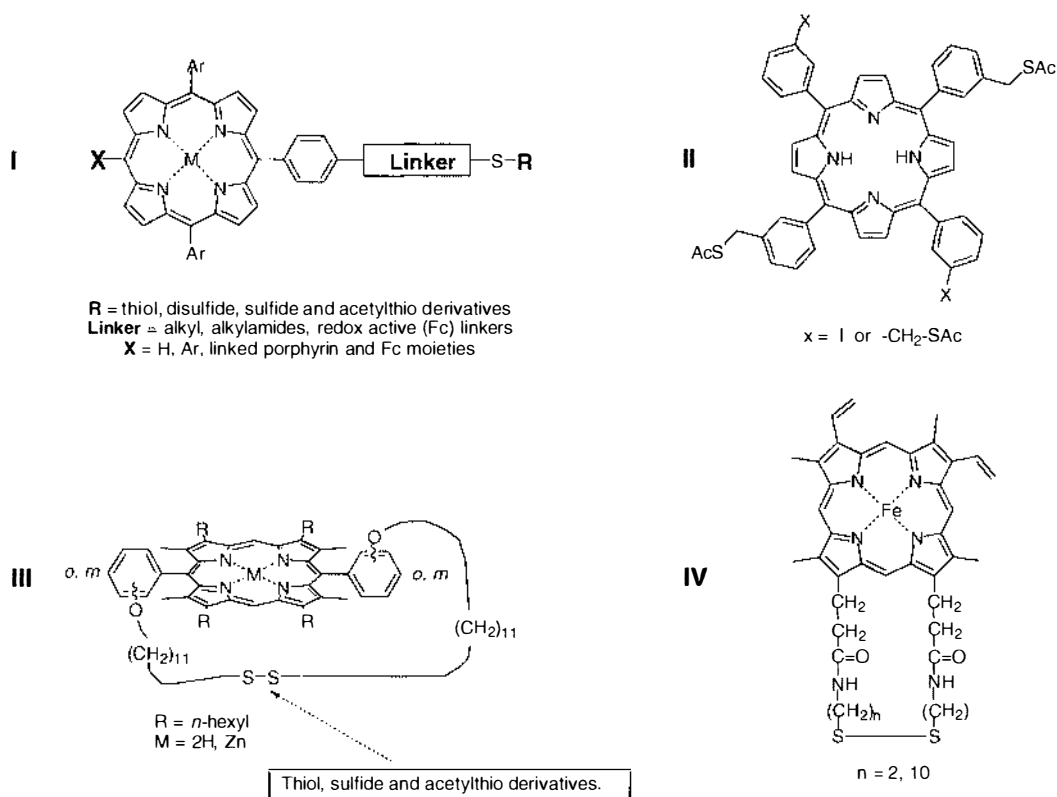
Figure 6-1. Examples of covalently linked sulfur-functionalised porphyrins.

Sulfur-functionalised porphyrins attached through linkers at the β-pyrrolic position are rare; a few modified natural heme derivatives, prepared by Willner et al.[64] and Kobayashi et al.[65], are known (Figure 6-1, **IV**). Our extensive experience with TAPps Wittig chemistry developed in this laboratory and familiarity with classical porphyrin forming condensation reactions, presented an opportunity to synthesise simple novel thiol-functionalised porphyrins for attachment to both GaAs and Au surfaces. These functionalised surfaces are of interest for the study of photo-initiated charge transfer process and potential devices thereof (i.e. photoelectronic molecular and alternative light harvesting devices).

The simplest route proposed to thiol-functionalised porphyrins with our TAP Wittig chemistry would involve the Wittig reaction of 4-mercaptobenzaldehyde **131** with TXPps **5** (Figure 6-2) forming the β-styryl thiol derivative **132**.

131

a) Wittig,
b) Isomerisation

TXPps
5

132
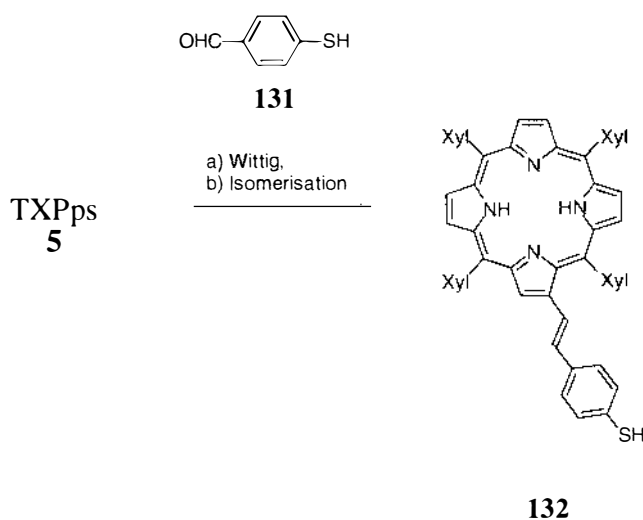
Figure 6-2. Direct synthesis of β-styryl thiol porphyrin derivative **132**.

However, it was clear from previous work that the use of disulfides over thiols for the preparation, purification and attachment to surfaces is preferred due to their greater stability and ease of synthesis; others have reported problems handling free thiols.[72,192] By using building block methodology, the disulfide approach also offers the flexibility to allow the co-adsorption of either two similar or two dissimilar chromophore species (R_1/R_2, Figure 6-3), or perhaps a chromophore and an anti-aggregation molecule onto a surface in a controlled ratio.
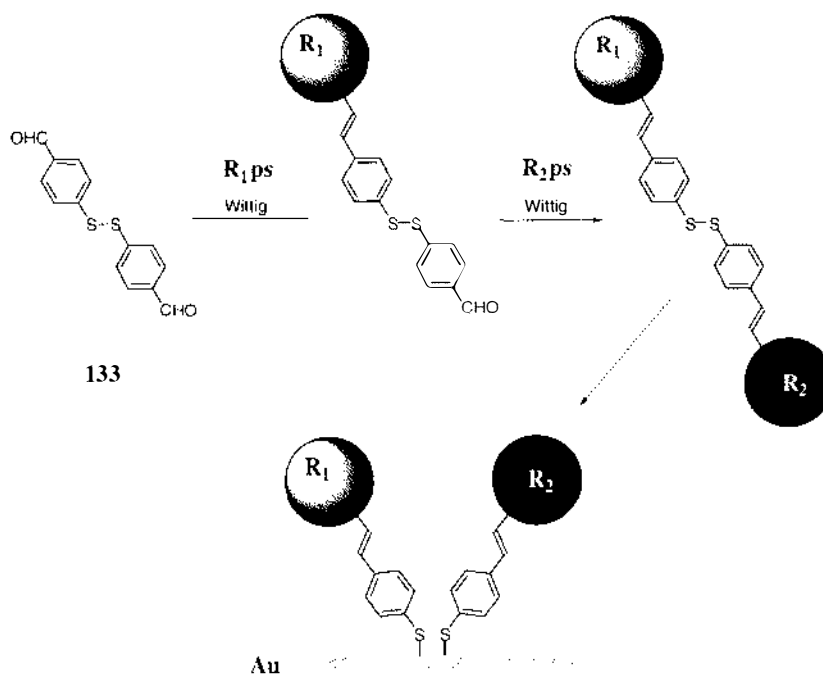
Figure 6-3. Disulfide building block approach.

6.1.2 Thienylporphyrins

Not only are thiophene-appended porphyrins of significance for binding to Au surfaces[53], but they also exhibit substantial potential in polymer research currently under investigation in our laboratories. A variety of thienylporphyrins exist in the literature; a representative collection of some of those suitable for both Au binding and polymerisation are illustrated in Figure 6-4. The most common examples are the tetra-*meso*-substituted 2- or 3-thienylporphyrins, these include tetra-(mono-[98,193-196], bi-[193] and ter-thiophene[193])porphyrin variants (Figure 6-4, **I**).
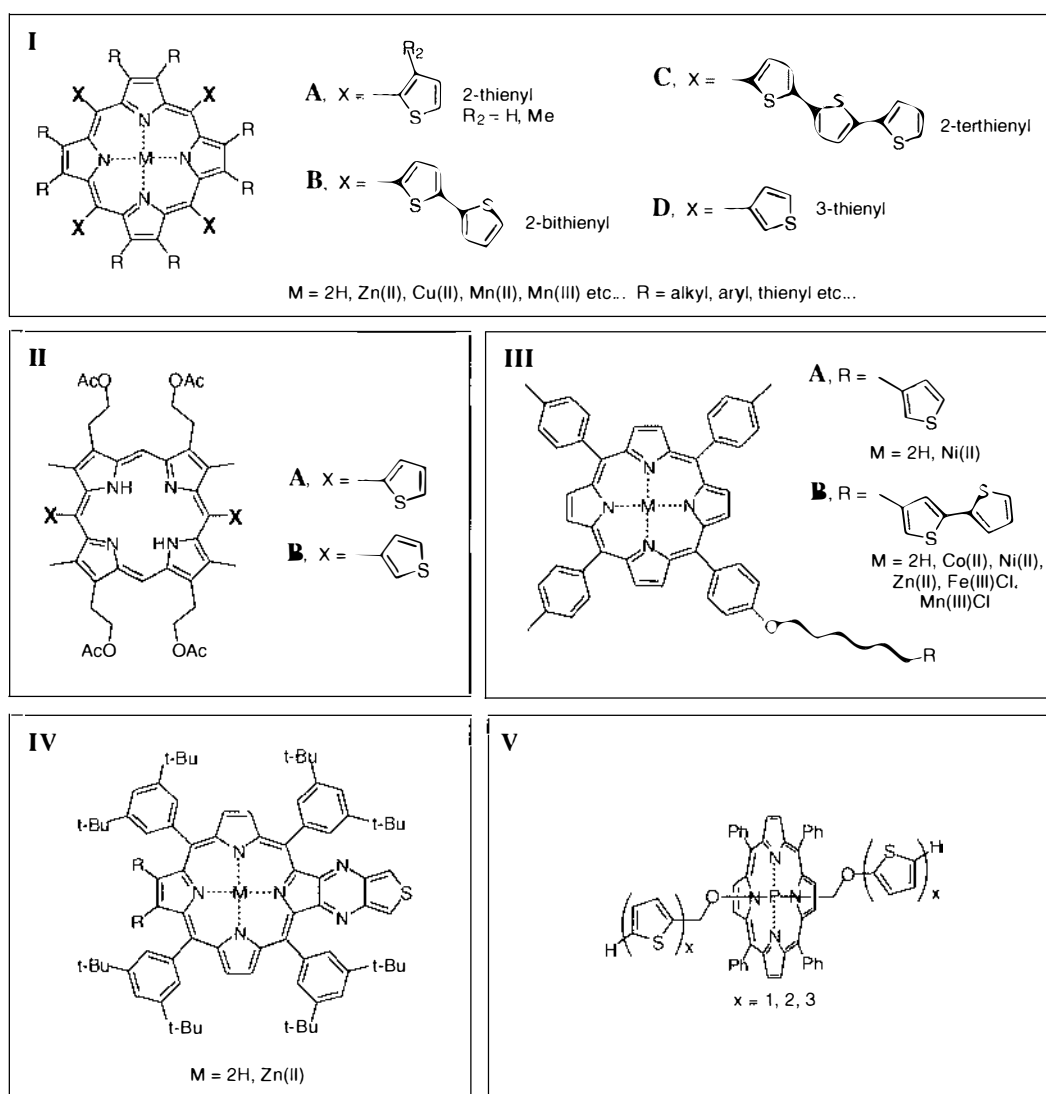
Figure 6-4. Thienylporphyrins.

The only examples of *trans*-bis-substituted 2- and 3-thienylporphyrins are those of Armiger et al. (Figure 6-4, **II**).[197] A couple of *meso*-alkyl-linked examples exist, these having either a single 3-thiophene prepared by Ballarin and co workers[198] or a single 3-bithiophene unit reported by Schaferling et al.[199] (Figure 6-4, **III**). Crossley's group has synthesised a number of mono and diporphyrin thiophene-appended derivatives primarily for binding to Au, where the sulfur is fully conjugated with the porphyrin ring (Figure 6-4, **IV**).[54] Attaching thiophenes axially through a phosphorus(V) porphyrin has been carried out by Shimidzu et al.[200] They have made various mono-, bi- and terthiophene monomers and polymerised these to fabricate so-called "molecular wires" (Figure 6-4, **V**).

Again, our experience with porphyrin and Wittig chemistry has provided the opportunity to make some new 2- and 3-thiophene-appended porphyrins, such as *trans*-bis-2-thienylporphyrin **134** and *trans*-bis-3-thienylporphyrin **135** (Figure 6-5). It has been shown that thiophene binds orthogonal to a Au surface.[201,202] Therefore, 2-thienyl derivative **134** offers potential to bind the porphyrin planar to a Au surface, whereas the 3-thienyl derivative may adopt a more vertical mono-coordinated arrangement.

Bis-2-thienylporphyrin
M-134

Bis-3-thienylporphyrin
M-135

R = *n*-Butyl
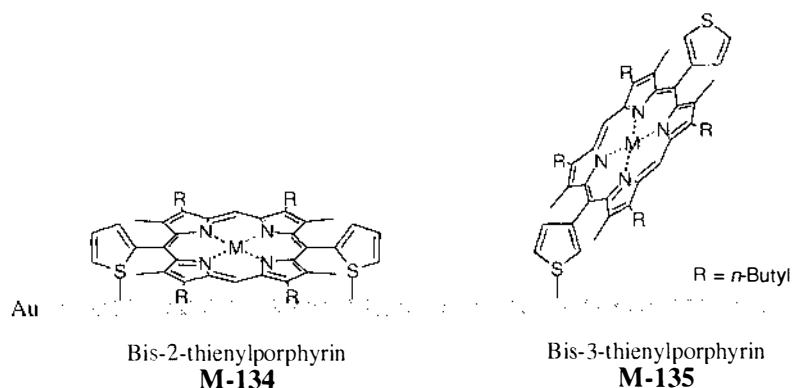
Figure 6-5. The binding of proposed 2- and 3-thienylporphyrin derivatives.

A synthesis of 3'-formylterthiophene **136** was developed in our laboratories by Collis (Figure 6-6).[203] This aldehyde **136** was made to provide a common building block for a wide variety of functionalised polythiophenes. Aldehyde **136** was also clearly useful for porphyrin synthesises. By utilising established TAPps Wittig chemistry and classical porphyrin condensation forming reactions, the synthesis of mono-, bis- and tetra-substituted terthienylporphyrins **137**, **138** and **139** was proposed (Figure 6-6). It

has been shown that thiophene can bind to a Au surface[204] therefore these types of compounds are of interest for Au surfaces binding as well as polymerisation studies.
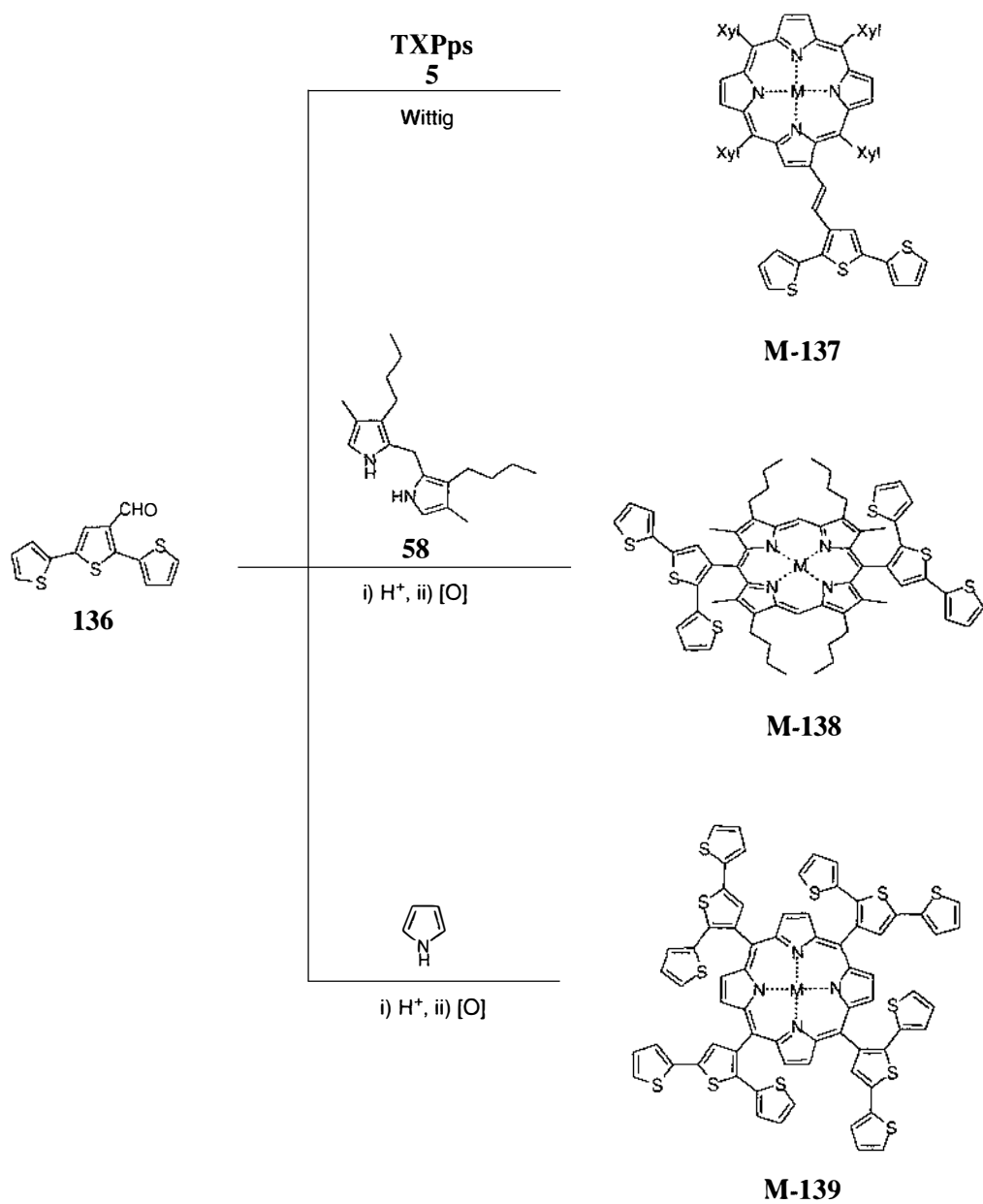
Figure 6-6. Proposed 3'-terthiophene porphyrins.

6.2   Synthesis and Characterisation

6.2.1   Synthesis of Disulfide- and Thiol-appended Porphyrins

An efficient high yielding synthesis of 4,4'-dithiobisbenzaldehyde **133** has been reported. by Dickman et al. from 4-(*tert*-butylsulfanyl)benzaldehyde **140**, which gives **133** in 92% yield (Figure 6-7). [205,206]
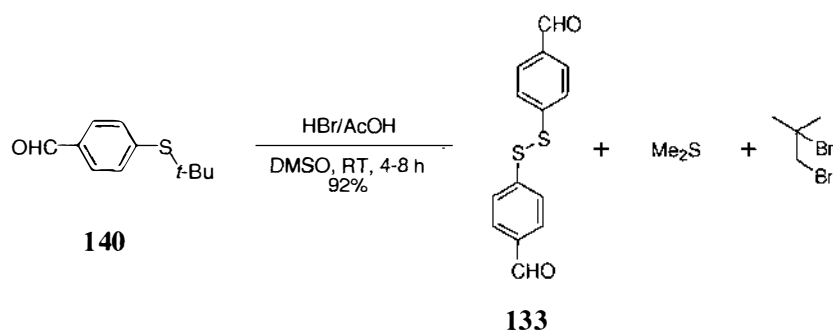
Figure 6-7. Synthesis of bisformyl-disulfide **133**.[206]

However with the availability of 4-mercaptotoluene in our laboratory and extensive experience with benzaldehyde formation for porphyrin synthesis, an alternative synthesis of disulfide **133** was investigated via bromination and Sommelet oxidation of the tolyldisulfide **141** (Figure 6-8).
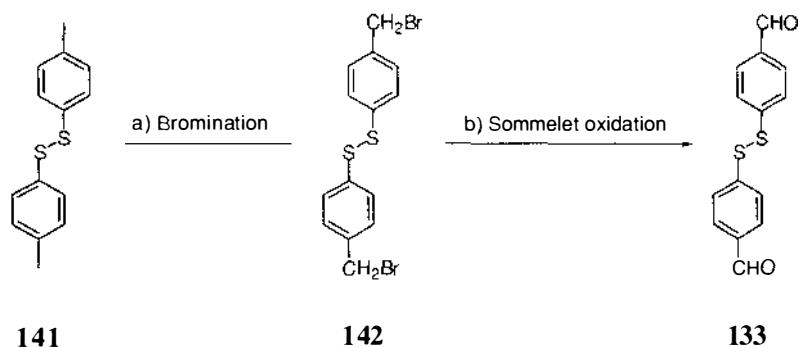
Figure 6-8. Alternative synthesis of bisformyl-disulfide **133**.

The alternative approach to the synthesis of disulfide **133** was carried out. 4,4'-Dithiobis-toluene **141** was prepared in quantitative yield from the oxidation of *p*-toluenethiol **143** with active MnO$_2$[95] by the method of Papadopoulos et al. (Figure 6-9).[207] The ^{1}H NMR data was consistent with that quoted previously.[208] The bromination of **141** gave a mixture of bromomethylphenyl disulfides **144**, **142** and **145** (identified by ^{1}H NMR spectroscopy and mass spectrometry). Separation of this mixture by column chromatography proved difficult, therefore this mixture was subjected to Sommelet[209] oxidation 'as is'. Both 4,4'-dithiobisbenzaldehyde **133** (21% from **141**) and 4-*p*-tolyldisulfanylbenzaldehyde **146** (14% from **141**) were isolated by column chromatography. Additional ^{1}H, ^{13}C NMR and HRMS data for **133** was obtained, as these do not appear in the literature.[206] The melting point is consistent with that reported.

a) MnO$_2$ (1.0 eq), CHCl$_3$, RT (15 min). b) Br$_2$ (4.0 eq, drop-wise), hv, CCl$_4$, argon, reflux. c) i) HMTA, EtOH/H$_2$O, reflux (6 h). ii) Conc. HCl, reflux (30 min).
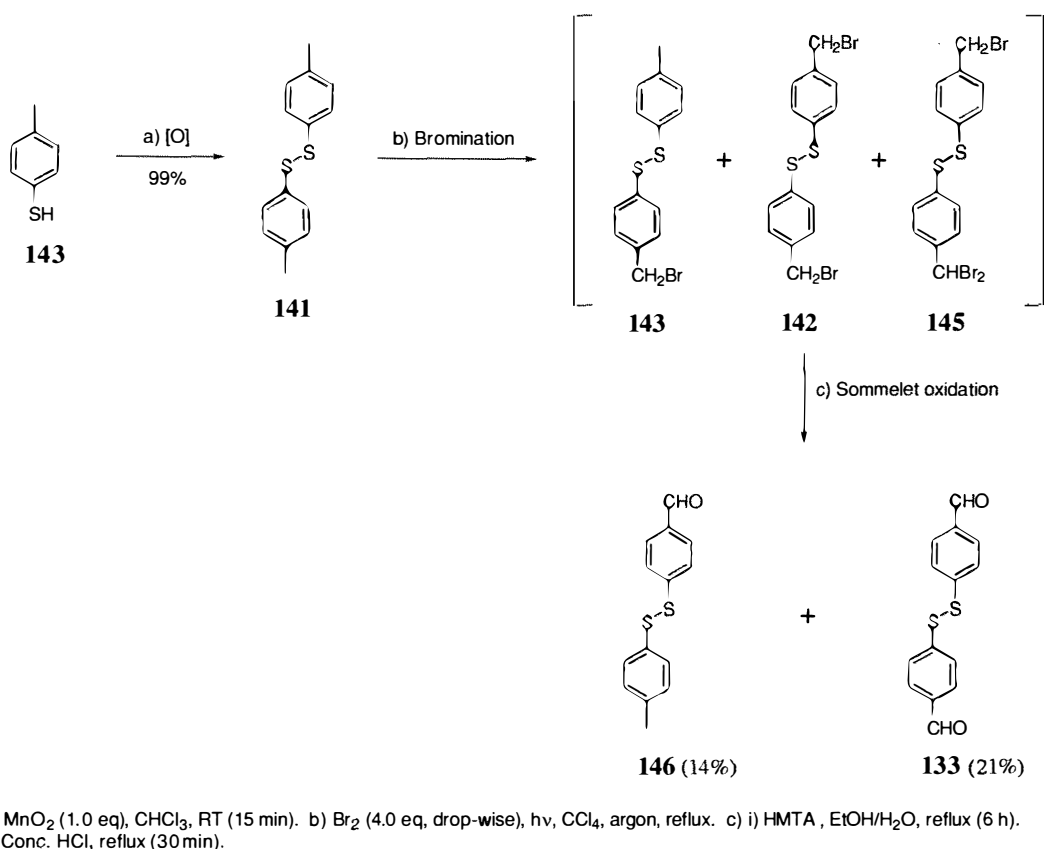
Figure 6-9. Synthesis of formyl-disulfides **146** and **133**.

Monoformyl disulfide **146** has not been described or characterised in the literature as of yet, and was characterised by ^{1}H, ^{13}C NMR spectroscopy and EI mass spectrometry.

The ^{1}H NMR was typical of a *para*-substituted benzaldehyde and toluene, showing the two expected sets of AB quartets from each aryl group, and the methyl and aldehyde resonances. Both **146** and **133** were used for the synthesis of disulfide functionalised porphyrins.

The Wittig reactions of TXPps **5** with mono- and di-formyl disulfides **146** and **133** were undertaken. The treatment of the diformyl disulfide **133** with 2.0 equivalents of TXPps **5** gave a mixture of mono- and di-Wittig products **147** and **148** respectively (Figure 6-10). Standard I$_2$ isomerisation conditions were employed, ensuring only *trans* products resulted. The Wittig reaction presumably would have been driven towards the diporphyrin product **148** if an excess of TXPps **5** had been employed; alternatively using less **5** could have resulted in a higher yield of the mono product **147**. However, the mono Wittig product **147** offers access to unsymmetrical diporphyrinyl disulfides (see Figure 6-3), although this is yet to be pursued. Metallation of diporphyrin **148** with nickel(II) gave **Ni$_2$-148** in near quantitative yield.

a) DBU (3 eq), toluene, reflux (15 min), N$_2$. b) i) I$_2$ (3 eq), CHCl$_3$, RT (3 h). ii) Sat. Na$_2$S$_2$O$_3$. c) Ni(OAc)$_2$·4H$_2$O (30 eq), CHCl$_3$/MeOH, reflux (16 h), N$_2$.
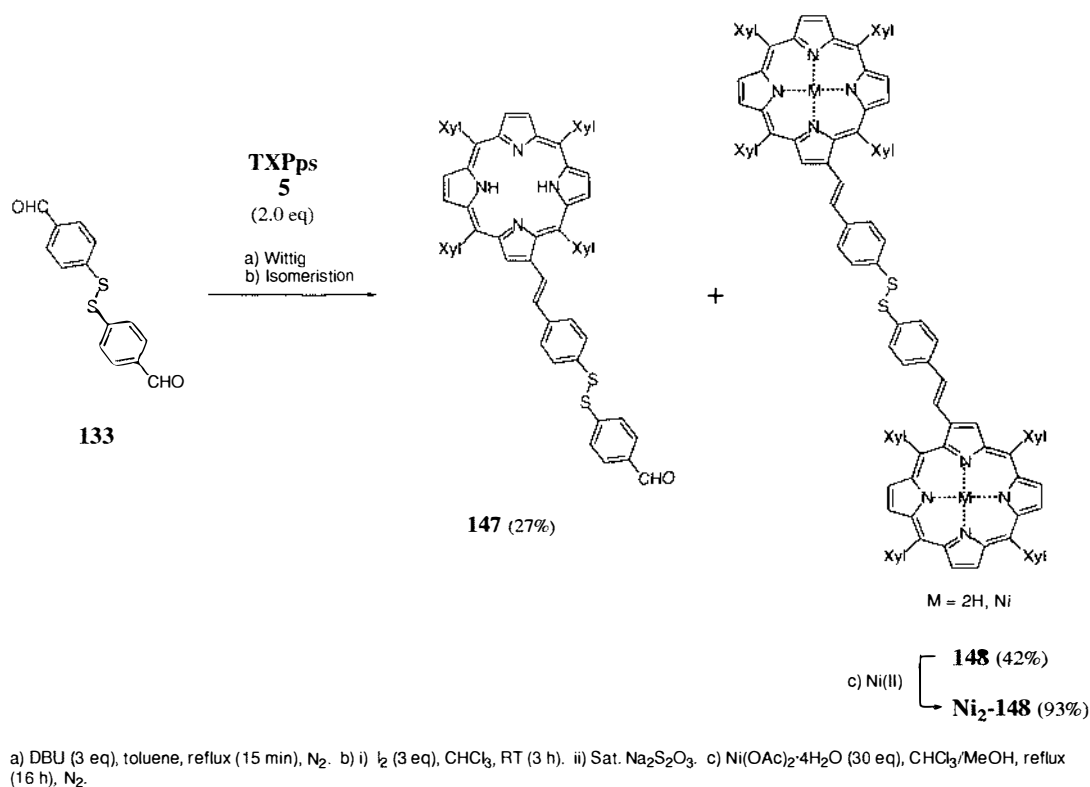
Figure 6-10. Synthesis of mono and di-Wittig TXP disulfides **147** and **148**.

The disulfide porphyrins **147** and **148** were characterised by ^{1}H NMR and UV-vis spectroscopy and FAB HRMS. Both **147** and **148** gave typical β-styryl substituted TXP ^{1}H NMR and UV-vis spectra. The unsymmetrical building block **147** displaying appropriate coupling in COSY spectra amongst doublets associated with the styryl aromatic protons, and amongst the doublets for the benzaldehyde aryl protons.

The Wittig reaction of tolyl monoformyl disulfide **146** with TXPps **5** gave what appeared to be mixtures by TLC, and column chromatography was ineffective due to band smearing. To aid isolation, metallation of the mixture with zinc(II) was carried out affording pure **Zn-149** in low yield (24%) after column chromatography (Figure 6-11). This Wittig reaction was then repeated, but the crude product was directly metallated with nickel(II). This gave better chromatographic resolution of products on the silica gel column. Both disulfide **Ni-149** and reduced thiol derivative **Ni-132** were isolated and characterised as the major porphyrin components of the reaction. Both **Ni-149** and **Ni-132** together accounted for only 52% of the theoretical product yield. No other products were isolated from the reaction mixture and the reaction conditions were not optimised at this time.
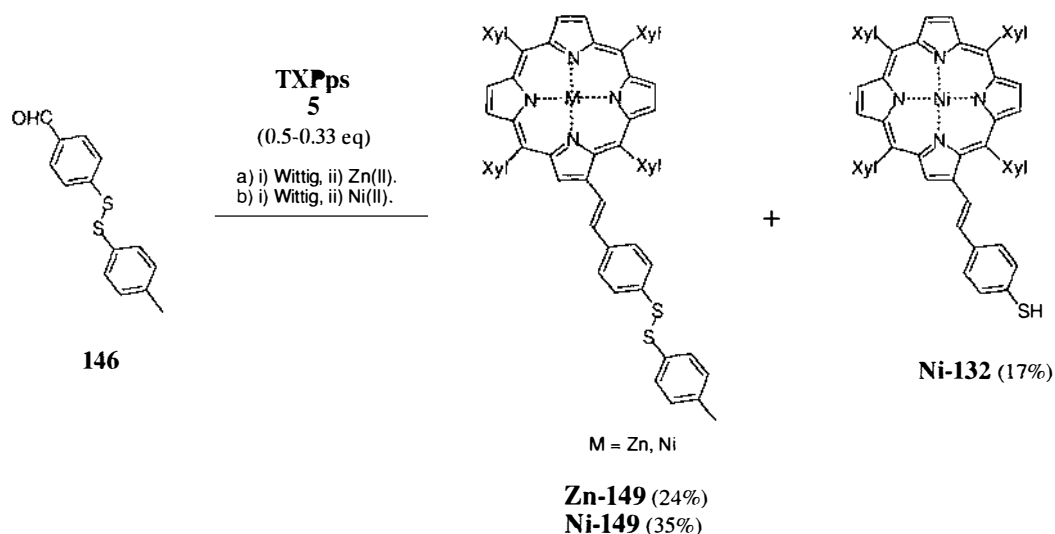
a) i) **5** (0.33 eq), DBU (5 eq), toluene, reflux (20 min), N$_2$. ii) Zn(OAc)$_2$·2H$_2$O (2.0 eq), CH$_2$Cl$_2$/MeOH, RT (20 min), N$_2$. b) i) **5** (0.5 eq), DBU (5 eq), CHCl$_3$, reflux (20 min), N$_2$. ii) Ni(OAc)$_2$·4H$_2$O (30 eq), CHCl$_3$/MeOH, reflux (13 h), N$_2$.

Figure 6-11. Synthesis of tolyl disulfide porphyrin **M-149** and thiol porphyrin **Ni-132**.

Both **M-149** and **Ni-132** gave typical β-styryl substituted TXP ^{1}H NMR and UV-vis spectra and correct FAB HRMS data. The unsymmetrical disulfides **Zn-149** and **Ni-**

149 displayed appropriate coupling in the COSY spectra amongst two sets of doublets associated with the styryl and tolyl aryl protons. The methyl tolyl resonance was observed at 2.37 ppm for both compounds. The thiol proton of **Ni-132** was not observed in the ^{1}H NMR spectrum, but the correct parent molecular ion was obtained in the FAB HRMS.

The use of tolyl monoformyl disulfide **146** in dipyrrylmethane condensation chemistry was explored, and a new bis(tolyldisulfide)porphyrin (BDP) **150** formed (Figure 6-12). This was achieved initially by condensing DPM **58**[106,107] with 4-*p*-tolyldisulfanyl-benzaldehyde **146** using *p*-toluenesulfonic acid under similar conditions to that of Gunter et al.[115], to give the porphyrinogen. Oxidation with *p*-chloranil in DCM then afforded **150** in 70% yield.

146

58

a) H$^+$
b) [O]

M = 2H, Zn

c) Zn(II) **150** (70%)

→ **Zn-150** (87%)

a) i) *p*-TsOH·H$_2$O (0.25 eq), MeOH (0.08 M), RT (22.5 h), N$_2$. b) i) *p*-Chloranil (2.0 eq), CH$_2$Cl$_2$, RT (2.5 h). ii) Sat. Na$_2$S$_2$O$_3$ /Et$_3$N (excess), RT (30 min). c) Zn(OAc)$_2$·2H$_2$O (2.0 eq), MeOH/CH$_3$Cl, RT (15 min).
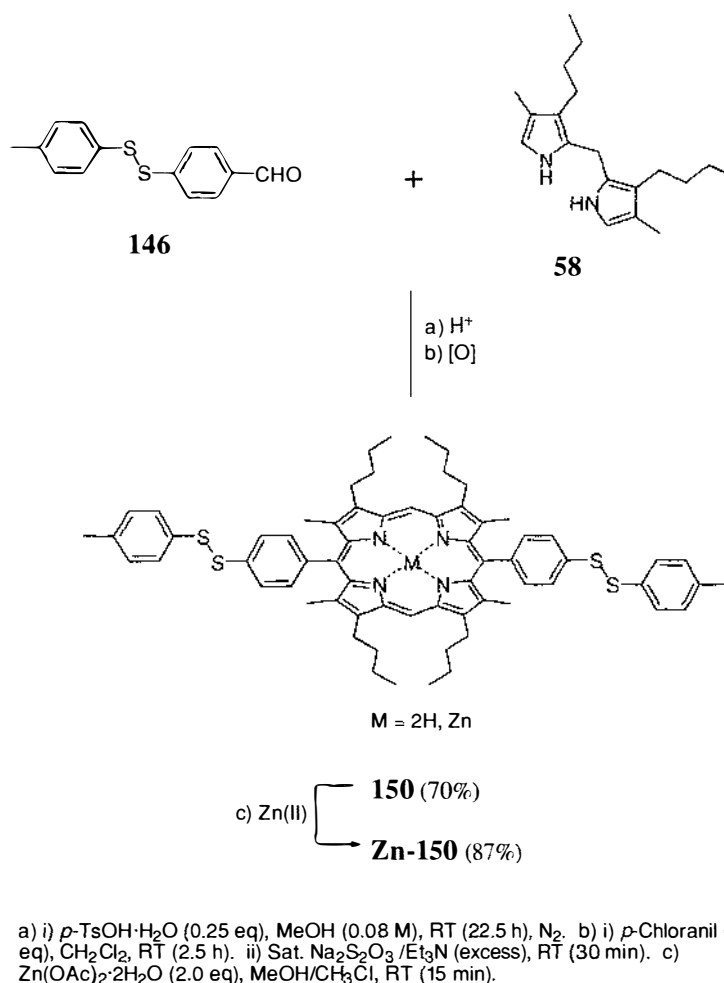
Figure 6-12. Synthesis of bisdisulfide porphyrins (BDPs) **M-150.**

Metallation of BDP **150** with Zn(II) by using the acetate method[60] gave **Zn-150** in 87% yield.

The bisdisulfide porphyrins **150** and **Zn-150** were characterised by ^{1}H, ^{13}C NMR and UV-vis spectroscopy and FAB HRMS. Both **150** and **Zn-150** gave typical TBMP ^{1}H NMR and UV-vis spectra. In the ^{1}H NMR spectrum the tolyl aryl resonances were observed as separate doublets, and the aryl protons of the *meso*-attached phenyl rings were observed as AB quartets. Assignments in the ^{13}C NMR spectrum of **150** were aided with HETCOR spectra.
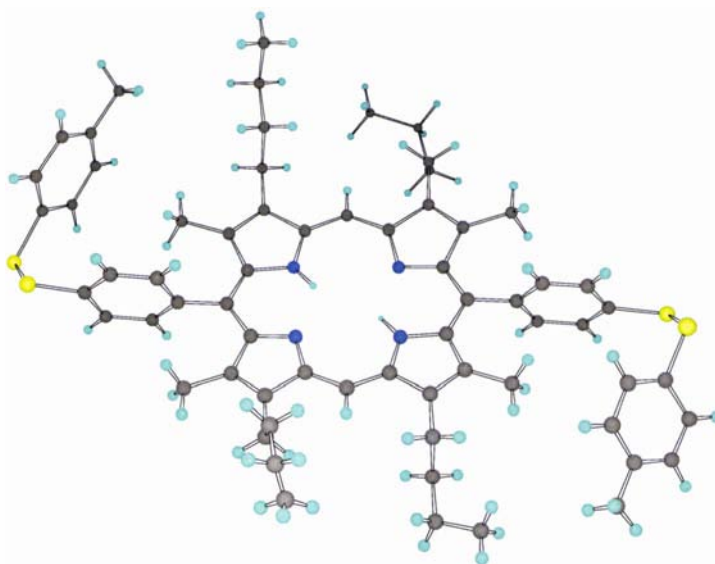
Figure 6-13. Chem3D representation of bisdisulfide porphyrin (BDP) **150** crystal structure.

X-ray quality crystals of **150** were grown from a diffusion mixture of CHCl$_3$/MeOH. The structure was solved by Professor A. K. Burrell and refined by B. Therrien (Figure 6-13). The crystal structure refinement data is tabulated in the appendix (Table 7-9, pg 335) and full crystallographic data has been submitted to *Acta Cryst. E.*[134] The FAB MS was typical of porphyrins; the most notable characteristic was intense molecular ion mass peaks, representing the porphyrin with cleavage at the disulfide bonds.

6.2.2   Synthesis of Thiophene-appended Porphyrins

With the ready availability of thiophene aldehydes in our laboratories, the syntheses of bis- and tetrathienylporphyrins were explored. The synthesis of bis-2-thienylporphyrin (B2TP) **134** was straightforward, using *p*-toluenesulfonic acid to catalyse the 2+2 condensation of 2-formylthiophene **151** with DPM **58** in MeOH using similar conditions employed for **150**. Subsequent oxidation of the porphyrinogen with *p*-chloranil gave **134** in 65% yield (Figure 6-14). **Zn-134** was obtained quantitatively from **134** using the acetate method.[60]

a) i) *p*-TsOH·H₂O (0.25 eq), MeOH (0.08 M), RT (12 h), N₂. b) i) *p*-Chloranil (2.2 eq), CH₂Cl₂, RT (2.5 h). ii) Sat. Na₂S₂O₃/Et₃N (excess), RT (1.5 h). c) Zn(OAc)₂·2H₂O (2.0 eq), MeOH/CH₂Cl₂, RT (10 min).
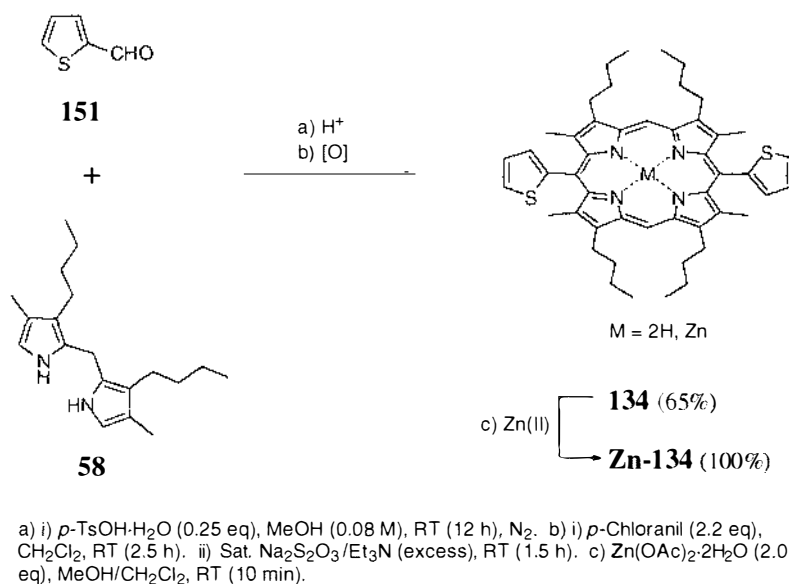
Figure 6-14. Synthesis of bis-2-thienylporphyrin (B2TP) **M-134**.

Complete characterisation of both the free-base and zinc(II) metallo derivatives by ¹H NMR, UV-vis, FAB HRMS gave spectra typical of bis-substituted TBMPs. X-ray quality crystals of both the free-base **134** (Figure 6-15) and Zn(II) derivative **Zn-134** (Figure 6-16) were obtained from a diffusion matrices of CHCl₃/MeOH. The structures was solved by Professor A. K. Burrell and refined by B. Therrien. Both **134** and **Zn-134** adopt typical non-distorted planar porphyrin geometries. Interestingly, only *anti* isomers are observed in the crystal structures. This is presumably due to more favourable crystal packing forces for this isomer. The crystal structure refinement data

for **134** and **Zn-134** is tabulated in the Appendix A (Table 7-6, pg 333 and Table 7-7, pg 334 respectively) and full crystallographic data has been submitted to *Acta Cryst. E.*[134].
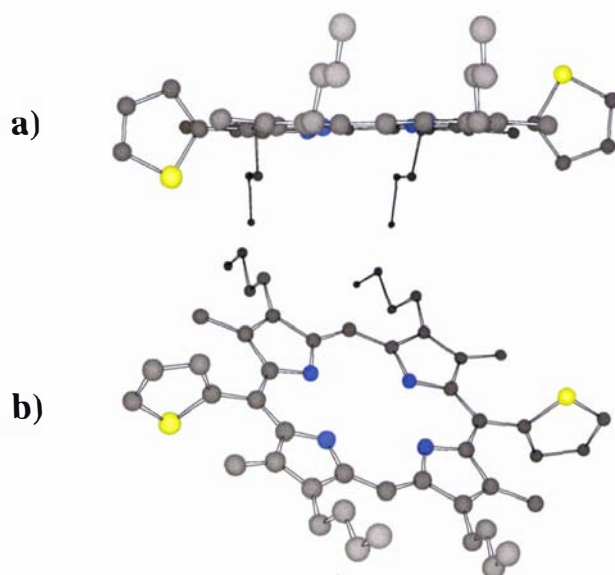
Figure 6-15. Chem3D representations of B2TP **134** crystal structure, a) side on view, b) tilted view (hydrogens omitted for clarity).
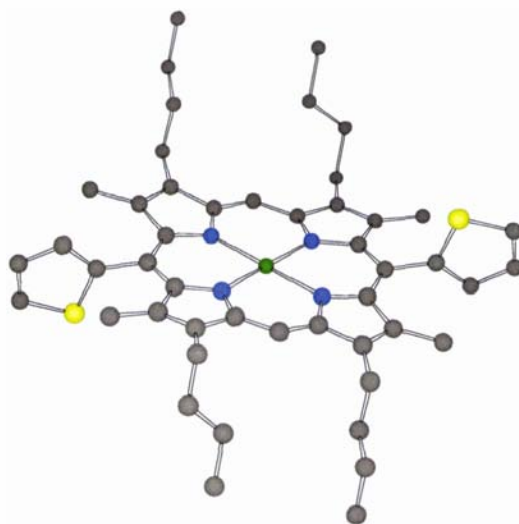
Figure 6-16. Chem3D representation of ZnB2TP **Zn-134** crystal structure (hydrogens omitted for clarity).

The synthesis of the bis-3-thienylporphyrin (B3TP) analogue **135** was then undertaken. Under the author's supervision, the synthesis was carried out as Bachelor of a Technology fourth year project by S. O'Connor. Employing the same conditions as for **134** to catalyse the 2+2 condensation of DPM **58** with 3-formylthiophene **152** gave poor

yields (23%) of porphyrin **135** after oxidation. By repeating the reaction under Lindsey conditions[114], using TFA as the acid catalyst followed by subsequent oxidation, the synthesis of **135** was achieved in a more respectable 53% yield (Figure 6-17).

a) i) TFA (1.0 eq), CH_2Cl_2 (10^2 M), RT (15 min), N_2. b) i) p-Chloranil (2.5 eq), CH_2Cl_2, RT (4 h). ii) Et_3N (excess), RT (1.75 h).
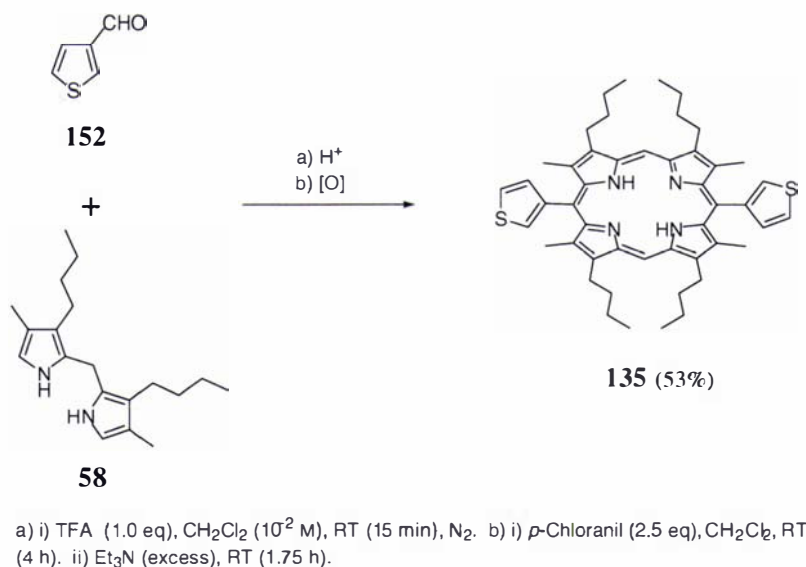
Figure 6-17. Synthesis of bis-3-thienylporphyrin (B3TP) **135**.

^{1}H and ^{13}C NMR, UV-vis, FAB HRMS spectra were again as expected for a bis substituted TBMP, being consistent with the 2-substituted thiophene derivative **M-134**. X-ray quality crystals of **135** were obtained from a diffusion matrix of $CHCl_3$/MeOH. The structure was solved by Professor A. K. Burrell and refined by B. Therrien. Again **135** adopted a typical non-distorted planar porphyrin geometry (Figure 6-18), with an *anti* configuration as previously observed for **M-134**. The crystal structure refinement data for **135** is tabulated in the Appendix A (Table 7-8, pg 334) and full crystallographic data has been submitted to *Acta Cryst. E.*[134].
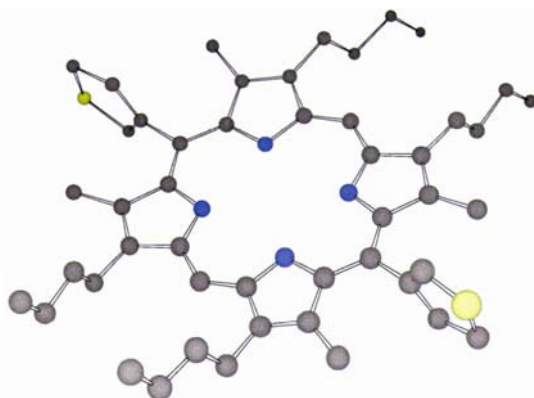
Figure 6-18. Chem3D representation of B3TP **135** crystal structure (hydrogens omitted for clarity).

Exploiting 3'-terthiophene aldehyde 136.

TAP-=-Terthiophenes

The TAPps Wittig reactions on thiophene aldehydes were first investigated in our laboratories by Allwood, Burrell and Officer with the synthesis of a 3-thienyl TPP derivative **153** (Figure 6-19).[210] This was later extended to give the β-vinyl 3'-terthienyl TPP derivative **154** (Figure 6-19).[211] The synthesis of the 3-thienyl TPP derivative **153** was achieved using Et$_3$N as the base and I$_2$ isomerisation of the resulting *cis/trans* mixture afforded the title compound. The terthiophene TPP derivative **154** was synthesised using the more usual base, DBU. Isomerisation of the resulting *cis/trans* mixture was achieved by refluxing at 80°C in front of a tungsten lamp over night.
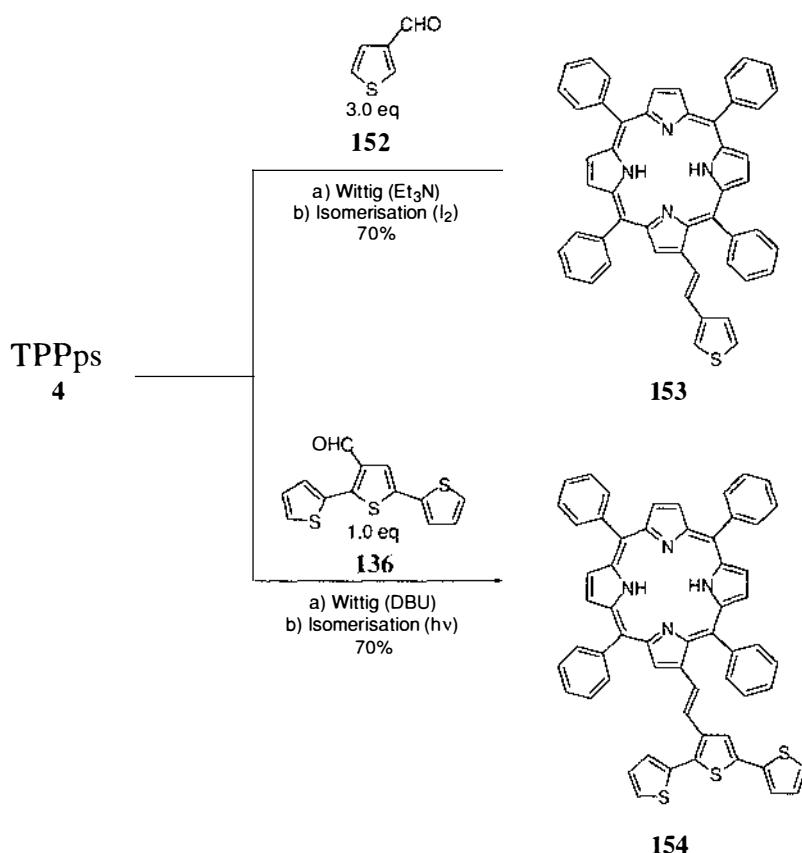
Figure 6-19. Synthesis of thienyl TPP derivatives **153**[210] and **154**[211].

When first synthesised by Reid et al. assignment of the ^{1}H NMR spectrum of **154** proved difficult due to the complication of overlapping *o,m,p*-phenyl and thiophene proton resonances, and so was not fully characterised. With the availability of the

TXPps **5** and the likelihood of obtaining a more soluble analogue of **154** suitable for characterisation, the synthesis of the TXP derivative **137** was carried out. Initially the synthesis of the terthiophene TXP derivative **137** was attempted by Wittig reaction of TXPps **5** and 3'-formylterthiophene **136** in dry refluxing CHCl$_3$. This gave a *cis/trans* mixture ($\approx$ 1:4.5 by ^{1}H NMR) in 70% yield. Isomerisation using standard conditions of 3.0 equivalent of iodine for 3 hours followed by the usual sat. Na$_2$S$_2$O$_3$ work-up was not successful. The ^{1}H NMR of the resulting product revealed a more complex structure than expected, consistent with multiple products. Since this was likely to have resulted from iodination of the appended thiophene moieties (as had been previously observed for the thiophene analogue **153**[211]), no further isolation or characterisation of this mixture was carried out. Instead, the Wittig reaction was attempted at a higher temperature in refluxing toluene. In this fashion, the amount of *cis* product was reduced and the thermodynamically stable *trans* product **137** was obtained in high yield (Figure 6-20). Metallation of **137** with zinc(II) afforded **Zn-137**.
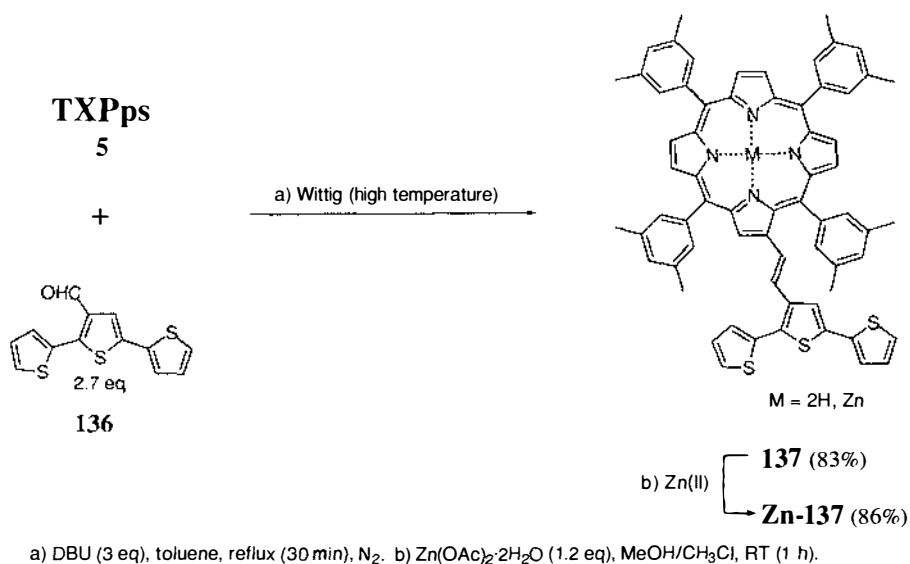
Figure 6-20. Synthesis of TXP-=-terthiophene derivatives **137** and **Zn-137**.

The interpretation of the ^{1}H NMR spectra of **137** and **Zn-137** was not straightforward due to the unsymmetrical nature of a single β-substitution at the porphyrin periphery and the overlapping multiplets from the unsymmetrical terthiophene moiety (Figure 6-21).

a)

b)

Figure 6-21. a) ^{1}H NMR and b) Long Range COSY spectra of TXP-=-terthiophene **137** (400 MHz in CDCl$_3$).
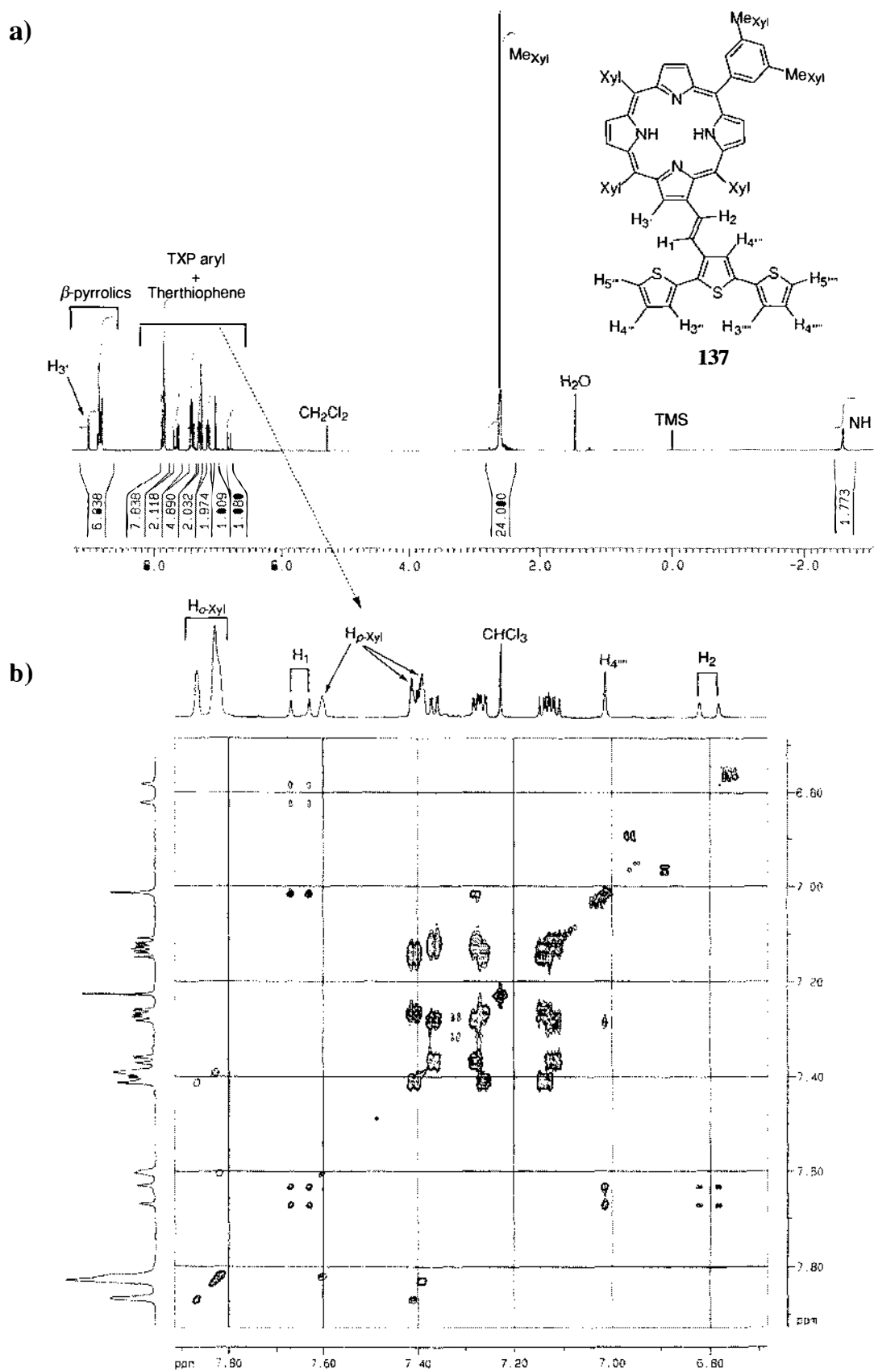
With the aid of COSY spectra, confident distinction can be made between the *meso*-aryl and thiophene protons. In the COSY spectrum a strong coupling is evident between the $H_{3'}$ β-pyrrolic and H_2 ethenyl proton signals. As the terthiophene proton signals demonstrate essentially first order splitting, a more detailed assignment of the terthiophene protons was possible (Figure 6-22), aided by long-range COSY spectra (Figure 6-21). The long-range COSY shows connectivity between the $H_{4'''}$ thienyl proton of the centre thiophene ring, and the H_1 ethenyl proton. In addition, a long-range coupling is observed from $H_{4'''}$ to $H_{3'''}$ of the third thiophene ring. This is consistent with that observed by Collis for the 3'-formylterthiophene **136** (Figure 6-23).[203]
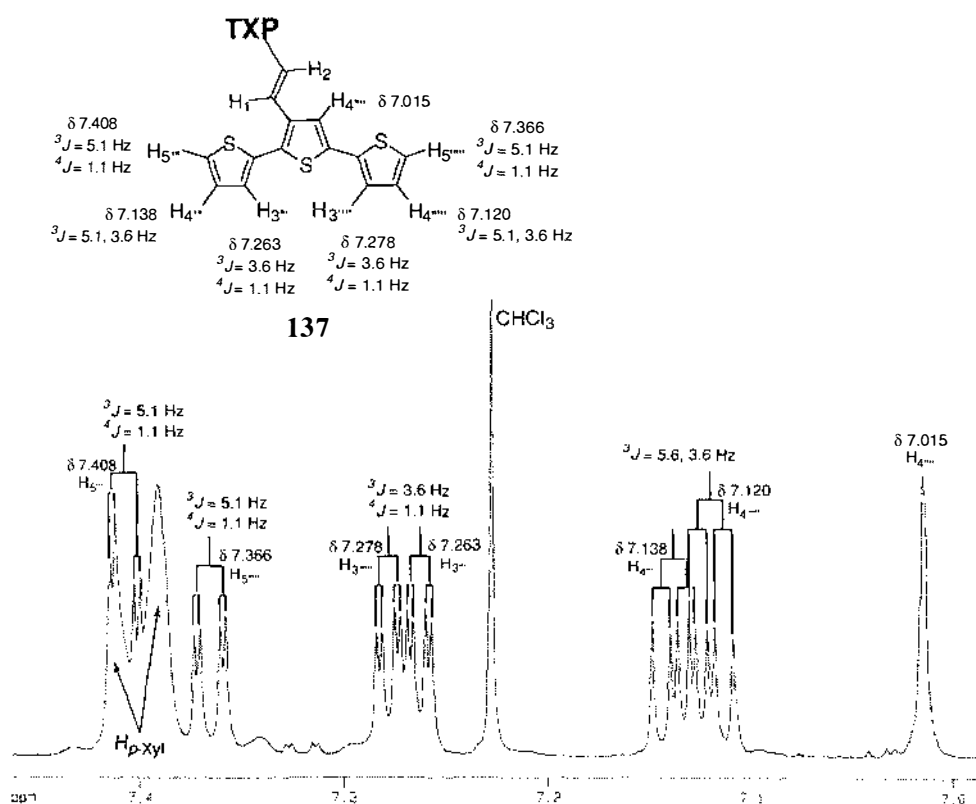
Figure 6-22. Expanded terthiophene region of TXP-=-terthiophene **137** (400 MHz ^{1}H NMR in CDCl$_3$).

From a detailed analysis of the long-range COSY and coupling constants of the thiophene signals in the ^{1}H NMR spectrum, all protons of the terthiophene moiety can be accounted for (Figure 6-22). The TPP derivative **154** of Reid displayed essentially the same terthiophene COSY spectral pattern, allowing full assignment by correlation. The spectra of zinc derivative **Zn-137** could not be fully assigned in the same fashion

since the thienyl signals overlapped and coupling between $H_{3''''}$ and $H_{4''''}$ could not be identified.
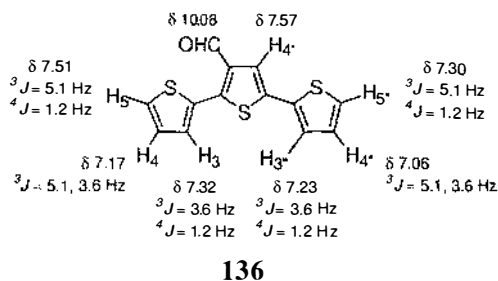
Figure 6-23. 3'-Formylterthiophene **136** 400 MHz ^1H NMR assignments in CDCl$_3$.

Bisterthienylporphyrins

Next, the use of 3'-formylterthiophene **136** in porphyrin-forming condensation reactions with dipyrrylmethane **58** and pyrrole was examined. As had previously been done for the synthesis of **135** under the authors supervision, the synthesis of the bis-3"-terthienylporphyrin **138** was carried out by S. O'Connor (see Figure 6-17). Performing the 2+2 condensation of DPM **58** with 3'-formylterthiophene **136** under Lindsey conditions[114] using TFA as the acid catalyst consequently gave **138** in 41% yield after oxidation with *p*-chloranil (Figure 6-24). Quantitative metallation of **138** with Zn(II) acetate by the author afforded **Zn-138**.

a) i) TFA (1.0 eq), CH$_2$Cl$_2$ (10^{-2} M), RT (15 min), N$_2$. ii) *p*-Chloranil (2.5 eq), CH$_2$Cl$_2$, RT (4 h).
iii) Et$_3$N (excess), RT (1.75 h). b) Zn(OAc)$_2$·2H$_2$O (1.2 eq), MeOH/CH$_3$Cl, RT (30 min).
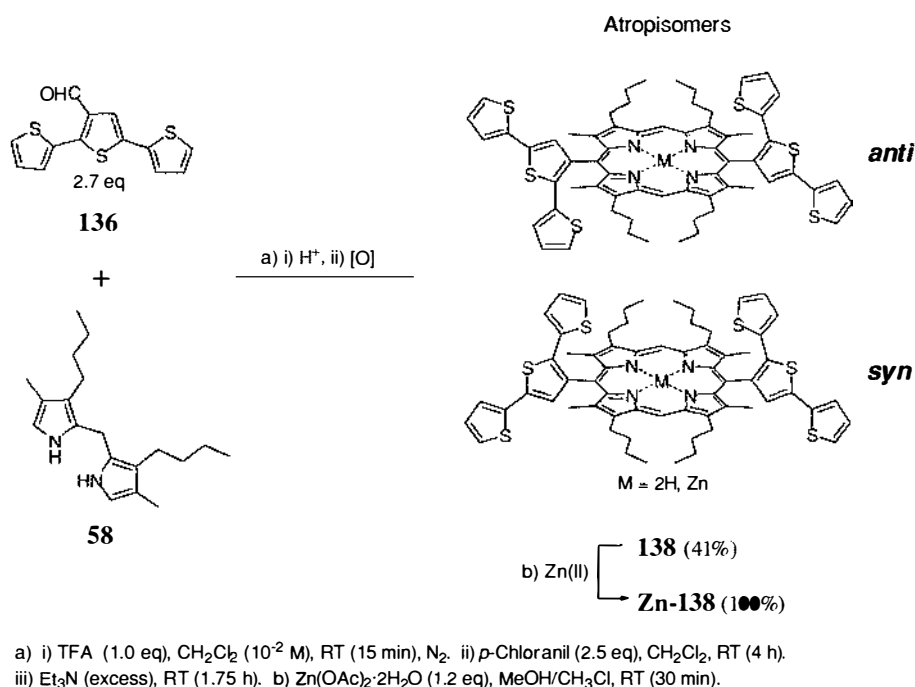
Figure 6-24. Synthesis of bisterthienylporphyrins (BTTP) **138** and **Zn-138**.

The products **138** and **Zn-138** appear to be a mixture of *syn* ($\alpha\alpha$ or $\beta\beta$) and *anti* ($\alpha\beta$ or $\beta\alpha$) atropisomers by ^{1}H NMR analysis (Figure 6-25). The room temperature 400 MHz ^{1}H NMR spectrum of **138** clearly shows splitting in the NH (-2.304, -2.315 ppm), H_{meso} (10.224, 10.230 ppm) and $H_{4''}$ (7.629, 7.631 ppm) proton signals into doublets, indicative of two atropisomers. In contrast, the room temperature 400 MHz ^{1}H NMR spectrum of **Zn-138** shows two well separated and resolved $H_{4''}$ proton resonances (7.674, 7.696 ppm) and no splitting in the H_{meso} proton resonance.
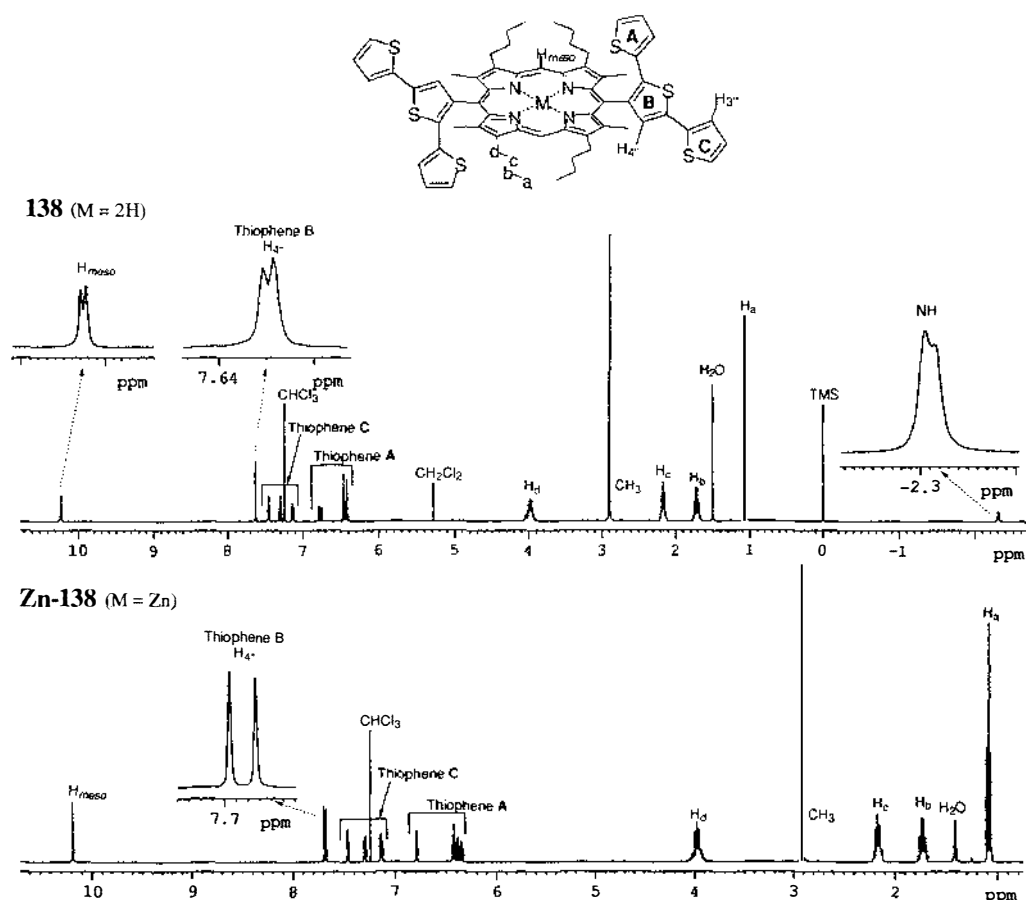
Figure 6-25. 400 MHz ^{1}H NMR of BTTPs **138** and **Zn-138** in $CDCl_3$.

While proton signals can be assigned to thiophene protons aided by COSY spectra, the assignment of the individual $\alpha\alpha$ or $\alpha\beta$ isomer proton signals cannot be made. The isomer ratio appears to be close to a statistical 1:1 based on ^{1}H NMR signal integrals of $H_{4''}$. The 101 MHz ^{13}C NMR spectroscopy also contained more signals than would be expected for only one isomer. Long-range coupling observed in the COSY spectrum allowed easy assignment of the $H_{4''}$ proton signal, seen coupled into $H_{3'''}$ of thiophene

ring **C**. Thiophene rings **A** and **C** are well separated due to the "ring-current effect" of the porphyrin ring. Thiophene **A** appearing up-field, experiencing shielding from the porphyrin ring, whereas the protons of thiophene **C** resonate at more typical positions (see Figure 6-21). ^{1}H NMR variable temperature experiments on the zinc(II) derivative **Zn-138** up to 55°C showed no coalescence of the H$_{4''}$ signals at 7.67 ppm, indicating a lack of rotation of the terthiophene moieties. Chem3D modelling supports a locked geometry, as significant steric interaction can be seen between thiophene ring **A** and the methyl groups of the porphyrin on rotation (Figure 6-26).
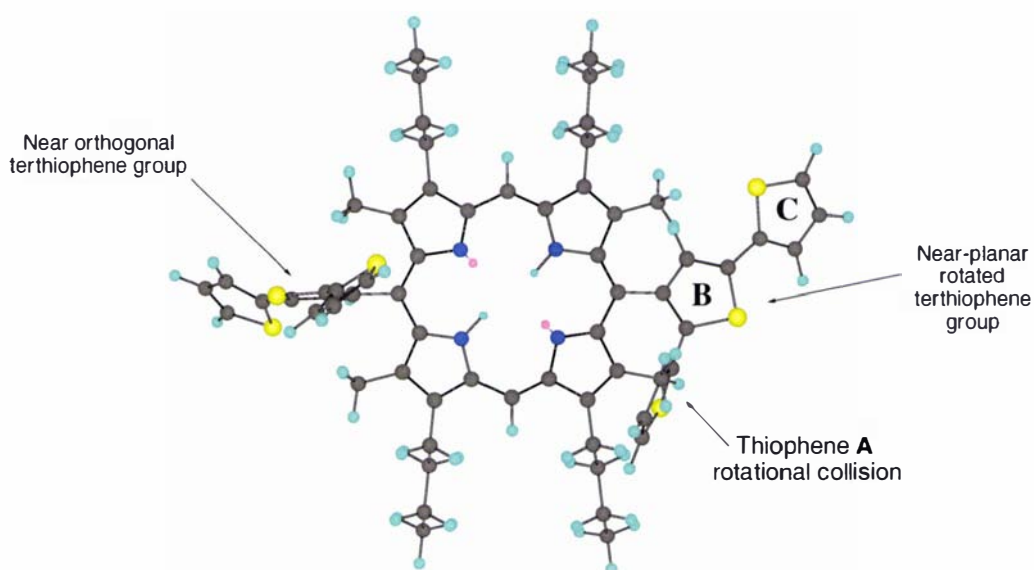
Figure 6-26. Illustration of steric interaction of terthiophene moiety in BTTP **138** (Chem3D MM2 minimised model).

Attempts to resolve the isomers chromatographically by HPLC were unsuccessful. Only one molecular ion is seen in each mass spectrum confirming the isomeric nature of the products. Typical free-base and metalloporphyrin UV-vis absorption spectra were seen for **138** and **Zn-138** respectively. Free-base **138** does however exhibit a broadening of the base of the Soret band into the UV region, presumably resulting from the terthiophene moieties. This resolves out into a well-separated strong absorption at 353 nm for the zinc derivative **Zn-138**. Unsubstituted terthiophene typically absorbs at 360 nm.[212.203]

Tetraterthienylporphyrins

The last terthiophene-appended porphyrin to be synthesised was the tetra-*meso*-terthienylporphyrin **139** (Figure 6-27). Initially the condensation between pyrrole and 3'-formylterthiophene **136** was carried out using TFA as the acid catalyst under Lindsey conditions.[114] This however gave a low yield (17%) of the desired product **139** after oxidation. Changing the acid catalyst to boron trifluoride diethyl etherate while still under Lindsey conditions, improved the yield to 34%.

a) i) BF$_3$·OEt$_2$ (0.1 eq), CH$_2$Cl$_2$ (10^{-2} M), RT (2 h), N$_2$. ii) *p*-Chloranil (0.75 eq), CH$_2$Cl$_2$, RT (2 h). iii) Et$_3$N (excess), RT (1.75 h). b) Zn(OAc)$_2$·2H$_2$O (2.0 eq), MeOH/CH$_3$Cl, RT (1 h) → reflux (1 h).
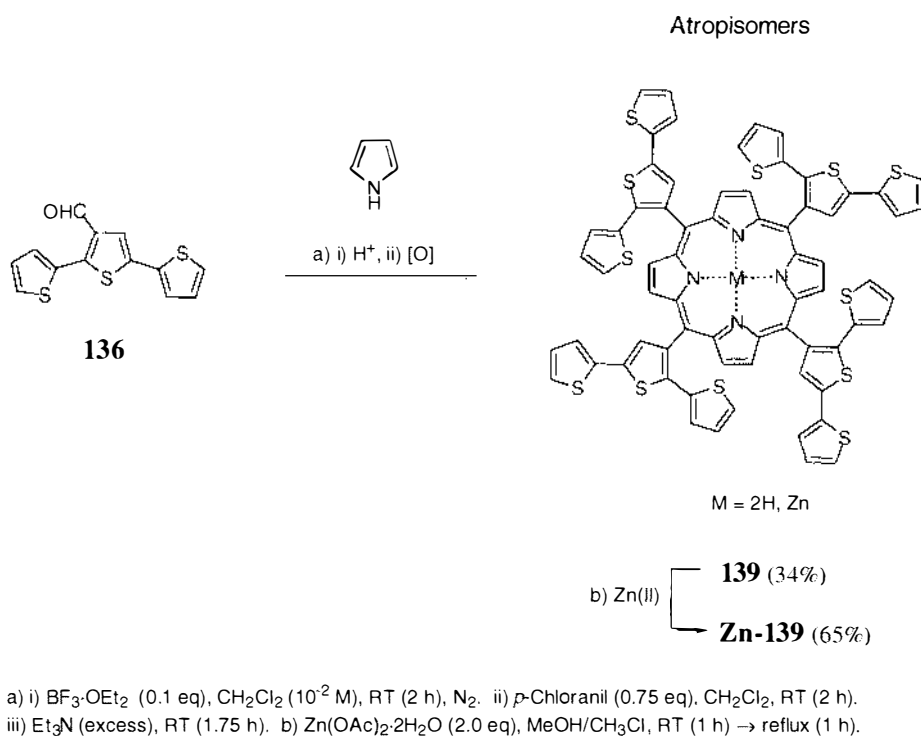
Figure 6-27. Synthesis of tetra-*meso*-terthienyl porphyrins (TTTPs) **139** and **Zn-139**.

Analysis of the product by 400 MHz ^{1}H NMR gave a spectrum consistent with multiple atropisomers. This was anticipated based on the results obtained for the bisterthienylporphyrin **M-138** and Chem3D modelling analysis. Chem3D modelling of **139** shows that even without the neighbouring methyls of **M-138**, there is still considerable steric interaction on rotation of the terthiophene moiety between the thiophene ring **A** and the β-pyrrolic protons (assuming a planar porphyrin moiety, Figure 6-28). Significant deformation would have to occur in the porphyrin ring and terthiophene moieties, to allow rotation.
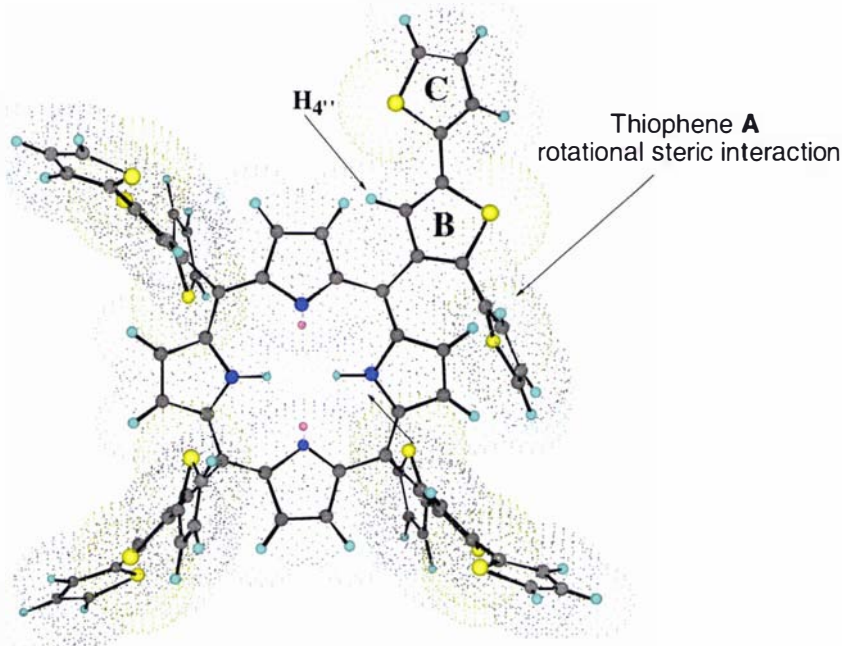
Figure 6-28. Steric interaction of terthienyl group and atropisomerism in TTTP **139** (Chem3D MM2 minimised model with electron density clouds).

Table 6-1. Atropisomers and expected proton signals for tetra-*meso*-porphyrins.

Atropisomers

[4,0]	[3,1]	[cis-2,2]	[trans-2,2]

Expected $H_{4''}$ ^{1}H NMR signals

1	3	1	1

The $H_{4''}$ proton signals are observed as six separate singlets in both $CDCl_3$ (Figure 6-29) and C_6D_6. These can be attributed to the four expected atropisomers, being the [4,0], [3,1], [cis-2,2] and [trans-2,2] as labelled by Beeston et al. (Table 6-1).[213] Variable temperature ^{1}H NMR spectroscopy (400 MHz, C_6D_6) up to 79°C was performed on **139** and no change in signals was observed upon heating or cooling. However, some signals were better resolved at the higher temperature, the **NH** signals were further split into 3 signals from the 2 observed at room temperature. It would be of interest to ascertain the

energy barrier to rotation of the terthiophene substituents by investigating the effect of higher temperatures on the isomer ratio.
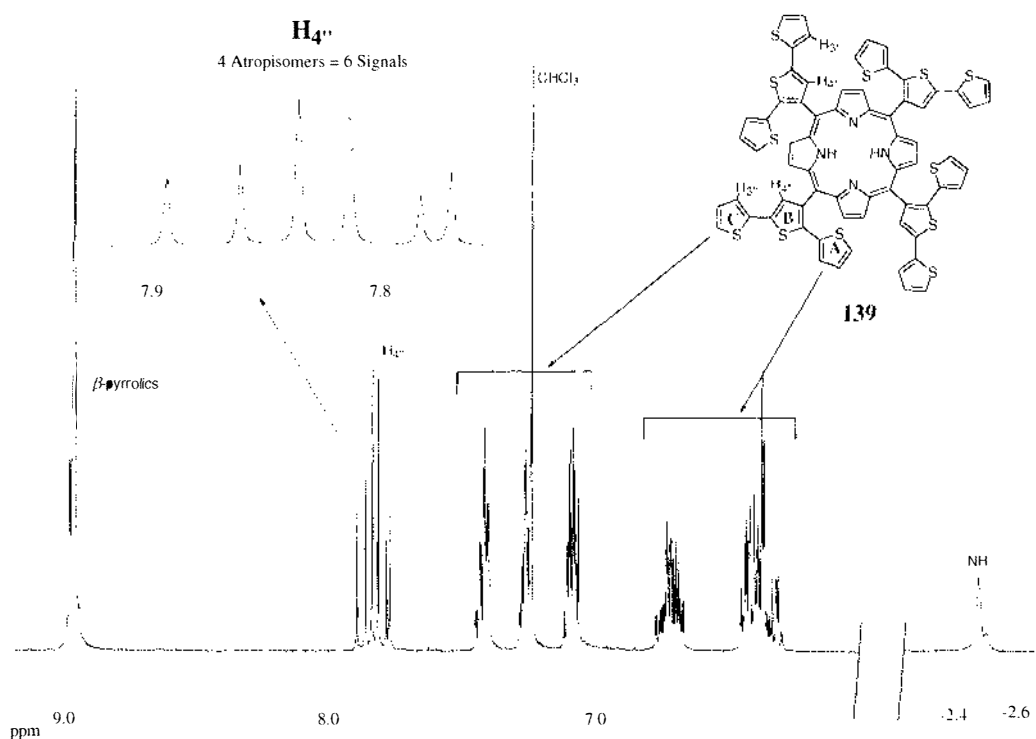
Figure 6-29. 270 MHz ^{1}H NMR spectrum of TTTP **139** in CDCl$_3$.

Metallation of **139** with zinc(II) acetate appeared slow when monitored by TLC. It appears that metallation of some of the atropisomers may be slower than others, possibly due to steric constraints imposed by the terthiophene moieties. Even after reflux with excess zinc(II) acetate, metallation was not totally complete by ^{1}H NMR. This is surprising as zinc insertion into most porphyrins under these conditions is usually rapid at room temperature. Complete separation by column chromatography was not obtained due to band smearing, and the final product contained about 5% of a non-metallated species. A longer reflux may have resulted in more complete conversion to metallated products **Zn-139**. It may therefore be possible to separate isomers by metallating at different temperatures, followed by careful column chromatography.

As in the case of bisterthienylporphyrin **M-138**, only one molecular ion ascribed to the title compounds **139** and **Zn-139** is seen in the mass spectra. Typical free-base and

metalloporphyrin UV-vis absorption spectra were seen for **139** and **Zn-139** respectively. Free-base **139** and zinc compound **Zn-139** both show a separate intense absorption at 357 and 352 nm respectively, presumably due to the appended terthiophene moieties. As might be expected the molar absorptivity of these bands are almost double that of the bisterthienylporphyrin **Zn-138** analogue.

6.3 Conclusion

Disulfides

The syntheses of a variety of new disulfide porphyrins were achieved. The development of the building block methodology to give bifunctionalised disulfide chromophores of the type **155** should be explored in the future. Surface binding of **M-155** on GaAs or Au could potentially result in controlled surface mixing of two synergistic molecules (Figure 6-30).
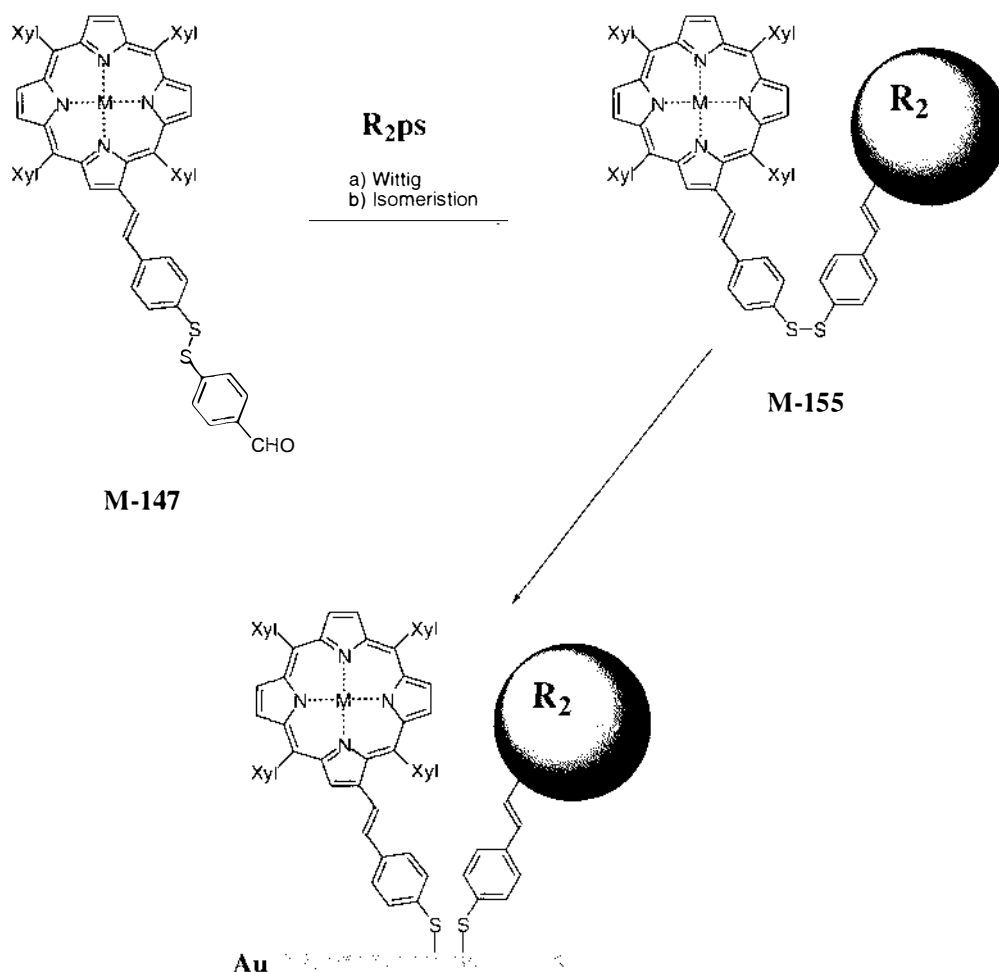
Figure 6-30. Mixed surface adsorption with bifunctional disulfides.

Currently the adsorption onto Au surfaces of a number of the disulfide porphyrins produced in this work is under investigation by Smela.[214]

Thienylporphyrins

New 2- and 3-thienylporphyrins were successfully synthesised for Au adsorption and polymerisation studies. X-ray quality crystals were obtained and the structures of **134**, **Zn-134** and **135** were solved. A new class of terthiophene-appended porphyrins was also synthesised. Using a combination of Wittig chemistry and classical condensation reactions, β-substituted, and bis- and tetra-*meso*-porphyrin variants were synthesised and characterised. Both the bis- and tetraterthienylpoprhyrins **M-138** and **M-139** were isolated as mixtures of atropisomers. Although, currently separation of the atropisomers could not be achieved by chromatographic techniques, careful metallation may resolve this. Polymerisation studies involving these compounds is currently being undertaken.

The value of employing different acid catalysts during pyrrole or dipyrrylmethane condensations is demonstrated in the synthesis of the thienylporphyrins. Marked variations in porphyrin yields were experienced depending on whether *p*-toluenesulfonic acid, trifluoroacetic acid or boron trifluoride diethyl etherate was employed as the acid catalyst.

Investigation into the immobilisation of these porphyrins (in particular **Zn-137**) onto TiO$_2$ by polymerisation should be investigated. This may not only allow excellent binding but also aid in preventing back electron transfer (dark currents).

Chapter 7

Experimental

7.1 *General*

Physical Measurements

^{1}H nuclear magnetic resonance (NMR) spectra were obtained at 270.19 MHz using a JEOL JMN-GX270 FT-NMR Spectrometer with Tecmag Libra upgrade, and at 400.132 MHz using Brucker 400 Avance running X-WIN-NMR software. The chemical shifts are relative to TMS or to the residual protium in deuterated solvents (CDCl$_3$, 7.25 ppm; pyridine-d$_5$, 7.00, 7.35, 8.50 ppm; DMSO-d$_6$, 2.50 ppm; MeOD-d$_4$, 3.35 ppm) when TMS is not present. ^{13}C NMR chemical shifts are relative to CDCl$_3$ (77.0 ppm), pyridine-d$_5$ (123.4, 135.3, 149.8 ppm), MeOD-d$_4$, (49.0 ppm).

Electronic absorption spectra were obtained on a Shimadzu UV-3101PC UV-VIS-NIR-Scanning Spectrophotometer. AR grade solvents were used unless otherwise specified.

Fast-atom-bombardment (FAB) mass spectra were recorded on a Varian VG70-250S double focusing magnetic sector mass spectrometer at Hort Research, Palmerston North. Samples analysed by FAB high resolution mass spectra (HRMS) were supported in a *p*-nitrobenzyl alcohol matrix unless otherwise stated. The data was put through VG-OPUS software to give ±5 ppm error formulations on molecular ions. Major fragmentations are given as percentages relative to the base peak intensity.

MALDI- TOF MS in Chapter 3 was carried out by Professor L. Li of the University of Alberta, Edmonton, Canada. Initially the samples were run on a Hewlett-Packard 2025 MALDI time-of-flight mass spectrometer. Later they were run on a homebuilt time-lag focusing or delayed extraction MALDI-TOF MS system which offered improved performance in terms of resolution and mass accuracy.

MALDI-TOF MS in Chapter 4 was carried out by the Author and were performed on a Micromass^{TM} ProteomeWorks^{TM} M@LDI-Reflectron mass spectrometer, fitted with a 337 nm nitrogen UV laser. Samples were prepared by a two-layer technique, where 1-2 μL of matrix (10 mg in 1 mL acetone) was deposited on the target plate and allowed to dry. Then 1-2 μL of porphyrin solution (~10^{-4} M) was applied on top of the matrix and

allowed to dry. The TXP triporphyrin **Ni$_3$-65** ($C_{160}H_{148}N_{12}Ni_3$ = 2411.0010) was used as a calibration standard.

ES-MS was carried out by G. Norris at Massey University, Palmerston North, New Zealand.

X-ray structures were solved by A. K. Burrell and refined by B. Therrien at Massey University, Palmerston North, New Zealand.

Melting point determinations were performed on a Cambridge Instruments Kofler hot-stage (calibration standards employed). All porphyrin derivatives in this thesis have melting points higher than the 280°C upper limit of this equipment.

Reagents

Solvent and reagents were supplied from many different sources, generally as AR grade unless otherwise stated. Chromatography solvents were distilled laboratory grade. H_2O refers to reverse osmosis (RO) or Milli Q for higher purity. Dry degassed DCM and DMF were prepared by distilling AR grade off CaH_2 under N_2 atmosphere. Dry toluene, ether, benzene and THF were prepared by passing argon-degassed solvent through activated alumina columns. p-Xylene was prepared by distillation from Na with benzophenone under argon atmosphere. N_2 (oxygen-free) was passed through a KOH drying column to remove moisture. Acetonitrile was HPLC grade. Glutaronitrile (98%), was dried over CaH_2 (large amount of gas evolution initially) for 2 days then vacuum distilled at 85°C (0.4 mm Hg).

Active MnO_2 was prepared according to the method of Attenburrow et al.[95] Argentic Oxide was prepared according to the method of Corey et al.[84] by the addition of aq. KOH to a solution of $AgNO_3$ (2.0 g, 12 mmol) and $KMnO_4$ (22 mg) in H_2O (5.0 mL) until no more precipitated was formed. The precipitate was then washed exhaustively with H_2O until washings were free of base and $KMnO_4$. The product was then washed with THF and dried *in vacuo* to give AgO (624 mg, 42%) as a grey solid. 5% Pd/BaSO$_4$ was obtained from Sigma. NaI (>99.5%) was prepared anhydrous by heated to 70°C for 12 hours under high vacuum.

Methyl 2-formylbenzoate **26** was prepared using a procedure essentially the same as Osuka et al. via alkylation of the methyl 2-formylbenzoic acid (Aldrich, 97%) metal salt in DMF.[215,216] Attempted acid catalysed esterification with MeOH was not successful; a product was obtained with a proton NMR consistent with the acetal 3-methoxyphthalide.[217] Methyl 3-formylbenzoate **27** was purchased from Fluka (≥ 98%, HPLC). Methyl 4-formylbenzoate **28** was prepared from 4-formylbenzoic acid **7** using a similar method to that described in Vogel for methyl benzoates.[218,219] Removal of excess MeOH by azeotrope distillation with ether prior to an aqueous Na_2CO_3 workup, was used to get an acetal-free product (94% yield). Trimethyl trimesate **44** was prepared from trimesic acid using a similar method to that described in Vogel for methyl benzoates in 83% yield.[218,219]

4,4'-Dithiobis-toluene **141** was prepared quantitatively from *p*-toluenethiol **143** using the method that Papadopoulos et al. used to prepare phenyl disulfide from benzenethiol.[207] ^{1}H NMR data was consistent with that reported in the literature.[208]

3'-formyl-2,2':5',2"-terthiophene **136** was prepared by Collis.[203]

Bis(3-butyl-4-methyl-2-pyrryl)methane (DPM) **58** was prepared according to Sessler et al.[106,107] TPPps **4**, TXPps **5**, and TBPps **6** were prepared according to Reid[79] and Belcher et al.[83] TEP **85** and TCP **8** were synthesised according to established literature procedures.[120,220] The metallo derivatives CuTEP **Cu-85** and ZnTCP **Zn-8** were prepared by the acetate method.[60]

Experimental procedures

Column chromatography employed silica gel (0.032-0.063 mm, Merck Kieselgel 60) or equivalent. Thin layer chromatography (TLC) was performed using precoated silica gel plates (Merck Kieselgel 60F$_{254}$). The term "chromatographed" hereby implies that it (the mixture or crude product) has been subjected to either gravity or flash chromatography. Where a dual solvent system is used, gradient elution is implied, collecting the major band unless otherwise stated. All fractions or solutions containing

a single spot by TLC with the same R_f were combined, filtered and solvent removed *in vacuo* (rotary evaporation followed by high vacuum), unless otherwise stated.

All solid precipitates were separated by filtration or centrifugation, rinsing with the precipitating solvent, then dried under high vacuum overnight unless otherwise stated. All porphyrin reactions were in general carried out shielded from ambient light, under a nitrogen or argon atmosphere and using dry degassed solvents.

Equations used for calculating moles in mixtures

Equation 7-1. Two component mixtures [X:Y].

$$X_{mol} = \frac{Total\ Mass\ (g)}{\left(X_{Mr} + Y_{Mr}\left[\frac{Y}{X}\right]\right)} \quad \text{and} \quad Y_{mol} = X_{mol}\left[\frac{Y}{X}\right]$$

Equation 7-2. Three component mixtures [X:Y:Z].

$$X_{mol} = \frac{Total\ Mass\ (g)}{\left(X_{Mr} + Y_{Mr}\left[\frac{Y}{X}\right] + Z_{Mr}\left[\frac{Z}{X}\right]\right)} \quad \text{and} \quad Y_{mol} = X_{mol}\left[\frac{Y}{X}\right], \ Z_{mol} = X_{mol}\left[\frac{Z}{X}\right]$$

Equation 7-3. Equation 7-1 and Equation 7-2 are derived from:

$$Total\ Mass = X_{mol}X_{Mr} + Y_{mol}Y_{Mr} + ...$$

$$\therefore \frac{Y_{mol}}{X_{mol}} = \left[\frac{Y}{X}\right]$$

where $\left[\frac{Y}{X}\right]$ is the molar ratio calculated from the integrals of ^1H NMR spectra.

Nomenclature

Generally, any styrylporphyrin has been named using a protocol whereby the substituent has been given naming priority over the alkene or porphyrin. Naming these porphyrins in this way allows the systematic naming of larger arrays. All alkenes are *trans* unless otherwise stated.

7.2   Chapter 2: Synthesis of Benzoic Acid Porphyrins

ZnTPP-=-PhCO₂H, Zn-9.

4-(*Trans*-2'-(2"-(5",10",15",20"-tetraphenylporphyrinato zinc(II))yl)ethen-1'-yl)-1-benzoic acid.

$C_{53}H_{34}N_4O_2Zn$
Exact Mass: 822.1973
Mol. Wt.: 824.2528
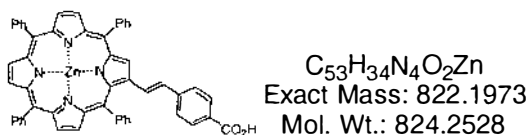
KOH (107 mg, 1.91 mmol, 20 eq) in MeOH (22 mL) and H_2O (2.2 mL) was added to a solution of ester **Zn-10** (80.0 mg, 95.4 μmol) in THF (22 mL). The mixture was refluxed for 17.5 h under N_2. On cooling to RT, H_2O (30 mL), $CHCl_3$ (40 mL) and 2.0 M H_3PO_4 (aq) (1.0 mL, 21 eq) were added with stirring. The resulting red coloured organic layer was washed with H_2O (50 ml x 3), and then separated carefully and the solvent removed *in vacuo*. Recrystallisation from $CHCl_3$/hexane gave **Zn-9** (75.2 mg, 96%) as a purple powder. ^{1}H NMR (400 MHz, DMSO-d₆, TMS): δ 7.084 and 7.340 (ABq, 2H, ^3J = 16.0, 15.9 Hz, $H_{2',1'}$), 7.353 (d, 2H, ^3J = 8.0 Hz, H_{styryl}), 7.76-7.95 (m, 12H, $H_{m,p-Ph}$), 7.910 (d, 2H, ^3J = 8.4 Hz, H_{styryl}), 8.16-8.23 (m, 8H, H_{o-Ph}), 8.659 and 8.725 (ABq, 2H, ^3J = 4.6, 4.7 Hz, $H_{\beta-pyrrolic}$), 8.740 (s, 2H, $H_{\beta-pyrrolic}$), 8.727 and 8.763 (ABq, 2H, ^3J = 4.7, 4.7 Hz, $H_{\beta-pyrrolic}$), 9.018 (s, 1H, $H_{3"}$ (β-pyrrolic)). *Assignments aided by COSY spectra.* UV-vis (THF): λ_{max} [nm] (ε x 10^{-3}) 437 (218), 565 (21.0), 602 (8.73). FAB-LRMS: m/z (%, assignment) cluster at 822-829, 824 (100, M⁺). HRMS: Calcd for M⁺ ($C_{53}H_{34}N_4O_2Zn$): 822.1973, found: 822.1934.

NiTPP-=-PhCO₂H, Ni-9.

4-(*Trans*-2'-(2"-(5",10",15",20"-tetraphenylporphyrinato nickel(II))yl)ethen-1'-yl)-1-benzoic acid.

$C_{53}H_{34}N_4NiO_2$
Exact Mass: 816.2035
Mol. Wt.: 817.5562
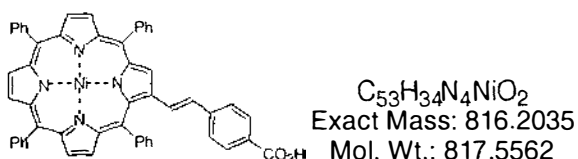
*Originally synthesised by Grant[81] from the Wittig reaction of NiTPPps **Ni-4** with 4-formylbenzoic acid 7 followed by I_2 isomerization. Presented here is a modified*

synthesis of the original (Method A) and the new method from the hydrolysis of the methyl ester (Method B).

Method A: A solution of NiTPPps **Ni-4** (107 mg, 109 μmol) and methyl 4-formylbenzoic acid **7** (49 mg, 330 μmol, 3 eq) in toluene (7.0 mL) was heated to reflux under N_2. DBU (81 μL, 5.0 eq) was added, and after 15 min TLC analysis indicated that all the starting material **Ni-4** had been consumed. After cooling to RT the solvent was removed *in vacuo*. The residue was column chromatographed (silica, 18 mm$_{dia}$ x 200 mm, CH_2Cl_2:MeOH (50:1→25:1)). Recrystallisation from CH_2Cl_2:MeOH gave *trans* **Ni-9** (52.6 mg, 59%) as a red/purple powder.

Method B: KOH (35.7 mg, 636 μmol, 16 eq) in MeOH (10.1 mL) and H_2O (1.1 mL) was added to a solution of porphyrin ester **Ni-10** (33.1 mg, 39.8 μmol) in THF (11.8 mL). The mixture was refluxed for 9 h under N_2. On cooling to RT, 2.0 M HCl$_{(aq)}$ (0.50 mL) was added to adjust the acidity to pH ≈ 1. The aqueous layer was extracted with Et_2O (100 mL). The resulting organic layer was washed with H_2O (2 x 50 mL), and then separated carefully and the solvent removed *in vacuo*. The residue was column chromatographed (silica, 27 mm$_{dia}$ x 100 mm, CH_2Cl_2:MeOH (25:1)). Recrystallisation from CH_2Cl_2:MeOH gave *trans* **Ni-9** (29.9 mg, 92%) as a red/purple powder.

A broadened ^1H NMR spectra due to very poor solubility was obtained, a suitable solvent was not found. The major difference in the overall spectrum (ca. NiTPP-=-CO$_2$Me, Ni-10) is the absence of the methyl ester (CO$_2$CH$_3$) proton resonance. Identical ^1H NMR spectra were obtained for both methods A and B in CDCl$_3$. ^1H NMR (270 MHz, CDCl$_3$, TMS): δ 7.000 and 7.149 (br ABq, 2H, ^3J = 16.2, 15.9 Hz, H$_{2',1'}$), 7.21-28 (m, CHCl$_3$ + 2H$_{styryl}$), 7.63-7.78 (m, 12H, H$_{m,p\text{-Ph}}$), 7.94-8.06 (m, 10H, 2H$_{styryl}$ + 8H$_{o\text{-Ph}}$), 8.66-8.72 (m, 6H, H$_{\beta\text{-pyrrolic}}$), 8.915 (br s, 1H, H$_{3''\,(\beta\text{-pyrrolic})}$). UV-vis (CH$_2Cl_2$): λ_{max} [nm] (ε x 10^{-3}) 429 (197), 540 (18.4), 577 (13.0). FAB-LRMS: *m/z* (%, assignment) cluster at 815-822, 816 (98, M$^+$). HRMS: Calcd for M$^+$ (C$_{53}$H$_{34}$N$_4$NiO$_2$): 816.2035, found: 816.1977.

TPP-=-PhCO₂Me, 10.

Methyl 4-(*trans*-2'-(5",10",15",20"-tetraphenylporphyrin-2"-yl)ethen-1'-yl)-1-benzoate.

$C_{54}H_{38}N_4O_2$
Exact Mass: 774.2995
Mol. Wt.: 774.9053
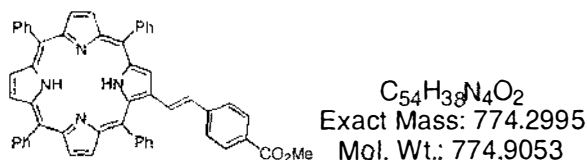
TPP-=-PhCO₂Me **10** was made according to the method of D. K. Grant[81] using Wittig chemistry between TPPps **4** and methyl 4-formylbenzoate **28** followed by I_2 isomerization to give a purple powder (134 mg, 64%). The spectra is consistent with that already reported. New data is given below. ^{1}H NMR (400 MHz, CDCl₃, TMS): δ - 2.597 (br s, 2H, NH), 3.954 (s, 3H, CO₂CH₃), 7.090 and 7.290 (ABq, 2H, ^3J = 16.0, 15.5 Hz, H$_{2',1'}$), 7.283 (d, 2H, ^3J = 8.5 Hz, H$_{styryl}$), 7.71-7.85 (m, 12H, H$_{m,p\text{-}Ph}$), 7.998 (d, 2H, ^3J = 8.4 Hz, H$_{styryl}$), 8.17-8.26 (m, 8H, H$_{o\text{-}Ph}$), 8.722 and 8.777 (ABq, 2H, ^3J = 4.8, 4.9 Hz, H$_{\beta\text{-pyrrolic}}$), 8.783 (d, 1H, ^3J = 4.8 Hz, H$_{\beta\text{-pyrrolic}}$), 8.81-8.84 (m, 3H, H$_{\beta\text{-pyrrolic}}$), 9.010 (s, 1H, H$_{3"\ (\beta\text{-pyrrolic})}$). *Assignments aided by COSY spectra.* FAB-LRMS: *m/z* (%, assignment) cluster at 773-778, 775 (100, MH⁺). HRMS: Calcd for MH⁺ ($C_{54}H_{39}N_4O_2$): 775.3073, found: 775.2994.

ZnTPP-=-PhCO₂Me, Zn-10.

Methyl 4-(*trans*-2'-(2"-(5",10",15",20"-tetraphenylporphyrinato zinc(II))yl)ethen-1'-yl)-1-benzoate.

$C_{54}H_{36}N_4O_2Zn$
Exact Mass: 836.2130
Mol. Wt.: 838.2794
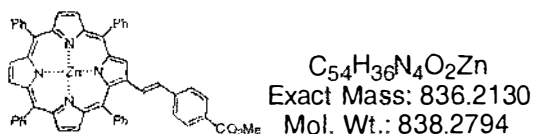
A solution of Zn(OAc)₂·2H₂O (34 mg, 155 μmol, 1.2 eq) in MeOH (1.5 mL) was added to a solution of ester **10** (100 mg, 129 μmol) in CHCl₃ (10 mL) with stirring at RT. After 1.75 h, UV-vis analysis indicated that the reaction was complete. Precipitation using MeOH gave **Zn-10** (107 mg, 99%) as a purple microcrystalline solid. ^{1}H NMR (400 MHz, CDCl₃, TMS): δ 3.825 (s, 3H, CO₂CH₃), 7.111 (dd, 1H, ^3J = 16.0 Hz, ^4J = 0.8, 0.7 Hz, H$_2$), 7.239 (d, 1H, ^3J = 15.6 Hz, H$_1$), 7.248 (d, 2H, ^3J = 8.4 Hz, H$_{styryl}$), 7.71-7.82 (m, 12H, H$_{m,p\text{-}Ph}$), 7.854 (d, 2H, ^3J = 8.3 Hz, H$_{styryl}$), 8.16-8.26 (m, 8H, H$_{o\text{-}Ph}$), 8.811 and 8.889 (ABq, 2H, ^3J = 4.7, 4.8 Hz, H$_{\beta\text{-pyrrolic}}$), 8.910 (s, 2H, H$_{\beta\text{-pyrrolic}}$), 8.902 and 8.932 (ABq, 2H, ^3J = 4.8, 4.7 Hz, H$_{\beta\text{-pyrrolic}}$), 9.116 (d, 1H, ^4J = 0.7 Hz, H$_{3"\ (\beta\text{-pyrrolic})}$).

Assignments aided by COSY spectra. UV-vis (CH$_2$Cl$_2$): λ_{max} [nm] (ϵ x 10^{-3}) 433 (248), 560 (23.4), 597 (10.0). FAB-LRMS: *m/z* (%, assignment) cluster at 835-843, 836 (100, M$^+$). HRMS: Calcd for M$^+$ (C$_{54}$H$_{36}$N$_4$O$_2$Zn): 836.2130, found: 836.2085.

NiTPP-=-PhCO$_2$Me, Ni-10.

Methyl 4-(*trans*-2'-(2"-(5",10",15",20"-tetraphenylporphyrinato nickel(II))yl)ethen-1'-yl)-1-benzoate.

C$_{54}$H$_{36}$N$_4$NiO$_2$
Exact Mass: 830.2192
Mol. Wt.: 831.5828
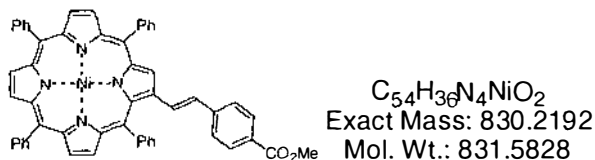
A solution of Ni(OAc)$_2$·4H$_2$O (266 mg, 1.07 mmol, 12 eq) in MeOH (1.5 mL) was added to a refluxing solution of ester **10** (69 mg, 89 μmol) in CHCl$_3$ (10 mL) with stirring under N$_2$ atmosphere. Reflux was continued for 15 h. On cooling to RT the product was precipitated with MeOH to give **Ni-10** (59 mg, 80%) as a purple microcrystalline solid. ^{1}H NMR (270 MHz, CDCl$_3$, TMS): δ 3.937 (s, 3H, CO$_2$CH$_3$), 6.959 (dd, 1H, ^3J = 15.9 Hz, ^4J = 0.6 Hz, H$_{2'}$), 7.118 (d, 1H, ^3J = 15.9 Hz, H$_{1'}$), 7.199 (d, 2H, ^3J = 8.5 Hz, H$_{styryl}$), 7.60-7.78 (m, 12H, H$_{m,p\text{-Ph}}$), 7.92-8.40 (m, 10H, 8H$_{o\text{-Ph}}$ + 2H$_{styryl}$), 8.66-8.71 (m, 6H, H$_{\beta\text{-pyrrolic}}$), 8.895 (d, 1H, ^4J = 0.6 Hz, H$_{3"\,(\beta\text{-pyrrolic})}$). UV-vis (CH$_2Cl_2$): λ_{max} [nm] (ϵ x 10^{-3}) 429 (189), 540 (17.8), 576 (12.4). FAB-LRMS: *m/z* (%, assignment) cluster at 829-836, 830 (100, M$^+$). HRMS: Calcd for M$^+$ (C$_{54}$H$_{36}$N$_4$NiO$_2$): 830.2192, found: 830.2162.

TXP-=-PhCO$_2$H, 15.

4-(*Trans*-2'-(5",10",15",20"-tetrakis(3"',5"'-dimethylphenyl)porphyrin-2"-yl)ethen-1'-yl)-1-benzoic acid.

C$_{61}$H$_{52}$N$_4$O$_2$
Exact Mass: 872.4090
Mol. Wt.: 873.0913
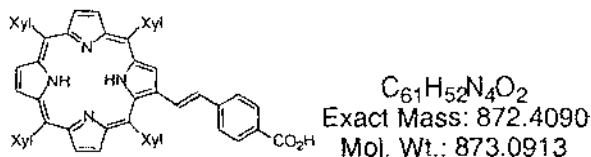
KOH (253 mg, 4.5 mmol, 20 eq) in MeOH (60 mL) and H$_2$O (6.0 mL) was added to a solution of ester **23** (200 mg, 225 μmol) in THF (60 mL). The mixture was refluxed for 14.5 h under N$_2$. After cooling to RT, H$_2$O (150 mL), CHCl$_3$ (80 mL) and 2.0 M H$_3$PO$_4$ (aq) (2.37 mL, 21 eq) were added with stirring. The resulting brown organic layer was

washed with H_2O (3 x 150 mL), and then separated carefully and the solvent removed *in vacuo*. The residue was column chromatographed (silica, 37 mm_{dia} x 70 mm, $CHCl_3$) to give **15** (190 mg, 96%) as a purple solid. ^1H NMR (270 MHz, $CDCl_3$ + Et_3N, TMS): δ -2.623 (br s, 2H, NH), 2.514 (s, 6H, H_{Me-Xyl}), 2.597 (s, 12H, H_{Me-Xyl}), 2.626 (s, 6H, H_{Me-Xyl}), 7.086 (d, 1H, ^3J = 16.2 Hz, $H_{2'}$), 7.28-7.47 (m, 7H, $1H_{1'}$ + $2H_{styryl}$ + $4H_{p-Xyl}$), 7.78-7.86 (m, 8H, H_{o-Xyl}), 8.058 (d, 2H, ^3J = 8.2 Hz, H_{styryl}), 8.77-8.86 (m, 6H, $H_{\beta-pyrrolic}$), 9.018 (s, 1H, $H_{3'' (\beta-pyrrolic)}$). *Et_3N was required to solubilize porphyrin.* UV-vis (CH_2Cl_2): λ_{max} [nm] (ε x 10^{-3}) 430 (243), 526 (22.1), 566 (13.1), 601, (8.46), 657 (3.81). FAB-LRMS: *m/z* (%, assignment) cluster at 871-876, 873 (100, M^+). HRMS: Calcd for M^+ ($C_{61}H_{52}N_4O_2$): 872.4062, found: 872.4090.

CuTXP-=-PhCO$_2$H, Cu-15.

4-(*Trans*-2'-(2''-(5'',10'',15'',20''-tetrakis(3''',5'''-dimethylphenyl)porphyrinato copper(II))yl)ethen-1'-yl)-1-benzoic acid.
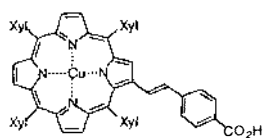
$C_{61}H_{50}CuN_4O_2$
Exact Mass: 933.3330
Mol. Wt.: 934.6215

A solution of $Cu(OAc)_2 \cdot H_2O$ (3.8 mg, 19 μmol, 1.1 eq) in MeOH (1.0 mL) was added to a refluxing solution of acid **15** (15.0 mg, 17.2 μmol) in $CHCl_3$ (5 mL) with stirring. After 15 min, TLC analysis indicated that all the starting material **15** had been consumed. After cooling to RT, the organic layer was washed with 1.0 M $H_3PO_{4(aq)}$ (60 mL) carefully separated and the solvent removed *in vacuo*. The residue was column chromatographed (silica, 20 mm_{dia} x 50 mm, $CHCl_3$) to give **Cu-15** (14.5 mg, 90%) as a red/purple solid. UV-vis (CH_2Cl_2): λ_{max} [nm] (ε x 10^{-3}) 429 (248), 549 (23.5), 586 (12.0). FAB-LRMS: *m/z* (%, assignment) cluster at 932-938, 933 (100, M^+). HRMS: Calcd for M^+ ($C_{61}H_{50}CuN_4O_2$): 933.3230, found: 933.3218.

ZnTXP-=-PhCO$_2$H, Zn-15.

4-(*Trans*-2'-(2''-(5'',10'',15'',20''-tetrakis(3''',5'''-dimethylphenyl)porphyrinato zinc(II))yl)ethen-1'-yl)-1-benzoic acid.
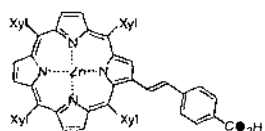

$C_{61}H_{50}N_4O_2Zn$
Exact Mass: 934.3225
Mol. Wt.: 936.4655

KOH (177 mg, 3.15 mmol, 20 eq) in MeOH (42 mL) and H_2O (4.2 mL) was added to a solution of ester **Zn-23** (150 mg, 158 μmol) in THF (42 mL). The mixture was refluxed for 14.5 h under N_2. After cooling to RT, H_2O (100 mL), $CHCl_3$ (60 mL) and 2.0 M $H_3PO_{4(aq)}$ (1.66 mL, 21 eq) were added with stirring. The resulting red/green coloured organic layer was washed with H_2O (3 x 100 mL), and then separated carefully and the solvent removed *in vacuo.* The residue was column chromatographed (silica, 37 mm$_{dia}$ x 70 mm, $CHCl_3$) to give **Zn-15** (143 mg, 96%) as a purple solid. ^{1}H NMR (270 MHz, DMSO-d$_6$): δ 2.516 (s, 6H, H$_{Me-Xyl}$), 2.579 (s, 12H, H$_{Me-Xyl}$), 2.605 (s, 6H, H$_{Me-Xyl}$), 7.125 and 7.344 (ABq, 2H, ^3J = 16.2, 15.9 Hz, H$_{2',1'}$), 7.39-7.47 (m, 5H, 2H$_{styryl}$ + 3H$_{p-Xyl}$), 7.550 (s, 1H, H$_{p-Xyl}$), 7.779 (s, 6H, H$_{o-Xyl}$), 7.817 (s, 2H, H$_{o-Xyl}$), 7.943 (d, 2H, ^3J = 8.2 Hz, H$_{styryl}$), 8.72-8.79 (m, 6H, H$_{\beta\text{-pyrrolic}}$), 9.021 (s, 1H, H$_{3''}$ $_{(\beta\text{-pyrrolic})}$). UV-vis ($CH_2Cl_2$): λ_{max} [nm] (ε x 10^{-3}) 433 (245), 558 (24.0), 595 (11.0). FAB-LRMS: m/z (%, assignment) cluster at 933-941, 934 (100, M$^+$). HRMS: Calcd for M$^+$ (C$_{61}$H$_{50}$N$_4$O$_2$Zn): 934.3225, found: 934.3240.

NiTXP-CHO, Ni-16.

2-Formyl-5,10,15,20-tetrakis(3',5'-dimethylphenyl)porphyrinato nickel(II).

C$_{53}$H$_{44}$N$_4$NiO
Exact Mass: 810.2869
Mol. Wt.: 811.6362
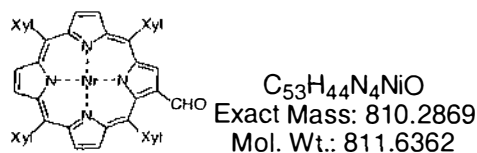
To a solution of porphyrin aldehyde **Ni-14** (20.0 mg, 22 μmol) in acetone (1.5 mL) was added KMnO$_4$ (5.2 mg, 1.5 eq) and the reaction stirred at RT. After 4 h, TLC displayed a new spot at higher R_f than the starting material **Ni-17**. The reaction was driven to completion by adding another 3.0 eq of KMnO$_4$ over 50 min. The solvent was removed *in vacuo* and the residue filtered through a silica gel plug using CH_2Cl_2:hexane (2:1) to give **Ni-16** (15.6 mg, 88%) as a purple solid. ^{1}H NMR (270 MHz, CDCl$_3$): δ 2.49-2.56 (m, 24H, H$_{Me-Xyl}$), 7.30-7.37 (m, 4H, H$_{p-Xyl}$), 7.55-7.66 (m, 8H, H$_{o-Xyl}$), 8.67-8.80 (m, 6H, H$_{\beta\text{-pyrrolic}}$), 9.188 (s, 1H, H$_{3}$ $_{(\beta\text{-pyrrolic})}$), 9.306 (s, 1H, CHO). FAB-LRMS: m/z (%, assignment) cluster at 809-816, 810 (100%, M$^+$).

TXP-=-PhCO₂Me, 23.

Methyl 4-(*trans*-2'-(5",10",15",20"-tetrakis(3'",5'"-dimethylphenyl)porphyrin-2"-yl)ethen-1'-yl)-1-benzoate.

$C_{62}H_{54}N_4O_2$
Exact Mass: 886.4247
Mol. Wt.: 887.1179
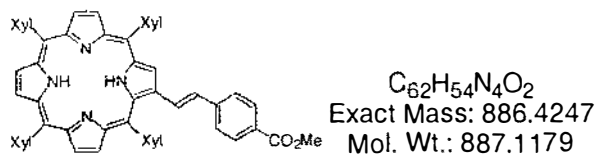
A solution of TXPps **5** (600 mg, 578 μmol) and methyl 4-formylbenzoate **28** (380 mg, 2.31 mmol, 4.0 eq) in CHCl₃ (58 mL) was heated to reflux under N₂. DBU (259 μL, 3.0 eq) was added. After 15 min, TLC analysis indicated that all of the starting material **5** had been consumed. The crude isomeric mixture was precipitated with MeOH to give a purple powder (413 mg, ≈ 15% *cis* by ¹H NMR). The crude product was dissolved in CH₂Cl₂ (60 mL) and I₂ (355 mg, 25.4 mmol, 3.0 eq) added. After stirring at RT for 3 h in darkness, excess sat. Na₂S₂O₃ was added and stirring continued for 30 min. The organic layer was separated, dried (MgSO₄) and the solvent removed *in vacuo*. The residue was column chromatographed (silica, 25 mm$_{dia}$ x 40 mm, CH₂Cl₂). Recrystallisation from CH₂Cl₂/MeOH gave *trans* ester **23** (375 mg, 73%) as a purple powder. ¹H NMR (270 MHz, CDCl₃, TMS): δ -2.628 (br s, 2H, NH), 2.523 (s, 6H, H$_{Me-Xyl}$), 2.598 (s, 12H, H$_{Me-Xyl}$), 2.628 (s, 6H, H$_{Me-Xyl}$), 3.975 (s, 3H, CO₂CH₃), 7.145 and 7.312 (ABq, 2H, ^3J = 15.9, 15.6 Hz, H$_{2',1'}$), 7.355 (d, 2H, ^3J = 8.2 Hz, H$_{styryl}$), 7.38-7.48 (m, 4H, H$_{p-Xyl}$), 7.79-7.87 (m, 8H, H$_{o-Xyl}$), 8.023 (d, 2H, ^3J = 8.2 Hz, H$_{styryl}$), 8.78-8.86 (m, 6H, H$_{\beta-pyrrolic}$), 9.026 (s, 1H, H$_{3"\,(\beta-pyrrolic)}$). UV-vis (CH₂Cl₂): λ_{max} [nm] (ε x 10⁻³) 430 (268), 526 (24.4), 567 (14.1), 601 (9.03), 658 (3.99). FAB-LRMS: *m/z* (%, assignment) cluster at 885-890, 887 (100, M⁺). HRMS: Calcd for M⁺ ($C_{62}H_{54}N_4O_2$): 886.4247, found: 886.4250.

ZnTXP-=-PhCO₂Me, Zn-23.

Methyl 4-(*trans*-2'-(2"-(5",10",15",20"-tetrakis(3'",5'"-dimethylphenyl)porphyrinato zinc(II))yl)ethen-1'-yl)-1-benzoate.

$C_{62}H_{52}N_4O_2Zn$
Exact Mass: 948.3382
Mol. Wt.: 950.4920
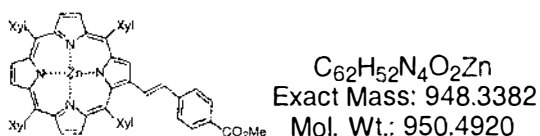
A solution of Zn(OAc)$_2$·2H$_2$O (29.7 mg, 135 μmol, 1.2 eq) in MeOH (1.0 mL) was added to a solution of ester **23** (100 mg, 113 μmol) in CHCl$_3$ (10 mL) with stirring at RT. After 20 min, UV-vis analysis indicated that the reaction was complete. Precipitation with MeOH gave **Zn-23** (103 mg, 97%) as a purple powder. ^{1}H NMR (270 MHz, CDCl$_3$, TMS): δ 2.503 (s, 6H, H$_{Me\text{-}Xyl}$), 2.595 (s, 12H, H$_{Me\text{-}Xyl}$), 2.631 (s, 6H, H$_{Me\text{-}Xyl}$), 3.866 (s, 3H, CO$_2$CH$_3$), 7.168 and 7.265 (ABq, 2H, ^3J = 16.2, 16.5 Hz, H$_{2',1'}$), 7.325 (d, 2H, ^3J = 8.2 Hz, H$_{styryl}$), 7.398 (br s, 2H, H$_{p\text{-}Xyl}$), 7.432 (br s, 2H, H$_{p\text{-}Xyl}$), 7.76-7.94 (m, 10H, 8H$_{o\text{-}Xyl}$ + 2H$_{styryl}$), 8.023 (d, 2H, ^3J = 8.2 Hz, H$_{styryl}$), 8.89-8.98 (m, 6H, H$_{\beta\text{-}pyrrolic}$), 9.138 (s, 1H, H$_{3''\ (\beta\text{-}pyrrolic)}$). UV-vis (CH$_2Cl_2$): λ_{max} [nm] (ε x 10^{-3}) 433 (281), 558 (26.6), 595 (11.9). FAB-LRMS: m/z (%, assignment) cluster at 947-955, 948 (100, M$^+$). HRMS: Calcd for M$^+$ (C$_{62}$H$_{52}$N$_4$O$_2$Zn): 948.3382, found: 948.3460.

NiTXP-=-PhCO$_2$Me, Ni-23.

Methyl 4-(*trans*-2'-(2''-(5'',10'',15'',20''-tetrakis(3''',5'''-dimethylphenyl)porphyrinato nickel(II))yl)ethen-1'-yl)-1- benzoate.

C$_{62}$H$_{52}$N$_4$NiO$_2$
Exact Mass: 942.3444
Mol. Wt.: 943.7954
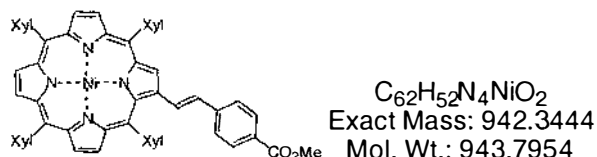
To a solution of porphyrin aldehyde **Ni-14** (20.0 mg, 22 μmol) in THF:MeOH (1:5, 6.0 mL) was added NaCN (21.6 mg, 20 eq) and the reaction stirred at RT for 30 min. Active MnO$_2$ (143 mg, 75 eq) was added and the reaction heated to reflux for 18 h. A spot at higher R_f appears by TLC (silica, R_f = 0.83, CH$_2$Cl$_2$). On cooling to RT the mixture was filtered through a celite plug and the solvent removed *in vacuo*. The residue was column chromatographed (silica, 17 mm$_{dia}$ x 210 mm, CH$_2$Cl$_2$:hexane (1:1)) to give **Ni-23** (15.3 mg, 74%) as a purple solid. ^{1}H NMR (400 MHz, CDCl$_3$, TMS): δ 2.450 (s, 6H, H$_{Me\text{-}Xyl}$), 2.531 (s, 12H, H$_{Me\text{-}Xyl}$), 2.559 (s, 6H, H$_{Me\text{-}Xyl}$), 3.955 (s, 3H, CO$_2$CH$_3$), 7.029 and 7.146 (ABq, 2H, ^3J = 16.0, 16.0 Hz, H$_{2',1'}$), 7.273 (d, 2H, ^3J = 8.3 Hz, H$_{styryl}$), 7.314 (s, 2H, H$_{p\text{-}Xyl}$), 7.351 (s, 1H, H$_{p\text{-}Xyl}$), 7.366 (s, 1H, H$_{p\text{-}Xyl}$), 7.580 (s, 2H, H$_{o\text{-}Xyl}$), 7.613 (s, 4H, H$_{o\text{-}Xyl}$), 7.633 (s, 2H, H$_{o\text{-}Xyl}$), 7.983 (d, 2H, ^3J = 8.3 Hz, H$_{styryl}$), 8.69-8.73 (m, 6H, H$_{\beta\text{-}pyrrolic}$), 8.912 (s, 1H, H$_{3''\ (\beta\text{-}pyrrolic)}$). *Assignments aided by COSY spectra.* UV-vis (CH$_2$Cl$_2$): λ_{max} [nm] (ε x 10^{-3}) 430 (211), 540 (20.1), 577 (13.3). FAB-LRMS:

m/z (%, assignment) cluster at 940-948, 943 (100, M$^+$). HRMS: Calcd for M$^+$ (C$_{62}$H$_{52}$N$_4$NiO$_2$): 942.3444, found: 942.3456.

TXP-=-Ph$_s$C●$_2$Me, 29.

Methyl 2-(*trans*-2'-(5",10",15",20"-tetrakis(3''',5'''-dimethylphenyl)porphyrin-2"-yl)ethen-1'-yl)-1-benzoate.

C$_{62}$H$_{54}$N$_4$O$_2$
Exact Mass: 886.4247
Mol. Wt.: 887.1179
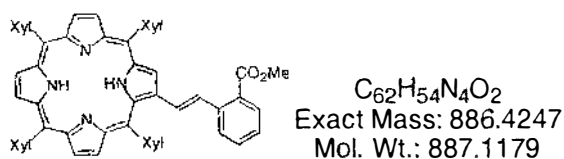
A solution of TXPps **5** (80.9 mg, 78.0 μmol) and methyl 2-formylbenzoate **26** (51.2 mg, 312 μmol, 4.0 eq) in CHCl$_3$ (78 mL) was heated to reflux under N$_2$. DBU (35 μL, 3.0 eq) was added and after 15 min, TLC analysis indicated that all of **5** had been consumed. The crude isomeric product was precipitated with MeOH to give a purple powder (61.5 mg, ≈15% *cis* by ^{1}H NMR). The crude product was dissolved in CH$_2$Cl$_2$ (10 mL) and I$_2$ (53 mg, 209 μmol, 3.0 eq) was added. After stirring at RT for 3 h in darkness, excess sat. Na$_2$S$_2$O$_3$ was added and stirring continued for 30 min. The organic layer was separated, dried (MgSO$_4$) and the solvent removed *in vacuo*. The residue was column chromatographed (silica, 19 mm$_{dia}$ x 80 mm, CH$_2$Cl$_2$) to give *trans* ester **29** (55.3 mg, 80%) as a purple powder. ^{1}H NMR (270 MHz, CDCl$_3$, TMS): δ -2.634 (br s, 2H, NH), 2.515 (s, 6H, H$_{Me-Xyl}$), 2.58-2.61 (m, 12H, H$_{Me-Xyl}$), 2.624 (s, 6H, H$_{Me-Xyl}$), 3.927 (s, 3H, CO$_2$CH$_3$), 6.933 (d, 1H, ^3J = 15.9 Hz, H$_2$), 7.27-7.52 (m, 7H, 4H$_{p-Xyl}$ + H$_{3,4,5}$), 7.79-7.93 (m, 9H, 8H$_{o-Xyl}$ + H$_6$), 8.048 (d, 1H, ^3J = 15.9 Hz, H$_1$), 8.782 and 8.799 (ABq, 2H, ^3J = 4.9, 4.9 Hz, H$_{\beta-pyrrolic}$), 8.835 (s, 2H, H$_{\beta-pyrrolic}$), 8.853 (s, 2H, H$_{\beta-pyrrolic}$), 9.044 (s, 1H, H$_{3" (\beta-pyrrolic)}$). *Assignments aided by COSY spectra.* UV-vis (CH$_2$Cl$_2$): λ$_{max}$ [nm] (ε x 10^{-3}) 428 (245), 525 (19.0), 563 (9.56), 600 (6.36), 659 (3.32). FAB-LRMS: m/z (%, assignment) cluster at 886-891, 887 (100, MH$^+$). HRMS: Calcd for MH$^+$ (C$_{62}$H$_{54}$N$_4$O$_2$): 887.4325, found: 887.4297.

ZnTXP-=-Ph$_o$CO$_2$Me, Zn-29.

Methyl 2-(*trans*-2'-(2"-(5",10",15",20"-tetrakis(3"',5"'-dimethylphenyl)porphyrinato zinc(II)}yl)ethen-1'-yl)-1-benzoate.

C$_{62}$H$_{52}$N$_4$O$_2$Zn
Exact Mass: 948.3382
Mol. Wt.: 950.4920
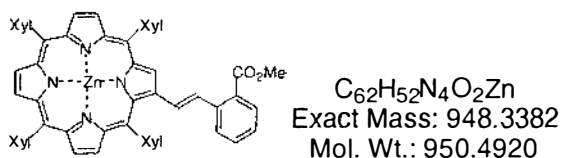
A solution of Zn(OAc)$_2$·2H$_2$O (15.0 mg, 68.3 μmol, 1.2 eq) in MeOH (500 μL) was added to a solution of porphyrin ester **29** (50.6 mg, 57.0 μmol) in CHCl$_3$ (5.0 mL) with stirring at RT. After 30 min, TLC analysis indicated that all of **28** had been consumed with the appearance of a single new spot at lower R_f. The solvent was removed *in vacuo* and the residue column chromatographed (silica, 19 mm$_{dia}$ x 100 mm, CHCl$_3$) to give **Zn-29** (44.2 mg, 82%) as a purple solid. ^{1}H NMR (270 MHz, CDCl$_3$, TMS): δ 2.506 (s, 6H, H$_{Me-Xyl}$), 2.595 (s, 12H, H$_{Me-Xyl}$), 2.620 (s, 6H, H$_{Me-Xyl}$), 3.916 (s, 3H, CO$_2$CH$_3$), 6.956 (d, 1H, ^3J = 15.9 Hz, H$_{2'}$), 7.27-7.52 (m, 7H, 4H$_{p-Xyl}$ + H$_{3,4,5}$), 7.77-7.91 (m, 9H, 8H$_{o-Xyl}$ + H$_6$), 7.986 (d, 1H, ^3J = 15.9 Hz, H$_{1'}$), 8.87-8.97 (m, 6H, H$_{\beta-pyrrolic}$), 9.135 (s, 1H, H$_{3"\,(\beta-pyrrolic)}$). *Assignments aided by COSY spectra.* UV-vis (CH$_2$Cl$_2$): λ_{max} [nm] (ε x 10^{-3}) 430 (253), 556 (19.5), 593 (5.50). FAB-LRMS: *m/z* (%, assignment) cluster at 948-954, 948 (100, M$^+$). HRMS: Calcd for M$^+$ (C$_{62}$H$_{52}$N$_4$O$_2$Zn): 948.3382, found: 948.3403.

TXP-=-Ph$_m$CO$_2$Me, 30.

Methyl 3-(*trans*-2'-(5",10",15",20"-tetrakis(3"',5"'-dimethylphenyl)porphyrin-2"-yl)ethen-1'-yl)-1-benzoate.

C$_{62}$H$_{54}$N$_4$O$_2$
Exact Mass: 886.4247
Mol. Wt.: 887.1179
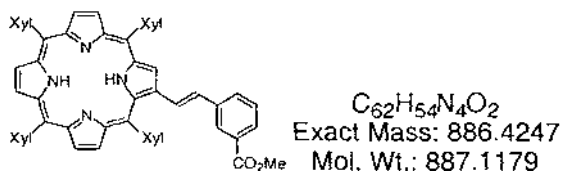
A solution of TXPps **5** (81.4 mg, 78.4 μmol) and methyl 3-formylbenzoate **27** (51.5 mg, 314 μmol, 4.0 eq) in CHCl$_3$ (7.8 mL) was heated to reflux under N$_2$. DBU (35 μL, 3.0 eq) was added and after 15 min, TLC analysis indicated that all of **5** had been consumed. The solvent was removed *in vacuo* and the residue column chromatographed (silica, 19 mm$_{dia}$ x 80 mm, CH$_2$Cl$_2$:hexane (1:1)). The isomeric product (63.8 mg) was dissolved in CH$_2$Cl$_2$ (10 mL) and I$_2$ (55 mg, 217 μmol, 3.0 eq)

added. After stirring at RT for 3 h in darkness, excess sat. $Na_2S_2O_3$ was added and stirring continued for 30 min. The organic layer was separated, dried ($MgSO_4$) and the solvent removed *in vacuo*. The residue was column chromatographed (silica, 19 mm$_{dia}$ x 80 mm, CH_2Cl_2) to give *trans* ester **30** (51.8 mg, 74%) as a purple powder. ^{1}H NMR (270 MHz, $CDCl_3$, TMS): δ -2.635 (br s, 2H, NH), 2.511 (s, 6H, H$_{Me-Xyl}$), 2.595 (s, 12H, H$_{Me-Xyl}$), 2.629 (s, 6H, H$_{Me-Xyl}$), 4.038 (s, 3H, CO_2CH_3), 7.002 and 7.296 (ABq, 2H, ^3J = 15.9, 16.2 Hz, H$_{2',1'}$), 7.38-7.52 (m, 5H, 4H$_{p-Xyl}$ + H$_5$), 7.78-7.87 (m, 9H, 8H$_{o-Xyl}$ + H$_{4 or 6}$), 7.944 (dt, 1H, ^3J = 7.3 Hz, ^4J = 1.5 Hz,, H$_{6 or 4}$), 7.994 (s, 1H, H$_2$), 8.78-8.86 (m, 6H, H$_{\beta-pyrrolic}$), 9.001 (s, 1H, H$_{3'' (\beta-pyrrolic)}$). *Assignments aided by COSY spectra.* UV-vis (CH_2Cl_2): λ_{max} [nm] (ε x 10^{-3}) 427 (238), 524 (19.3), 562 (10.2). FAB-LRMS: *m/z* (%, assignment) cluster at 886-891, 887 (100, MH$^+$). HRMS: Calcd for MH$^+$ ($C_{62}H_{55}N_4O_2$): 887.4325, found: 887.4325.

ZnTXP-=-Ph$_m$CO$_2$Me, Zn-30.

Methyl 3-(*trans*-2'-(2"-(5''',10",15",20"-tetrakis(3''',5'''-dimethylphenyl)porphyrinato zinc(II))yl)ethen-1'-yl)-1-benzoate.

$C_{62}H_{52}N_4O_2Zn$
Exact Mass: 948.3382
Mol. Wt.: 950.4920
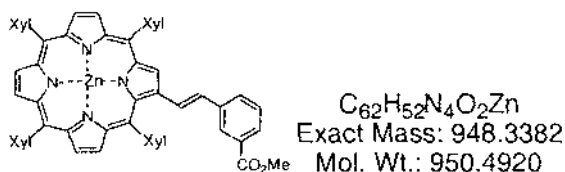
A solution of Zn(OAc)$_2$·2H$_2$O (14.1 mg, 64.2 μmol, 1.2 eq) in MeOH (0.5 mL) was added to a solution of ester **30** (47.6 mg, 53.7 μmol) in CHCl$_3$ (5.0 mL) with stirring at RT. After 30 min, TLC analysis indicated that starting material **30** had been consumed, and a single new spot had appeared at lower R_f. The solvent was removed *in vacuo* and the residue column chromatographed (silica, 19 mm$_{dia}$ x 100 mm, CHCl$_3$) to give **Zn-30** (37.9 mg, 74%) as a purple solid. ^{1}H NMR (270 MHz, CDCl$_3$, TMS): δ 2.499 (s, 6H, H$_{Me-Xyl}$), 2.595 (s, 12H, H$_{Me-Xyl}$), 2.628 (s, 6H, H$_{Me-Xyl}$), 4.017 (s, 3H, CO_2CH_3), 7.030 and 7.257 (ABq, 2H, ^3J = 16.2, 15.9 Hz, H$_{2',1'}$), 7.37-7.52 (m, 5H, 4H$_{p-Xyl}$ + H$_5$), 7.77-7.87 (m, 9H, 8H$_{o-Xyl}$ + H$_{4 or 6}$), 7.907 (d, 1H, ^3J = 7.6 Hz, H$_{6 or 4}$), 7.997 (s, 1H, H$_2$), 8.90-8.98 (m, 6H, H$_{\beta-pyrrolic}$), 9.106 (s, 1H, H$_{3'' (\beta-pyrrolic)}$). *Assignments aided by COSY spectra.* UV-vis (CH_2Cl_2): λ_{max} [nm] (ε x 10^{-3}) 431 (251), 557 (19.8), 592 (6.05). FAB-LRMS: *m/z* (%, assignment) cluster at 947-955, 948 (100, M$^+$). HRMS: Calcd for M$^+$ ($C_{62}H_{52}N_4O_2Zn$): 948.3382, found: 948.3373.

TBP-=-PhCO₂Me, 31.

Methyl 4-(*trans*-2'-(5",10",15",20"-tetrakis(3'",5'"-di-*tert*-butylphenyl)porphyrin-2"-yl)ethen-1'-yl)-1-benzoate.
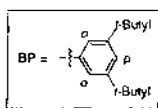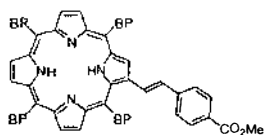
$C_{86}H_{102}N_4O_2$
Exact Mass: 1222.8003
Mol. Wt.: 1223.7558

A solution of TBPps **6**[79] (250 mg, 182 μmol) and methyl 4-formylbenzoate **28** (119 mg, 728 μmol, 4.0 eq) in CHCl₃ (18 mL) was heated to reflux under N₂. DBU (82 μL, 3.0 eq) was added and after 15 min TLC analysis indicated that all **6** had been consumed. The crude product was quantitatively precipitated with MeOH to give a purple powder. This material was dissolved in CH₂Cl₂ (17 mL) and I₂ (150 mg, 591 μmol, 3.0 eq) was added. After stirring at RT for 3 h in darkness, excess sat. Na₂S₂O₃ was added and stirring continued for 30 min. The organic layer was separated, dried (MgSO₄) and the solvent removed *in vacuo*. The residue was column chromatographed (silica, 37 mm$_{dia}$ x 120 mm, CH₂Cl₂:hexane (1:1)). Recrystallisation from CH₂Cl₂/MeOH gave *trans* ester **31** (117 mg, 53%) as a purple powder. ¹H NMR (400 MHz, CDCl₃, TMS): δ -2.535 (br s, 2H, NH), 1.421 (s, 18H, H$_{Me-BP}$), 1.518 (s, 18H, H$_{Me-BP}$), 1.523 (s, 18H, H$_{Me-BP}$), 1.561 (s, 18H, H$_{Me-BP}$), 3.967 (s, 3H, CO₂CH₃), 7.039 and 7.261 (ABq, 2H, ^3J = 15.9, 15.2 Hz, H$_{2',1'}$), 7.271 (d, 2H, ^3J = 8.4 Hz, H$_{styryl}$), 7.783 (t, 2H, ^4J = 1.7 Hz, H$_{p-BP}$), 7.824 (t, 1H, ^4J = 1.8 Hz, H$_{p-BP}$), 7.859 (t, 1H, ^4J = 1.8 Hz, H$_{p-BP}$), 7.972 (d, 2H, ^3J = 8.3 Hz, H$_{styryl}$), 8.060 (d, 2H, ^4J = 1.8 Hz, H$_{o-BP}$), 8.078 (app t, 4H, ^4J = 2.0 Hz, H$_{o-BP}$), 8.140 (d, 2H, ^4J = 1.8 Hz, H$_{o-BP}$), 8.807 and 8.851 (ABq, 2H, ^3J = 4.8, 5.0 Hz, H$_{\beta-pyrrolic}$), 8.85-8.89 (m, 4H, H$_{\beta-pyrrolic}$), 9.069 (s, 1H, H$_{3" (\beta-pyrrolic)}$). *Assignments aided by COSY spectra.* UV-vis (CH₂Cl₂): λ_{max} [nm] (ϵ x 10⁻³) 431 (239), 527 (22.9), 567 (14.4), 601 (9.29), 658 (5.63). FAB-LRMS: *m/z* (%, assignment) cluster at 1222-1227, 1224 (100, M⁺). HRMS: Calcd for M⁺ ($C_{86}H_{103}N_4O_2$): 1222.8003, found: 1222.7991.

ZnTBP-=-PhCO₂Me, Zn-31.

Methyl 4-(*trans*-2'-(2"-(5",10",15",20"-tetrakis(3'",5'"-di-*tert*-butylphenyl)porphyrinato zinc(II))yl)ethen-1'-yl)-1-benzoate.
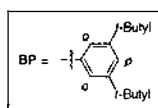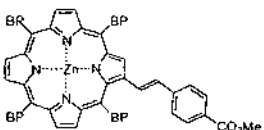
$C_{86}H_{100}N_4O_2Zn$
Exact Mass: 1284.7138
Mol. Wt.: 1287.1300

A solution of Zn(OAc)$_2$·2H$_2$O (22 mg, 98 μmol, 1.2 eq) in MeOH (1.5 mL) was added to a solution of ester **31** (100 mg, 81.7 μmol) in CHCl$_3$ (10 mL) with stirring at RT. After 1.75 h, UV-vis analysis indicated that the reaction was complete. The product was precipitated with MeOH to give **Zn-31** (103 mg, 98%) as a purple microcrystalline powder. ^{1}H NMR (400 MHz, CDCl$_3$, TMS): δ 1.418 (s, 18H, H$_{Me-BP}$), 1.520 (s, 18H, H$_{Me-BP}$), 1.524 (s, 18H, H$_{Me-BP}$), 1.561 (s, 18H, H$_{Me-BP}$), 3.961 (s, 3H, CO$_2$CH$_3$), 7.083 (dd, 1H, ^3J = 15.9 Hz, ^4J = 0.7 Hz, H$_{2'}$), 7.247 (d, 1H, ^3J = 15.8 Hz, H$_{1'}$), 7.281 (d, 2H, ^3J = 8.4 Hz, H$_{styryl}$), 7.782 (app q, 2H, ^4J = 1.8 Hz, H$_{p-BP}$), 7.820 (t, 1H, ^4J = 1.8 Hz, H$_{p-BP}$), 7.854 (t, 1H, ^4J = 1.8 Hz, H$_{p-BP}$), 7.967 (d, 2H, ^3J = 8.3 Hz, H$_{styryl}$), 8.059 (d, 2H, ^4J = 1.9 Hz, H$_{o-BP}$), 8.088 (app t, 4H, ^4J = 1.6 Hz, H$_{o-BP}$), 8.144 (d, 2H, ^4J = 1.9 Hz, H$_{o-BP}$), 8.899 and 8.967 (ABq, 2H, ^3J = 4.7, 4.4 Hz, H$_{\beta-pyrrolic}$), 8.978 (s, 2H, H$_{\beta-pyrrolic}$), 8.993 and 9.008 (ABq, 2H, ^3J = 4.7, 4.7 Hz, H$_{\beta-pyrrolic}$), 9.188 (d, 1H, ^4J = 0.7 Hz, H$_{3'' (\beta-pyrrolic)}$). *Assignments aided by COSY spectra.* UV-vis (CH$_2$Cl$_2$): λ_{max} [nm] (ε x 10^{-3}) 437 (225), 561 (19.7), 598 (8.05). FAB-LRMS: *m/z* (%, assignment) cluster at 1284-1293, 1287 (100, M$^+$). HRMS: Calcd for M$^+$ (C$_{86}$H$_{100}$N$_4$O$_2$Zn): 1284.7138, found: 1284.7221.

ZnTXP-=-Ph$_o$CO$_2$H, Zn-32.

2-(*Trans*-2'-(2''-(5''',10''',15''',20'''-tetrakis(3'''',5''''-dimethylphenyl)porphyrinato zinc(II))yl)ethen-1'-yl)-1-benzoic acid.

C$_{61}$H$_{50}$N$_4$O$_2$Zn
Exact Mass: 934.3225
Mol. Wt.: 936.4655
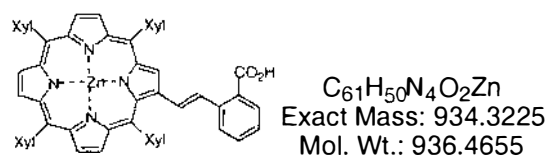
KOH (89.9 mg, 1.60 mmol, 35 eq) in MeOH (13.2 mL) and H$_2$O (1.2 mL) was added to a solution of ester **Zn-29** (43.1 mg, 45.3 μmol) in THF (12.2 mL). The mixture was refluxed for 23.5 h under N$_2$. After cooling to RT, H$_2$O (25 mL), CH$_2$Cl$_2$ (25 mL) and 2.0 M H$_3$PO$_{4 (aq)}$ (0.82 mL, 36 eq) were added with stirring. The resulting coloured organic layer was washed with H$_2$O (2 x 40 mL), and then separated. The solvent was removed *in vacuo* to give **Zn-32** (40.5 mg, 95%) as a purple solid. ^{1}H NMR (270 MHz, acetone-d$_6$, TMS): δ 2.537 (s, 6H, H$_{Me-Xyl}$), 2.602 (s, 12H, H$_{Me-Xyl}$), 2.626 (s, 6H, H$_{Me-Xyl}$), 7.121 (d, 1H, ^3J = 16.0 Hz, H$_{2'}$), 7.35-7.64 (m, 7H, 4H$_{p-Xyl}$ + H$_{3,4,5}$), 7.77-7.90 (m, 8H, H$_{o-Xyl}$), 7.994 (app d, 1H, ^3J = 8.1 Hz, H$_6$), 8.281 (d, 1H, ^3J = 15.9 Hz, H$_{1'}$), 8.78-8.88(m, 6H, H$_{\beta-pyrrolic}$), 9.145 (s, 1H, H$_{3'' (\beta-pyrrolic)}$). *Assignments aided by COSY spectra.* UV-vis (CH$_2$Cl$_2$): λ_{max} [nm] (ε x 10^{-3}) 436 (214), 566 (18.2), 604 (6.51). FAB-LRMS: *m/z* (%,

assignment) cluster at 934-940, 934 (100, M$^+$). HRMS: Calcd for M$^+$ (C$_{61}$H$_{50}$N$_4$O$_2$Zn): 934.3225, found: 934.3256.

ZnTXP-=-Ph$_m$CO$_2$H, Zn-33.

3-(*Trans*-2'-(2"-(5",10",15",20"-tetrakis(3''',5'''-dimethylphenyl)porphyrinato zinc(II))yl)ethen-1'-yl)-1-benzoic acid.

C$_{61}$H$_{50}$N$_4$O$_2$Zn
Exact Mass: 934.3225
Mol. Wt.: 936.4655
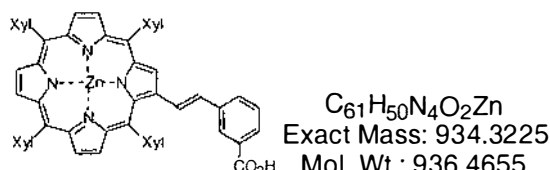
KOH (43.3 mg, 772 μmol, 20 eq) in MeOH (10.4 mL) and H$_2$O (1.4 mL) was added to a solution of ester **Zn-30** (36.7 mg, 38.6 μmol) in THF (10.4 mL). The mixture was refluxed for 16.5 h under N$_2$. After cooling to RT, H$_2$O (25 mL), CH$_2$Cl$_2$ (25 mL) and 2.0 M H$_3$PO$_4$ $_{(aq)}$ (430 μL, 21 eq) were added with stirring. The resulting red/green coloured organic layer was washed with H$_2$O (2 x 40 ml), and then separated. The solvent was removed *in vacuo*, giving **Zn-33** (35.7 mg, 99%) as a purple solid. ^{1}H NMR (270 MHz, acetone-d$_6$, TMS): δ 2.531 (s, 6H, H$_{Me-Xyl}$), 2.603 (s, 12H, H$_{Me-Xyl}$), 2.621 (s, 6H, H$_{Me-Xyl}$), 7.130 and 7.352 (ABq, 2H, ^3J = 15.9, 16.2 Hz, H$_{2',1'}$), 7.41-7.60 (m, 5H, 4H$_{p-Xyl}$ + H$_5$), 7.78-7.88 (m, 9H, 8H$_{o-Xyl}$ + H$_{4 or 6}$), 7.933 (d, 1H, ^3J = 7.7 Hz, H$_{6 or 4}$), 8.046 (s, 1H, H$_2$), 8.81-8.88 (m, 6H, H$_{\beta-pyrrolic}$), 9.143 (s, 1H, H$_{3" (\beta-pyrrolic)}$). *Assignments aided by COSY spectra.* UV-vis (THF): λ_{max} [nm] (ϵ x 10^{-3}) 436 (238), 565 (19.7), 602 (7.13). FAB-LRMS: *m/z* (%, assignment) cluster at 933-941, 934 (100, M$^+$). HRMS: Calcd for M$^+$ (C$_{61}$H$_{50}$N$_4$O$_2$Zn): 934.3225, found: 934.3244.

ZnTBP-=-PhCO$_2$H, Zn-34.

4-(*Trans*-2'-(2"-(5",10",15",20"-tetrakis(3''',5'''-di-*tert*-butylphenyl)porphyrinato zinc(II))yl)ethen-1'-yl)-1-benzoic acid.

C$_{85}$H$_{98}$N$_4$O$_2$Zn
Exact Mass: 1270.6981
Mol. Wt.: 1273.1034
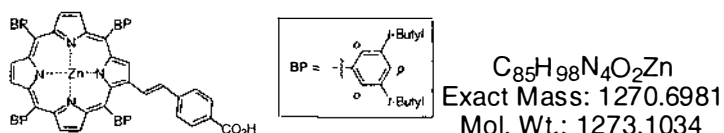
KOH (69.7 mg, 1.24 mmol, 20 eq) in MeOH (15 mL) and H$_2$O (1.5 mL) was added to a solution of ester **Zn-31** (80.0 mg, 62.2 μmol) in THF (15 mL). The mixture was refluxed for 19.5 h under N$_2$. After cooling to RT, H$_2$O (30 mL), CHCl$_3$ (40 mL) and

2.0 M H_3PO_4 (aq) (0.65 mL, 21 eq) were added with stirring. The resulting red/green coloured organic layer was washed with H_2O (3 x 50 mL), then separated carefully and the solvent removed *in vacuo*. Recrystallisation from $CHCl_3$/hexane gave acid **Zn-34** (74.1 mg, 94%) as a purple powder. ^{1}H NMR (400 MHz, CDCl$_3$, 55°C, TMS): δ 1.433 (s, 18H, H$_{\text{Me-BP}}$), 1.522 (s, 18H, H$_{\text{Me-BP}}$), 1.527 (s, 18H, H$_{\text{Me-BP}}$), 1.566 (s, 18H, H$_{\text{Me-BP}}$), 7.167 and 7.246 (ABq, 2H, ^3J = 16.0, 15.7 Hz, H$_{2',1'}$), 7.304 (d, 2H, ^3J = 8.4 Hz, H$_{\text{styryl}}$), 7.794 (app q, 2H, ^4J = 1.8 Hz, H$_{p\text{-BP}}$), 7.833 (t, 1H, ^4J = 1.8 Hz, H$_{p\text{-BP}}$), 7.869 (t, 1H, ^4J = 1.8 Hz, H$_{p\text{-BP}}$), 8.014 (d, 2H, ^3J = 8.2 Hz, H$_{\text{styryl}}$), 8.063 (d, 2H, ^4J = 1.8 Hz, H$_{o\text{-BP}}$), 8.079 (app t, 4H, ^4J = 1.9 Hz, H$_{o\text{-BP}}$), 8.140 (d, 2H, ^4J = 1.8 Hz, H$_{o\text{-BP}}$), 8.851 and 8.930 (ABq, 2H, ^3J = 4.7, 4.8 Hz, H$_{\beta\text{-pyrrolic}}$), 8.939 (s, 2H, H$_{\beta\text{-pyrrolic}}$), 8.964 and 8.971 (ABq, 2H, ^3J = 5.0, 4.9 Hz, H$_{\beta\text{-pyrrolic}}$), 9.183 (s, 1H, ^4J = 0.7 Hz, H$_{3''\ (\beta\text{-pyrrolic})}$). UV-vis (THF): λ_{max} [nm] (ε x 10^{-3}) 440 (251), 567 (24.6), 604 (11.2). FAB-LRMS: *m/z* (%, assignment) cluster at 1271-1278, 1273 (100, M$^+$). HRMS: Calcd for M$^+$ (C$_{85}$H$_{98}$N$_4$O$_2$Zn): 1270.6981, found: 1270.6895.

ZnTXP-=-PhCO$_2^-$ Na$^+$, Zn-35.

Sodium 4-(*trans*-2'-(2''-(5'',10'',15'',20''-tetrakis(3''',5'''-dimethylphenyl)porphyrinato zinc(II))yl)ethen-1'-yl)-1-benzoate.


C$_{61}$H$_{49}$N$_4$NaO$_2$Zn
Exact Mass: 956.3045
Mol. Wt.: 958.4473
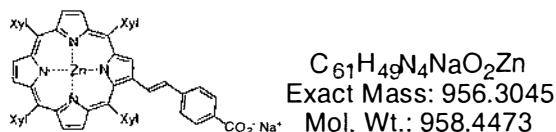
Aqueous NaOH (0.8 M, 188 μL, 4.0 eq) was added to a suspension of acid **Zn-15** (35.0 mg, 37.4 μmol) in MeOH (5.0 mL) at RT. After 15 min, TLC analysis indicated that all the starting material had been consumed. The solvent was removed *in vacuo*, the residue was dissolved in benzene ($\approx$ 40 mL) and then dried (Na$_2$SO$_4$). The solvent was removed *in vacuo* to give **Zn-35** (33.8 mg, 94%) as a purple solid. ^{1}H NMR (270 MHz, MeOD-d$_4$, TMS): δ 2.537 (s, 6H, H$_{\text{Me-Xyl}}$), 2.577 (s, 12H, H$_{\text{Me-Xyl}}$), 2.606 (s, 6H, H$_{\text{Me-Xyl}}$), 7.167 and 7.207 (ABq, 2H, ^3J = 15.9, 16.2 Hz, H$_{2',1'}$), 7.297 (d, 2H, ^3J = 8.3 Hz, H$_{\text{styryl}}$), 7.390 (s, 2H, H$_{p\text{-Xyl}}$), 7.433 (s, 1H, H$_{p\text{-Xyl}}$), 7.502 (s, 1H, H$_{p\text{-Xyl}}$), 7.792 (s, 6H, H$_{o\text{-Xyl}}$), 7.833 (s, 2H, H$_{o\text{-Xyl}}$), 7.932 (d, 2H, ^3J = 8.1 Hz, H$_{\text{styryl}}$), 8.75-8.82(m, 6H, H$_{\beta\text{-pyrrolic}}$), 9.002 (s, 1H, H$_{3''(\beta\text{-pyrrolic})}$). UV-vis (CH$_2Cl_2$): λ_{max} [nm] (ε x 10^{-3}) 429 (186), 559 (17.8), 595 (7.45). FAB-LRMS: *m/z* (%, assignment) cluster at 934-940, 934 (100, [M – Na + H]$^+$). HRMS: Calcd for [M – Na + H]$^+$ (C$_{61}$H$_{50}$N$_4$O$_2$Zn): 934.3225, found: 934.3191.

ZnTXP-=-PhCO₂⁻ (*n*-Bu)₄N⁺, Zn-36.

Tetra-*n*-butylammonium 4-(*trans*-2'-(2"-(5",10",15",20"-tetrakis(3'",5'"-dimethylphenyl)-porphyrinato zinc(II))yl)ethen-1'-yl)-1-benzoate.

$C_{77}H_{85}N_5O_2Zn$
Exact Mass: 1175.5995
Mol. Wt.: 1177.9213

Aqueous tetra-*n*-butylammonium hydroxide (100 μL of 40% w/w, 152 μmol, 4.0 eq) was added to a suspension of acid **Zn-15** (35.0 mg, 37.4 μmol) in MeOH (5.0 mL) at RT. After 30 min, TLC analysis indicated that all the starting material had been consumed. The solvent was removed *in vacuo* and the resulting oily residue was then dissolved in CH_2Cl_2 (70 mL) before washing with H_2O (3 x 150 mL). The organic layer was then separated carefully and the solvent removed *in vacuo* to give **Zn-36** (41.6 mg, 95%) as a purple solid. ¹H NMR (270 MHz, MeOD-d₄, TMS): δ 0.948 (t, 12H, $CH_2CH_2CH_2CH_3$), 1.273 (sext, 8H, $CH_2CH_2CH_2CH_3$), 1.40-1.54 (m, 8H, $CH_2CH_2CH_2CH_3$), 2.531 (s, 6H, H_{Me-Xyl}), 2.583 (s, 12H, H_{Me-Xyl}), 2.610 (s, 6H, H_{Me-Xyl}), 2.95-3.05 (m, 8H, $CH_2CH_2CH_2CH_3$), 7.190 (s, 2H, $H_{1',2'}$), 7.289 (d, 2H, ^3J = 8.3 Hz, H_{styryl}), 7.402 (s, 2H, H_{p-Xyl}), 7.441 (s, 1H, H_{p-Xyl}), 7.501 (s, 1H, H_{p-Xyl}), 7.798 (s, 6H, H_{o-Xyl}), 7.836 (s, 2H, H_{o-Xyl}), 7.914 (d, 2H, ^3J = 8.1 Hz, H_{styryl}), 8.775 and 8.808 (ABq, 2H, ^3J = 4.6, 4.6 Hz, $H_{\beta-pyrrolic}$), 8.776 (s, 2H, $H_{\beta-pyrrolic}$), 8.790 (s, 2H, $H_{\beta-pyrrolic}$), 9.020 (s, 1H, $H_{3"}$ $_{(\beta-pyrrolic)}$). UV-vis (CH_2Cl_2): λ_{max} [nm] (ε x 10⁻³) 433 (253), 520 (5.95), 558 (24.4), 595 (10.8). FAB-LRMS: *m/z* (%, assignment) cluster at 934-940, 934 (15, [M – (*n*-Bu)₄N + H]⁺), 242 (100, (*n*-Bu)₄N⁺). HRMS: Calcd for [M – (*n*-Bu)₄N + H]⁺ ($C_{61}H_{50}N_4O_2Zn$): 934.3225, found: 934.3243.

ZnTXP-=-Ph_m(CO₂H)₂, Zn-37.

5-(*trans*-2'-(2"-(5",10",15",20"-tetrakis(3'",5'"-dimethylphenyl)porphyrinato zinc(II))yl)ethen-1'-yl))-1,3-benzenedicarboxylic acid.
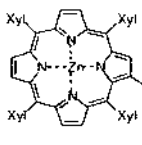
$C_{62}H_{50}N_4O_4Zn$
Exact Mass: 978.3124
Mol. Wt.: 980.4750

KOH (51.0 mg, 909 μmol, 20 eq) in MeOH (13.0 mL)/H_2O (1.30 mL) was added to a solution of diester **Zn-50** (45.8 mg, 45.4 μmol) in THF (13.0 mL). The mixture was heated to reflux under N_2 for 17 h. After cooling to RT, H_2O (30 mL) was added

followed by H_3PO_4 (480 μL, 2.0 M) and CH_2Cl_2 (30 mL). The pH of the aqueous layer was 3. The organic layer was washed with H_2O (2 x 40 mL), and then carefully separated and the solvent removed *in vacuo*. The residue was dissolved in minimal CH_2Cl_2 and on standing a precipitate formed, which was separated by filtration and dried *in vacuo* to give diacid **Zn-37** (38.0 mg, 85%) as a purple powder. ^{1}H NMR (270 MHz, acetone-d_6, Et$_3$N, TMS): δ 0.991 (t, 20H, ^3J = 7.3 Hz, Et$_3$N), 2.375 (s, 6H, H$_{Me-Xyl}$), 2.53-2.64 (m, 31H, 18H$_{Me-Xyl}$ + 13H Et$_3$N), 6.965 and 7.244 (ABq, 2H, ^3J = 15.9, 15.9 Hz, H$_{2',1'}$), 7.34-7.42 (m, 4H, H$_{p-Xyl}$), 7.516 (br s, 2H, H$_{4,6}$), 7.714 (br s, 2H, H$_{o-Xyl}$), 7.834 (br s, 6H, H$_{o-Xyl}$), 8.081 (br s, 1H, H$_2$), 8.77-8.85 (m, 6H, H$_{\beta\text{-pyrrolic}}$), 9.164 (s, 1H, H$_{3''\,(\beta\text{-pyrrolic})}$). *^{1}H NMR assignments were made with the aid of long range couplings observed in COSY spectra. Et$_3$N was added to the NMR solvent to improve solubility. Subtraction of the Et$_3$N integral values gave the correct integral values for the porphyrin moiety.* UV-vis (THF): λ_{max} [nm] (ε x 10^{-3}) 437 (257), 566 (21.4), 603 (7.71). FAB-LRMS: *m/z* (%, assignment) cluster at 978-984, 978 (100, M$^+$). HRMS: Calcd for M$^+$ (C$_{62}$H$_{50}$N$_4$O$_4$Zn): 978.3124, found: 978.3120.

Dimethyl 5-formyl-1,3-benzenedioate, 40.

MeO$_2$C ⟋⟍ CO$_2$Me

CHO
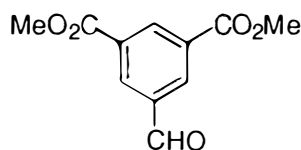
C$_{11}$H$_{10}$O$_5$
Exact Mass: 222.0528
Mol. Wt.: 222.1941   [164073-80-7]

Rosenmund Reduction.[218]

A mixture of acyl chloride **46** (7.746 g, 30.2 mmol) and 5% palladium on barium sulfate (595 mg) in dry *p*-xylene (87 mL) was heated to reflux temperature while bubbling H$_2$ into the solution. The liberated HCl was titrated with NaOH (1.009 M) using Bromothymol Blue as the indicator. The reaction was deemed complete after 3 h with no further HCl liberated (29.9 mL of NaOH, 100%). The reaction was cooled to RT and CH_2Cl_2 (80 mL) then added. The mixture was filtered through celite, and then column chromatographed (silica, 55 mm$_{dia}$ x 60 mm, CH_2Cl_2). Recrystallisation from CH_2Cl_2/hexane gave dimethyl 5-formylisophthalate **40** (5.813 g, 90%) as a white solid. ^{1}H NMR (270 MHz, CDCl$_3$, TMS): δ 4.003 (s, 6H, CO$_2$CH$_3$), 8.717 (d, ^4J = 1.6 Hz, 2H, H$_{4,6}$), 8.917 (t, ^4J = 1.7 Hz, 1H, H$_2$), 10.134 (s, 1H, CHO). ^{13}C NMR (68 MHz, CDCl$_3$): δ 52.77, 131.73, 134.18, 135.58, 136.74, 165.00, 190.17. EI-LRMS: *m/z* (%, assignment) 222 (95, M$^+$), 191 (100, [M – OMe]$^+$), 163 (21, [M - CO$_2$Me]$^+$). HRMS:

Calcd for M^+ ($C_{11}H_{10}O_5$): 222.0528, found: 222.0528. *Data is in agreement with literature values.*[98,99]

Dimethyl 5-carboxy-1,3-benzenedioate, 45.

MeO$_2$C

CO$_2$H

CO$_2$Me

$C_{11}H_{10}O_6$
Exact Mass: 238.0477
Mol. Wt.: 238.1935   [38588-64-6]
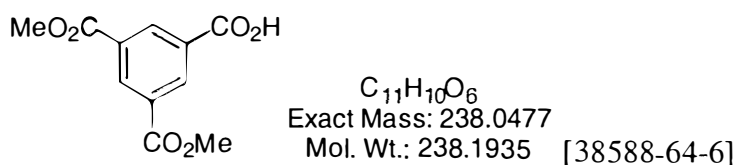
Trimethyl trimesate **44** (8.572 g, 33.98 mmol) was dissolved in MeOH (514 mL) using ultrasound and gentle heating. A solution of KOH (2.860 g, 51.0 mmol, 1.5 eq) in MeOH (171 mL) was added, and the reaction mixture heated to reflux for 16.5 h. After cooling to RT, H_3PO_4 (15 M, 3.40 mL), H_2O (2.2 L) and $CHCl_3$ (1.0 L) were added and the mixture stirred for 30 min. The organic layer was dried ($MgSO_4$) and the solvent removed *in vacuo* to give a crude mixture of starting material **44**, diester acid **45** and diacid ester **47** (4:94:2 by ^1H NMR) as a white solid (9.046 g). This mixture was column chromatographed (silica, 55 mm$_{dia}$ x 100 mm), first eluting with CH_2Cl_2:Et_2O (98:2) to give unreacted **44** as a white solid (475 mg, 5%), then CH_2Cl_2:Et_2O:MeOH (96:2:2) to give diester acid **45** as a white solid (7.271 g, 87%). ^1H NMR (270 MHz, MeOD-d$_4$): δ 3.998 (s, 6H, CO$_2$CH$_3$), 8.670 (t, 1H, ^4J = 1.8 Hz, ArH), 8.721 (d, 2H, ^4J = 1.5 Hz, ArH). ^{13}C NMR (68 MHz, MeOD-d$_4$) δ 53.13, 132.22, 133.15, 134.72, 135.18, 166.39, 167.30. EI-LRMS: *m/z* (%, assignment) 238 (16, M^+), 207 (100, $[M - OCH_3]^+$), 179 (15, $[M - CO_2CH_3]^+$). HRMS: Calcd for M^+ ($C_{11}H_{10}O_6$): 238.0477, found: 238.0478.

Dimethyl 5-chlorocarbonyl-1,3-benzenedioate, 46.

MeO$_2$C

CO$_2$Me

COCl

$C_{11}H_9ClO_5$
Exact Mass: 256.0139
Mol. Wt.: 256.6389   [68872-14-0]
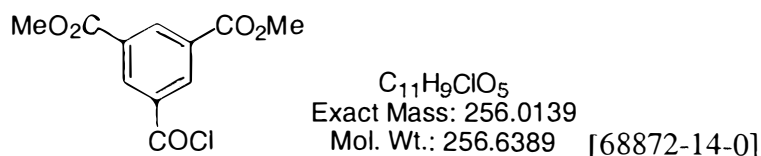
A suspension of diester acid **45** (7.047 g, 29.6 mmol) in dry benzene (190 mL) was reduced in volume to 70 mL under reduced pressure at 40°C. Oxalyl chloride (7.05 mL, 80.8 mmol, 2.7 eq) and DMF (141 μL) were added and the reaction stirred at RT under argon for 15 min, then 40°C for 15 min, then 60°C for 15 min. The solvent was then removed under reduced pressure. More benzene (100 mL) was added and then removed

in vacuo to give monochlorocarbonyl **46** (7.306 g, 96%) as a white solid. ^{1}H NMR (400 MHz, CDCl$_3$, TMS): δ 4.013 (s, 6H, CO$_2$CH$_3$), 8.924 (d, 2H, ^4J = 1.6 Hz, H$_{4,6}$), 8.965 (t, 1H, ^4J = 1.6 Hz, H$_2$). ^{13}C NMR (101 MHz, CDCl$_3$): δ 52.91, 131.89, 134.29, 135.75, 136.51, 164.70, 167.19. EI-LRMS: *m/z* (%, assignment) 256 (1, M$^+$), 225 (11, [M − OCH$_3$]$^+$), 221 (100, [M − Cl]$^+$), 193 (10, [M − COCl]$^+$). HRMS: Calcd for M$^+$ (C$_{11}$H$_9$ClO$_5$): 256.0139, found: 256.0151. *All data is in agreement with literature values.*[102]

Methyl 3,5-dicarboxybenzoate, 47.

MeO$_2$C $\diagdown$ $\diagup$ CO$_2$H

CO$_2$H
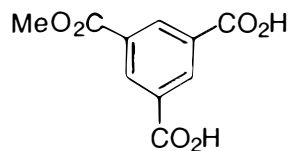
C$_{10}$H$_8$O$_6$
Exact Mass: 224.0321
Mol. Wt.: 224.1669   [18263-95-1]

Trimethyl 1,3,5-benzenetricarboxylate **44** (4.74 g, 18.8 mmol) was dissolved in MeOH (100 mL) aided by ultrasound and gentle heating. A solution of KOH (3.061 g, 55.6 mmol, 2.9 eq) in MeOH (90 mL) was added and the reaction mixture heated at reflux for 22 h. After cooling to RT, 15 M H$_3$PO$_4$ (14.2 mL) and H$_2$O (500 mL) were added. The aqueous solution was extracted with Et$_2$O (2 x 400 mL), and the extract dried (MgSO$_4$), filtered and the solvent removed *in vacuo* to give a mixture of products **45:47:48** (5:84:10 by ^{1}H NMR, 3.97 g) as a white solid. The crude product was adsorbed onto silica gel (40 g) and a soxhlet extraction was carried out with CH$_2$Cl$_2$ for 84 h. The solvent was removed *in vacuo* to give a mixture of diester acid and diacid ester **45:47** (9:91 by ^{1}H NMR, 816.4 mg) as a white solid. A pure sample of diacid ester **47** (151 mg) was isolated for characterisation using careful column chromatography (silica, CH$_2$Cl$_2$:Et$_2$O (9:1)). **47**: ^{1}H NMR (270 MHz, MeOD-d$_4$): δ 4.006 (s, 3H, CO$_2$CH$_3$), 8.774 (app d, 2H, ^4J = 1.9 Hz, ArH), 8.816 (app t, 1H, ^4J = 1.6 Hz, ArH). ^{13}C NMR (68 MHz, MeOD-d$_4$): δ 53.09, 132.19, 133.06, 135.09, 135.52, 166.60, 167.52. EI-LRMS: *m/z* (%, assignment) 224 (20, M$^+$), 193 (100, [M − OCH$_3$]$^+$), 165 (15, [M − CO$_2$CH$_3$]$^+$). HRMS: Calcd for M$^+$ (C$_{10}$H$_8$O$_6$): 224.0321, found: 224.0325.

TXP-=-Ph$_m$(CO$_2$Me)$_2$, 50.

Dimethyl 5-(*trans*-2'-(5",10",15",20"-tetrakis(3"',5"'-dimethylphenyl)porphyrin-2"-yl)ethen-1'-yl)-1,3-benzenedioate.

C$_{64}$H$_{56}$N$_4$O$_4$
Exact Mass: 944.4302
Mol. Wt.: 945.1540
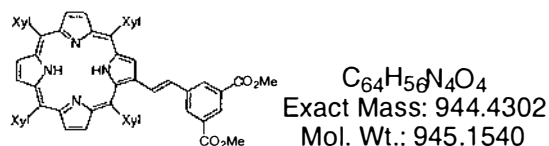
A solution of TXPps **5** (79.8 mg, 76.9 μmol) and dimethyl 5-formylisophthalate **40** (68.3 mg, 308 μmol, 4.0 eq) in CHCl$_3$ (7.8 mL) was heated to reflux under N$_2$. DBU (35 μL, 3.0 eq) was added and after 15 min, TLC analysis indicated that all **5** had been consumed. The solvent was removed *in vacuo* and the residue column chromatographed (silica, 19 mm$_{dia}$ x 80 mm, CH$_2$Cl$_2$:hexane (2:1)) to give a 1:9 *cis/trans* mixture of porphyrin **50** (70.0 mg, 96%) as a purple solid. The *cis/trans* mixture of **50** was dissolved in CH$_2$Cl$_2$ (10 mL) and I$_2$ (56 mg, 3.0 eq) was added. After stirring at RT for 3 h, sat. Na$_2$S$_2$O$_3$ (15 mL) was added and stirring continued for 30 min. The organic layer was separated, dried (MgSO$_4$) and the solvent removed *in vacuo*. The residue was column chromatographed as before to give the *trans* porphyrin diester **50** (59.4 mg, 85%, 82% overall) as a purple solid. ^{1}H NMR (270 MHz, CDCl$_3$, TMS): δ -2.637 (br s, 2H, NH), 2.514 (s, 6H, H$_{Me-Xyl}$), 2.599 (s, 12H, H$_{Me-Xyl}$), 2.636 (s, 6H, H$_{Me-Xyl}$), 4.065 (s, 6H, CO$_2$CH$_3$), 6.982 and 7.311 (ABq, 2H, ^3J = 15.9, 15.9 Hz, H$_{2',1'}$), 7.400 (br s, 2H, H$_{p-Xyl}$), 7.453 (br s, 1H, H$_{p-Xyl}$), 7.486 (br s, 1H, H$_{p-Xyl}$), 7.78-7.87 (m, 8H, H$_{o-Xyl}$), 8.159 (d, 2H, ^3J = 1.5 Hz, H$_{4,6}$), 8.582 (t, 1H, ^3J = 1.5 Hz, H$_2$), 8.79-8.88 (m, 6H, H$_{\beta\text{-pyrrolic}}$), 8.993 (s, 1H, H$_{3" (\beta\text{-pyrrolic})}$). *Cis/trans* mixture **50**: ^{1}H NMR (270 MHz, CDCl$_3$, TMS, selective data only): δ -2.71 (br s, NH *cis*), -2.64 (br s, NH *trans*), 6.35 and 6.57 (ABq, ^3J = 12 Hz, *cis* vinylic), 6.98 and 7.31 (ABq, ^3J = 15.9 Hz, *trans* vinylic). UV-vis (CH$_2$Cl$_2$): λ_{max} [nm] (ε x 10^{-3}) 428 (246), 524 (19.8), 563 (9.84), 600 (6.60), 658 (3.56). FAB-LRMS: *m/z* (%, assignment) cluster at 944-947, 945 (100, MH$^+$). HRMS: Calcd for MH$^+$ (C$_{64}$H$_{57}$N$_4$O$_4$): 945.4380, found: 945.4347.

ZnTXP-=-Ph$_m$(CO$_2$Me)$_2$, Zn-50.

Dimethyl 5-(trans-2'-(2"-(5",10",15",20"-tetrakis(3''',5'''-dimethylphenyl)porphyrinato zinc(II))yl)ethen-1'-yl))-1,3-benzenedioate.

C$_{64}$H$_{54}$N$_4$O$_4$Zn
Exact Mass: 1006.3437
Mol. Wt.: 1008.5281
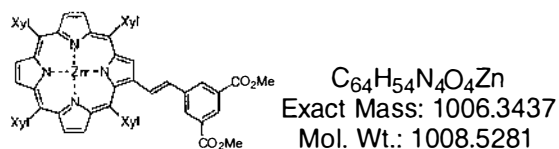
A solution of Zn(OAc)$_2$·2H$_2$O (15.3 mg, 70 μmol, 1.2 eq) in MeOH (500 μL) was added to a solution of diester **50** (54.8 mg, 58.0 μmol) in CHCl$_3$ (5.0 mL) with stirring at RT. After 30 min, TLC analysis indicated that all of **5** had been consumed with the appearance of a single coloured band at lower R_f. The solvent was removed *in vacuo* and the residue column chromatographed (silica, 19 mm$_{dia}$ x 100 mm, CH$_2$Cl$_2$:hexane (3:1)) to give the metalloporphyrin diester **Zn-50** (47.0 mg, 80%) as a purple solid. ^{1}H NMR (270 MHz, CDCl$_3$, TMS): δ 2.498 (s, 6H, H$_{Me-Xyl}$), 2.56-2.65 (m, 18H, H$_{Me-Xyl}$), 4.048 (s, 6H, CO$_2$CH$_3$), 7.015 and 7.273 (ABq, 2H, ^3J = 16.2, 16.2 Hz, H$_{2',1'}$), 7.36-7.50 (m, 4H, H$_{p-Xyl}$), 7.74-7.92 (m, 8H, H$_{o-Xyl}$), 8.159 (br s, 2H, H$_{4,6}$), 8.582 (br s, 1H, H$_2$), 8.90-8.99 (m, 6H, H$_{\beta-pyrrolic}$), 9.106 (s, 1H, H$_{3'' (\beta-pyrrolic)}$). UV-vis (CH$_2$Cl$_2$): λ_{max} [nm] (ε x 10^{-3}) 431 (250), 557 (19.7), 593 (6.15). FAB-LRMS: m/z (%, assignment) cluster at 1006-1012, 1006 (100, M$^+$). HRMS: Calcd for M$^+$ (C$_{64}$H$_{54}$N$_4$O$_4$Zn): 1006.3437, found: 1006.3463.

Methyl 3,5-diformylbenzoate, 51.

C$_{10}$H$_8$O$_4$
Exact Mass: 192.0423
Mol. Wt.: 192.1681   [126775-15-3]
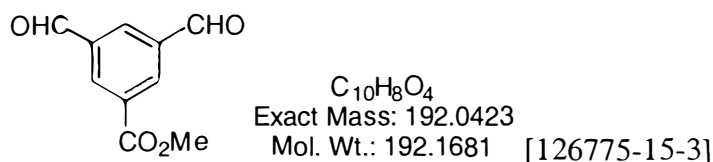
Two-component Rosenmund reduction:[218]

A mixture of acyl chlorides **46:56** (11:89, 780.3 mg, 5.658 mmol (-COCl)) and 5% palladium on BaSO$_4$ (59.9 mg) in dry *p*-xylene (10.0 mL) was heated to reflux while H$_2$ was bubbled into the solution. The liberated HCl was titrated with NaOH (0.3074 M) using Bromothymol Blue as the indicator. The reaction was stopped after 3.3 h at which point 16.25 mL of NaOH had been consumed (88%). The reaction was cooled to RT and then filtered through celite, rinsing with CH$_2$Cl$_2$ and removing the solvent *in vacuo*. The resulting solid was dissolved in CH$_2$Cl$_2$:hexane (1:1, 50 mL) and column

chromatographed (silica, 25 mm$_{dia}$ x 170 mm, CH$_2$Cl$_2$:hexane (4:1)), to give an inseparable mixture of dimethyl 5-formylisophthalate **40** and the desired product methyl 3,5-diformylbenzoate **51** (10:90 by ^{1}H NMR, 448.7 mg, 77%) as a white solid. A pure sample of methyl 3,5-diformylbenzoate **51** was isolated for characterisation using careful column chromatography (silica, CH$_2$Cl$_2$:hexane (3:1)). **51**, ^{1}H NMR (270 MHz, CDCl$_3$, TMS): δ 4.025 (s, 3H, CO$_2$CH$_3$), 8.586 (t, ^4J = 1.7 Hz, 1H, H$_4$), 8.782 (d, ^4J = 1.5 Hz, 2H, H$_{2,6}$), 10.177 (s, 2H, CHO). ^{13}C NMR (68 MHz, CDCl$_3$): δ 52.87, 132.30, 133.33, 135.31, 137.17, 164.72, 189.91. EI-LRMS: *m/z* (%, assignment) 192 (68, M$^+$), 161 (100, [M – OMe]$^+$), 133 (52, [M – (OMe, CHO)]$^+$), 104 (12, [M – (OMe, CHO, CHO)]$^+$). HRMS: Calcd for M$^+$ (C$_{10}$H$_8$O$_4$): 192.0423, found: 192.0428. **40**, *^{1}H NMR data was consistent with that previously obtained.*

(TXP-=-)$_2$PhCO$_2$Me, 52.

Methyl 3,5-bis(*trans*-2'-(5",10",15",20"-tetrakis(3''',5'''-dimethylphenyl)-porphyrin-2"-yl)ethen-1'-yl)benzoate.

C$_{116}$H$_{100}$N$_8$O$_2$
Exact Mass: 1636.7969
Mol. Wt.: 1638.0879
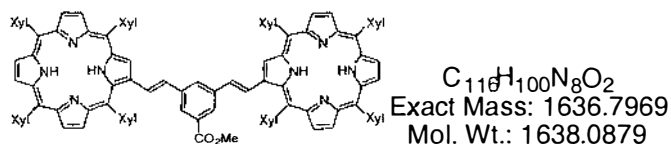
To a solution of aldehydes **40**:**51** (1:9, 15.0 mg, 7.70:69.0 µmol, 146 µmol of CHO) and TXPps salt **5** (227 mg, 219 µmol, 1.5 eq per CHO) in CH$_2$Cl$_2$ (5.0 mL), was added DBU (65.5 µL, 438 µmol, 2.0 eq) under N$_2$ at RT. After stirring for 15 min the solvent was removed *in vacuo* and the residue was column chromatographed (silica, 30 mm$_{dia}$ x 160 mm), first eluting with CH$_2$Cl$_2$:hexane (1:2) to give TXP-Me **57** (32.5 g, 20%) as a purple solid. Elution with 3:2-2:1 gave an isomeric mixture of diporphyrin **52** (132.4 mg) as a purple solid. Further elution gave TXP-=-Ph$_m$(CO$_2$Me)$_2$ **50** (5.4 mg, 74%) as a purple solid. The isomeric mixture of **52** and I$_2$ (61.5 mg, 242 µmol, ≈ 2 eq) were dissolved in CH$_2$Cl$_2$ (15 mL). After stirring at RT for 3 h, sat. Na$_2$S$_2$O$_3$ (15 mL) was added and stirring continued for 30 min. The organic layer was separated and dried (MgSO$_4$), then the solvent removed *in vacuo*. The residue was column chromatographed (silica, 30 mm$_{dia}$ x 120 mm, CH$_2$Cl$_2$:hexane (3:1)) to give the all *trans* diporphyrin ester **52** (89.0 mg, 78%) as a purple solid. *Both TXP-Me 57 and the TXP-diester 50 were identified by ^{1}H NMR.* ^{1}H NMR (270 MHz, CDCl$_3$, TMS): δ -2.565 (br s, 4H, NH), 2.520 (s, 12H, H$_{Me-Xyl}$), 2.610 (s, 24H, H$_{Me-Xyl}$), 2.677 (s, 12H, H$_{Me-Xyl}$), 4.187

(s, 3H, CO_2CH_3), 7.120 and 7.400 (ABq, 4H, ^3J = 16.2, 16.2 Hz, $H_{2',1'}$), 7.347-7.513 (m, 9H, ArH), 7.775-7.956 (m, 18H, ArH), 8.795-8.888 (m, 12H, $H_{\beta\text{-pyrrolic}}$), 9.181 (s, 2H, $H_{3''}$ $_{(\beta\text{-pyrrolic})}$). *A cis:trans ratio of about 88:8:4 was determined by integral ratios from NH signals seen at −2.565, -2.654 and −2.702 ppm, attributed to trans:trans, trans:cis and cis:cis supported by cis vinylic signals at 6.431 and 6.585 ppm (ABq, ^3J = 12.2 Hz, vinylic). $H_{2'}$ and $H_{1'}$ vinylic and $H_{3''}$ β-pyrrolic signals assigned from short and long-range COSY experiments.* UV-vis (CH_2Cl_2): λ_{max} [nm] (ε x 10^{-3}) 429 (440), 525 (41.7), 565 (23.7), 600 (15.3), 657 (7.07). FAB-LRMS: *m/z* (%, assignment) cluster at 1636-1642, 1638 (100, MH^+). HRMS: Calcd for MH^+ ($C_{116}H_{101}N_8O_2$): 1637.8048, found: 1637.8002.

(ZnTXP-=-)$_2$PhCO$_2$Me, Zn-52.

Methyl 3,5-bis(*trans*-2'-(2''-(5'',10'',15'',20''-tetrakis(3''',5'''-dimethylphenyl)-porphyrinato zinc(II))yl)ethen-1'-yl)benzoate.

$C_{116}H_{96}N_8O_2Zn_2$
Exact Mass: 1760.6239
Mol. Wt.: 1764.8362
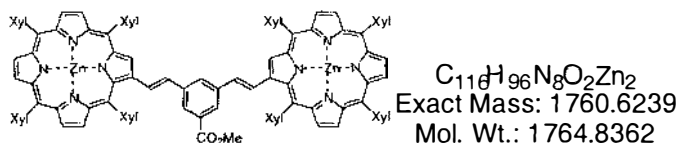
A solution of $Zn(OAc)_2 \cdot 2H_2O$ (20.4 mg, 93.1 μmol, 2.2 eq) dissolved in MeOH (500 μL) was added to a solution of ester **52** (69.3 mg, 42.3 μmol) in $CHCl_3$ (10 mL) with stirring at RT. After 30 min, TLC analysis indicated that no starting material remained with the appearance of a new brown band at lower R_f. The solvent was removed *in vacuo* and the residue column chromatographed (silica, 17 mm$_{dia}$ x 80 mm, CH_2Cl_2) to give the diporphyrin ester **Zn-52** (68.9 mg, 92%) as a purple solid. ^{1}H NMR (270 MHz, CDCl$_3$, TMS): δ 2.524 (s, 12H, $H_{Me\text{-}Xyl}$), 2.609 (s, 24H, $H_{Me\text{-}Xyl}$), 2.672 (s, 12H, $H_{Me\text{-}Xyl}$), 4.156 (s, 3H, CO_2CH_3), 7.155 (d, 2H, ^3J = 15.9 Hz, $H_{2'}$), 7.337-7.428 (m, 7H, 5ArH + 2$H_{1'}$), 7.488 (s, 4H, ArH), 7.860 (br s, 14H, ArH), 7.945 (s, 4H, ArH), 8.92-9.00 (m, 12H, $H_{\beta\text{-pyrrolic}}$), 9.299 (s, 2H, $H_{3''}$ $_{(\beta\text{-pyrrolic})}$). UV-vis ($CH_2Cl_2$): λ_{max} [nm] (ε x 10^{-3}) 430 (552), 558 (57.4), 594 (23.6). FAB-LRMS: *m/z* (%, assignment) cluster at 1761-1771, 1765 (100, M^+). HRMS: Calcd for M^+ ($C_{116}H_{96}N_8O_2Zn_2$): 1760.6239, found: 1760.6320.

(ZnTXP-=-)₂PhCO₂H, Zn-53.

3,5-Bis(*trans*-2'-(2"-(5",10",15",20"-tetrakis(3"',5"'-dimethylphenyl)porphyrinato zinc(II))yl)ethen-1'-yl)benzoic acid.

$C_{115}H_{94}N_8O_2Zn_2$
Exact Mass: 1746.6083
Mol. Wt.: 1750.8096
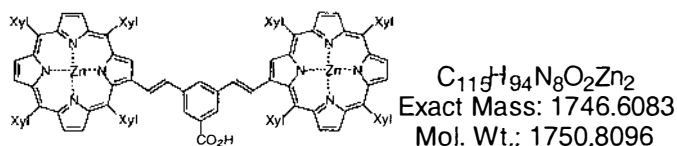
KOH (31.8 mg, 567 mmol, 20 eq) in MeOH (7.6 mL) and H_2O (760 μL) was added to a solution of ester **Zn-52** (50.0 mg, 28.3 μmol) in THF (7.6 mL). The mixture was heated to reflux for 17 h under N_2. After cooling to RT, H_2O (25 mL) was added followed by 2.0 M H_3PO_4 (300 μL, 21 eq) and CH_2Cl_2 (25 mL). The pH of the aqueous layer was 3. The organic layer was then washed further with 8.0 mM $H_3PO_{4(aq)}$ (25 mL), then separated and dried (MgSO₄), and the solvent removed *in vacuo*. The residue was column chromatographed (silica, 17 mm$_{dia}$ x 50 mm) first eluting with CH_2Cl_2 to give unreacted ester **Zn-52** (8.7 mg, 17%), then CH_2Cl_2:Et₂O (20:1) to give the desired acid **Zn-53** (33.2 mg, 67%) as a purple solid. ¹H NMR (400 MHz, CDCl₃, TMS): δ 2.598-2.619 (m, 36H, H$_{Me-Xyl}$), 2.697 (s, 12H, H$_{Me-Xyl}$), 7.245 and 7.452 (ABq, 4H, ^3J = 15.9, 15.9 Hz, H$_{2',1'}$), 7.415 (s, 4H, ArH), 7.486 (s, 1H, ArH), 7.515 (s, 2H, ArH), 7.592 (s, 2H, ArH), 8.865 (s, 8H, ArH), 8.915 (s, 4H, ArH), 8.968 (s, 4H, ArH), 8.052 (s, 2H, ArH), 8.96-9.01 (m, 12H, H$_{\beta-pyrrolic}$), 9.343 (s, 2H, H$_{3" (\beta-pyrrolic)}$). UV-vis (CH_2Cl_2): λ_{max} [nm] (ε x 10^{-3}) 430 (470), 558 (4.96), 594 (2.05). FAB-LRMS: *m/z* (%, assignment) cluster at 1745-1757, 1751 (100, M⁺). HRMS: Calcd for M⁺ ($C_{115}H_{94}N_8O_2Zn_2$): 1746.6083, found: 1746.6000.

Methyl 3,5-bis(chlorocarbonyl)benzoate, 56.

$C_{10}H_6Cl_2O_4$
Exact Mass: 259.9643
Mol. Wt.: 261.0576   [170160-27-7]
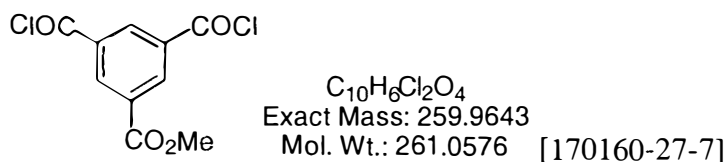
A mixture containing acid esters **45:47** (774.9 mg, 9:91, 0.308:3.11 mmol) in dry benzene (60.0 mL) was reduced in volume to about 30 mL *in vacuo* at 40°C. Oxalyl chloride (854 μL, 9.79 mmol 1.5 eq per CO_2H) and DMF (15 μL) was added and the reaction heated under argon to 60°C for 15 min and then 70°C for 30 min. The solvent was then removed under reduced pressure. Benzene (60 mL) was added and then

removed *in vacuo* to give a mixture of the chlorocarbonyl derivatives of **46:56** (11:89 by ¹H NMR, 833.0 mg, 93%) as a pale yellow solid. A pure sample of **56** was obtained in 95% yield for characterisation from the acylation of a pure sample of **47** using the above procedure. **56**, ¹H NMR (400 MHz, CDCl₃, TMS): δ 4.022 (s, 3H, CO₂CH₃), 8.982 (t, 1H, ⁴J = 1.8 Hz, H₄), 9.028 (d, 2H, ⁴J = 1.8 Hz, H₂,₆). ¹³C NMR (68 MHz, CDCl₃): δ 53.23, 132.52, 134.83, 136.54, 137.34, 163.87, 166.47. EI-LRMS: *m/z* (%, assignment) 260 (<1, M⁺), 225 (100, [M – Cl]⁺), 162 (13, [M – COCl]⁺). HRMS: Calcd for [M – Cl]⁺ (C₁₀H₆Cl₁O₄): 224.9955, found: 224.9944.

4-(1',3'-Dioxa-2'-cyclopentyl)benzaldehyde, 59.

OHC—⟨benzene ring⟩—CH⟨O—CH₂ / O—CH₂⟩   C₁₀H₁₀O₃
Exact Mass: 178.0630
Mol. Wt.: 178.1846
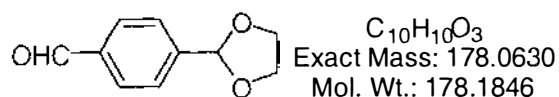
1,2-Ethanediol (9.36 mL, 173 mmol) was added to a mixture of terephthalaldehyde **22** (15.000 g, 111.8 mmol) and *p*-TsOH·H₂O (300 mg, 1.58 mmol) in CH₂Cl₂ (10.0 mL). The reaction vessel was sealed and stirred at RT for 12.5 h. The reaction was then neutralised by stirring with K₂CO₃₍ₛ₎ (900 mg) for 15 min. Sat. K₂CO₃ (20 mL) was added and the reaction stirred vigorously for 30 min. The organic layer was diluted with CH₂Cl₂ (20 mL) and washed with aq. K₂CO₃ (2 x 50 mL), separated and dried (K₂CO₃). The suspension was the filtered through a plug of celite and the solvent removed *in vacuo* to give a pale lemon coloured oil (19.005 g). ¹H NMR was consistent with three products in a molar ratio of 19:69:11, assigned as the dialdehyde **22**, monoacetal **59** and diacetal **70** products respectively. The dialdehyde **22** component was removed from the mixture by sublimation at 45°C under high vacuum (0.01 mm Hg, water jacketed cold finger) until the first sign of dampness appeared on the cold finger. Next collecting fractions A to D by short path vacuum distillation at 50°C: these containing mostly the desired monoacetal **59** product as major component: Fraction (mass, **22:59:70**), A (2.158 g, 4:96:1), B (2.833 g, 3:95:2), C (2.571 g, 0:97:3), D (1.561 g, 0:88:12). **59** (Fraction C): ¹H NMR (270 MHz, CDCl₃, TMS): δ 3.99-4.14 (m, 4H, ArCH(OCH₂)₂), 5.860 (s, 1H, ArCH(OCH₂)₂), 7.632 and 7.882 (ABq, 4H, ³J = 8.5, 8.3 Hz, H₀,ₘ-ₐᵣ), 10.014 (s, 1H, CHO). ¹³C NMR (68 MHz, CDCl₃, TMS): δ 65.996 (ArCH(OCH₂)₂), 103.313 (ArCH(OCH₂)₂), 127.574 (Ar), 130.235 (Ar), 137.337 (Ar), 144.865 (Ar), 192.327 (CHO). EI-LRMS: *m/z* (%, assignment) 177 (100%, (M-H)⁺), 178 (35%, M⁺). HRMS: Calcd for M⁺ (C₁₀H₁₀O₃): 178.0630, found: 178.0614. *¹H*

NMR is consistent with the 60 MHz data and LRMS data reported by Castells et al.[111] *The molar amounts of the monoacetal **59** in any given mixture of **22:59:70** were calculated from equations 2-1 and 2-3 (Page 225) using the integrals ratios from the* ^1H *NMR spectrum.*

TBMP{-PhCO₂Me}₂, 60.

5,15-Bis(methyl 4"-benzoate)-2,8,12,18-tetrabutyl-3,7,13,17-tetramethylporphyrin.

$C_{56}H_{66}N_4O_4$
Exact Mass: 858.5084
Mol. Wt.: 859.1478
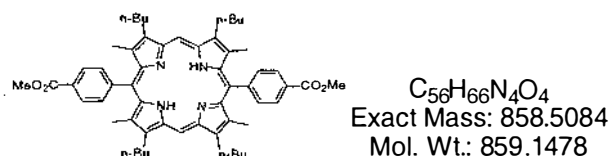
Originally synthesised by Kuciauskas et al.[108] *in 52% yield using the method of Osuka et al.*[109] *and as a by-product from the synthesis of **61***. *It was also synthesised here directly using p-TsOH·H₂O in MeOH under similar conditions to that of Gunter et al.*[115]

Methyl 4-formylbenzoate **28** (40 mg, 244 μmol) and dipyrrylmethane **58** (70 mg, 244 μmol, 1.0 eq) were dissolved in MeOH (3.0 mL, 0.08 M) under N_2. To this was added *p*-TsOH·H₂O (12 mg, 0.25 eq, 63 μmol). The reaction mixture was sealed and stirred for 20 h at RT, before removing the solvent *in vacuo*. The resulting residue was dissolved in CH_2Cl_2 (5.0 mL) and *p*-chloranil (108 mg, 0.9 eq) was added. The resulting mixture was stirred for 3.5 h at RT giving a deep green solution. The organic layer was washed with sat. $NaHCO_3$ (2 x 30 mL), separated, dried (K_2CO_3) and the solvent removed *in vacuo*. The residue was chromatographed (neutral Al_2O_3, 17 mm$_{dia}$ x 150 mm, CH_2Cl_2:hexane (1:1)) to give **60** (67 mg, 64%) as a purple solid.

ZnTBMP(-PhCO₂Me)₂, Zn-60.

5,15-Bis(4"-methoxycarbonylphenyl)-2,8,12,18-tetra-*n*-butyl-3,7,13,17-tetramethyl-porphyrinato zinc(II).

$C_{56}H_{64}N_4O_4Zn$
Exact Mass: 920.4219
Mol. Wt.: 922.5219
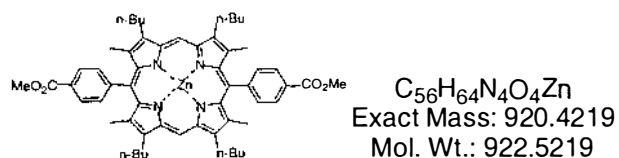
A solution of Zn(OAc)₂·2H₂O (25 mg, 114 μmol, 1.2 eq) in MeOH (1.5 mL) was added to a solution of bisester porphyrin **60**[108] (81.2 mg, 94.5 μmol) in $CHCl_3$ (10 mL) with stirring at RT. After 30 min, TLC analysis indicated that the reaction was complete

with the appearance of a new spot at higher R_f. The solvent was removed *in vacuo* and the residue column chromatographed (silica, 30 mm$_{dia}$ x 100 mm, CH$_2$Cl$_2$:hexane (2:1)). Recrystallisation from CHCl$_3$/MeOH gave **Zn-60** (69.7 mg, 80%) as a red solid. ^{1}H NMR (400 MHz, CDCl$_3$, TMS): δ 1.090 (t, 12H, ^3J = 7.4 Hz, CH$_2$CH$_2$CH$_2$CH$_3$), 1.721 (app sext, 8H, ^3J = 7.4 Hz, CH$_2$CH$_2$CH$_2$CH$_3$), 2.093 (app pent, 8H, ^3J = 7.8 Hz, CH$_2$CH$_2$CH$_2$CH$_3$), 2.340 (s, 12H, H$_{Me\text{-}TBMP}$), 3.814 (app t, 8H, ^3J = 7.9 Hz, CH$_2$CH$_2$CH$_2$CH$_3$), 4.129 (s, 6H, CO$_2$CH$_3$) 8.126 (d, 4H, ^3J = 8.0 Hz, ArH$_{Ester}$), 8.417 (d, 4H, ^3J = 8.4 Hz, ArH$_{Ester}$), 9.999 (s, 2H, H$_{meso}$). *Assignments aided by COSY spectra.* UV-vis (CH$_2$Cl$_2$): λ_{max} [nm] (ε x 10^{-3}) 412 (370), 503 (3.34), 540 (19.4), 575 (10.4). FAB-LRMS: *m/z* (%, assignment) cluster at 920-927, 920 (100, M$^+$). HRMS: Calcd for M$^+$ (C$_{56}$H$_{64}$N$_4$O$_4$Zn): 920.4219, found: 920.4247.

TBMP(-PhCO$_2$Me)$_2$, 60.

5,15-Bis(4'-methoxycarbonylphenyl)-2,8,12,18-tetrabutyl-3,7,13,17-tetramethylporphyrin.

C$_{56}$H$_{66}$N$_4$O$_4$
Exact Mass: 858.5084
Mol. Wt.: 859.1478
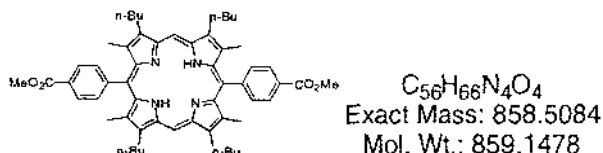
and (OCH$_2$)$_2$CH-Ph-TBMP-PhCO$_2$Me, 61.

5-(4'-Methoxycarbonylphenyl)-15-(4"-(1''',3'''-Dioxacyclopent-2'''-yl)phenyl)-2,8,12,18-tetrabutyl-3,7,13,17-tetramethylporphyrin.

C$_{57}$H$_{68}$N$_4$O$_4$
Exact Mass: 872.5241
Mol. Wt.: 873.1744
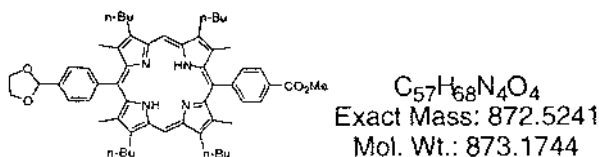
and TBMP(-PhCH(OCH$_2$)$_2$)$_2$, 62.

5,15-Bis(4'-(1",3"-dioxacyclopent-2"-yl)phenyl)-2,8,12,18-tetrabutyl-3,7,13,17-tetramethylporphyrin.

C$_{58}$H$_{70}$N$_4$O$_4$
Exact Mass: 886.5397
Mol. Wt.: 887.2010
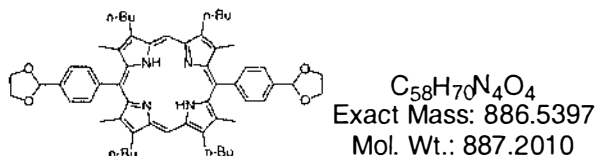
To acetals **59:70** (95:5, 116.0 mg, 611 μmol **59**), methyl 4-formylbenzoate **28** (100.3 mg, 611 μmol) and dipyrrylmethane **58** (350 mg, 1.22 mmol) in degassed CH_2Cl_2 (122 mL) under N_2 at RT, was added TFA (97 μL, 1.22 mmol, 1.0 eq). At the first sign of baseline material by TLC (CH_2Cl_2, 25 min) the reaction was quenched with DBU (188 μL, 1.22 mmol, 1.0 eq). *p*-Chloranil (752 mg, 2.5 eq) was added and the solution stirred for 6 h at reflux temperature. After cooling to RT, the solvent was removed *in vacuo* and the residue filtered through a silica gel plug using CH_2Cl_2:MeOH (97:3) to give a mixture of 3 products by TLC (R_f = 0.5, 0.4 & 0.25, CH_2Cl_2:Et_2O (39:1)) as a purple solid (599 mg). The residue was column chromatographed (silica, 37 mm_{dia} x 210 mm), first eluting with CH_2Cl_2:Et_2O (200:1) to give bisester porphyrin **60**[108] (117 mg, 22%) as a purple solid. The ^1H NMR spectra of the bisester porphyrin **60** is consistent with Kuciauskas et al.[108]

Further elution gave then the title acetal/ester porphyrin **61** (146 mg, 27%, precipitated from CH_2Cl_2 using MeOH) as a purple solid. **61**: ^1H NMR (270 MHz, $CDCl_3$, TMS): δ -2.413 (s, 2H, NH), 1.083 (t, 12H, ^3J = 7.3 Hz, $CH_2CH_2CH_3CH_3$), 1.728 (sext, 8H, ^3J = 7.3 Hz, $CH_2CH_2CH_2CH_3$), 2.152 (app pent, 8H, ^3J = 7.3 Hz, $CH_2CH_2CH_2CH_3$), 2.444 (s, 6H, $H_{Me-TBMP}$), 2.464 (s, 6H, $H_{Me-TBMP}$), 3.964 (t, 8H, ^3J = 7.6 Hz, $CH_2CH_2CH_2CH_3$), 4.123 (s, 3H, CO_2CH_3), 4.19-4.38 (m, 4H, $-CH(OCH_2)_2$), 6.156 (s, 1H, $-CH(OCH_2)_2$), 7.856 and 8.083 (ABq, 4H, ^3J = 7.8, 8.1 Hz, ArH_{Acetal}), 8.168 and 8.423 (ABq, 4H, ^3J = 8.4, 8.1 Hz, ArH_{Ester}), 10.233 (s, 2H, H_{meso}). *AB quartets were assigned from the known spectra of the bisacetal porphyrin **62** (7.859 and 8.094 (ABq, ^3J = 7.9, 8.2 Hz, ArH_{Acetal})) and the bisester porphyrin **60**[108] (8.164 and 8.427 (ABq, ^3J = 8.1, 8.4 Hz, ArH_{Ester})).* ^{13}C NMR (101 MHz, $CDCl_3$): δ 14.21, 14.82, 23.29, 26.45, 35.46, 52.41, 65.52, 97.13, 104.04, 116.47, 117.65, 125.91, 128.76, 130.01, 132.83, 133.15, 135.70, 136.36, 138.03, 141.42, 141.54, 143.25, 143.41, 143.54, 144.45, 145.10, 147.50, 167.40. UV-vis (CH_2Cl_2): λ_{max} [nm] (ε x 10^{-3}) 409 (230), 507 (18.2), 541 (5.63), 574 (7.39), 626 (1.63). FAB-LRMS: *m/z* (%) cluster at 872-876, 873 (100, M^+). HRMS: Calcd for M^+ ($C_{57}H_{68}N_4O_4$): 872.5241, found: 872.5249.

Further elution using CH_2Cl_2:MeOH (49:1) gave the bisacetal porphyrin **62** (79 mg, 15%) as a purple solid. ^1H NMR (270 MHz, $CDCl_3$, TMS): δ -2.462 (br s, 2H, NH), 1.081 (t, 12H, ^3J = 7.3 Hz, $CH_2CH_2CH_2CH_3$), 1.726 (app sext, 8H, ^3J = 7.3 Hz,

CH$_2$CH$_2$CH$_2$CH$_3$), 2.09-2.21 (m, 8H, CH$_2$CH$_2$CH$_2$CH$_3$), 2.470 (s, 12H, H$_{Me-TBMP}$), 3.971 (t, 8H, ^3J = 7.3 Hz, CH$_2$CH$_2$CH$_2$CH$_3$), 4.199-4.391 (m, 8H, -CH(OCH$_2$)$_2$), 6.162 (s, 2H, -CH(OCH$_2$)$_2$), 7.859 and 8.094 (ABq, 8H, ^3J = 7.9, 8.2 Hz, ArH$_{Acetal}$), 10.231 (s, 2H, H$_{meso}$). ^{13}C NMR (68.1 MHz, CDCl$_3$, TMS): δ 15.01, 15.61, 24.06, 27.223, 36.22, 66.22, 97.64, 104.71, 118.03, 126.49, 133.47, 136.79, 138.57, 142.01, 143.89, 145.57. UV-vis (CH$_2$Cl$_2$): λ_{max} [nm] (ε x 10^{-3}) 409 (205), 507 (16.6), 541 (4.8), 574 (6.49), 625 (1.06). FAB-LRMS: m/z (%, assignment) cluster at 885.5-889.6, 887.5 (100, MH$^+$). HRMS: Calcd for MH$^+$ (C$_{58}$H$_{71}$N$_4$O$_4$): 887.5475, found: 887.5424.

CHO-Ph-TBMP-PhCO$_2$Me, 63.

5-(4'-Formylphenyl)-15-(4''-methoxycarbonylphenyl)-2,8,12,18-tetra-n-butyl-3,7,13,17-tetramethylporphyrin.

C$_{55}$H$_{64}$N$_4$O$_3$
Exact Mass: 828.4978
Mol. Wt.: 829.1218
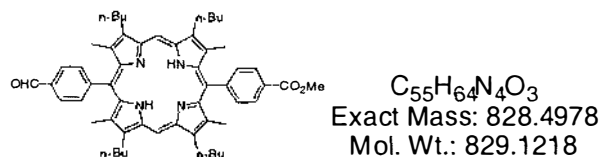
A solution of acetal/ester porphyrin **61** (110 mg, 126 μmol) and p-TsOH·H$_2$O (144 mg, 756 μmol, 6 eq) in acetone (40 mL) was heated to reflux under N$_2$. The reaction was deemed complete after 1.5 h with the appearance of a single new green band of higher R_f than **61**. The reaction was cooled to RT, and quenched with Et$_3$N (123 μL, 882 μmol, 1.2 eq). The crude product in the resulting suspension was separated by filtration then dissolved in minimal CH$_2$Cl$_2$ and precipitated using MeOH to give formyl/ester porphyrin **63** as a purple powder (104 mg, 99%). ^{1}H NMR (400 MHz, CDCl$_3$, TMS): δ -2.412 (s, 2H, NH), 1.087 (t, 12H, ^3J = 7.4 Hz, CH$_2$CH$_2$CH$_2$CH$_3$), 1.730 (sext, 8H, ^3J = 7.3 Hz, CH$_2$CH$_2$CH$_2$CH$_3$), 2.150 (app pent, 8H, ^3J = 7.3 Hz, CH$_2$CH$_2$CH$_2$CH$_3$), 2.410 (s, 6H, H$_{Me-TBMP}$), 2.433 (s, 6H, H$_{Me-TBMP}$), 3.956 (t, 8H, ^3J = 7.7 Hz, CH$_2$CH$_2$CH$_2$CH$_3$), 4.124 (s, 3H, CO$_2$CH$_3$), 8.143 (d, 2H, ^3J = 8.2 Hz, ArH$_{Ester}$), 8.212 (s, 4H, ArH$_{CHO}$), 8.415 (d, 2H, ^3J = 8.1 Hz, ArH$_{Ester}$), 10.238 (s, 2H, H$_{meso}$), 10.357 (s, 1H, CHO). ^{13}C NMR (101 MHz, CDCl$_3$): δ 14.20 (CH$_3$), 14.81 (CH$_3$), 14.84 (CH$_3$), 23.29 (CH$_2$CH$_2$CH$_2$CH$_3$), 26.44 (CH$_2$CH$_2$CH$_2$CH$_3$), 35.46 (CH$_2$CH$_2$CH$_2$CH$_3$), 52.42 (COCH$_3$), 97.33 (CH$_{meso}$), 116.23, 116.86, 128.81, 130.08, 133.08, 133.74 08, 135.58, 135.93, 136.17, 141.54, 141.60, 143.69, 143.76, 144.35, 144.63, 147.30, 149.09, 167.35 (CO$_2$CH$_3$), 192.42 (CHO). *Assignments aided by HETCOR and COSY spectra.* UV-vis (CH$_2$Cl$_2$): λ_{max} [nm] (ε x 10^{-3}) 410 (219), 508 (17.8), 541 (5.64), 575 (7.11), 626 (1.61).

FAB-LRMS: m/z (%) cluster at 827-832, 829 (95, M$^+$). HRMS: Calcd for M$^+$ (C$_{55}$H$_{64}$N$_4$O$_3$): 828.4978, found: 828.4942.

ZnTXP-=-Ph-ZnTBMP-PhCO$_2$Me, Zn$_2$-64.

5-(4'-Methoxycarbonylphenyl)-15-(4"-(*trans*-2'''-(2''''-(5'''''',10'''''',15'''''',20''''''-tetrakis(3''''''',5'''''''-dimethylphenyl)porphyrinato zinc(II))yl)ethen-1'''-yl)phenyl)-2,8,12,18-tetra-*n*-butyl-3,7,13,17-tetramethylporphyrinato zinc(II).

C$_{108}$H$_{106}$N$_8$O$_2$Zn$_2$
Exact Mass: 1674.7022
Mol. Wt.: 1678.8300
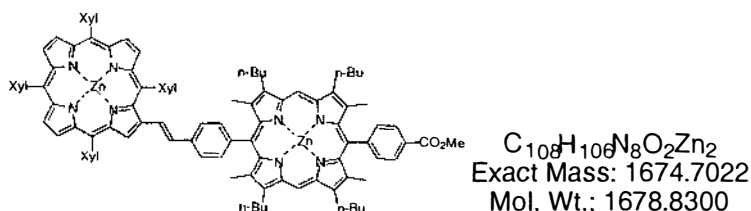
A solution of formyl/ester porphyrin **63** (45.0 mg, 54.3 μmol) and TXPps **5** (84.5mg, 81.4 μmol, 1.5 eq) in CHCl$_3$ (5.0 mL) was heated to reflux temperature under N$_2$. DBU (16.2 μL, 2.0 eq) was added and after 20 min, TLC analysis indicated that no **63** remained. The solvent was removed *in vacuo* and the residue column chromatographed (silica, 30 mm$_{dia}$ x 100 mm, CH$_2$Cl$_2$:CHCl$_3$ (1:1)) to give a mixture of free-base diporphyrin ester **64** and other organic residues (possibly PPh$_3$O, 106 mg) as a purple solid. A solution of Zn(OAc)$_2$·2H$_2$O (15.3 mg, 70 μmol, 1.2 eq) in MeOH (0.5 mL) was added to a solution of the crude **64** in CHCl$_3$ (5.0 mL) with stirring at RT. After 30 min, TLC analysis indicated that the metallation was complete with the appearance of a new single red band at higher R_f. The solvent was removed *in vacuo* and the residue column chromatographed (silica, 30 mm$_{dia}$ x 130 mm, CH$_2$Cl$_2$:hexane (3:1 => 2:1)) to give the metallodiporphyrin ester **Zn$_2$-64** (74.3 mg, 82%) as a purple solid. *Metallation with zinc(II) was carried out after Wittig to aid in the separation of the mixture.* **64**: ^{1}H NMR (270 MHz, CDCl$_3$, TMS, selected data only): δ -2.339 (br s, 2H, NH$_{TXP}$), -2.456 (br d, 2H, NH$_{TBMP}$), 9.187 (s, 1H, H$_{3''''(\beta\text{-pyrrolic})}$). **Zn$_2$-64**: ^{1}H NMR (400 MHz, CDCl$_3$, TMS): δ 1.123 (t, 6H, ^3J = 7.4 Hz, CH$_2$CH$_2$CH$_2$CH$_3$), 1.145 (t, 6H, ^3J = 7.4 Hz, CH$_2$CH$_2$CH$_2$CH$_3$), 1.780 (app oct, 8H, ^3J = 7.3 Hz, CH$_2$CH$_2$CH$_2$CH$_3$), 2.12-2.27 (m, 8H, CH$_2$CH$_2$CH$_2$CH$_3$), 2.413 (s, 6H, H$_{Me\text{-}TBMP}$), 2.61-2.70 (m, 30H, 24H$_{Me\text{-}Xyl}$ + 6H$_{Me\text{-}TBMP}$), 3.930 (app t, 4H, ^3J = 7.5 Hz, CH$_2$CH$_2$CH$_2$CH$_3$), 3.999 (app t, 4H, ^3J = 7.5 Hz, CH$_2$CH$_2$CH$_2$CH$_3$), 4.104 (s, 3H, CO$_2$CH$_3$), 7.38-7.50 (m, 5H, 4H$_{p\text{-}Xyl}$ + 1H$_{2'''}$), 7.624 (d, 1H, ^3J = 16.0 Hz, H$_{1'''}$), 7.721 (d, 2H, ^3J = 8.0 Hz, H$_{styryl}$), 7.871 (s, 4H, H$_{o\text{-}Xyl}$), 7.958 (s, 4H, H$_{o\text{-}Xyl}$), 8.052 (d, 2H, ^3J = 8.0 Hz, H$_{styryl}$), 8.190 (d, 2H, ^3J = 8.2 Hz, ArH$_{Ester}$), 8.411

(d, 2H, ^3J = 8.2 Hz, ArH$_{Ester}$), 8.96-9.01 (m, 6H, H$_{\beta\text{-pyrrolic}}$), 9.303 (s, 1H, H$_{3''''(\beta\text{-pyrrolic})}$), 10.172 (s, 2H, H$_{meso}$). UV-vis (CH$_2Cl_2$): λ_{max} [nm] ($\varepsilon \times 10^{-3}$) 411 (361), 430 (326), 554 (35.1), 591 (12.7). FAB-LRMS: m/z (%) cluster at 1673-1685, 1679 (100, M$^+$). HRMS: Calcd for M$^+$ (C$_{108}$H$_{106}$N$_8$O$_2$Zn$_2$): 1674.7022, found: 1674.7007.

ZnTXP-=-Ph-ZnTBMP-PhCO$_2$H, Zn$_2$-66.

5-(4'-Carboxyphenyl)-15-(4"-(*trans*-2'''-(2''''-(5'''',10'''',15'''',20''''-tetrakis(3''''',5'''''-dimethylphenyl)porphyrinato zinc(II))yl)ethen-1'''-yl)phenyl)-2,8,12,18-tetra-*n*-butyl-3,7,13,17-tetramethylporphyrinato zinc(II).
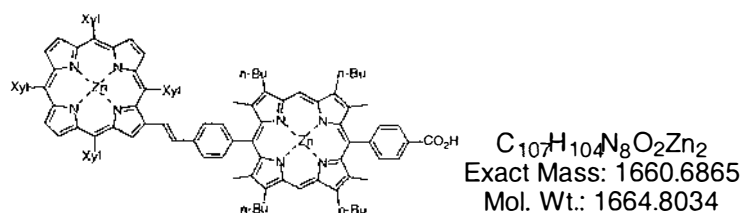

C$_{107}$H$_{104}$N$_8$O$_2$Zn$_2$
Exact Mass: 1660.6865
Mol. Wt.: 1664.8034

KOH (50.1 mg, 980 μmol, 30 eq) in MeOH:H$_2$O (8.0:0.80 mL) was added to a solution of diporphyrin ester **Zn$_2$-64** (50.0 mg, 29.8 μmol) in THF (8.0 mL). The mixture was heated to reflux for 5 h under N$_2$. After cooling to RT, H$_2$O (30 mL) was added followed by 2.0 M H$_3$PO$_4$ (0.48 mL, 32 eq) and CH$_2$Cl$_2$ (50 mL). The pH of the aqueous layer was 3. The organic layer was then washed with 8.0 mM H$_3$PO$_4$ (25 mL), and then separated and dried (MgSO$_4$), and solvent removed *in vacuo*. The residue was column chromatographed (silica, 30 mm$_{dia}$ x 50 mm, CH$_2$Cl$_2$:MeOH (49:1)) to give diporphyrin acid **Zn$_2$-66** (46.5 mg, 94%) as a purple solid. ^{1}H NMR (400 MHz, CDCl$_3$, TMS): δ 1.148 (t, 6H, ^3J = 7.4 Hz, CH$_2$CH$_2$CH$_2$CH$_3$), 1.160 (t, 6H, ^3J = 7.4 Hz, CH$_2$CH$_2$CH$_2$CH$_3$), 1.803 (app hept, 8H, ^3J = 7.6 Hz, CH$_2$CH$_2$CH$_2$CH$_3$), 2.16-2.25 (m, 8H, CH$_2$CH$_2$CH$_2$CH$_3$), 2.474 (s, 6H, H$_{Me\text{-TBMP}}$), 2.61-2.70 (m, 30H, 24H$_{Me\text{-Xyl}}$ + 6H$_{Me\text{-TBMP}}$), 3.96-4.03 (m, 8H, CH$_2$CH$_2$CH$_2$CH$_3$), 7.419 (br s, 2H, H$_{p\text{-Xyl}}$), 7.49-7.50 (m, 2H, H$_{p\text{-Xyl}}$), 7.417 and 7.634 (ABq, 2H, ^3J = 15.9, 15.9 Hz, H$_{2''',1'''}$), 7.741 (d, 2H, ^3J = 8.1 Hz, H$_{styryl}$), 7.872 (s, 4H, H$_{o\text{-Xyl}}$), 7.962 (s, 4H, H$_{o\text{-Xyl}}$), 8.075 (d, 2H, ^3J = 7.9 Hz, H$_{styryl}$), 8.275 (d, 2H, ^3J = 7.9 Hz, ArH$_{Ester}$), 8.546 (d, 2H, ^3J = 7.9 Hz, ArH$_{Ester}$), 8.97-9.01 (m, 6H, H$_{\beta\text{-pyrrolic}}$), 9.303 (s, 1H, H$_{3'''(\beta\text{-pyrrolic})}$), 10.257 (s, 2H, H$_{meso}$). UV-vis (CH$_2Cl_2$): λ_{max} [nm] ($\varepsilon \times 10^{-3}$) 411 (384), 430 (353), 554 (38.4), 591 (14.4). FAB-LRMS: m/z (%) cluster at 1659-1670, 1665 (100, M$^+$). HRMS: Calcd for M$^+$ (C$_{107}$H$_{104}$N$_8$O$_2$Zn$_2$): 1660.6865, found: 1660.6786.

TXP-=-PhOH, 72.

4-(*Trans*-2'-(5",10",15",20"-tetrakis(3'",5'"-dimethylphenyl)porphyrin-2"-yl)ethen-1'-yl)phenol.

$C_{60}H_{52}N_4O$
Exact Mass: 844.4141
Mol. Wt.: 845.0812
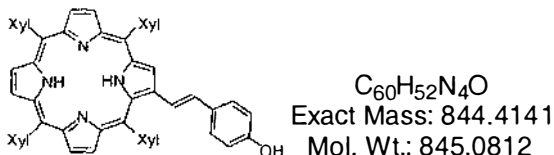
A solution of TXPps **5** (250 mg, 241 μmol) and 4-formylphenol **71** (88.2 mg, 723 μmol, 3.0 eq) in toluene (12.5 mL) was heated to reflux under N_2. DBU (108 μL, 3.0 eq) was added. After 30 min, TLC analysis indicated that all **5** had been consumed. The solvent was removed *in vacuo*. The residue was dissolved in CH_2Cl_2 (60 mL) and the organic layer washed with aqueous 7.4 mM H_3PO_4 (100 mL), and then H_2O (2 x 100 mL). The organic layer was separated, dried (MgSO$_4$) and the solvent removed *in vacuo*. The residue was column chromatographed (silica, 37 mm$_{dia}$ x 110 mm, CH_2Cl_2) to give *trans* phenol porphyrin **72** (107 mg, 52%) as a purple solid.

^{1}H NMR (270 MHz, CDCl$_3$, TMS): δ -2.638 (br s, 2H, NH), 2.514 (s, 6H, H$_{Me-Xyl}$), 2.593 (s, 12H, H$_{Me-Xyl}$), 2.620 (s, 6H, H$_{Me-Xyl}$) 6.771 (d, 2H, ^3J = 8.5 Hz, H$_{styryl}$), 6.863 and 7.234 (ABq, 2H, ^3J = 16.2, 15.7 Hz, H$_{2',1'\text{ or }1',2'}$), 7.184 (d, 2H, ^3J = 8.4 Hz, H$_{styryl}$), 7.391 (s, 2H, H$_{p-Xyl}$), 7.423 (m, 2H, H$_{p-Xyl}$), 7.785 (s, 2H, H$_{o-Xyl}$), 7.823 (s, 4H, H$_{o-Xyl}$), 7.847 (s, 2H, H$_{o-Xyl}$), 8.772 and 8.813 (ABq, 2H, ^3J = 4.9, 4.9 Hz, H$_{\beta\text{-pyrrolic}}$), 8.785 (s, 2H, H$_{\beta\text{-pyrrolic}}$), 8.853 (s, 2H, H$_{\beta\text{-pyrrolic}}$), 8.976 (s, 1H, H$_{3"\ (\beta\text{-pyrrolic})}$). UV-vis (CH$_2Cl_2$): λ_{max} [nm] (ε x 10^{-3}) 425 (216), 526 (18.6), 565 (11.0), 600 (6.66), 657 (2.23). FAB-LRMS: *m/z* (%, assignment) cluster at 844-848, 845 (100, MH$^+$). HRMS: Calcd for MH$^+$ (C$_{60}$H$_{53}$N$_4$O): 845.4219, found: 845.4185.

ZnTXP-=-PhOH, Zn-72.

4-(*Trans*-2'-(2"-(5",10",15",20"-tetrakis(3'",5'"-dimethylphenyl)porphyrinato zinc(II))yl)ethen-1'-yl)phenol.

$C_{60}H_{50}N_4OZn$
Exact Mass: 906.3276
Mol. Wt.: 908.4554
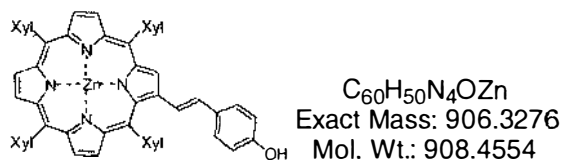
A solution of Zn(OAc)$_2$·2H$_2$O (11 mg, 50 μmol, 2.0 eq) in MeOH (1.0 mL) was added to a solution of porphyrin **72** (20.7 mg, 24.5 μmol) in CHCl$_3$ (5.0 mL) with stirring at

RT. After 15 min, TLC analysis indicated that the reaction was complete with the appearance of a new band at higher R_f. The solvent was removed *in vacuo* and the residue dissolved in minimal CH_2Cl_2 before passing through a plug of silica gel to give **Zn-72** (20.8 mg, 93%) as a purple solid. ^1H NMR (270 MHz, $CDCl_3$, TMS): δ 2.506 (s, 6H, H_{Me-Xyl}), 2.593 (s, 12H, H_{Me-Xyl}), 2.620 (s, 6H, H_{Me-Xyl}) 4.752 (s, 1H, ArOH), 6.771 (d, 2H, ^3J = 8.7 Hz, H_{styryl}), 6.884 and 7.188 (ABq, 2H, ^3J = 15.9, 15.9 Hz, $H_{2',1' \text{ or } 1',2'}$), 7.187 (d, 2H, ^3J = 8.7 Hz, H_{styryl}), 7.37-7.45 (m, 4H, H_{p-Xyl}), 7.783 (s, 2H, H_{o-Xyl}), 7.831 (s, 4H, H_{o-Xyl}), 7.855 (s, 2H, H_{o-Xyl}), 8.88-8.97 (m, 2H, $H_{\beta\text{-pyrrolic}}$), 9.072 (s, 1H, $H_{3'' (\beta\text{-pyrrolic})}$). UV-vis ($CH_2Cl_2$): λ_{max} [nm] (ε x 10^3) 427 (239), 557 (20.9), 592 (7.53). FAB-LRMS: *m/z* (%, assignment) cluster at 906-912, 906 (100, M$^+$). HRMS: Calcd for M$^+$ ($C_{60}H_{50}N_4OZn$): 906.3276, found: 906.3275.

ZnTBMP(-PhCO$_2$H)$_2$, Zn-73.

5,15-Bis(4"-carboxyphenyl)-2,8,12,18-tetra-*n*-butyl-3,7,13,17-tetramethyl-porphyrinato zinc(II).

$C_{54}H_{60}N_4O_4Zn$
Exact Mass: 892.3906
Mol. Wt.: 894.4688
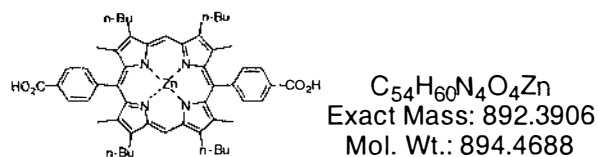
KOH (91.2 mg, 1.63 mmol, 15 eq per CO$_2$Me) in MeOH:H$_2$O (9.0:0.90 mL) was added to a solution of bisester **Zn-60** (50.0 mg, 54.2 μmol) in THF (9.0 mL). The mixture was heated to reflux for 22 h under N$_2$. After cooling to RT, the solvent was removed *in vacuo*. The residue was dissolved in MeOH ($\approx$ 50 mL) and acidified with 2.0 M H$_3$PO$_4$ (800 μL). The resulting precipitate was separated by filtration. Recrystallisation from THF/(MeOH:H$_2$O (1:1)) gave **Zn-73** (47.2 mg, 97%) as a red solid. ^1H NMR (400 MHz, DMSO-d$_6$, TMS): δ 1.083 (t, 12H, ^3J = 7.4 Hz, CH$_2$CH$_2$CH$_2$CH$_3$), 1.705 (app sext, 8H, ^3J = 7.3 Hz, CH$_2$CH$_2$CH$_2$CH$_3$), 2.094 (app pent, 8H, ^3J = 7.1 Hz, CH$_2$CH$_2$CH$_2$CH$_3$), 2.355 (s, 12H, $H_{Me-TBMP}$), 3.924 (app t, 8H, ^3J = 7.4 Hz, CH$_2$CH$_2$CH$_2$CH$_3$), 8.165 and 8.349 (ABq, 8H, ^3J = 8.0, 8.1 Hz, ArH$_{Ester}$), 10.069 (s, 2H, H_{meso}), 13.212 (br s, 2H, CO$_2$H). *Assignments aided by COSY spectra.* UV-vis (THF): λ_{max} [nm] (ε x 10^3) 417 (399), 506 (3.13), 546 (21.5), 580 (8.10). FAB-LRMS: *m/z* (%, assignment) cluster at 892-897, 892 (100, M$^+$). HRMS: Calcd for M$^+$ ($C_{54}H_{60}N_4O_4Zn$): 892.3906, found: 892.3948.

P(Ph$_m$(CO$_2$Me)$_2$)$_4$, 74.

5,10,15,20-Tetrakis(3',5'-dimethoxycarbonylphenyl)porphyrin.

C$_{60}$H$_{46}$N$_4$O$_{16}$
Exact Mass: 1078.2909
Mol. Wt.: 1079.0246
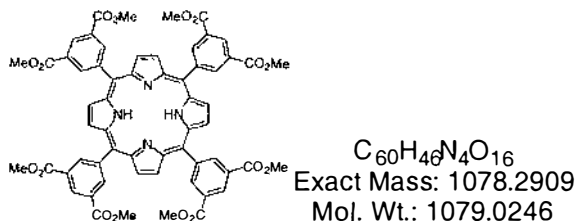
To a solution of dimethyl 5-formylisophthalate **40** (1.58 g, 7.09 mmol) and pyrrole (492 μL, 7.09 mmol) in dry degassed CH$_2$Cl$_2$ (709 mL) under N$_2$ at RT was added BF$_3$·OEt$_2$ (75 μL, 0.71 mmol, 0.1 eq). After 3 h p-chloranil (1.31 g, 0.75 eq) was added and the solution heated to reflux for 2 h in air. Excess Et$_3$N (3.0 mL) was added and the reaction mixture cooled to RT. The solvent was removed *in vacuo* and the residue column chromatographed (silica, 80 mm$_{dia}$ x 55 mm, CH$_2$Cl$_2$:Et$_2$O (25:1)). On reducing the volume under reduced pressure, the product precipitated out of solution to give the octaester **74** (330 mg, 17%) as a purple powder. ^{1}H NMR (270 MHz, CDCl$_3$, TMS): δ - 2.808 (s, 2H, NH), 4.039 (s, 24H, CO$_2$CH$_3$), 8.776 (s, 8H, H$_{\beta\text{-pyrrolic}}$), 9.077 (d, 8H, ^3J = 1.8 Hz, H$_{2',6'}$), 9.164 (t, 4H, ^3J = 1.5 Hz, H$_{4'}$). ^{13}C NMR (68 MHz, CDCl$_3$): δ 52.7, 118.3, 129.5, 130.3, 138.4, 142.5, 166.2. UV-vis (CH$_2$Cl$_2$): λ_{max} [nm] (ϵ x 10^{-3}) 421 (448), 515 (21.8), 550 (7.44), 590 (6.78), 646 (3.08). FAB-LRMS: m/z (%, assignment) cluster at 1078-1081, 1078 (75, M$^+$). HRMS: Calcd for M$^+$ (C$_{60}$H$_{46}$N$_4$O$_{16}$): 1078.2909, found: 1078.2882.

ZnP(Ph$_m$(CO$_2$Me)$_2$)$_4$, Zn-74.

5,10,15,20-Tetrakis(3',5'-dimethoxycarbonylphenyl)porphyrinato zinc(II).

C$_{60}$H$_{44}$N$_4$O$_{16}$Zn
Exact Mass: 1140.2044
Mol. Wt.: 1142.3987
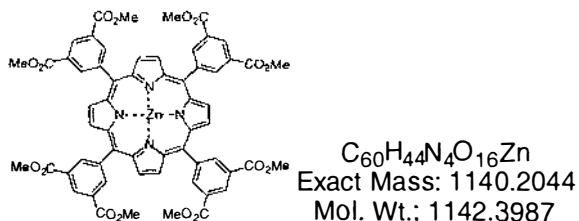
A solution of Zn(OAc)$_2$·2H$_2$O (27 mg, 123 μmol, 1.2 eq) in MeOH (2.0 mL) was added with stirring to a refluxing solution of octaester porphyrin **74** (111 mg, 103 μmol) in CHCl$_3$ (20 mL). After 30 min, TLC analysis indicated that the reaction was complete with the appearance of a new spot at higher R_f. The solvent was removed *in vacuo* and the residue column chromatographed (silica, 30 mm$_{dia}$ x 80 mm, CH$_2$Cl$_2$:Et$_2$O (25:2)) to

give **Zn-74** (113 mg, 96%) as a purple solid. ^{1}H NMR (400 MHz, CDCl$_3$, TMS): δ 4.018 (s, 24H, CO$_2$CH$_3$), 8.861 (s, 8H, H$_{\beta\text{-pyrrolic}}$), 9.065 (d, 8H, ^3J = 1.6 Hz, H$_{2',6'}$), 9.143 (t, 4H, ^3J = 1.6 Hz, H$_{4'}$). UV-vis (CH$_2$Cl$_2$): λ_{max} [nm] (ε x 10^{-3}) 426 (498), 554 (22.9), 594 (4.10). FAB-LRMS: m/z (%, assignment) cluster at 1140-1147, 1140 (90, M$^+$). HRMS: Calcd for M$^+$ (C$_{60}$H$_{44}$N$_4$O$_{16}$Zn): 1140.1974, found: 1140.2082.

ZnP(Ph$_m${(CO$_2$H)$_2$)$_4$, Zn-75.

5,10,15,20-Tetrakis(3',5'-dicarboxylatephenyl)porphyrinato zinc(II).

C$_{52}$H$_{28}$N$_4$O$_{16}$Zn
Exact Mass: 1028.0792
Mol. Wt.: 1030.1861
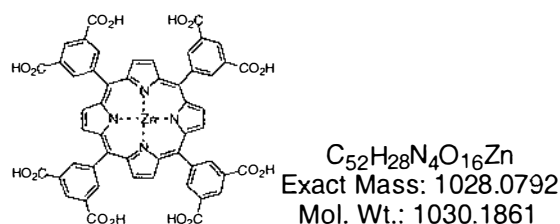
KOH (589 mg, 10.5 mmol, 15 eq per CO$_2$Me) in MeOH:H$_2$O (60:0:6.0 mL) was added to a solution of octaester **Zn-74** (100 mg, 87.5 μmol) in THF (60 mL). The mixture was heated to reflux for 18 h under N$_2$. After cooling to RT, the solvent was removed *in vacuo*. The residue was dissolved in H$_2$O ($\approx$ 50 mL) and acidified with 2.0 M H$_3$PO$_4$ (5.3 mL). The resulting precipitate was then washed with H$_2$O, and freeze dried to give octaacid **Zn-75** (82.3 mg, 91%) as a purple solid. ^{1}H NMR (400 MHz, DMSO-d$_6$, TMS): δ 8.825 (s, 8H, H$_{\beta\text{-pyrrolic}}$), 8.903 (d, 8H, ^3J = 1.5 Hz, H$_{2',6'}$), 8.950 (t, 4H, ^3J = 1.6 Hz, H$_{4'}$), 13.5 (br s, 8H, CO$_2$H). UV-vis (THF): λ_{max} [nm] (ε x 10^{-3}) 428 (442), 558 (20.7), 597 (6.07). FAB-LRMS: m/z (%, assignment) cluster at 1029-1033, 1029 (100, MH$^+$).

7.3 Chapter 3: Synthesis of Mixed-Metal and Mixed-Porphyrin Arrays

7.3.1 Bisformylporphyrin (BFP)

BAcP, 62.

5,15-Bis(4'-(1",3"-dioxacyclopent-2"-yl)phenyl)-2,8,12,18-tetrabutyl-3,7,13,17-tetramethylporphyrin.

$C_{58}H_{70}N_4O_4$
Exact Mass: 886.5397
Mol. Wt.: 887.2010
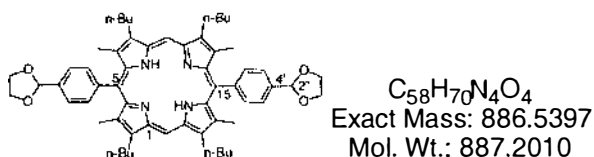
To a solution of 4-(1',3'-dioxa-2'-cyclopentyl)benzaldehyde **59** (1.18 g, 6.60 mmol) and dipyrrylmethane **58**[106,107] (1.89 g, 6.60 mmol) in dry degassed CH_2Cl_2 (660 mL, 10^{-2} M) under N_2 at RT, was added TFA (509 μL, 6.60 mmol, 1.0 eq). At the first sign of polar material by TLC (20 min, silica, CH_2Cl_2), the reaction was quenched with DBU (988 μL, 6.60 mmol, 1.0 eq). *p*-Chloranil (4.06 g, 16.5 mmol, 2.5 eq) was added and the solution stirred for 4 h at RT, then heated to reflux for 45 min. Et_3N (684 μL) was added and reaction stirred for 1.5 h. Then excess Et_3N (4.5 mL) was added and reaction stirred for an additional 15 min. The product was then precipitated out of solution with MeOH, to give bisacetal **62** (1.87 g, 64%) as a purple powder. *The ^1H NMR was consistent with that previously characterised in Chapter 2.*

BAcP, Ni-62.

5,15-Bis(4'-(1",3"-dioxacyclopent-2"-yl)phenyl)-2,8,12,18-tetrabutyl-3,7,13,17-tetramethylporphyrinato nickel(II).

$C_{58}H_{68}N_4NiO_4$
Exact Mass: 942.4594
Mol. Wt.: 943.8785
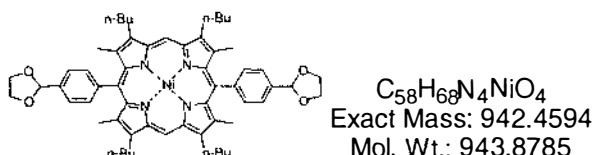
A solution of $Ni(OAc)_2 \cdot 4H_2O$ (701 mg, 2.82 mmol, 10 eq) in MeOH (5.0 mL) was added to a refluxing solution of bisacetal **62** (250 mg, 282 μmol) in $CHCl_3$ (50 mL) with

stirring under N_2. After 8 min, TLC analysis indicated that all starting material **62** had been consumed. After cooling to RT the crude product was precipitated with MeOH. The resulting solid was dissolved in CH_2Cl_2 and filtered through a plug of silica gel. Recrystallisation from CH_2Cl_2/MeOH gave bisacetal **Ni-62** (248 mg, 93%) as a purple microcrystalline solid. ^{1}H NMR (270 MHz, $CDCl_3$, TMS): δ 1.037 (t, 12H, $^3J = 7.3$ Hz, $CH_2CH_2CH_2CH_3$), 1.613 (sext, 8H, $^3J = 7.3$ Hz, $CH_2CH_2CH_2CH_3$), 1.978 (app pent, 8H, $^3J = 7.3$ Hz, $CH_2CH_2CH_2CH_3$), 2.213 (s, 12H, $H_{Me\text{-}TBMP}$), 3.637 (t, 8H, $^3J = 7.6$ Hz, $CH_2CH_2CH_2CH_3$), 4.149-4.333 (m, 8H, $-CH(OCH_2)_2$), 6.074 (s, 2H, $-CH(OCH_2)_2$), 7.742 and 7.868 (ABq, 8H, $^3J = 7.9, 8.2$ Hz, ArH_{Acetal}), 9.426 (s, 2H, H_{meso}). UV-vis (CH_2Cl_2): λ_{max} [nm] (ε x 10^{-3}) 407 (219), 529 (13.8), 564 (18.7). FAB-LRMS: m/z (%, assignment) cluster at 942-947, 942 (100, M^+). HRMS: Calcd for M^+ ($C_{58}H_{68}N_4O_4Ni$): 942.4594, found: 942.4556.

BFP, 76.

5,15-Bis(4'-formylphenyl)-2,8,12,18-tetrabutyl-3,7,13,17-tetramethylporphyrin.
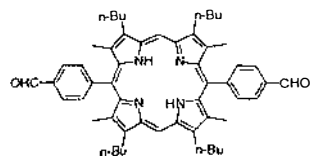
$C_{54}H_{62}N_4O_2$
Exact Mass: 798.4873
Mol. Wt.: 799.0958

A solution of bisacetal **62** (212 mg, 238 μmol) and p-TsOH·H_2O (271 mg, 1.42 mmol, 6 eq) in acetone (79 mL) was heated to reflux under N_2. After 1.5 h, TLC analysis ($R_f = 0.38$; silica gel, MeOH:CH_2Cl_2 (1:50)) indicated that all the starting material **62** had been consumed. The reaction was cooled to RT, and quenched with Et_3N (300 μL, 2.15 mmol). The solvent was removed *in vacuo*, and the residue dissolved in minimal CH_2Cl_2 and then filtered. Recrystallisation from CH_2Cl_2/MeOH gave bisformylporphyrin **76** (179 mg, 94%) as a purple microcrystalline solid. ^{1}H NMR (270 MHz, $CDCl_3$, TMS): δ -2.411 (br s, 2H, N**H**), 1.087 (t, 12H, $^3J = 7.3$ Hz, $CH_2CH_2CH_2CH_3$), 1.728 (sext, 8H, $^3J = 7.3$ Hz, $CH_2CH_2CH_2CH_3$), 2.146 (app pent, 8H, $^3J = 7.6$ Hz, $CH_2CH_2CH_2CH_3$), 2.393 (s, 12H, $H_{Me\text{-}TBMP}$), 3.949 (t, 8H, $^3J = 7.6$ Hz, $CH_2CH_2CH_2CH_3$), 8.178 (s, 8H, ArH_{CHO}), 10.237 (s, 2H, H_{meso}), 10.337 (s, 2H, C**H**O). ^{13}C NMR (68 MHz, $CDCl_3$): δ 14.99 (**C**H$_3$), 15.62 (**C**H$_3$), 24.08 (CH$_2$**C**H$_2$CH$_2$CH$_3$), 27.21 (CH$_2$CH$_2$**C**H$_2$CH$_3$), 36.22 (**C**H$_2$CH$_2$CH$_2$CH$_3$), 98.02 (C_{meso}), 117.02, 129.40, 134.26, 136.28, 136.79, 142.19, 144.39, 144.98, 149.57, 192.857 (CHO). UV-vis (CH_2Cl_2): λ_{max} [nm] (ε x 10^{-3}) 411 (209), 508 (18.2), 542 (6.43), 575 (7.80), 626 (2.53).

FAB-LRMS: m/z (%, assignment) cluster at 797-802, 799 (100, MH$^+$). HRMS: Calcd for MH$^+$ (C$_{54}$H$_{63}$N$_4$O$_2$): 799.4951, found: 799.4893.

BFP, Ni-76.

5,15-Bis(4'-formylphenyl)-2,8,12,18-tetrabutyl-3,7,13,17-tetramethylporphyrinato nickel(II).

C$_{54}$H$_{60}$N$_4$NiO$_2$
Exact Mass: 854.4070
Mol. Wt.: 855.7734
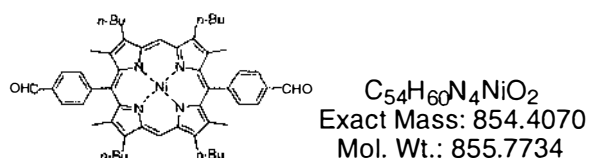
A solution of bisacetal **Ni-62** (239 mg, 253 μmol) and p-TsOH·H$_2$O (192 mg, 1.01 mmol, 4 eq) in acetone (80 mL) was heated to reflux under N$_2$. After 15 min, TLC analysis (R_f = 0.33; silica, CH$_2$Cl$_2$:hexane (2:1)) indicated that starting material **Ni-62** had been consumed. The reaction was cooled to RT, and quenched with Et$_3$N (200 μL, 1.43 mmol). The solvent was removed *in vacuo* and the residue dissolved in minimal CH$_2$Cl$_2$ and then filtered. Recrystallisation from CH$_2$Cl$_2$/MeOH gave bisformylporphyrin **Ni-76** (211 mg, 97%) as a brick-red microcrystalline solid. ^{1}H NMR (270 MHz, CDCl$_3$, TMS): δ 1.044 (t, 12H, ^3J = 7.3 Hz, CH$_2$CH$_2$CH$_2$CH$_3$), 1.619 (app sext, 8H, ^3J = 7.3 Hz, CH$_2$CH$_2$CH$_2$CH$_3$), 1.980 (app pent, 8H, ^3J = 7.3 Hz, CH$_2$CH$_2$CH$_2$CH$_3$), 2.187 (s, 12H, H$_{Me\text{-}TBMP}$), 3.643 (t, 8H, ^3J = 7.6 Hz, CH$_2$CH$_2$CH$_2$CH$_3$), 8.042 and 8.147 (ABq, 8H, ^3J = 7.9, 8.2 Hz, ArH$_{CHO}$), 9.458 (s, 2H, H$_{meso}$), 10.296 (s, 2H, CHO). UV-vis (CH$_2$Cl$_2$): λ_{max} [nm] (ε x 10^{-3}) 350 (20.4), 410 (196), 529 (15.2), 565 (19.9). FAB-LRMS: m/z (%, assignment) cluster at 853-859, 854 (100, M$^+$). HRMS: Calcd for M$^+$ (C$_{54}$H$_{60}$N$_4$O$_2$Ni): 854.4070, found: 854.4051.

BFP, Zn-76.

5,15-Bis(4'-formylphenyl)-2,8,12,18-tetrabutyl-3,7,13,17-tetramethylporphyrinato zinc(II).

C$_{54}$H$_{60}$N$_4$O$_2$Zn
Exact Mass: 860.4008
Mol. Wt.: 862.4700
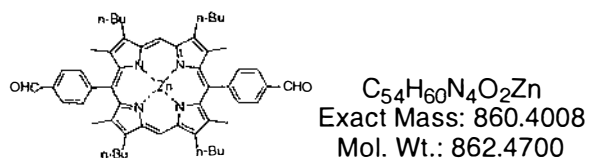
A solution of Zn(OAc)$_2$·2H$_2$O (61 mg, 278 μmol, 1.5 eq) in MeOH (500 μL) was added to a solution of bisformylporphyrin **76** (149 mg, 186 μmol) in CH$_2$Cl$_2$ (10 mL) with

stirring at RT. After 20 min, TLC analysis indicated that starting material **76** had been consumed. Precipitation using MeOH gave **Zn-76** (149 mg, 93%) as a brick-red microcrystalline solid. ^{1}H NMR (270 MHz, CDCl$_3$, TMS): δ 1.101 (t, ^3J = 7.3 Hz, 12H, CH$_2$CH$_2$CH$_2$CH$_3$), 1.738 (sext, 8H, ^3J = 7.3 Hz, CH$_2$CH$_2$CH$_2$CH$_3$), 2.130 (app pent, 8H, ^3J = 7.8 Hz, CH$_2$CH$_2$CH$_2$CH$_3$), 2.387 (s, 12H, H$_{Me\text{-}TBMP}$), 3.899 (t, 8H, ^3J = 7.7 Hz, CH$_2$CH$_2$CH$_2$CH$_3$), 7.742 (s, 8H, ArH$_{CHO}$), 10.127 (s, 2H, H$_{meso}$), 10.400 (s, 2H, CHO); UV-vis (CH$_2$Cl$_2$): λ_{max} [nm] (ε x 10^{-3}) 346 (21.6), 412 (343), 504 (3.66), 539 (20.2), 575 (12.0). FAB-LRMS: *m/z* (%, assignment) cluster at 859-866, 860 (100, M$^+$). HRMS: Calcd for M$^+$ (C$_{54}$H$_{60}$N$_4$O$_2$Zn): 860.4031, found: 860.3978.

BFP, Ag-76.

5,15-Bis(4'-formylphenyl)-2,8,12,18-tetrabutyl-3,7,13,17-tetramethylporphyrinato silver(II).

C$_{54}$H$_{60}$AgN$_4$O$_2$
Exact Mass: 903.3767
Mol. Wt.: 904.9482
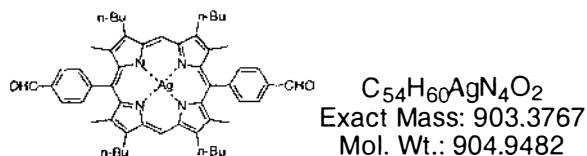
A suspension of bisformylporphyrin **76** (5.3 mg, 6.6 μmol) and AgO[84] (9.0 mg, 73 μmol, 5.5 eq) in THF (1.8 mL) and H$_2$O (200 μL) was stirred at RT. After 21 h, a single new compound at higher R_f than the starting material **76** was evident by TLC. The suspension was filtered and the solvent removed *in vacuo*. The residue was then dissolved in CH$_2$Cl$_2$ and filtered through a plug of silica gel. The solvent was removed in vacuo to give bisformylporphyrin **Ag-76** (5.1 mg, 85%) as a red solid. UV-vis (CH$_2$Cl$_2$): λ_{max} [nm] (ε x 10^{-3}) 418 (293), 532 (18.0), 64 (11.6). FAB-LRMS: *m/z* (%, assignment) cluster at 903-907, 905 (100, M$^+$). HRMS: Calcd for M$^+$ (C$_{54}$H$_{60}$Ag^{109}N$_4$O$_2$): 903.3767, found: 903.3785.

7.3.2 Diporphyrin Building Block C and Triporphyrins

ZnTXP-ZnTBMP-CHO Diporphyrin Building Block C, Zn/Zn-77

5-(4'-formylphenyl)-15-(4"-(*trans*-2"'-(2""-(5""',10"",15""',20""'-tetrakis(3""",5"""-dimethylphenyl)porphyrinato zinc(II))yl)ethen-1"'-yl)phenyl)-2,8,12,18-tetra-*n*-butyl-3,7,13,17-tetramethylporphyrinato zinc(II).

$C_{107}H_{104}N_8OZn_2$
Exact Mass: 1644.6916
Mol. Wt.: 1648.8040
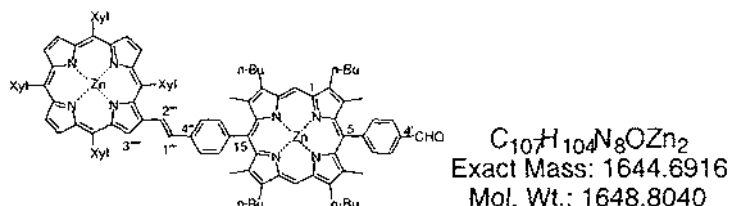
and ZnTXP-ZnTBMP-ZnTXP Triporphyrin, Zn/Zn/Zn-65.

5,15-Bis(4'-(*trans*-2"-(2"'-(5"',10"',15"',20"'-tetrakis(3"",5""-dimethylphenyl)porphyrinato zinc(II))yl)ethen-1"-yl)phenyl)-2,8,12,18-tetra-*n*-butyl-3,7,13,17-tetramethylporphyrinato zinc(II).

$C_{160}H_{148}N_{12}Zn_3$
Exact Mass: 2428.9824
Mol. Wt.: 2435.1380
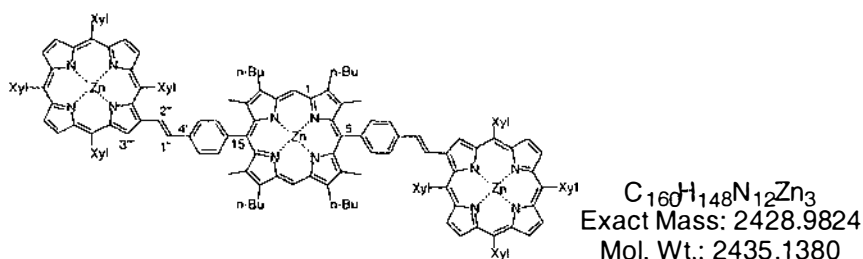
To a solution of bisformylporphyrin **76** (16.0 mg, 20.0 μmol) and TXPps **5** (20.8 mg, 20.0 μmol) in CH_2Cl_2 (2.0 mL) was added DBU (32 μL, 110 μmol, 5.5 eq) at RT under N_2. After 10 min, TLC analysis indicated that starting material **5** had been consumed. Precipitation from CH_2Cl_2/MeOH gave a mixture (by ^1H NMR) of inseparable products (20.8 mg) as a purple powder. Unreacted **76** (5.1 mg, 32%) was recovered as a purple solid from the filtrate by further volume reduction. Metallation with zinc(II) was then carried out to aid in the separation of the mixture. A solution of $Zn(OAc)_2·2H_2O$ (17.6 mg, 80 μmol, > 2 eq) in MeOH (0.5 mL) was added to a solution of the mixture in CH_2Cl_2 (2.0 mL) with stirring at RT. After 15 min, TLC analysis indicated that the metallation was complete with the appearance of two separable red bands. Et_3N (1 drop) was added and the solvent was removed *in vacuo*. The residue was column chromatographed (silica, 25 mm$_{dia}$ x 130 mm, CH_2Cl_2:hexane (1:1)) to give triporphyrin

Zn/Zn/Zn–65 (3.6 mg, 7.4% based on **76**, recrystallised from CH_2Cl_2/MeOH) as a purple powder. ^1H NMR (270 MHz, $CDCl_3$, TMS): δ 1.167 (t, 12H, ^3J = 7.3 Hz, $CH_2CH_2CH_2CH_3$), 1.75-1.90 (m, 8H, $CH_2CH_2CH_2CH_3$), 2.18-2.32 (m, 8H, $CH_2CH_2CH_2CH_3$), 2.58-2.730 (m, 60H, $12H_{Me\text{-}TBMP}$ + $48H_{Me\text{-}Xyl}$), 4.01-4.12 (m, 8H, $CH_2CH_2CH_2CH_3$), 7.421 (d, 2H, ^3J = 16.2 Hz, $H_{ethenyl}$), 7.399-7.439 (m, 4H $H_{p\text{-}Xyl}$), 7.479-7.524 (m, 4H, $H_{p\text{-}Xyl}$), 7.639 (d, 2H, ^3J = 15.9 Hz, $H_{ethenyl}$), 7.748-8.101 (ABq, 8H, ^3J = 8.2, 7.9 Hz, H_{styryl}), 7.871 (br s, 8H, $H_{o\text{-}Xyl}$), 7.962 (br s, 8H, $H_{o\text{-}Xyl}$), 8.935-9.029 (m, 12H, $H_{\beta\text{-pyrrolic}}$), 9.306 (s, 2H, $H_{3''' (\beta\text{-pyrrolic})}$), 10.284 (s, 2H, H_{meso}). UV-vis (CH_2Cl_2): λ_{max} [nm] (ε x 10^{-3}) 412 (273), 431 (410), 557 (48.8), 592 (20.5). FAB-LRMS: m/z (%, assignment) cluster at 2428-2443, 2435 (100, M^+). HRMS: Calcd for M^+ ($C_{160}H_{148}N_{12}Zn_3$): 2428.9824, found: 2429.0169.

Further elution gave the title diporphyrin **Zn/Zn-77** (9.2 mg, 28% based on **76**, recrystallised from CH_2Cl_2/MeOH) as a purple powder. ^1H NMR (270 MHz, $CDCl_3$, TMS): δ 1.09-1.18 (m, 12H, $CH_2CH_2CH_2CH_3$), 1.69-1.89 (m, 8H, $CH_2CH_2CH_2CH_3$), 2.10-2.29 (m, 8H, $CH_2CH_2CH_2CH_3$), 2.419 (s, 6H, $H_{Me\text{-}TBMP}$), 2.59-2.72 (m, 30H, $6H_{Me\text{-}TBMP}$ + $24H_{Me\text{-}Xyl}$), 3.89-4.08 (m, 8H, $CH_2CH_2CH_2CH_3$), 7.37-7.52 (m, 5H, $1H_{ethenyl}$ (^3J = 15.9 Hz) + $4H_{p\text{-}Xyl}$), 7.628 (d, ^3J = 16.2 Hz, 1H, $H_{ethenyl}$), 7.739-8.069 (ABq, ^3J = 7.9, 7.9 Hz, 4H, H_{styryl}), 7.869 (br s, 4H, $H_{o\text{-}Xyl}$), 7.957 (br s, 4H, $H_{o\text{-}Xyl}$), 8.27-8.23 (m, 4H, ArH_{CHO}), 8.945-9.027 (m, 6H, $H_{\beta\text{-pyrrolic}}$), 9.306 (s, 1H, $H_{3''' (\beta\text{-pyrrolic})}$), 10.201 (s, 2H, H_{meso}), 10.394 (s, 1H, CHO). UV-vis (CH_2Cl_2): λ_{max} [nm] (ε x 10^{-3}) 412 (321), 430 (312), 591 (12.9), 552 sh (33.8). FAB-LRMS: m/z (%, assignment) cluster at 1644-1654, 1645 (55, M^+). HRMS: Calcd for M^+ ($C_{107}H_{104}N_8OZn_2$): 1644.6916, found: 1644.6897.

TXP-ZnTBMP-CHO Diporphyrin Building Block C, 2H/Zn-77

5-(4'-formylphenyl)-15-(4"-(*trans*-2'''-(2''''-(5''''',10''''',15''''',20'''''-tetrakis(3''''',5'''''-dimethylphenyl)porphyrinyl)ethen-1'''-yl)phenyl)-2,8,12,18-tetra-*n*-butyl-3,7,13,17-tetramethylporphyrinato zinc(II).

$C_{107}H_{106}N_8OZn$
Exact Mass: 1582.7781
Mol. Wt.: 1585.4299

and TXP-ZnTBMP-TXP Triporphyrin, 2H/Zn/2H-65.

5,15-Bis(4'-(*trans*-2"-(2'''-(5''',10''',15''',20'''-tetrakis(3'''',5''''-dimethylphenyl)porphyrinyl)ethen-1"-yl)phenyl)-2,8,12,18-tetra-*n*-butyl-3,7,13,17-tetramethylporphyrinato zinc(II).
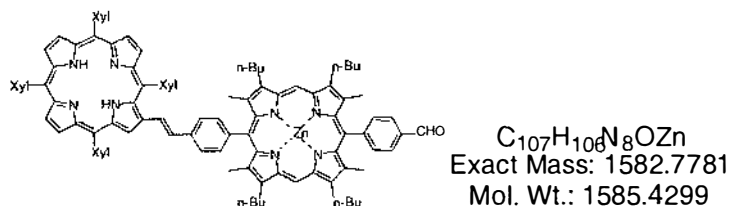

$C_{160}H_{152}N_{12}Zn$
Exact Mass: 2305.1554
Mol. Wt.: 2308.3898
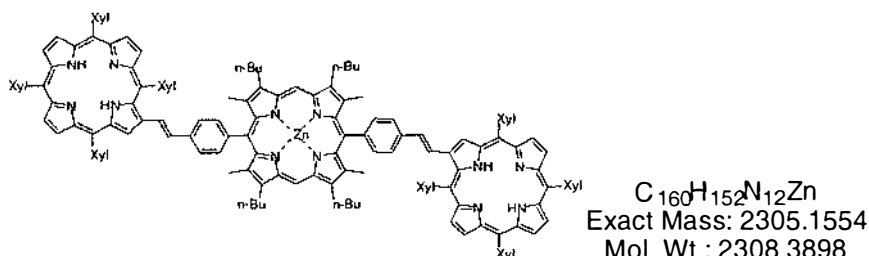
A solution of bisformylporphyrin **Zn-76** (95.4 mg, 111 μmol) and TXPps **5** (115 mg, 111 μmol) in dry toluene (14.3 mL) was heated to reflux under N_2. DBU (99 μL, 666 μmol) was added and reaction refluxed for 1 h. The solution was cooled and then the solvent removed *in vacuo.* The residue was then column chromatographed (silica, 37 mm$_{dia}$ x 150 mm) first eluting with CH_2Cl_2:hexane (1:1) to give triporphyrin **2H/Zn/2H-65** (32 mg, 13%) as a purple solid. ^{1}H NMR (270 MHz, CDCl$_3$, TMS, selected data only): δ -2.538 (br s, NH), 1.164 (t, ^3J = 7.3 Hz, CH$_2$CH$_2$CH$_2$CH$_3$), 1.821 (app sext, ^3J = 7.0 Hz, CH$_2$CH$_2$CH$_2$CH$_3$), 2.17-2.32 (m, CH$_2$CH$_2$CH$_2$CH$_3$), 2.54-2.73 (m, H$_{Me\text{-}TBMP}$ + H$_{Me\text{-}Xyl}$), 4.00-4.11 (m, CH$_2$CH$_2$CH$_2$CH$_3$), 7.34-7.53 (m, H$_{p\text{-}Xyl}$ + H$_{ethenyl}$), 7.63-8.00 (m, H$_{ethenyl}$ (7.684 (d, ^3J = 15.9 Hz)) + H$_{o\text{-}Xyl}$), 7.741 and 8.102 (ABq, ^3J = 7.9, 7.9 Hz, H$_{styryl}$), 8.62-8.93 (m, H$_{\beta\text{-pyrrolic}}$), 9.206 (s, H$_{3''' (\beta\text{-pyrrolic})}$), 10.272 (s, H$_{meso}$). UV-vis (CH$_2Cl_2$): λ_{max} [nm] (ε x 10^{-3}) 420 (530), 531 (47.1), 567 (31.2), 597 (15.8), 655 (6.69). FAB-LRMS: *m/z* (%, assignment) cluster at 2305-2314, 2308 (100, MH$^+$). HRMS: Calcd for MH$^+$ (C$_{160}$H$_{153}$N$_{12}$Zn): 2306.1633, found: 2306.1655.

Further elution gave diporphyrin **2H/Zn-77** (54 mg, 31%, recrystallised from CH$_2$Cl$_2$/MeOH) as a purple powder. ^{1}H NMR (270 MHz, CDCl$_3$, TMS): δ -2.547 (br s, 2H, NH), 1.09-1.17 (m, 12H, CH$_2$CH$_2$CH$_2$**CH$_3$**), 1.68-1.88 (m, 8H, CH$_2$CH$_2$**CH$_2$**CH$_3$), 2.09-2.27 (m, 8H, CH$_2$**CH$_2$**CH$_2$CH$_3$), 2.391 (s, 6H, H$_{Me\text{-}TBMP}$), 2.57-2.73 (m, 30H, 6H$_{Me\text{-}TBMP}$ + 24H$_{Me\text{-}Xyl}$), 3.900 (app t, 4H, ^3J = 7.4 Hz, **CH$_2$**CH$_2$CH$_2$CH$_3$), 3.986 (app t, 4H, ^3J = 7.6 Hz, **CH$_2$**CH$_2$CH$_2$CH$_3$), 7.34-7.52 (m, 5H, 1H$_{ethenyl}$ + 4H$_{p\text{-}Xyl}$), 7.670 (d, 1H, ^3J = 16.2 Hz, H$_{ethenyl}$), 7.729 and 8.067 (ABq, 4H, ^3J = 8.1, 7.7 Hz, H$_{styryl}$), 7.862 (br s, 4H, H$_{o\text{-}Xyl}$), 7.94-7.98 (m, 4H, H$_{o\text{-}Xyl}$), 8.273 (s, 4H, ArH$_{CHO}$ (ROESY TPPI shows coupling to δ 2.391 ppm)), 8.82-8.91 (m, 6H, H$_{\beta\text{-pyrrolic}}$), 9.201 (s, 1H, H$_{3'''' (\beta\text{-pyrrolic})}$), 10.153 (s, 2H, H$_{meso}$), 10.393 (s, 1H, CHO). UV-vis (CH$_2$Cl$_2$): λ$_{max}$ [nm] (ε x 10^{-3}) 412 (342), 426 (323), 536 (37.7), 569 (23.2), 599 (8.99), 656 (3.30). FAB-LRMS: m/z (%, assignment) cluster at 1581-1591, 1585 (100, M$^+$). HRMS: Calcd for M$^+$ (C$_{107}$H$_{106}$N$_8$OZn): 1582.7781, found: 1582.7709.

Additional elution with CH$_2$Cl$_2$ gave unreacted starting material **Zn-76** (38.6 mg, 40%) as a purple solid.

NiTXP-ZnTBMP-CHO Diporphyrin Building Block C, Ni/Zn-77.

5-(4'-formylphenyl)-15-(4"-(*trans*-2'''-(2''''-(5''''',10''''',15''''',20'''''-tetrakis(3'''''',5''''''-dimethylphenyl)porphyrinato nickel(II))yl)ethen-1'''-yl)phenyl)-2,8,12,18-tetra-*n*-butyl-3,7,13,17-tetramethylporphyrinato zinc(II).
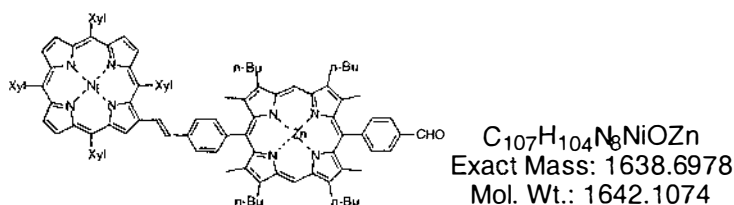

C$_{107}$H$_{104}$N$_8$NiOZn
Exact Mass: 1638.6978
Mol. Wt.: 1642.1074

A solution of Ni(OAc)$_2$·4H$_2$O (35 mg, 141 μmol, 10 eq) in MeOH (500 μL) was added to a refluxing solution of **2H/Zn-77** (22.3 mg, 14.1 μmol) in CHCl$_3$ (7.0 mL) with stirring under N$_2$. After 15 h, by TLC all starting material **2H/Zn-77** had been metallated. After cooling to RT, the solvent was removed *in vacuo* and the residue was column chromatographed (silica, 17 mm$_{dia}$ x 150 mm, CH$_2$Cl$_2$:hexane (1:1)). Recrystallisation from CH$_2$Cl$_2$/MeOH gave diporphyrin **Ni/Zn-77** (18.3 mg, 79%) as a purple powder. ^{1}H NMR (270 MHz, CDCl$_3$, TMS): δ 1.08-1.18 (m, 12H, CH$_2$CH$_2$CH$_2$**CH$_3$**), 1.773 (app hept, 8H, ^3J = 7.3 Hz, CH$_2$CH$_2$**CH$_2$**CH$_3$), 2.09-2.27 (m,

8H, CH$_2$**CH$_2$**CH$_2$CH$_3$), 2.410 (s, 6H, H$_{Me-TBMP}$), 2.53-2.65 (m, 30H, 6H$_{Me-TBMP}$ + 24H$_{Me-Xyl}$), 3.963 (app pent, 8H, ^3J = 7.6 Hz, CH$_2$CH$_2$**CH$_2$**CH$_3$), 7.251 and 7.488 (ABq, 2H, ^3J = 16.2, 15.9 Hz, H$_{ethenyl}$), 7.32-7.43 (m, 4H, H$_{p-Xyl}$), 7.61-7.67 (m, 6H, 4H$_{o-Xyl}$ + 2H$_{styryl}$), 7.732 (br s, 4H, H$_{o-Xyl}$), 8.028 (d, 2H, ^3J = 7.9 Hz, H$_{styryl}$), 8.289 (s, 4H, ArH$_{CHO}$), 8.73-8.82 (m, 6H, H$_{\beta\text{-pyrrolic}}$), 9.072 (s, 1H, H$_{3'''\ (\beta\text{-pyrrolic})}$), 10.182 (s, 2H, H$_{meso}$), 10.406 (s, 1H, CHO). UV-vis (CH$_2$Cl$_2$): λ_{max} [nm] (ε x 10^{-3}) 328 (34.6), 412 (355), 428 (299), 540 (43.8), 575 (26.8). FAB-LRMS: m/z (%, assignment) cluster at 1638-1648, 1641 (100, M$^+$). HRMS: Calcd for M$^+$ (C$_{107}$H$_{104}$N$_8$NiOZn): 1638.6978, found: 1638.7114.

NiTXP-ZnTBMP-TPP Triporphyrin, Ni/Zn/2H-82.

5-(4'-(*trans*-2"-(2'''-(5''',10''',15''',20'''-tetraphenylporphyrinyl)ethen-1"-yl)phenyl)-15-(4''''-(*trans*-2'''''-(2''''''-(5'''''',10'''''',15'''''',20''''''-tetrakis(3'''''''',5''''''''-dimethylphenyl)-porphyrinato nickel(II))yl)ethen-1'''''-yl)phenyl)-2,8,12,18-tetra-*n*-butyl-3,7,13,17-tetramethylporphyrinato zinc(II).

C$_{152}$H$_{134}$N$_{12}$NiZn
Exact Mass: 2248.9499
Mol. Wt.: 2252.8546
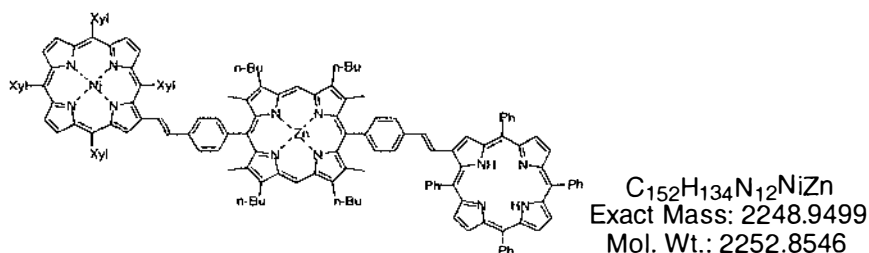
A solution of diporphyrin **Ni/Zn-77** (11.5 mg, 7.00 μmol) and TPPps **4** (8.9 mg, 8.6 μmol, 1.2 eq) in dry toluene (3 mL) was heated to reflux under N$_2$. DBU (48 μL, 0.32 mmol, 46 eq) was added and reaction refluxed for 1 h. The solution was cooled and then the solvent removed *in vacuo*. The residue was then column chromatographed (silica, 17 mm$_{dia}$ x 150 mm, CH$_2$Cl$_2$:hexane (1:1)). Recrystallisation from CH$_2$Cl$_2$/MeOH gave *cis/trans*-**Ni/Zn/2H-82** (9.9 mg, 63%) in a ratio of 1:4 (based on **NH** ^{1}H NMR integrals) as a purple powder. ^{1}H NMR (270 MHz, CDCl$_3$, TMS, selected data only): δ -2.653 (br s, NH$_{cis}$), -2.524 (br s, NH$_{trans}$), 6.586 and 6.812 (ABq, ^3J = 13.5, 13.2 Hz, H$_{cis\text{-ethenyl}}$).

Isomerisation

cis/trans-**Ni/Zn/2H-82** (9.5 mg, 4.2 μmol) was dissolved in toluene (5 mL) and heated to reflux under N$_2$ for 28 h. The solution was then cooled and the solvent removed *in vacuo*. Recrystallisation from CH$_2$Cl$_2$/MeOH then CH$_2$Cl$_2$/hexane gave all *trans*

Ni/Zn/2H-82 (8.2 mg, 86%) as a purple powder. ^{1}H NMR (270 MHz, CDCl$_3$, TMS): δ -2.527 (br s, 2H, NH), 1.159 (t, 12H, ^3J = 7.3 Hz, CH$_2$CH$_2$CH$_2$CH$_3$), 1.773 (app sext, 8H, ^3J = 7.6 Hz, CH$_2$CH$_2$CH$_2$CH$_3$), 2.235 (app pent, 8H, ^3J = 7.3 Hz, CH$_2$CH$_2$CH$_2$CH$_3$), 2.52-2.67 (m, 36H, 12H$_{Me-TBMP}$ + 24H$_{Me-Xyl}$), 3.98-4.10 (m, 8H, CH$_2$CH$_2$CH$_2$CH$_3$), 7.258 and 7.500 (ABq, 2H, ^3J = 15.6, 15.9 Hz, H$_{ethenyl}$), 7.291 (d, 1H, ^3J = 15.9 Hz, H$_{ethenyl}$), 7.338 (br s, 2H, ArH), 7.38-7.44 (m, 2H, ArH), 7.60-7.70 (m, 9H, 8ArH + 1H$_{ethenyl}$ (Coupled to doublet at δ 7.291 ppm)), 7.72-7.81 (m, 10H, ArH), 7.84-7.90 (m, 6H, ArH), 8.02-8.10 (m, 4H, ArH), 8.21-8.28 (m, 4H, ArH), 8.31-8.38 (m, 4H, ArH), 8.73-8.89 (m, 12H, H$_{\beta\text{-pyrrolic}}$), 9.080 (s, 1H, H$_{3''''' (\beta\text{-pyrrolic-TXP})}$), 9.185 (s, 1H, H$_{3''' (\beta\text{-pyrrolic-TPP})}$), 10.250 (s, 2H, H$_{meso}$). UV-vis (CH$_2Cl_2$): λ$_{max}$ [nm] (ε x 10^{-3}) 412$_{TBMP}$ (385), 429$_{TAP}$ (458), 538 (57.1), 571 (37.0), 598 (15.4), 653 (3.61). FAB-LRMS: m/z (%, assignment) cluster at 2248-2260, 2252 (100, M$^+$). HRMS: Calcd for M$^+$ (C$_{152}$H$_{134}$N$_{12}$NiZn): 2248.9499, found: 2248.9500.

NiTXP-NiTBMP-CHO Diporphyrin Building Block C, Ni/Ni-77

5-(4'-formylphenyl)-15-(4"-(*trans*-2'''-(2''''-(5''''',10''''',15''''',20'''''-tetrakis(3''''',5'''''-dimethylphenyl)porphyrinato nickel(II))yl)ethen-1'''-yl)phenyl)-2,8,12,18-tetra-*n*-butyl-3,7,13,17-tetramethylporphyrinato nickel (II).


C$_{107}$H$_{104}$N$_8$Ni$_2$O
Exact Mass: 1632.7040
Mol. Wt.: 1635.4108
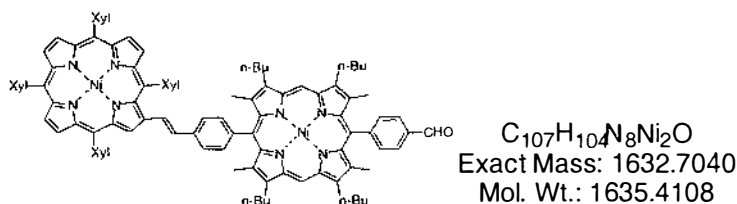
and NiTXP-NiTBMP-NiTXP Triporphyrin, Ni/Ni/Ni-65.

5,15-Bis(4'-(*trans*-2"-(2'''-(5''',10''',15''',20'''-tetrakis(3'''',5''''-dimethylphenyl)porphyrinato nickel (II))yl)ethen-1"-yl)phenyl)-2,8,12,18-tetra-*n*-butyl-3,7,13,17-tetramethylporphyrinato nickel (II).

C$_{160}$H$_{148}$N$_{12}$Ni$_3$
Exact Mass: 2411.0010
Mol. Wt.: 2415.0482
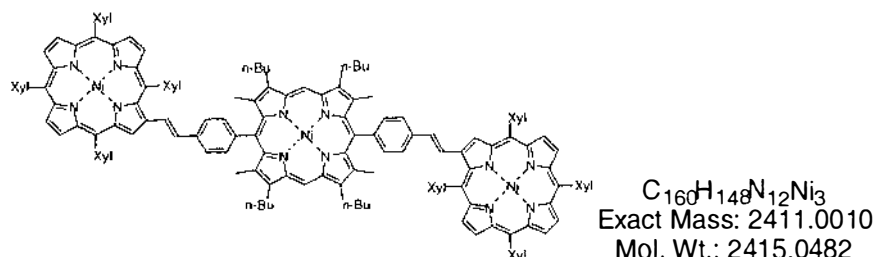
A solution of bisformylporphyrin **Ni-76** (276.0 mg, 323 μmol) and TXPps **5** (255.8 mg, 247 μmol) in toluene (45 mL) was heated to reflux under argon. DBU (210 μL, 5.7 eq) was added, and after 50 min starting material **5** had been consumed by TLC. After cooling to RT the solvent was removed *in vacuo*. The residue was dissolved in CH_2Cl_2 and filtered through a plug of silica gel before removing the solvent *in vacuo*. A solution of $Ni(OAc)_2 \cdot 4H_2O$ (631 mg, 2.54 mmol, 10 eq) in MeOH (6.0 mL) was added to a refluxing solution of the residue in $CHCl_3$ (75 mL) under N_2. After 13.5 h, the red solution was cooled to RT and the crude product precipitated with MeOH. The solid was column chromatographed (silica, 52 mm_{dia} x 160 mm), collecting three major porphyrin bands. First eluting with CH_2Cl_2:hexane (1:1) gave *cis/trans*-**Ni/Ni/Ni-65** (51.7 mg, 6.6%, recrystallised from CH_2Cl_2/MeOH) in a ratio of 1:4 (based on H_{meso} ^1H NMR integrals) as a purple powder. ^1H NMR (270 MHz, $CDCl_3$, TMS, selected data only): δ 6.372 and 6.598 (ABq, $^3J = 12.5$, 12.8 Hz, $H_{cis\text{-ethenyl}}$), 7.185 and 7.399 (ABq, $^3J = 16.2$, 16.2 Hz, $H_{trans\text{-ethenyl}}$), 9.404 (s, $H_{cis\text{-meso}}$), 9.512 (s, $H_{trans\text{-meso}}$).

Further elution gave diporphyrin *cis/trans*-**Ni/Ni-77**, (183 mg, 35%, recrystallised from CH_2Cl_2/MeOH) in a ratio of 1:6 (based on H_{meso} ^1H NMR integrals) as a purple powder. ^1H NMR (270 MHz, $CDCl_3$, TMS, selected data only): δ 6.355 and 6.592 (ABq, $^3J = 12.5$, 12.5 Hz, $H_{cis\text{-ethenyl}}$), 7.172 and 7.381 (ABq, $^3J = 16.2$, 16.2 Hz, $H_{trans\text{-ethenyl}}$), 9.377 (s, $H_{cis\text{-meso}}$), 9.485 (s, $H_{trans\text{-meso}}$), 10.274 (s, CHO_{cis}), 10.315 (s, CHO_{trans}).

Additional elution with CH_2Cl_2:hexane (2:1) gave the recovered starting material **Ni-76** (109 mg, 39%, recrystallised from CH_2Cl_2/MeOH) as a purple powder.

Isomerisation

cis/trans-**Ni/Ni-77** (172 mg, 105 μmol) was dissolved in CH_2Cl_2 (34 mL) and I_2 (65.2 mg, 257 μmol, 2.4 eq) added. After stirring at RT for 4.5 h in darkness, excess sat. $Na_2S_2O_3$ was added and stirring continued for 30 min. The organic layer was separated and dried ($MgSO_4$). Recrystallisation from CH_2Cl_2/MeOH gave *trans* **Ni/Ni-77** (172 mg, 100%) as a purple powder. ^1H NMR (270 MHz, $CDCl_3$, TMS): δ 1.061 (t, 6H, $^3J = 7.3$ Hz, $CH_2CH_2CH_2CH_3$), 1.079 (t, 6H, $^3J = 7.3$ Hz, $CH_2CH_2CH_2CH_3$), 1.652 (app hept, 8H, $^3J = 7.3$ Hz, $CH_2CH_2CH_2CH_3$), 1.927-2.105 (m, 8H, $CH_2CH_2CH_2CH_3$), 2.211 (s, 6H, $H_{Me\text{-TBMP}}$), 2.366 (s, 6H, $H_{Me\text{-TBMP}}$), 2.521 (s, 6H, $H_{Me\text{-Xyl}}$), 2.548 (s, 12H, $H_{Me\text{-Xyl}}$),

2.607 (s, 6H, H_{Me-Xyl}), 3.618-3.758 (m, 8H, $CH_2CH_2CH_2CH_3$), 7.171 and 7.381 (ABq, 2H, ^3J = 15.9, 15.9 Hz, $H_{ethenyl}$), 7.331 (br s, 1H, H_{p-Xyl}), 7.389 (br s, 3H, H_{p-Xyl}), 7.522 and 7.795 (ABq, 4H, ^3J = 8.2, 8.2 Hz, H_{styryl}), 7.639 (br s, 4H, H_{o-Xyl}), 7.698 (br s, 4H, H_{o-Xyl}), 8.085 and 8.172 (ABq, 4H, ^3J = 8.2, 8.2 Hz, ArH_{CHO}), 8.732 and 8.773 (ABq, 2H, ^3J = 4.9, 4.9 Hz, $H_{\beta-pyrrolic}$), 8.743-8.758 (m, 4H, $H_{\beta-pyrrolic}$), 9.013 (s, 1H, $H_{3''' (\beta-pyrrolic)}$), 9.485 (s, 2H, H_{meso}), 10.315 (s, 1H, CHO). UV-vis (CH_2Cl_2): λ_{max} [nm] (ε x 10^{-3}) 429 (249), 535 (28.2), 566 (26.4). FAB-LRMS: m/z (%, assignment) cluster at 1632-1641, 1635 (100, M$^+$). HRMS: Calcd for M$^+$ ($C_{107}H_{104}N_8Ni_2O$): 1632.7040, found: 1632.7013.

cis/trans-**Ni/Ni/Ni-65** (51.7 mg, 21.4 μmol) was dissolved in CH_2Cl_2 (7 mL) and I_2 (13.6 mg, 53.6 μmol, 2.5 eq) was added. After stirring at RT for 4.5 h in darkness, excess sat. $Na_2S_2O_3$ was added and stirring continued for 30 min. The organic layer was separated, dried (MgSO$_4$) and the solvent removed *in vacuo*. The residue was then column chromatographed (silica, 17 mm$_{dia}$ x 130 mm, CH_2Cl_2:hexane (1:4)). Recrystallisation from CH_2Cl_2/MeOH gave all *trans* **Ni/Ni/Ni-65** (42.8 mg, 83%) as a purple powder. ^1H NMR (270 MHz, CDCl$_3$, TMS): δ 1.096 (t, 12H, ^3J = 7.6 Hz, $CH_2CH_2CH_2CH_3$), 1.684 (sext, 8H, ^3J = 7.3 Hz, $CH_2CH_2CH_2CH_3$), 2.058 (app pent, 8H, ^3J = 7.3 Hz, $CH_2CH_2CH_2CH_3$), 2.383 (s, 12H, $H_{Me-TBMP}$), 2.490-2.571 (m, 36H, H_{Me-Xyl}), 2.615 (s, 12H, H_{Me-Xyl}), 3.618-3.758 (m, 8H, $CH_2CH_2CH_2CH_3$), 7.180 and 7.399 (ABq, 4H, ^3J = 15.9, 15.9 Hz, $H_{ethenyl}$), 7.317-7.366 (m, 6H, H_{p-Xyl}), 7.397 (br s, 2H, H_{p-Xyl}), 7.537 and 7.826 (ABq, 8H, ^3J = 8.2, 8.2 Hz, H_{styryl}), 7.645 (br s, 8H, H_{o-Xyl}), 7.703 (br s, 8H, H_{o-Xyl}), 8.739 and 8.785 (ABq, 4H, ^3J = 4.9, 4.9 Hz, $H_{\beta-pyrrolic}$), 8.757 (app d, 8H, ^3J = 1.2 Hz, $H_{\beta-pyrrolic}$), 9.024 (s, 2H, $H_{3''' (\beta-pyrrolic)}$), 9.511 (s, 2H, H_{meso}). UV-vis (CH_2Cl_2): λ_{max} [nm] (ε x 10^{-3}) 430 (553), 537 (66.4), 568 (52.4). FAB-LRMS: m/z (%, assignment) cluster at 2410-2420, 2414 (100, M$^+$). HRMS: Calcd for M$^+$ ($C_{160}H_{148}N_{12}Ni_3$): 2411.0010, found: 2411.0108.

7.3.3   Pentaporphyrins

Linear Pentaporphyrin, Ni/Ni/2H/Ni/Ni-83.
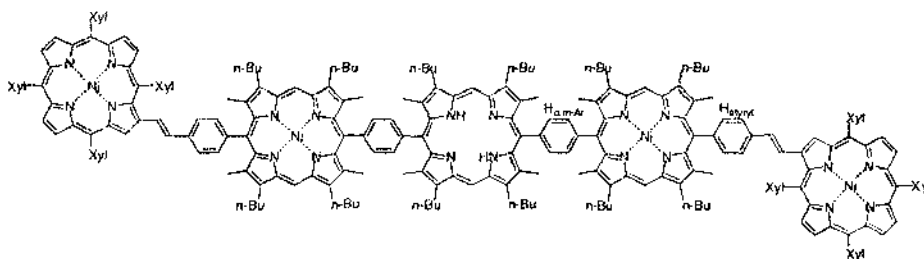
$C_{252}H_{258}N_{20}Ni_4$
Exact Mass: 3795.8217
Mol. Wt.: 3801.6533

To a solution of **Ni/Ni-77** (71.9 mg, 44.0 μmol) and dipyrrylmethane **58** (13.9 mg, 48.4 μmol, 1.1 eq) in dry degassed CH_2Cl_2 (2.9 mL, 10^{-2} M) and MeOH (1.5 mL) under N_2 at RT, was added TFA (5.1 μL, 66 μmol, 1.5 eq). After 1 h the reaction was quenched by adding Et_3N (9.8 μL, 69 μmol, 1.0 eq). *p*-Chloranil (37.8 mg, 154 μmol, 3.5 eq) was added and the solution stirred for 140 min at RT. Excess Et_3N (0.1 mL, 717 μmol) was added and stirring continued for 20 min. The crude product was then precipitated out with MeOH, and the resulting residue was chromatographed (silica, 37 mm_{dia} x 60 mm). Elution with CH_2Cl_2:Hexane (1:1) gave unreacted starting material **Ni/Ni-77** (17.2 mg, 24%, recrystallised from CH_2Cl_2/MeOH) as a purple powder. Further elution with CH_2Cl_2:MeOH (100:1) gave **Ni/Ni/2H/Ni/Ni-83** (53.1 mg, 64%, recrystallised from CH_2Cl_2/MeOH) as a purple powder. ^{1}H NMR (270 MHz, $CDCl_3$, TMS): δ -1.620 (br s, 1H, NH), 1.126 (t, 12H, ^3J = 7.3 Hz, $CH_2CH_2CH_2CH_3$), 1.163 (t, 12H, ^3J = 7.3 Hz, $CH_2CH_2CH_2CH_3$), 1.197 (t, 12H, ^3J = 7.3 Hz, $CH_2CH_2CH_2CH_3$), 1.645-1.955 (m, 24H, $CH_2CH_2CH_2CH_3$), 2.019-2.372 (m, 24H, $CH_2CH_2CH_2CH_3$), 2.401 (s, 12H, $H_{Me-TBMP}$), 2.554 (s, 36H, H_{Me-Xyl}), 2.620 (s, 12H, H_{Me-Xyl}), 2.958 (s, 12H, $H_{Me-TBMP}$), 3.059 (s, 12H, $H_{Me-TBMP}$), 3.652-3.932 (m, 16H, $CH_2CH_2CH_2CH_3$), 4.038-4.235 (m, 8H, $CH_2CH_2CH_2CH_3$), 7.192 and 7.403 (ABq, 4H, ^3J = 15.9, 16.2 Hz, $H_{ethenyl}$), 7.334 (s, 4H, H_{p-Xyl}), 7.369 (s, 2H, H_{p-Xyl}), 7.402 (s, 2H, H_{p-Xyl}), 7.551 and 7.845 (ABq, 8H, ^3J = 8.2, 8.2 Hz, H_{styryl}), 7.649 (br s, 8H, H_{o-Xyl}), 7.710 (br s, 8H, H_{o-Xyl}), 8.296 and 8.423 (ABq, 8H, ^3J = 7.9, 7.9 Hz, $H_{o,m-Ar}$), 8.744 and 8.792 (ABq, 4H, ^3J = 4.9, 4.9 Hz, $H_{\beta-pyrrolic}$), 8.760 (app d, 8H, ^3J = 0.6 Hz, $H_{\beta-pyrrolic}$), 9.032 (s, 2H, $H_{3\,(\beta-pyrrolic)}$), 9.538 (s, 4H, H_{meso}), 10.399 (s, 2H, H_{meso}). UV-vis (CH_2Cl_2): λ_{max} [nm] (ε x 10^{-3}) 431 (674), 510 sh (46.1),

536 (68.8), 571 (61.5). FAB-LRMS: m/z (%, assignment) 3800 (100, M$^+$). Calcd for

M$^+$ (C$_{252}$H$_{258}$N$_{20}$Ni$_4$): 3799. Hewlett-Packard 2025 MALDI-TOF MS (all-*trans*-retinoic

acid): m/z = 3801 (M$^+$). Time lag focusing MALDI-TOF MS: m/z = 3800 (M$^+$, 100%),

Calcd avg mass for M$^+$ (C$_{252}$H$_{258}$N$_{20}$Ni$_4$): 3802.

Linear Pentaporphyrin, Ni/Ni/Zn/Ni/Ni-83.
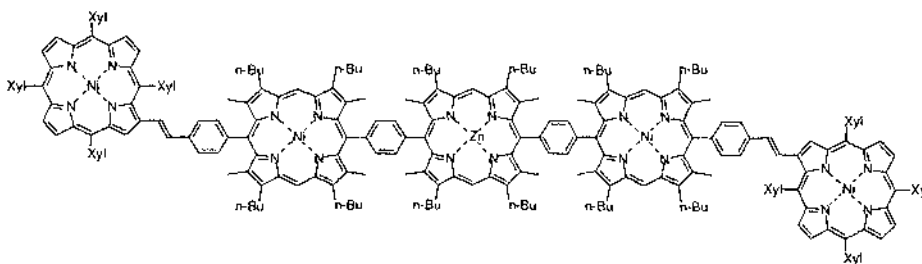
C$_{252}$H$_{256}$N$_{20}$Ni$_4$Zn
Exact Mass: 3857.7352
Mol. Wt.: 3865.0274

A solution of Zn(OAc)$_2$·2H$_2$O (1.6 mg, 7.3 μmol, 2.0 eq) in MeOH (200 μL) was added

to a solution of **Ni/Ni/2H/Ni/Ni-83** (14.0 mg, 3.68 μmol) in CH$_2$Cl$_2$ (2.0 mL) with

stirring at RT. After 15 min, TLC analysis indicated that all the starting material

Ni/Ni/2H/Ni/Ni-83 had been metallated. The solvent was removed *in vacuo* and the

residue dissolved in CH$_2$Cl$_2$ then filtered through a plug of basic alumina.

Recrystallisation from CH$_2$Cl$_2$/hexane then CH$_2$Cl$_2$/MeOH gave **Ni/Ni/Zn/Ni/Ni-83**

(12.4 mg, 87%) as a brick-red powder. ^{1}H NMR (270 MHz, CDCl$_3$, TMS): δ 1.088-

1.202 (m, 36H, CH$_2$CH$_2$CH$_2$CH$_3$), 1.634-1.942 (m, 24H, CH$_2$CH$_2$CH$_2$CH$_3$), 2.019-2.344

(m, 24H, CH$_2$CH$_2$CH$_2$CH$_3$), 2.398 (s, 12H, H$_{Me-TBMP}$), 2.554 (s, 36H, H$_{Me-Xyl}$), 2.619 (s,

12H, H$_{Me-Xyl}$), 3.019 (br s, 24H, H$_{Me-TBMP}$), 3.657-3.910 (m, 16H, CH$_2$CH$_2$CH$_2$CH$_3$),

3.992-4.158 (m, 8H, CH$_2$CH$_2$CH$_2$CH$_3$), 7.190 and 7.403 (ABq, 4H, ^3J = 15.9, 16.2 Hz,

H$_{ethenyl}$), 7.334 (s, 4H, H$_{p-Xyl}$), 7.369 (s, 2H, H$_{p-Xyl}$), 7.401 (s, 2H, H$_{p-Xyl}$), 7.553 and 7.848

(ABq, 8H, ^3J = 7.9, 7.9 Hz, H$_{styryl}$), 7.648 (s, 8H, H$_{o-Xyl}$), 7.707 (s, 8H, H$_{o-Xyl}$), 8.316 and

8.458 (ABq, 8H, ^3J = 7.9, 7.9 Hz, H$_{o,m-Ar}$), 8.742 and 8.790 (ABq, 4H, ^3J = 5.2, 5.2 Hz,

H$_{\beta-pyrrolic}$), 8.759 (s, 8H, H$_{\beta-pyrrolic}$), 9.030 (s, 2H, H$_{3\ (\beta-pyrrolic)}$), 9.524 (s, 4H, H$_{meso}$), 10.276

(s, 2H, H$_{meso}$). UV-vis (CH$_2$Cl$_2$): λ_{max} [nm] (ε x 10^{-3}) 433 (940), 540 (111), 572 (84.5).

ES-MS (CHCl$_3$:MeOH (3:2)): m/z = 1932.7, 1288.8, 966.9, Calcd avg mass for

C$_{252}$H$_{256}$N$_{20}$Ni$_4$Zn: [M + 2H]$^{2+}$ = 1933.5, [M + 3H]$^{3+}$ = 1289.3, [M + 4H]$^{4+}$ = 967.3. ES-

MS (CHCl$_3$:MeOH (3:2) + formic acid): m/z = 1901.7, 1267.8, Calcd avg mass for

C$_{252}$H$_{256}$N$_{20}$Ni$_4$Zn: [M - Zn + 4H]$^{2+}$ = 1901.8, [M - Zn + 5H]$^{3+}$ = 1268.2. Hewlett-

Packard 2025 MALDI-TOF MS (all-*trans*-retinoic acid): m/z = 3861 (M$^+$). Time lag focusing MALDI-TOF MS: m/z = 3861 (M$^+$, 100%). Calcd avg mass for M$^+$ ($C_{252}H_{256}N_{20}Ni_4Zn$): 3865.

7.3.4 Nonaporphyrins

Star Nonaporphyrin, (Ni/Ni)$_4$-Zn-84.

$C_{444}H_{420}N_{36}Ni_8Zn$
Exact Mass: 6782.8091
Mol. Wt.: 6795.2654
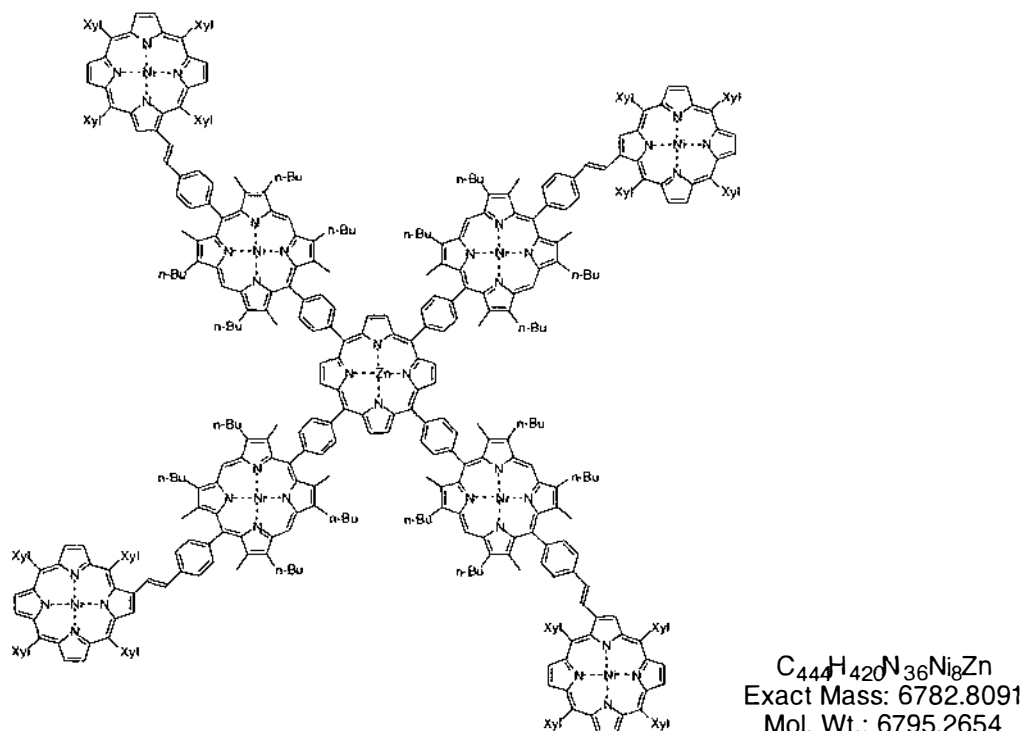
BF$_3$·OEt$_2$ (98.0 μL of 236 mM in CH$_2$Cl$_2$, 11.4 μmol, 0.2 eq) was added to a solution of **Ni/Ni-77** (94.9 mg, 58.0 μmol) and pyrrole (101 μL of 577 mM in CH$_2$Cl$_2$, 58.0 μmol, 1.0 eq) in dry degassed CH$_2$Cl$_2$ (5.8 mL) and EtOH (43.5 μL, 0.75%) under argon at RT (10^{-2} M). After 1.5 h, two new bands of higher R_f than starting material **Ni/Ni-77** were evident by TLC. *p*-Chloranil (21.6 mg, 89.2 μmol, 1.5 eq) was added and the solution refluxed for 1 h. After cooling the reaction to RT, excess Et$_3$N (200 μL, 1.4 mmol) was added and the solution stirred for 20 minutes. The crude product was then precipitated out with MeOH. To aid purification a solution of Zn(OAc)$_2$·2H$_2$O (13 mg, 59 μmol) in MeOH (2.0 mL) was added to a solution of the precipitate in CH$_2$Cl$_2$ (15 mL) at RT. After 15 min a solid was precipitated from CH$_2$Cl$_2$ with MeOH (twice). This resulting solid was dissolved in CH$_2$Cl$_2$ and filtered through a plug of silica gel. The solvent was

removed *in vacuo* and the residue column chromatographed (basic alumina, 37 mm$_{dia}$ x 100 mm, CH_2Cl_2). Recrystallisations from CH_2Cl_2/MeOH, CH_2Cl_2/hexane and CH_2Cl_2/MeOH gave **(Ni/Ni)$_4$-Zn-84** (21.6 mg, 22%) as a brick-red powder. ^{1}H NMR (270 MHz, CDCl$_3$, TMS): δ 1.168 (t, 24H, ^3J = 7.3 Hz, CH$_2$CH$_2$CH$_2$CH$_3$), 1.239 (t, 24H, ^3J = 7.3 Hz, CH$_2$CH$_2$CH$_2$CH$_3$), 1.686-1.944 (m, 32H, CH$_2$CH$_2$CH$_2$CH$_3$), 2.077-2.342 (m, 32H, CH$_2$CH$_2$CH$_2$CH$_3$), 2.455 (s, 24H, H$_{Me-TBMP}$), 2.538-2.594 (m, 72H, H$_{Me-Xyl}$), 2.632 (s, 24H, H$_{Me-Xyl}$), 3.019 (s, 24H, H$_{Me-TBMP}$), 3.737-4.055 (m, 32H, CH$_2$CH$_2$CH$_2$CH$_3$), 7.214 (d, 4H, ^3J = 15.9 Hz, H$_{ethenyl}$), 7.338 (s, 8H, H$_{p-Xyl}$), 7.375-7.428 (m, 10H, 8H$_{p-Xyl}$ + 2H$_{ethenyl}$), 7.463 (s, 2H, H$_{ethenyl}$), 7.582 and 7.888 (ABq, 16H, ^3J = 8.2, 8.2 Hz, H$_{styryl}$), 7.657 (s, 16H, H$_{o-Xyl}$), 7.724 (s, 16H, H$_{o-Xyl}$), 8.467 (d, 8H, ^3J = 7.9 Hz, H$_{o,m-Ar}$), 8.723-8.822 (m, 23H, 24H$_{\beta-pyrrolic}$ + 8H$_{o,m-Ar}$), 9.051 (s, 4H, H$_{3\,(\beta-pyrrolic)}$), 9.661 (br s, 16H, 8H$_{meso}$ + 8H$_{\beta-pyrrolic}$). *Assignments aided by COSY spectra.* UV-vis (CH$_2$Cl$_2$): λ$_{max}$ [nm] (ε x 10^{-3}) 412 sh (876), 434 (1671), 537 (156), 564 (152). Hewlett-Packard 2025 MALDI-TOF MS (all-*trans*-retinoic acid): m/z = 6791 (M$^+$, 100%). Time lag focusing MALDI-TOF MS: m/z = 6800 (M$^+$, 100%). Calcd avg mass for M$^+$ (C$_{444}$H$_{420}$N$_{36}$Ni$_8$Zn): 6795.

7.4 Chapter 4: Synthesis of "Sticky" Porphyrin Arrays

7.4.1 Trans-BMBEP

ZnBMBEP, Zn-88.

5,15-Bis(4'-methylcarboxyphenyl)-10,20-bis(4"-methoxyphenyl)porphyrinato zinc(II).

$C_{50}H_{36}N_4O_6Zn$
Exact Mass: 852.1926
Mol. Wt.: 854.2342
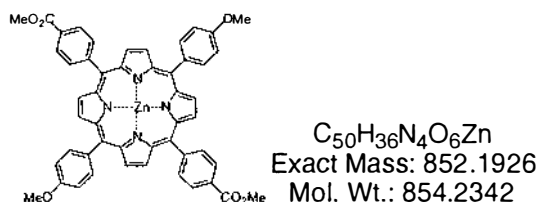
Methyl 4-formylbenzoate (2.50 g, 15.2 mmol) in CH_2Cl_2 (87 mL) was added drop wise over 1 h to a mixture of $Zn(OAc)_2 \cdot 2H_2O$ (4.33 g, 19.7 mmol) and DPM **91** (3.844 g, 15.25 mmol) in propanoic acid (216 mL) at 0°C. After stirring for 2 h at 0°C then 17.5 h at RT, the mixture was heated at reflux for 2 h. During the last hour, O_2 was bubbled through the refluxing solution. The volume was reduced *in vacuo* and the crude product was precipitated with hexane and then separated by filtration. The solid was then dissolved in CH_2Cl_2 and filtered (#2 sintered glass). The organic layer was then washed with dilute aq. ammonia before drying ($MgSO_4$) and removing the solvent *in vacuo*. This residue was then filtered through a plug of silica gel with $CHCl_3$ and the solvent again removed *in vacuo*. Recrystallisation from toluene/hexane (3 times), then from $CHCl_3$/hexane, gave **Zn-88** as purple crystalline solid (1.44 g, 22%). ^{1}H NMR (400 MHz, CDCl$_3$, TMS): δ 4.080 (s, 12H, 6H ArOCH$_3$ + 6H CO$_2$CH$_3$), 7.272 (d, 4H, ^3J = 8.8 Hz, ArH) , 8.115 (d, 4H, ^3J = 8.6 Hz, ArH), 8.296 and 8.403 (ABq, 8H, ^3J = 8.2, 8.3 Hz, ArH), 8.883 and 8.999 (ABq, 8H, ^3J = 4.7, 4.7 Hz, H$_{\beta\text{-pyrrolic}}$). UV-vis (CH$_2$Cl$_2$): λ_{max} [nm] (ε x 10^{-3}) 424 (470), 552 (21.0), 595 (6.93). FAB-LRMS: *m/z* (%, assignment) cluster at 851-859, 852 (100, M$^+$). HRMS: Calcd for M$^+$ ($C_{50}H_{36}N_4O_6Zn$): 852.1926, found: 852.2017.

CuBMBEP, Cu-88.

5,15-Bis(4'-methylcarboxyphenyl)-10,20-bis(4"-methoxyphenyl)porphyrinato copper(II).

$C_{50}H_{36}CuN_4O_6$
Exact Mass: 851.2031
Mol. Wt.: 852.3902
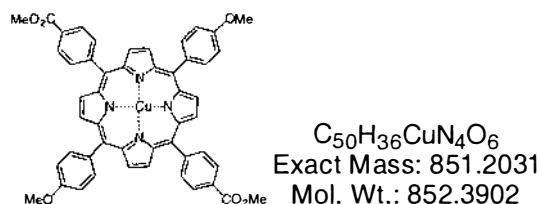
A mixture of ZnBMBEP **Zn-88** (440 mg, 468 μmol), $Cu(OAc)_2 \cdot H_2O$ (467 mg, 2.34 mmol, 5 eq) and conc. HCl (100 μL, > 2.2 eq) in acetone:MeOH (1:1, 50 mL) was heated to reflux for 1 h. The reaction mixture turned from green to red as metallation proceeded. The mixture was cooled to RT and the precipitate collected by filtration to give **Cu-88** as a purple/blue crystalline solid (360.6 mg, 90 %). UV-vis (CH_2Cl_2): λ_{max} [nm] (ε x 10^{-3}) 418 (461), 540 (21.9), 577 (3.71). FAB-LRMS: m/z (%, assignment) cluster at 851-856, 851 (100, M$^+$). HRMS: Calcd for M$^+$ ($C_{50}H_{36}N_4O_6Cu$): 851.1931, found: 851.1888.

BMBEP-CHO, 89.

2- and 3-formyl-(5,15-bis(4'-methylcarboxyphenyl)-10,20-bis(4"-methoxyphenyl))-porphyrin.

$C_{51}H_{38}N_4O_7$
Exact Mass: 818.2741
Mol. Wt.: 818.8702
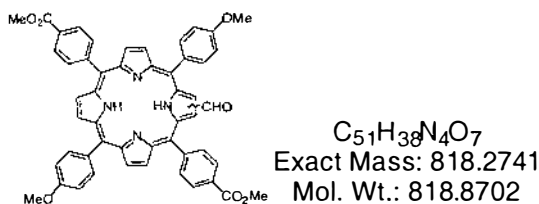
A Vilsmeier complex was prepared by adding $POCl_3$ (2.08 mL, 22.3 mmol) slowly to dry DMF (2.60 mL, 35.6 mmol) at 0°C under argon. After 35 min the viscous oil was added to a cold (0°C), stirred solution of **Cu-88** (300 mg, 352 μmol) in dry 1,2-DCE (24 mL) under argon. After stirring the mixture for 20 min it was warmed to RT over 20 min. The argon source was replaced with a drying tube ($CaCl_2$) and the reaction was heated to reflux for 7 h. On cooling to RT, conc. H_2SO_4 (4.5 mL) was added to the vigorously stirred mixture. After stirring for 10 min the mixture was poured onto a cold (0°C) solution of aqueous NaOH (6.2 g in 100 mL). $CHCl_3$ (100 mL) was added and the aqueous layer was decanted off. The organic layer was washed with sat. aq. $NaHCO_3$ ($\approx$ 100 mL) and then H_2O (100 mL). The organic layer was separated and

dried (MgSO$_4$). The residue was column chromatographed (silica, 27 mm$_{dia}$ x 150 mm, CH$_2$Cl$_2$:MeOH (200:1)). Recrystallisation from CHCl$_3$/MeOH gave the mixture **89** (162 mg, 56%) as a purple powder. *Selected data only:* ^{1}H NMR (270 MHz, CDCl$_3$, TMS): δ -2.57 (br s, NH), 9.314 (s, CHO). ^{1}H NMR (270 MHz, C$_6$D$_6$, TMS): δ -2.07 (s, NH), 9.537 (s, CHO), 9.623 (s, CHO). FAB-LRMS: *m/z* (%, assignment) cluster at 818-821, 819 (100, MH$^+$). Calcd for MH$^+$ (C$_{51}$H$_{39}$N$_4$O$_7$): 819.

DPM, 91.

5-(4'-Methoxyphenyl)dipyrrylmethane.
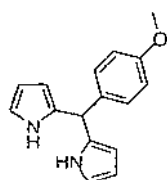
C$_{16}$H$_{16}$N$_2$O
Exact Mass: 252.1263
Mol. Wt.: 252.3111

p-Methoxybenzaldehyde **90** (4.00 g, 29.4 mmol) was added to pyrrole (143 mL, 2.06 mol, 70 eq) and the resulting solution degassed with argon for 10 min. TFA (226 μL, 2.94 mmol, 0.1 eq) was then added and the reaction stirred at RT. After 15 min, all of the aldehyde had been consumed, by TLC. The reaction was quenched with Et$_3$N (451 μL, 3.24 mmol, 0.11 eq) and excess pyrrole removed by vacuum distillation at 60°C. The residue was column chromatographed (silica, 37 mm$_{dia}$ x 200 mm, CH$_2$Cl$_2$:hexane:Et$_3$N (400:100:0.2)), collecting the first major fraction (R_f = 0.2, CH$_2$Cl$_2$:hexane (4:1)). The solvent was removed *in vacuo* to yield the title compound **91** as a pale yellow solid (4.57 g, 62% based on *p*-methoxybenzaldehyde). ^{1}H NMR (270 MHz, CDCl$_3$, TMS): δ 3.737 (s, 3H, ArOCH$_3$), 5.314 (s, 1H, H CH$_{methine}$), 5.825-5.874 (m, 2H, H$_{pyrrole}$), 6.084 -6.137 (m, 2H, H$_{pyrrole}$), 6.561-6.603 (m, 2H, H$_{pyrrole}$), 6.803 (d, 2H, ^3J = 8.8 Hz, ArH), 7.065 (d, 2H, ^3J = 8.6 Hz, ArH), 7.782 (br s, 2H, NH). ^{13}C NMR (68 MHz, CDCl$_3$, TMS): δ 43.72, 55.91, 107.64, 108.87, 114.49, 117.72 129.90, 133.44, 134.78, 158.91. FAB-LRMS: *m/z* (%, assignment) 252 (100, M$^+$). HRMS: Calcd for M$^+$ (C$_{16}$H$_{16}$N$_2$O): 252.1263, found: 252.1254. All spectral assignments are in agreement with the literature, and additional HRMS data is reported here.[140]

ZnBMBCP, Zn-92.

5,15-Bis(4'-carboxyphenyl)-10,20-bis(4"-methoxyphenyl)porphyrinato zinc(II).
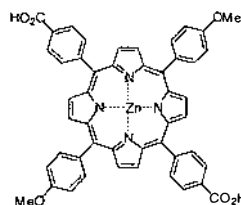
$C_{48}H_{32}N_4O_6Zn$
Exact Mass: 824.1613
Mol. Wt.: 826.1810

KOH (197 mg, 3.51 mmol, 15 eq per CO_2Me) in $MeOH{:}H_2O$ (10:1 22.0 mL) was added to a solution of bisester **Zn-88** (100.0 mg, 117 μmol) in THF (20 mL). The mixture was heated to reflux under N_2. After 5 h, the reaction was complete by TLC with the appearance of a single spot at lower R_f than the starting material. After cooling to RT, the reaction mixture was acidified with 2.0 M H_3PO_4 (1.8 mL). The aqueous layer was extracted with $CHCl_3$ ($\approx$ 50 mL) and carefully separated before removing the solvent *in vacuo*. The residue was dissolved in $CHCl_3{:}THF$ (1:1, 100 mL) and column chromatographed (silica, 45 mm$_{dia}$ x 65 mm, $CH_2Cl_2{:}AcOH$ (99:1)). Recrystallisation from THF/hexane gave bisacid **Zn-92** (94.1 mg, 97%) as a red solid. ^{1}H NMR (400 MHz, DMSO-d$_6$, TMS): δ 4.033 (s, 6H, ArOCH$_3$), 7.346 (d, 4H, ^3J = 8.7 Hz, H$_{3",5"}$) , 8.086 (d, 4H, ^3J = 8.6 Hz, H$_{2",6"}$), 8.297 and 8.362 (ABq, 8H, ^3J = 8.2, 8.2 Hz, H$_{2',6'\ and\ 3',5'}$), 8.769 and 8.834 (ABq, 8H, ^3J = 4.7, 4.7 Hz, H$_{3,7,13,17\ and\ 2,8,12,18\ \beta\text{-pyrrolic}}$), 13.3 (br s, CO$_2$H). *Assignments aided by long range COSY spectra.* UV-vis (THF): λ_{max} [nm] (ε x 10^{-3}) 426 (472), 557 (20.9), 599 (9.38). FAB-LRMS: *m/z* (%, assignment) cluster at 824-830, 824 (100, M$^+$). HRMS: Calcd for M$^+$ (C$_{48}$H$_{32}$N$_4$O$_6$Zn): 824.1613, found: 824.1637.

7.4.2   T3EPps

T3EP, 93.

5,10,15,20-Tetra(3'-methoxycarbonylphenyl)porphyrin.
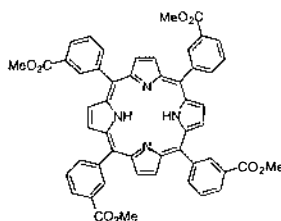
$C_{52}H_{38}N_4O_8$
Exact Mass: 846.2690
Mol. Wt.: 846.8803

To a solution of methyl 3-formylbenzoate **27** (1.16 g, 7.09 mmol) and pyrrole (492 μL, 7.09 mmol) in dry degassed CH_2Cl_2 (709 mL) under N_2 at RT was added $BF_3 \cdot OEt_2$ (75 μL, 710 μmol, 0.1 eq). After stirring for 3 h, p-chloranil (1.31 g, 0.75 eq) was added and the solution heated at reflux for 2 h. Excess Et_3N (3.0 mL) was added and the reaction cooled to RT. The solution was column chromatographed (silica, 80 mm_{dia} x 75 mm, CH_2Cl_2:Et_2O (49:1)) collecting a red band. Recrystallisation from CH_2Cl_2/MeOH gave porphyrin **93** (647 mg, 43%) as a purple powder. ^{1}H NMR and UV-vis data is consistent with that in the literature.[144,145] Additional ^{13}C NMR data has been supplied. ^{1}H NMR (270 MHz, $CDCl_3$, TMS): δ -2.795 (s, 2H, NH), 3.988 (s, 12H, CO_2CH_3), 7.852 (t, 4H, ^3J = 7.6 Hz, $H_{5'}$), 8.404 (d of t, 4H, ^3J = 8.2 Hz, ^4J = 1.2 Hz, $H_{4' \, or \, 6'}$), 8.490 (d of t, 4H, ^3J = 7.9 Hz, ^4J = 1.2 Hz, $H_{6' \, or \, 4'}$), 8.803 (s, 8H, $H_{\beta\text{-pyrrolic}}$), 8.90 (t, 4H, ^4J = 1.2 Hz, $H_{2'}$). ^{13}C NMR (68 MHz, $CDCl_3$): δ 52.37 (CO_2CH_3), 119.15, 126.86, 128.86, 129.09, 134.81, 138.34, 142.15, 167.09 (CO_2CH_3). UV-vis (CH_2Cl_2): λ_{max} [nm] (ε x 10^{-3}) 418 (440), 515 (21.1), 549 (7.62), 589 (6.23), 645 (3.61).

CuT3EP, Cu-93.

5,10,15,20-Tetra(3'-methoxycarbonylphenyl)porphyrinato copper(II).

$C_{52}H_{36}CuN_4O_8$
Exact Mass: 907.1929
Mol. Wt.: 908.4104
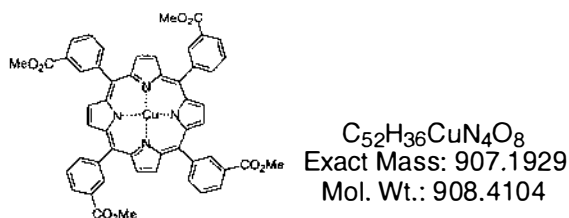
A solution of $Cu(OAc)_2 \cdot H_2O$ (200 mg, 1.06 mmol, 1.2 eq) in MeOH (25 mL) was added to a refluxing solution of T3EP **93** (750 mg, 886 μmol) in $CHCl_3$ (100 mL). The reaction was adjudged complete by TLC after 1 h. On cooling to RT, the volume was reduced *in vacuo*. Recrystallisation from $CHCl_3$/MeOH (twice) quantitatively gave **Cu-93** (828 mg) as a red powder. UV-vis (CH_2Cl_2): λ_{max} [nm] (ε x 10^{-3}) 415 (424), 539 (23.3). FAB-LRMS: m/z (%, assignment) cluster at 907-912, 907 (97, M^+). HRMS: Calcd for M^+ ($C_{52}H_{36}N_4O_8Cu_1$): 907.1829, found: 907.1846.

ZnT3EP, Zn-93.

5,10,15,20-Tetra(3'-methoxycarbonylphenyl)porphyrinato zinc(II).

$C_{52}H_{36}N_4O_8Zn$
Exact Mass: 908.1825
Mol. Wt.: 910.2544
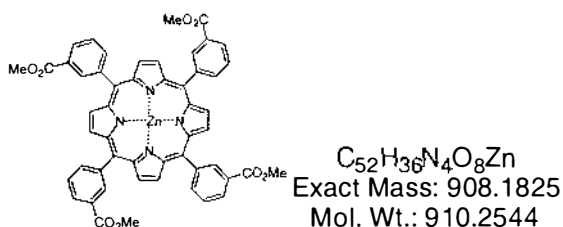
A solution of $Zn(OAc)_2 \cdot 2H_2O$ (34.2 mg, 156 μmol, 1.2 eq) in MeOH (2.0 mL) was added to a refluxing solution of ester **93** (110 mg, 130 μmol) in $CHCl_3$ (20 mL). After 1 h, TLC analysis indicated metallation was complete. On cooling to RT, the solvent was removed *in vacuo*. The residue was then column chromatographed (silica, 30 mm$_{dia}$ x 60 mm, CH_2Cl_2:Et_2O (25:1)). Recrystallisation from CH_2Cl_2/hexane quantitatively gave porphyrin **Zn-93** (118 mg, 100%) as a purple powder. ^{1}H NMR (400 MHz, CDCl$_3$, 40°C, TMS): δ 3.909 (s, 12H, CO$_2$CH$_3$), 7.805 (t, 4H, ^3J = 7.7 Hz, H$_{5'}$), 8.394 (app t, 8H, ^3J = 7.7 Hz, H$_{4',6'}$), 8.83-8.88 (m, 12H, 4H$_{2'}$ + 8H$_{\beta\text{-pyrrolic}}$). UV-vis (CH_2Cl_2): λ_{max} [nm] (ε x 10^{-3}) 422 (471), 551 (21.1), 593 (4.01). FAB-LRMS: m/z (%, assignment) cluster at 908-914, 908 (100, M$^+$). HRMS: Calcd for M$^+$ (C$_{52}$H$_{36}$N$_4$O$_8$Zn): 908.1825, found: 908.1820. *^{1}H NMR and UV-vis is consistent with that reported in the literature[145], extra FAB-HRMS data is presented here.*

T3EPps, 94.

(5,10,15,20-Tetra(3'-methoxycarbonylphenyl)porphyrin-2-yl)methyltriphenyl-phosphonium chloride.

$C_{71}H_{54}ClN_4O_8P$
Exact Mass: 1156.3368
Mol. Wt.: 1157.6371
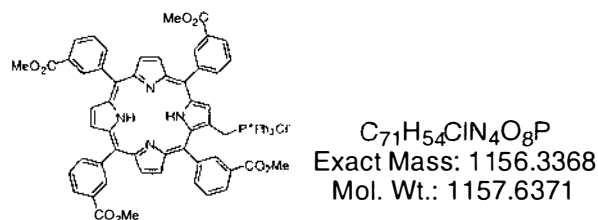
Chloromethyl porphyrin **98** (331 mg, 369 μmol) and PPh$_3$ (1.94 g, 7.38 mmol, 20 eq) in $CHCl_3$ (16 mL) were heated to reflux under argon. The reaction was adjudged complete by TLC after 5 h with the formation of a single spot of higher polarity than the starting material. The solvent was removed *in vacuo* and the residue column chromatographed (silica, 37 mm$_{dia}$ x 60 mm, CH_2Cl_2:MeOH (32:1)) to give the title phosphonium salt **94** (423 mg, 99%) as a purple solid. ^{1}H NMR (400 MHz, C$_6$D$_6$, 85°C, TMS): δ -2.213 (br

s, 2H, NH), 3.72-3.82 (m, 12H, CO$_2$CH$_3$), 4.8 (br s, CH$_2$), 6.6-8.8 (m, 38H), 9.128 (br d, 2H, ^3J = 13 Hz). ^{31}P NMR (162 MHz, C$_6$D$_6$, H$_3$PO$_4$): ≈ 22°C = 24.29, 23.95 ppm, 85°C = 24.34 ppm. UV-vis (CH$_2$Cl$_2$): λ_{max} [nm] (ε x 10^{-3}) 425 (391), 520 (21.7), 553 (9.70), 595 (8.80), 651 (7.77). FAB-LRMS: m/z (%, assignment) 1121 (100, [M – Cl]$^+$), 859 (75, [M – (P$^+$Ph$_3$Cl$^-$)]$^+$). HRMS (2-nitrophenyl octyl ether matrix): Calcd for [M – Cl]$^+$ (C$_{71}$H$_{54}$N$_4$O$_8$P$_1$): 1121.3679, found: 1121.3632.

ZnT3CP, Zn-95.

5,10,15,20-Tetra(3'-carboxyphenyl)porphyrinato zinc(II).

C$_{48}$H$_{28}$N$_4$O$_8$Zn
Exact Mass: 852.1199
Mol. Wt.: 854.1481
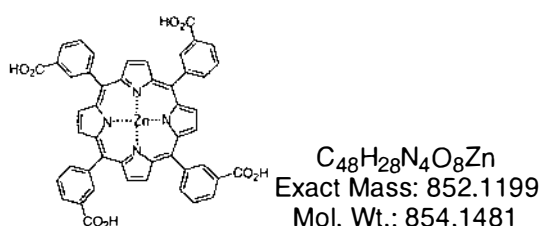
Zn-93 (100.0 mg, 110 μmol) and KOH (369 mg, 6.58 mmol, 15 eq per CO$_2$Me) in MeOH:H$_2$O (30:3.0 mL) was heated to reflux under N$_2$. The reaction was deemed complete after 2.5 h by TLC, with the appearance of a single spot of higher polarity than the starting material. After cooling to RT, the reaction mixture was acidified with 2.0 M H$_3$PO$_4$ (3.3 mL) and the volume reduced *in vacuo*. The resulting red precipitate was separated by filtration and washed with H$_2$O (≈ 50 mL) then dried *in vacuo* at 60°C to give **Zn-95** (90.7 mg, 97%) as a red solid. ^{1}H NMR (400 MHz, DMSO-d$_6$, TMS): δ 7.948 (t, 4H, ^3J = 7.7 Hz, H$_{5'}$), 8.39-8.49 (m, 8H, H$_{4',6'}$), 8.70-8.72 (m, 4H, H$_{2'}$), 8.791 (s, 8H, H$_{\beta\text{-pyrrolic}}$), 13.27 (br s, 4H, CO$_2$H). UV-vis (THF): λ_{max} [nm] (ε x 10^{-3}) 425 (483), 557 (26.3), 596 (7.70). FAB-LRMS: m/z (%, assignment) cluster at 852-857, 852 (100, M$^+$). HRMS: Calcd for M$^+$ (C$_{48}$H$_{28}$N$_4$O$_8$Zn): 852.1199, found: 852.1208.

T3EP-CHO, 96.

2-Formyl-5,10,15,20-tetra(3'-methoxycarbonylphenyl)porphyrin.

C$_{53}$H$_{38}$N$_4$O$_9$
Exact Mass: 874.2639
Mol. Wt.: 874.8904
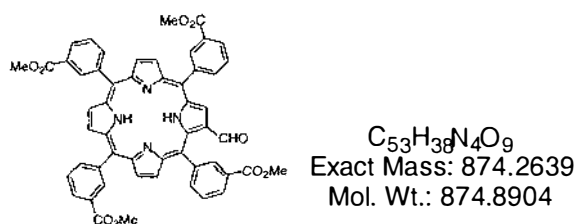
A Vilsmeier complex was prepared by adding $POCl_3$ (796 μL) slowly to dry DMF (996 μL) at 0°C under argon. After 35 min the viscous oil was added to a cold (0°C), stirred solution of **Cu-93** (100 mg, 118 μmol) in dry 1,2-DCE (8.5 mL) under argon. After for 20 min, the reaction was warmed to RT. The argon source was replaced with a drying tube ($CaCl_2$) and the reaction was heated to reflux for 24 h. On cooling to RT, conc. H_2SO_4 (1.41 mL) was added to the vigorously stirred mixture. After stirring for 15 min the mixture was diluted with H_2O (70 mL) and extracted into CH_2Cl_2 (70 mL). The aqueous layer was separated and the organic layer washed with H_2O (2 x 70 mL) then sat. aq. $NaHCO_3$ (70 mL). The organic layer was dried ($MgSO_4$) and the solvent removed *in vacuo*. The residue was column chromatographed (silica, 35 mm_{dia} x 85 mm), first eluting with CH_2Cl_2:Et_2O (49:1) to give demetallated starting material **93** (16 mg, 17%), then CH_2Cl_2:Et_2O (19:1) to give the title compound **96** (67.3 mg, 70%, recrystallised from CH_2Cl_2/MeOH) as a purple powder. ^{1}H NMR (400 MHz, $CDCl_3$, TMS): δ -2.566 (br s, 2H, NH), 3.999 (s, 12H, CO_2CH_3), 7.83-7.90 (m, 4H, $H_{5'}$), 8.37-8.55 (m, 8H, $H_{4',6'}$), 8.730 (s, 2H, $H_{\beta\text{-pyrrolic}}$), 8.80-8.98 (m, 8H, $4H_{\beta\text{-pyrrolic}}$ + $4H_{2'}$), 9.325 (s, 1H, CHO [coupled to δ 189]), 9.347 (s, 1H, $H_{3,\ \beta\text{-pyrrolic}}$ [coupled to δ 137]). ^{1}H NMR (400 MHz, C_6D_6, 70°C, TMS): δ -2.013 (br s, 2H, NH), 3.68-3.73 (m, 12H, CO_2CH_3), 7.42-7.57 (m, 4H, $H_{5'}$), 8.10-8.23 (m, 4H, $H_{4'\text{ or }6'}$), 8.50-8.60 (m, 4H, $H_{6'\text{ or }4'}$), 8.76-8.81 (m, 6H, $H_{\beta\text{-pyrrolic}}$), 9.13-9.19 (m, 4H, $H_{2'}$), 9.656 (s, 1H, $H_{3,\ \beta\text{-pyrrolic}}$ [coupled to δ 137]), 9.719 (s, 1H, CHO [coupled to δ 187]). *Assignments aided by ^1H-^{13}C HETCOR and COSY spectra.* UV-vis (CH_2Cl_2): λ_{max} [nm] (ε x 10^{-3}) 431 (315), 525 (17.7), 566 (6.75), 604 (5.54), 662 (6.43). FAB-LRMS: *m/z* (%, assignment) cluster at 874-878, 875 (100, MH^+). HRMS: Calcd for MH^+ ($C_{53}H_{39}N_4O_9$): 875.2717, found: 875.2689.

T3EP-CH$_2$OH, 97.

2-Hydroxymethyl-5,10,15,20-tetra(3'-methoxycarbonylphenyl)porphyrin.
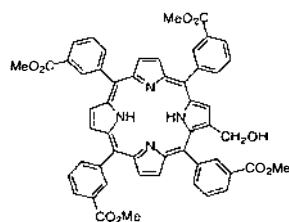
$C_{53}H_{40}N_4O_9$
Exact Mass: 876.2795
Mol. Wt.: 876.9063

A mixture of porphyrin aldehyde **96** (500 mg, 572 μmol) and $NaBH_4$ (491 mg, 13.0 mmol, 23 eq) in THF (42 mL) and H_2O (850 μL) was stirred at RT. After 45 min TLC

analysis indicated that the starting material had been consumed with the appearance of a new more polar red band. Excess H_2O ($\approx$ 100 mL) was added and the aqueous layer extracted with CH_2Cl_2 (250 mL). The organic layer was washed with H_2O (250 mL), sat. aq. $NaHCO_3$ (250 mL), then separated and dried ($MgSO_4$) and the solvent removed *in vacuo*. The residue was column chromatographed (silica, 45 mm$_{dia}$ x 55 mm, CH_2Cl_2:Et_2O (9:1)). Recrystallisation from CH_2Cl_2/hexane gave the alcohol **97** (475 mg, 95%) as a purple powder. ^{1}H NMR (400 MHz, $CDCl_3$, 55°C, TMS): δ -2.698 (br s, 2H, NH), 1.888 (br s, 1H, CH_2OH), 3.95-3.97 (m, 12H, CO_2CH_3), 4.895 (br s, 2H, CH_2OH), 7.79-7.84 (m, 4H, H$_{5'}$), 8.10-8.54 (m, 10H), 8.68-8.77 (m, 6H), 8.85-8.87 (m, 4H). ^{1}H NMR (400 MHz, C_6D_6, 75°C, TMS): δ -2.160 (br s, 2H, NH), 1.163 (br s, 1H, CH_2OH), 3.59-3.62 (m, 12H, CO_2CH_3), 4.670 (br s, 2H, CH_2OH), 7.32-7.46 (m, 4H, H$_{5'}$), 7.931(br d, 1H, ^3J = 7.3 Hz, H$_{4' \text{ or } 6'}$), 8.154 (br d, 2H, ^3J = 7.5 Hz, H$_{6' \text{ or } 4'}$), 8.204 (br d, 1H, ^3J = 7.1 Hz, H$_{4' \text{ or } 6'}$), 8.42-8.53 (m, 5H), 8.71-8.79 (m, 5H), 8.889 (br s, 1H), 9.03-9.11(m, 4H). UV-vis (CH_2Cl_2): λ_{max} [nm] (ϵ x 10^{-3}) 419 (420), 515 (20.5), 548 (6.09), 590 (5.75), 650 (5.01). FAB-LRMS: *m/z* (%, assignment) cluster at 876-880, 876 (87, M$^+$). HRMS: Calcd for M$^+$ ($C_{53}H_{40}N_4O_9$): 876.2795, found: 876.2776.

T3EP-CH$_2$Cl, 98.

2-Chloromethyl-5,10,15,20-tetra(3'-methoxycarbonylphenyl)porphyrin.

$C_{53}H_{39}ClN_4O_8$
Exact Mass: 894.2456
Mol. Wt.: 895.3516
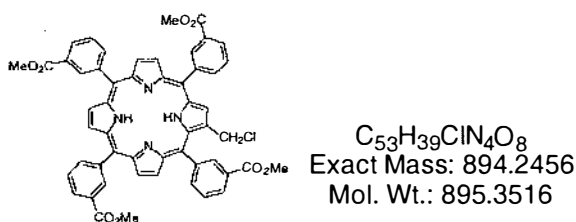
$SOCl_2$ (170 μL, 2.3 mmol) was added to a solution of alcohol **97** (490 mg, 559 μmol) and dry pyridine (0.43 mL, 5.3 mmol) in dry CH_2Cl_2 (60 mL) at 0°C under argon. After stirring at 0°C for 15 min, the solution was warmed to RT. After 105 min no starting material remained by TLC and a new red band of lower polarity was evident. The reaction was poured into $CHCl_3$ (100 mL) and stirred for 15 min. The resulting green solution was washed with H_2O (5 x 70 mL) then sat. aq. $NaHCO_3$ (70 mL). The red-brown organic layer was separated and dried ($MgSO_4$) and the solvent removed *in vacuo*. The residue was column chromatographed (silica, 45 mm$_{dia}$ x 75 mm, CH_2Cl_2:Et_2O (49:1)) to give the title compound **98** (350 mg, 70%) as a purple solid. ^{1}H

NMR (400 MHz, C_6D_6, 75°C, TMS): δ -2.213 (br s, 2H, NH), 3.58-3.62 (m, 12H, CO_2CH_3), 4.675 (s, 2H, CH_2Cl), 7.35-7.46 (m, 4H, $H_{5'}$), 8.05-8.16 (m, 4H, $H_{4' \, or \, 6'}$), 8.42-8.49 (m, 4H, $H_{6' \, or \, 4'}$), 8.529 (d, 1H, ^3J = 4.8 Hz, $H_{\beta\text{-pyrrolic}}$), 8.675 (d, 1H, ^3J = 4.8 Hz, $H_{\beta\text{-pyrrolic}}$), 8.69-8.73 (m, 4H, $H_{\beta\text{-pyrrolic}}$), 8.96-9.07 (m, 5H, $4H_{2'}$ + $1H_{3, \, \beta\text{-pyrrolic}}$). *Assignments aided by COSY spectra.* UV-vis (CH_2Cl_2): λ_{max} [nm] (ε x 10^{-3}) 420 (404), 516 (18.0), 548 (6.44), 592 (5.03), 642 (2.28). FAB-LRMS: m/z (%, assignment) cluster at 894-899, 894 (75, M^+). HRMS: Calcd for M^+ ($C_{53}H_{39}Cl_1N_4O_8$): 894.2456, found: 894.2447.

7.4.3   T3EP Arrays

Diporphyrins

ZnT3CP–ZnTXP diporphyrin, Zn_2-99.

1-(*Trans*-2'-(2''-(5'',10'',15'',20''-Tetra(3'''-carboxyphenyl)porphyrinato zinc(II))yl)ethen-1'-yl)-4-(*trans*-2''''-(2'''''-(5''''',10''''',15''''',20'''''-tetrakis(3''''''',5'''''''-dimethylphenyl)-porphyrinato zinc(II))yl)ethen-1''''-yl)benzene.
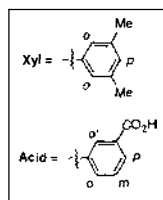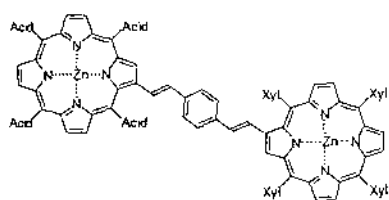
$C_{110}H_{78}N_8O_8Zn_2$
Exact Mass: 1766.4526
Mol. Wt.: 1770.6254

KOH (38.0 mg, 677 μmol, 15 eq per CO_2Me) in $MeOH:H_2O$ (10:1, 4.0 mL) was added to a solution of porphyrin ester Zn_2-102 (20.6 mg, 11.3 μmol) in THF (2.0 mL). The mixture was refluxed for 6.5 h under N_2. On cooling to RT the solvent was removed *in vacuo*. The residue was dissolved in a solution of H_2O (10 mL) and $H_3PO_{4 \, (aq)}$ (360 μL, 2.0 M, 16 eq), forming a dark green precipitate. The pH of the aqueous layer was ≈ 2. The precipitate was washed with H_2O (10 mL) then dried *in vacuo* at 60°C giving acid Zn_2-99 (20.1 mg, 100%) as a purple solid. ^{1}H NMR (400 MHz, acetone-d_6, TMS): δ 2.619 (s, 12H, H_{Me-Xyl}), 2.655 (s, 6H, H_{Me-Xyl}), 2.695 (s, 3H, H_{Me-Xyl}), 2.738 (s, 3H, H_{Me-Xyl}), 7.09-7.54 (m, 12H, $4H_{ethenyl}$ + $4H_{p-Xyl}$ + $4H_{styryl}$), 7.85-7.89 (m, 8H, H_{o-Xyl}), 7.95-8.03 (m, 3H, H_{m-Acid}), 8.14-8.17 (m, 1H, H_{m-Acid}), 8.50-8.58 (m, 7H, $H_{o,p-Acid}$), 8.80-8.93 (m, 17H, $H_{o'-Acid}$ + $H_{\beta\text{-pyrrolic}}$ + $H_{o \, or \, p-Acid}$), 9.170 (s, 2H, $H_{o'-Acid}$ or $H_{\beta\text{-pyrrolic}}$). From the COSY

spectrum the multiplet at 7.09-7.54 ppm can be assigned as 7.116 and 7.432 (ABq, ^3J = 18, 18 Hz, $H_{ethenyl}$), 7.160 and 7.339 (ABq, ^3J = 16 Hz, $H_{ethenyl}$), 7.253 and 7.312 (ABq, ^3J = 8.1 Hz, H_{styryl}), 7.498 (s, H_{p-Xyl}), 7.536 (s, 1H, H_{p-Xyl}). UV-vis (THF): λ_{max} [nm] (ε x 10^{-3}) 434 (353), 569 (50.8), 608 (35.2). FAB-LRMS: m/z (%) cluster at 1766-1777, 1771 (75, M$^+$). HRMS: Calcd for M$^+$ ($C_{110}H_{78}N_8O_8Zn_2$): 1766.4526, found: 1766.4581.

ZnT3CP-ZnT3CP diporphyrin, Zn$_2$-100.

1,4-Bis(*trans*-2'-(2"-(5",10",15",20"-tetra(3'''-carboxyphenyl)porphyrinato zinc(II))yl)-ethen-1'-yl)benzene.
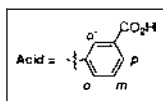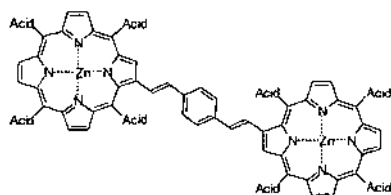
$C_{106}H_{62}N_8O_{16}Zn_2$
Exact Mass: 1830.2867
Mol. Wt.: 1834.4508

KOH (102 mg, 1.82 mmol, 19 eq CO$_2$Me) in MeOH:H$_2$O (10:1, 10.0 mL) was added to a solution of ester **Zn$_2$-103** (23.2 mg, 11.9 μmol) in THF (4.0 mL). The mixture was heated to reflux for 4.5 h under N$_2$. On cooling to RT the solvent was removed *in vacuo*. The residue was dissolved in H$_2$O (10 mL) and H$_3$PO$_{4\,(aq)}$ (910 μL, 2.0 M, 19 eq) added, forming a dark green precipitate. The pH of the aqueous layer was $\approx$ 2. The precipitate was washed with H$_2$O (10 mL) then dried *in vacuo* at 60°C to give porphyrin acid **Zn$_2$-100** (19.5 mg, 89%) as a purple solid. ^{1}H NMR (400 MHz, acetone-d$_6$, TMS): δ 7.03-7.11 (m, 2H), 7.220 (br s, 4H, H_{styryl}), 7.414 (app d, 2H, ^3J = 16.3 Hz, $H_{ethenyl}$), 7.90-8.20 (m, 8H, H_{m-Acid}), 8.43-8.54 (m, 16H, $H_{o,p-Acid}$), 8.74-8.96 (m, 18H), 9.04-9.06 (m, 2H), 9.167 (br s, 2H). *Assignments H_{m-Acid} and $H_{o,p-Acid}$ aided by COSY spectra.* UV-vis (THF): λ_{max} [nm] (ε x 10^{-3}) 433 (300), 568 (43.4), 608 (30.0). FAB-LRMS: m/z (%) cluster at 1829-1840, 1834 (10, M$^+$). HRMS: Calcd for M$^+$ ($C_{106}H_{62}N_8O_{16}Zn_2$): 1830.2867, found: 1830.2913.

T3EP–=–PhCHO "Building Block A", 101.

4-(*Trans*-2'-(5'',10'',15'',20''-Tetra(3'''-methoxycarbonylphenyl)porphyrin-2''-yl)ethen-1'-yl)benzaldehyde
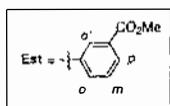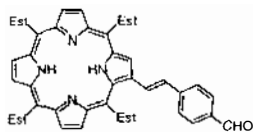
$C_{61}H_{44}N_4O_9$
Exact Mass: 976.3108
Mol. Wt.: 977.0236

A solution of T3EPps **94** (150.0 mg, 130 μmol) and terephthaldicarboxaldehyde **22** (86.9 mg, 648 μmol, 5.0 eq) in $CHCl_3$ (8.0 mL) was heated to reflux under N_2. DBU (58 μL, 3.0 eq) was added. After 20 min, TLC analysis indicated all **94** had been consumed. The solvent was removed *in vacuo* and the residue column chromatographed (silica, 37 mm$_{dia}$ x 65 mm, CH_2Cl_2:Et_2O (1:0 to 24:1)) collecting the major red/brown band. Recrystallisation from CH_2Cl_2/MeOH gave *trans*-**101** (113.4 mg, 90%) as a purple solid. ^{1}H NMR (400 MHz, $CDCl_3$, 70°C, TMS): δ -2.488 (br s, 2H, NH), 3.880 (s, 3H, CO_2CH_3), 3.96-3.99 (m, 9H, CO_2CH_3), 7.051 and 7.209 (ABq, 2H, ^3J = 16.0, 16.0 Hz, H$_{ethenyl}$), 7.303 (d, 2H, ^3J = 8.1 Hz, H$_{styryl}$), 7.76-7.89 (m, 6H, 4H$_{m-Est}$ + 2H$_{styryl}$), 8.24-8.47 (m, 8H, H$_{o,p-Est}$), 8.650 (d, 1H, ^3J = 4.9 Hz, H$_{\beta-pyrrolic}$), 8.70-8.75 (m, 5H, H$_{\beta-pyrrolic}$), 8.85-8.90 (m, 5H, 1H$_{\beta-pyrrolic}$ + 4H$_{o'-Est}$), 10.010 (s, 1H, CHO). *Assignments aided by COSY spectra.* UV-vis (CH_2Cl_2): λ_{max} [nm] (ϵ x 10^{-3}) 429 (218), 524 (19.8), 564 (11.3), 599 (7.63), 656 (2.54). FAB-LRMS: *m/z* (%) cluster at 976-979, 977 (100, M$^+$). HRMS: Calcd for M$^+$ ($C_{61}H_{44}N_4O_9$): 976.3108, found: 976.3109.

T3EP–TXP diporphyrin, 102.

1-(*Trans*-2'-(5'',10'',15'',20''-Tetra(3'''-methoxycarbonylphenyl)porphyrin-2''-yl)ethen-1'-yl)-4-(*trans*-2''''-(5'''''',10'''''',15'''''',20''''''-tetrakis(3'''''',5''''''-dimethylphenyl)porphyrin-2''''''-yl)ethen-1''''-yl)benzene.
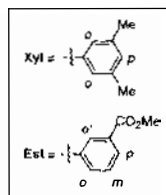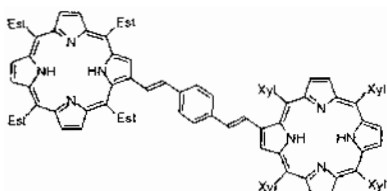
$C_{114}H_{90}N_8O_8$
Exact Mass: 1698.6882
Mol. Wt.: 1699.9835

A solution of T3EP building block **101** (32.8 mg, 33.6 μmol) and TXPps **5** (52.2 mg, 50.4 μmol, 1.5 eq) in $CHCl_3$ (4.0 mL) was heated to reflux under N_2. DBU (22.6 μL, 3.0 eq per **5**) in $CHCl_3$ (660 μL) was added at 220 μL per h via a syringe pump. On

cooling to RT the solvent was removed *in vacuo* and the residue column chromatographed (silica, 37 mm$_{dia}$ x 90 mm, CH_2Cl_2:Et_2O (50:1)). The major brown band was collected and the solvent removed *in vacuo*. Recrystallisation from CH_2Cl_2/MeOH gave *trans*-**102** (54.7 mg, 91%) as a purple powder. ^1H NMR (400 MHz, $CDCl_3$, TMS): δ -2.578 (br s, 4H, NH), 2.61-2.67 (m, 24H, H$_{Me-Xyl}$), 3.93-4.07 (m, 12H, CO_2CH_3), 6.964 and 7.338 (ABq, 2H, ^3J = 16.4, 15.9 Hz, H$_{ethenyl}$), 7.078 and 7.354 (ABq, 2H, ^3J = 16.0, 16.0 Hz, H$_{ethenyl}$), 7.207 and 7.295 (ABq, 4H, ^3J = 8.1, 8.1 Hz, H$_{styryl}$), 7.409 (s, 2H, H$_{p-Xyl}$), 7.483 (s, 1H, H$_{p-Xyl}$), 7.651 (s, 1H, H$_{p-Xyl}$), 7.84-7.99 (m, 12H, 4H$_{m-Est}$ + 8H$_{o-Xyl}$), 8.36-8.96 (m, 25H, H$_{o,o',p-Est \; and \; \beta-pyrrolic}$), 9.168 (s, 1H, H$_{o'-Est \; or \; \beta-pyrrolic}$). ^1H NMR (400 MHz, C_6D_6, TMS, selected data only): δ -1.975 (br s, 2H, NH), -1.653 (br s, 2H, NH). *Assignments aided by COSY spectra.* UV-vis (CH_2Cl_2): λ$_{max}$ [nm] (ε x 10^{-3}) 426 (381), 523 (55.8), 574 (38.1), 601 (28.0), 660 (6.06). FAB-LRMS: *m/z* (%) cluster at 1699-1704, 1700 (100, M$^+$). HRMS: Calcd for M$^+$ ($C_{114}H_{90}N_8O_8$): 1698.6882, found: 1698.6795.

ZnT3EP–ZnTXP diporphyrin, Zn$_2$-102.

1-(*Trans*-2'-(2''-(5'',10'',15'',20''-Tetra(3'''-methoxycarbonylphenyl)porphyrinato zinc(II))yl)ethen-1'-yl)-4-(*trans*-2''''-(2'''''-(5''''',10''''',15''''',20'''''-tetrakis(3''''''',5'''''''-dimethylphenyl)porphyrinato zinc(II))yl)ethen-1''''-yl)benzene.

$C_{114}H_{86}N_8O_8Zn_2$
Exact Mass: 1822.5152
Mol. Wt.: 1826.7318
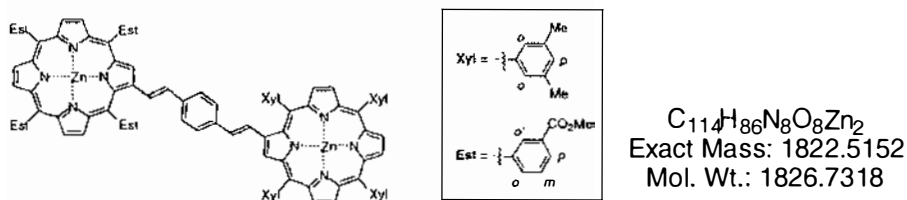
A solution of $Zn(OAc)_2$·$2H_2O$ (14.1 mg, 64.1 μmol, 2.4 eq) in MeOH (1.0 mL) was added to a solution of diporphyrin **102** (45.4 mg, 26.7 μmol) in $CHCl_3$ (10 mL) with stirring at RT. After 1 h, TLC analysis indicated all **102** had been consumed with the appearance of a new band of higher polarity than the starting material. The solvent was removed *in vacuo* and the residue column chromatographed (silica, 30 mm$_{dia}$ x 80 mm, CH_2Cl_2:Et_2O (50:1)). The major red/brown band was collected and the solvent removed *in vacuo*. Recrystallisation from CH_2Cl_2/MeOH gave **Zn$_2$-102** (29.2 mg, 60%) as a purple powder. ^1H NMR (400 MHz, $CDCl_3$, TMS): δ 2.61-2.66 (m, 24H, H$_{Me-Xyl}$), 3.92-3.97 (m, 12H, CO_2CH_3), 6.968 (d, 1H, ^3J = 15.0 Hz, H$_{ethenyl}$), 7.095 (d, 1H, ^3J = 15.9 Hz, H$_{ethenyl}$), 7.184 (d, 2H, ^3J = 8.0 Hz, H$_{styryl}$), 7.26-7.33 (m, 4H, 2H$_{ethenyl}$ + 2H$_{styryl}$), 7.410 (s,

2H, $H_{p\text{-Xyl}}$), 7.478 (s, 1H, $H_{p\text{-Xyl}}$), 7.632 (s, 1H, $H_{p\text{-Xyl}}$), 7.81-7.97 (m, 12H, $4H_{m\text{-Est}}$ + $8H_{o\text{-Xyl}}$), 8.40-8.50 (m, 7H, $H_{o,p\text{-Est}}$), 8.641 (br d, 1H, ^3J = 8.0 Hz, $H_{o \text{ or } p\text{-Est}}$), 8.80-8.98 (m, 16H, $H_{o'\text{-Est}}$ + $H_{\beta\text{-pyrrolic}}$), 9.034 (s, 1H, $H_{o'\text{-Est}}$ or $H_{\beta\text{-pyrrolic}}$), 9.168 (s, 1H, $H_{o'\text{-Est}}$ or $H_{\beta\text{-pyrrolic}}$). *Assignments aided by COSY spectra.* UV-vis (CH$_2$Cl$_2$): λ_{max} [nm] (ε x 10^{-3}) 430 (382), 563 (51.2), 604 (36.4). FAB-LRMS: *m/z* (%) cluster at 1822-1831, 1827 (100, M$^+$). HRMS: Calcd for M$^+$ (C$_{114}$H$_{86}$N$_8$O$_8$Zn$_2$): 1822.5152, found: 1822.5235.

T3EP–T3EP diporphyrin, 103.

1,4-Bis(*trans*-2'-(5",10",15",20"-tetra(3'''-methoxycarbonylphenyl)porphyrin-2"-yl)ethen-1'-yl)benzene.
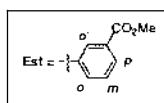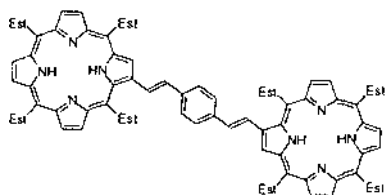
$C_{114}H_{82}N_8O_{16}$
Exact Mass: 1818.5849
Mol. Wt.: 1819.9152

A solution of porphyrin building block **101** (30.0 mg, 30.7 μmol) and T3EPps **94** (42.6 mg, 36.8 μmol, 1.2 eq) in CHCl$_3$ (3.0 mL) was heated to reflux under N$_2$. DBU (5.5 μL, 1.2 eq) was added and reflux continued for 60 min. On cooling to RT, the solvent was removed *in vacuo* and the residue column chromatographed (silica, 37 mm$_{dia}$ x 100 mm, CH$_2$Cl$_2$:Et$_2$O (50:1 to 17:1)). The major red/brown band was collected and the solvent removed *in vacuo*. Recrystallisation from CH$_2$Cl$_2$/MeOH give *trans*-diporphyrin **103** (39.1 mg, 70%) as a brown solid. ^{1}H NMR (400 MHz, CDCl$_3$, TMS): δ -2.582 (br s, 4H, NH), 3.98-4.07 (m, 24H, CO$_2$CH$_3$), 6.945 (d, 2H, ^3J = 16.0 Hz, $H_{ethenyl}$), 7.303 (s, 4H, H_{styryl}), 7.315 (dd, 2H, ^3J = 16.0, ^4J = 2.5 Hz, $H_{ethenyl}$), 7.83-8.04 (m, 8H, $H_{m\text{-Est}}$), 8.41-8.99 (m, 38H, $14H_{\beta\text{-pyrrolic}}$ + $24H_{o,o',p\text{-Est}}$). *Assignments aided by COSY spectra.* UV-vis (CH$_2$Cl$_2$): λ_{max} [nm] (ε x 10^{-3}) 425 (382), 522 (53.7), 572 (34.4), 600 (26.7), 658 (4.97). FAB-LRMS: *m/z* (%) cluster at 1818-1825, 1821 (100, M$^+$). HRMS: Calcd for M$^+$ (C$_{114}$H$_{82}$N$_8$O$_{16}$): 1818.5849, found: 1818.5795.

ZnT3EP–ZnT3EP diporphyrin, Zn$_2$-103.

1,4-Bis(*trans*-2'-(2''-(5'',10'',15'',20''-tetra(3'''-methoxycarbonylphenyl)porphyrinato zinc(II))yl)ethen-1'-yl)benzene.

$C_{114}H_{78}N_8O_{16}Zn_2$
Exact Mass: 1942.4119
Mol. Wt.: 1946.6634
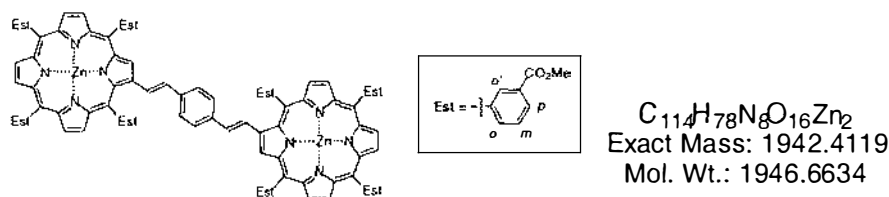
A solution of Zn(OAc)$_2$·2H$_2$O (5.6 mg, 26 µmol, 1.3 eq) in MeOH (1.0 mL) was added to a solution of freebase diporphyrin **103** (38.0 mg, 20.9 µmol) in CHCl$_3$ (10 mL) while stirring at RT. After 50 min, TLC analysis indicated on new major band of higher polarity than the starting material. The solvent was removed *in vacuo* and the residue was column chromatographed (silica, 30 mm$_{dia}$ x 70 mm, CH$_2$Cl$_2$:Et$_2$O (25:1)). Recrystallisation from CH$_2$Cl$_2$/MeOH gave **Zn$_2$-103** (31.7 mg, 78%) as a purple solid. ^{1}H NMR (400 MHz, CDCl$_3$, 55°C, TMS): δ 3.91-3.98 (m, 24H, CO$_2$CH$_3$), 6.971 and 7.221 (ABq, 4H, ^3J = 15.4, 15.4 Hz, H$_{ethenyl}$), 7.137 (s, 4H, H$_{styryl}$), 7.80-7.96 (m, 8H, H$_{m-Est}$), 8.38-9.01 (m, 38H, 14H$_{\beta\text{-pyrrolic}}$ + 24H$_{o,o',p\text{-Est}}$). *Assignments aided by COSY spectra.* UV-vis (CH$_2$Cl$_2$): λ$_{max}$ [nm] (ε x 10^{-3}) 430 (488), 563 (63.9), 604 (45.7). FAB-LRMS: m/z (%) cluster at 1942-1952, 1948 (100, M$^+$). HRMS: Calcd for M$^+$ (C$_{114}$H$_{78}$N$_8$O$_{16}$Zn$_2$): 1942.4119, found: 1942.4132.

Triporphyrins

ZnT3CP–ZnTBMP–ZnTXP, Zn$_3$-104.

5-(4'-(*Trans*-2''-(2'''-(5''',10''',15''',20'''-tetra(3''''-carboxyphenyl)porphyrinato zinc(II))yl)ethen-1''-yl)phenyl)-15-(4'''''-(*trans*-2'''''-(2''''''-(5'''''',10'''''',15'''''',20''''''-tetrakis(3'''''''',4''''''''-dimethylphenyl)porphyrinato zinc(II))yl)ethen-1''''''-yl)phenyl)-2,8,12,18-tetra-*n*-butyl-3,7,13,17-tetramethylporphyrinato zinc(II).


$C_{156}H_{132}N_{12}O_8Zn_3$
Exact Mass: 2492.8165
Mol. Wt.: 2498.9634
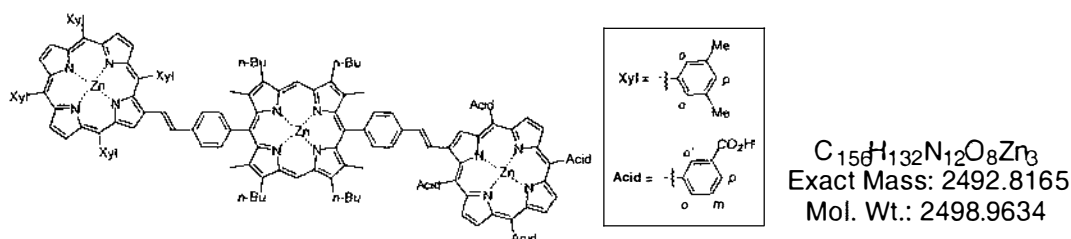
KOH (34.6 mg, 617 μmol, 15 eq per CO_2Me) in MeOH (8.0 mL) and H_2O (800 μL) was added to a solution of triporphyrin Zn_3-107 (26.3 mg, 10.3 μmol) in THF (8.0 mL). The mixture was refluxed for 6.5 h under N_2. On cooling to RT, H_2O (40 mL) and 2.0 M H_3PO_4 (aq) (310 μL, 1.1 eq) were added forming a dark green precipitate. The aqueous layer was extracted with Et_2O (25 mL). The resulting organic layer was washed with 25 mM $H_3PO_4(aq)$ (25 mL), then carefully separated and the solvent removed *in vacuo*. Recrystallisation from THF/hexane gave Zn_3-104 (24.8 mg, 96%) as a purple solid. ^{1}H NMR (Broadened spectrum, 400 MHz, $CDCl_3$, 55°C, TMS): δ 1.05-1.35 (m, $CH_2CH_2CH_2CH_3$), 1.70-1.95 (m, $CH_2CH_2CH_2CH_3$), 2.15-2.35 (m, $CH_2CH_2CH_2CH_3$), 2.55-2.85 (m, $H_{Me-TBMP}$ + H_{Me-Xyl}), 3.90-4.20 (m, $CH_2CH_2CH_2CH_3$), 7.43-9.31 (m), 10.258 (br s, H_{meso}). UV-vis (THF): λ_{max} [nm] (ε x 10^{-3}) 418 (304), 436 (455), 564 (53.3), 601 (19.2). FAB-LRMS: *m/z* (%) cluster at 2493-2506, 2499 (35, M^+). HRMS: Calcd for MH^+ ($C_{156}H_{133}N_{12}O_8Zn_3$): 2493.8244, found: 2493.8295.

ZnT3CP–ZnTBMP–ZnT3CP, Zn_3-105.

5,15-Bis(4'-(*trans*-2''-(2'''-(5''',10''',15''',20'''-tetra(3''''-carboxyphenyl)porphyrinato zinc(II))yl)ethen-1''-yl)phenyl)-2,8,12,18-tetra-*n*-butyl-3,7,13,17-tetramethyl-porphyrinato zinc(II).

$C_{152}H_{116}N_{12}O_{16}Zn_3$
Exact Mass: 2556.6507
Mol. Wt.: 2562.7887
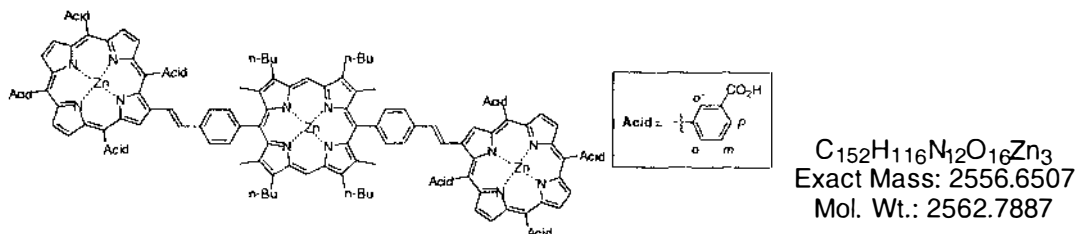
KOH (26.4 mg, 471 μmol, 15 eq per CO_2Me) in MeOH (4.0 mL) and H_2O (400 μL) was added to a solution of porphyrin Zn_3-108 (11 mg, 3.9 μmol) in THF (4.0 mL). The mixture was refluxed for 4 h under N_2. On cooling to RT, H_2O (20 mL) and 2.0 M H_3PO_4 (aq) (260 μL, 1.1 eq) was added forming a dark green precipitate. The aqueous layer was extracted with Et_2O (25 mL). The resulting organic layer was washed with 21 mM $H_3PO_4(aq)$ (25 mL), then separated carefully and the solvent removed *in vacuo*. Recrystallisation from THF/hexane gave Zn_3-105 (11 mg, quantitative) as a purple powder. ^{1}H NMR (selected data only, 400 MHz, DMSO-d_6, RT): δ 10.139 (s, H_{meso}), 13.278 (br s, CO_2H). ^{1}H NMR (selected data only, 400 MHz, DMSO-d_6, 100°C): δ 7.359 and 7.599 (ABq, ^3J = 16.1, 16.3 Hz, $H_{ethenyl}$), 10.139 (s, H_{meso}). UV-vis (THF):

λ_{max} [nm] (ε x 10^{-3}) 418 sh (292), 435 (450), 563 (50.4), 599 (18.0). FAB-LRMS: m/z (%) cluster at 2557-2569, 2563 (100, M$^+$). HRMS: Calcd for M$^+$ ($C_{152}H_{116}N_{12}O_{16}Zn_3$): 2556.6507, found: 2556.6418.

T3EP–TBMP–CHO, "Building Block C", 106.

5-(4'-(*Trans*-2"-(2'''-(5''',10''',15''',20'''-tetra(3''''-methoxycarbonylphenyl)porphyrin)yl)-ethen-1"-yl)phenyl)-15-(4'-formylphenyl)-2,8,12,18-tetra-*n*-butyl-3,7,13,17-tetramethyl-porphyrin.

$C_{107}H_{100}N_8O_9$
Exact Mass: 1640.7613
Mol. Wt.: 1641.9874
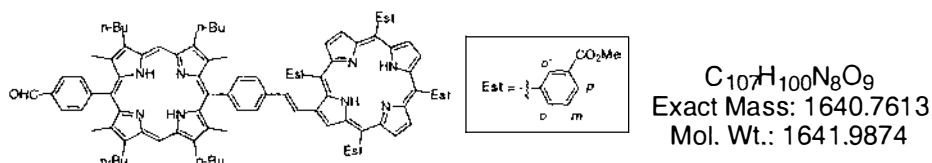
A solution of T3EPps **94** (75 mg, 65 μmol) and BFP **76** (250 mg, 324 μmol, 5.0 eq) in CHCl$_3$ (8.0 mL) was heated to reflux under N$_2$. DBU (58 μL, 6.0 eq) was added. After 20 min, TLC analysis indicated all **94** had been consumed. On cooling to RT the solvent was removed *in vacuo* and the residue column chromatographed (silica, 37 mm$_{dia}$ x 110 mm, CH$_2$Cl$_2$:Et$_2$O (50:1→33:1)). Unreacted starting material BFP **76** was eluted first (170 mg, 79% recovered after recrystallised from CH$_2$Cl$_2$/MeOH) as a red solid. Further elution gave a *cis/trans* (< 5% *cis* by ^{1}H NMR) mixture of the title compound **106** (88.3 mg, 83%, recrystallised from CH$_2$Cl$_2$/MeOH) as a purple solid. ^{1}H NMR (400 MHz, CDCl$_3$, 55°C, TMS): δ -2.556 (s, 2H, NH), -2.450 (br s, 2H, NH), 1.09-1.17 (m, 12H, CH$_2$CH$_2$CH$_2$CH$_3$), 1.73-1.83 (m, 8H, CH$_2$CH$_2$CH$_2$CH$_3$), 2.16-2.28 (m, 8H, CH$_2$CH$_2$CH$_2$CH$_3$), 2.446 (s, 6H, H$_{Me-TBMP}$), 2.599 (s, 6H, H$_{Me-TBMP}$), 3.85-4.04 (m, 20H, 8H CH$_2$CH$_2$CH$_2$CH$_3$ + 12H CO$_2$CH$_3$), 7.226 (d, 1H, ^3J = 10.4 Hz, H$_{ethenyl}$), 7.534 (d, 1H, ^3J = 16.0 Hz, H$_{ethenyl}$), 7.566 (d, 2H, ^3J = 8.7 Hz, H$_{styryl}$), 7.81-7.92(m, 4H, H$_{m-Est}$), 7.997 (d, 2H, ^3J = 7.7 Hz, H$_{styryl}$), 8.18-8.24 (m, 4H, ArH$_{CHO}$), 8.39-8.55 (m, 8H, H$_{o,p-Est}$), 8.72-8.79 (m, 6H, H$_{\beta-pyrrolic}$), 8.907 (s, 2H, 2H$_{o'-Est}$), 8.99-9.00 (m, 2H, 2H$_{o'-Est}$), 9.032 (m, 1H, H$_{3''' (\beta-pyrrolic)}$), 10.264 (s, 2H, H$_{meso}$), 10.366 (m, 1H, CHO). *Assignments aided by COSY spectra.* UV-vis (CH$_2$Cl$_2$): λ_{max} [nm] (ε x 10^{-3}) 423 (353), 511 (36.7), 571 (17.1), 593 sh (9.22), 624 sh (2.68), 652 (1.42). FAB-LRMS: m/z (%) cluster at 1639-1646, 1642 (100, MH$^+$). HRMS: Calcd for M$^+$ ($C_{107}H_{100}N_8O_9$): 1640.7613, found: 1640.7541.

T3EP–TBMP–TXP, 107.

5-(4'-(*Trans*-2''-(2'''-(5''',10''',15''',20'''-tetra(3''''-methoxycarbonylphenyl)porphyrinyl))-ethen-1''-yl)phenyl)-15-(4'''''-(*trans*-2''''''-(2'''''''-(5''''''',10''''''',15''''''',20'''''''-tetrakis-(3''''''',4'''''''-dimethylphenyl)porphyrinyl))ethen-1'''''''-yl)phenyl)-2,8,12,18-tetra-*n*-butyl-3,7,13,17-tetramethylporphyrin.

$C_{160}H_{146}N_{12}O_8$
Exact Mass: 2363.1387
Mol. Wt.: 2364.9473
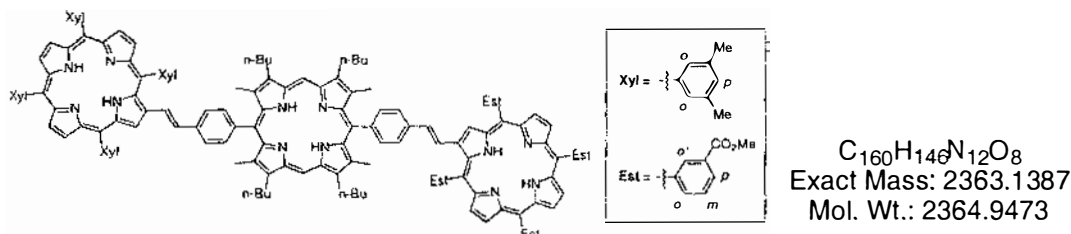
A solution of building block **106** (35 mg, 21 μmol) and TXPps **5** (33 mg, 32 μmol, 1.5 eq) in CHCl$_3$ (4.0 mL) was heated to reflux under N$_2$. DBU (19 μL, 4.0 eq per **5**) in CHCl$_3$ (1.0 mL) was added at 250 μL h^{-1} via a syringe pump. On cooling to RT the solvent was removed *in vacuo* and the residue column chromatographed (silica, 30 mm$_{dia}$ x 230 mm, CH$_2$Cl$_2$:Et$_2$O (33:1)). The major red/brown band was collected and the solvent removed *in vacuo*. Recrystallisation from CH$_2$Cl$_2$/MeOH gave *trans*-triporphyrin **107** (44 mg, 82%) as a purple powder. ^{1}H NMR (400 MHz, CDCl$_3$, 55°C, TMS): δ -2.446 (s, 4H, NH), -2.195 (br s, 2H, NH), 1.159 (t, 12H, ^3J = 7.3 Hz, CH$_2$CH$_2$CH$_2$CH$_3$), 1.819 (app sext, 8H, ^3J = 7.3 Hz, CH$_2$CH$_2$CH$_2$CH$_3$), 2.268 (app pent, 8H, ^3J = 7.2 Hz, CH$_2$CH$_2$CH$_2$CH$_3$), 2.60-2.69 (m, 36H, 12H$_{Me-TBMP}$ + 24H$_{Me-Xyl}$), 3.96-4.06 (m, 20H, 8H CH$_2$CH$_2$CH$_2$CH$_3$ + 12H CO$_2$CH$_3$), 7.22-7.64 (m, 10H, [7.259 and 7.566 (ABq, 2H, ^3J = 16.0, 16.0 Hz, H$_{ethenyl}$) + 7.402 and 7.619 (ABq, 2H, ^3J = 16.2, 16.3 Hz, H$_{ethenyl}$) + 7.397 (br s, 2H, H$_{p-Xyl}$) + 7.484 (br s, 2H, H$_{p-Xyl}$) + 7.612 (d, 2H, ^3J = 8.0 Hz, H$_{styryl}$)]), 7.721 (d, 2H, ^3J = 7.3 Hz, H$_{styryl}$), 7.82-7.88 (m, 6H, 4H$_{o-Xyl}$ + 2H$_{m-Est}$), 7.92-7.95 (m, 6H, 4H$_{o-Xyl}$ + 2H$_{m-Est}$), 8.062 (app t, 4H, [8.052 (d, 2H, ^3J = 7.8 Hz, H$_{styryl}$) + 8.071 (d, 2H, ^3J = 7.7 Hz, H$_{styryl}$)]), 8.40-8.58 (m, 8H, H$_{o,p-Est}$), 8.71-8.87 (m, 12H, H$_{\beta-pyrrolic}$), 8.913 (br s, 2H, H$_{o'-Est}$), 9.008 (br s, 2H, H$_{o'-Est}$), 9.049 (s, 1H, H$_{3''' (\beta-pyrrolic)-T3EP}$), 9.172 (s, 1H, H$_{3'''''' (\beta-pyrrolic)-TXP}$), 10.296 (s, 2H, H$_{meso}$). *Assignments aided by COSY spectra.* UV-vis (CH$_2$Cl$_2$): λ_{max} [nm] (ε x 10^{-3}) 427 (588), 518 (63.7), 568 (35.9), 598 (20.7), 656 (5.81). FAB-LRMS: *m/z* (%) cluster at 2362-2368, 2365 (100, MH$^+$). HRMS: Calcd for M$^+$ (C$_{160}$H$_{146}$N$_{12}$O$_8$): 2363.1387, found: 2363.1220.

ZnT3EP–ZnTBMP–ZnTXP, Zn₃-107.

5-(4'-(*Trans*-2"-(2'''-(5''',10''',15''',20'''-tetra(3''''-methoxycarbonylphenyl)porphyrinato zinc(II))yl)ethen-1"-yl)phenyl)-15-(4'''''-(*trans*-2''''''-(2'''''''-(5'''''''',10'''''''',15'''''''',20''''''''-tetrakis(3'''''''',4''''''''-dimethylphenyl)porphyrinato zinc(II))yl)ethen-1'''''''-yl)phenyl)-2,8,12,18-tetra-*n*-butyl-3,7,13,17-tetramethylporphyrinato zinc(II).

$C_{160}H_{140}N_{12}O_8Zn_3$
Exact Mass: 2548.8791
Mol. Wt.: 2555.0697
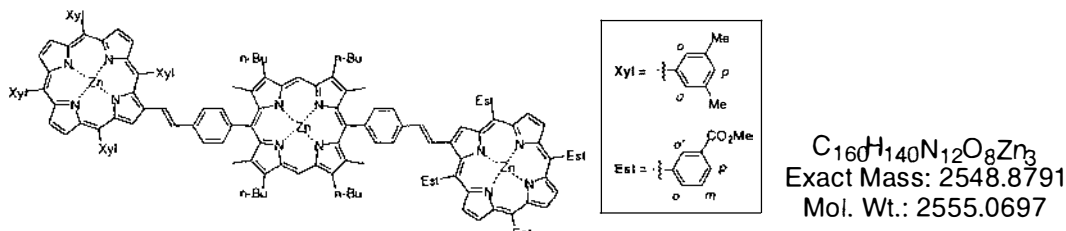
A solution of $Zn(OAc)_2 \cdot 2H_2O$ (15 mg, 68 μmol, 4.0 eq) in MeOH (1.0 mL) was added to a solution of triporphyrin **107** (40.3 mg, 17 μmol) in $CHCl_3$ (5.0 mL) with stirring at RT. The reaction was deemed complete after 3 h by TLC, with the appearance of a new band of higher polarity than starting material **107**. The solvent was removed *in vacuo* and the residue column chromatographed (silica, 30 mm$_{dia}$ x 110 mm, CH_2Cl_2:Et_2O (99:1)) to give **Zn₃-107** (32.8 mg, 75%) as a purple solid. ^1H NMR (400 MHz, $CDCl_3$, 55°C, TMS): δ 1.174 (t, 12H, ^3J = 7.4 Hz, $CH_2CH_2CH_2CH_3$), 1.829 (app sext, 8H, ^3J = 7.3 Hz, $CH_2CH_2CH_2CH_3$), 2.270 (app pent, 8H, ^3J = 7.1 Hz, $CH_2CH_2CH_2CH_3$), 2.60-2.69 (m, 36H, 12H$_{Me-TBMP}$ + 24H$_{Me-Xyl}$)), 3.94-4.07 (m, 20H, 8H $CH_2CH_2CH_2CH_3$ + 12H CO_2CH_3)), 7.28-7.63 (m, 10H, [7.303 and 7.546 (ABq, 2H, ^3J = 15.9, 15.8 Hz, H$_{ethenyl}$) + 7.396 (br s, 2H, H$_{p-Xyl}$) + 7.456 and 7.613 (ABq, 2H, ^3J = 16.2, 16.0 Hz, H$_{ethenyl}$) + 7.483 (br s, 2H, H$_{p-Xyl}$) + 7.619 (d, 2H, ^3J = 7.9 Hz, H$_{styryl}$)]), 7.733 (d, 2H, ^3J = 7.9 Hz, H$_{styryl}$), 7.81-7.86 (m, 6H, 4H$_{o-Xyl}$ + 2H$_{m-Est}$), 7.91-7.95 (m, 6H, 4H$_{o-Xyl}$ + 2H$_{m-Est}$), 8.072 (app t, 4H, [8.062 (d, 2H, ^3J = 8.3 Hz, H$_{styryl}$) + 8.083 (d, 2H, ^3J = 8.7 Hz, H$_{styryl}$)]), 8.41-8.58 (m, 8H, H$_{o,p-Est}$), 8.84-8.99 (m, 16H, 12H$_{\beta-pyrrolic}$ + 4H$_{o'-Est}$), 9.163 (s, 1H, H$_{3''' (\beta-pyrrolic)-T3EP}$), 9.295 (s, 1H, H$_{3'''''' (\beta-pyrrolic)-TXP}$), 10.262 (s, 2H, H$_{meso}$). *Assignments aided by COSY spectra.* UV-vis (CH_2Cl_2): λ_{max} [nm] (ε x 10^{-3}) 412 (421), 433 (643), 558 (72.6), 593 (26.3). FAB-LRMS: *m/z* (%) cluster at 2548-2563, 2555 (100, MH$^+$). HRMS: Calcd for M$^+$ ($C_{160}H_{140}N_{12}O_8Zn_3$): 2548.8791, found: 2548.8767.

T3EP–TBMP–T3EP, 108.

5,15-Bis(4'-(*trans*-2"-(2"'-(5"',10"',15"',20"'-tetra(3""-methoxycarbonylphenyl)-porphyrin)yl)ethen-1"-yl)phenyl)-2,8,12,18-tetra-*n*-butyl-3,7,13,17-tetramethyl-porphyrin.

$C_{160}H_{138}N_{12}O_{16}$
Exact Mass: 2483.0354
Mol. Wt.: 2484.8790
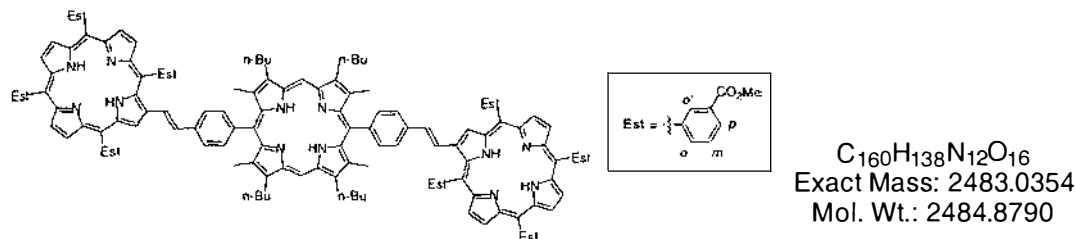
A solution of building block **106** (19 mg, 12 μmol) and T3EPps **94** (16 mg, 14 μmol, 1.2 eq) in CHCl$_3$ (4.0 mL) was heated to reflux under N$_2$. DBU (7.8 μL, 4.0 eq per **94**) in CHCl$_3$ (1.0 mL) was added at 250 μL h^{-1} via a syringe pump. On cooling to RT the solvent was removed *in vacuo* and the residue column chromatographed (silica, 30 mm$_{dia}$ x 120 mm, CH$_2$Cl$_2$:Et$_2$O (20:1)). The major red/brown band was collected and the solvent removed *in vacuo*. Recrystallisation from CHCl$_3$/MeOH gave all *trans*-**108** (19 mg, 66%) as a purple powder. ^{1}H NMR (400 MHz, CDCl$_3$, 55°C, TMS): δ -2.446 (s, 4H, NH$_{T3EP}$), -2.210 (s, 2H, NH$_{TBMP}$), 1.162 (t, 12H, ^3J = 7.3 Hz, CH$_2$CH$_2$CH$_2$CH$_3$), 1.821 (app sext, 8H, ^3J = 7.3 Hz, CH$_2$CH$_2$CH$_2$CH$_3$), 2.268 (app pent, 8H, ^3J = 7.3 Hz, CH$_2$CH$_2$CH$_2$CH$_3$), 2.624 (s, 12H, H$_{Me\text{-}TBMP}$), 3.91-4.05 (m, 32H, 8H CH$_2$CH$_2$CH$_2$CH$_3$ + 24H CO$_2$CH$_3$), 7.241 and 7.557 (ABq, 4H, ^3J = 15.9, 16.2 Hz, H$_{ethenyl}$), 7.591 (d, 4H, ^3J = 7.9 Hz, H$_{styryl}$), 7.834 (app t, 4H, ^3J = 7.4 Hz, H$_{m\text{-}Est}$), 7.90-7.96 (m, 4H, H$_{m\text{-}Est}$), 8.034 (d, 4H, ^3J = 7.5 Hz, H$_{styryl}$), 8.40-8.59 (m, 16H, H$_{o,p\text{-}Est}$), 8.72-8.79 (m, 12H, H$_{\beta\text{-pyrrolic}}$), 8.912 (s, 4H, H$_{o'\text{-}Est}$), 9.006 (s, 4H, H$_{o'\text{-}Est}$), 9.047 (s, 2H, H$_{3"'(\beta\text{-pyrrolic})\text{-}T3EP}$), 10.295 (s, 2H, H$_{meso}$). *Assignments aided by COSY spectra.* UV-vis (CH$_2$Cl$_2$): λ$_{max}$ [nm] (ε x 10^{-3}) 426 (496), 518 (55.0), 565 (31.0), 595 (20.9), 648 (7.37). FAB-LRMS: *m/z* (%) cluster at 2482-2489, 2485 (100, MH$^+$). HRMS: Calcd for MH$^+$ ($C_{160}H_{139}N_{12}O_{16}$): 2484.0432, found: 2484.0247.
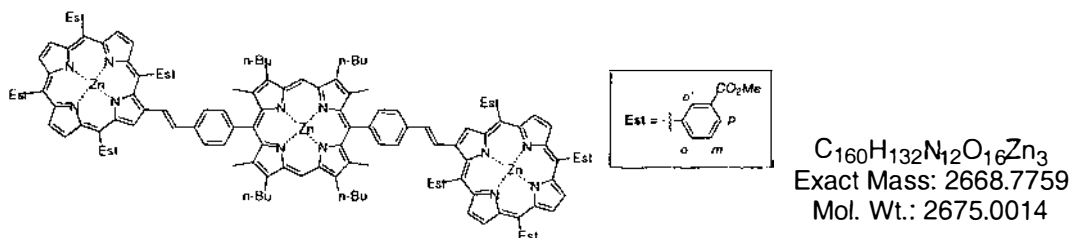
ZnT3EP–ZnTBMP–ZnT3EP, Zn₃-108.

5,15-Bis(4'-(*trans*-2"-(2'''-(5''',10''',15''',20'''-tetra(3''''-methoxycarbonylphenyl)-porphyrinato zinc(II))yl)ethen-1"-yl)phenyl)-2,8,12,18-tetra-*n*-butyl-3,7,13,17-tetramethylporphyrinato zinc(II).

$C_{160}H_{132}N_{12}O_{16}Zn_3$
Exact Mass: 2668.7759
Mol. Wt.: 2675.0014

A solution of $Zn(OAc)_2 \cdot 2H_2O$ (6.9 mg, 31 μmol, 4.0 eq) in MeOH (1.0 mL) was added to a solution of triporphyrin **108** (19.4 mg, 7.8 μmol) in $CHCl_3$ (5.0 mL) with stirring at RT. The reaction was deemed complete after 3 h, by TLC with the appearance of a new band of higher polarity than the starting material **108**. The solvent was removed *in vacuo* and the residue column chromatographed (silica, 20 mm$_{dia}$ x 70 mm, CH_2Cl_2:Et_2O (24:1)). Recrystallisation from CH_2Cl_2/hexane gave **Zn₃-108** (15.1 mg, 72%) as a red powder. ^{1}H NMR (400 MHz, CDCl$_3$, 55°C, TMS): δ 1.174 (t, 12H, ^3J = 7.3 Hz, $CH_2CH_2CH_2CH_3$), 1.855 (app sext, 8H, ^3J = 7.3 Hz, $CH_2CH_2CH_2CH_3$), 2.267 (app pent, 8H, ^3J = 7.3 Hz, $CH_2CH_2CH_2CH_3$), 2.611 (s, 12H, H$_{Me-TBMP}$), 3.91-4.05 (m, 32H, 8H $CH_2CH_2CH_2CH_3$) + 24H CO_2CH_3), 7.286 and 7.532 (ABq, 4H, ^3J = 16.0, 15.9 Hz, H$_{ethenyl}$), 7.599 (d, 4H, ^3J = 6.9 Hz, H$_{styryl}$), 7.820 (app t, 4H, ^3J = 7.4 Hz, H$_{m-Est}$), 7.918 (app t, 4H, ^3J = 7.2 Hz, H$_{m-Est}$), 8.044 (d, 4H, ^3J = 7.4 Hz, H$_{styryl}$), 8.40-8.52 (m, 16H, H$_{o,p-Est}$), 8.83-8.90 (m, 16H, 12H$_{\beta-pyrrolic}$ + 4H$_{o'-Est}$), 8.977 (s, 4H, H$_{o'-Est}$), 9.156 (s, 2H, H$_{3'''-\beta-pyrrolic-T3EP}$), 10.255 (s, 2H, H$_{meso}$). *Assignments aided by COSY spectra.* UV-vis (CH$_2$Cl$_2$): λ_{max} [nm] (ϵ x 10^{-3}) 413 (411), 433 (618), 557 (68.5), 592 sh (25.3). FAB-LRMS: *m/z* (%) cluster at 2669-2682, 2675 (100, M$^+$). HRMS: Calcd for M$^+$ (C$_{160}$H$_{132}$N$_{12}$O$_{16}$Zn$_3$): 2668.7759, found: 2668.7863.

Pentaporphyrins

TXP Star Pentaporphyrin, 109.

5,10,15,20-Tetra(4'-(*trans*-2"-(2'"-(5'",10'",15'",20'"-tetrakis(3"",5""-dimethylphenyl)-porphyrinyl)ethenyl-1"-yl)phenyl)porphyrin.

$C_{260}H_{214}N_{20}$
Exact Mass: 3615.7360
Mol. Wt.: 3618.6160
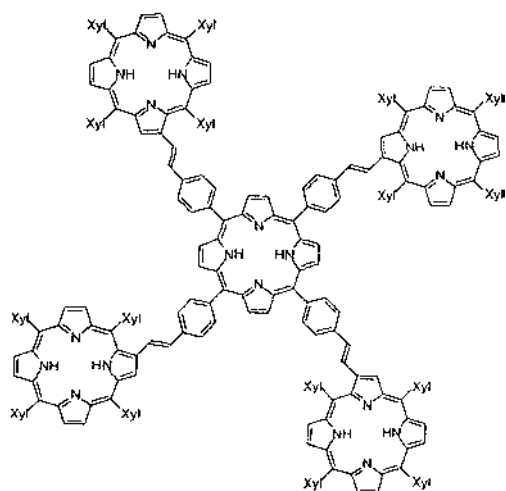
A solution of TFP **110** (20 mg, 28 μmol) and TXPps **5** (143 mg, 138 μmol, 5.0 eq) in CHCl$_3$ (8.0 mL) was heated to reflux under N$_2$. DBU (93 μL, 4.5 eq per **5**) in CHCl$_3$ (1.0 mL) was added at 220 μL h^{-1} via a syringe pump. On cooling to RT the solvent was removed *in vacuo* and the residue column chromatographed (silica, 37 mm$_{dia}$ x 120 mm, CH$_2$Cl$_2$:hexane (2:1)). The major yellow/brown band was collected and the solvent removed *in vacuo*. Recrystallisation from CH$_2$Cl$_2$/MeOH gave the crude product **109** (75 mg). This material was dissolved in CH$_2$Cl$_2$ (10 mL) and I$_2$ (62.4 mg, $\approx$ 3.0 eq per ethenyl) added. The reaction was stirred at RT in the dark for 3 h. Sat. Na$_2$S$_2$O$_3$ (10 mL) was added and mixture stirred vigorously for 30 min. The organic layer was separated and the solvent removed *in vacuo*. Further column chromatography (silica, 30 mm$_{dia}$ x 130 mm, CH$_2$Cl$_2$:hexane (2:1)) followed by recrystallisation from CH$_2$Cl$_2$/hexane then CH$_2$Cl$_2$/MeOH, gave all *trans*-**109** (43.5 mg, 43% based on TFP) as a purple powder. ^{1}H NMR (400 MHz, CDCl$_3$, 30°C, TMS): δ -2.529 (s, 8H, NH), -2.469 (s, 2H, NH), 2.596 (s, 24H, H$_{Me-Xyl}$), 2.608 (s, 24H, H$_{Me-Xyl}$), 2.680-2.685 (m, 48H, H$_{Me-Xyl}$), 7.400 and 7.648 (ABq, 8H, ^3J = 15.7, 16.0 Hz, H$_{2",1"-ethenyl}$), 7.399 (s, 8H, H$_{p-Xyl}$), 7.491 (s, 4H, H$_{p-Xyl}$), 7.574 (s, 4H, H$_{p-Xyl}$), 7.783 (d, 8H, ^3J = 8.2 Hz, H$_{3',5'-styryl}$), 7.845 (s, 16H, H$_{o-Xyl}$), 7.944 (s, 8H, H$_{\bullet-Xyl}$), 7.956 (s, 8H, H$_{o-Xyl}$), 8.325 (d, 8H, ^3J = 8.2 Hz, H$_{2',6'-styryl}$), 8.82-8.86 (m, 24H, H$_{\beta-pyrrolic-TXP}$), 9.112 (s, 8H, H$_{\beta-pyrrolic}$), 9.194 (m, 4H,

$H_{3''' - \beta\text{-pyrrolic-TXP}}$). *Assignments aided by COSY (short and long range) spectra.* UV-vis (CH$_2$Cl$_2$): λ_{max} [nm] (ε x 10^{-3}) 428 (945), 525 (118), 568 (91.9), 599 (49.6), 654 (26.8). MALDI-TOF MS (α-cyano-4-hydroxycinnamic acid): *m/z* (%) cluster at 3615-3624, centred at 3619.7 (100, MH$^+$). Calcd avg mass for MH$^+$ (C$_{260}$H$_{215}$N$_{20}$): 3619.6.

TFP, 110.

5,10,15,20-Tetra(4'-formylphenyl)porphyrin.
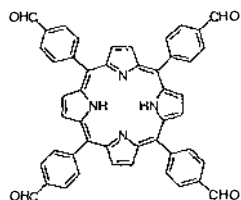
C$_{48}$H$_{30}$N$_4$O$_4$
Exact Mass: 726.2267
Mol. Wt.: 726.7764

A solution of tetra-acetal **114** (332 mg, 310 μmol) in CH$_2$Cl$_2$:TFA:H$_2$O (3:3:1, 61 mL) was stirred at RT for 1.8 h. H$_2$O (500 mL) and CH$_2$Cl$_2$ (400 mL) were added followed by excess sat. NaHCO$_3$. The green solution turned red. After evolution of gas had ceased ($\approx$ 20 min) the organic layer was washed with H$_2$O (2 x 1 L) and sat. NaHCO$_3$ (1 L), then dried (MgSO$_4$). After reducing the volume *in vacuo* the product was precipitated using MeOH to give TFP **110** (211 mg, 94%) as a purple microcrystalline powder. ^{1}H NMR (400 MHz, CDCl$_3$, TMS): δ -2.779 (s, 2H, NH), 8.305 and 8.400 (ABq, 16H, ^3J = 7.9, 7.9 Hz, ArH), 8.831 (s, 8H, H$_{\beta\text{-pyrrolic}}$), 10.398 (s, 4H, CHO). ^{13}C NMR (101 MHz, CDCl$_3$): 119.25, 128.12, 135.11, 135.79, 148.04, 192.26 (CHO). UV-vis (CH$_2$Cl$_2$): λ_{max} [nm] (ε x 10^{-3}) 422 (476), 516 (22.5), 552 (10.9), 591 (7.05), 646 (4.46). FAB-LRMS: *m/z* (%) cluster at 726-730, 726 (72, M$^+$). HRMS: Calcd for M$^+$ (C$_{48}$H$_{30}$N$_4$O$_4$): 726.2267, found: 726.2294.

T3CP$_4$ Star Pentaporphyrin, Zn$_5$-111.

5,10,15,20-Tetra(4'-(*trans*-2''-(2'''-(5''',10''',15''',20'''-tetra(3''''-carboxyphenyl)-porphyrinato zinc(II)yl)ethenyl-1''-yl)phenyl)porphyrinato zinc(II).


$C_{244}H_{140}N_{20}O_{32}Zn_5$
Exact Mass: 4180.6400
Mol. Wt.: 4190.7880
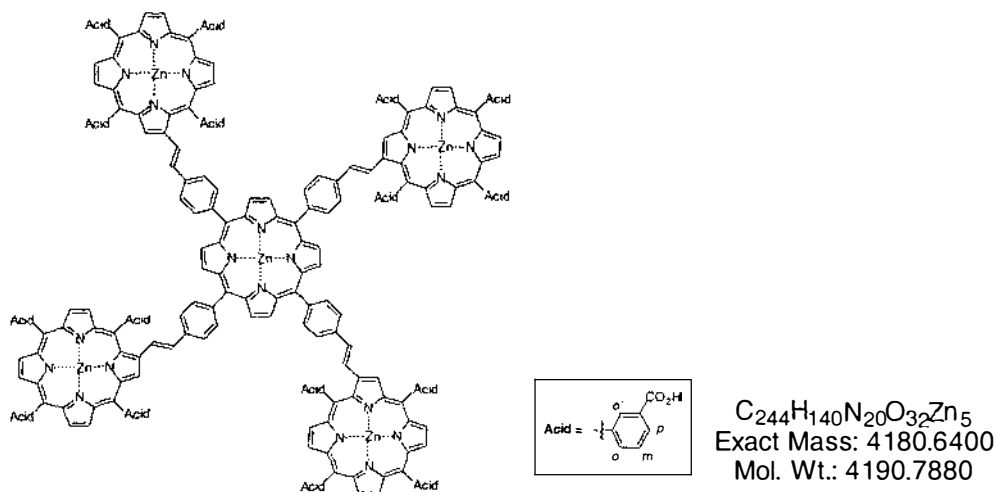
A solution of TFP **110** (10 mg, 14 μmol) and T3EPps **94** (79.7 mg, 70 μmol, 5.0 eq) in CHCl$_3$ (4.0 mL) was heated to reflux under N$_2$. DBU (46.3 μL, 4.5 eq per **94**) in CHCl$_3$ (1.0 mL) was added at 220 μL h^{-1} via a syringe pump. On cooling to RT, the crude solid was precipitated out of solution with MeOH to give a purple solid (61.7 mg). The solid was dissolved in CHCl$_3$ (20 mL) and a solution of Zn(OAc)$_2$·2H$_2$O (21.1 mg, 96 μmol) in MeOH (1.0 mL) added. The mixture was heated at reflux for 1 h. On cooling to RT the solvent was removed *in vacuo* and the residue column chromatographed (silica, 30 mm$_{dia}$ x 160 mm, CH$_2$Cl$_2$:MeOH (50:1)). The major red band was collected and the solvent removed *in vacuo*. Recrystallisation from CH$_2$Cl$_2$/MeOH gave a purple powder (53.0 mg). Metallated ester was identified by MALDI (all-*trans*-retinoic acid): m/z (%) cluster 4406-4424 centred at 4415 (100, M$^+$), Calcd avg mass for M$^+$ (C$_{260}$H$_{172}$N$_{20}$O$_{32}$Zn$_5$): 4415. The purple powder was dissolved in THF (15 mL) and treated with KOH (214 mg, 3.8 mmol, 20 eq per CO$_2$Me) in MeOH:H$_2$O (10:1, 4.0 mL). The mixture was refluxed for 8.5 h under N$_2$. On cooling to RT the solvent was removed *in vacuo*. The residue was dissolved in a solution of H$_2$O (10 mL) and 2.0 M H$_3$PO$_4$$_{(aq)}$ (2.5 mL), forming a dark green precipitate. The pH of the aqueous layer was $\approx$ 1.5. The precipitate was washed with H$_2$O (10 mL) then dried under high vacuum at 60°C to give a purple solid (48.6 mg). This solid was dissolved in THF (20 mL), adding Zn(OAc)$_2$·2H$_2$O (5.6 mg) in H$_2$O (2.0 mL) the mixture was refluxed for 30 min under N$_2$. On cooling to RT, 182 mM KOH$_{(aq)}$ (5.0 mL) was added and the solvent was removed *in vacuo*. The residue was dissolved in H$_2$O (10 mL) and the pH adjusted to $\approx$

3 with acetic acid, forming a dark green precipitate. The precipitate was washed with H_2O (10 mL) then dried *in vacuo* at 70°C to give porphyrin acid **Zn$_5$-111** (48.6 mg, 84%). ^{1}H NMR (400 MHz, DMSO-d_6, RT, TMS): δ 7.2-9.2 (m, 124H), 13.27 (br s, 16H, CO_2H). ^{1}H NMR (400 MHz, DMSO-d_6, 80°C, TMS): δ 7.311 and 7.616 (ABq, 8H, ^3J = 15.5, 15.5 Hz, H$_{ethenyl}$), 7.717 and 8.234 (ABq, 16H, ^3J = 7.8, 7.6 Hz, H$_{styryl}$), 7.89-7.94 (m, 8H, H$_{m\text{-Acid}}$), 8.010 (app t, 4H, ^3J = 7.5 Hz, H$_{m\text{-Acid}}$), 8.086 (app t, 4H, ^3J = 7.4 Hz, H$_{m\text{-Acid}}$), 8.37-8.59 (m, 32H), 8.72-8.82 (m, 40H), 9.038 (br s, 8H), 9.101 (br s, 4H), 12.7 (very br s, 16H, CO_2H). *Assignments aided by COSY spectra.* UV-vis (THF): λ_{max} [nm] (ε x 10^{-3}) 435 (784), 565 (102), 606 (60.8). ES-MS (-ve, THF:MeOH (1:1)): *m/z* = clusters centred at 2094.42, 1395.86, Calcd avg masses ($C_{244}H_{140}N_{20}O_{32}Zn_5$), [M − 2H]$^{2-}$ = 2094.39, [M − 3H]$^{3-}$ = 1395.93. MALDI-TOF MS (all-*trans*-retinoic acid): *m/z* (%) cluster 4180-4202 centred at 4190.8 (100, M$^+$), Calcd avg mass for M$^+$ ($C_{244}H_{140}N_{20}O_{32}Zn_5$): 4190.9.

Diporphyrinyl Trialdehyde, 112.

5,10,15-Tri(4'-formylphenyl)-20-(4"-(*trans*-2"'-(2""-(5"""',10"""',15"""',20"'-tetra(3"""-methoxycarbonylphenyl)porphyrinyl)ethenyl-1"'-yl)phenyl)porphyrin.
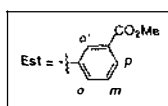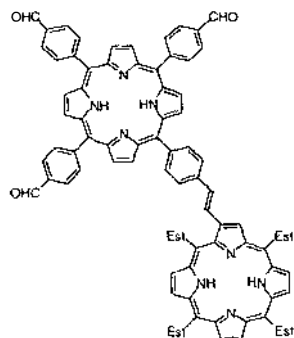
$C_{101}H_{68}N_8O_{11}$
Exact Mass: 1568.5008
Mol. Wt.: 1569.6679

A solution of T3EPps **94** (11.7 mg, 10.1 μmol) and TFP **110** (44.1 mg, 60.6 μmol, 6.0 eq) in 1,2-dichloroethane (8.0 mL) was heated to reflux under N_2. DBU (4.5 μL, 3.0 eq per **94**) in 1,2-dichloroethane (500 μL) was added at 170 μL h^{-1} via a syringe pump. On cooling to RT the solvent was removed *in vacuo* and the residue column chromatographed (silica, 30 mm$_{dia}$ x 55 mm). Elution with CH_2Cl_2:Et$_2$O (25:1) gave TFP **110** (34.5 mg, 87% recovered) after recrystallisation from CH_2Cl_2/MeOH. Further elution with CH_2Cl_2:Et$_2$O:MeOH (20:2:0.1) gave the title compound *trans*-**112** (9.7 mg, 61%) after recrystallisation from CHCl$_3$/MeOH as a purple solid. ^{1}H NMR (400 MHz, CDCl$_3$, 55°C, TMS): δ -2.622 (s, 2H, NH), -2.472 (s, 2H, NH), 3.887 (s, 3H, CO_2CH_3),

3.984 and 3.993 (m, 6H, CO_2CH_3), 4.024 (s, 3H, CO_2CH_3), 7.179 and 7.502 (ABq, 2H, ^3J = 15.6, 15.9 Hz, $H_{ethenyl}$), 7.582 (d, 2H, ^3J = 7.7 Hz, H_{styryl}), 7.82-7.85 (m, 2H, $H_{m\text{-Est}}$), 7.91-7.93 (m, 2H, $H_{m\text{-Est}}$), 8.161 (d, 2H, ^3J = 7.9 Hz, H_{styryl}), 8.26-8.30 (m, 6H, ArH_{CHO}), 8.38-8.55 (m, 14H, $6ArH_{CHO}$ + $8H_{o,p\text{-Est}}$), 8.71-9.00 (m, 19H, $15H_{\beta\text{-pyrrolic}}$ + $4H_{o'\text{-Est}}$), 10.378 and 10.389 (app d, 3H, CHO). *Assignments aided by COSY spectra.* UV-vis (CH_2Cl_2): λ_{max} [nm] (ε x 10^{-3}) 425 (493), 520 (42.9), 558 (25.6), 596 (15.8), 649 (7.74). FAB-LRMS: *m/z* (%) cluster at 1568-1574, 1569 (100, MH^+). HRMS: Calcd for M^+ ($C_{101}H_{68}N_8O_{11}$): 1568.5008, found: 1568.4957.

ZnTXP$_3$,ZnT3CP Star Pentaporphyrin, Zn$_5$-113.

5-(4'-(*Trans*-2"-(2"'-(5"',10"',15"',20"'-tetra(3""-carboxyphenyl)porphyrinato zinc(II)yl)-ethenyl-1"-yl)phenyl)- 10,15,20-tris(4""'-(*trans*-2""""-(2"""""-(5""""",10""""",15""""",20"""""-tetrakis-(3""""""',5""""""'-dimethylphenyl)porphyrinato zinc(II)yl)ethenyl-1"""""-yl)phenyl)-porphyrinato zinc(II).

$C_{256}H_{188}N_{20}O_8Zn_5$
Exact Mass: 3989.1376
Mol. Wt.: 3999.3119
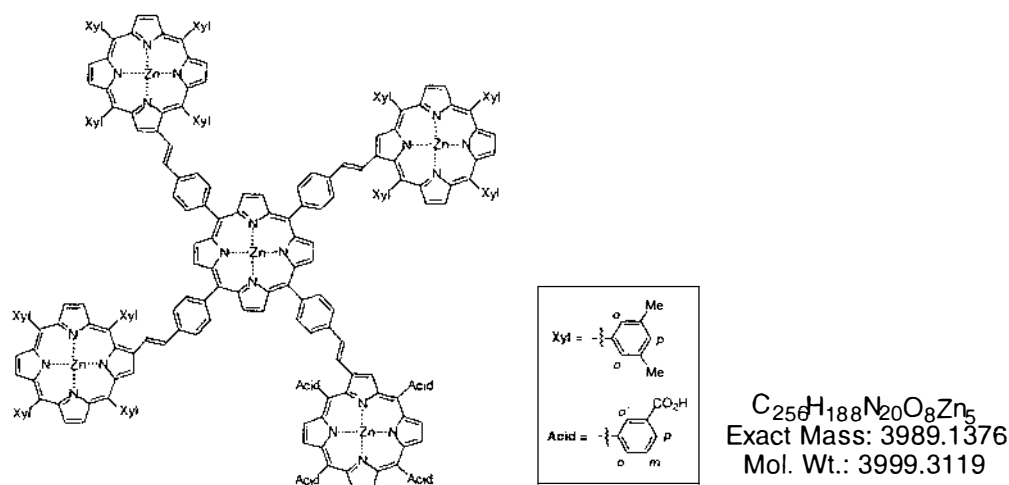
KOH (15.5 mg, 276 μmol, 31 eq per CO_2Me) in MeOH (1.0 mL) and H_2O (100 μL) was added to a solution of pentaporphyrin Zn$_5$-115 (8.8 mg, 2.2 μmol) in THF (1.5 mL). The mixture was refluxed for 4 h under N_2. On cooling to RT, H_2O (20 mL) and 2.0 M H_3PO_4 (aq) (150 μL, 1.1 eq) were added forming a dark green precipitate. The aqueous layer was extracted with Et_2O (15 mL). The resulting organic layer was washed with 20 mM $H_3PO_{4(aq)}$ (15 mL), then separated and dried (K_2CO_3) and the solvent removed *in vacuo*. Recrystallisation from THF/H_2O (rinsing with MeOH) and then CH_2Cl_2/hexane gave Zn$_5$-113 (7.3 mg, 84%) as a purple solid. ^{1}H NMR (400 MHz, $CDCl_3$, 55°C, TMS): δ 2.2-2.8 (m, 72H, $H_{Me\text{-Xyl}}$), 7.1-9.4 (m, 112H). UV-vis (THF): λ_{max} [nm] (ε x 10^{-3}) 436 (1040), 565 (138), 606 (84.5). MALDI-TOF MS (all-

trans-retinoic acid): *m/z* (%) cluster at 3991-4008, centred at 4000 (100, MH$^+$), Calcd avg mass for MH$^+$ (C$_{256}$H$_{188}$N$_{20}$O$_8$Zn$_5$): 4000.4.

TAcP, 114.

5,10,15,20-Tetrakis(4'-(5",5"-dimethyl-1",3"-dioxane-2"-yl)phenyl)porphyrin.
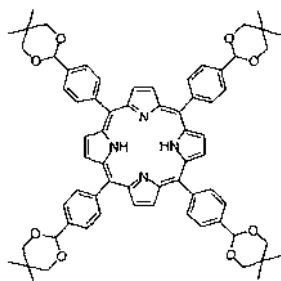
C$_{68}$H$_{70}$N$_4$O$_8$
Exact Mass: 1070.5194
Mol. Wt.: 1071.3056

Synthesis of **114** was carried out according to Lindsey et al.[120] The mono-protected dialdehyde 4-(5',5'-dimethyl-1',3'-dioxane-2'-yl)benzaldehyde *p-79* was prepared from 4-bromobenzaldehyde according to Nierengarten et al.[147] Additional data: UV-vis (CH$_2$Cl$_2$): λ_{max} [nm] (ε x 10^{-3}) 418 (448), 515 (18.1), 551 (8.28), 591 (6.35), 645 (4.77).

TXP$_3$,T3EP Mixed Star Pentaporphyrin, 115.

5-(4'-(*Trans*-2"-(2'"-(5"",10"",15"",20""-tetra(3""'-methoxycarbonylphenyl)porphyrinyl)-ethenyl-1"-yl)phenyl)- 10,15,20-tris(4""''-(*trans*-2"""''-(2"""''"-(5"""''"'",10"""''"'",15"""''"'",20"""''"'"-tetrakis(3"""''"'"",5"""''"'""-dimethylphenyl)porphyrinyl)ethenyl-1"""''-yl)phenyl)porphyrin.
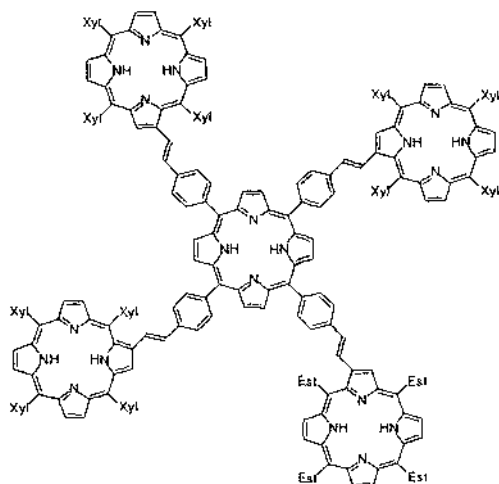
C$_{260}$H$_{206}$N$_{20}$O$_8$
Exact Mass: 3735.6327
Mol. Wt.: 3738.5476

A solution of diporphyrinyl trialdehyde **112** (8.7 mg, 5.5 μmol) and TXPps **5** (25.9 mg, 24.9 μmol, 4.5 eq) in CHCl$_3$ (3.0 mL) was heated to reflux under N$_2$. DBU (17 μL, 4.5 eq per **5**) in CHCl$_3$ (1.0 mL) was added at 220 μL h^{-1} via a syringe pump. On cooling to RT the solvent was removed *in vacuo* and the residue column chromatographed (silica,

30 mm$_{dia}$ x 55 mm, CH$_2$Cl$_2$:Et$_2$O (200:1)). The major yellow/brown band was collected and the solvent removed *in vacuo*. Recrystallisation from CH$_2$Cl$_2$/MeOH gave all *trans*-**115** (11.2 mg, 54%) as a purple powder. ^{1}H NMR (400 MHz, CDCl$_3$, 55°C, TMS): δ - 2.463 (s, 8H, NH), -2.413 (s, 2H, NH), 2.589 (s, 18H, H$_{Me-Xyl}$), 2.601 (s, 18H, H$_{Me-Xyl}$), 2.672 (s, 36H, H$_{Me-Xyl}$), 3.965 (s, 3H, CO$_2$CH$_3$), 3.976 (s, 3H, CO$_2$CH$_3$), 3.990 (m, 3H, CO$_2$CH$_3$), 4.029 (s, 3H, CO$_2$CH$_3$), 7.293 and 7.610 (ABq, 2H, ^3J = 16.0, 16.0 Hz, H$_{ethenyl-T3EP}$), 7.385 (br s, 6H, H$_{p-Xyl}$), 7.416 and 7.621 (ABq, 6H, ^3J = 15.9, 15.9 Hz, H$_{ethenyl-TXP}$), 7.472 (br s, 3H, H$_{p-Xyl}$), 7.550 (br s, 3H, H$_{p-Xyl}$), 7.661 (d, 2H, ^3J = 7.6 Hz, H$_{styryl-T3EP}$), 7.771 (d, 6H, ^3J = 7.2 Hz, H$_{styryl-TXP}$), 7.80-8.02 (m, 28H, [7.833 (br s, 12H, H$_{o-Xyl}$) + 7.933 (br s, 12H, H$_{o-Xyl}$) + 4H$_{m-Est}$]), 8.283 (d, 2H, ^3J = 7.6 Hz, H$_{styryl-T3EP}$), 8.308 (d, 6H, ^3J = 7.2 Hz, H$_{styryl-TXP}$), 8.38-8.63 (m, 8H, H$_{o,p-Est}$), 8.73-9.17 (m, 40H, 36H$_{\beta-pyrrolic}$ + 4H$_{o-Est}$). *Assignments aided by COSY spectra.* UV-vis (CH$_2$Cl$_2$): λ$_{max}$ [nm] (ε x 10^{-3}) 428 (1400), 524 (171), 568 (130), 599 (71.6), 654 (37.7). MALDI-TOF MS (all-*trans*-retinoic acid): *m/z* (%) cluster at 3734-3746, centred at 3740 (100, MH$^+$). Calcd avg mass for MH$^+$ (C$_{260}$H$_{207}$N$_{20}$O$_8$): 3739.6.

ZnTXP$_3$,ZnT3EP Star Pentaporphyrin, Zn$_5$-115.

5-(4'-(*Trans*-2"-(2"'-(5"',10"',15"',20"'-tetra(3""-methoxycarbonylphenyl)porphyrinato zinc(II)yl)ethenyl-1"-yl)phenyl)- 10,15,20-tris(4""'-(*trans*-2"""'-(2"""'-
(5"""",10"""",15"""",20""""-tetrakis(3""""',5""""'-dimethylphenyl)porphyrinato zinc(II)yl)-
ethenyl-1"""'-yl)phenyl)porphyrinato zinc(II).

C$_{260}$H$_{196}$N$_{20}$O$_8$Zn$_5$
Exact Mass: 4045.2002
Mol. Wt.: 4055.4182
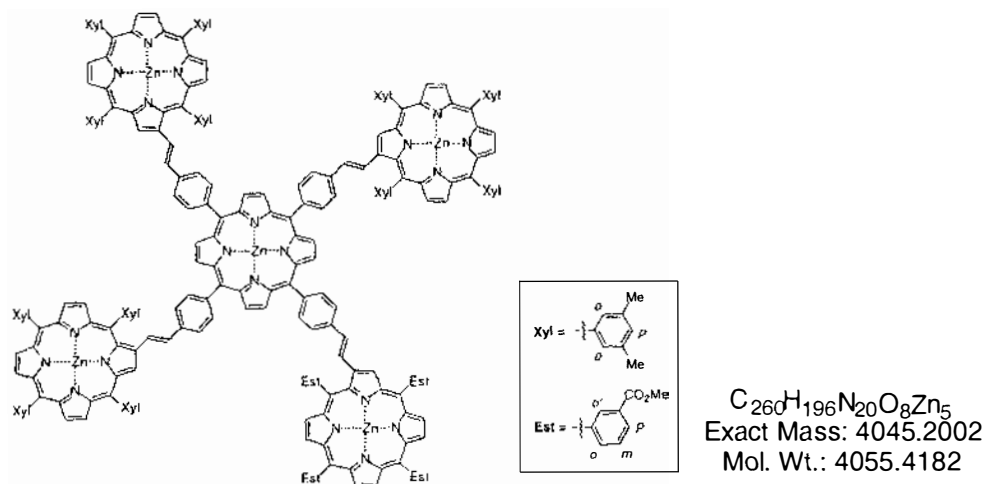
A solution of Zn(OAc)$_2$·2H$_2$O (7.2 mg, 33 μmol, 12 eq) in MeOH (1.0 mL) was added to a solution of pentaporphyrin **115** (10.2 mg, 2.7 μmol) in CHCl$_3$ (5.0 mL) with stirring at RT. The reaction was deemed complete after 3 h by TLC, with the appearance of a

new band of higher polarity than the starting material **115**. The solution was washed with H_2O (25 mL) and then sat. $NaHCO_3$ (25 mL). The organic layer was separated and dried (K_2CO_3). The product was then precipitated out of solution with MeOH giving **Zn$_5$-115** (9.6 mg, 87%) as a purple powder. ^{1}H NMR (400 MHz, $CDCl_3$, 55°C, TMS): δ 2.588 (s, 18H, H_{Me-Xyl}), 2.601 (s, 18H, H_{Me-Xyl}), 2.672 (s, 36H, H_{Me-Xyl}), 3.94-4.00 (m, 12H, CO_2CH_3), 7.25-8.05 (m, 22H, [7.277 and 7.543 (ABq, 2H, ^3J = 16.4, 16.4 Hz, $H_{ethenyl-T3EP}$) + 7.380 (br s, 6H, H_{p-Xyl}) + 7.414 and 7.597 (ABq, 6H, ^3J = 16.2, 16.2 Hz, $H_{ethenyl-TXP}$) + 7.470 (br s, 3H, H_{p-Xyl}) + 7.546 (br s, 3H, H_{p-Xyl}) + 7.662 (d, 2H, ^3J = 7.4 Hz, $H_{styryl-T3EP}$)]), 7.725-8.00 (m, 34H, [7.781 (d, 6H, ^3J = 8.0 Hz, $H_{styryl-TXP}$) + 7.844 (br s, 12H, H_{o-Xyl}) + 7.944 (br s, 12H, H_{o-Xyl}) + $4H_{m-Est}$)]), 8.28-8.33 (m, 8H, [8.293 (d, 2H, ^3J = 7.4 Hz, $H_{styryl-T3EP}$) + 8.317 (d, 6H, ^3J = 8.0 Hz, $H_{styryl-TXP}$)]), 8.39-8.67 (m, 8H, $H_{o,p-Est}$), 8.87-8.99 (m, 28H, $H_{\beta-pyrrolic}$), 9.10-9.29 (m, 12H, $8H_{\beta-pyrrolic}$ + $4H_{o'-Est}$). *Assignments aided by COSY spectra.* UV-vis (THF): λ_{max} [nm] (ε x 10^{-3}) 436 (995), 565 (131), 606 (84.8). MALDI-TOF MS (all-*trans*-retinoic acid): *m/z* (%) cluster at 4048-4064, centred at 4055 (100, M^+). Calcd avg mass for M^+ ($C_{260}H_{196}N_{20}O_8Zn_5$): 4055.49.

7.5   *Chapter 5: Porphyrins as Sensitisers in a Grätzel Cell*

7.5.1   Test Equipment

Diagrams and illustrations of this test equipment are given in Section 5.2. All test equipment (sensors and cell holders etc.) was designed and fabricated by the author with the exception of the light source. This was fabricated to the authors own design by IFS Mechanical and Electronic Workshops.[174]

Light Source

Philips Halotone Master Line Plus, GU 5.3, 12V/50W Halogen Bulb, 24° Beam (UV Block) powered by a 230/12V electronic transformer.

The optics of an old microscope were replaced with an adjustable brass tube containing the halogen bulb. Ventilation holes were placed around the bulb to minimise overheating. The X-Y-Z stage was left inplace to allow alignment of cell holders under the light source and fine adjustment of light intensity.

Sensors

LDR1 and LDR2: CdS light dependent resistor (Dick Smith Electronics, Z-4801), Dark resistance > 10 MΩ, 10 lux 48-140 kΩ, peak spectral response 560-620 nm.
DPT1 and DPT2: Silicon Darlington phototransistor (MEL 12 NPN).

LDR   DPT
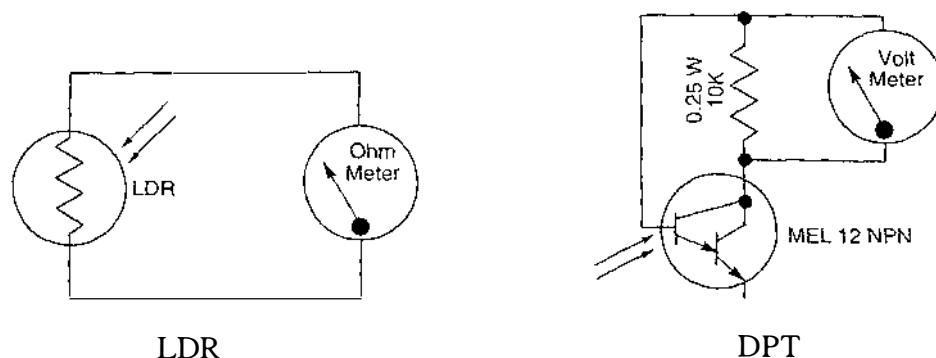
Figure 7-1. Circuit diagrams for DPT and LDR sensors.

The sensors were connected as displayed in the circuit diagrams of Figure 7-1. The sensor components were super-glued to a pre-cut glass microscope slide (the optical lens of the phototransistor was sanded flat first). The backs of both sensors LDR and DPT were then embedded in 5 minute epoxy resin using rubber moulding techniques (see Figure 5-24 and Figure 5-25, pg. 153, 154).

A second set of sensors (LDR2 and DPT2) were fabricated and calibrated for use as backups to LDR1 and DPT1. The cross-reference calibration values for these sensors in the dummy cell holder are:

- ❖ LDR1 (158 Ω), LDR2 (159 Ω).
- ❖ DPT1 (130 mV), DPT2 (125 mV).

Cell Holders (CH1, CH2 and CH3)

Construction of the cell holders is detailed in the text (see Section 5.2, pg 154).

Power Conditioner

Sola 230V/50Hz mains power conditioner (required a 2 hour warm up period).

Multimeters

Dick Smith Electronics Multimeter (Q-1563).

Digitech 3.5 Dig Multimeter with a PC RSC232 interface (QM-1350).

7.5.2   TiO$_2$-coated Plates Used

During the course of testing cells, different batches of TiO$_2$ (PA-PD) were used as supplied by Sustainable Technologies Australia Ltd (STA), NSW, Australia. STA is licensed to produce the Grätzel cells. Different plates from within the same batch set supplied are also designated by an additional identification number, i.e. PA1, PA2 etc.

7.5.3   Electrolytes Used

A number of electrolyte systems (A-G) were prepared, evaluated and used over the course of this research work:

   A.   (0.6 M LiI, 0.1 M I_2 in glutaronitrile).

   B.   (0.6 M LiI, 0.01 M I_2 in glutaronitrile).

   C.   (0.6 M LiI, 0.1 M I_2 in 3-methoxypropionitrile).

   D.   (0.6 M LiI, 0.1 M I_2, 4-t-butylpyridine (1.0 mM) in glutaronitrile).

   E.   (0.5 M NaI, 0.05 M I_2, in glutaronitrile).

   F.   (0.5 M NaI, 0.05 M I_2 in ethylene glycol).

   G.   (0.5 M NaI, 0.05 M I_2, 4-t-butylpyridine (0.01 mol L^{-1}) in glutaronitrile).

Cells using electrolytes (A-D) took a long time to stabilise. It was later found that the LiI obtained to make these electrolytes was not anhydrous as assumed. NaI was then chosen, as it was easier to obtain and prepare in its anhydrous form, thereby eliminating any possible problems associated with solvated H_2O affecting the cell performance. Electrolyte G in dry glutaronitrile with 4-t-butylpyridine as an additive gave the best results, allowing the cells to rapidly stabilise to a SS I_{sc} condition. A small amount of fine white precipitate formed on storage of E and G, so the electrolyte was shaken prior to use.

7.5.4   Refined Solar Cell Testing Procedure

The sequence of steps that were required for PEC testing are:

   A. TiO_2 electrode preparation (cutting, pre-treatment and dye adsorption).

   B. Platinum counter electrode preparation.

   C. Cell assembly and electrolyte introduction in cell holder **CH3**.

   D. Calibration of light source and testing.

   E. Data acquisition.

A. TiO$_2$ Electrode Preparation

Cutting and Pre-treatment

Using a cutting guide the TiO$_2$ plates were prepared by cutting 10 x 15 mm sections of the TiO$_2$ coated glass. The TiO$_2$ surface was placed face down on lint-free tissue paper, taking care not to damage the surface during cutting. Cutting with a standard glasscutter was found easier using hexane (in place of kerosene) inside the glasscutter. One edge of the TiO$_2$ layer was then scraped back for an electrode contact point, leaving about a 10 x 10 mm TiO$_2$ square, with the TiO$_2$ extending fully to 3 edges (see Figure 5-29, pg 158). The TiO$_2$ plates were then pre-treated by washing with ethanol (30 min), hexane (30 min), Milli Q water (30 min) and then rinsed with ethanol prior to drying and firing at 480°C for 30 min. All TiO$_2$ plates were carefully handled with tweezers and powder-free gloves to avoid contamination.

Dye Adsorption

Prior to dye adsorption, the plates were fired again at 480°C for 30 min and then immersed in the dye solution while still warm. The plates were immersed in a sealed container of dye solution (10^{-4} M) for over night adsorption (12-20 hours) prior to testing. Most dye adsorptions were carried out using 3.3 to 5.0 mL per 1.0 cm^2 of TiO$_2$ area. The concentration was based on moles of porphyrin units per dye molecule, not the whole molecule. The TiO$_2$ plates were removed from the dye solution directly before testing and the excess solvent removed by blotting on lint-free tissue paper. Generally, the electrodes were not rinsed but if rinsing was carried out, it was done in the same solvent as the dye was adsorbed, for 5 minutes before blotting dry. These dyed plates were then dried under high vacuum for 5 minutes prior to cell assembly in cell holder **CH3**.

B. Platinum Counter Electrode Preparation

The 13 x 12 mm Pt counter electrode was stored in ethanol until required. The cell side was polished by rubbing on lint-free paper wetted with acetone on a flat glass surface. The electrode was then air-dried for 5 minutes prior to each cell test.

C. Cell Assembly and Electrolyte Introduction in Cell Holder CH3

Prior to assembling and during assembly of the cell, the cell holder electrodes were short-circuited (to prevent any damaging V_{oc} conditions within the cell before testing). Assembly of the cell in holder **CH3** involved clamping the dyed TiO_2 electrode into the modified Bull Dog clip. Next the Pt counter electrode was placed against the TiO_2 layer while releasing the counter electrode contact support onto the Pt plate. Electrolyte was then introduced by capillary action into the cell between the two cell electrode surfaces and any excess electrolyte removed with a paper towel.

D. Calibration of Light Source and Testing

The bulb assembly required a 15 minute warm up before testing, to stabilise any thermal drift. After checking calibration of the light source with DPT1 (130 mV, adjusting the vertical hight of the X-Y-Z stage if necessary) the lamp was momentarily turned off while the assembled cell holder was placed into the testing rig and connected up to the multimeter, in a closed circuit current (I_{sc}) reading mode. I_{sc} readings were taken as soon as the light source was turned on. Figure 5-30 (pg 159) shows the final illuminated cell holder **CH3** set-up in the testing apparatus.

E. Data Acquisition

The data collection system comprised of a Digitech Multimeter with a PC RSC232 interface, collecting the data directly on a computer. I_{sc} data was recorded automatically every 30 seconds, and V_{oc} readings were performed for 10 seconds (V_{oc} reading times were kept short to eliminate any damaging open circuit conditions) as required. V_{oc} readings were generally taken after a SS I_{sc} value was observed, the cell current was then allowed time to recover before any more V_{oc} readings were performed. All I_{sc} values recorded in the final set-up using cell holder **CH3** were corrected to mA cm^{-2} by accurately measuring the TiO_2 area with vernier calipers after testing.

In general, the protocol for the final screening of porphyrins involved the fabrication and testing of three separate identical cells for each compound. If two consistent results (<10% deviation in I_{sc}) were not obtained, extra cells were constructed and tested,

calculating the average I_{sc} and V_{oc} results of these. Any cell results that appeared as outliers were discarded; if this was a result of poor cell mechanics (i.e. short circuiting between electrodes or damaged TiO_2 layer) generally a low V_{oc} resulted, allowing a confident exclusion of this result. For cells that never reached a steady state (SS) I_{sc} value, their maximum I_{sc} values are used.

7.5.5   TiO$_2$ Electrode Inconsistencies

Evaluation of TiO$_2$ Consistency by Dye Binding (Batch PB vs. PC).

Zn-15 dye binding to electrodes of the same area was carried out on a series of pre-treated PC TiO_2-coated electrodes, and compared to an older PB TiO_2 electrode (Table 7-1). The TiO_2 area was scraped to 7 x 7 mm for all plates, and then fired at 480°C for 30 min. On cooling *in vacuo* the TiO_2-coated plates were immersed in a solution of **Zn-15** (3 mL, 10^{-5} M, THF) dye for 18 h. Excess dye was rinsed off with THF (3 mL, 5 min) the electrode. The bound dye was then desorbed from the electrode using Et_3N (3 x 2 mL) giving TiO_2 layers free of discolouration. The resulting dye solutions were made up to a standard volume (10.0 mL, Et_3N). The UV-vis absorption spectra were acquired and the maximum absorbance values of the Soret band recorded.

Table 7-1. TiO_2 pre-treatment versus adsorption of **Zn-15** dye.

#	TiO$_2$ Plate	Pre-treatment	UV-vis Absorbance (λ_{max})
1	PB	None	0.246
2	PC	None	0.111
3	PC	H$_2$O (5 mL), 2 hr	0.192
4	PC	aq. Et$_3$N (5 mL, 0.1 M), 2 hr	0.192
5	PC	HCl (7 mL, 0.03 M), 2 hr	0.173

Evaluation of Non-Uniformity of TiO$_2$ Thickness by UV-vis Spectroscopy.

This UV-vis method was used after testing a series of cells containing Grätzel's strongly binding Ru_{red} **118** dye, to see if the differences in I_{sc} readings was reflected in the amount of dye adsorbed onto the electrodes. UV-vis analysis was carried out on two TiO_2 Ru_{red} PD electrodes that showed a large difference in I_{sc} values. Solar cells (203 and 207) were fabricated and tested as described above, using electrolyte E to give maximum I_{sc} values as quoted in Table 7-2. After testing, the cells were dismantled and

the dye coated TiO_2 electrode rinsed free of electrolyte with acetonitrile. The dye was desorbed with 0.1 M methanolic NaOH (2 x 1.5 mL). The solvent was then removed *in vacuo*. A standard solution of 2.0 mL was made up in MeOH and the UV-vis absorption spectrum obtained. The strongest absorption band at 308 nm was recorded giving the following results (Table 7-2).

Table 7-2. TiO_2 thickness variations.

Cell # (Plate)	I_{sc} (mA cm^{-2})	V_{oc} (mV)	Absorbance (A cm^{-2} TiO_2)
203 (PD1)	4.54	580	0.475
207 (PD1)	5.21	590	0.551

7.6 Chapter 6: Synthesis of Sulfur Functionalised Porphyrins

7.6.1 Thiol and Disulfide Porphyrins

4-*p*-Tolyldisulfanylbenzaldehyde, 146

$C_{14}H_{12}OS_2$
Exact Mass: 260.0330
Mol. Wt.: 260.3765

and 4,4'-Dithiobisbenzaldehyde, 133.

$C_{14}H_{10}O_2S_2$
Exact Mass: 274.0122
Mol. Wt.: 274.3600
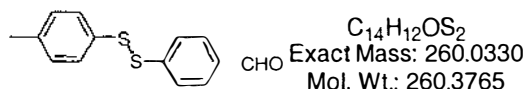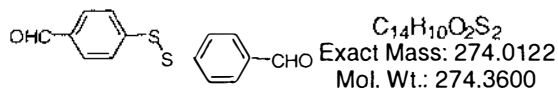
Bromination.

A solution of 4,4'-dithiobistoluene[208] **141** (962 mg, 3.91 mmol) in CCl_4 (4.8 mL) was heated to reflux under argon using a 275 W tungsten heat lamp. Br_2 (0.8 mL, 4.0 eq) was added drop-wise (at such a rate that no permanent brown colour persisted) over 3.5 h. On cooling to RT, the solution was washed with sat. $Na_2HCO_{3(aq)}$ (50 mL). The organic layer was dried ($MgSO_4$), filtered and the solvent removed *in vacuo*. The residue was dissolved in CH_2Cl_2:hexane (1:1) and filtered through a plug of silica gel until all the brown colour had disappeared. Removal of the solvent *in vacuo* gave a pale yellow solid (1.25 g) which was identified as a mixture of bromomethyl products by ^{1}H NMR and mass spectrometry. ^{1}H NMR (270 MHz, CDCl$_3$, Selected data only): δ 2.331 (s, ArCH$_3$), 4.467 (s, ArCH$_2$Br), 6.617 (s, ArCHBr$_2$).

4-*p*-Tolyldisulfanylbromomethylbenzene, **144**.

$C_{14}H_{13}BrS_2$
Exact Mass: 323.9642
Mol. Wt.: 325.2890
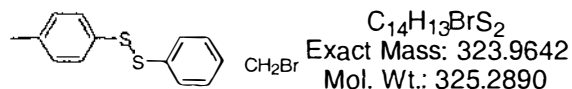
EI$^+$-LRMS: *m/z* (%, assignment) cluster at 323-327, 325 (55, M$^+$). HRMS: Calcd for M$^+$ ($C_{14}H_{13}BrS_2$): 324.9543, found: 324.9549.

4,4'-Dithiobisbromomethylbenzene, **142**.

$C_{14}H_{12}Br_2S_2$
Exact Mass: 401.8747
Mol. Wt.: 404.1851
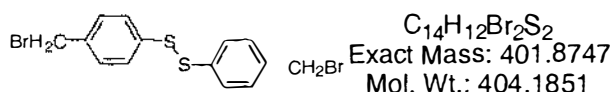
EI$^+$-LRMS: m/z (%, assignment) cluster at 401-408, 404 (25, M$^+$). HRMS: Calcd for M$^+$ (C$_{14}$H$_{12}$Br$_2$S$_2$): 403.8727, found: 403.8720.

4-p-Bromomethylphenyldisulfanyl-dibromomethylbenzene, **145**.

BrH$_2$C—⟨benzene⟩—S—S—⟨benzene⟩—CHBr$_2$ C$_{14}$H$_{10}$Br$_4$S$_2$
Exact Mass: 557.6957
Mol. Wt.: 561.9772

EI$^+$-LRMS: m/z (%, assignment) cluster at 479-487, 484 (2, M$^+$). HRMS: Calcd for M$^+$ (C$_{14}$H$_{11}$Br$_3$S$_2$): 483.7811, found: 483.7791.

Sommelet Reaction.[209]

The crude mixture (1.25 g), HMTA (1.7 g, 12.4 mmol), EtOH (3.5 mL) and H$_2$O (3.5 mL) were heated at reflux for 6 h. Conc. HCl (1.1 mL) was added carefully and reflux continued for a further 30 min. On cooling to RT, H$_2$O (20 mL) was added and mixture extracted with CHCl$_3$ (2 x 50 mL). The organic layer was washed with sat. Na$_2$HCO$_{3(aq)}$ (100 mL), separated and dried (MgSO$_4$) then filtered and solvent removed *in vacuo*. The residue was chromatographed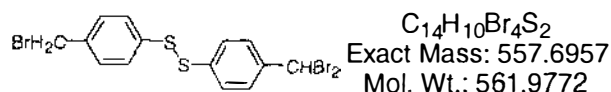 (silica, 150 mm x 27 mm$_{dia}$), collecting two major bands (TLC; R_f = 0.75, 0.4, CH$_2$Cl$_2$). Elution with CH$_2$Cl$_2$:hexane (1:1) giving 4-p-tolyldisulfanylbenzaldehyde **146** (145 mg, 14%) as a pale yellow oil. ^{1}H NMR (270 MHz, CDCl$_3$): δ 2.298 (s, 3H, ArCH$_3$), 7.099 and 7.368 (ABq, 4H, ^3J = 8.2, 8.2 Hz, ArH$_{tolyl}$), 7.637 and 7.777 (ABq, 4H, ^3J = 8.6, 8.5 Hz, ArH$_{CHO}$), 9.922 (s, 1H, CHO). ^{13}C NMR (68.1 MHz, CDCl$_3$): δ 21.024 (**CH$_3$**), 125.947, 128.256, 129.844, 129.947, 132.196, 134.446, 137.857, 145.297, 190.789 (**CHO**). EI$^+$-LRMS: m/z (%, assignment) 260 (95, M$^+$), 123 (100, [M – SPhCHO]$^+$): HRMS: Calcd for M$^+$ (C$_{14}$H$_{12}$OS$_2$): 260.0335, found: 260.0330.

Further elution with CH$_2$Cl$_2$:hexane (3:1) gave 4,4'-dithiobisbenzaldehyde **133** (220 mg, 21%) as a pale yellow solid. ^{1}H NMR (270 MHz, CDCl$_3$): δ 7.578 and 7.776 (ABq, 8H, ^3J = 8.5, 8.5 Hz, ArH), 9.909 (s, 2H, CHO). ^{13}C NMR (68.1 MHz, CDCl$_3$): δ 126.050, 130.138, 134.872, 143.518, 190.657 (**CHO**). EI$^+$-LRMS: m/z (%, assignment) 136 (16, [M – SPhCHO]$^+$), 274 (100, M$^+$): HRMS: Calcd for M$^+$ (C$_{14}$H$_{10}$O$_2$S$_2$): 274.0122, found: 274.0121. mp: 102-104°C (lit, 107°C)[206].

TXP-=-Ph-SS-PhCHO, 147.

1-(4'-Formylphenyldisulfanyl)-4-(*trans*-2''-(2'''-(5''',10''',15''',20'''-tetrakis(3'''',5''''-dimethylphenyl)porphyrin)yl)ethen-1''-yl)benzene.

$C_{67}H_{56}N_4OS_2$
Exact Mass: 996.3896
Mol. Wt.: 997.3199
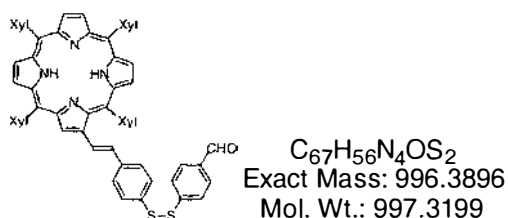
and TXP-=-Ph-SS-Ph-=-TXP, 148.

Bis-4-(*trans*-2'-(2''-(5'',10'',15'',20''-tetrakis(3''',5'''-dimethylphenyl)porphyrin)yl)ethen-1'-yl)-phenyl disulfide.

$C_{120}H_{102}N_8S_2$
Exact Mass: 1718.7669
Mol. Wt.: 1720.2798
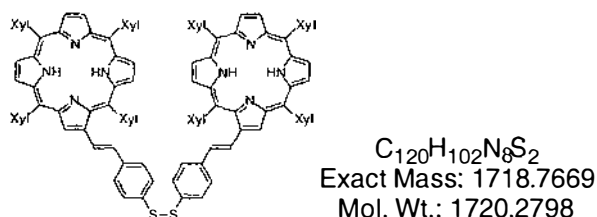
DBU (127 μL, 847 μmol, 2.9 eq) was added to a refluxing solution of disulfide **133** (39.7 mg, 145 μmol) and TXPps salt **5** (300 mg, 289 μmol, 2.0 eq) in toluene (15 mL) under N_2. After 15 min, TLC analysis indicated that all starting material **5** had been consumed. On cooling to RT, the solution was passed through a silica gel plug, then the solvent was removed *in vacuo*. The residue and I_2 (188 mg, 741 μmol, 2.5 eq) were dissolved in CH_2Cl_2 (15 mL) and stirred at RT for 3 h. Next excess sat. $Na_2S_2O_3$ was added and stirring continued for 20 min. The organic layer was separated and dried ($MgSO_4$), then the solvent removed *in vacuo*. The residue was column chromatographed (silica, 37 mm_{dia} x 130 mm), eluting with 2:1 (CH_2Cl_2:hexane) to give the diporphyrin **148** (106 mg, 42%, recrystallised from CH_2Cl_2/MeOH) as a purple powder. ^{1}H NMR (270 MHz, $CDCl_3$, TMS): δ -2.598 (br s, 4H, NH), 2.559 (s, 12H, H_{Me-Xyl}), 2.61-2.65 (m, 36H, H_{Me-Xyl}), 7.076 and 7.301 (ABq, 4H, ^3J = 16.2, 15.4 Hz, $H_{2',1'}$), 7.318 and 7.567 (ABq, 8H, ^3J = 8.9, 8.7 Hz, H_{styryl}), 7.418 (br s, 4H, H_{p-Xyl}), 7.45-7.47 (m, 4H, H_{p-Xyl}), 7.81-7.89 (m, 16H, H_{o-Xyl}), 8.79-8.87 (m, 12H, $H_{\beta-pyrrolic}$), 9.038 (s, 2H, $H_{3''\,(\beta-pyrrolic)}$). UV-vis ($CH_2Cl_2$): λ_{max} [nm] (ε x 10^{-3}) 301 (50.4), 427 (441), 526 (41.8), 567 (26.0), 600 (15.6), 657 (5.66). FAB-LRMS: *m/z (%, assignment)* cluster at 1717-1724, 1721 (100, MH$^+$). HRMS: Calcd for MH$^+$ ($C_{120}H_{103}N_8S_2$): 1719.7747, found: 1719.7646.

Further elution with CH_2Cl_2 gave the formyl monoporphyrin **147** (39.4 mg, 27%, recrystallised from CH_2Cl_2/MeOH) as a purple powder. ^{1}H NMR (270 MHz, $CDCl_3$, TMS): δ -2.618 (br s, 2H, NH), 2.50-2.64 (m, 24H, $H_{Me\text{-}Xyl}$), 7.022 (d, 1H, ^3J = 15.8 Hz, $H_{2''}$), 7.225 (d, 2H, ^3J = 7.6 Hz, H_{styryl}), 7.41-7.50 (m, 7H, $2H_{styryl}$ + $4H_{p\text{-}Xyl}$ + $H_{1''}$), 7.725 (d, 2H, ^3J = 8.2 Hz, ArH_{CHO}), 7.79-7.89 (m, 10H, $2ArH_{CHO}$ + $8H_{o\text{-}Xyl}$), 8.78-8.87 (m, 6H, $H_{\beta\text{-pyrrolic}}$), 8.999 (s, 1H, $H_{3''\ (\beta\text{-pyrrolic})}$), 9.993 (s, 1H, CHO). UV-vis (CH_2Cl_2): λ_{max} [nm] (ε x 10^{-3}) 297 (36.6), 427 (230), 526 (21.6), 567 (12.9), 600 (8.05), 657 (3.25). FAB-LRMS: m/z (%, assignment) cluster at 996-1002, 998 (100, MH^+). HRMS: Calcd for MH^+ ($C_{67}H_{57}N_4OS_2$): 997.3974, found: 997.3944.

NiTXP-=-Ph-SS-Ph-=-NiTXP, Ni$_2$-148 .

Bis-4-(*trans*-2'-(2''-(5'',10'',15'',20''-tetrakis(3''',5'''-dimethylphenyl)porphyrinato nickel(II))yl)-ethen-1'-yl)phenyl disulfide.

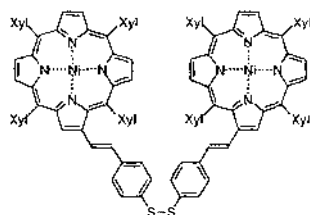$C_{120}H_{98}N_8Ni_2S_2$
Exact Mass: 1830.6063
Mol. Wt.: 1833.6348

A solution of $Ni(OAc)_2 \cdot 4H_2O$ (280 mg, 1.23 mmol, 30 eq) in MeOH (2.0 mL) was added to a refluxing solution of diporphyrin **148** (65.0 mg, 37.8 μmol) in $CHCl_3$ (15 mL) with stirring under N_2. After 16 h, TLC analysis indicated that all of **148** had been consumed. After cooling to RT, the crude product was precipitated with MeOH. The resulting solid was dissolved in CH_2Cl_2 and filtered through a plug of silica gel. Recrystallisation from CH_2Cl_2/MeOH gave **Ni-148** (65.0 mg, 93%) as a pink powder. ^{1}H NMR (270 MHz, $CDCl_3$, TMS): δ 2.470 (s, 12H, $H_{Me\text{-}Xyl}$), 2.54-2.57 (m, 36H, $H_{Me\text{-}Xyl}$), 6.937 and 7.118 (ABq, 4H, ^3J = 16.2, 15.4 Hz, $H_{2',1'}$), 7.219 and 7.505 (ABq, 8H, ^3J = 8.7, 8.4 Hz, H_{styryl}), 7.328 (br s, 4H, $H_{p\text{-}Xyl}$), 7.359 (br s, 4H, $H_{p\text{-}Xyl}$), 7.58-7.65 (m, 16H, $H_{o\text{-}Xyl}$), 8.69-8.75 (m, 12H, $H_{\beta\text{-pyrrolic}}$), 8.910 (s, 2H, $H_{3''\ (\beta\text{-pyrrolic})}$). UV-vis ($CH_2Cl_2$): λ_{max} [nm] (ε x 10^{-3}) 311 (49.2), 428 (367), 540 (36.1), 576 (25.1). FAB-LRMS: m/z (%, assignment) cluster at 1829-1838, 1833 (100, M^+). HRMS: Calcd for M^+ ($C_{120}H_{98}N_8Ni_2S_2$): 1830.6063, found: 1830.6095.

ZnTXP-=-Ph-SS-Tolyl, Zn-149.

1-(p-Tolyldisulfanyl)-4-(*trans*-2'-(2''-(5'',10'',15'',20''-tetra(3''',5'''-dimethylphenyl)-porphyrinato zinc(II))yl)ethen-1'-yl)benzene.
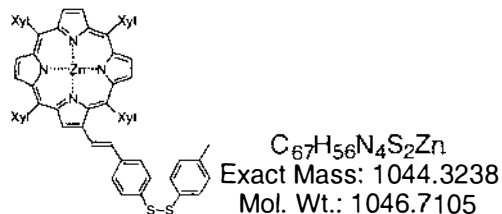
$C_{67}H_{56}N_4S_2Zn$
Exact Mass: 1044.3238
Mol. Wt.: 1046.7105

DBU (122 μL, 816 μmol, 5.0 eq) was added to a refluxing solution of tolyl formylphenyl disulfide **146** (127 mg, 491 μmol) and TXPps salt **5** (170 mg, 164 μmol, 0.33 eq) in toluene (10 mL) under N_2. After 20 min, TLC analysis indicated that all **5** had been consumed, and on cooling to RT the solvent was removed *in vacuo*. The residue was dissolved in minimal CH_2Cl_2 (20 mL) then passed through a plug of silica gel. A solution of Zn(OAc)$_2$·2H$_2$O (72 mg, 328 μmol, 2.0 eq) in MeOH (1.0 mL) was added. After stirring for 20 min at RT, the solution was again filtered through a plug of silica gel and the solvent removed *in vacuo*. The residue was column chromatographed (silica, 27 mm$_{dia}$ x 180 mm, CH_2Cl_2:hexane (1:2)). The first major band was collected and solvent removed to give **Zn-149** (41.3 mg, 24%) as a purple solid. ^{1}H NMR (270 MHz, CDCl$_3$, TMS): δ 2.372 (s, 3H, H$_{Me\text{-}Tolyl}$), 2.536 (s, 6H, H$_{Me\text{-}Xyl}$), 2.644 (s, 12H, H$_{Me\text{-}Xyl}$), 2.672 (s, 6H, H$_{Me\text{-}Xyl}$), 7.080 and 7.230 (ABq, 2H, ^3J = 16.2, 15.7 Hz, H$_{2',1'}$), 7.157 (d, 2H, ^3J = 7.9 Hz, H$_{styryl}$ or ArH$_{Tolyl}$), 7.241 (d, 2H, ^3J = 8.6 Hz, H$_{styryl}$ or ArH$_{Tolyl}$), 7.40-7.50 (m, 8H, 2H$_{Tolyl}$ + 2H$_{styryl}$ + 4H$_{p\text{-}Xyl}$), 7.836 (br s, 2H, H$_{o\text{-}Xyl}$), 7.89-7.95 (m, 6H, H$_{o\text{-}Xyl}$), 8.95-9.03 (m, 6H, H$_{\beta\text{-}pyrrolic}$), 9.162 (s, 1H, H$_{3''\ (\beta\text{-}pyrrolic)}$). UV-vis ($CH_2Cl_2$): λ_{max} [nm] (ε x 10^{-3}) 308 (20.9), 431 (227), 558 (20.7), 594 (8.44). FAB-LRMS: m/z (%, assignment) cluster at 1044-1051, 1044 (100, M$^+$). HRMS: Calcd for M$^+$ ($C_{67}H_{56}N_4S_2Zn$): 1044.3238, found: 1044.3253.

NiTXP-=-Ph-SS-Tolyl, Ni-149.

1-(p-Tolyldisulfanyl)-4-(*trans*-2'-(2"-(5",10",15",20"-tetrakis(3"',5"'-dimethylphenyl)-porphyrinato nickel(II)'}yl)ethen-1'-yl)benzene.

C$_{67}$H$_{56}$N$_4$NiS$_2$
Exact Mass: 1038.3300
Mol. Wt.: 1040.0139
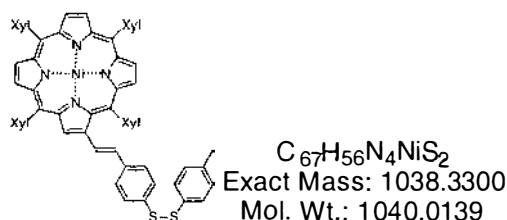
and NiTXP-=-PhSH, Ni-132.

4-(*Trans*-2'-(2"-(5",10",15",20"-tetrakis(3"',5"'-dimethylphenyl)porphyrinato nickel(II))yl)-ethen-1'-yl)benzenethiol.

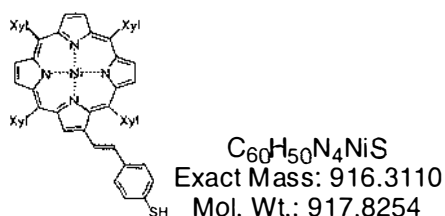C$_{60}$H$_{50}$N$_4$NiS
Exact Mass: 916.3110
Mol. Wt.: 917.8254

DBU (130 μL, 869 μmol, 5.0 eq) was added to a refluxing solution of tolyl formylphenyl disulfide **146** (100 mg, 384 μmol) and TXPps salt **5** (178 mg, 172 μmol, 0.45 eq) in CHCl$_3$ (10 mL) under N$_2$ for 20 min. A solution of Ni(OAc)$_2$·4H$_2$O (640 mg, 2.57 mmol, 15 eq) in MeOH (3.0 mL) was added via the reflux condenser. After stirring for 13 h at reflux, the solution was cooling to RT, and the crude product was precipitated with MeOH. TLC analysis indicated two red bands of lower polarity than **146** and **5**. The residue was column chromatographed (silica, 38 mm$_{dia}$ x 130 mm, CH$_2$Cl$_2$:hexane (1:3)) to give porphyrin disulfide **Ni-149** (61.6 mg, 35%) as a red/purple solid. ^{1}H NMR (270 MHz, CDCl$_3$, TMS): δ 2.368 (s, 3H, H$_{Me\text{-}Tolyl}$), 2.444 (s, 6H, H$_{Me\text{-}Xyl}$), 2.550 (s, 12H, H$_{Me\text{-}Xyl}$), 2.571 (s, 6H, H$_{Me\text{-}Xyl}$), 6.900 and 7.082 (ABq, 2H, ^3J = 16.2, (^4J = 0.9), 15.7 Hz, H$_{2',1'}$), 7.13-7.22 (m, 4H, H$_{styryl}$ + ArH$_{Tolyl}$), 7.31-7.37 (m, 4H, H$_{p\text{-}Xyl}$), 7.444 (d, 2H, ^3J = 8.2 Hz, H$_{styryl}$ or ArH$_{Tolyl}$), 7.458 (d, 2H, ^3J = 8.6 Hz, H$_{styryl}$ or ArH$_{Tolyl}$), 7.569 (br s, 2H, H$_{o\text{-}Xyl}$), 7.61-7.66 (m, 6H, H$_{o\text{-}Xyl}$), 8.68-8.75 (m, 6H, H$_{\beta\text{-pyrrolic}}$), 8.885 (s, 1H, ^4J = 0.9 Hz , H$_{3"\ (\beta\text{-pyrrolic})}$). UV-vis (CH$_2Cl_2$): λ_{max} [nm] (ϵ x 10^{-3}) 313 (20.7), 428 (188), 540 (15.6), 578 (10.2). FAB-LRMS: *m/z* (%, assignment) cluster at 1038-1045, 1038 (100, M$^+$). HRMS: Calcd for M$^+$ (C$_{67}$H$_{56}$N$_4$NiS$_2$): 1038.3300, found: 1038.3246.

Further elution gave the porphyrin thiol **Ni-132** (26.6 mg, 17%) as a red/purple solid. ^{1}H NMR (270 MHz, CDCl$_3$, TMS): δ 2.480 (s, 6H, H$_{Me-Xyl}$), 2.53-2.58 (m, 18H, H$_{Me-Xyl}$), 6.949 and 7.130 (ABq, 2H, ^{3}J = 16.2, 15.9 Hz, H$_{2',1'}$), 6.228 and 7.510 (ABq, 2H, ^{3}J = 8.7, 8.1 Hz, H$_{styryl}$), 7.337 (br s, 2H, H$_{p-Xyl}$), 7.369 (br s, 2H, H$_{p-Xyl}$), 7.600 (br s, 2H, H$_{o-Xyl}$), 7.63-7.68 (m, 6H, H$_{o-Xyl}$), 8.70-8.78 (m, 6H, H$_{\beta-pyrrolic}$), 8.922 (s, 1H, H$_{3''\,(\beta-pyrrolic)}$). UV-vis (CH$_2$Cl$_2$): λ$_{max}$ [nm] (ε x 10^{-3}) 316 (19.8), 428 (165), 539 (16.2), 576 (10.2). FAB-LRMS: m/z (%, assignment) cluster at 914-921, 916 (100, M^{+}). HRMS: Calcd for M^{+} (C$_{60}$H$_{50}$N$_4$NiS): 916.3110, found: 916.3120.

BDP, 150.

2,8,12,18-Tetrabutyl-5,15-di(4-p-tolyldisulfanyl)-3,7,13,17-tetramethylporphyrin.

C$_{66}$H$_{74}$N$_4$S$_4$
Exact Mass: 1050.4796
Mol. Wt.: 1051.5847
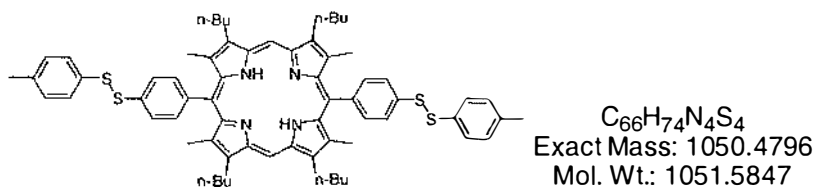
4-p-Tolyldisulfanyl-benzaldehyde **146** (250 mg, 0.960 mmol) and dipyrrylmethane[106,107] **58** (302 mg, 1.06 mmol) were dissolved in MeOH (12 mL, 0.08 M). To this was added p-TsOH·H$_2$O (45.6 mg, 0.25 eq). The reaction mixture was sealed and stirred for 22.5 h at RT, before removing the solvent under reduced pressure. The resulting residue was dissolved in CH$_2$Cl$_2$ (20 mL) and p-chloranil (472 mg, 2.0 eq) added. The resulting mixture was stirred for 2.5 h at RT resulting in a deep green solution. Next, a solution of Na$_2$S$_2$O$_3$·5H$_2$O (3.0 g in 50 mL of H$_2$O) and Et$_3$N (1.0 mL) was added and the mixture stirred vigorously for 30 min. The organic layer was separated and dried (K$_2$CO$_3$), filtered and solvent removed *in vacuo*. The residue was chromatographed (silica, 160 mm x 20 mm$_{dia}$, CH$_2$Cl$_2$), collecting the major green band. The crude product was precipitated from CH$_2$Cl$_2$ with MeOH. Filtration through a plug of basic alumina with CH$_2$Cl$_2$:hexane (1:1) followed by recrystallisation from CH$_2$Cl$_2$/MeOH gave porphyrin **150** (355 mg, 70%) as a pink solid. ^{1}H NMR (270 MHz, CDCl$_3$): δ -2.305 (br s, 2H, NH), 1.232 (t, 12H, ^{3}J = 7.3 Hz, CH$_2$CH$_2$CH$_2$CH$_3$), 1.860 (app sext, 8H, ^{3}J = 7.3 Hz, CH$_2$CH$_2$CH$_2$CH$_3$), 2.22-2.36 (m, 8H, CH$_2$CH$_2$CH$_2$CH$_3$), 2.496 (s, 18H, 6H$_{Me-tolyl}$ + 12H$_{Me-TBMP}$), 4.039 (t, 8H, ^{3}J = 7.9 Hz, CH$_2$CH$_2$CH$_2$CH$_3$), 7.290 (d, 4H, ^{3}J = 8.1 Hz, ArH$_{tolyl}$), 7.610 (d, 4H, ^{3}J = 8.1 Hz, ArH$_{tolyl}$), 7.828 and 7.898 (ABq, 8H, ^{3}J = 8.4, 7.8 Hz, ArH), 10.307 (s, 2H, H$_{meso}$). ^{1}H NMR (270 MHz, C$_6$D$_6$, TMS): δ -1.584 (s, 2H,

NH), 1.084 (t, 12H, ^3J = 7.3 Hz, CH$_2$CH$_2$CH$_2$CH$_3$), 1.726 (app sext, 8H, ^3J = 7.3 Hz,

CH$_2$CH$_2$CH$_2$CH$_3$), 2.032 (s, 6H, H$_{Me\text{-tolyl}}$), 2.14-2.29 (m, 8H, CH$_2$CH$_2$CH$_2$CH$_3$), 2.516 (s,

12H, H$_{Me\text{-TBMP}}$), 3.961 (t, 8H, ^3J = 7.6 Hz, CH$_2$CH$_2$CH$_2$CH$_3$), 6.930 (d, 4H, ^3J = 7.8 Hz,

ArH$_{tolyl}$), 7.563 (d, 4H, ^3J = 8.4 Hz, ArH$_{tolyl}$), 7.577 and 7.694 (ABq, 8H, ^3J = 8.4, 8.4

Hz, ArH), 10.459 (s, 2H, H$_{meso}$). ^{13}C NMR (68.1 MHz, CDCl$_3$): δ 14.349(CH$_3$), 14.849

(CH$_3$), 21.260 (C$_{Me\text{-Tolyl}}$), 23.421 (CH$_2$CH$_2$CH$_2$CH$_3$), 26.509 (CH$_2$CH$_2$CH$_2$CH$_3$), 35.566

(CH$_2$CH$_2$CH$_2$CH$_3$), 96.967 (CH$_{meso}$), 116.728 (C$_{meso}$), 127.256 (C$_{Ar}$), 129.314 (C$_{Ar\text{-Tolyl}}$),

129.829 (C$_{Ar\text{-Tolyl}}$), 133.196, 133.564 (C$_{Ar}$), 135.828, 137.328, 137.887, 141.209,

141.327, 143.224, 144.827. *Assignments aided by COSY & HETCOR spectra.* UV-vis

(CH$_2$Cl$_2$): λ_{max} [nm] (ε x 10^{-3}) 410 (263), 508 (19.7), 541 (5.16), 574 (7.58), 627 (1.10).

FAB-LRMS: *m/z* (%, assignment) cluster at 1049-1055, 1051 (100, MH$^+$). HRMS:

Calcd for MH$^+$ (C$_{66}$H$_{75}$N$_4$S$_4$): 1051.4875, found: 1051.4864.

ZnBDP, Zn-150.

2,8,12,18-Tetrabutyl-5,15-di(4-*p*-tolyldisulfanyl)-3,7,13,17-tetramethylporphyrinato

zinc(II).
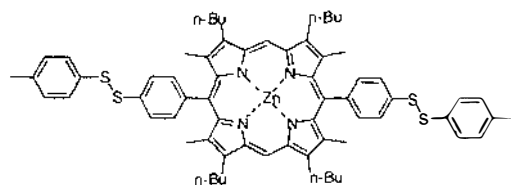
C$_{66}$H$_{72}$N$_4$S$_4$Zn
Exact Mass: 1112.3931
Mol. Wt.: 1114.9588

A solution of Zn(OAc)$_2$·2H$_2$O (37 mg, 170 μmol, 2.0 eq) in MeOH (1.0 mL) was added

to a solution of porphyrin **150** (85.7 mg, 83.7 μmol) in CHCl$_3$ (5.0 mL) with stirring at

RT. The reaction was deemed complete by TLC after 15 min with the appearance of a

new coloured band at higher R_f than **150**. The product was precipitated with MeOH to

give **Zn-150** (81.2 mg, 87%) as a pink powder. ^{1}H NMR (270 MHz, CDCl$_3$): δ 1.103 (t,

12H, ^3J = 7.3 Hz, CH$_2$CH$_2$CH$_2$CH$_3$), 1.737 (app sext, 8H, ^3J = 7.3 Hz,

CH$_2$CH$_2$CH$_2$CH$_3$), 2.06-2.19 (m, 8H, CH$_2$CH$_2$CH$_2$CH$_3$), 2.41-2.43 (m,[2.413 (s), 2.423

(s), 18H, 6H$_{Me\text{-tolyl}}$ + 12H$_{Me\text{-TBMP}}$]), 3.888 (t, 8H, ^3J = 7.6 Hz, CH$_2$CH$_2$CH$_2$CH$_3$), 7.248 (d,

4H, ^3J = 8.1 Hz, ArH$_{tolyl}$), 7.585 (d, 4H, ^3J = 7.8 Hz, ArH$_{tolyl}$), 7.868 and 7.962 (ABq,

8H, ^3J = 8.4, 8.4 Hz, ArH), 10.079 (s, 2H, H$_{meso}$). UV-vis (CH$_2$Cl$_2$): λ_{max} [nm] (ε x 10^{-3})

412 (439), 539 (19.7), 575 (10.3). FAB-LRMS: *m/z* (%, assignment) cluster at 1111-

1120, 1112 (100, M$^+$). HRMS: Calcd for M$^+$ (C$_{66}$H$_{72}$N$_4$S$_4$Zn): 1112.3931, found:

1112.3937.

7.6.2 Thienylporphyrins

B2TP, 134.

5,15-Bis(2'-thienyl)-2,8,12,18-tetra-*n*-butyl-3,7,13,17-tetramethylporphyrin.
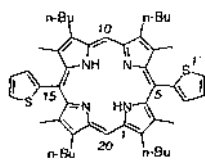
$C_{48}H_{58}N_4S_2$
Exact Mass: 754.4103
Mol. Wt.: 755.1331

p-TsOH·H$_2$O (30.2 mg, 159 μmol, 0.25 eq) was added to a solution of 2-formylthiophene **151** (71.2 mg, 635 μmol) and dipyrrylmethane **58** (200 mg, 698 μmol, 1.1 eq) in MeOH (8 mL) at RT. The reaction was sealed and stirred for 12 h in the dark. The solvent was removed *in vacuo*. The residue was dissolved in CH$_2$Cl$_2$ (20 mL) and *p*-chloranil (342 mg, 1.39 mmol, 2.2 eq) was added and the mixture stirred at RT for 2.5 h. Next sat. Na$_2$S$_2$O$_3$ (50 mL) containing Et$_3$N (500 μL) was added and the mixture stirred vigorously for 1.5 h. The organic layer was separated and dried (MgSO$_4$) and the product precipitated out CH$_2$Cl$_2$ with MeOH (twice), to give product **134** (155 mg, 65%) as a dark purple powder. ^{1}H NMR (270 MHz, CDCl$_3$, TMS): δ -2.31 (br s, 2H, NH), 1.10 (t, 12H, ^3J = 7.3 Hz, CH$_2$CH$_2$CH$_2$CH$_3$), 1.75 (app sex, 8H, ^3J = 7.3 Hz, CH$_2$CH$_2$CH$_2$CH$_3$), 2.10-2.25 (m, 8H, CH$_2$CH$_2$CH$_2$CH$_3$), 2.72 (s, 12H, H$_{Me\text{-}TBMP}$), 4.00 (t, 8H, ^3J = 7.6 Hz, CH$_2$CH$_2$CH$_2$CH$_3$), 7.48 (dd, 2H, ^3J = 5.2, 3.4 Hz, H$_{4', thienyl}$), 7.75 (dd, 2H, ^3J = 3.4, ^4J = 0.9 Hz, H$_{3', thienyl}$), 7.82 (dd, 2H, ^3J = 5.2, ^4J = 0.9 Hz, H$_{5', thienyl}$), 10.25 (s, 2H, H$_{meso}$). UV-vis (CH$_2$Cl$_2$): λ$_{max}$ [nm] (ε x 10^{-3}) 409 (194), 510 (14.2), 545 (6.74), 578 (5.81), 629 (3.36). FAB-LRMS: *m*/z (%, assignment) 756 (100, MH$^+$). HRMS: Calcd for MH$^+$ (C$_{48}$H$_{59}$N$_4$S$_2$): 755.4181, found: 755.4130.

ZnB2TP, Zn-134.

5,15-Bis(2'-thienyl)-2,8,12,18-tetra-*n*-butyl-3,7,13,17-tetramethylporphyrinato zinc(II).
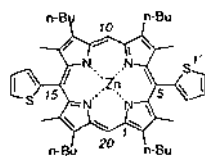
$C_{48}H_{56}N_4S_2Zn$
Exact Mass: 816.3238
Mol. Wt.: 818.5072

A solution of Zn(OAc)$_2$·2H$_2$O (35 mg, 159 μmol, 2.0 eq) in MeOH (1.0 mL) was added to a solution of porphyrin **134** (60.0 mg, 79.5 μmol) in CHCl$_3$ (10 mL) at RT. The reaction mixture was monitored by TLC and judged complete after 10 min by the

absence of **134**. The product was precipitated out of solution with MeOH, and dried under high vacuum to give product **Zn-134** (65.7 mg, 100 %) as a purple microcrystalline solid. ^{1}H NMR (270 MHz, CDCl$_3$, TMS): δ 1.11 (t, 12H, ^3J = 7.3 Hz, CH$_2$CH$_2$CH$_2$CH$_3$), 1.74 (app sex, 8H, ^3J = 7.3 Hz, CH$_2$CH$_2$CH$_2$CH$_3$), 2.06-2.22 (m, 8H, CH$_2$CH$_2$CH$_2$CH$_3$), 2.66 (s, 12H, H$_{Me\text{-}TBMP}$), 3.90 (t, 8H, ^3J = 7.6 Hz, CH$_2$CH$_2$CH$_2$CH$_3$), 7.49 (dd, 2H, ^3J = 5.2, 3.4 Hz, H$_{4', thiophene}$), 7.74 (dd, 2H, ^3J = 3.4, ^4J = 0.9 Hz, H$_{3', thienyl}$), 7.82 (dd, 2H, ^3J = 5.2, ^4J = 1.2 Hz, H$_{5', thienyl}$), 10.07 (s, 2H, H$_{meso}$). UV-vis (CH$_2$Cl$_2$): λ$_{max}$ [nm] (ε x 10^{-3}) 350 (17.9), 412 (369), 541 (17.5), 580 (14.7). FAB-LRMS: m/z (%, assignment) 817 (22, M$^+$), 756 (100, [M − Zn + 2H]$^+$). HRMS: Calcd for M$^+$ (C$_{48}$H$_{56}$N$_4$S$_2$Zn$_4$): 816.3238, found: 816.3217.

B3TP, 135.

5,15-Bis(3'-thienyl)-2,8,12,18-tetra-*n*-butyl-3,7,13,17-tetramethylporphyrin.

C$_{48}$H$_{58}$N$_4$S$_2$
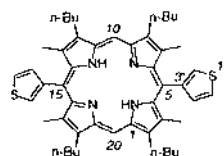Exact Mass: 754.4103
Mol. Wt.: 755.1331

3-Formylthiophene **152** (30.6 μL, 349 μmol) and dipyrrylmethane **58** (100 mg, 349 μmol) were dissolved in degassed anhydrous CH$_2$Cl$_2$ (35 mL) at RT. TFA (26.9 μL, 349 μmol, 1.0 eq) was added and the solution stirred under N$_2$. At the first sign of baseline material by TLC (≈ 15 minutes; silica gel, CH$_2$Cl$_2$) the reaction was quenched by the addition of DBU (52.2 μL, 349 μmol, 1.0 eq). Then *p*-chloranil (214.5 mg, 873 μmol, 2.5 eq) was added and the solution stirred for 4 h at RT. Next Et$_3$N (36 μL, 258 μmol) was added and reaction stirred vigorously for 1.5 h. Then excess Et$_3$N (723 μL, 5.190 mmol) was added and reaction stirred for 15 min. The product was then precipitated out of solution with MeOH giving porphyrin **135** (69.3 mg, 53%) as a purple crystalline solid. ^{1}H NMR (270 MHz, CDCl$_3$, TMS): δ -2.41 (br s, 2H, NH), 1.12 (t, 12H, ^3J = 7.3 Hz, CH$_2$CH$_2$CH$_2$CH$_3$), 1.78-1.90 (app sex, 8H, ^3J = 7.3 Hz, CH$_2$CH$_2$CH$_2$CH$_3$), 2.13-2.28 (m, 8H, CH$_2$CH$_2$CH$_2$CH$_3$), 2.66 (s, 12H, H$_{Me\text{-}TBMP}$), 4.03 (t, 8H, ^3J = 7.6Hz, CH$_2$CH$_2$CH$_2$CH$_3$), 7.77 (s, 6H, H$_{thienyl}$), 10.26 (s, 2H, H$_{meso}$). ^{13}C NMR (68.1 MHz, CDCl$_3$): δ 13.7, 14.3, 23.4, 26.5, 35.6, 97.0, 111.7, 124.4, 126.8, 132.6, 136.2, 141.3, 142.0, 143.1, 145.4; UV-vis (CH$_2$Cl$_2$): λ$_{max}$ [nm] (ε x 10^{-3}) 408 (208), 507 (19.8), 542 (9.1), 574 (10.5), 627 (5.4), 674 (3.7). FAB-LRMS: m/z = (%) cluster at 755 (100%, MH$^+$). HRMS: Calcd for MH$^+$ (C$_{48}$H$_{59}$N$_4$S$_2$): 755.4181, found: 755.4162.

TXP-=-Terthiophene, 137.

Trans-1-(2'-(5',10',15',20'-tetrakis(3",5"-dimethylphenyl)porphyrinyl))-2-([2''',2'''':5'''',2'''''-terthiophen]-3''''-yl)ethene.

$C_{66}H_{54}N_4S_3$
Exact Mass: 998.3511
Mol. Wt.: 999.3599

A solution of TXPps **5** (100 mg, 96.4 μmol) and 3'-formyl-2,2':5',2''-terthiophene **136** (71.9 mg, 260 μmol, 2.7 eq) in dry toluene (5.0 mL) was heated to reflux. DBU (43 μL, 288 μmol, 3 eq) was added and reaction refluxed for 30 min. The solution was cooled and the solvent removed in vacuo. The residue was column chromatographed (100 mm x 27 mm$_{dia}$, CH$_2$Cl$_2$:hexane (3:4)) collecting the major purple band (R_f = 0.50, CH$_2$Cl$_2$:hexane (1:1)). Recrystallisation from CH$_2$Cl$_2$/MeOH give porphyrin **137** (80.3 mg, 83%) as a purple powder. ^{1}H NMR (400 MHz, CDCl$_3$, TMS): δ -2.598 (br s, 2H, NH), 2.592 (s, 18H, H$_{Me-Xyl}$), 2.609 (s, 6H, H$_{Me-Xyl}$), 6.803 (d, 1H, ^3J = 16.0 Hz, H$_{1, ethenyl}$), 7.015 (s, 1H, H$_{4''', thienyl}$), 7.120 (dd, 1H, ^3J = 5.1, 3.6 Hz, H$_{4'''', thienyl}$), 7.138 (dd, 1H, ^3J = 5.1, 3.6 Hz, H$_{4''', thienyl}$), 7.263 (dd, 1H, ^3J = 3.6, ^4J = 1.1 Hz, H$_{3'', thienyl}$), 7.278 (dd, 1H, ^3J = 3.6, ^4J = 1.1 Hz, H$_{3'''', thienyl}$), 7.366 (dd, 1H, ^3J = 5.1, ^4J = 1.1 Hz, H$_{5'''', thienyl}$), 7.408 (dd, 1H, ^3J = 5.1, ^4J = 1.1 Hz, H$_{5''', thienyl}$), 7.38-7.42 (m, 3H, H$_{p-Xyl}$), 7.602 (br s, 1H, H$_{p-Xyl}$), 7.650 (d, 1H, ^3J = 16.0 Hz, H$_{2, ethenyl}$), 7.829 (br s, 5H, H$_{o-Xyl}$), 7.867 (br s, 3H, H$_{o-Xyl}$), 8.804 and 8.814 (ABq, 2H, ^3J = 4.8 Hz, H$_{7', 8', \beta-pyrrolic}$), 8.833 and 8.862 (ABq, 2H, ^3J = 4.8 Hz, H$_{17', 18', \beta-pyrrolic}$), 8.849 (s, 2H, H$_{12', 13', \beta-pyrrolic}$), 9.017 (s, 1H, H$_{3', \beta-pyrrolic}$). *Assignments aided by short and long-range COSY spectra.* UV-vis (CH$_2$Cl$_2$): λ_{max} [nm] (ε x 10^{-3}) 311 (34.4), 426 (255), 527 (23.6), 568 (14.5), 601 (9.20), 660 (3.94). FAB-LRMS: *m/z* (%, assignment) cluster at 998-1002, 999 (100, MH$^+$). HRMS: Calcd for MH$^+$ (C$_{66}$H$_{55}$N$_4$S$_3$): 999.3589, found 999.3534.

ZnTXP-=-Terthiophene, Zn-137.

Trans-1-(2'-(5',10',15',20'-tetrakis(3",5"-dimethylphenyl)porphyrinato zinc(II)yl))-2-([2''',2'''':5'''',2'''''-terthiophen]-3''''-yl)ethene.

$C_{66}H_{52}N_4S_3Zn$
Exact Mass: 1060.2646
Mol. Wt.: 1062.7340
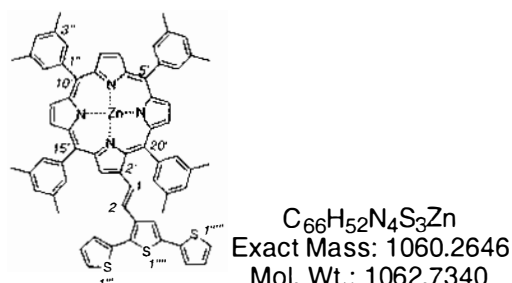
A solution of $Zn(OAc)_2 \cdot 2H_2O$ (11.9 mg, 54 μmol, 1.2 eq) in MeOH (1.0 mL) was added to a solution of terthienylporphyrin **137** (45.0 mg, 45.0 μmol) in $CHCl_3$ (4.5 mL) with stirring at RT for 1 h. The crude product was precipitated with MeOH, and the resulting solid was recrystallised from CH_2Cl_2/MeOH giving **Zn-137** (41.3 mg, 86%) as a purple microcrystalline solid. ^{1}H NMR (400 MHz, $CDCl_3$, TMS): δ 2.589 (s, 6H, H_{Me-Xyl}), 2.598 (s, 12H, H_{Me-Xyl}), 2.613 (s, 6H, H_{Me-Xyl}), 6.817 (dd, 1H, $^3J = 15.7$ Hz, $^4J = 0.7$ Hz, $H_{1,\ ethenyl}$), 7.035 (s, 1H, $H_{4''',\ thienyl}$), 7.12-7.15 (m, 2H, $H_{thienyl}$), 7.26-7.28 (m, 2H, $H_{thienyl}$), 7.37-7.41 (m, 2H, $_{,}H_{thienyl}$), 7.39-7.42 (m, 3H, H_{p-Xyl}), 7.606 (s, 1H, H_{p-Xyl}), 7.621 (d, 1H, $^3J = 15.7$ Hz, $H_{2,\ ethenyl}$), 7.817 (s, 2H, H_{o-Xyl}), 7.838 (s, 4H, H_{o-Xyl}), 7.874 (s, 2H, H_{o-Xyl}), 8.92 and 8.95 (m, 4H, $H_{\beta-pyrrolic}$), 8.971 and 8.999 (ABq, 2H, $^3J = 4.7$ Hz, $H_{17',18',\ \beta-pyrrolic}$), 9.127 (d, 1H, $^4J = 0.8$ Hz, $H_{3',\ \beta-pyrrolic}$). *Assignments aided by COSY spectra.* UV-vis (CH_2Cl_2): λ_{max} [nm] (ε x 10^{-3}) 310 (34.7), 353 (31.1), 430 (227), 561 (23.4), 597 (10.7). FAB-LRMS: *m/z* (%, assignment) cluster at 1060-1066, 1060 (85, M$^+$). HRMS: Calcd for M$^+$ ($C_{66}H_{52}N_4S_3Zn$): 1060.2646, found: 1060.2542.

BTTP, 138.

5,15-Bis([2',2'':5'',2'''-terthiophen]-3''-yl)-2,8,12,18-tetra-*n*-butyl-3,7,13,17-tetramethyl-porphyrin.

$C_{64}H_{66}N_4S_6$
Exact Mass: 1082.3612
Mol. Wt.: 1083.6318
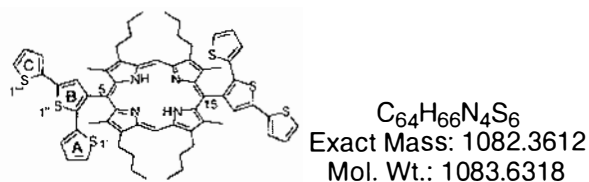
3'-Formyl-2,2':5',2''-terthiophene **136** (96.5 mg, 349 μmol) and dipyrrylmethane **58** (100 mg, 349 μmol) were dissolved in degassed dry CH_2Cl_2 (35 mL) at RT. TFA (26.9 μL,

349 μmol, 1.0 eq) was added and the solution stirred under N_2. At the first sign of baseline material by TLC ($\approx$ 15 minutes; silica gel, CH_2Cl_2) the reaction was quenched by the adding DBU (52.2 μL 349 μmol, 1.0 eq). Then *p*-chloranil (214.5 mg, 873 μmol, 2.5 eq) was added and the solution stirred for 4 h at RT. Next Et_3N (36 μL, 258 μmol) was added and reaction stirred vigorously for 1 h. Excess Et_3N (723 μL, 5.190 mmol) was added and reaction stirred for 15 min. The product was then precipitated out of solution with MeOH, to give product **138** (76.9 mg, 41%) as a brownish-purple solid. ^{1}H NMR (400 MHz, CDCl$_3$, TMS): δ -2.309 (br d, 4H, [-2.304 (NH$_{(\alpha\alpha\ or\ \alpha\beta)}$), -2.314 (NH$_{(\alpha\beta\ or\ \alpha\alpha)}$)]), 1.067 (t, 24H, ^3J = 7.3 Hz, CH$_2$CH$_2$CH$_2$CH$_3$), 1.65-1.78 (app sext, 16H, CH$_2$CH$_2$CH$_2$CH$_3$), 2.11-2.26 (app pent, 16H, CH$_2$CH$_2$CH$_2$CH$_3$), 2.898 (s, 24H, H$_{Me-TBMP}$), 3.90-4.10 (m, 16H, CH$_2$CH$_2$CH$_2$CH$_3$), 6.40-6.48 (m, 8H, H$_{4',\ 5',\ thienyl\ A}$), 6.753 (dd, 2H, ^3J = 3.4, ^4J = 1.5 Hz, H$_{3'\ (\alpha\beta\ or\ \alpha\alpha),\ thienyl\ A}$), 6.786 (dd, 2H, ^3J = 3.4, ^4J = 1.5 Hz, H$_{3'\ (\alpha\alpha\ or\ \alpha\beta),\ thienyl\ A}$), 7.12-7.15 (4H, [7.129 (dd, ^3J = 5.1, 3.6 Hz, H$_{4'''\ (\alpha\alpha\ or\ \alpha\beta)}$), 7.136 (dd, ^3J = 5.1, 3.6 Hz, H$_{4'''\ (\alpha\beta\ or\ \alpha\alpha)}$)]), H$_{thienyl\ C}$), 7.29-7.31 [4H, [7.294 (dd, ^3J = 5.2 Hz, ^4J = 1.1 Hz, H$_{5'''\ (\alpha\alpha\ or\ \alpha\beta)}$), 7.304 (dd, ^3J = 5.2 Hz, ^4J = 1.1 Hz, H$_{5'''\ (\alpha\beta\ or\ \alpha\alpha)}$)]), H$_{thienyl\ C}$), 7.44-7.46 (4H, [7.448 (dd, ^3J = 3.7 Hz, ^4J = 1.1 Hz, H$_{3'''\ (\alpha\alpha\ or\ \alpha\beta)}$), 7.458 (dd, ^3J = 3.7 Hz, ^4J = 1.1 Hz, H$_{3'''\ (\alpha\beta\ or\ \alpha\alpha)}$), H$_{thienyl\ C}$], 7.630 (app d, 4H, [7.629 (H$_{4''\ (\alpha\alpha\ or\ \alpha\beta)}$), 7.631 (H$_{4''\ (\alpha\beta\ or\ \alpha\alpha)}$)], H$_{thienyl\ B}$), 10.227 (app d, 4H, [10.224 (H$_{10,\ 20\ (\alpha\alpha\ or\ \alpha\beta)}$), 10.230 (H$_{10,\ 20\ (\alpha\beta\ or\ \alpha\alpha)}$)], H$_{meso}$). *Assignments aided by COSY spectra.* ^{13}C NMR (101 MHz): δ 13.71, 13.72, 14.2, 23.3, 26.5, 35.6, 97.2, 108.6, 110.18, 110.21, 124.1, 124.2, 124.8, 124.9, 125.4, 126.2, 126.3, 128.1, 130.0, 130.1, 134.1, 134.2, 135.4, 135.5, 136.0, 136.1, 136.5, 137.2, 138.5, 141.9, 143.5, 145.4, 145.5. UV-vis (CH$_2$Cl$_2$): λ_{max} [nm] (ε x 10^{-3}) 415 (203), 511 (17.8), 546 (7.06), 577 (7.59), 630 (3.23). FAB-LRMS: *m/z* (%, assignment) 1083 (100, MH$^+$). HRMS: Calcd for MH$^+$ (C$_{64}$H$_{67}$N$_4$S$_6$): 1083.3690, found: 1083.3719.

ZnBTTP, Zn-138.

5,15-Bis([2',2":5",2'''-terthiophen]-3"-yl)-2,8,12,18-tetra-*n*-butyl-3,7,13,17-tetramethyl-porphyrinato zinc(II).
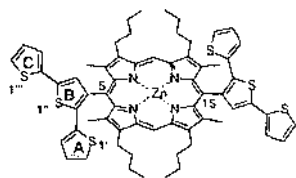
C$_{64}$H$_{64}$N$_4$S$_6$Zn
Exact Mass: 1144.2747
Mol. Wt.: 1147.0059

A solution of Zn(OAc)$_2$·2H$_2$O (42.9 mg, 196 μmol, 1.2 eq) in MeOH (1.0 mL) was added to a solution of bisterthienylporphyrin **138** (177 mg, 163 μmol) in CHCl$_3$ (18 mL) with stirring at RT. The reaction was deemed complete by TLC (R_f = 0.25, silica, CH$_2$Cl$_2$:hexane (1:2)) after 30 min. The crude product was precipitated with MeOH and the resulting solid was recrystallised from CH$_2$Cl$_2$/MeOH giving **Zn-138** (189 mg, 100%) as a brick-red powder. ^{1}H NMR (400 MHz, CDCl$_3$, TMS) δ 1.085 (t, 24H, ^3J = 7.3 Hz, CH$_2$CH$_2$CH$_2$CH$_3$), 1.68-1.79 (app sex, 16H, CH$_2$CH$_2$CH$_2$CH$_3$), 2.13-2.21 (app pent, 16H, CH$_2$CH$_2$CH$_2$CH$_3$), 2.915 (s, 24H, H$_{Me-TBMP}$), 3.90-4.05 (m, 16H, CH$_2$CH$_2$CH$_2$CH$_3$), 6.34-6.44 (m, 8H, H$_{thienyl\ A}$), 6.78-6.80 (m, 4H, H$_{thienyl\ A}$), 7.12-7.15 (4H, [7.135 (dd, ^3J = 5.1, 3.7 Hz, H$_{4'''\ (\alpha\alpha\ or\ \alpha\beta)}$), 7.137 (dd, ^3J = 5.1, 3.7 Hz, H$_{4'''\ (\alpha\beta\ or\ \alpha\alpha)}$)]), H$_{thienyl\ C}$), 7.28-7.31 [4H, [7.293 (dd, ^3J = 5.3 Hz, ^4J = 1.2 Hz, H$_{5'''\ (\alpha\alpha\ or\ \alpha\beta)}$), 7.298 (dd, ^3J = 5.3 Hz, ^4J = 1.2 Hz, H$_{5'''\ (\alpha\beta\ or\ \alpha\alpha)}$)]), H$_{thienyl\ C}$), 7.45-7.47 (4H, [7.459 (dd, ^3J = 3.6 Hz, ^4J = 1.3 Hz, H$_{3'''\ (\alpha\alpha\ or\ \alpha\beta)}$), 7.463 (dd, ^3J = 3.6 Hz, ^4J = 1.3 Hz, H$_{3'''\ (\alpha\beta\ or\ \alpha\alpha)}$), H$_{thienyl\ C}$], 7.674 (s, 2H, H$_{4''\ (\alpha\alpha\ or\ \alpha\beta),\ thienyl\ B}$), 7.696 (s, 2H, H$_{4''\ (\alpha\beta\ or\ \alpha\alpha),\ thienyl\ B}$), 10.188 (s, 4H, H$_{10,\ 20,\ meso}$). *Assignments aided by COSY spectra.* ^{13}C NMR (101 MHz): δ 14.2, 14.3, 23.3, 26.5, 35.6, 97.8, 111.4, 111.5, 124.0, 124.1, 124.58, 124.63, 124.7, 125.4, 126.02, 126.09, 128.1, 130.4, 130.5, 133.86, 133.92, 135.5, 135.6, 136.7, 137.4, 137.89, 137.92, 140.1, 143.7, 146.84, 146.86, 148.1. UV-vis (CH$_2$Cl$_2$): λ_{max} [nm] (ε x 10^{-3}) 353 (63.2), 418 (336), 504 (4.51), 543 (21.6), 581 (13.4). FAB-LRMS: m/z (%, assignment) cluster at 1143-1151, 1144 (80, M$^+$). HRMS: Calcd for M$^+$ (C$_{64}$H$_{64}$N$_4$S$_6$Zn): 1144.2747, found: 1144.2791.

TTTP, 139.

5,10,15,20-Tetrakis([2',2'':5'',2'''-terthiophen]-3''-yl)porphyrin.
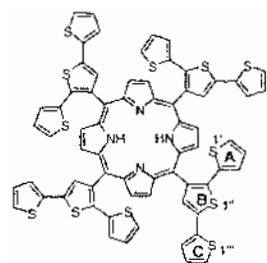
C$_{68}$H$_{38}$N$_4$S$_{12}$
Exact Mass: 1293.9745
Mol. Wt.: 1295.8483

Procedure A

3'-Formyl-2,2':5',2''-terthiophene **136** (158 mg, 572 μmol) and pyrrole (39.6 μL, 572 μmol) were dissolved in degassed anhydrous CH$_2$Cl$_2$ (57 mL, 10^{-2} M) under N$_2$ at RT. Then TFA (44.0 μL, 572 μmol, 1.0 eq) was added and the solution stirred in dark for

1.5 hours. *p*-Chloranil (105 mg, 429 μmol, 0.75 eq) was added and the solution stirred for 2 h at RT. Next excess Et$_3$N was added and the crude product was precipitated out from solution with MeOH. The solid was column chromatographed (silica, 100 mm x 37 mm$_{dia}$, CH$_2$Cl$_2$) collecting the first major porphyrin coloured band (R_f = 0.15, CH$_2$Cl$_2$:hexane (1:1)). The product was then repetitively recrystallised from CH$_2$Cl$_2$/MeOH (20 times), to give porphyrin **139** (31.2 mg, 17%) as a purple powder. *^{1}H NMR is consistent with the four possible isomer products.*

Procedure B

3'-Formyl-2,2':5',2''-terthiophene **136** (158 mg, 572 μmol) and pyrrole (39.7 μL, 572 μmol) were dissolved in degassed anhydrous CH$_2$Cl$_2$ (57 mL) under N$_2$ at RT. BF$_3$·OEt$_2$ (7.0 μL, 57 μmol, 0.1 eq) was added and the solution stirred in dark for 2 h. *p*-Chloranil (105 mg, 429 μmol, 0.75 eq) was added and the solution stirred at reflux for 2 h. Next excess Et$_3$N was added and the solvent removed *in vacuo*. The residue was subjected to column chromatography (80 mm x 37 mm$_{dia}$, CH$_2$Cl$_2$:hexane (1:1)) collecting the first major coloured band (R_f = 0.15, CH$_2$Cl$_2$:hexane (1:1)). Recrystallisation from CH$_2$Cl$_2$/MeOH giving porphyrin **139** (62.4 mg, 34%) as a purple powder containing an inseparable mixture of atropisomers by ^{1}H NMR. *^{1}H NMR is consistent with the four possible isomer products.* ^{1}H NMR (270 MHz, CDCl$_3$, TMS): δ -2.52-2.44 (2H, [-2.47 (br s), -2.50 (br s)], NH), 6.30-6.47 (m, 8H, H$_{thienyl\,A}$), 6.66-6.79 (m, 4H, H$_{thienyl\,A}$), 7.06-7.13 (m, 4H, H$_{thienyl\,C}$), 7.23-7.30 (m, 4H, H$_{thienyl\,C}$), 7.39-7.46 (m, 4H, H$_{thienyl\,C}$), 7.76-7.90 (4H, [7.772 (s), 7.784 (s), 7.818 (s), 7.840 (s), 7.869 (s), 7.897 (s)], H$_{4'',\,thienyl}$), 8.93-9.00 (m, 8H, H$_{\beta\text{-pyrrolic}}$). UV-vis (CH$_2$Cl$_2$): λ_{max} [nm] (ε x 10^{-3}) 252 (43.2), 357 (100), 426 (220), 525 (21.4), 561 (6.39), 596 (7.46), 654 (1.67). FAB-LRMS: *m/z* (%, assignment) cluster at 1294-1300, 1295 (100, MH$^+$). HRMS: Calcd for MH$^+$ (C$_{68}$H$_{39}$N$_4$S$_{12}$): 1294.9823, found: 1294.9798.

ZnTTTP, Zn-139.

5,10,15,20-Tetrakis([2',2'':5'',2'''-terthiophen]-3''-yl)porphyrinato zinc(II).
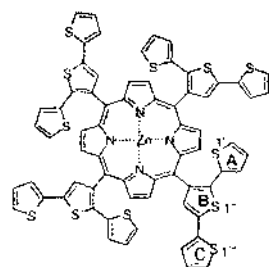
C$_{68}$H$_{36}$N$_4$S$_{12}$Zn
Exact Mass: 1355.8880
Mol. Wt.: 1359.2224

A solution of Zn(OAc)$_2$·2H$_2$O (9.3 mg, 42 μmol, 1.2 eq) in MeOH (1.0 mL) was added to a solution of *meso*-tetraterthienylporphyrin **139** (45.9 mg, 35.4 μmol) in CHCl$_3$ (4.5 mL) with stirring at RT. After 1 h, two close running coloured bands were observed by TLC (Possibly a mixture of metallated and non-metallated products). More Zn(OAc)$_2$·2H$_2$O (6.2 mg, 28 μmol, 0.8 eq) in MeOH (0.5 mL) was added and the reaction mixture was heated to reflux for 1 h. The two bands were still evident by TLC. On cooling to RT the solvent was removed *in vacuo* and the residue column chromatographed (silica, 30 mm$_{dia}$ x 200 mm, CH$_2$Cl$_2$:hexane (1:1)) first collecting fraction A. Recrystallistion from CH$_2$Cl$_2$/MeOH gave unmetallated porphyrins (3.4 mg, **NH** resonances of the correct integral present in ^{1}H NMR spectrum). Further elution gave fraction B, and recrystallisation from CH$_2$Cl$_2$/MeOH gave **Zn-139** (31.5 mg, 65%) as a purple powder. ^{1}H NMR (400 MHz, CDCl$_3$, TMS): δ 6.26-6.44 (m, 8H, H$_{thienyl A}$), 6.74-6.83 (m, 4H, H$_{thienyl A}$), 7.06-7.11 (m, 4H, H$_{thienyl C}$), 7.22-7.28 (m, 4H, H$_{thienyl C}$), 7.40-7.44 (m, 4H, H$_{thienyl C}$), 7.82-7.94 (4H, [7.830 (s), 7.840 (s), 7.900 (s), 7.906 (s), 7.933 (s), 7.939 (s)], H$_{4'', thienyl}$), 9.05-9.09 (m, 8H, H$_{\beta\text{-pyrrolic}}$). UV-vis (CH$_2$Cl$_2$): λ_{max} [nm] (ε x 10^{-3}) 352 (97.3), 434 (264), 521 (7.91), 559 (28.3), 598 (6.18). FAB-LRMS: *m/z* (%, assignment) cluster at 1356-1364, 1356 (55, M$^+$). HRMS: Calcd for M$^+$ (C$_{68}$H$_{36}$N$_4$S$_{12}$Zn): 1355.8880, found: 1355.8801.

TPP-=-Terthiophene, 154.

Trans-1-(5',10',15',20'-tetraphenylporphyrin-2'-yl)-2-((2'',2''':5''',2''''-terthiophen)-3'''-yl)ethene.
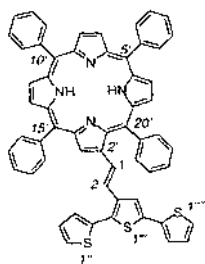
C$_{58}$H$_{38}$N$_4$S$_3$
Exact Mass: 886.2259
Mol. Wt.: 887.1473

Synthesised by D. C. W. Reid and characterised by G. E. Collis and the author.[211]

3'-Formyl-2,2':5',2''-terthiophene **136** (234.6 mg, 848 μmol) and TPPps **4** (786 mg, 849 μmol) were dissolved in dry DCE (50 mL) under N$_2$. DBU (254 μL, 1.70 mmol, 2.0 eq) was added and reaction stirred at RT for 15 min. The solution was refluxed in front of a

tungsten lamp overnight to ensure only the *trans* isomer was present. The solvent was removed *in vacuo* and the residue recrystallised from hot $CHCl_3$/MeOH to give porphyrin **154** (527 mg, 70%) as a purple solid. ^{1}H NMR (270 MHz, $CDCl_3$, TMS): δ - 2.62 (br s, 2H, NH), 6.81 (d, 1H, ^3J = 16.0 Hz, $H_{1, ethenyl}$), 6.95 (s, 1H, $H_{4''', thienyl}$), 7.10-7.20 (m, 2H, $H_{4'', 4'''', thienyl}$), 7.25 (dd, 1H, ^3J = 3.4, ^4J = 1.2 Hz, $H_{3'', thienyl}$), 7.28 (dd, 1H, ^3J = 3.4, ^4J = 1.2 Hz, $H_{3'''', thienyl}$), 7.39 (dd, 1H, ^3J = 5.2, ^4J = 1.2 Hz, $H_{5'''', thienyl}$), 7.44 (dd, 1H, ^3J = 5.2, ^4J = 1.2 Hz, $H_{5'', thienyl}$), 7.66 (d, 1H, ^3J = 16.0 Hz, $H_{2, ethenyl}$), 7.70-7.91 (m, 15H, H_{Ph}), 7.95-8.04 (m, 1H, H_{Ph}), 8.16-8.30 (m, 8H, H_{Ph}), 8.73-8.89 (m, 6H, $H_{\beta-pyrrolic}$), 8.90 (s, 1H, $H_{3', \beta-pyrrolic}$). UV-vis (CH_2Cl_2): λ_{max} [nm] (ε x 10^{-3}) 311 sh (26), 423 (188), 524 (17.3), 567 (11.2), 600 (7.56), 657 (3.61). FAB-LRMS: *m/z* (%, assignment) cluster at 886-890, 887 (100, MH$^+$). HRMS: Calcd for MH$^+$ ($C_{58}H_{39}N_4S_3$): 887.2337, found: 887.2373.

Crystal Structure Refinement Data

BFP 76
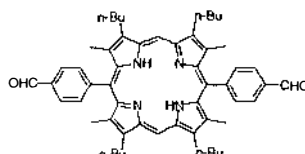
Table 7-3. Crystal data and structure refinement for **76**.

|	
Empirical formula	$C_{54}H_{62}N_4O_2$
Formula weight	799.08
Temperature	203(2) K
Wavelength	0.71073 Å
Crystal system	Triclinic
Space group	P-1
Unit cell dimensions	a = 7.13830(10) Å α = 70.7560(10)°.
	b = 10.8185(2) Å β = 77.5550(10)°.
	c = 15.7130(2) Å γ = 89.5880(10)°.
Volume	1116.04(3) Å^3
Z	1
Density (calculated)	1.189 Mg/m^3
Absorption coefficient	0.072 mm^{-1}
F(000)	430
Crystal size	0.40 x 0.16 x 0.11 mm^3
Theta range for data collection	1.41 to 26.35°.
Index ranges	-8<=h<=8, -13<=k<=13, -19<=l<=19
Reflections collected	10109
Independent reflections	4414 [R(int) = 0.0691]
Absorption correction	Semi-empirical from equivalents
Max. and min. transmission	0.992 and 0.971
Refinement method	Full-matrix least-squares on F^2
Data / restraints / parameters	4414 / 0 / 276
Goodness-of-fit on F^2	0.925
Final R indices [I>2sigma(I)]	R1 = 0.0709, wR2 = 0.1690
R indices (all data)	R1 = 0.1235, wR2 = 0.2062
Extinction coefficient	0.059(8)
Largest diff. peak and hole	0.481 and -0.399 e.Å^{-3}

Diporphyrin Building Block, Zn/Zn-77
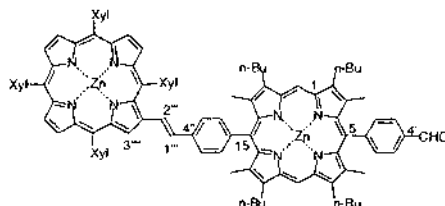
Table 7-4. Crystal data and structure refinement for **Zn/Zn-77**.

Empirical formula	$C_{116}H_{123}Cl_3N_8O_3Zn_2$
Formula weight	1914.31
Temperature	203(2) K
Wavelength	0.71073 Å
Crystal system	monoclinic
Space group	P2(1)/c
Unit cell dimensions	a = 13.1533(2) Å α = 90°.
	b = 26.89110(10) Å β = 93.0560(10)°.
	c = 28.7840(4) Å γ = 90°.
Volume	10166.6(2) Å^3
Z	4
Density (calculated)	1.251 Mg/m^3
Absorption coefficient	0.607 mm^{-1}
F(000)	4040
Crystal size	0.1 x 0.13 x 0.21 mm^3
Theta range for data collection	1.04 to 20.00°.
Index ranges	-12<=h<=11, -25<=k<=25, -24<=l<=27
Reflections collected	32252
Independent reflections	9495 [R(int) = 0.0816]
Refinement method	Full-matrix least-squares on F^2
Data / restraints / parameters	9495 / 0 / 1189
Goodness-of-fit on F^2	1.033
Final R indices [I>2sigma(I)]	R1 = 0.0817, wR2 = 0.2102
R indices (all data)	R1 = 0.1325, wR2 = 0.2488
Largest diff. peak and hole	0.589 and -0.879 e.Å^{-3}

CuBMBEP, Cu-88
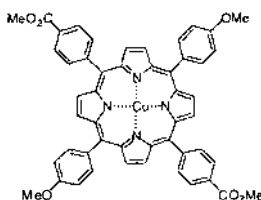
Table 7-5. Crystal data and structure refinement for **Cu-88**.

Empirical formula	$C_{50}H_{36}Cu_1N_4O_6$
Formula weight	852.37
Temperature	200(2) K
Wavelength	0.71073 Å
Crystal system	Monoclinic
Space group	C2/c
Unit cell dimensions	a = 36.2425(6) Å α = 90°.
	b = 9.3553(2) Å β = 114.2190(10)°.

|		
	c = 15.38210(10) Å	$\gamma = 90°$.
Volume	4756.40(13) Å^3	
Z	4	
Density (calculated)	1.190 Mg/m^3	
Absorption coefficient	0.509 mm^{-1}	
F(000)	1764	
Crystal size	0.36 x 0.28 x 0.12 mm^3	
Theta range for data collection	1.23 to 25.43°.	
Index ranges	-43<=h<=43, -11<=k<=11, -18<=l<=18	
Reflections collected	18798	
Independent reflections	4364 [R(int) = 0.0756]	
Completeness to theta = 25.43°	99.0 %	
Absorption correction	Semi-empirical from equivalents	
Max. and min. transmission	0.9415 and 0.8380	
Refinement method	Full-matrix least-squares on F^2	
Data / restraints / parameters	4364 / 0 / 277	
Goodness-of-fit on F^2	0.963	
Final R indices [I>2sigma(I)]	R1 = 0.0624, wR2 = 0.1678	
R indices (all data)	R1 = 0.0860, wR2 = 0.1791	
Largest diff. peak and hole	0.979 and -0.845 e.Å^{-3}	

B2TP, 134
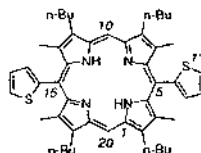
Table 7-6. Crystal data and structure refinement for **134**.

|		
Empirical formula	C$_{48}$H$_{58}$N$_4$S$_2$	
Formula weight	755.10	
Temperature	203(2) K	
Wavelength	0.71073 Å	
Crystal system	triclinic	
Space group	P-1	
Unit cell dimensions	a = 8.84340(10) Å	108.1950(10)°.
	b = 10.1415(3) Å	$\beta = 92.9350(10)°$.
	c = 12.8459(3) Å	$\gamma = 105.4490(10)°$.
Volume	1043.52(4) Å^3	
Z	1	
Density (calculated)	1.202 Mg/m^3	
Absorption coefficient	0.166 mm^{-1}	
F(000)	406	
Crystal size	0.22 x 0.12 x 0.09 mm^3	
Theta range for data collection	1.69 to 26.79°.	
Index ranges	-10<=h<=11, -12<=k<=12, -16<=l<=16	
Reflections collected	9421	
Independent reflections	4159 [R(int) = 0.1098]	
Max. and min. transmission	0.9852 and 0.9644	
Refinement method	Full-matrix least-squares on F^2	
Data / restraints / parameters	4159 / 0 / 247	
Goodness-of-fit on F^2	0.919	
Final R indices [I>2sigma(I)]	R1 = 0.1194, wR2 = 0.2733	
R indices (all data)	R1 = 0.2254, wR2 = 0.3403	
Largest diff. peak and hole	0.561 and -1.011 e.Å^{-3}	

ZnB2TP, Zn-134
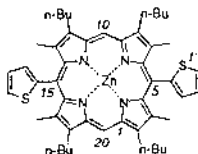
Table 7-7. Crystal data and structure refinement for **Zn-134**.

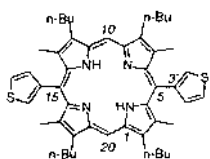| Empirical formula	$C_{48}H_{56}N_4S_2Zn$	
Formula weight	818.46	
Temperature	203(2) K	
Wavelength	0.71073 Å	
Crystal system	triclinic	
Space group	P-1	
Unit cell dimensions	a = 5.54780(10) Å	$\alpha = 89.8010(10)°.$
	b = 12.4150(10) Å	$\beta = 88.9690(10)°.$
	c = 30.4332(4) Å	$\gamma = 81.6080(10)°.$
Volume	2073.30(5) Å^3	
Z	2	
Density (calculated)	1.311 Mg/m^3	
Absorption coefficient	0.732 mm^{-1}	
F(000)	868	
Crystal size	0.45 x 0.08 x 0.07 mm^3	
Theta range for data collection	1.34 to 25.00°.	
Index ranges	-6<=h<=6, -14<=k<=14, -36<=l<=36	
Reflections collected	16750	
Independent reflections	7201 [R(int) = 0.0624]	
Completeness to theta = 25.00°	98.4 %	
Max. and min. transmission	0.9505 and 0.7341	
Refinement method	Full-matrix least-squares on F^2	
Data / restraints / parameters	7201 / 0 / 515	
Goodness-of-fit on F^2	1.232	
Final R indices [I>2sigma(I)]	R1 = 0.0896, wR2 = 0.1917	
R indices (all data)	R1 = 0.1361, wR2 = 0.2162	
Largest diff. peak and hole	1.034 and -0.775 e.Å^{-3}	

B3TP, 135

Table 7-8. Crystal data and structure refinement for **135**.

Empirical formula	$C_{48}H_{56}N_4S_2$	
Formula weight	753.09	
Temperature	200(2) K	
Wavelength	0.71073 Å	
Crystal system	Triclinic	
Space group	P - 1	
Unit cell dimensions	a = 8.8717(2) Å	$\alpha = 109.2670(10)°.$
	b = 10.1934(2) Å	$\beta = 92.7790(10)°.$
	c = 12.6873(2) Å	$\gamma = 104.5030(10)°.$
Volume	1037.72(4) Å^3	

| Z	1
Density (calculated)	1.205 Mg/m^3
Absorption coefficient	0.167 mm^{-1}
F(000)	404
Crystal size	0.45 x 0.21 x 0.11 mm^3
Theta range for data collection	1.72 to 27.52°.
Index ranges	-11<=h<=11, -13<=k<=13, -16<=l<=16
Reflections collected	9691
Independent reflections	4494 [R(int) = 0.0224]
Absorption correction	Semi-empirical from equivalents
Max. and min. transmission	0.9819 and 0.9288
Refinement method	Full-matrix least-squares on F^2
Data / restraints / parameters	4494 / 0 / 246
Goodness-of-fit on F^2	1.031
Final R indices [I>2sigma(I)]	R 1 = 0.0536, wR2 = 0.1382
R indices (all data)	R 1 = 0.0696, wR2 = 0.1507
Largest diff. peak and hole	0.472 and -0.407 e.Å^{-3}

BDP, 150
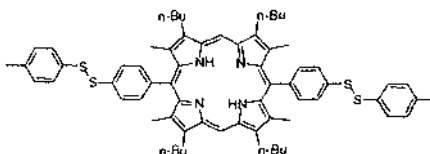
Table 7-9. Crystal data and structure refinement for **150**.

Empirical formula	$C_{66}H_{74}N_4S_4$	
Formula weight	1051.53	
Temperature	203(2) K	
Wavelength	0.71073 Å	
Crystal system	Monoclinic	
Space group	P2(1)/c	
Unit cell dimensions	a = 14.7912(6) Å	$\alpha = 90°$.
	b = 25.5383(11) Å	$\beta = 106.9040(10)°$.
	c = 16.0662(6) Å	$\gamma = 90°$.
Volume	5806.7(4) Å^3	
Z	4	
Density (calculated)	1.203 Mg/m^3	
Absorption coefficient	0.207 mm^{-1}	
F(000)	2248	
Crystal size	0.38 x 0.14 x 0.09 mm^3	
Theta range for data collection	1.44 to 26.45°.	
Index ranges	-18<=h<=18, -29<=k<=32, -14<=l<=20	
Reflections collected	29215	
Independent reflections	11698 [R(int) = 0.2355]	
Completeness to theta = 26.45°	97.8 %	
Absorption correction	Semi-empirical from equivalents	
Max. and min. transmission	0.992 and 0.971	
Refinement method	Full-matrix least-squares on F^2	
Data / restraints / parameters	11698 / 27 / 715	
Goodness-of-fit on F^2	0.757	
Final R indices [I>2sigma(I)]	R 1 = 0.0778, wR2 = 0.1324	
R indices (all data)	R 1 = 0.3022, wR2 = 0.1952	
Largest diff. peak and hole	0.283 and -0.423 e.Å^{-3}	

Appendix B

Solar Cell Data (Thesis Results)

* Data omitted as an outlier.

BDM implies Before Digital Multimeter (computer interfaced).

Effect of Dye Adsorption Time and Temperature

Adsorption Conditions	Compound #	I_{sc} (mA)	Avg I_{sc}	StdDev I_{sc}	% StdDev I_{sc}	V_{oc} (mV)	Avg V_{oc}	StdDev V_{oc}	% StdDev V_{oc}	Solvent (μM)	Electrolyte	Plate	Rinsing (solvent)	Cell #	Sample #	TiO_2 Colour	Cell Behaviour	Isc (max or SS)
9 hours, RT	Zn-15	0.476				462				THF (10)	E	PA	Rinse (CH_2Cl_2)	52	wax823	Pale Green	BDM	max Isc
	Zn-15	0.496	0.486	0.014	3	456	459	4	1	"	"	"	"	53	"	"	"	"
22 hours, RT	Zn-15	0.380				418				CH_2Cl_2 (10)	E	PA	Rinse (CH_2Cl_2)	48	wax823	Green/orange	BDM	max Isc
	Zn-15	0.373	0.377	0.005	1	415	417	2	1	"	"	"	"	49	"	"	"	"
3 hours. Reflux	Zn-15	0.182				373				CH_2Cl_2 (10)	E	PA	Rinse (CH_2Cl_2)	50	wax823	Red	BDM	max Isc
	Zn-15	0.200	0.191	0.013	7	387	380	10	3	"	"	"	"	51	"	"	"	"

Cell Holder CHI

Plate area 7 x 7 mm

Pt counter 8 x 8 mm

DPTI (124 mV)

Effect of Adsorption Solvent Type

Solvent	Compound #	I_{sc} (mA)	Avg I_{sc}	StdDev I_{sc}	% StdDev I_{sc}	V_{oc} (mV)	Avg V_{oc}	StdDev V_{oc}	% StdDev V_{oc}	Solvent (μM)	Electrolyte	Plate	Rinsing (solvent)	Cell #	Sample #	TiO_2 Colour	Cell Behaviour	Isc (max or SS)
CH_2Cl_2	Zn-15	0.476				462				THF (10)	E	PA	Rinse (CH_2Cl_2)	52	wax823	Pale Green	BDM	max Isc
"	Zn-15	0.496	0.486	0.014	3	456	459	4	1	"	"	"	"	53	"	"	"	"
THF	Zn-15	0.728				478				THF (10)	E	PA	Rinse (THF)	54	wax823	Green	BDM	max Isc
"	Zn-15	0.724	0.726	0.003	0	478	478	0	0	"	"	PA1	"	58	"	"	"	"
THF + Pyridine (12 mmol)	Zn-15	0.699				503				THF (10)	E	PA1	Rinse (THF + Pyridine (12 mM))	60	wax823	Green	BDM	max Isc
Triethylamine	Zn-15	0.313				425				THF (10)	E	PA1	Rinse (Et3N)	59	wax823	Pale Green	BDM	max Isc
Ethanol	Zn-15	0.300				395				THF (10)	E	PA1	Rinse (EtOH)	62	wax823	Green/orange	BDM	max Isc
Benzonitrile	Zn-15	0.053				333				THF (10)	E	PA1	Rinse (Benzonitrile)	61	wax823	Pale Green	BDM	max Isc
1,4-Dioxane	Zn-15	0.268				391				THF (10)	E	PA1	Rinse (1,4-Dioxane)	63	wax823	Green/orange	BDM	max Isc

Cell Holder CHI

Plate area 7 x 7 mm

Pt counter 8 x 8 mm

DPTI (124 mV)

Adsorption time (9-13 h)

Effect of Dye Concentration and Rinsing

Dye Concentration (mol/L)	Compound #	I_{sc} (mA)	Avg I_{sc}	StdDev I_{sc}	% StdDev I_{sc}	V_{oc} (mV)	Avg V_{oc}	StdDev V_{oc}	% StdDev V_{oc}	Solvent (μM)	Electrolyte	Plate	Rinsing (solvent)	Cell #	Sample #	TiO_2 Colour	Cell Behaviour	Isc (max or SS)
1.1×10^6	Zn-15	0.046				292				THF (1.1)	E	PA1	Rinse (THF)	65	wax823	Very Pale Green	BDM	max Isc
5.5×10^6	Zn-15	0.262				397				THF (5.5)	E	PA1	Rinse (THF)	64	wax823	Pale Green	BDM	max Isc
1.1×10^5	Zn-15	0.728				478				THF (10)	E	PA	Rinse (THF)	54	wax823	Green	BDM	max Isc

	Compound #	I_{sc} (mA)	Avg I_{sc}	StdDev I_{sc}	% StdDev I_{sc}	V_{oc} (mV)	Avg V_{oc}	StdDev V_{oc}	% StdDev V_{oc}	Solvent (μM)	Electrolyte	Plate	Rinsing (solvent)	Cell #	Sample #	TiO₂ Colour	Cell Behaviour	Isc (max or SS)
.	Zn-15	0.724	0.726	0.003	0	478	478	0	0	"	"	PA1	"	58	"	"	"	"
1.1×10^{-4}	Zn-15	0.863				459				THF (110)	E	PA1	Rinse (THF)	66	wax823	Green	BDM	max Isc
1.1×10^{-4} (No Rinse)	Zn-15	0.758				468				THF (110)	E	PA1	No Rinse	67	wax823	Green	BDM	max Isc

Cell Holder **CH1**

Plate area 7 x 7 mm

Pt counter 8 x 8 mm

DPT1 (124 mV)

Adsorption time (9 h)

Acid Salt Effect on Dye Efficiency

Dye	Compound #	I_{sc} (mA)	Avg I_{sc}	StdDev I_{sc}	% StdDev I_{sc}	V_{oc} (mV)	Avg V_{oc}	StdDev V_{oc}	% StdDev V_{oc}	Solvent (μM)	Electrolyte	Plate	Rinsing (solvent)	Cell #	Sample #	TiO₂ Colour	Cell Behaviour	Isc (max or SS)
ZnTXP-=-PhCOOH	Zn-15	0.728				478				THF (10)	E	PA	Rinse (THF)	54	wax823	Green	BDM	max Isc
"	Zn-15	0.724	0.726	0.003	0	478	478	0	0	"	"	PA1	"	58	"	"	"	"
ZnTXP-=-PhCOO⁻ Na⁺	Zn-35	0.274				388				THF (10)	E	PA1	Rinse (THF)	70	wax829A	Green	BDM	max Isc
ZnTXP-=-PhCOO⁻ n-Bu₄N⁺	Zn-36	0.065				287				THF (10)	E	PA1	Rinse (THF)	71	wax838	Pale Green	BDM	max Isc
.	Zn-36	0.067	0.066	0.001	2	297	292	7	2	"	"	"	"	72	"	"	"	"

Cell Holder **CH1**

Plate area 7 x 7 mm

Pt counter 8 x 8 mm

DPT1 (124 mV)

Adsorption time (9 h)

Effect of Electrolyte Composition on Cell Performance

Dye	Compound #	I_{sc} (mA cm⁻²)	Avg I_{sc}	StdDev I_{sc}	% StdDev I_{sc}	V_{oc} (mV)	Avg V_{oc}	StdDev V_{oc}	% StdDev V_{oc}	Solvent (μM)	Electrolyte	Plate	Rinsing (solvent)	Cell #	Sample #	TiO₂ Colour	Cell Behaviour	Isc (max or SS)
ZnTXP-=-PhCOOH	Zn-15	0.824				464				THF (100)	E	PD1, 2	No Rinse	209	wax823	green	*Type II*	SS Isc
"	Zn-15	0.860				442				"	"	"	"	210	"	"	"	"
	Zn-15	0.956	0.880	0.068	8	440	449	13	3	"	"	-	"	256	"	"	"	"
ZnTXP-=-PhCOOH (4-*t*-butylpyridine)	Zn-15	0.744				434				THF (100)	G	PD2	No Rinse	266	wax823	green	*Type I*	SS Isc
"	Zn-15	0.729				407				"	"	"	"	267	"	"	"	"
"	Zn-15	0.888				417				"	"	"	"	268	"	"	"	"
"	Zn-15	0.708	0.767	0.082	11	429	422	12	3	"	"	"	"	269	"	"	"	"
Ru_red (Electrolyte E)	118	4.110				601				Acetonitrile	E	PD1	No Rinse	202		orange	*Type II*	max Isc
"	118	4.540				580				"	"	"	"	203	"	"	"	"
"	118	4.470				593				"	"	"	"	204	"	"	"	"
"	118	3.910				595				"	"	"	"	205	"	"	"	"
"	118	5.210	4.448	0.498	11	590	592	8	1	"	"	"	"	207	"	"	"	"
Ru_red (Electrolyte F)	118	1.310				545				Acetonitrile	F	PD1	No Rinse	206		orange	*Type II*	max Isc

Cell Holder **CH3**

Pt counter 13 x 12 mm

DPT1 (130 mV)

Adsorption time (over night, 12-20 h)

<u>Metalloporphyrins (M = 2H, Zn & Cu)</u>

Dye	Compound #	I_{sc} (mA)	Avg I_{sc}	StdDev I_{sc}	% StdDev I_{sc}	V_{oc} (mV)	Avg V_{oc}	StdDev V_{oc}	% StdDev V_{oc}	Solvent (µM)	Electrolyte	Plate	Rinsing (solvent)	Cell #	Sample #	TiO2 Colour	Cell Behaviour	Isc (max or SS)
ZnTXP-=-Ph-COOH	Zn-15	1.266				465				THF (10)	E	PA2	Rinse (THF)	73	wax823	Green	BDM	max Isc
-	Zn-15	1.154	1.210	0.079	7	453	459	8	2	"	"	-	"	74	"	"	"	"
CuTXP-=-Ph-COOH	Cu-15	0.591				456				THF (10)	E	PA2	Rinse (THF)	80	wax882	Brown	BDM	max Isc
"	Cu-15	0.633	0.612	0.030	5	463	460	5	1	"	"	"	-	81	"	"	"	"
NiTPP-=-Ph-COOH	Ni-9	0.076				318				THF (10)	E	PA2	Rinse (THF)	82	wax769B	Red	BDM	max Isc
'	Ni-9	0.069	0.073	0.005	7	317	318	1	0	"	"	"	"	83	"	"	"	"
H2TXP-=-Ph-COOH	15	0.017				188				THF (10)	E	PA2	Rinse (THF)	75	wax822	Brown	BDM	max Isc
"	15	0.019	0.018	0.001	8	208	198	14	7	"	"	"	"	76	"	"	"	"
H2TXP-=-Ph-COOH + (Zn(OAc)2, MeOH)	Zn-15	0.489				567				THF (10)	E	PA2	Rinse (THF)	77 (76 + Zn(OAc)2)	wax822	Green	BDM	max Isc

Cell Holder **CH1**

Plate area 7 x 7 mm

Pt counter 8 x 8 mm

DPT1 (124 mV)

Adsorption time (9-11 h)

<u>o,m,p-Carboxylic Acids of ZnTXP-=-Ph(COOH).</u>

Dye	Compound #	I_{sc} (mA)	Avg I_{sc}	StdDev I_{sc}	% StdDev I_{sc}	V_{oc} (mV)	Avg V_{oc}	StdDev V_{oc}	% StdDev V_{oc}	Solvent (µM)	Electrolyte	Plate	Rinsing (solvent)	Cell #	Sample #	TiO2 Colour	Cell Behaviour	Isc (max or SS)
ZnTXP-=-Ph-pCOOH	Zn-15	0.828				427				THF (10)	E	PB	Rinse (THF)	86	wax823	green	BDM	max Isc (25 min)
	Zn-15	0.904	0.866	0.054	6	416	422	8	2	"	"	"	"	87	"	"	"	"
ZnTXP-=-Ph-mCOOH	Zn-33	0.665				450				THF (10)	E	PB	Rinse (THF)	88	wax889	green/orange	BDM	max Isc (35 min)
	Zn-33	0.664	0.665	0.001	0	422	436	20	5	"	"	"	-	89	"	"	"	"
ZnTXP-=-Ph-oCOOH	Zn-32	0.009				209				THF (10)	E	PB	Rinse (THF)	90	wax890	pale green	BDM	max Isc (30 min)
	Zn-32	0.0094	0.0092	0.000	3	209	209	0	0	"	"	"	"	91	"	"	"	"
ZnTXP-=-Ph-3,5-(COOH)2	Zn-37	0.728				440				THF (10)	E	PB	Rinse (THF)	92	wax891	green/orange	BDM	max Isc (80 min)
	Zn-37	0.738	0.733	0.007	1	455	448	11	2	"	"	"	"	93	"	"	"	"

Cell Holder **CH1**

Plate area 7 x 7 mm

Pt counter 8 x 8 nun

DPT1 (124 mV)

Adsorption time (9-10 h)

Benzoic Acid versus Phenol Binding Group

Dye	Compound #	I_{sc} (mA)	Avg I_{sc}	StdDev I_{sc}	% StdDev I_{sc}	V_{oc} (mV)	Avg V_{oc}	StdDev V_{oc}	% StdDev V_{oc}	Solvent (μM)	Electrolyte	Plate	Rinsing (solvent)	Cell #	Sample #	TiO$_2$ Colour	Cell Behaviour	Isc (max or SS)
ZnTXP-=-PhCOOH	Zn-15	1.266				465				THF (10)	E	PA2	Rinse (THF)	73	wax823	Green	BDM	max Isc
"	Zn-15	1.154	1.210	0.079	7	453	459	8	2	"	"	"	"	74	"	"	"	"
ZnTXP-=-PhOH	Zn-72	0.087				313				THF (10)	E	PA2	Rinse (THF)	84	wax826	Pale Green	BDM	max Isc
"	Zn-72	0.088	0.088	0.001	1	330	322	12	4	"	"	"	"	85	"	"	"	"

BDM implies before computer interfaced digital multimeter

Cell Holder CH1

Plate area 7 x 7 mm

Pt counter 8 x 8 mm

DPT1 (124 mV)

Adsorption time (9-11 h)

ZnTXP-=-ArCOOH vs. Grätzel's Ru$_{bd}$ Dye

Dye	Compound #	I_{sc} (mA cm^{-1})	Avg I_{sc}	StdDev I_{sc}	% StdDev I_{sc}	V_{oc} (mV)	Avg V_{oc}	StdDev V_{oc}	% StdDev V_{oc}	Solvent (μM)	Electrolyte	Plate	Rinsing (solvent)	Cell #	Sample #	TiO$_2$ Colour	Cell Behaviour	Isc (max or SS)
Ru$_{bd}$	118	4.110				601				Acetonitrile	E	PD1	No Rinse	202		orange	Type II	max Isc
"	118	4.540				580				"	"	"	"	203		"	"	"
"	118	4.470				593				"	"	"	"	204		"	"	"
"	118	3.910				595				"	"	"	"	205		"	"	"
"	118	5.210	4.448	0.498	11	590	592	8	1	"	"	"	"	207		"	"	"
ZnTXP-=-PhCOOH	Zn-15	0.824				464				THF (100)	E	PD1	No Rinse	209	wax823	green	Type II	SS Isc
"	Zn-15	0.860	0.842	0.025	3	442	453	16	3	"	"	"	"	210	"	"	"	"

Cell Holder CH3

Pt counter 13 x 12 mm

DPT1 (130 mV)

Adsorption time (over night, 12-20 h)

TPP vs. TXP vs. TBP derivatives of ZnTAP-=-PhCOOH

Dye	Compound #	I_{sc} (mA cm^{-1})	Avg I_{sc}	StdDev I_{sc}	% StdDev I_{sc}	V_{oc} (mV)	Avg V_{oc}	StdDev V_{oc}	% StdDev V_{oc}	Solvent (μM)	Electrolyte	Plate	Rinsing (solvent)	Cell #	Sample #	TiO$_2$ Colour	Cell Behaviour	Isc (max or SS)
ZnTPP-=-PhCOOH	Zn-9	1.012				433				THF (100)	G	PD2	No Rinse	270	wax1008	green	Type I	SS Isc
"	Zn-9	1.108				437				"	"	"	"	271	"	"	"	"
"	Zn-9	1.140				438				"	"	"	"	272	"	"	"	"
"	Zn-9	1.026	1.072	0.062	6	428	434	5	1	"	"	"	"	273	"	"	"	"
ZnTXP-=-PhCOOH	Zn-15	0.744				434				THF (100)	G	PD2	No Rinse	266	wax823	green	Type I	SS Isc
"	Zn-15	0.729				407				"	"	"	"	267	"	"	"	"
"	Zn-15	0.888*				417*				"	"	"	"	268	"	"	"	"
"	Zn-15	0.708	0.727	0.018	2	429	423	14	3	"	"	"	"	269	"	"	"	"
ZnTBP-=-PhCOOH	Zn-34	0.649				406				THF (100)	G	PD2	No Rinse	274	wax1009	green	Type I	SS Isc
"	Zn-34	0.627				401				"	"	"	"	275	"	"	"	"

| | Zn-34 | 0.695 | | | | 403 | | | | | | | | 276 | " | - | " | " |
| " | Zn-34 | 0.601 | 0.643 | 0.040 | 6 | 403 | 403 | 2 | 1 | " | " | " | " | 277 | " | " | " | " |

Cell Holder **CH3**

Pt counter 13 x 12 mm

DPTI (130 mV)

Adsorption time (over night, 12-20 h)

Screening of Monoporphyrin Acids

Dye	Compound #	I_{sc} (mA cm^{-2})	Avg I_{sc}	StdDev I_{sc}	% StdDev I_{sc}	V_{oc} (mV)	Avg V_{oc}	StdDev V_{oc}	% StdDev V_{oc}	Solvent (μM)	Electrolyte	Plate	Rinsing (solvent)	Cell #	Sample #	TiO$_2$ Colour	Cell Behaviour	Isc (max or SS)
ZnTXP-=-PhCOOH	Zn-15	0.824				464				THF (100)	E	PD1	No Rinse	209	wax823	green	Type II	SS Isc
"	Zn-15	0.860	0.842	0.025	3	442	453	16	3	"	-	-	"	210	"	"	"	"
HOOCPh-ZnTBTMP-PhCOOH	Zn-73	0.045*				178*				THF (100)	E	PD1	No Rinse	231	wax996	orange	Type I	SS Isc
"	Zn-73	0 014				113				"	"	"	"	232	"	"	"	"
"	Zn-73	0.022	0.018	0.006	31	123	118	7	6	-	"	"	"	233	"	-	"	"
5,15-Bis(PhOMe)-10,20-Bis(PhCOOH)ZnP	Zn-92	0.201				299				THF (100)	E	PD1	No Rinse	221	wax999	bright green	Type I	SS Isc
"	Zn-92	0 012*				113*				-	-	"	"	222	"	"	"	"
ZnT3CP	Zn-95	0.301*				377*				THF (100)	E	PD1	No Rinse	234	wax1001	green/orange	Type I	SS Isc
"	Zn-95	0.421				369				"	"	"	"	235	"	"	"	"
"	Zn-95	0.403	0.412	0.013	3	356	363	9	3	"	"	"	"	236	"	"	"	"
ZnTCP (MeOH)	Zn-8	0.079				202				THF (100)	E	PD1	No Rinse	223	wax992	green/orange	Type II	SS Isc
"	Zn-8	0.079	0.079	0.000	0	206	204	3	1	"	"	"	"	224	"	"	"	"
ZnT3,5CP	Zn-75	0.160				292				THF (100)	E	PD1	No Rinse	219	wax1000	pale green	Type I	SS Isc
"	Zn-75	0.133	0.147	0.019	13	278	285	10	3	"	"	"	"	220	"	"	"	"

Cell Holder **CH3**

Pt counter 13 x 12 mm

DPTI (130 mV)

Adsorption time (over night, 12-20 h)

Screening of Array Porphyrin Acids

Dye	Compound #	I_{sc} (mA cm^{-2})	Avg I_{sc}	StdDev I_{sc}	% StdDev I_{sc}	V_{oc} (mV)	Avg V_{oc}	StdDev V_{oc}	% StdDev V_{oc}	Solvent (μM)	Electrolyte	Plate	Rinsing (solvent)	Cell #	Sample #	TiO$_2$ Colour	Cell Behaviour	Isc (max or SS)
ZnTXP-=-PhCOOH	Zn-15	0.824				464				THF (100)	E	PD1	No Rinse	209	wax823	green	Type II	SS Isc
-	Zn-15	0 860	0.842	0.025	3	442	453	16	3	"	"	"	"	210	"	"	"	"
3,5-Bis(ZnTXP-=-)PhCOOH	Zn$_2$-53	0.067*				291*				THF (100)	E	PD1	No Rinse	225	wax916B	pale green	Type I	SS Isc
"	Zn$_2$-53	0.095				315				"	"	"	"	226	"	"	"	"
"	Zn$_2$-53	0.120	0.108	0.018	16	299	307	11	4	"	"	"	"	227	"	-	"	"
ZnTXP-=-Ph-ZnTBMP-PhCOOH	Zn$_2$-66	0.084				245				THF (100)	E	PD1	No Rinse	228	wax926	tan	Type I	SS Isc
"	Zn$_2$-66	0.090				240				"	"	-	"	229	"	"	"	"
"	Zn$_2$-66	0.092	0 089	0.004	5	248	244	4	2	"	"	-	"	230	"	-	-	"
ZnT3CP-ZnTXP	Zn$_2$-99	0.265				331				THF (100)	E	PD1	No Rinse	238	wax975	dark green	Type II	SS Isc

Dye	Compound #	I_{sc} (mA cm⁻²)	Avg I_{sc}	StdDev I_{sc}	% StdDev I_{sc}	V_{oc} (mV)	Avg V_{oc}	StdDev V_{oc}	% StdDev V_{oc}	Solvent (μM)	Electrolyte	Plate	Rinsing (solvent)	Cell #	Sample #	TiO₂ Colour	Cell Behaviour	Isc (max or SS)
"	Zn₁-99	0.267	0.266	0.001	1	332	332	1	0	"	"	"	"	239	"	"	"	"
ZnT3CP-ZnT3CP	Zn₃-100	0.135				302				THF (100)	E	PD1	No Rinse	240	wax974	dark green	Type II	SS Isc
"	Zn₃-100	0.184*				310*				"	"	"	"	241	"	"	"	"
"	Zn₃-100	0.110	0.123	0.018	14	291	297	8	3	"	"	"	"	242	"	"	"	"
ZnT3CP-ZnTBTMP-ZnTXP	Zn₃-104	0.360				365				THF (100)	E	PD1	No Rinse	244	wax983	brown	Type IV	max Isc
"	Zn₃-104	0.335	0.348	0.018	5	362	364	2	1	"	"	"	"	245	"	"	"	"
ZnT3CP-ZnTBTMP-ZnTXP (EtOH)	Zn₃-104	0.315				380				EtOH (50)	E	PD1	Rinse (EtOH)	249	wax983	brown	Type IV	max Isc
ZnT3CP-ZnTBTMP-ZnT3CP	Zn₃-105	0.245				352				THF (100)	E	PD1	No Rinse	246	wax984	brown	Type III	max Isc
"	Zn₃-105	0.204				331				"	"	"	"	247	"	"	"	"
"	Zn₃-105	0.225	0.225	0.021	9	346	343	11	3	"	"	"	"	248	"	"	"	"
(ZnT3CP),(ZnTXP),ZnP	Zn₅-113	0.259				347				THF (100)	E	PD1	No Rinse	250	wax988	dark green	Type III	max Isc
"	Zn₅-113	0.370*				377*				"	"	"	"	251	"	"	"	"
"	Zn₅-113	0.260	0.260	0.001	0	351	349	3	1	"	"	"	"	252	"	"	"	"
(ZnT3CP),ZnP	Zn₅-111	0.289				368				THF (100)	E	PD1	No Rinse	253	wax976D	dark green	Type III	max Isc
"	Zn₅-111	0.275				365				"	"	"	"	254	"	"	"	"
"	Zn₅-111	0.295	0.286	0.010	4	354	362	7	2	"	"	"	"	255	"	"	"	"

Cell Holder CH3

Pt counter 13 x 12 mm

DPT1 (130 mV)

Adsorption time (overnight, 12-20 h)

343

Effect of 4-t-butylpyridine on Zn₅-111 cell performance
* Implies Outlier

Dye	Compound #	I_{sc} (mA cm⁻²)	Avg I_{sc}	StdDev I_{sc}	% StdDev I_{sc}	V_{oc} (mV)	Avg V_{oc}	StdDev V_{oc}	% StdDev V_{oc}	Solvent (μM)	Electrolyte	Plate	Rinsing (solvent)	Cell #	Sample #	TiO₂ Colour	Cell Behaviour	Isc (max or SS)
(ZnT3CP),ZnP	Zn₅-111	0.289				368				THF (100)	E	PD1	No Rinse	253	wax976D	dark green	Type III	max Isc
"	Zn₅-111	0.275				365				"	"	"	"	"	"	"	"	"
"	Zn₅-111	0.295	0.286	0.010	4	354	362	7	2	"	"	"	"	"	"	"	"	"
(ZnT3CP),ZnP (4-t-butylpyridine)	Zn₅-111	0.296				367				THF (100)	G	PD2	No Rinse	263	wax976D	dark green	Type III	max Isc
"	Zn₅-111	0.242	0.269	0.038	14	395	381	20	5	"	"	"	"	"	"	"	"	"
(ZnT3CP),ZnP (soaked in 4-t-butylpyridine)	Zn₅-111	0.177				395				THF (100)	G	PD2	No Rinse	264	wax976D	bright green	Type I	SS Isc

Cell Holder CH3

Pt counter 13 x 12 mm

DPT1 (130 mV)

Adsorption time (overnight, 12-20 h)

Solar Cell Data (Grätzel's Results)

Zn₂-53
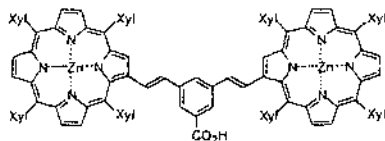
Cell Name: Marie_Oct 12#11

Measurement Date	: Thu, Oct 12, 2000 / 10:43:08 AM
Type of cell	: 2.5micr
Cell Active Area	: 0.44 cm²
Dye Sensitiser	: WAX916
Additional Remarks	: 15h
Electrolyte Solution	: 955
SemiConductor Layer	: 2.5μm
Layer Thickness, Porosity	: 2.5 μm, 63 %
Working Electrode Glass	: NSG 10Ω/cm
Counter Electrode Type	: FlachGlas/Pt refl/Pt°
Data FileName	: Marie_Oct 12#11
Current Compliance	: 2 mA
Settling Time	: 0.04 s
Voltage Increment	: 5 mV

	1.5% Sun	9.4% Sun	51.5% Sun	98.5% Sun
Thermopile_ref	29.895 mSun	65.158 mSun	418.968 mSun	806.866 mSun
Current_ref	-52.351 μA	-337.236 μA	-1.849 mA	-3.535 mA
Power_in	1.458 mW/cm²	9.394 mW/cm²	51.503 mW/cm²	98.468 mW/cm²
Norm. Std. Dev.	27.72	2.29	0.79	0.45
Module U_oc	291.05 mV	420.30 mV	473.93 mV	470.32 mV
Cell U_oc	291.05 mV	420.30 mV	473.93 mV	470.32 mV
I_sc	-4.107 μA	-30.315 μA	-196.796 μA	-468.424 μA
J_sc	-7.95 μA/cm²	-70.41 μA/cm²	-460.21 μA/cm²	-1.08 mA/cm²
U_pmax	157.93 mV	330.48 mV	379.37 mV	368.58 mV
I_pmax	-4.7 μA/cm²	-56.6 μA/cm²	-399.0 μA/cm²	-958.9 μA/cm²
Power_out	739.76 nW/cm²	18.36 μW/cm²	151.37 μW/cm²	353.41 μW/cm²
Total Power_out	325.50 nW	8.08 μW	66.60 μW	155.50 μW
Fill Factor	0.272	0.634	0.714	0.706
Efficiency η	0.05%	0.20%	0.29%	0.36%

IPCE @ 550 nm : -7.8316 %
Slope ∂V_oc/∂ln(I_sc) : 44.293 mV

Calibration File: Mowgli:Igor Applications:DataScan Data:cal_Tue, Aug 25, 1998

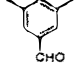© RAHB: KIDAQnew   Measured by Marie

Date: Thu, Oct 12, 2000
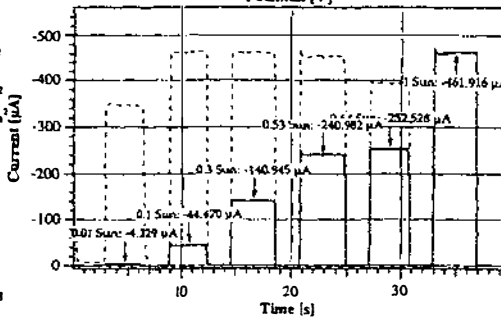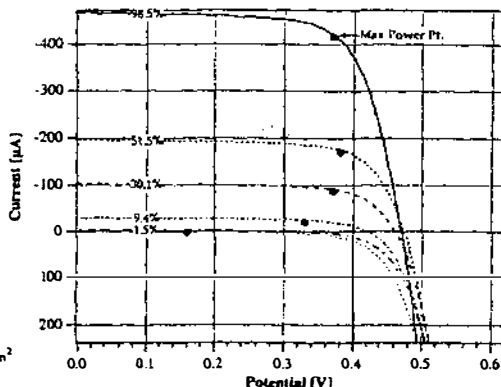
Zn₂-66
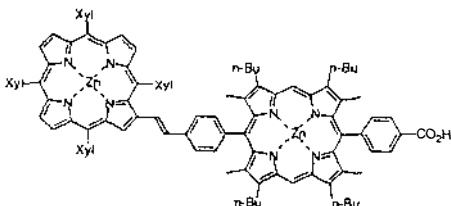
Cell Name: Marie_Oct 10#11

Measurement Date	: Tue, Oct 10, 2000 / 10:17:36 AM
Type of cell	: Robin 3micr
Cell Active Area	: 0.44 cm^2
Dye Sensitiser	: WAX 926
Additional Remarks	: 15h
Electrolyte Solution	: 955
SemiConductor Layer	: Robin 3μm
Layer Thickness, Porosity	: 3 μm, 63%
Working Electrode Glass	: NSG 10Ω/cm
Counter Electrode Type	: FlachGlas / Pt refl / Pt*
Data File Name	: Marie_Oct 10#11
Current Compliance	: 2 mA
Settling Time	: 0.04 s
Voltage Increment	: 5 mV

	1.4% Sun	9.5 % Sun	51.5% Sun	97.3% Sun
Thermopile$_{ref}$	29.372 mSun	75.214 mSun	429.612 mSun	826.913 mSun
Current$_{ref}$	-51.832 μA	-388.073 μA	-1.848 mA	-3.492 mA
Power$_{in}$	1.444 mW/cm^2	9.278 mW/cm^2	51.479 mW/cm^2	97.269 mW/cm^2
Norm. Std .Dev.	1141.28	7.85	2.17	1.46
Module U$_{oc}$	99.62 mV	388.47 mV	456.96 mV	476.57 mV
Cell U$_{oc}$	99.62 mV	388.47 mV	456.96 mV	476.57 mV
I$_{sc}$	-1.656 μA	-13.457 μA	-86.620 μA	-170.839 μA
I$_{sc}$	-3.24 μA/cm^2	-36.35 μA/cm^2	-202.66 μA/cm^2	-399.32 μA/cm^2
U$_{pmax}$	Nan V	296.62 mV	366.62 mV	386.03 mV
I$_{pmax}$	4.2 mA/cm^2	-22.1 μA/cm^2	-159.8 μA/cm^2	-326.5 μA/cm^2
Power$_{out}$	2.41 mW/cm^2	6.56 μW/cm^2	58.60 μW/cm^2	126.06 μW/cm^2
Total Power$_{out}$	1.06 mW	2.88 μW	25.78 μW	55.46 μW
Fill Factor	Nan	0.480	0.651	0.681
Efficiency η	166.74%	0.07%	0.11%	0.13%

IPCE @ 550 nm : -7.8316 %
Slope ∂V$_{oc}$/∂ln(I$_{sc}$) : 88.599 mV

Calibration File: Mowgli:Igor Applications:DataScan Data:cal_Tue, Aug 25, 1998

© RAHB: KIBAQnew   Measured by Marie
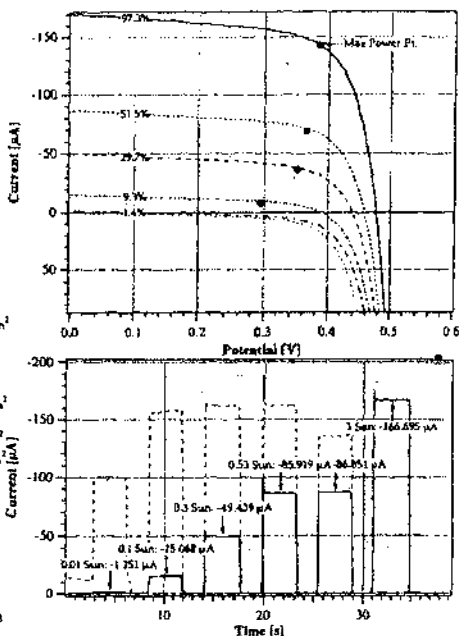
Date: Tue, Oct 10, 2000

Incident Photon to Current Conversion Efficiency

Measurement Date	: Tue, Oct 10, 2000/10:14:20 AM
Type of cell	: double 13micr
Cell N°.	: Marie_Oct 10#11
Cell Active Area	: 0.44 cm^2
Dye Sensitiser	: WAX-926
Additional Remarks	: 15h
Electrolyte Solution	: 1190
SemiConductor Layer	: double 13micr
Layer Thickness, Porosity	: 13 μm, 60 %
Working Electrode Glass	: NSG 10Ω/cm
Cell Temperature	: 298 K
Counter Electrode Type	: FlachGlas/Pt refl /Pt*
Data File Name	: Marie_Oct 10#11
Calibration File	: Quadra70:Igor Applications:DataScan Data:cal_Thu, Aug 10, 2000
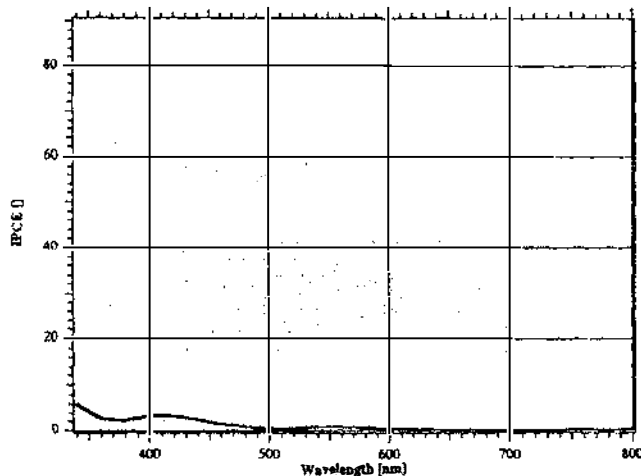
IPCE @ 540 nm (init) is 1 %

IPCE @ 550 nm (meas) is 1 %
IPCE @ 700 nm (meas) is 0 %

Integrated Current (AM 1.5 G ;1000W/m²) from 340 to 800nm is 172.3 μA/cm²

© RAHB   Measured by Marie

Date: Tue, Oct 10, 2000

Zn₂-99
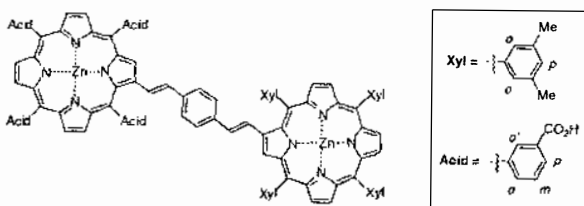
EPFL — Cell Name: Marie_Oct 12#09

	:
Measurement Date	: Thu, Oct 12, 2000 / 10:20:50 AM
Type of cell	: 8.8micr
Cell Active Area	: 0.44 cm²
Dye Sensitiser	: WAX975
Additional Remarks	: 15h
Electrolyte Solution	: 955
SemiConductor Layer	: 8.8μm
Layer Thickness, Porosity	: 8.8 μm, 63 %
Working Electrode Glass	: NSG 10Ω/cm
Counter Electrode Type	: FlachGlas/Pt refl/Pt°
Data File Name	: Marie_Oct 12#09
Current Compliance	: 2 mA
Settling Time	: 0.04 s
Voltage Increment	: 5 mV

	1.5% Sun	9.4% Sun	51.5% Sun	98.4% Sun
Thermopile_ref	25.193 mSun	68.684 mSun	416.029 mSun	808.041 mSun
Current_ref	-52.534 μA	-337.475 μA	-1.849 mA	-3.532 mA
Power_in	1.463 mW/cm²	9.400 mW/cm²	51.516 mW/cm²	98.391 mW/cm²
Norm. Std. Dev.	7.64	0.74	0.31	0.30
Module U_oc	342.22 mV	430.47 mV	488.20 mV	508.83 mV
Cell U_oc	342.22 mV	430.47 mV	488.20 mV	508.83 mV
I_sc	-12.071 μA	-135.399 μA	-881.739 μA	-1.807 mA
J_sc	-23.28 μA/cm²	-314.25 μA/cm²	-2.06 mA/cm²	-4.17 mA/cm²
U_pmax	255.10 mV	345.36 mV	384.29 mV	382.86 mV
J_pmax	-18.2 μA/cm²	-273.2 μA/cm²	-1.8 mA/cm²	-3.7 mA/cm²
Power_out	4.64 μW/cm²	94.35 μW/cm²	704.61 μW/cm²	1.43 mW/cm²
Total Power_out	2.04 μW	41.51 μW	310.03 μW	630.26 μW
Fill Factor	0.494	0.712	0.720	0.686
Efficiency η	0.32%	1.00%	1.37%	1.46%

IPCE @ 550 nm : -7.8316%
Slope ∂V_oc/∂ln(I_sc) : 39.524 mV
Ideality Factor @ 1 Sun : 1.37
Series Resistance @ 1 Sun 24.61 Ω ± 1.2 %, (10.83 Ω.cm2)

Calibration File: Mowgli:Igor Applications:DataScan Data:cal_Tue, Aug 25, 1998

© RAHB: KIDAQnew   Measured by Marie
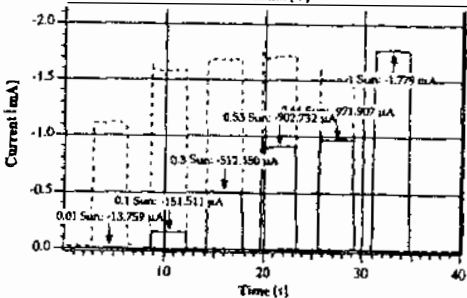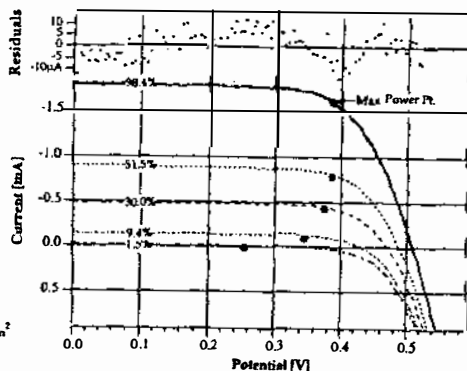
Date: Thu, Oct 12, 2000

EPFL — Cell Name: Marie_Oct 12#10

	:
Measurement Date	: Thu, Oct 12, 2000 / 10:31:53 AM
Type of cell	: 8.8micr
Cell Active Area	: 0.44 cm²
Dye Sensitiser	: WAX975
Additional Remarks	: 15h
Electrolyte Solution	: 955
SemiConductor Layer	: 8.8μm
Layer Thickness, Porosity	: 8.8 μm, 63 %
Working Electrode Glass	: NSG 10Ω/cm
Counter Electrode Type	: FlachGlas/Pt refl/Pt°
Data File Name	: Marie_Oct 12#10
Current Compliance	: 2 mA
Settling Time	: 0.04 s
Voltage Increment	: 5 mV

	1.5% Sun	9.4% Sun	52% Sun	98.7% Sun
Thermopile_ref	30.482 mSun	68.684 mSun	418.968 mSun	808.041 mSun
Current_ref	-52.940 μA	-337.682 μA	-1.867 mA	-3.543 mA
Power_in	1.475 mW/cm²	9.406 mW/cm²	52.004 mW/cm²	98.696 mW/cm²
Norm. Std. Dev.	12.91	1.05	0.41	0.26
Module U_oc	315.93 mV	408.21 mV	464.72 mV	483.62 mV
Cell U_oc	315.93 mV	408.21 mV	464.72 mV	483.62 mV
I_sc	-14.059 μA	-150.196 μA	-966.402 μA	-2.006 mA
J_sc	-26.90 μA/cm²	-348.38 μA/cm²	-2.24 mA/cm²	-4.62 mA/cm²
U_pmax	230.31 mV	324.97 mV	364.08 mV	364.55 mV
J_pmax	-18.4 μA/cm²	-300.6 μA/cm²	-2.0 mA/cm²	-4.1 mA/cm²
Power_out	4.23 μW/cm²	97.69 μW/cm²	727.50 μW/cm²	1.51 mW/cm²
Total Power_out	1.86 μW	42.98 μW	320.10 μW	663.14 μW
Fill Factor	0.419	0.701	0.713	0.684
Efficiency η	0.29%	1.04%	1.40%	1.53%

IPCE @ 550 nm : -7.8316 %
Slope ∂V_oc/∂ln(I_sc) : 39.883 mV
Ideality Factor @ 1 Sun : 1.38
Series Resistance @ 1 Sun 18.88 Ω ± 1.3 %, (8.31 Ω.cm2)

Calibration File: Mowgli:Igor Applications:DataScan Data:cal_Tue, Aug 25, 1998

© RAHB: KIDAQnew   Measured by Marie
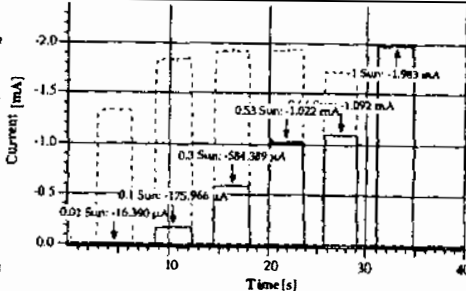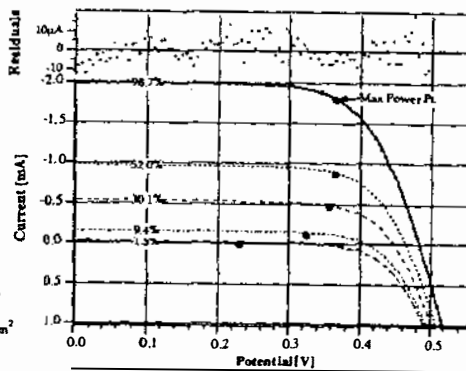
Date: Thu, Oct 12, 2000
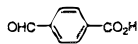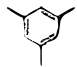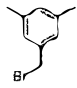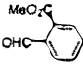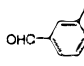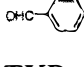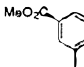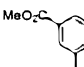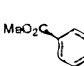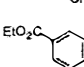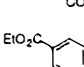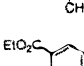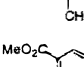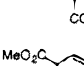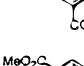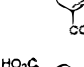
Appendix C

Compound Number Index

1	TPP	27	OHC—⟨benzene⟩—CO$_2$Me
2	TXP	28	OHC—⟨benzene⟩—CO$_2$Me
3	TBP	29	TXP-=-Ph$_o$CO$_2$Me
4	TPPps	30	TXP-=-Ph$_m$CO$_2$Me
5	TXPps	31	TBP-=-PhCO$_2$Me
6	TBPps	32	TXP-=-Ph$_o$CO$_2$H
7	OHC—⟨benzene⟩—CO$_2$H	33	TXP-=-Ph$_m$CO$_2$H
8	TCP	34	TBP-=-PhCO$_2$H
9	TPP-=-PhCO$_2$H	35	TXP-=-PhCO$_2^-$Na$^+$
10	TPP-=-PhCO$_2$Me	36	TXP-=-PhCO$_2^-$(n-Bu)$_4$N$^+$
11	TPP-=-PhCO$_2$TIPs	37	TXP-=-Ph$_m$(CO$_2$H)$_2$
12	TPP-=-PhCO$_2$CH$_2$CCl$_3$	38	MeO$_2$C—⟨benzene⟩—CO$_2$Me (CH$_3$)
13	TPP-=-PhCHO	39	MeO$_2$C—⟨benzene⟩—CO$_2$Me (CH$_2$Br)
14	TXP-=-PhCHO	40	MeO$_2$C—⟨benzene⟩—CO$_2$Me (CHO)
15	TXP-=-PhCO$_2$H	41	EtO$_2$C—⟨benzene⟩—CO$_2$Et (CO$_2$Et)
16	TXP-CHO	42	EtO$_2$C—⟨benzene⟩—CO$_2$Et (CH$_2$OH)
17	⟨structure⟩	43	EtO$_2$C—⟨benzene⟩—CO$_2$Et (CHO)
18	⟨structure, Br⟩	44	MeO$_2$C—⟨benzene⟩—CO$_2$Me (CO$_2$Me)
19	⟨structure, CHO⟩	45	MeO$_2$C—⟨benzene⟩—CO$_2$Me (CO$_2$H)
20	TXP-CH$_2$OH	46	MeO$_2$C—⟨benzene⟩—CO$_2$Me (COCl)
21	TXP-CH$_2$Cl	47	HO$_2$C—⟨benzene⟩—CO$_2$H (CO$_2$Me)
22	OHC—⟨benzene⟩—CHO		
23	TXP-=-PhCO$_2$Me		
24	TPP-Me		
25	TPP-CHO		
26	MeO$_2$C / OHC—⟨benzene⟩		

347

48

49

50 TXP-=-Ph$_m$(CO$_2$Me)$_2$

51

52

53

54

55

56

57 TXP-Me

58

59

60

61

62

BAcP

63

64

65

TXP-TBMP-TXP

66

67

68

69

70

71

72 TXP-=-PhOH

73

74

75

76

BFP

77

Building Block C

78

79 CHO *o,m,p*

8 0

o,m,p

81 *o,m,p*
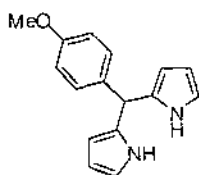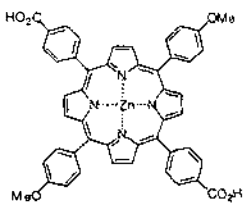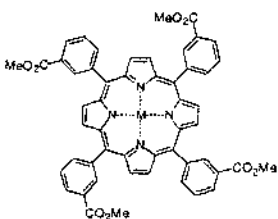
82

TXP-TBMP-TPP

83
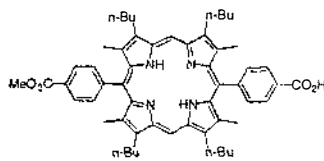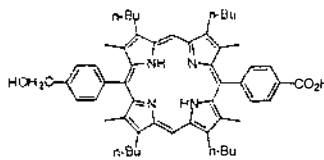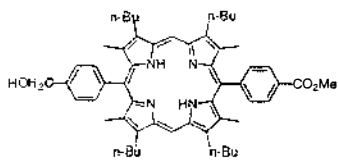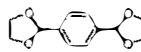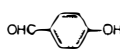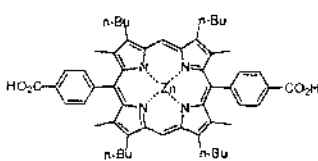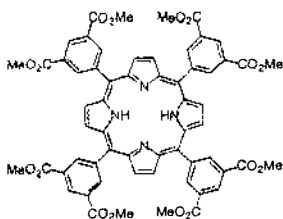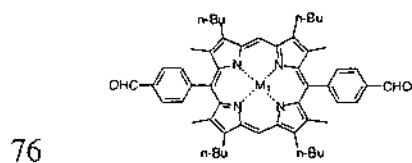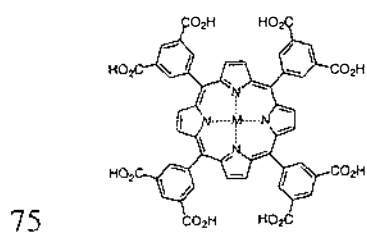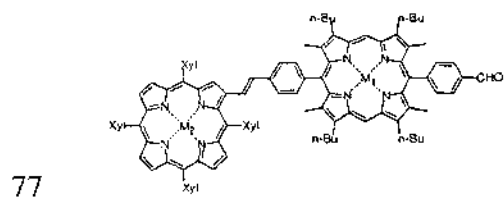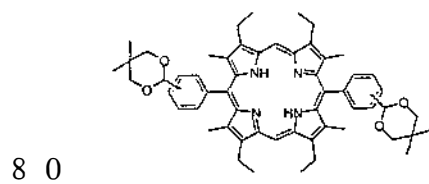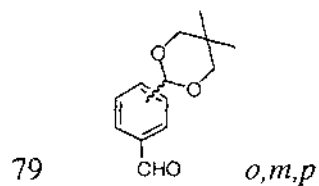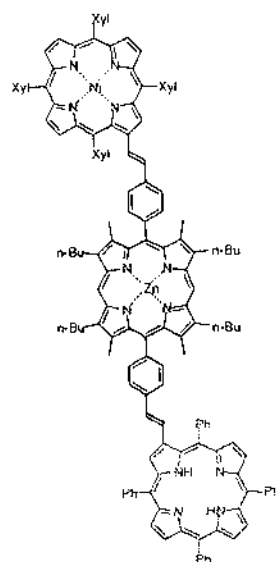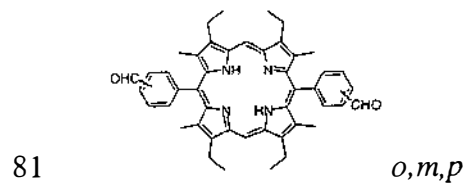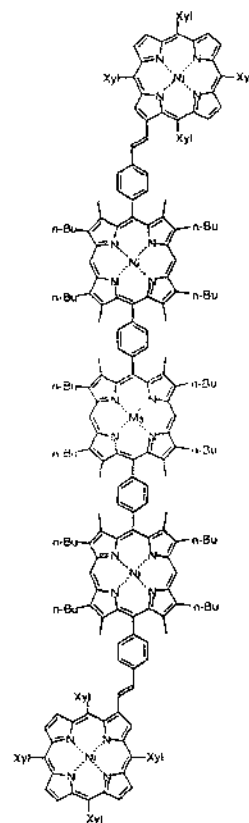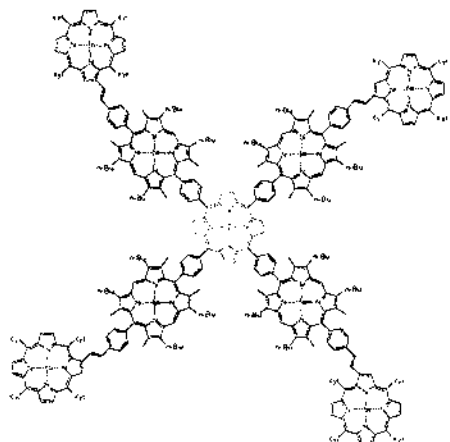
84

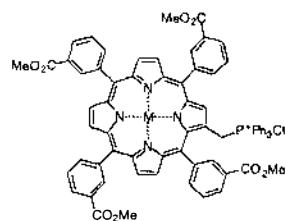85   TEP

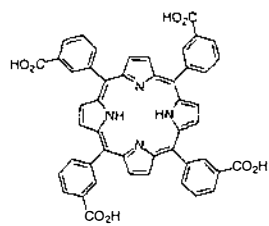86   TEPps
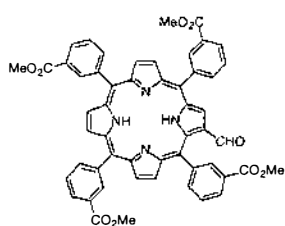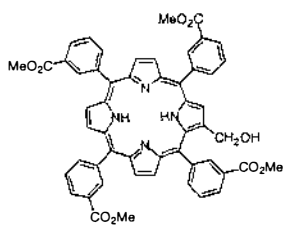
87   TEP-CHO
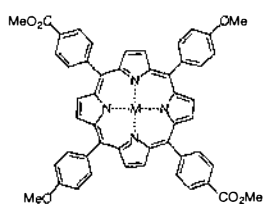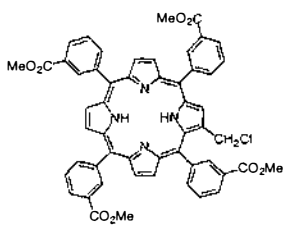

88
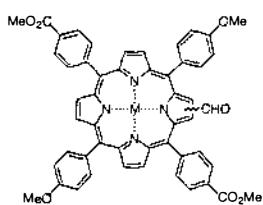
89
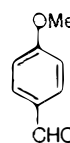
90

91
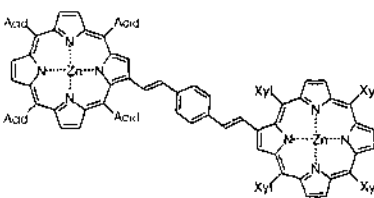

92

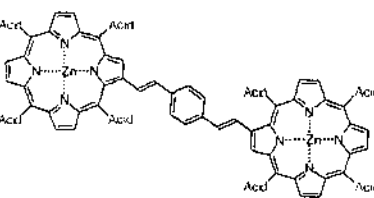
93   T3EP

9   4

T3EPps

95   T3CP

96   T3EP-

CHO

97   T3EP-

CH₂OH

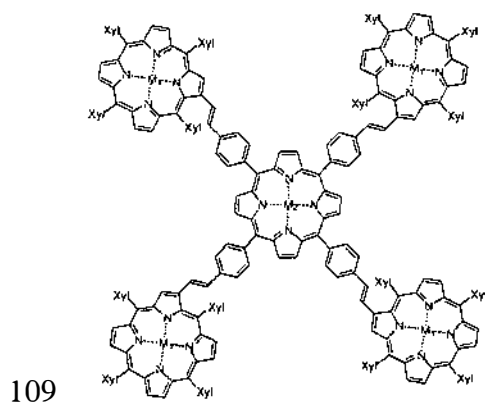98   T3EP-

CH₂Cl

99

100

101

T3EP-=-PhCHO

102

103

104

105

106

107

108

109

110 TFP

111

112

113

114 TAcP

115

116

117

118

119

120 M = Zn^{II}, Sb^{V} (O, Cl)

121 Acceptor R = ◊—N$^+$

M = Zn, Pd

122 Donor R = ◊—OH **122**

M = 2H

123

R = ⟨benzene-C₈H₁₇⟩ **123**

TOPP, M = 2H

124

Dimer A (M₁ = 2H, M₂ = Zn)
2H/Zn-124

Dimer B (M₁ = Zn, M₂ = 2H)
Zn/2H-124

125

P_Zn-P

125

126

M = 2H, Zn

P, P_Zn

127 PC

128

129 ZnTsPP

130 GaTsPc

131

132

133

134

135

136

137

138

139

140
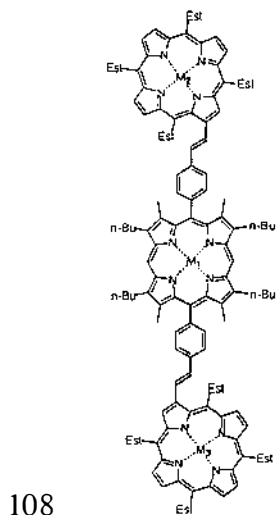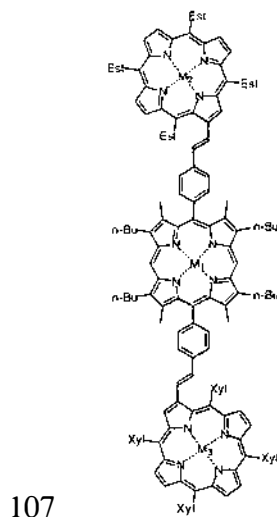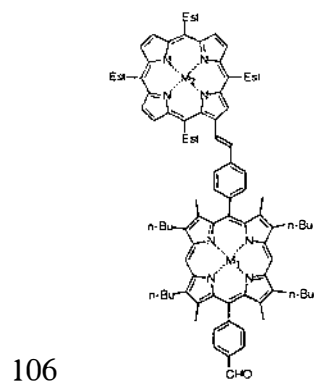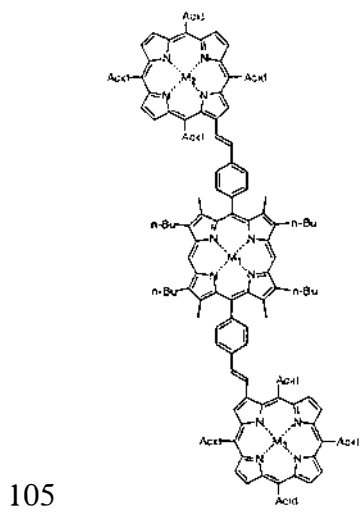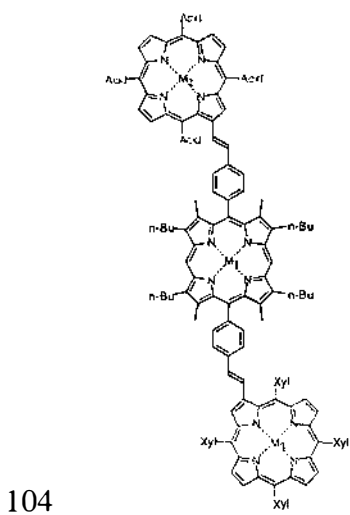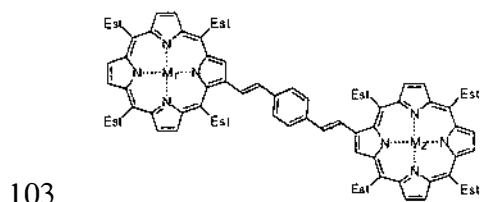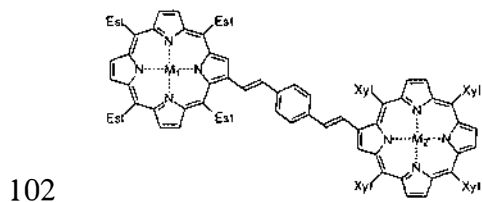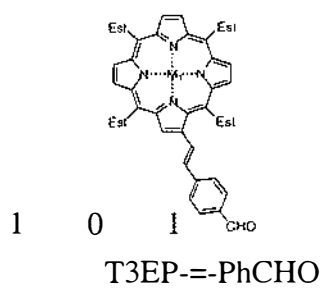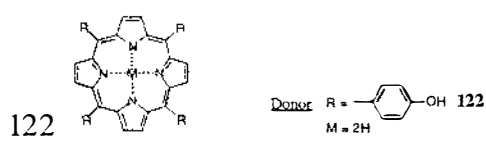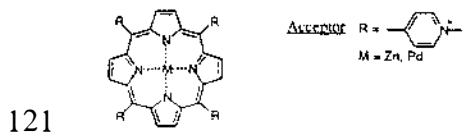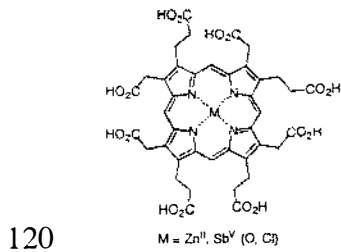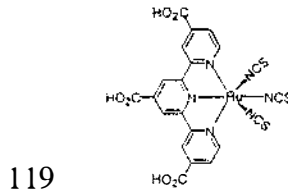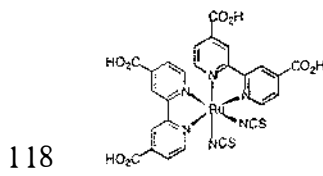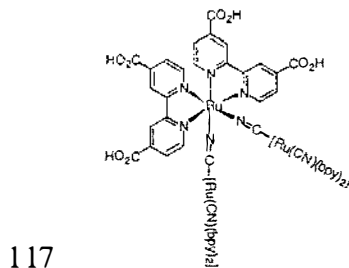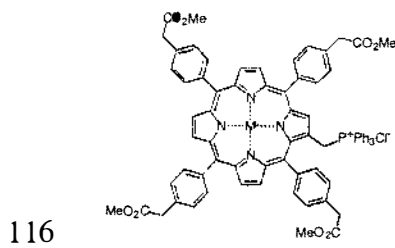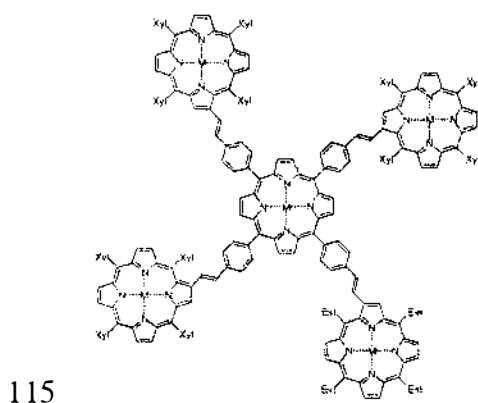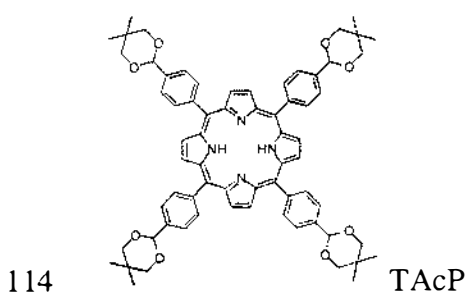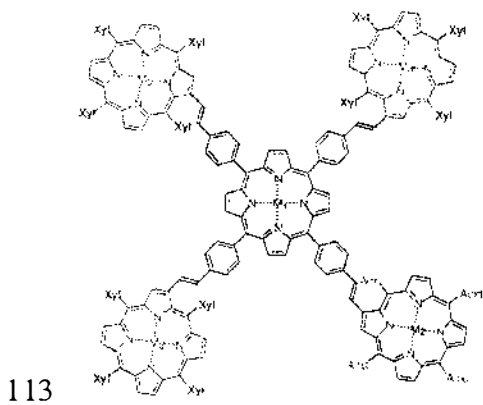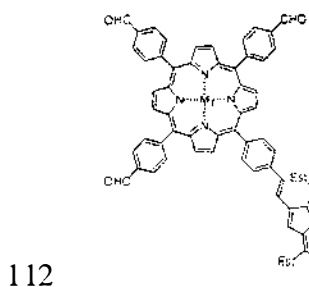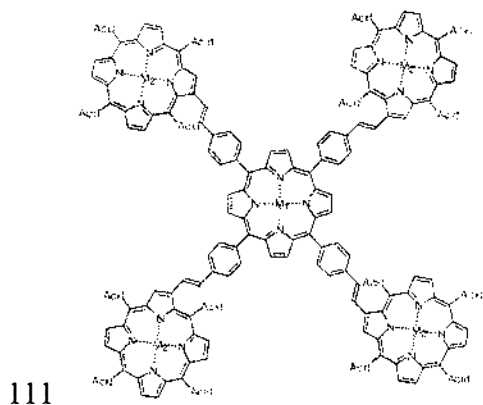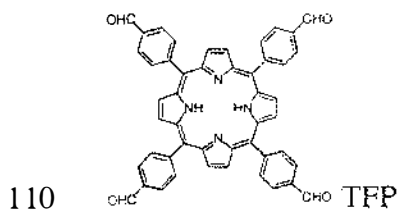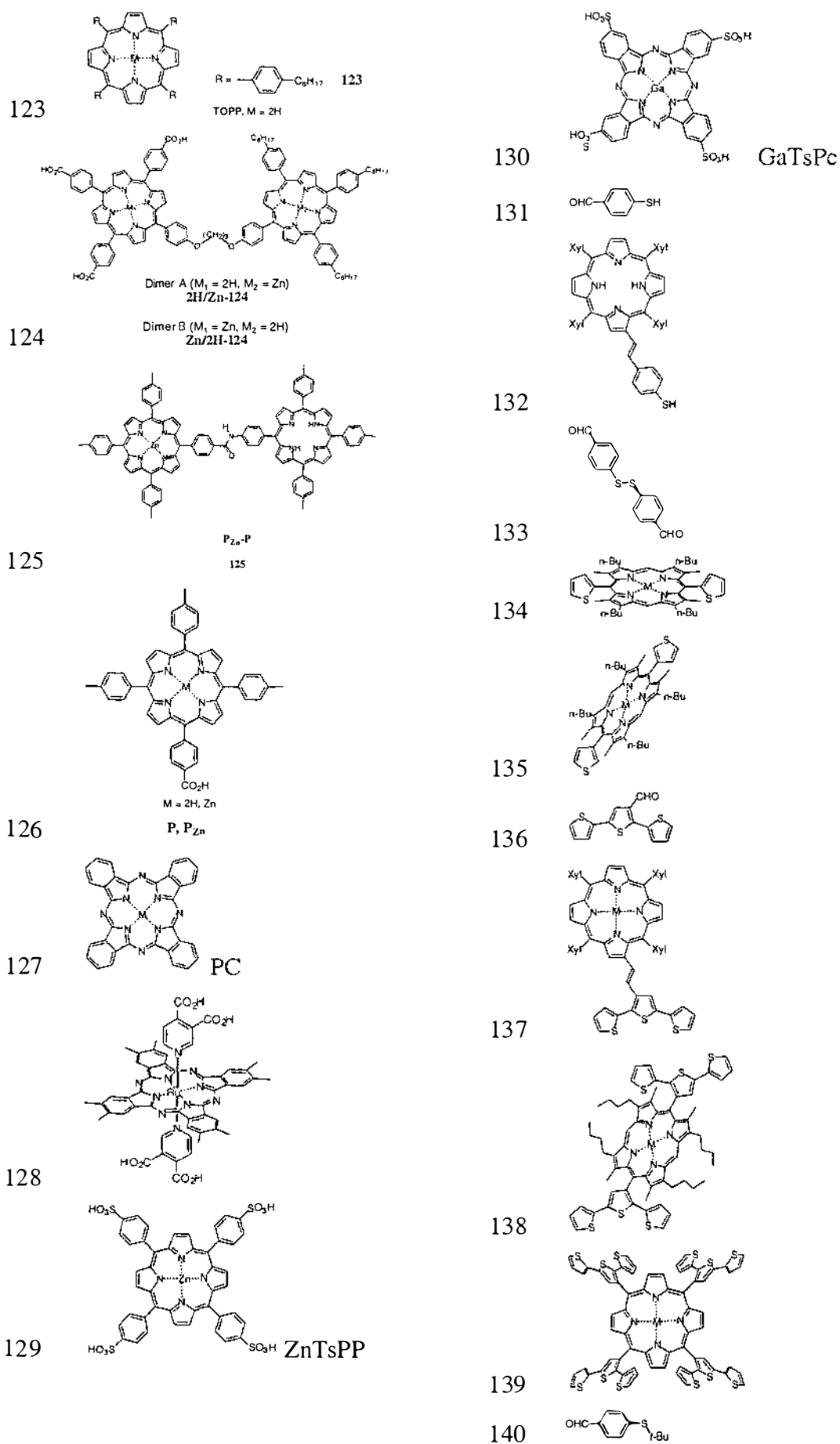
141
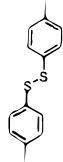
142
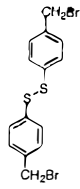
143

144
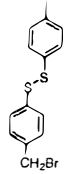
145

146

147

148

149

150

M = 2H, Zn
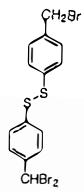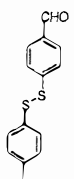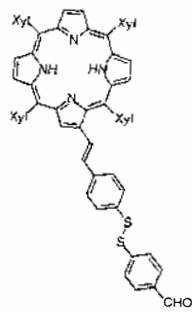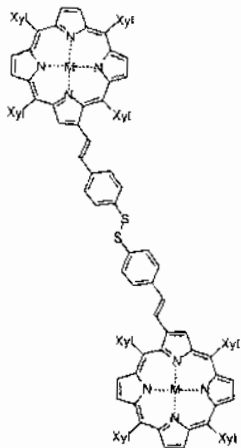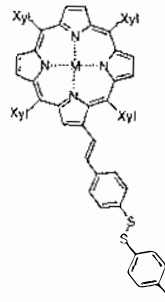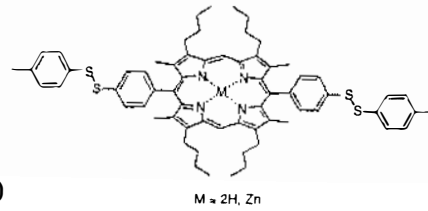
151
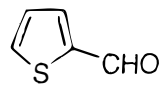
152
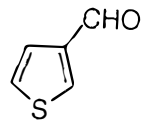
153
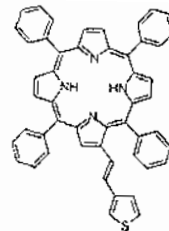
154
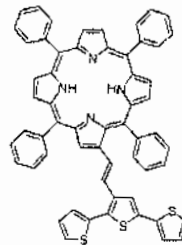
155
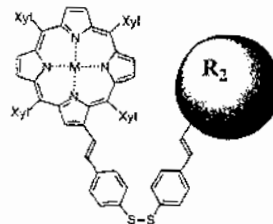
References and Notes

(1)   Mirkin, C. A.; Xu, F.; Zhu, J. *Adv. Mater.*, **1997**, *9*, 167-173.

(2)   Kamat, P. V. *Prog. Inorg. Chem.*, **1997**, *44*, 273-343.

(3)   Ulman, A. *Chem. Rev.*, **1996**, *96*, 1533-1554.

(4)   Ogawa, M. *Annu. Rep. Prog. Chem., Sect. C: Phys. Chem.*, **1998**, *94*, 209-257.

(5)   Schanze, K. S.; Schmehl, R. H. *J. Chem. Educ.*, **1997**, *74*, 633-635.

(6)   Bignozzi, C. A.; Schoonover, J. R.; Scandola, F. *Prog. Inorg. Chem.*, **1997**, *44*, 1-95.

(7)   Bignozzi, C. A.; Argazzi, R.; Kleverlaan, C. J. *Chem. Soc. Rev.*, **2000**, *29*, 87-96.

(8)   Kalyanasundaram, K.; Grätzel, M. *Coord. Chem. Rev.*, **1998**, *177*, 347-414.

(9)   Hagfeldt, A.; Grätzel, M. *Acc. Chem. Res.*, **2000**, *33*, 269-277.

(10)   Wienke, J.; Schaafsma, T. J.; Goossens, A. *J. Phys. Chem. B*, **1999**, *103*, 2702-2708.

(11)   Gerfin, T.; Grätzel, M.; Walder, L. *Prog. Inorg. Chem.*, **1997**, *44*, 345-393.

(12)   Moser, J. E.; Bonhote, P.; Walder, L.; Grätzel, M. *Chimia*, **1997**, *51*, 28-30.

(13)   Grätzel, M. *Coord. Chem. Rev.*, **1998**, *171*, 245-250.

(14)   Deb, S. K.; Lee, S. H.; Edwin Tracy, C.; Roland Pitts, J.; Gregg, B. A.; Branz, H. M. *Electrochim. Acta*, **2001**, *46*, 2125-2130.

(15)   Bechinger, C.; Ferrere, S.; Zaban, A.; Sprague, J.; Gregg, B. A. *Nature*, **1996**, *383*, 608-609.

(16)   Grätzel, M. *Nature*, **2001**, *409*, 575-576.

(17)   Will, G.; Sotomayer, J. S.; Rao, N.; Fitzmaurice, D. *J. Mater. Chem.*, **1999**, *9*, 2297-2299.

(18)   Hoffmann, M. R.; Martin, S. T.; Choi, W.; Bahnemann, D. W. *Chem. Rev.*, **1995**, *95*, 69-96.

(19)   Linsebigler, A. L.; Lu, G.; Yates, J. T., Jr. *Chem. Rev.*, **1995**, *95*, 735-758.

(20)   Treadway, J. A.; Moss, J. A.; Meyer, T. J. *Inorg. Chem.*, **1999**, *38*, 4386-4387.

(21)   Mills, A.; Le Hunte, S. *J. Photochem. Photobiol., A*, **1997**, *108*, 1-35.

(22)   Grätzel, M.; Hagfeldt, A. *Chem. Rev.*, **1995**, *95*, 49-68.

(23)   Gartsman, K.; Cahen, D.; Kadyshevitch, A.; Libman, J.; Moav, T.; Naaman, R.; Shanzer, A.; Umansky, V.; Vilan, A. *Chem. Phys. Lett.*, **1998**, *283*, 301-306.

(24) Wu, D. G.; Ashkenasy, G.; Shvarts, D.; Ussyshkin, R. V.; Naaman, R.; Shanzer, A.; Cahen, D. *Angew. Chem., Int. Ed.*, **2000**, *39*, 4496-4500.

(25) Imahori, H.; Norieda, H.; Yamada, H.; Nishimura, Y.; Yamazaki, I.; Sakata, Y.; Fukuzumi, S. *J. Am. Chem. Soc.*, **2001**, *123*, 100-110.

(26) Yamada, H.; Imahori, H.; Nishimura, Y.; Yamazaki, I.; Fukuzumi, S. *Chem. Commun.*, **2000**, 1921-1922.

(27) Willner, I.; Willner, B. *J. Mater. Chem.*, **1998**, *8*, 2543-2556.

(28) Braun, J. H. *J. Coat. Technol.*, **1997**, *69*, 59-72.

(29) Data ploted for AM1.0 and AM1.5 spectra were downloaded from National Renewable Energy Laboratories (NREL, USA), (retrieved March 2001), http://rredc.nrel.gov/solar.

(30) Haque, S. A.; Tachibana, Y.; Willis, R. L.; Moser, J. E.; Grätzel, M.; Klug, D. R.; Durrant, J. R. *J. Phys. Chem. B*, **2000**, *104*, 538-547.

(31) Huang, S. Y.; Schlichthorl, G.; Nozik, A. J.; Grätzel, M.; Frank, A. J. *J. Phys. Chem. B*, **1997**, *101*, 2576-2582.

(32) Zaban, A.; Chen, S. G.; Chappel, S.; Gregg, B. A. *Chem. Commun.*, **2000**, 2231-2232.

(33) Nazeeruddin, M.; Kay, A.; Rodicio, I.; Humphry-Baker, R.; Muller, E.; Liska, P.; Vlachopolous, N.; Grätzel, M. *J. Am. Chem. Soc.*, **1993**, *115*, 6382-6390.

(34) Deng, H.; Zhou, Y.; Mao, H.; Lu, Z. *Synth. Met.*, **1998**, *92*, 269-274.

(35) Hiemer, T. A.; D'Arcangelis, S. T.; Farzad, F.; Stipkala, J. M.; Meyer, G. J. *Inorg. Chem.*, **1996**, *35*, 5319-5324.

(36) Burfeindt, B.; Hannappel, T.; Storck, W.; Willig, F. *J. Phys. Chem.*, **1996**, *100*, 16463-16465.

(37) Moser, J.; Grätzel, M. *J. Am. Chem. Soc.*, **1984**, *106*, 6557-6564.

(38) Abe, R.; Hara, K.; Sayama, K.; Domen, K.; Arakawa, H. *J. Photochem. Photobiol., A*, **2000**, *137*, 63-69.

(39) Sayama, K.; Sugino, M.; Sugihara, H.; Abe, Y.; Arakawa, H. *Chem. Lett.*, **1998**, 753-754.

(40) Hoyle, R.; Will, G.; Fitzmaurice, D. *J. Mater. Chem.*, **1998**, *8*, 2033-2036.

(41) Rehm, J. M.; McLendon, G. L.; Nagasawa, Y.; Yoshihara, K.; Moser, J.; Grätzel, M. *J. Phys. Chem.*, **1996**, *100*, 9577-9578.

(42) Smestad, G. P.; Grätzel, M. *J. Chem. Educ.*, **1998**, *75*, 752-756.

(43) Falaras, P. *Sol. Energy Mater. Sol. Cells*, **1998**, *53*, 163-175.

(44) Duffy, N. W.; Dobson, K. D.; Gordon, K. C.; Robinson, B. H.; McQuillan, A. J. *Chem. Phys. Lett.*, **1997**, *266*, 451-455.

(45) Pechy, P.; Rotzinger, F. P.; Nazeeruddin, M. K.; Kohle, O.; Zakeeruddin, S. M.; Humphry-Baker, R.; Grätzel, M. *J. Chem. Soc., Chem. Commun.*, **1995**, 1093.

(46) Pechy, P.; Rotzinger, F. P.; Nazeeruddin, M. K.; Kohle, O.; Zakeeruddin, S. M.; Humphry-Baker, R.; Grätzel, M. *J. Chem. Soc., Chem. Commun.*, **1995**, 65-66.

(47) Argazzi, R.; Bignozzi, C. A.; Heimer, T. A.; Meyer, G. J. *Inorg. Chem.*, **1997**, *36*, 2-3.

(48) Heimer, T. A.; D'Arcangelis, S. T.; Farzad, F.; Stipkala, J. M.; Meyer, G. J. *Inorg. Chem.*, **1996**, *35*, 5319-5324.

(49) Vilan, A.; Ussyshkin, R.; Gartsman, K.; Cahen, D.; Naaman, R.; Shanzer, A. *J. Phys. Chem. B*, **1998**, *102*, 3307-3309.

(50) Zhang, J.; Wang, D.; Bai, Y.; Sun, H.; Shen, D.; Li, T. *J. Photochem. Photobiol., A*, **1998**, *112*, 225-229.

(51) Ashkenasy, G.; Kalyuzhny, G.; Libman, J.; Rubinstein, I.; Shanzer, A. *Angew. Chem., Int. Ed.*, **1999**, *38*, 1257-1261.

(52) Shin, C. K.; Lee, H.; Jung, C.; Kim, D.; Rhee, B. K. *Mol. Cryst. Liq. Cryst. Sci. Technol., Sect. A*, **2000**, *349*, 167-170.

(53) Dishner, M. H.; Hemminger, J. C.; Feher, F. J. *Langmuir*, **1996**, *12*, 6176-6178.

(54) Crossley, M. J.; Prashar, J. K. *Tetrahedron Lett.*, **1997**, *38*, 6751-6754.

(55) Liu, S.-G.; Echegoyen, L.; Martineau, C.; Raimundo, J.-M.; Roncali, J. *Chem. Commun.*, **2001**, 913-914.

(56) Kambe, S.; Murakoshi, K.; Kitamura, T.; Wada, Y.; Yanagida, S.; Kominami, H.; Kera, Y. *Sol. Energy Mater. Sol. Cells*, **2000**, *61*, 427-441.

(57) Balzani, V.; Campagna, S.; Denti, G.; Juris, A.; Serroni, S.; Venturi, M. *Acc. Chem. Res.*, **1998**, *31*, 26-34.

(58) Constable, E. C.; Harverson, P.; Ramsden, J. J. *Chem. Commun.*, **1997**, 1683-1684.

(59) Crossley, M. J.; Harding, M. M.; Sternhell, S. *J. Am. Chem. Soc.*, **1992**, *114*, 3266-3272.

(60) Smith, K. M.; Editor *Porphyrins and Metalloporphyrins*; 2nd Ed.; Elsevier: Amsterdam, **1975**.

(61) Kay, A.; Grätzel, M. *J. Phys. Chem.*, **1993**, *97*, 6272-6277.

(62) Kay, A.; Humphry-Baker, R.; Grätzel, M. *J. Phys. Chem.*, **1994**, *98*, 952-959.

(63) Kalyanasundaram, K.; Shelnutt, J. A.; Grätzel, M. *Inorg. Chem.*, **1988**, *27*, 2820-2825.

(64) Willner, I.; Katz, E.; Patolsky, F.; Buckmann, A. F. *J. Chem. Soc., Perkin Trans. 2*, **1998**, 1817-1822.

(65) Kobayashi, K.; Imabayashi, S. i.; Fujita, K.; Nonaka, K.; Kakiuchi, T.; Sasabe, H.; Knoll, W. *Bull. Chem. Soc. Jpn.*, **2000**, *73*, 1993-2000.

(66) Kanayama, N.; Kanbara, T.; Kitano, H. *J. Phys. Chem. B*, **2000**, *104*, 271-278.

(67) Yamamoto, H.; Liu, H.; Waldeck, D. H. *Chem. Commun.*, **2001**, 1032-1033.

(68) Nazeeruddin, M. K.; Humphry-Baker, R.; Grätzel, M.; Murrer, B. A. *Chem. Commun.*, **1998**, 719-720.

(69) Koehorst, R. B. M.; Boschloo, G. K.; Savenije, T. J.; Goossens, A.; Schaafsma, T. J. *J. Phys. Chem. B*, **2000**, *104*, 2371-2377.

(70) Fungo, F.; Otero, L.; Durantini, E. N.; Silber, J. J.; Sereno, L. E. *J. Phys. Chem. B*, **2000**, *104*, 7644-7651.

(71) Fungo, F.; Otero, L. A.; Sereno, L.; Silber, J. J.; Durantini, E. N. *J. Mater. Chem.*, **2000**, *10*, 645-650.

(72) Clausen, C.; Gryko, D. T.; Yasseri, A. A.; Diers, J. R.; Bocian, D. F.; Kuhr, W. G.; Lindsey, J. S. *J. Org. Chem.*, **2000**, *65*, 7371-7378.

(73) McDermott, G.; Prince, S. M.; Freer, A. A.; Hawthornthwaite-Lawless, A. M.; Papiz, M. Z.; Cogdell, R. J.; Isaacs, N. W. *Nature*, **1995**, *374*, 517-521.

(74) Kuehlbrandt, W. *Nature*, **1995**, *374*, 497-498.

(75) Kalyanasundaram, K. *Photochemistry of Polypyridine and Porphyrin Complexes*; Academic Press Limited, England, **1992**.

(76) Watts, R. J. *J. Chem. Educ.*, **1983**, *60*, 834-842.

(77) McCallien, D. W. J.; Burn, P. L.; Anderson, H. L. *J. Chem. Soc., Perkin Trans. 1*, **1997**, 2581-2586.

(78) Bonfantini, E. E.; Burrell, A. K.; Officer, D. L.; Reid, D. C. W.; McDonald, M. R.; Cocks, P. A.; Gordon, K. C. *Inorg. Chem.*, **1997**, *36*, 6270-6278.

(79) Reid, D. C. W., *A Building Block Approach to Porphyrin Arrays*, **1998**, PhD Thesis, IFS Chemistry, Massey University, Palmerston North, New Zealand.

(80) Longo, F. R.; Finarelli, M. G.; Kim, J. B. *J. Heterocycl. Chem.*, **1969**, *6*, 927-931.

(81)   Grant, D. K., *Synthetic Studies Toward Ionisable Porphyrin Derivatives*, **1997**, Honours Report, Department of Chemistry, Massey University, Palmerston North, New Zealand.

(82)   Burrell, A. K.; Officer, D. L. *Synlett*, **1998**, 1297-1307.

(83)   Belcher, W. J.; Burrell, A. K.; Campbell, W. M.; Officer, D. L.; Reid, D. C. W.; Wild, K. Y. *Tetrahedron*, **1999**, *55*, 2401-2418.

(84)   Corey, E. J.; Gilman, N. W.; Ganem, B. E. *J. Am. Chem. Soc.*, **1968**, *90*, 5616-5617.

(85)   Hudlicky, M. *Oxidations in Organic Chemistry*; American Chemical Society: Washington DC, **1990**, p 175, 179.

(86)   Dalcanale, E.; Montanari, F. *J. Org. Chem.*, **1986**, *51*, 567-569.

(87)   Banerjee, A.; Hazra, B.; Bhattacharya, A.; Banerjee, S.; Banerjee, G. C.; Sengupta, S. *Synthesis*, **1989**, 765-766.

(88)   Clezy, P. S.; Fookes, C. J. R. *Aust. J. Chem.*, **1977**, *30*, 609-620.

(89)   Iihama, T.; Fu, J.-M.; Bourguignon, M.; Snieckus, V. *Synthesis*, **1989**, *3*, 184-188.

(90)   Crossley, M. J., The University of Sydney, Personal communication, **1990**.

(91)   March, J. *Advanced Organic Chemistry: Reactions, Mechanisms, and Structure.*; 3rd Ed.; John Wiley & Sons: New York, **1985**, p 629 & 1072.

(92)   Sala, T.; Sargent, M. V. *J. Chem. Soc., Chem. Commun.*, **1978**, 253-254.

(93)   Sam, D. J.; Simmons, H. E. *J. Amer. Chem. Soc.*, **1972**, *94*, 4024-4025.

(94)   Lai, G.; Anderson, W. K. *Synth. Commun.*, **1997**, *27*, 1281-1283.

(95)   Attenburrow, J.; Cameron, A. F. B.; Chapman, J. H.; Evans, R. M.; Hems, B. A.; Jansen, A. B. A.; Walker, T. *J. Chem. Soc.*, **1952**, 1094-1111.

(96)   Fuhrhop, J.-H.; Vos, J. G.; Nakamura, A.; Ruhlmann, L. *Inorg. Chem.*, **1998**, *37*, 6052-6059.

(97)   Voegtle, F.; Gross, J.; Seel, C.; Nieger, M. *Angew. Chem.*, **1992**, *104*, 1112-1114. (See also Angew. Chem., Int. Ed. Engl., **1992**, 31(8), 1069-71).

(98)   Bonar-Law, R. P. *J. Org. Chem.*, **1996**, *61*, 3623-3634.

(99)   Gross, J.; Harder, G.; Siepen, A.; Harren, J.; Voegtle, F.; Stephan, H.; Gloe, K.; Ahlers, B.; Cammann, K.; Rissanen, K. *Chem.--Eur. J.*, **1996**, *2*, 1585-1595.

(100) Fudickar, W.; Zimmermann, J.; Ruhlmann, L.; Schneider, J.; Roeder, B.; Siggel, U.; Fuhrhop, J.-H. *J. Am. Chem. Soc.*, **1999**, *121*, 9539-9545.

(101) Kasina, S.; Nematollahi, J. *Tetrahedron Lett.*, **1978**, 1403-1406.

(102) Melvin, T.; Schuster, G. B. *Photochem. Photobiol.*, **1990**, *51*, 155-160.

(103) Keana, J. F. W.; Pou, S. *Org. Prep. Proced. Int.*, **1989**, *21*, 303-308.

(104) Atwell, G. J.; Yaghi, B. M.; Turner, P. R.; Boyd, M.; O'Connor, C. J.; Ferguson, L. R.; Baguley, B. C.; Denny, W. A. *Bioorg. Med. Chem.*, **1995**, *3*, 679-691.

(105) Von Pechmann, H. *Liebigs Ann. Chem.*, **1891**, *264*, 261.

(106) Sessler, J. L.; Johnson, M. R.; Creager, S. E.; Fettinger, J. C.; Ibers, J. A. *J. Am. Chem. Soc.*, **1990**, *112*, 9310-9329.

(107) Sessler, J. L.; Hugdahl, J.; Johnson, M. R. *J. Org. Chem.*, **1986**, *51*, 2838-2840.

(108) Kuciauskas, D.; Liddell, P. A.; Lin, S.; Stone, S. G.; Moore, A. L.; Moore, T. A.; Gust, D. *J. Phys. Chem. B*, **2000**, *104*, 4307-4321.

(109) Osuka, A.; Nagata, T.; Kobayashi, F.; Maruyama, K. *J. Heterocycl. Chem.*, **1990**, *27*, 1657-1659.

(110) Ichimura; Kunihiro; Yatabemachi; Tsukuba-gun; Ibaragi-ken, **1982**, US Patent Patent 4350833.

(111) Castells, J.; Font, J.; Virgili, A. *J. Chem. Soc., Perkin Trans. 1*, **1979**, 1-6.

(112) Blankespoor, R. L.; Smart, R. P.; Batts, E. D.; Kiste, A. A.; Lew, R. E.; Van der Vliet, M. E. *J. Org. Chem.*, **1995**, *60*, 6852-6859.

(113) Ponde, D. E.; Deshpande, V. H.; Bulbule, V. J.; Sudalai, A.; Gajare, A. S. *J. Org. Chem.*, **1998**, *63*, 1058-1063.

(114) Lindsey, J. S.; Hsu, H. C.; Schreiman, I. C. *Tetrahedron Lett.*, **1986**, *27*, 4969-4970.

(115) Gunter, M. J.; Mander, L. N. *J. Org. Chem.*, **1981**, *46*, 4792-4795.

(116) Vinogradov, S. A.; Wilson, D. F. *Tetrahedron Lett.*, **1998**, *39*, 8935-8938.

(117) Patel, B. R.; Suslick, K. S. *J. Am. Chem. Soc.*, **1998**, *120*, 11802-11803.

(118) Niedballa, U.; Weinmann, H. J.; Gries, H.; Conrad, J.; Hofmann, S.; Speck, U., **1994**, US Patent 5284647.

(119) Niedballa, U.; Gries, H.; Conrad, J.; Hofmann, S.; Weinmann, H. J.; Speck, U., **1989**, DE Patent 3809671.

(120) Lindsey, J. S.; Schreiman, I. C.; Hsu, H. C.; Kearney, P. C.; Marguerettaz, A. M. *J. Org. Chem.*, **1987**, *52*, 827-836.

(121) Frauenkron, M.; Berkessel, A.; Gross, J. H. *Eur. Mass Spectrom.*, **1997**, *3*, 427-438.

(122) Burrell, A. K.; Officer, D. L.; Plieger, P. G.; Reid, D. C. W. *Chem. Rev.*, **2001**, *101*, 2751-2796.

(123)   Wagner, R. W.; Lindsey, J. S.; Seth, J.; Palaniappan, V.; Bocian, D. F. *J. Am. Chem. Soc.*, **1996**, *118*, 3996-3997.

(124)   Lammi, R. K.; Ambroise, A.; Balasubramanian, T.; Wagner, R. W.; Bocian, D. F.; Holten, D.; Lindsey, J. S. *J. Am. Chem. Soc.*, **2000**, *122*, 7579-7591.

(125)   Mongin, O.; Papamicael, C.; Hoyler, N.; Gossauer, A. *J. Org. Chem.*, **1998**, *63*, 5568-5580.

(126)   Burrell, A. K.; Officer, D. L.; Reid, D. C. W.; Scott, S. M.; Gordon, K. C. *J. Porphyrins Phthalocyanines*, **2000**, *4*, 626-633.

(127)   Officer, D. L.; Burrell, A. K.; Reid, D. C. W. *Chem. Commun.*, **1996**, 1657-1658.

(128)   Takagi, S.; Inoue, H. *Multimetallic and Macromolecular Inorganic Photochemistry; Molecular and Supramolecular Photochemistry of Porphyrins and Metalloporphyrins*; Marcel Dekker, Inc.: New York, **1999**; Vol. 4.

(129)   Hammel, D.; Kautz, C.; Muellen, K. *Chem. Ber.*, **1990**, *123*, 1353-1356.

(130)   Higashida, S.; Imahori, H.; Kaneda, T.; Sakata, Y. *Chem. Lett.*, **1998**, 605-606.

(131)   Jiang, B.; Yang, S.; Niver, R.; Jones, W. E., Jr. *Synth. Met.*, **1998**, *94*, 205-210.

(132)   Balaban, T. S.; Eichhofer, A.; Lehn, J.-M. *Eur. J. Org. Chem.*, **2000**, 4047-4057.

(133)   Leo, L.; Mele, G.; Rosso, G.; Stasi, G.; Valli, L.; Vasapollo, G. *Sens. Microsyst., Proc. Ital. Conf., 4th*, **2000**, 202-206.

(134)   Burrell, A. K.; Campbell, W. M.; Therrien, B.; Officer, D. L., Manuscript in preparation, *Acta Cryst. E*, **2001.**

(135)   Burrell, A. K.; Officer, D. L.; Reid, D. C. W. *Angew. Chem., Int. Ed. Engl.*, **1995**, *34*, 900-902.

(136)   Lindsey, J. S.; Wagner, R. W. *J. Org. Chem.*, **1989**, *54*, 828-836.

(137)   Burrell, A. K.; Officer, D. L.; Scott, S. M., Unpublished results from these laboratories.

(138)   Bonfantini, E. E.; Officer, D. L. *Tetrahedron Lett.*, **1993**, *34*, 8531-8534.

(139)   Lee, C.-H.; Lindsey, J. S. *Tetrahedron*, **1994**, *50*, 11427-11440.

(140)   Littler, B. J.; Miller, M. A.; Hung, C.-H.; Wagner, R. W.; O'Shea, D. F.; Boyle, P. D.; Lindsey, J. S. *J. Org. Chem.*, **1999**, *64*, 1391-1396.

(141)   Wallace, D. M.; Leung, S. H.; Senge, M. O.; Smith, K. M. *J. Org. Chem.*, **1993**, *58*, 7245-7257.

(142)   Setsune, J.-i.; Hashimoto, M.; Shiozawa, K.; Hayakawa, J.; Ochi, T.; Masuda, R. *Tetrahedron*, **1998**, *54*, 1407-1424.

(143) Lavallee, D. K. *Coord. Chem. Rev.*, **1985**, *61*, 55-96.

(144) Datta-Gupta, N.; Jones, E.; Thomas, L. K.; Malakar, D. *J. Indian Chem. Soc.*, **1981**, *58*, 1171-1172.

(145) Bonar-Law, R. P.; Sanders, J. K. M. *J. Chem. Soc., Perkin Trans. 1*, **1995**, 3085-3096.

(146) Osuka, A.; Liu, B. L.; Maruyama, K. *Chem. Lett.*, **1993**, 949-952.

(147) Eckert, J.-F.; Nicoud, J.-F.; Nierengarten, J.-F.; Liu, S.-G.; Echegoyen, L.; Barigelletti, F.; Armaroli, N.; Ouali, L.; Krasnikov, V.; Hadziioannou, G. *J. Am. Chem. Soc.*, **2000**, *122*, 7467-7479.

(148) Nierengarten, J.-F.; Eckert, J.-F.; Nicoud, J.-F.; Ouali, L.; Krasnikov, V.; Hadziioannou, G. *Chem. Commun.*, **1999**, 617-618.

(149) Developed by Spectrolab (Division of Hughes Electronics Corporation) and National Renewable Energy Laboratory (NREL); Spectrolab Incorporated 12500 Gladstone Avenue, Sylmar, CA 91342-5373, USA.

(150) Nazeeruddin, M. K.; Pechy, P.; Renouard, T.; Zakeeruddin, S. M.; Humphry-Baker, R.; Comte, P.; Liska, P.; Cevey, L.; Costa, E.; Shklover, V.; Spiccia, L.; Deacon, G. B.; Bignozzi, C. A.; Grätzel, M. *J. Am. Chem. Soc.*, **2001**, *123*, 1613-1624.

(151) Bach, U.; Lupo, D.; Comte, P.; Moser, J. E.; Weissortel, F.; Salbeck, J.; Spreitzer, H.; Grätzel, M. *Nature*, **1998**, *395*, 583-585.

(152) Matsumoto, M.; Wada, Y.; Kitamura, T.; Shigaki, K.; Inoue, T.; Ikeda, M.; Yanagida, S. *Bull. Chem. Soc. Jpn.*, **2001**, *74*, 387-393.

(153) Tanaka, S. *Jpn. J. Appl. Phys., Part 1*, **2001**, *40*, 97-107.

(154) Stathatos, E.; Lianos, P.; Krontiras, C. *J. Phys. Chem. B*, **2001**, *105*, 3486-3492.

(155) Kelly, C. A.; Meyer, G. J. *Coord. Chem. Rev.*, **2001**, *211*, 295-315.

(156) Grätzel, M., (2000), *Ruthenium Dye Photocurrent Action Spectra Picture*, Retrieved 2001, http://dcwww.epfl.ch/icp/ICP-2/solarcellE.html.

(157) Khairutdinov, R. F.; Serpone, N. *J. Phys. Chem.*, **1995**, *99*, 11952-11958.

(158) Matsumura, M.; Mitsuda, K.; Yoshizawa, N.; Tsubomura, H. *Bull. Chem. Soc. Jpn.*, **1981**, *54*, 692-695.

(159) Kalyanasundaram, K.; Vlachopoulos, N.; Krishnan, V.; Monnier, A.; Grätzel, M. *J. Phys. Chem.*, **1987**, *91*, 2342-2347.

(160) Dabestani, R.; Bard, A. J.; Campion, A.; Fox, M. A.; Mallouk, T. E.; Webber, S. E.; White, J. M. *J. Phys. Chem.*, **1988**, *92*, 1872-1878.

(161) Boschloo, G. K.; Goossens, A. *J. Phys. Chem.*, **1996**, *100*, 19489-19494.

(162) Cherian, S.; Wamser, C. C. *J. Phys. Chem. B*, **2000**, *104*, 3624-3629.

(163) He, J.; Lindstrom, H.; Hagfeldt, A.; Lindquist, S. E. *J. Phys. Chem. B*, **1999**, *103*, 8940-8943.

(164) Tachibana, Y.; Haque, S. A.; Mercer, I. P.; Durrant, J. R.; Klug, D. R. *J. Phys. Chem. B*, **2000**, *104*, 1198-1205.

(165) Malinka, E. A.; Kamalov, G. L.; Vodzinskii, S. V.; Melnik, V. I.; Zhilina, Z. I. *J. Photochem. Photobiol., A*, **1995**, *90*, 153-158.

(166) Schaafsma, T. J. *Sol. Energy Mater. Sol. Cells*, **1995**, *38*, 349-351.

(167) Giraudeau, A.; Fan, F.-R. F.; Bard, A. J. *J. Am. Chem. Soc.*, **1980**, *102*, 5137-5142.

(168) Yanagi, H.; Chen, S.; Lee, P. A.; Nebesny, K. W.; Armstrong, N. R.; Fujishima, A. *J. Phys. Chem.*, **1996**, *100*, 5447-5451.

(169) Gregg, B. A. *Chem. Phys. Lett.*, **1996**, *258*, 376-380.

(170) Kajihara, K.; Tanaka, K.; Hirao, K.; Soga, N. *Jpn. J. Appl. Phys., Part 1*, **1996**, *35*, 6110-6116.

(171) Inigo, A. R.; Xavier, F. P.; Goldsmith, G. J. *Mater. Res. Bull.*, **1997**, *32*, 539-546.

(172) Fang, J.; Su, L.; Wu, J.; Shen, Y.; Lu, Z. *New J. Chem.*, **1997**, *21*, 1303-1307.

(173) Deng, H.; Zhang, H.; Liang, B.; Lu, Z. *Jpn. J. Appl. Phys., Part 2*, **1998**, *37*, L132-L135.

(174) IFS Mechanical & Electronic Workshops, Massey University, New Zealand.

(175) Philips Halotone Master Line Plus, GU 5.3, 12V/50W Halogen bulb, 24° Beam (UV Block).

(176) Emission spectra supplied courtesy of Philips Lighting, New Zealand.

(177) Evans, N., *Quantitative and Spectral Studies of Porphyrin Adsorbed Titanium Dioxide Photocells*, **2000**, 23.319 Chemistry Project Report, IFS, Massey University, New Zealand, Palmerston North.

(178) The light stainless steel spring for **CH3** was obtained from an automotive distributor cap.

(179) Nazeeruddin, M. K.; Zakeeruddin, S. M.; Humphry-Baker, R.; Jirousek, M.; Liska, P.; Vlachopoulos, N.; Shklover, V.; Fischer, C.-H.; Grätzel, M. *Inorg. Chem.*, **1999**, *38*, 6298-6305.
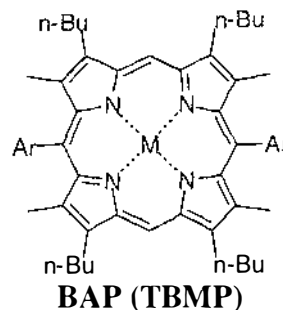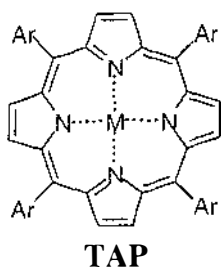
(180) Stanley, A.; Verity, B.; Matthews, D. *Sol. Energy Mater. Sol. Cells*, **1998**, *52*, 141-154.

(181) Nazeeruddin, M. K.; Kay, A.; Rodicio, I.; Humphry-Baker, R.; Mueller, E.; Liska, P.; Vlachopoulos, N.; Grätzel, M. *J. Am. Chem. Soc.*, **1993**, *115*, 6382-6390.

(182) Deb, S. K.; Ferrere, S.; Frank, A. J.; Gregg, B. A.; Huang, S. Y.; Nozik, A. J.; Schlichthoerl, G.; Zaban, A. *Conf. Rec. IEEE Photovoltaic Spec. Conf.*, **1997**, *26th*, 507-510.

(183) Schlichthoerl, G.; Huang, S. Y.; Sprague, J.; Frank, A. J. *J. Phys. Chem. B*, **1997**, *101*, 8139-8153.

(184) Uhlendorf, I.; Lauermann, I. *Proc. - Electrochem. Soc.*, **1997**, *97-20*, 126-129.

(185) Huang, S. Y.; Schlichthoerl, G.; Nozik, A. J.; Grätzel, M.; Frank, A. J. *J. Phys. Chem. B*, **1997**, *101*, 2576-2582.

(186) Sharma, C. V. K.; Broker, G. A.; Szulczewski, G. J.; Rogers, R. D. *Chem. Commun.*, **2000**, 1023-1024.

(187) Imahori, H.; Fukuzumi, S.; Nishimura, Y.; Yamazaki, I.; Norieda, H.; Karita, H.; Sakata, Y. *Chem. Commun.*, **2000**, 661-662.

(188) Yamada, H.; Imahori, H.; Fukuzumi, S.; Nishimura, Y.; Yamazaki, I. *Chem. Commun.*, **2000**, 1921-1922.

(189) Uosaki, K.; Kondo, T.; Zhang, X.-Q.; Yanagida, M. *J. Am. Chem. Soc.*, **1997**, *119*, 8367-8368.

(190) Gryko, D. T.; Zhao, F.; Yasseri, A. A.; Roth, K. M.; Bocian, D. F.; Kuhr, W. G.; Lindsey, J. S. *J. Org. Chem.*, **2000**, *65*, 7356-7362.

(191) Gryko, D. T.; Clausen, C.; Lindsey, J. S. *J. Org. Chem.*, **1999**, *64*, 8635-8647.

(192) Redman, J. E.; Sanders, J. K. M. *Org. Lett.*, **2000**, *2*, 4141-4144.

(193) Segawa, H.; Wu, F. P.; Nakayama, N.; Maruyama, H.; Sagisaka, S.; Higuchi, N.; Fujitsuka, M.; Shimidzu, T. *Synth. Met.*, **1995**, *71*, 2151-2154.

(194) Nagai, K.; Iyoda, T.; Fujishima, A.; Hashimoto, K. *Synth. Met.*, **1997**, *85*, 1701-1702.

(195) Kelemen, M.; Wachter, C.; Winter, H.; Dormann, E.; Gompper, R.; Hermann, D. *Mol. Phys.*, **1997**, *90*, 407-413.

(196) Ono, N.; Miyagawa, H.; Ueta, T.; Ogawa, T.; Tani, H. *J. Chem. Soc., Perkin Trans. 1*, **1998**, 1595-1602.

(197) Armiger, Y. L. S. T.; Lash, T. D. *J. Heterocycl. Chem.*, **1992**, *29*, 523-527.

(198) Ballarin, B.; Seeber, R.; Tassi, L.; Tonelli, D. *Synth. Met.*, **2000**, *114*, 279-285.

(199) Schaferling, M.; Bauerle, P. *Synth. Met.*, **1999**, *101*, 38-39.

(200) Shimidzu, T. *Synth. Met.*, **1996**, *81*, 235-241.

(201) Nakajima, M.; Onodera, O.; Matsuura, T.; Takamura, T.; Shimoyama, Y. *Hyomen Kagaku*, **2000**, *21*, 590-594.

(202) Dishner, M. H.; Taborek, P.; Hemminger, J. C.; Feher, F. J. *Langmuir*, **1998**, *14*, 6676-6680.

(203) Burrell, A. K.; Collis, G. E.; Officer, D. L. *Tetrahedron Lett.*, **2001**. Submitted for publication.

(204) Matsuura, T.; Takamura, T.; Shimoyama, Y. *Jpn. J. Appl. Phys., Part 1*, **1999**, *38*, 2874-2877.

(205) Young, R. N.; Gauthier, J. Y.; Coombs, W. *Tetrahedron Lett.*, **1984**, *25*, 1753-1756.

(206) Dickman, D. A.; Chemburkar, S.; Konopacki, D. B.; Elisseou, E. M. *Synthesis*, **1993**, 573-574.

(207) Papadopoulos, E. P.; Jarrar, A.; Issidorides, C. H. *J. Org. Chem.*, **1966**, *31*, 615-616.

(208) Hirano, M.; Yakabe, S.; Chikamori, H.; Clark, J. H.; Morimoto, T. *J. Chem. Res., Synop.*, **1998**, 310-311.

(209) Newman, M. S.; Lee, L. F. *J. Org. Chem.*, **1972**, *37*, 4468-4469.

(210) Too, C. O.; Wallace, G. G.; Burrell, A. K.; Collis, G. E.; Officer, D. L.; Boge, E. W.; Brodie, S. G.; Evans, E. J. *Synth. Met.*, **2001**, *123*, 53-60.

(211) Unpublished results from these laboratories.

(212) Nakayama, J.; Konishi, T.; Murabayashi, S.; Hoshino, M. *Heterocycles*, **1987**, *26*, 1793-1796.

(213) Beeston, R. F.; Stitzel, S. E.; Rhea, M. A. *J. Chem. Educ.*, **1997**, *74*, 1468-1471.

(214) Smela, E., University of Maryland.

(215) Osuka, A.; Nakajima, S.; Maruyama, K. *J. Org. Chem.*, **1992**, *57*, 7355-7359.

(216) Kim, H. S.; Chung, Y. M.; Park, Y. J.; Kim, J. N. *Bull. Korean Chem. Soc.*, **2000**, *21*, 371-372.

(217) Shim, S. C.; Lee, D. Y.; Choi, H. J.; Doh, C. H.; Huh, K. T. *Bull. Korean Chem. Soc.*, **1994**, *15*, 772-774.

(218) Furniss, B. S.; Hannaford, A. J.; Smith, P. W. G.; Tatchell, A. R. *Vogel's Textbook of Practical Organic Chemistry*; 5th Ed.; Longman Scientific & Technical: Essex, **1989**, 1077.

(219) Pouchert, C. J. *The Aldrich Library of NMR Spectra: Aldrich Chemical Company*; 2nd Ed.; Aldrich Chemical Company Inc: Milwaukee, **1983**.

(220) Keinan, E.; Benory, E.; Sinha, S. C.; Sinha-Bagchi, A.; Eren, D.; Eshhar, Z.; Green, B. S. *Inorg. Chem.*, **1992**, *31*, 5433-5438.

TAP and BAP Index

TAP

BAP (TBMP)

TAP	Ar	#
TPP	Ph	1
TXP	Xyl	2
TBP	BP	3
TEP	—CO$_2$Me	85
TCP	—CO$_2$H	8
T3EP	CO$_2$Me, Est	93
T3CP	CO$_2$H, Acid	95
T3,5EP	CO$_2$Me / CO$_2$Me	74
T3,5CP	CO$_2$H / CO$_2$H	75
TAcP		114
TFP	—CHO	110
TTTP		139

BAP	Ar	#
BAcP		62
BFP	—CHO	76
BEP	—CO$_2$Me	60
BCP	—CO$_2$H	73
BDP	—S—S— Me	150
B2TP		134
B3TP		135
BTTP		138